Ride and Handling Assessment of Vehicles Using Four-post Rig Testing and Simulation

L. J. Bennett

A thesis submitted in partial fulfilment of the requirements of Oxford Brookes University for the degree of Doctor of Philosophy

In association with Honda R&D Europe

October 2012

Abstract

The tuning of production road car suspension parameters in the development stage of a vehicle can be a lengthy and expensive procedure and commonly relies on the subjective judgements of test drivers to assess various aspects of ride and handling. The work in this thesis aims to create a testing and tuning technique using four-post rig testing and vehicle simulation to significantly reduce the amount of physical and subjective testing required within the development stage.

A four-post rig testing technique is developed using modal sine sweep inputs to acquire the response of the vehicle in the heave, pitch, roll and warp modes of excitation. An analysis and parameter estimation method is developed based on four-post data and a 7 degree-of-freedom model, with four-post test data used to validate the parameter estimation and vehicle model simultaneously, obtaining satisfactory results in all but the roll mode of excitation.

The BS 6841 [1] discomfort acceleration weightings are applied to the modal responses, with road input PSDs representative of standardised roads and driving cycles used to produce a comfort index value for a tested vehicle or setup.

A novel performance index is created to estimate grip loss due to static and dynamic tyre properties for each axle, which allows the prediction of road input effects on the total grip and balance of the vehicle, as well as a driver requirement of steering input.

MATLAB code is constructed for the parameter estimation procedure and for three general user interfaces to assist with the testing, tuning and benchmarking procedure.

An objective-subjective validation exercise is carried out using a single vehicle with four different component setups which are tested on the four-post rig to determine comfort and performance index values, as well as recording the subjective assessments of three test drivers on two drive routes in the UK and Germany. The results show fair to good correlation for comfort measures but generally poor correlation to the performance index, mostly because of large variations between the drivers' subjective assessment criteria.

Contents

Acknowledgements

There are many people that I would like thank for their help and support during my journey from starting this project to the final thesis, but I will aim to keep at least this section of the thesis short.

Firstly, I would like to thank the people at Honda R&D Europe for setting me the task of creating the testing and analysis method that this thesis details and funding the research. Special thanks to Blake Siegler (formally of Honda R&D Europe) and John Hargreaves who have been my supervisors at Honda throughout the project and who provided me with cars and components to test, as well as their advice.

I would like to thank my supervisors James Balkwill, Anand Thite and Denise Morrey for all of their supervision through the project, for help and encouragement when there seemed to be no solutions to some of the problems I encountered, and for providing me with critical but fair feedback of my work.

I would also like to thank other staff at Oxford Brookes University for their help, especially John Ward and Ian Spacksman who were always willing to help with setting up of the rig or changing components on the test vehicles.

I would like to say a big thank you to all my close family (Mum, Dad, Matt, Adam, Rebecca, Evie and Charlie) and friends who have been there to support me during the project and who have had to put up with me often not being free to socialise, especially during the writing up stage. My girlfriend Ruth deserves a special mention for her support and encouragement, for cooking me dinner when I was too busy and for understanding that when I say ‘I’ll have finished my PhD by the end of next weekend’, that it probably isn’t true.

Nomenclature

α – Slip Angle (degrees)

δ – Steering Angle (radians)

δ_{Ack} – Ackermann Steering Ratio (-)

δ_{HW} – Steering Angle at Hand Wheel (radians)

$\dot{\delta}$ - Steering Velocity (radians/s)

ζ – Damping Ratio (-)

γ - Coherence (-) and Camber (degrees)

ρ - Coherence Exponent (-)

ρ_{act} – Instantaneous Curvature (1/m)

ρ_{nom} – Desired Curvature (1/m)

θ – Phase (radians) and Pitch Angular Rotation (radians)

$\ddot{\theta}_2$ – Sprung Mass Pitch Rotational Acceleration (radians/s^2)

κ – Longitudinal Slip Ratio (-)

λ_{Fy} – Lateral Force Scaling Factor (-)

φ – Roll Angular Rotation (radians)

φ_0 – Input Roll Angular Rotation (radians)

φ_2 – Sprung Mass Roll Angular Rotation (radians)

Ω – Angular Wheel Velocity (radians/s)

ω – Angular Frequency (radians/s)

ω_n – Natural Frequency (radians/s and Hz)

a – Longitudinal Distance between Front Axle Centre Line and CofG (m) and Acceleration (m/s^2)

a_{max} – Maximum Sweep Rate (Hz/min)

$a_w s$ – Weighted Seat Acceleration RMS (m/s^2)

a_wp – Weighted Platform Acceleration RMS (m/s^2)

b – Longitudinal Distance between Rear Axle Centre Line and CofG (m)

d – Denominator Coefficients (-)

f – Frequency (Hz)

f_0 – Starting Frequency (Hz)

f_n – Resonance Frequency (Hz)

h – CofG Height (m)

k – Radius of Gyration (m) and Frequency Increase Exponent (-)

k_{dyn} – Dynamic Stiffness (N/m)

k_r – Roll Stiffness (N/m)

k_s – Spring Stiffness (N/m)

k_t – Tyre Stiffness (N/m)

k_{tm} – Top Mount Stiffness (N/m)

k_{Eng} – Engine Mounting Stiffness (N/,m)

l – Wheelbase (m)

l_{Eng} – Distance between Sprung Mass CofG and Engine CofG (m)

m – Mass (kg)

m_1 – Unsprung Mass (kg)

n – Spatial Frequency (cycles/m) and Numerator Coefficients (-)

n_0 – Reference Spatial Frequency (cycles/m)

r – Loaded Radius (m) and Yaw Velocity (radians/s)

r_e – Effective Rolling Radius (m)

$\dot{r}$ – Yaw Acceleration (radians/s^2)

t – Time (s)

t_r – Track Width (m) and Rear Track Width (m)

t_f – Front Track (m)

u – Longitudinal Velocity (m/s)

v – Lateral Velocity (m/s)

$\dot{v}$ – Lateral Acceleration (m/s^2)

w – Roughness Exponent (-)

w_1 – Low Wavenumber Roughness Exponent (-)

w_2 – High Wavenumber Roughness Exponent (-)

x – Displacement (m)

$\dot{x}$ - Velocity (m/s)

$\ddot{x}$ - Acceleration (m/s^2)

x_0 – Rig Actuator Displacement (m)

$\dot{x}_0$ – Rig Actuator Velocity (m/s)

$\ddot{x}_0$ – Rig Actuator Acceleration (m/s^2)

x_1 – Hub Displacement (m)

$\dot{x}_1$ – Hub Velocity (m/s)

$\ddot{x}_1$ – Hub Acceleration (m/s^2)

$x_{1.5}$ - Displacement of Top Mount Interface (m)

x_2 – Sprung Mass Displacement (m)

$\dot{x}_2$ – Sprung Mass Velocity (m/s)

$\ddot{x}_2$ – Sprung Mass Acceleration (m/s^2)

$\ddot{x}_{2v}$ – Sprung Mass Vertical Acceleration at CofG (m/s^2)

xSus – Suspension Displacement (m)

A – Suspension Displacement Amplitude (m)

A_{Fz} – Vertical Force Variation Amplitude (N)

$A_{FzDynamic}$ – Dynamically Scaled Equivalent of A_{Fz} (N)

C – Road Roughness Coefficient (m^3) and Damper Coefficient (N-sec/m)

C_{Eng} – Engine Mounting Damping (N-sec/m)

CPL – Contact Patch Load (N)

E – Energy Dissipated in a Cycle (W)

F – Force (N)

F_1 – Contact Patch Force (N)

F_{ksr} – Front Roll Stiffness (N/m)

F_x – Longitudinal Force (N)

F_y – Lateral Force (N)

$F_{yLoss\ Static}$ – Average Lateral Force Loss (%)

$F_{yLoss\ Static\_400}$ – $F_{yLossStatic}$ for 400kg Normal Load (%)

F_{y_Var} – Lateral Force Variation (N)

F_z – Vertical Force (N)

$F_{zStatic}$ – Static Vertical Force (N)

$F_{zStaticFactor}$ – Multiplication Factor for Normal Loads (-)

F_{z_Norm} – Static Mass Normalised Force Variation (%)

$F_{z\_Norm\_Dynamic}$ – Dynamically Weighted Equivalent of F_{z_Norm} (%)

$F_{z\_Norm\_Dynamic\_Combined}$ – Combined Version of $F_{z\_Norm\_Dynamic}$ (%)

G_d – Spatial Frequency Displacement PSD (m^3)

G_A – Acceleration PSD ((m/s^2)/Hz) or ((m/s^2)/n)

J – Mass Moment of Inertia ($kg.m^2$)

$J\varphi_2$ – Sprung Mass Roll Moment of Inertia ($kg.m^2$)

$J\varphi_{(Ground)}$ – Total Mass Roll Moment of Inertia about Ground Plane ($kg.m^2$)

J_{2p} – Sprung Mass Pitch Moment of Inertia ($kg.m^2$)

J_{2r} – Sprung Mass Roll Moment of Inertia ($kg.m^2$)

K – Steering Gain (-)

M – Mass (kg)

M_2 – Sprung Mass (kg)

M_z – Aligning Moment (Nm)

M_{Eng} – Engine Mass (kg)

M_T – Total Vehicle Mass (kg)

Q – Dynamic Amplification (-)

R – Inertia Coupling Ratio (-) and Signal Magnitude (-)

R_{ksr} – Rear Roll Stiffness (N/m)

RC_{CofG} – Roll Axis Height at CofG (m)

RC_F – Front Roll Centre Height (m)

RC_R – Rear Roll Centre Height (m)

S – Time Frequency Displacement PSD (m^2/Hz)

S_{max} – Maximum Sweep Rate (Octaves/min)

S_v – Time Frequency Velocity PSD ((m/s^2)/Hz)

S_{Hz} – Frequency Increase Rate (Hz/cycle)

T_w – Track Width (m)

V – Forward Velocity (m/s)

V_{sx} – Longitudinal Slip Velocity (m/s)

V_x – Longitudinal Velocity at Wheel Centre (m/s)

V_y – Lateral Velocity at Wheel Centre (m/s)

V_{Steer} – Steering Velocity Requirement (radians/s)

Wd_F – Fraction of vehicle Mass on Front Axle (-)

WT_F – Front Weight Transfer (N)

WT_R – Rear Weight Transfer (N)

$\dot{X}_{amp}$ – Constant Peak Velocity Amplitude (m/s)

Z – Complex Signal (-)

Z_0 – Input Displacement (m)

$\ddot{Z}_0$ – Input Acceleration (m/s^2)

Z_1 – Hub Displacement (m)

$\ddot{Z}_1$ – Hub Acceleration (m/s^2)

$_L$ – Suffix used to denote Left

$_R$ – Suffix used to denote Right

$_{FL}$ – Suffix used to denote Front Left Corner

$_{FR}$ – Suffix used to denote Front Right Corner

$_{RL}$ – Suffix used to denote Rear Left Corner

$_{RR}$ – Suffix used to denote Rear Right Corner

$_{Heave}$ – Suffix used to denote Heave Input of Output

$_{Pitch}$ – Suffix used to denote Pitch Input of Output

$_{Roll}$ – Suffix used to denote Roll Input of Output

$_{Warp}$ – Suffix used to denote Warp Input of Output

Abbreviations

BS – British Standards Institution

CofG – Centre of Gravity

CPL – Contact Patch Load

DoE – Design of Experiments

DoF – Degree-of-freedom

DSP – Digital Signal Processor

EVDV – Estimated Vibration Dose Value

FE – Finite Element

GPS – Global Positioning System

GUI – General User Interface

ICS – Iterative Control System

IMU – Inertial Measurement Unit

IRI – International Roughness Index

ISO – International Organization for Standardization

K&C – Kinematics and Compliance

MIRA – Motor Industry Research Association

MSDV – Motion Sickness Dose Value

NCHRP - National Cooperative Highway Research Program

NVH – Noise Vibration and Harshness

PC – Personal Computer

PSD – Power Spectral Density

PTFE - Polytetrafluoroethylene

R&D – Research and Development

RMQ – Root Mean Quad

RMS – Root Mean Square

SEAT – Seat Effective Amplitude Transmissibility

USB – Universal Serial Bus

VDV – Vibration Dose Value

VPG – Virtual Proving Ground

List of Figures

List of Tables

1 – Introduction

The ride and handling area of vehicle dynamics has been a topic of interest in the automotive industry for a number of years. One of the first engineers to investigate vehicle suspension behaviour in detail was Maurice Olley in the 1930's. Since then, the analysis and understanding of the way in which vehicle suspension behaves and the effect that it has on the vehicle motion and the passengers feelings has progressed immensely.

For modern road cars vehicle simulations are used substantially during the design stage of the vehicle. These models can vary from simple single-degree-of-freedom systems intended to simulate the behaviour of one corner of the vehicle bouncing on its suspension, to highly complex full vehicle models with hundreds of degrees-of-freedom, with realistic non-linear tyre behaviour.

These simulations are used in the design stage of the vehicle, to provide indications of suspension characteristics, and to model parameters, to provide desirable dynamic behaviour of a vehicle.

Once at the prototype stage of a vehicle a number of different tools are used to test various components of the vehicle as well as the whole vehicle itself. One common tool is the four-post rig, which is the main focus of this thesis. The four-post rig is a hydraulic rig used to vertically excite the road wheels of a vehicle, so that the vertical dynamics of the vehicle system can be measured. It is known that four-post test rigs are used widely within the automotive industry, yet very little information is published on the subject in general, and considerably less on road cars. This is most probably due to manufactures wanting to keep their proprietary test methods secret from their competition.

Even with the use of these complex simulations and rig testing a large amount of time and money is spent using test drivers and many different configurations of suspension parameters in order to determine the final suspension parameter setup of a vehicle before full production. In order to undertake this testing many low volume high cost components must be manufactured to be tested. The vehicles and test drivers will also be transported and tested to a variety of locations, which is costly to the manufacturer. Another downside with this method is that the amount of time spent in the tuning stage will delay the introduction of the vehicle into the market. For these reasons it is desirable for the manufacturer to have the subjective tuning part of the vehicle program as short as possible.

Honda had found success in using external consultant's four-post rig facilities and expertise to help in the tuning stage of a vehicle along with subjective test drives. However, they wished to have their own four-post rig testing technique and objective measures that they could relate to their test drivers subjective feeling. In addition it was also desired that a model be built that

would simulate the vehicle on the four-post rig so that simulations could be carried out, without the need to build physical components.

At the start of this project three main aims were set by Honda R&D Europe, these were:

1. Creation of a four-post rig testing technique and vehicle parameter estimation method.
2. Creation of a method of quantifying 'Performance' and 'Comfort' of a vehicle from four-post test measurements.
3. Creation of a model and simulation tool capable of allowing the engineer to optimise the vehicle suspension for 'best performance', 'best comfort' or a defined 'best compromise'.

To fulfil aim 1 a testing technique is developed that uses information from published literature to create a set of modal rig inputs suitable for characterising the response of a vehicle, In addition, a parameter estimation technique is created that was found suitably accurate to allow a 7 degree-of-freedom model to simulate four-post test derived vehicle responses with satisfactory accuracy with the exception of the roll excitation. The parameter estimation is not only useful for tuning purposes, but also allows the responses and parameters of competitor's cars to be estimated for benchmarking.

In order to fulfil aim 2 a comfort index is created that uses the vehicle responses and BS 6841 [1] discomfort weighting functions to create comfort responses which are then weighted using novel modal weighting PSDs for a specific road characteristic and speed profile. A novel performance index is created that uses literature on tyre behaviour to develop a method of estimating grip, car balance changes and driver steering requirements due to road inputs, that are used along with the model weighting PSDs to provide the final 'Performance Index' value. To assist the efficiency and consistency of the testing technique, MATLAB code is generated to carry out the signal processing and parameter estimation, which is run through the use of a general user interface. A second general user interface is created to allow efficient comparison between results from different setups and vehicles.

To validate the performance and comfort indices a subjective-objective test is carried out that finds fair to good correlation between objective and subjective comfort measures, but poor correlation between objective and subjective performance measures. However, in the same investigation large variations are obtained for the subjective driver assessments of the same vehicle setup, highlighting the difficulty of using subjective optimisation of vehicles.

To fulfil aim 3 a 8-degree-of-freedom model is developed along with MATLAB code and a general user interface that allows the user to sweep any of the vehicle parameters through a range of values, either independently or in pairs and note the effect on performance, comfort and a user adjusted compromise indices.

The method created has the potential to significantly reduce the amount of on-road testing required for subjective assessment and with it the time and financial costs associated with test driving.

2 - Literature Review

In this section of the thesis existing literature relevant to different aspects of the project is reviewed. The specific areas of research reviewed are:

- Road Surfaces
- Human Discomfort
- Vehicle Suspension Design Principals
- Vehicle Performance Optimisation
- Multi-post Rig Testing
- Parameter Determination
- Vehicle Modelling
- Subjective – Objective Vehicle Assessment

Some areas of the literature already have a large background of research, such as road surfaces and human discomfort. However, there is very little published on the use of multi-post rig testing for vehicle dynamics analysis. This is one area in which this thesis aims to add new and original contributions to the subject.

Another area in which this thesis aims to add contribution is in the objective vehicle assessment field. Currently there is a large gap in performance assessment of vehicles between using simple RMS (Root Mean Square) values of parameters such as contact patch load and complex assessment, such as full car models undertaking handling manoeuvres. One of the aims of this thesis is to produce performance assessments that are more relevant to real road and driving situations than the simple RMS, yet less complex and specific than handling manoeuvres.

2.1 – Road Surfaces

When designing and tuning a dynamic system it is vital to know the structure of the inputs that the system is likely to encounter during operation. For road cars the main source of excitation is the road surface. There are various ways to measure the road surface. Profilers explained in 'The little book of profiling' by Sayers and Karamihas [2] include:

1. Rod and Level, as used in general surveying.
2. A device called the 'Dipstick', which is walked along the path to be profiled and includes an accurate inclinometer and on-board computer to calculate the road profile.
3. The Inertial profiler, where a vehicle is instrumented with accelerometers to measure changes in vehicle height and a laser, infrared or ultrasonic sensor, used to measure the distance between the vehicle and road.

Other methods use indirect measurement of the road surface from vehicle sensors, such as work by Imine, Delanne and Sirdi [3], where a sliding mode observer was used to determine the road displacement using an instrumented vehicle and compared to measurements taken at the same time using well established profilers.

The ISO 8608 and BS 7853 standard [4], specifies a uniform way of reporting measured road profile data for both one-track and multi-track profiles so that profiles from various sources can be compared.

To create a generalised description of the road profile a curve is fitted to the displacement PSD (Power Spectral Density) over a specified range and in the form of equation (2-1).

$$G_d(n) = G_d(n_0) \times \left(\frac{n}{n_0} \right)^{-w} \tag{2-1}$$

Where:

G_d – Displacement PSD

n – Spatial frequency (cycles/m)

n_0 – Reference spatial frequency (0.1 cycles/m)

w – Exponent

An example presentation of road profile data from the standard is shown in Figure 2-1.

The standard explains that in the case where the exponent is equal to 2, the velocity PSD is constant along both frequency and spatial frequency domains. The standard presents a classification of road surfaces A to H which all have an exponent of 2. The profiles A to E represent: ‘Very Good’, ‘Good’, ‘Average’, ’Poor’, and ‘Very Poor’ roads respectively. Figure 2-2 presents the road profile classification levels from the standard.

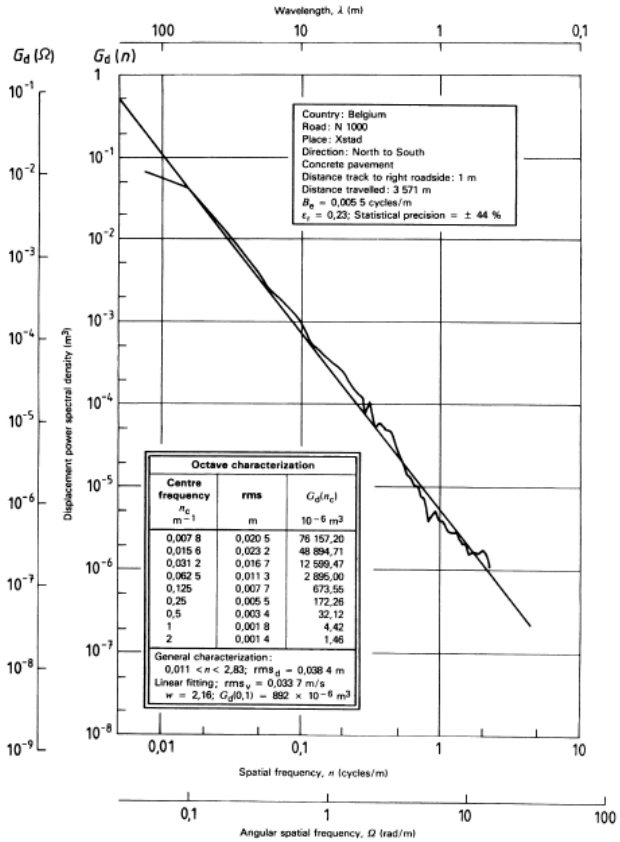

Figure 2-1– Example road profile displacement PSD and information – ISO 8608 [4]

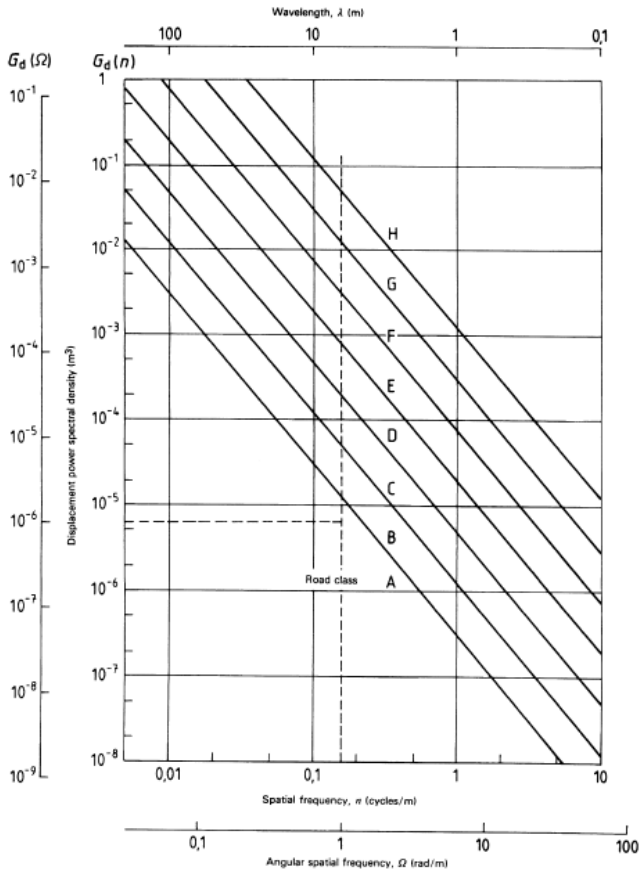

Figure 2-2 – Road profile classification – ISO 8608 [4]

In 2000, Rouillard, Bruscella and Sek [5] wrote a paper introducing a universal road profile classification method with special attention to the non-Gaussian and non-stationary properties of the profiles. The authors created nine classification parameters to describe the spatial acceleration of the road profile, based on the statistical characteristics of the transients and stationary segments.

Another method of road classification commonly used in research is the IRI (International Roughness Index). In 1995, Sayers [6] wrote a paper on the use of the IRI and its calculation from a longitudinal road profile and the IRI is explained by Sayers and Karamihas [2]. The IRI uses a linear two-degree-of-freedom quarter car model with specified dynamic properties known as 'The Golden Car', which is simulated over the road profile at fixed forward velocity of 80 kph (22 m/s). The IRI is a measure of cumulative suspension displacement of the vehicle normalised by the length of the profile, in units of mm/m.

In 2005, Kropac and Mucka [7] wrote a paper investigating the use of the IRI on different road surfaces. In this paper the authors created 7 different inputs an IRI of 2.21, but with different spectral properties representative of road surfaces. The authors found that the IRI was

insufficient to define a road profile if the profile is to be used for comfort assessment and the road does not conform to the standard spatial frequency exponent of 2.

In 2006, Andrén [8] wrote a paper exploring different ways that PSD approximations of road profiles have been created in the past 40-50 years. Nine different methods were presented, with four of the approximations being fitted to longitudinal road profile data from the entire Swedish state road network. The author found that the single gradient ISO 8608 [4] fit had the largest error. The most appropriate approximation was the two-split method, where a single roughness coefficient was used, but with 3 different exponents relating to different spatial frequency ranges.

For the simulation of vehicles travelling over road profiles, it is very common to assume that the rear wheels encounter the same inputs as the front wheels lagged by an amount of time specified by the forward velocity of the vehicle and the wheelbase. This is the case in a number of papers and books including Hassan and Lashine (2002) [9], Robson (1979) [10] and Gillespie (1992) [11]. However, it is often not possible to assume that the left and right tracks of a vehicle encounter the same road profile. A number of papers look into the correlation of the inputs to the left and right wheels of a vehicle and how these inputs affect the vibration of the vehicle.

In 1978, Kamash and Robson [12] and again in 1979, Robson [10] proposed the use of isotropy to describe the road surface. The model of isotropy is used to determine the coherence between the left and right wheel tracks of a vehicle and in-turn can be used to generate road inputs. However, the validity of the isotropic model is not particularly impressive. Robson notes that ‘it has to be admitted that close agreement between isotropy-based coherencies and measurement-based coherencies has not been demonstrated.’ Despite this fact, the isotropic assumption has been quite widely used to describe the road surface for vehicle modelling purposes. Figure 2-3 shows an example of the isotropy-based and measurement-based coherence for 3 different road types.

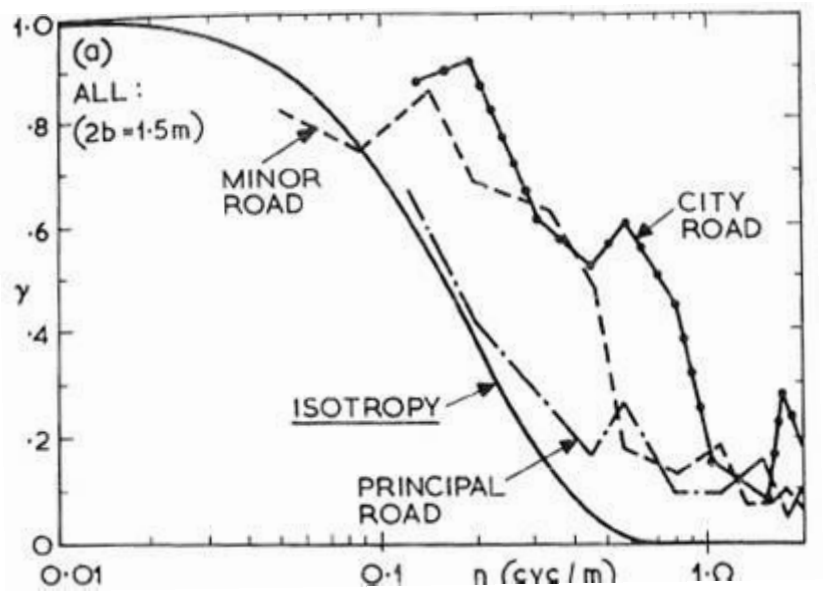

Figure 2-3 – Comparison of isotropy-based coherence to measured coherence – Robson (1979) [10]

In 1986, Sayers [13] wrote about the power spectral density functions of vertical and roll components of road roughness.

Sayers noted that for a typical road profile PSD with an exponent of 2 (as explained in ISO 8608 [4]), the constant velocity PSD can be defined as 'white noise' and with a given road roughness and forward speed, can be used as a PSD input to frequency domain transfer functions, which can be used to predict output PSDs for certain parameters important to road car comfort and safety.

The paper identifies the road inputs in terms of modal inputs to the vehicle in heave and roll, as well as coherence between left and right, vertical and roll inputs. Sayers found that the coherences had the following characteristics:

- Left-right coherence close to 1 for low wavenumbers, dropping to almost 0 at high wavenumbers.
- Left-vertical coherence close to 1 for low wavenumbers, dropping to 0.5 at high wavenumbers.
- Left-roll coherence close to 0 for low wavenumbers, but increases to 0.5 at high wavenumbers.
- Vertical-roll coherence close to 0 for all wavenumbers.

Sayers explains that the use of Parkhilovskii's model (Robson (1978) [14]) is possible, as this model assumes zero coherence between vertical and roll excitations at all wavenumbers. Rill

[15] has suggested that a single-pole high-pass filter can be used for this purpose and for the road surfaces investigated in Sayers [13], this was found to be more representative.

Bogsjo (2008) [16] studied the coherence functions for 20 measured roads of the Swedish road network. Coherences were compared for significantly different road spectrums and found to be surprisingly similar (Figure 2-4). Bogsjo compared the isotropic model coherence to a parametric exponentially decreasing model with a constant ρ fitted from the road coherence (Figure 2-5). The author found the exponential model superior in its representation of measured coherence compared to the isotropy model. However, one problem with this model is that it requires both wheel tracks to be measured and reported to calculate ρ, which the isotropic model does not. Obviously a general value can be used when only one wheel track is available, but this potentially reduces the validity of the modelling method.

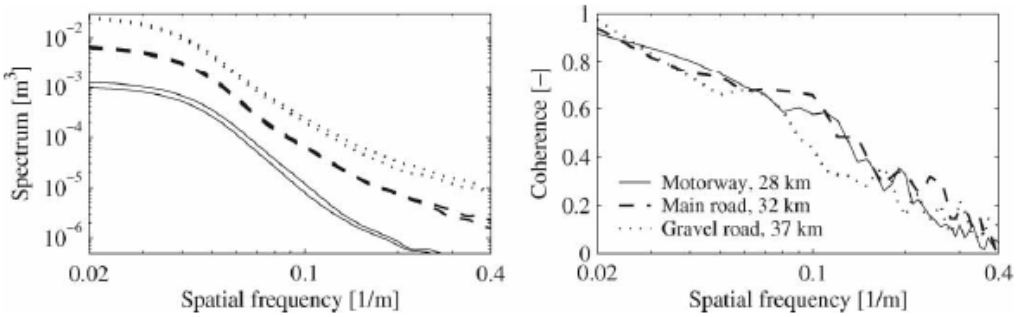

Figure 2-4 – Spectrum and coherence of different roads - Bogsjo (2008) [16]

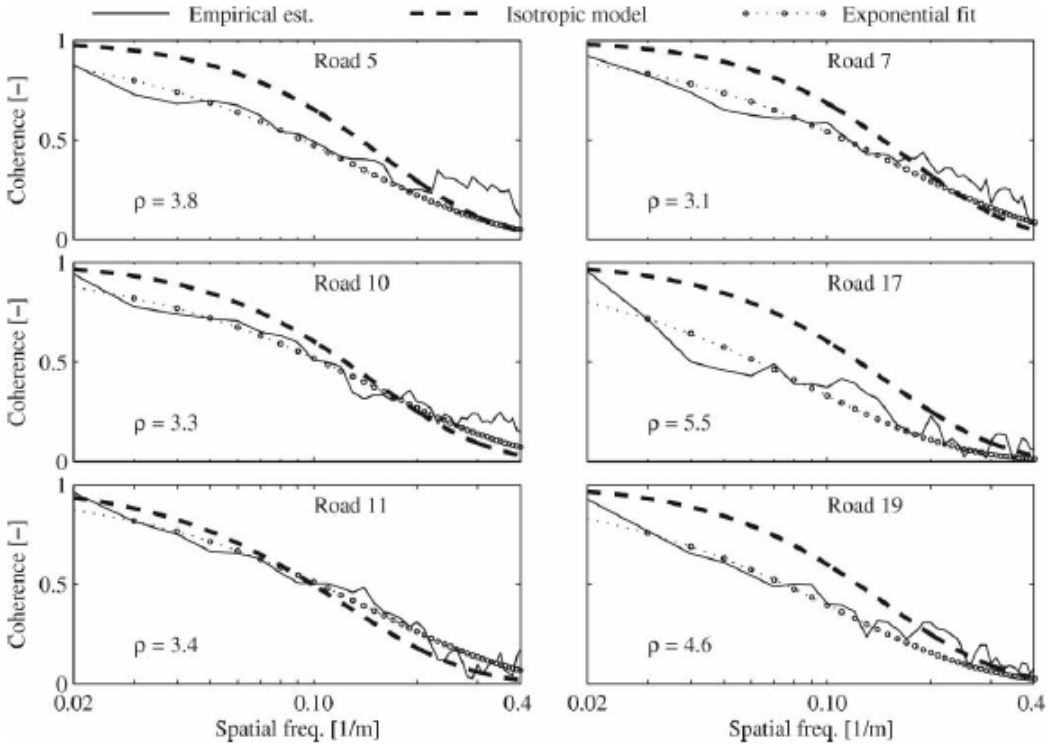

Figure 2-5 – Comparison of measured coherence, isotropic model and exponential model for 6 different road profiles – Bogsjo (2008) [16]

Rill (1984) [15] used 5 different complexity road models relating to both left to right and front to rear correlations, to investigate their influence on vehicle vibration. The road models were used as time domain inputs to a 19 degree-of-freedom vehicle model. Simulated vertical accelerations along the length and width of the vehicle body were compared and in conclusion, the author noted that, 'for improved investigations no simplifications in road modelling are justified'.

Mucka (2004) [17] investigated the effect of road roughness in different spatial frequency ranges. The author used a simple two degree-of-freedom quarter car model to assess the changes in the dynamic tyre force of a heavy commercial vehicle with varying exponents in the high and low spatial frequency range. The author found that changing the exponents, but maintaining the same roughness had a significant effect on the dynamic tyre force (Figure 2-6). Mucka noted that for small deviations from an exponent of 2 (1.9 to 2.1) the influence of the exponent is small and only the roughness coefficient is important, but also noted that 'Simple use of a time-integrated white-noise signal could cause marked errors in random response prediction in comparison with the response of the vehicle in real conditions'.

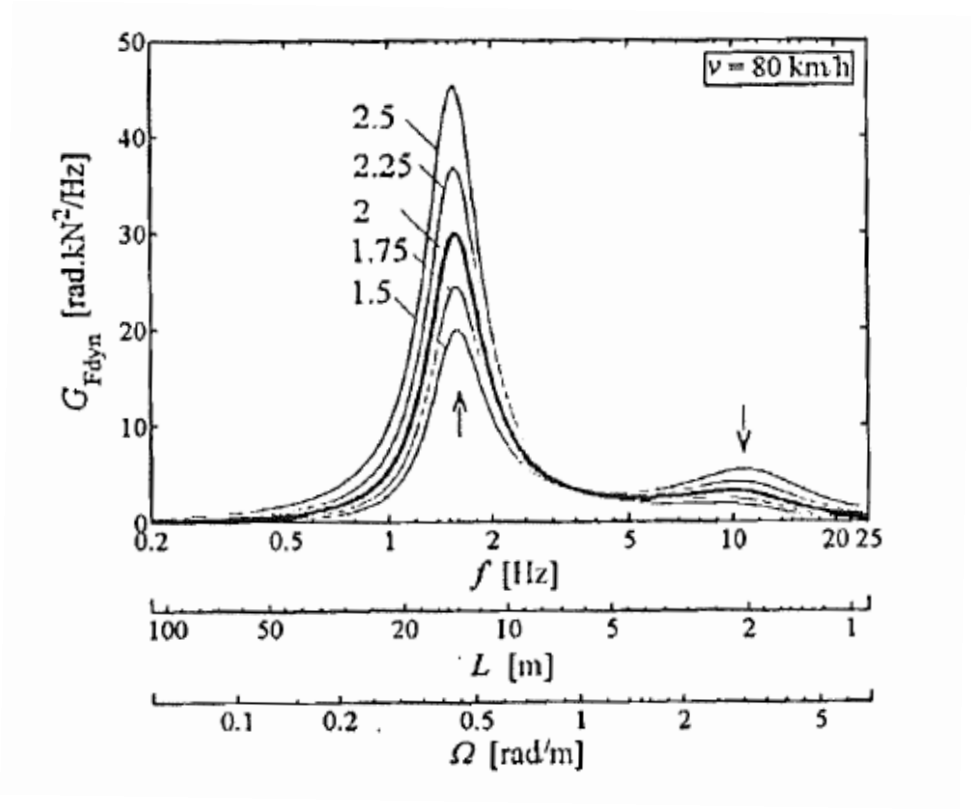

Figure 2-6 – Effect of exponent on the dynamic tyre force response – Mucka (2004) [17]

In 2008, Kropac and Mucka [18] investigated the effect that adding randomly distributed and random amplitude cosines (obstacles) to a high quality random road had on the input PSD, as well as the response of a passenger vehicle and 3-axle truck dynamic models (as used in Kropac and Mucka (2005) [7]). The authors found that adding the cosines effectively turned the straight line displacement PSD into a split between high and low wavelengths (Figure 2-7) and presented a similar effect to that of measured road data. The addition of obstacles also significantly effected the weighted driver's seat acceleration, increasing the RMS to almost 6 times with 64 added components.

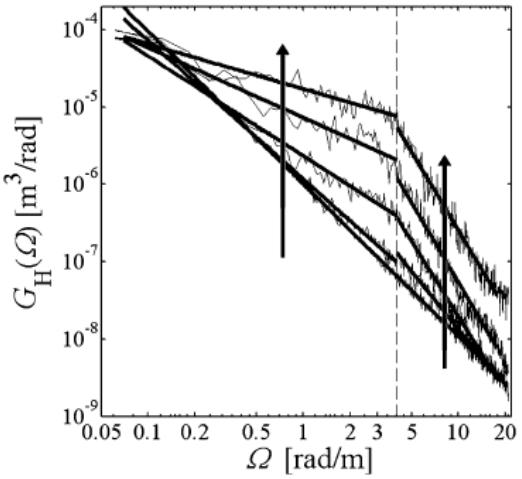

Figure 2-7 – Effect of obstacles on road displacement PSD- Kropac and Mucka (2008) [18]

Rouillard, Sek and Bruscella (2001) [19] presented a technique for the simulation of the road surface using similar details to their previous paper [5]. Again the road surface is separated into two fundamental components, the steady-state road surface irregularities and the transient events. The surface profile is created using an inverse Fourier transform to create the steady-state characteristics, with the normally distributed transients being added to create the final result. The authors found that this process 'faithfully represents the non-stationary, transient-laden nature of road surface profiles'.

In 1984, Cebon and Newland [20] used the inverse FFT method to generate an artificial three-dimensional road surface. In this paper the aim was to create not just a single track input, but a number of correlated parallel tracks and a complete two-dimensional random surface. In the paper, the theory of isotropy was used to describe a road surface. The author used a two-dimensional Fourier transform to create a 3 dimensional road profile.

2.2 – Human Discomfort

The comfort or discomfort of passengers in vehicles is a large subject area for a number of years. Many investigations have been carried out in an attempt to quantify discomfort due to vehicle vibrations, some of which are described in this section. In addition to quantifying discomfort, researchers and vehicle manufacturers are continually searching for characteristics that provide a desirable feeling for passengers. In 2004, Kushiro, Yasuda and Doi [21], carried out an investigation into the pitch and bounce motion of a vehicle requiring high performance ride comfort. The authors used a 6 degree-of-freedom simulator to establish that passengers found pitch around 1.5 times more uncomfortable than bounce bellow 1Hz, but the pitch sensitivity had reduced to 1/3 by 1.4Hz. A 2 degree-of-freedom half car model was used to analyse the pitch and bounce behaviour with natural frequency and damping ratio variations front and rear. The authors found that to minimise pitch at 100km/h the rear frequency ratio should be slightly higher than the front, but the rear damping ratio should be around twice the ratio of the front. However, with speed increased to 160 km/h, a frequency ratio closer to 1 was required and also a lower ratio of around 1.4 between the front and rear damping ratios. The authors carried out an experiment using the 'optimum' settings to compare against the original set-up. This found that the mean square pitch value had been reduced by over 20%, with the mean square bounce reduced by a small amount.

In 2000, Ebe and Griffin [22], [23] considered seat discomfort including both static and dynamic factors. Through subjective assessments using different seats the authors found that at low vibration magnitudes comfort was dominated by static stiffness, but as magnitude increased the dynamic factors became dominant. In the second paper [23] the authors created a model of seat discomfort that was able to correlate well with VDV (Vibration Dose Values) measured during testing.

In 1980, Leatherwood, Dempsey and Clevenson [24] created a tool for estimating passenger ride discomfort in complex ride environments. This was the culmination of a large series of studies and technical papers in which approximately 2200 test subjects were used. The aim was to obtain a single value to describe the discomfort for a certain complex vibration environment (e.g. a vehicle travelling over a road surface). In the method discomfort is calculated in single axis, combined and then corrected for noise and/or duration, before the single DISC value is obtained (Figure 2-8).

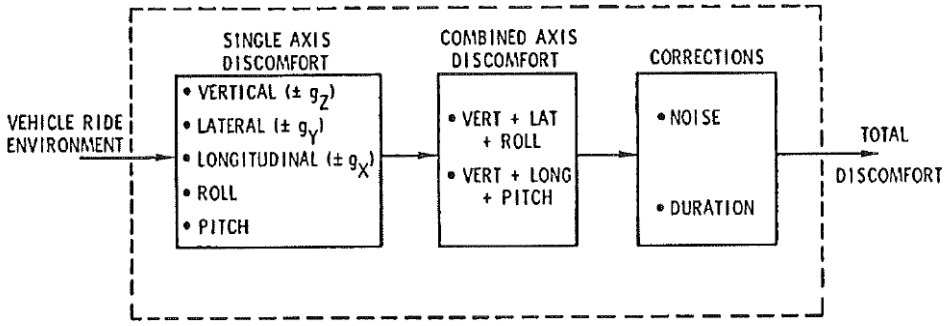

Figure 2-8 – DISC model concept - Leatherwood, Dempsey and Clevenson 1980 [24]

The authors found high levels of non-linearity in terms of both frequency and amplitude dependence. Figure 2-9 shows the equal discomfort curves across the frequency range for DISC values of 1 to 12 in the vertical axis.

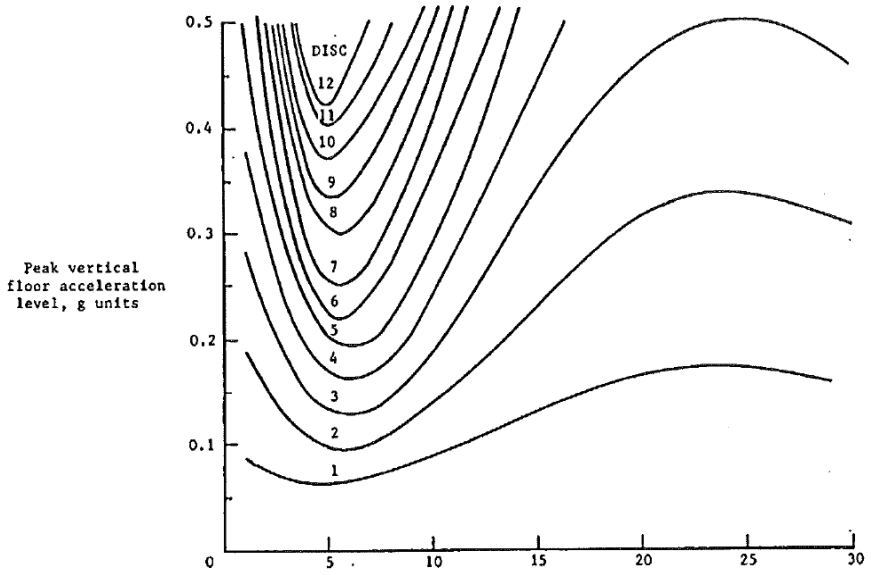

Figure 2-9 – Equal discomfort curves, sinusoidal vertical inputs - Leatherwood, Dempsey and Clevenson 1980 [24]

The authors identified a linear reduction in discomfort with increasing duration from 0 to 60 minutes, which then remained constant up to the maximum test time of 120 minutes. Examples of the application of the DISC method showed that the discomfort measure was relatively simple to apply.

M. J. Griffin has carried out a huge amount of work into ways of measuring and quantifying the discomfort of occupants in vehicles with many papers and multiple books published by himself and the Human Factors Research Unit in the Institute of Sound and Vibration Research at Southampton University. In 1986, Griffin [25] wrote a paper on the evaluation of human vibration.

This paper describes the various methods of quantifying discomfort of passengers in vehicles. Griffin defines the comfort model with 12 axes of vibration; 3 translations at the feet, seat surface and backrest and 3 rotations at the seat surface corresponding to roll, pitch and yaw. From studies of various different axes and positions a number of frequency weighting curves were created (6 in total). These frequency weightings were defined as transfer functions, with each frequency weighting also having multiplication factor depending on the location and axis of the vibration to be assessed. Figure 2-10 shows the frequency weighting functions.

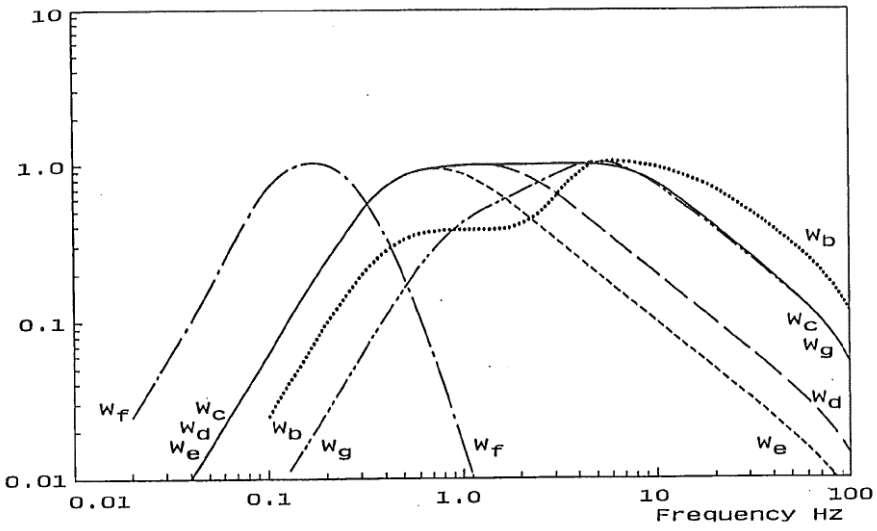

Figure 2-10 – Frequency Weighting Functions – Griffin 1986 [25]

In order to determine the level of discomfort due to a vibration input in a particular axis, Griffin suggests the use of the RMS of the frequency weighted vibration. In cases where there are high peak accelerations compared to the RMS (crest value of 6 times RMS), Griffin suggests the use of the RMQ (Root Mean Quad) rather than the RMS. In cases where there are many large transient inputs, the RMQ may be inappropriate to define discomfort, so Griffin defines a cumulative VDV (Vibration Dose Value). The paper presents approximate indications of weighted acceleration RMS values compared to subjective assessments of vibration from 0 to 5 (Figure 2-11).

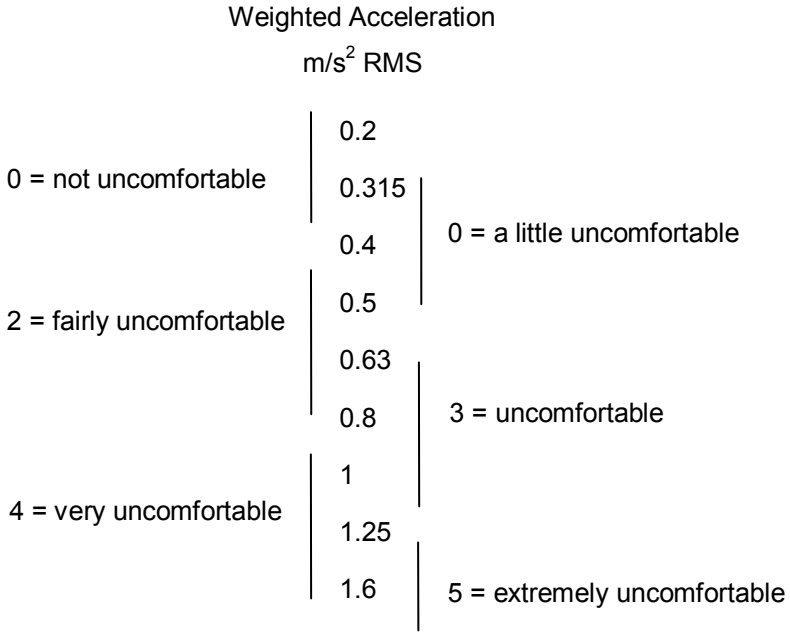

Figure 2-11 – Weighted Acceleration RMS compared to subjective assessments – Griffin 1986 [25]

In addition, Griffin also suggests a method for the assessment of seat performance using a measurement called SEAT (Seat Effective Amplitude Transmissibility). This is in essence the percentage of seat surface to seat input weighted accelerations. A value of 100% indicates that the passenger would have equal discomfort on the floor of the vehicle as the seat, whereas a value of less than 100% would mean that the seat provides a lower level of discomfort than the floor. Using these values, different seats can be assessed in terms of their performance and further explanation of differing levels of discomfort in different vehicles can be more fully understood.

Griffin's work in this paper forms the majority of the BS6841 standard [1]. The ISO 2631-1 standard [26] provides a very similar, but not identical, frequency weighting and comfort assessment.

In 2007, Griffin [27] wrote a paper describing the basics of assessing vehicle discomfort, from measurement, through frequency weighting and reporting results. One set of results presented shows some recent work on the equal discomfort curves across the frequency range for different magnitudes showing the non-linearity due to input magnitude (Figure 2-12).

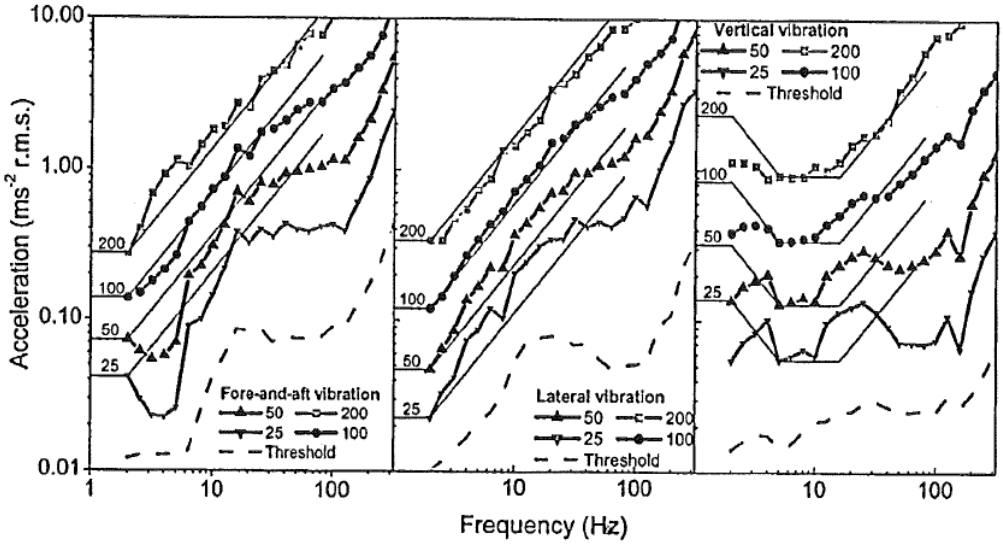

Figure 2-12 – Equal discomfort curves – Griffin 2007 [27]

Griffin explains that neither BS 6841 [1] nor ISO 2631 [26] standards account for non-linearity with respect to magnitude and that to do so would be complex. The author goes on to explain the slight differences in the vertical frequency weighting functions in BS 6841 (W_b) and ISO 2631 (W_k), as well as how the standards differ in their approach of quantifying discomfort for intermittent vibration or shocks.

Giacomin and Hacaambwa (2001) [28], evaluated the performance of the ISO 2631 [26] and BS6841 [1] standards in assessing passenger comfort in the x axis for three different road inputs at two levels of RMS input acceleration. The investigation found that the W_d weighting in both standards was necessary to produce any correlation between subjective assessment and that using VDVs significantly improved the correlation of the RMS acceleration to subjective assessment. However, the authors commented that the weighting method overestimates the perceived level of discomfort at low vibration levels, which is backed up by the results shown in Figure 2-12 (Griffin 2007 [27]), where the measured values of fore-and-aft acceleration for equal discomfort are generally lower than the weighting function values on 25 and 50 magnitude estimate lines.

The ISO 2631[26] and BS 6841 [1] standards provide frequency weightings and magnitude factors for a variety of locations and directions of vibration, but to create a single value of ride comfort from the different axis and location values a simple root-sum-squares equation is used. This implies no phase effect between the acceleration encountered at the feet and on the seat surface. A paper by Jang and Griffin (2000) [29], investigated this effect. The investigation found that the phase of the acceleration between the seat and feet did have an effect on discomfort, with a 180° phase difference producing more discomfort. However, as the frequency increased above 5Hz, the effect of phase decreased. The effect of phase also decreased with increasing

amplitude. This indicates that for low frequency, low amplitude accelerations, the introduction of a phase weighting would be beneficial to the discomfort assessment. However, the response of a road car seat is unlikely to have a significant phase angle at low frequency, so the phase difference expected is small.

The comfort papers explored in this literature review so far all relate to whole-body vibration, with weightings created from empirical testing of subjects on shaker rigs. To further understand the discomfort caused by vibration, some researchers have used biodynamic models of the human body to determine the response of different parts of the human body to an input excitation. Liang and Chiang [30] (2006) carried out a study with different biodynamic models ranging from simple single degree-of-freedom models (Figure 2-13, a) to an 11 degree-of-freedom non-linear model (Figure 2-13, b) and even a model of a pregnant female. The authors found the best estimation of STH (seat-to-head) transmissibility with a relatively simple 4 degree-of-freedom model. The use of biodynamic models requires the estimation of various parameters of the human body. As these are likely to change significantly from person to person, it may not be appropriate to use a single model to assess the comfort of a vehicle that would be used by many different people. The use of a biodynamic model also adds increased complexity to a vehicle model.

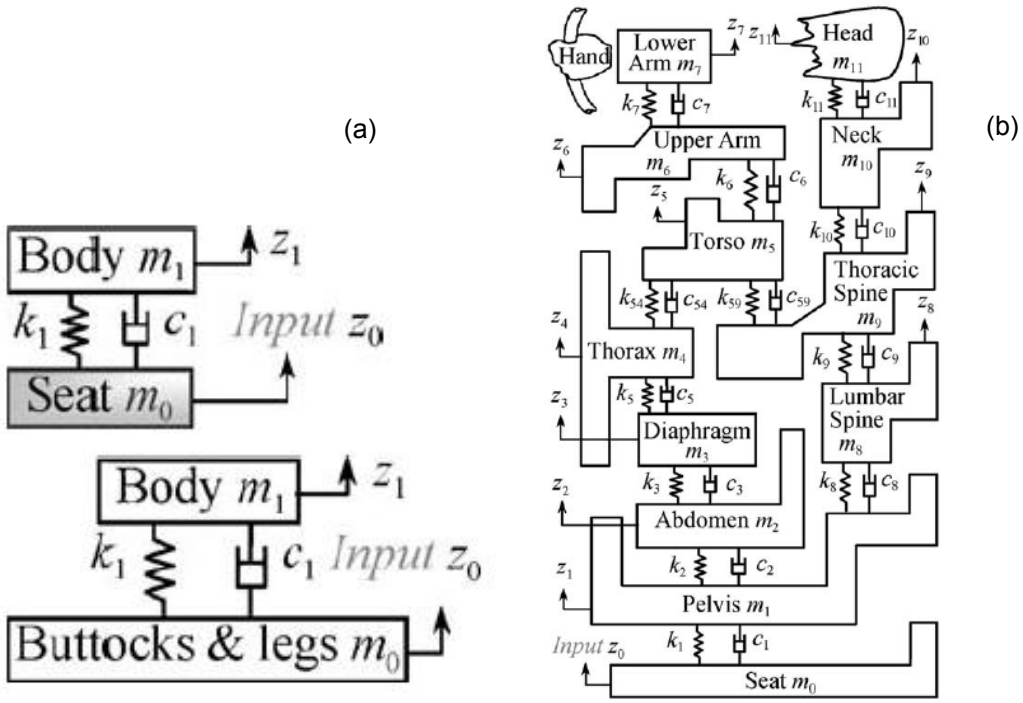

Figure 2-13 – 1 and 11 DoF biodynamic models - Liang and Chiang [30] (2006)

2.3 – Vehicle Suspension Design Principals

Many different parameters affect the handling and comfort performance of a road car. The suspension mounting positions control the movements of the wheel and tyre in 3 translations and 3 rotations through the suspension travel range, as well as the forces input to the chassis. These positions can have a significant effect on the handling performance of the car as well as tyre wear. Parameters such as the suspension stiffness and damping have a significant effect on the vibration of the vehicle when travelling over a road surface and therefore also have a significant effect on the passenger comfort. If the designer were to test and analyse all possibilities of all parameters to determine the final design of a vehicle, then it would take an extremely long time to design a road car. Instead, the designer relies on a number of different suspension design principals that have been developed over a number of years to provide a good starting point for the suspension design characteristics.

Barak (1991) [31] published a review paper named 'Magic numbers in design of suspensions for passenger cars'. The paper reviews many areas of vehicle suspension design and investigates typical values for significant parameters. For example, in the 'Ride' section of the paper, the author reviews information of the human response to vibration and determines that for good ride quality, the natural frequency of the vehicle body modes should be around 1Hz. The reasoning for this is that above this frequency the human body becomes more sensitive, and below this frequency, motion sickness is encountered. Also in this section, the author explains the ideal ratio between the radius of gyration and wheelbase, in order to reduce front-rear suspension interactions (as described in Thompson [32]) and the ideal front to rear suspension stiffness ratio used to achieve 'flat ride', in order to reduce the discomfort felt from pitching of the vehicle body. In the appendix of the paper, a large amount of information is provided on the typical parameter values used for a wide variety of suspension design areas such as general ride and handling, camber changes in bump and roll, roll centre heights, wheel rates and suspension compliances. The author claims that these magic numbers are timeless and that despite new technologies, the automotive industry will continue to use them, as the reality is that there is no substitute for past experience.

In 1999, Crolla and King [33] assessed the relevance of Olley's 'flat ride' to modern vehicles. The paper explains Olley's work and his significant contribution to early ride and handling analysis. Olley's 'flat ride' stated that the 'front suspension should have a 30% lower ride rate than the rear'. This approach has been commonplace in the design of road car suspension for a number of years. The authors point out that because the phase lag effect between front and rear wheels is forward speed dependant, while the pitch cancelation works well at one speed, the exact opposite could happen at another speed. The authors also point out that road inputs

are not deterministic in general, but random, so the flat ride concept may not work over more complicated input conditions. The authors used a 4 degree-of-freedom model of a 1990's Ford Granada to investigate the effect of different inputs on the vehicle, as this vehicle approximately followed Olley's 'flat ride' and inertia coupling ratio methodology. The authors conclude that when considering that only accelerations determine ride comfort, it could be confidently stated that the front-to-rear stiffness ratio has virtually no effect. However, if the pitch displacement is subjectively important, then there is value in the method. This is an issue of controversy in the absence of any evidence.

The findings of the paper are quite significant, indicating that a well-used theory that has been used in the suspension design of passenger cars for a number of years actually has no effect on overall ride comfort. However, if there is no effect when only considering accelerations, then there is no reason not to use a higher rear natural frequency (even though there is no evidence to support the effect of pitch displacement on ride) It is often desirable to have a stiffer rear suspension for other reasons, such as increased payload change compared to the front.

2.4 - Vehicle Performance Optimisation

The use of many different physical components and tests to optimise vehicle performance is an expensive and time consuming procedure. To reduce the monetary and time expense in the optimisation of vehicle parameters, the use of computer simulations to carry out optimisation routines has become commonplace in the automotive industry.

In 1973, Thompson [32] used a computer simulation of a 4 degree-of-freedom half-car model to investigate the effects of various model parameters on the body accelerations and suspension displacements of the simulated vehicle. Thompson wrote about the cases in which decoupling of the front and rear suspension systems occur and makes use of an inertia coupling ratio, equation (2-2).

$$R = \frac{k^2}{a \times b} \tag{2-2}$$

Where:

R – Inertia coupling ratio

k – Radius of gyration

a – Longitudinal distance between front axle centreline and CofG

b – Longitudinal distance between rear axle centreline and CofG

In the case that R=1, the system is said to be 'inertially decoupled'. In this case, the representation of the body mass can be replaced by two point masses located above the front and rear axles. If the ratio of front to rear spring stiffness is equal to the ratio a/b, then the system is said to be 'elastically decoupled'. If both decoupling situations are achieved, bounce and pitch motions are independent and any single input at the front wheel of the vehicle will only cause rotation about the rear wheel and vice-versa. Thompson later points out, that for the system to be completely non-interacting, the system must also have a relative front and rear damping coefficient ratio equal to a/b. Thompson presents equations for calculation of the optimum front damping to minimise tyre deflection (road holding performance) and body accelerations (comfort) independently. However, these equations only hold true for the R=1 case and for a random road with an exponent of 2. Thompson concludes that an R value of 1 represents the best compromise between the conflicting requirements of body acceleration and wheel travel. In order to equalise the body accelerations at the front and rear, the spring ratio and CofG position can be tuned to minimise pitch, and to reduce the level of acceleration. The

author also notes that careful CofG placement is a better approach than reducing damping levels, as it has less of an effect on road holding.

In reality it is unlikely that the manufacturer of a vehicle will define the location of the body CofG purely for ride reasons and the same is also true for the moment of inertia.

In 1983, Thompson [34] wrote a paper in which formulas were developed for the optimum spring and damper rates in a conventional passive suspension system. The formulas were based on the minimisation of the mean-squared tire forces. Thompson created an equation to find the optimum spring rate, assuming that the front and rear suspensions are virtually decoupled by R=1 and went on to create equations to determine the optimum damping coefficients. By using the equations created, Thompson changes the stiffness and damping rates of the vehicle quite significantly to achieve a small improvement in the combined performance index of around 7%.

In 2003, Vilela and Tamai [35] wrote a paper on the optimisation of ride comfort with simulation tools. The paper explains how traditional suspension tuning for ride comfort uses a series of physical prototype evaluations by skilled test drivers, who analyse the vehicle's performance in subjective terms. The authors point out that there are several problems with this method. Firstly, many of the suspension components are optimised independently, which ignores any factors due to the interaction between them, so the optimal set-up is often not achieved. Secondly, it requires the design and manufacture of prototype components, whose cost and construction lead times cannot be afforded in the current tight development cycles. Finally, the approach is prone to uncertainties due to its subjective nature.

Vilela and Tamai present an objective approach to the problem, using simulation tools to define optimised components for the suspension, without the need for prototypes. The vehicle model used in the investigation consisted of a multi-body model with around 20 degrees-of-freedom and non-linear properties. The software used in the investigation was a General Motors Brazil in-house developed program called Virtual Proving Ground (VPG), which had been found to provide accuracy to measured data within 3% error. The authors used ride measures from different road inputs to assess the vehicle performance for 8 different setups, finding good correlation to subjective assessment by test drivers for most of the measures used. The simulation model was used to determine the best parameters values, with improvements made for most of the ride comfort parameters, especially the harshness and absorption parameters.

In conclusion, the simulation tool created in the investigation proved to be a good basis for a new simulation tool to evaluate ride comfort with sufficient accuracy.

In 1983, Fukushima, Hidaka and Iwata [36] attempted to define the optimum damping characteristics for different driving conditions and road surfaces. The authors considered the force contribution of the springs and dampers of a vehicle during different manoeuvres and road inputs in order to determine the dependence on stiffness and damping for each type of input (Figure 2-14). An 8 degree-of-freedom vehicle model was used to investigate the effect of damping due to smooth road, rough road and ride harshness inputs. Comfort was measured using front and rear body accelerations, whilst performance was determined using two separate measures. The first was a measure of load fluctuation rate, defined as the ratio of RMS load variation to static wheel load. The second was a measure of the amount of time the tyre was in contact with the ground and was named the tire-ground contact rate. The authors determined an optimum damping rate and presented the effect of damping rate on the performance measures for the smooth and rough road surfaces (Figure 2-15), where the desireable damping coefficient on the rough road was 10 times that of the optimum on the smooth road. When tuning the damping coefficient for ride harshness inputs, the authors not only looked at overall damping coefficient, but also the ratio of compression and extension coefficients. They measured both peak-to-peak body acceleration and the amplitude of the initial peak to determine the 'desirable damping coefficient for this case', finding that a higher rate of extension to compression damping was desirable. The authors point out the need for the ideal damper to be not only velocity dependant, but also stoke dependant. The paper provides a good insight into the contradicting requirements of the damper and why the damper is such a critical component in the characteristic behaviour of a vehicle.

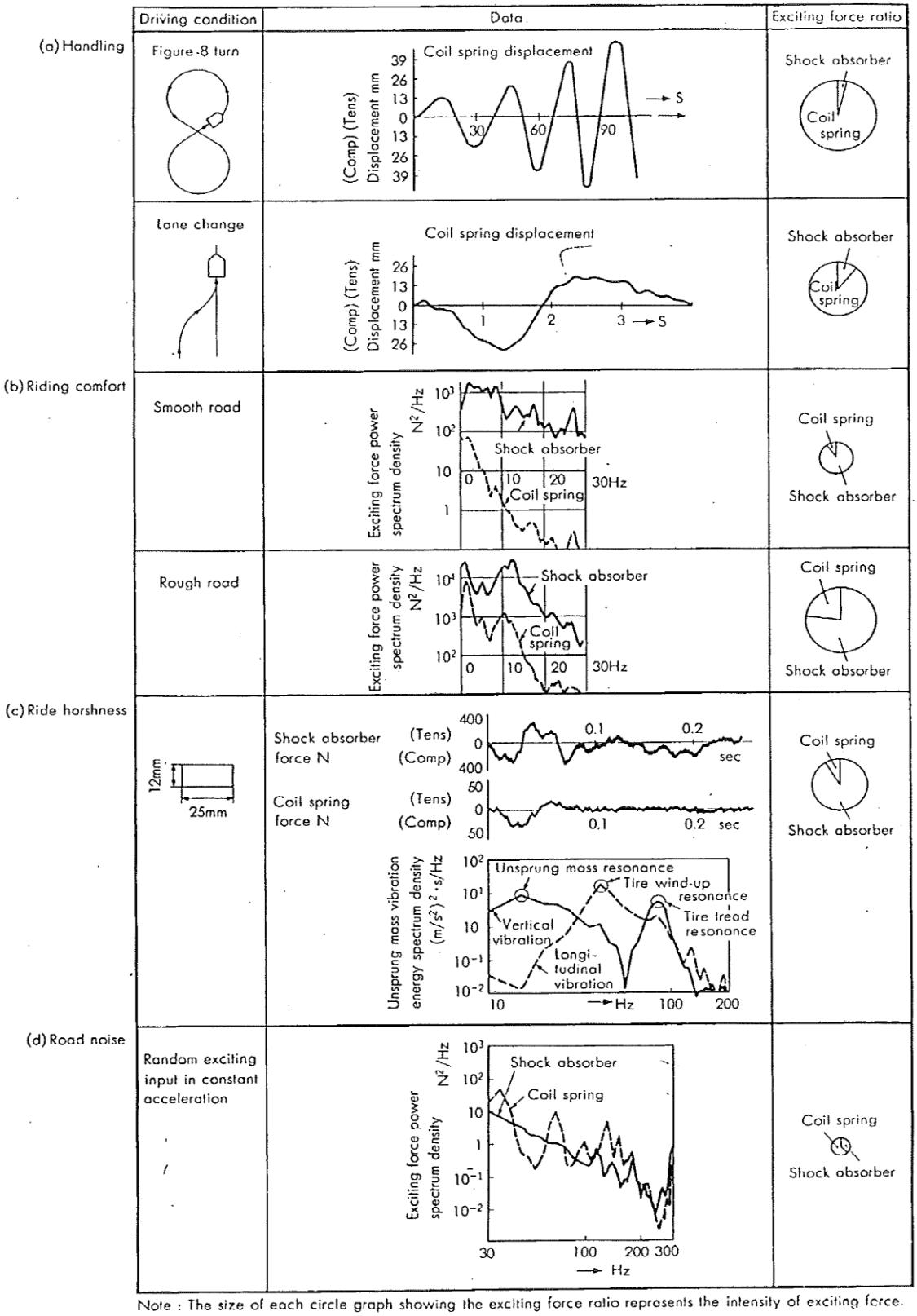

Note : The size of each circle graph showing the exciting force ratio represents the intensity of exciting force.

Figure 2-14 – Spring and Damper Force Contributions – Fukushima, Hidaka and Iwata (1983) [36]

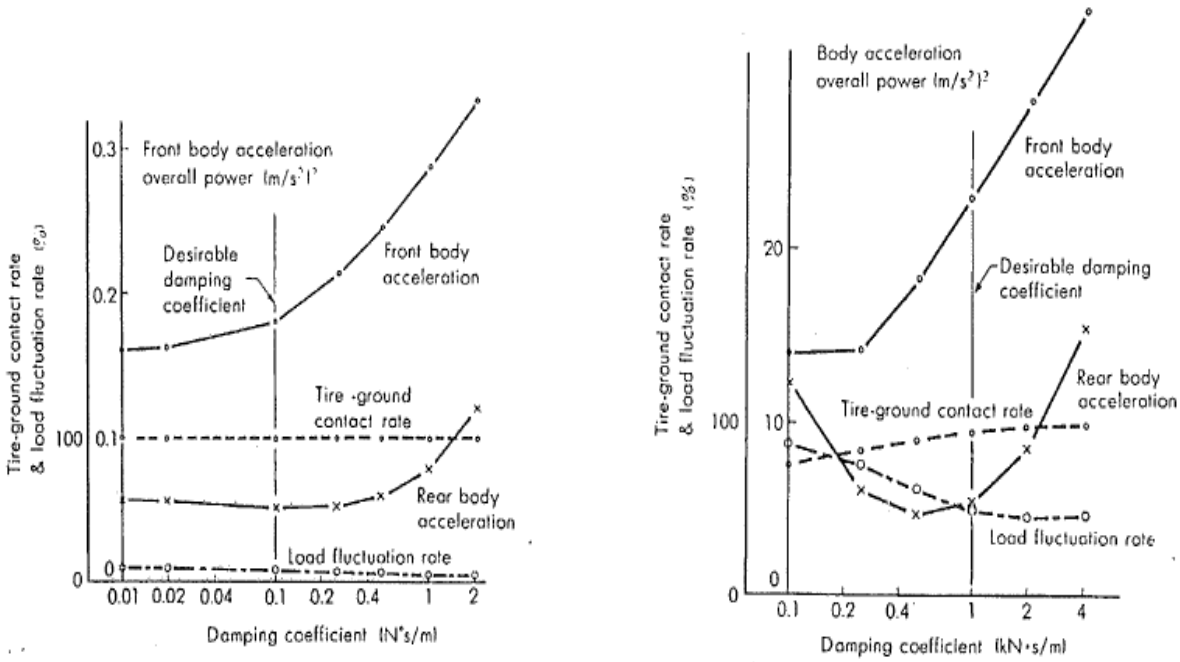

Smooth Road Rough Road

Figure 2-15 – Damping coefficient effects – Fukushima, Hidaka and Iwata (1983) [36]

Georgiou, Verros and Natsiavas (2007) [37], wrote a paper on the multi-objective optimisation of quarter-car models. The performance indices that the authors used within the optimisation were based on the absolute acceleration of the passengers for comfort, the tyre force for safety or performance and the suspension working space as a third criteria. The authors noted that as the performance indices are conflicting there is no single solution, but an infinite number of optimal solutions know as the Pareto-optimal or non-dominated solutions. In this case the combined solutions are optimal in the sense that the further improvement of one index will lead to the reduction in performance of one or more of the others. The authors use a method called the 'Strength Pareto Evolutionary Algorithm' to determine the optimal spring stiffness and damping coefficient of the simple linear model. The authors carried out investigations for both an isolated road irregularity and a random road surface.

This paper provides an insight into the possibilities of multi-objective optimisation. For vehicle dynamics engineers, there will always be a compromise between various factors of vehicle performance and this method allows the engineers to choose parameters based on a compromise, but in a way that allows an optimum compromise to be made when considering all performance indices.

Another paper with a similar approach to [38] but using a far more complex model with a larger amount of performance criteria was written by Gobbi, Mastinu and Doniselli (1999) [38]. In this paper the authors developed two different full car models. One model was used for the assessment of straight line running and a second model was used for steady state and transient manoeuvres. Both models were validated with measured car data with a good degree of accuracy.

A total of 17 different performance indices were used to asses the performance of the vehicle. The straight line model was used to perform rough road analysis and the other model to perform 6 driving manoeuvres such as J-turns and double lane changes.

A large sequence of suspension component variables were used to train an artificial neural network, in order to create an approximate model between vehicle parameters and performance indices. The model was found to have an error of only 0.7%.

Using this approximate model, the authors created a 17-dimensional Pareto-optimal set using an evolutionally genetic algorithm. A single Pareto-optimal solution was chosen and called the 'optimal car'. Results were impressive; in all performance indices the 'optimal car' either out performs the 'production car' or is equal to it. In some cases the improvements are as much as 16.7%, with the average around 6.6%. Performance indices relating to load variation were improved by 6.2% and 7.1% at the front and rear respectively. This shows that the 'production car' was not within the 'Pareto-optimal' otherwise the performance indices would be equal, or some would be higher, with others lower.

The authors noted that to complete the computations carried out in this investigation took around 24 hours on a 120 MHz Pentium PC. This would be expected to be reduced significantly by computing power available today.

This type of full vehicle ride and handling optimisation is obviously a very powerful tool. The work that was carried out using traditional methods would have taken many multiples of the time used by the method explained in the paper. In addition, the method actually performed better than the 'production setup' in everyway. This would have the potential to save car manufactures large amounts of time and money in the selection of component parameters for ride and handling.

2.5 – Multi-post Rig Testing

The literature review search on multi-post shaker rigs (4, 7 and 8-post) found only a small amount of material on the use of rigs for ride and handling assessment, with an especially small amount of material relating to passenger cars. This is despite the fact that they are known to be used widely in the automotive and motorsport industry. Car manufactures and motorsport teams may be reluctant to publish information on their proprietary testing and evaluation methods, to avoid competitors gaining some advantage from their published material.

In 2002, Vanhees and Maes [39] wrote a paper describing the test and evaluation methods used by Tenneco Automotive to characterise a vehicle on a four-post rig. The paper explains how the NVH behaviour of vehicles is divided into three main areas. The 0-25 Hz range is the Ride and Handling range, the 0-100 Hz is the Comfort and Harshness range and the 50-1000Hz range is the concerned with Structure Borne Noise from the vehicle. The authors explain the different inputs to the vehicle used to assess various areas of vehicle behaviour which include;

- Stepped sine inputs to assess the behaviour of the rigid body modes and wheel-hop.
- Single wheel input to simulate a vehicle driving over a bump or traffic ramp.
- Sleeping policeman (speed bump) test for both ride and comfort assessment.
- Tar strip test to assess harshness.
- 'Chuckle Test' used to determine Structure Borne Noise

The paper explains that a database of vehicles that have been benchmarked on the rig to reach general conclusions about different types of vehicle. The authors note that by using this benchmarking, improvements can be made in development of new suspension systems.

In 2002, Nuti, Garzeri and Orives [40] conducted an experiment to assess the effect of damper characteristics on comfort. In this paper the authors used a four-post rig to excite a vehicle using 3 different input types with 3 different damper specifications. The authors used an EEQ (Equivalent Exposure Measurement) from ISO 2631 [26] to measure comfort as well as subjective evaluation.

Also in 2002, the same three authors [41] wrote a paper on the compromise between head toss and roll motion of a vehicle. Again a four-post rig was used to excite a vehicle, but in this case using an increasing frequency roll sinusoid and step roll input. In addition subjective tests with a step-steer input were carried out. The authors investigated the effect of changing front spring stiffness and anti-roll stiffness, as well as low-speed damping. The authors concluded that the

increased low-speed damping reduced the roll motion at the natural frequency, but for very low frequency the higher damping increased the head toss behaviour (although this data is not presented).

Kowalczyk (2002) [42], wrote a paper describing the use of a 7-post rig (4 wheel actuators and 3 additional body actuators) at the ARC (Auto Research Centre). Inputs for the 7-post rig test and vehicle models were a constant peak velocity swept sine. The author notes that the set-up methodology of the team at the facility was to reduce the amount of bounce and pitch due to a pure heave input. The paper presents results for a 7 degree-of-freedom full car model's peak pitch and bounce sensitivity to front and rear damper changes. The results show that for the Champcar racing car simulated, the peak heave response is not minimised by the largest amount of suspension damping and it is not possible to achieve minimised heave and pitch responses simultaneously. The same approach was used with a real Champcar on the 7-post rig, where the maximum pitch response was reduced by 43%, for an 11% increase in bounce.

Again in 2002, Kowalczyk, along with Kelly and Oral [43], wrote a paper on the track simulation of vehicles using 7-post testing. Instead of using sine sweep inputs, the Servotest ICS (Iterative Control System) was used to determine inputs from measured on-car track data. Using the determined input, the authors tuned the suspension settings improving the front ride height variation by around 1mm (significant for aero-dependent racing cars) on some parts of the track The authors note that the realistic input obtained using the ICS helps the engineers to tune the vehicle more precisely than with a swept sine type input.

Although this system seems well suited to race cars, where the tuning of suspension for a particular circuit is desirable, it may not be well suited to road cars. Limiting the ICS inputs to only a few roads may lead to a vehicle setup that does not perform well on the majority of roads, yet creation of ICS profiles from a large number of different roads would require expensive and time-consuming collection of data.

A Vehicle Dynamics Expo 2007 conference presentation by Murray White [44] from the Multimatic Technical Centre explains 'Suspension measurements and characteristics – what learning can be shared between road and race cars'. White notes that although four-post rigs are widely used by automotive manufacturers, they are 'probably not used widely enough in the early development phase (too late to make use of the findings)'. White notes that four-post testing is good for:

- identifying vehicle properties and deficiencies;
- setting linear range suspension parameters;
- comparing ‘apples to apples’, albeit somewhat idealised apples…

The presentation briefly explains the use of a ‘Comfort’ calculation that uses the ISO comfort filter. White also notes that ‘The dynamic behaviour of the powertrain can have a dramatic effect on vehicle performance if not correctly handled’.

In 2001, Paul Haney [45] wrote a four part internet article on the Ohlins 7-post shaker rig. The rig works in much the same way as the rig in the Kowalczyk papers ([42], [43]). The author points out that the tuning focus for the Ohlins rig is finding the right compromise between pitch and grip. The input used on the rig is a randomised input with phase differences front-to-rear, left-to-right and diagonally. Ohlins engineers comment that their input is more realistic than a sine sweep type input due to the energy spectrum being very close to that seen in track data. The engineers completed a test matrix by adjusting the vehicle’s dampers incrementally until all combinations of front and rear damping have been achieved (49 total). Little detail is provided about the complexities of the analysis, but results are presented for the grip disturbance of all four wheels, as well as combined, front, rear, overall and dynamic pitch balance (Figure 2-16).

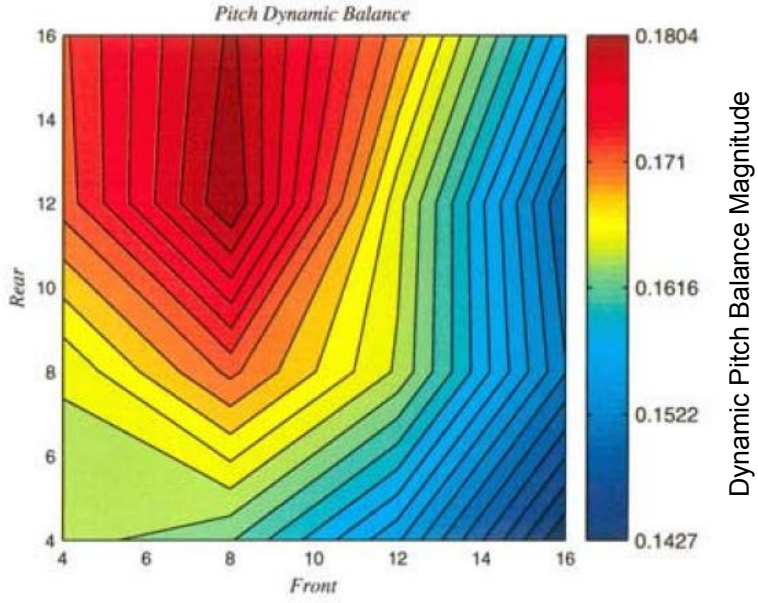

Figure 2-16 – Pitch Dynamic Balance – Haney (2001) [45]

In 2002 Miller [46], used the Ohlins rig to test an SAE racecar. Both Ohlins’ randomised inputs and sine sweeps were used to analyse the effect of anti-roll bar and damper adjustments. Analysis of the anti-roll bar and damper matrix results allowed the author to determine the most appropriate settings for the SAE car to minimise the grip disturbance.

2.6 – Parameter Determination

In order to model a physical system such as a road car, the parameter values of the model are required. In the early design stage of a vehicle these can simply be 'design values'. However, to accurately model the behaviour of the real vehicle it is essential that the parameters are verified from physical testing. In other circumstances where a manufacturer wishes to know the parameters of a competitor's vehicle, the values are simply not available. In this case the parameters should be determined from the physical vehicle. One method would be to disassemble the vehicle and identify the parameters of individual components or sub-systems. This is a time consuming and expensive process and without careful consideration of the kinematics of the system could still provide unsatisfactory results. Other methods focus on estimating the parameters based on the response of the complete vehicle to various inputs.

In 1977, Brueck and Ward [47], proposed a method for the identification of vehicle suspension parameters. The authors explain the requirement of accurate parametric data in order study the dynamic response of vehicles using computer simulations. In the paper the authors present a simplified method for obtaining the spring rates, damping characteristics and unsprung mass inertia properties of the vehicle suspension. The rig they used to carry out the parameter identification is almost a precursor to the four-post rig in that it uses hydraulic ram displacements as input to the vehicle to test the suspension system of the vehicle without the need for any disassembly (although the vehicle is mounted to a frame). They used the rig measurements to determine tyre stiffness, suspension stiffness, non-linear suspension damping and the unsprung mass roll moment of inertia. By simulating the response to the rig inputs using the acquired parameters in a time domain model, good agreement was seen between the simulated and measured signals.

In 2008-9, Boggs, Ahmadian and Southward [48] [49], from the Virginia Institute for Performance Engineering Research (VIPER), wrote two papers on the 'Application of System Identification for Efficient Suspension Tuning in High-Performance Vehicles'. In the first paper of the series [48], the authors use a linear quarter-car model with the addition of non-linear damping force model and a physical quarter-car rig to test the validity of the proposed method. The authors fitted fourth order transfer functions to non-parametric frequency responses determined from physical testing, which formed the linear part of the model. A validation exercise was then conducted with six different damper specifications used on the test rig and within the identified vehicle model (Figure 2-17). In all cases the general trend of measured signal standard deviations was similar for the model and test rig, indicating that the model is suitable for the tuning of the real system.

The second paper in the series [49], applies the identification method to a 7 degree-of-freedom full-car model, with the identification model developed to work with this more complicated system. Results for the time domain recreation and standard deviation of signals for different shock configurations showed good agreement between the full-car model and simplified identification model. However, no data was provided for the identification of a real vehicle tested on a 7/8-post rig that the system was designed for.

This type of system identification is quite desirable, since it does not rely on a fixed framework for the vehicle model as many other methods do. However, in some cases it may be desirable to know the estimated vehicle parameters such as spring rate, sprung mass and tyre stiffness, which this method will not provide. The method is also limited to the simulation of different damper characteristics for the particular model. When tuning a vehicle it is often desirable to also tune the spring stiffness and sometimes tyre pressures of the vehicle to achieve the desired response. Using this model, the system would have to be re-tested and re-indentified if these changes were made. Although not explicitly mentioned in the papers, it is assumed that the non-linear shock models are based on damper dynamometer test data of the real dampers. If this is the case then it is still a requirement for the dampers to be physically tested, which could take almost as much time as testing the whole quarter model or full-car on their respective rigs. In this case the model does offer some benefit, but not as much as would initially appear.

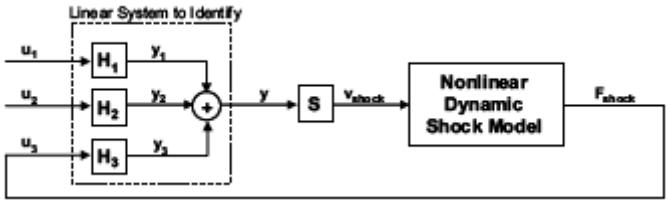

Figure 2-17 – Linear vehicle model with non-linear shock model – Boggs, Ahmadian and Southward (2008) [48]

In 2011, Thite, Banvidi, Ibicek and Bennett [50] created a suspension parameter estimation method using a matrix inversion approach in the frequency domain. In this paper, real data from a four-post rig test was used to determine parameters of a 4 degree-of-freedom half-car vehicle model. The paper presents results for the matrix inversion method used in both time and frequency domains. In the time domain results for body mass and pitch inertia were quite poor, as were results for damping coefficient. Conducting the parameter estimation in the frequency domain, the authors note that when dominant modes occur, parameters relating to that mode would be reliable, but results for some other parameters could become unreliable.

Yi and Hedrick (1993) [51], wrote a paper on the 'Observer based identification of nonlinear suspension parameters'. The authors used data from a 4 degree-of-freedom half-car rig. Instead of the traditional linear damping coefficient, the vehicle model and parameter estimation method used a bi-linear damper with one rate for extension and another for compression. The input to the half-car rig was a periodic step displacement input (Figure 2-18), which the authors noted is crucial to the parameter estimation method. Parameters were estimated for each period of the input. In total there were six iterations, but the solution had converged by the fourth iteration. Figure 2-19 shows the estimated damping coefficients. From the quality of the results and time taken to reach convergence, this parameter estimation method appears quite efficient, although no information is presented for how well the method would work for increased complexity in real vehicle systems.

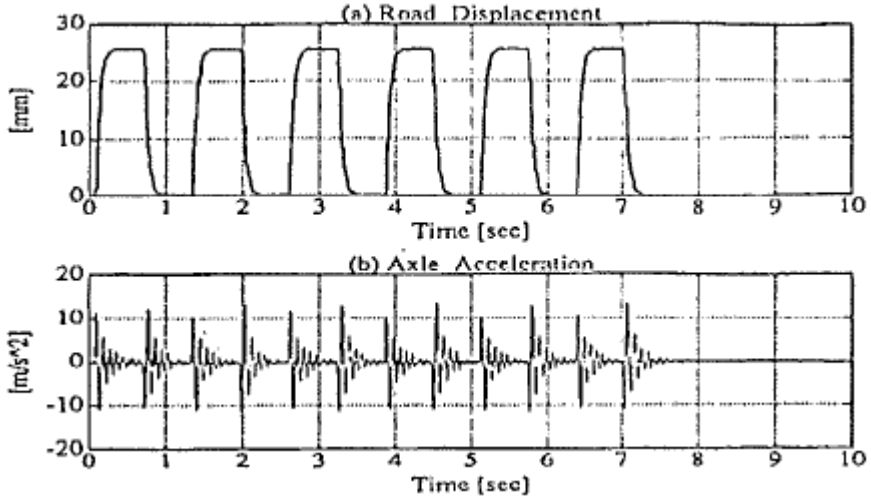

Figure 2-18 – Road displacement and axle acceleration signals – Yi and Hedrick (1993) [51]

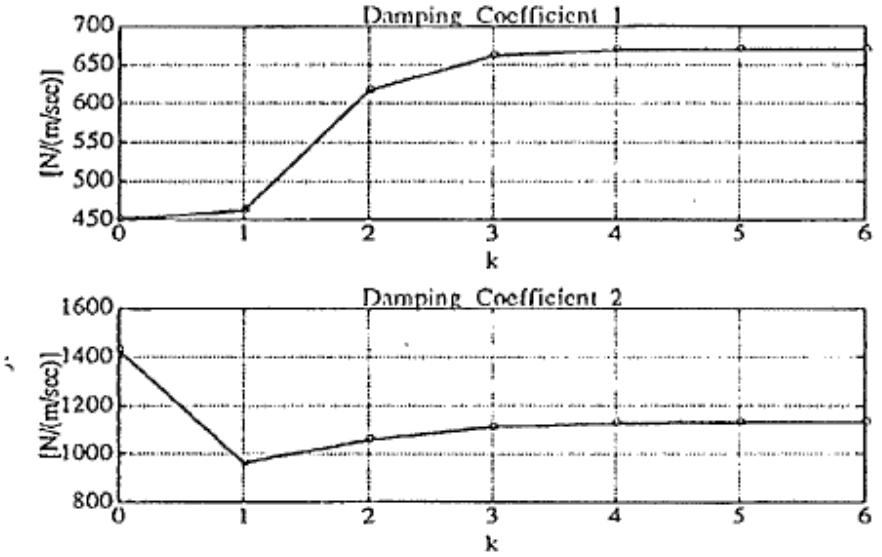

Figure 2-19 – Damper coefficient estimations – Yi and Hedrick (1993) [51]

2.7 – Vehicle Modelling

A variety of different complexity models are used for the assessment of vehicle characteristics in the automotive industry. These can vary from simple single or two-degree of freedom quarter-car models [48], to highly complex complete vehicle models with many degrees-of-freedom and complex non-linearity [63]. This section of the literature review details models used by different authors to assess and tune various aspects of vehicle performance.

Dixon, Franco-Jorge and Webb (2002) [52] described work carried out at MIRA using various different methods to model a vehicle for assessing handling and ride comfort. The paper focuses on two main models, an ADAMS model which is used mainly for handling development, along with a Simulink model which is used for ride assessment and development of control systems. Validation of the model was achieved by aligning vehicle testing with the simulation, for example validating the ADAMS model to MIRA K&C rig test results. The paper explains that with the use of Laser road profiling a complete accurate MIRA Virtual Proving Ground has been created. This allows the vehicle models to be simulated over the proving ground in exactly the same way as a real vehicle, even to the extent of the driven route on the track.

In 1952, Gallagher and Volterra [53] analysed the relaxation type of vehicle suspension. The suspension arrangement is similar to a standard spring-damper system, but in series with the damper is an additional spring. This type of suspension is commonly called ‘dual path’. The authors found that the maximum amplitude of the mass representing the vehicle body could be reduced by approximately 30% compared to standard spring-damper tyre suspension.

Kasprzak and Floyd (1994) [54], used a 4 degree-of-freedom model to simulate two different race cars (GTP and Indy Lights) on a four-post rig. They used a model in which it was possible to use both linear and non-linear damper curves derived from dynamometer testing of the dampers (three for each vehicle). The authors explain the sensitivity of aerodynamically dominated racing cars to ride height and pitch angle change. These are then used as the primary performance factors when tuning the dampers. To validate the model, the GTP car was simulated with non-linear damper curves and the acceleration response data compared to actual four-post testing of the same configuration. The simulation and rig test results provided similar characteristic curves, although there was some discrepancy in absolute magnitude.

In 1986, Rill [55] used an 11 degree-of-freedom non-linear vehicle model to study the effect of road roughness on steady-state cornering. A constant radius increasing speed test was used to determine the relationship between actual steering angle and ideal steering angle with lateral

acceleration (Figure 2-20). Rill used three different levels of random road: very good, good and poor. To model tyre behaviour, Rill used an approximation based on measured data. To drive the steering of the vehicle to follow the desired path, Rill used a simple steering velocity controller in the form of equation (2-3).

$$\dot{\delta} = (\rho_{nom} - \rho_{act}) \times K \times v \qquad \textbf{(2-3)}$$

Where:

$\dot{\delta}$ - Steering velocity

ρ_{nom} – Desired curvature (1/42.5)

ρ_{act} – Actual instantaneous curvature

K – Constant gain

v – Forward velocity

Although very simple, the steering controller worked very well and managed to maintain a precise curvature, even on the very rough road. Rill presented the steering characteristic curves for the three road surfaces (Figure 2-21). There were such large variations for the poor road that the original characteristic is almost lost completely. Results were also presented for the average steering velocity requirements at different levels of lateral acceleration, which reached a maximum of 67 °/s at 0.7 g on the poor road. Rill conducted investigations using the good road input with one damper defective and with all four dampers with reduced efficiency. The results showed that in both cases the steering activity requirement increased considerably. However, the steering characteristic curve shape was still comparable to the case with all dampers functioning correctly.

This paper identifies the significant effect that the road input and ride behaviour of the vehicle has on the required driver inputs. Typically the contact load variation is considered with respect to absolute grip for safety. However, this investigation makes it obvious that it has an influence on the driver's required inputs even when the vehicle is far from its maximum limitations. This influence could significantly affect the driver's perceived performance and comfort of a particular vehicle.

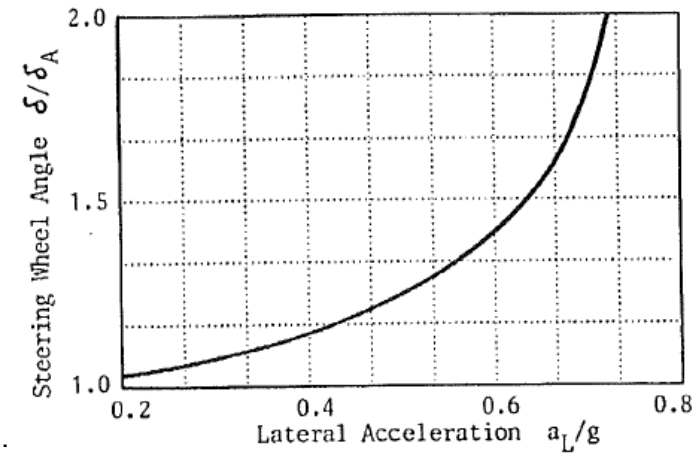

Figure 2-20 – Flat road steering wheel angle ratio vs. lateral acceleration – Rill (1986) [55]

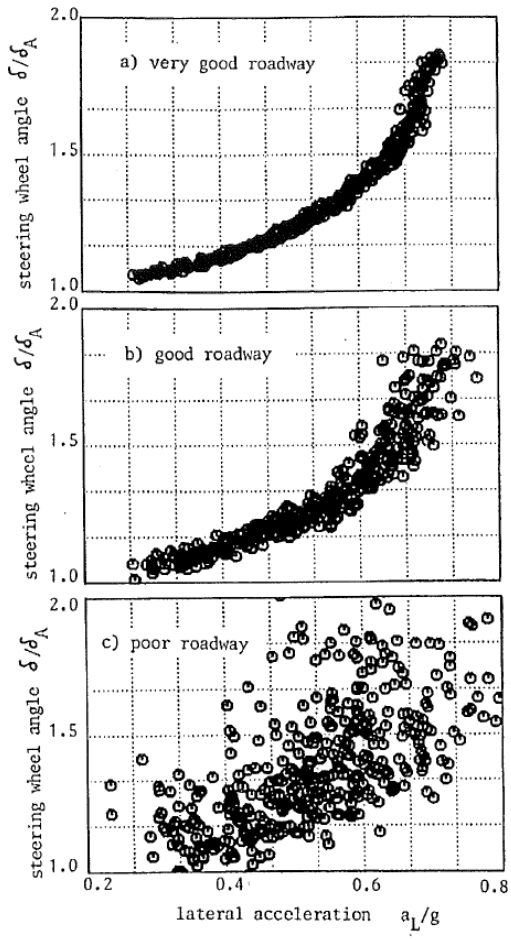

Figure 2-21 – Steering characteristics on different roads – Rill (1986) [55]

In 2005, Mashadi and Crolla [56] published the results of a similar investigation. The model used was a 10 degree-of-freedom full-car model, coupled with the well established 'Magic Formula' tyre model. Unlike Rill's investigation [55], an open loop steering control was used. The inputs to the vehicle were also different. Forward speed remained constant, whilst a step steer input was applied that corresponded to 0.55 g and 20m/s on a smooth road. Both sinusoidal and random road inputs were used during the investigation. Initial results for the sinusoidal inputs showed very little difference in mean lateral acceleration, yaw velocity or roll angle compared to a completely smooth road (max 1.7% difference). The authors expected that because of the lateral force reductions due to vertical load variations, the average lateral acceleration would decrease. However, it was determined that instead the mean slip angles of the tyres had increased 7% at the front and 10% at the rear (Figure 2-22). To evaluate the behaviour of the vehicle over different road surfaces for the entire lateral acceleration range, the authors made use of the understeer gradient measurement from an increasing steer angle test. The results from this part of the investigation were significant. For road surfaces with low to medium roughness, the effect on the understeer gradient with lateral acceleration (Figure 2-23) was only noticed above 0.6 g and only produced a slight reduction in the maximum lateral acceleration ability of the vehicle and a small change in the understeer gradient just before the limit. However, the roughest random road and sinusoidal inputs affected the understeer gradient from low lateral acceleration levels and the balance at the limit was oversteer.

This investigation shows the substantial effect that the ride of the vehicle can have on the handling and that not only does it reduce the maximum lateral capability, but also the handling behaviour of the car at lower lateral accelerations. A vehicle cannot be expected to be able to perform to the same limit of lateral accelerations when subjected to large road inputs, but it would be desirable for the handling characteristics to remain the same over different road surfaces for the ease and safety of the driver. It is then desirable to consider the setup of the car not only based on minimising overall load variations, but also taking into account the potential balance change due to different load variations.

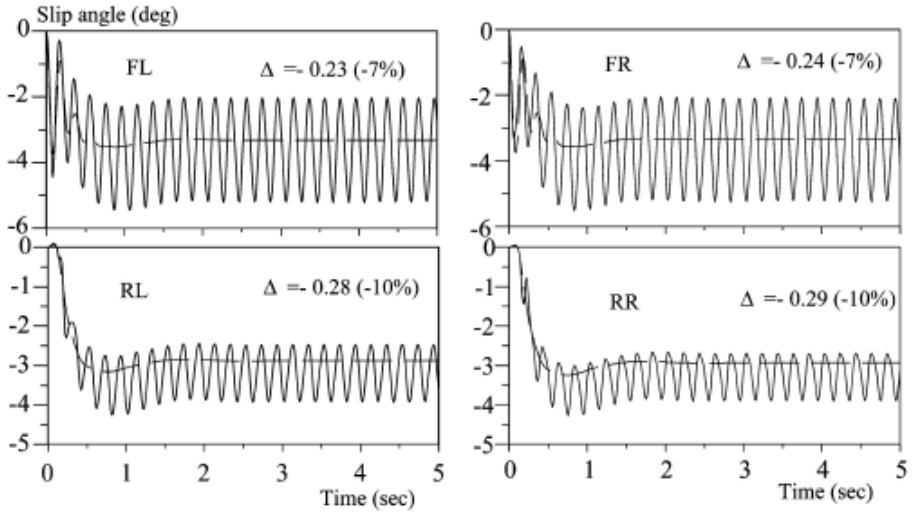

Figure 2-22 – Slip angles on sinusoidal road – Mashadi and Crolla (2005) [56]

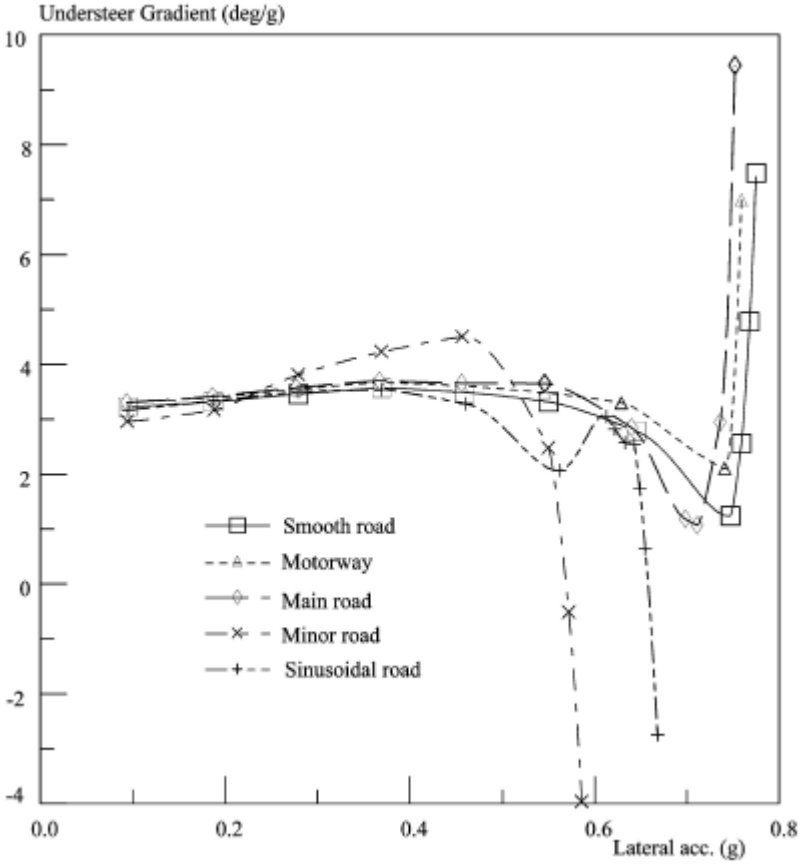

Figure 2-23 – Understeer gradient vs. lateral acceleration – Mashadi and Crolla (2005) [56]

Of the different tyre models available to vehicle dynamic engineers, the 'Magic Formula' tyre model is the most commonly used for simple handling analysis and vehicle modelling. In 1992, Pacejka and Bakker [57] presented version three of the model in a technical paper. The tyre model is an empirical model based on measured data, generally from tyre test rigs. The model has variable inputs of vertical load, lateral slip angle, longitudinal slip ratio and camber angle. A vast amount of parameters are used when creating the model to account for a number of different conditions, these are generally fitted to tyre data in order to produce a best fit. The general form of the shape equations is presented in equation (2-4).

$$y(x) = D\sin[C \times \arctan\{Bx - E(Bx - \arctan(Bx))\}] \tag{2-4}$$

Where:

y – Force

x – slip angle or ratio

B,C,D,E – Constant shape factors

Figure 2-24 shows the effects of some of the constants on the shape of the curve. Further explanation of the model as well as worked vehicle examples are presented in 'Tyre and Vehicle Dynamics', by Pacejka (2006) [58].

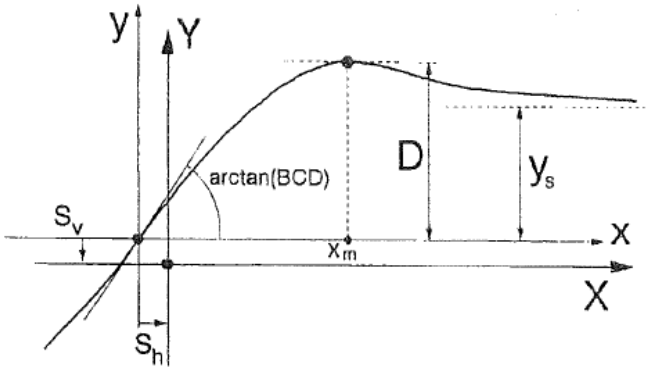

Figure 2-24 – Effect of shape constants – Pacejka and Bakker (1992) [57]

2.8 – Subjective – Objective Vehicle Assessment

Vilela and Tamai [35] explained that how traditional suspension tuning uses a series of physical prototype evaluations by skilled test drivers, who analyse the vehicle's performance in subjective terms. The cost and time involved in this process is large. Objective measurements from physical tests or computer simulations can be used to assist in the tuning procedure, but in order to do so the objective measures have to be linked to subjective feelings from the driver. A number of different investigations have been carried out in an attempt to determine these links, some of which are explained in this section of the literature review. The determination of strong links between various objective measures and driver's subjective feelings, allows confidence to be gained in the increased use of computer simulation results and the reduced use of subjective tests to reach a satisfactory end result. This has the effect of reducing the time and costs involved in the tuning stage of a vehicle.

In 1998, Crolla, Chen, Whitehead and Alstead [59], published a paper on handling assessment using a combined subjective-objective approach. They used information from a large data set acquired through testing conducted by Leeds University and MIRA. In the test, a passenger car was used with 16 different setup configurations (tyre pressures, anti-roll bars, dampers, as well as other components), along with an identical baseline car. The study used eight professional drivers, all with experience in vehicle dynamics testing and development. 46 different metrics were analysed from three different test types in order to characterise the vehicle objectively (Figure 2-26). Subjective assessment carried out by the drivers was performed using 49 different questions (Figure 2-27). Subjective assessments were made on a scale of 1 to 7 with reference to the baseline as it had been previously found that drivers were better at rating differences rather than absolute values. The authors stated that it was important that the vehicle parameter changes resulted in sufficiently different levels of performance that the drivers could perceive the differences subjectively.

The authors found that assessments between drivers had surprisingly poor consistency with the mean answers to most subjective questions for a single setup being able to be placed 'confidently' (95% confidence level) on the 'better' or 'worse' line of the baseline setup. The authors point out that this does not imply that the mean ratings are of no value, but it does reduce their significance. A simple linear regression was used to determine a relationship between measured metrics and mean subjective assessments, with 27 of the 49 questions found to have a correlation R^2 value of more than 0.7. The authors found that 11 of the subjective questions were consistent reliable indicators of measured performance and that there were 17 metrics that correlated consistently well with mean subjective assessments. These were separated into three categories, as presented in Figure 2-25.

The authors concluded that the work has contributed to the subjective-objective correlation debate significantly. However, they noted that there is still a long way to go in determining unequivocal links between subjective and objective ratings over a wide range of handling.

Unequivocal and Uniform Effect	Unequivocal Effect	Uniform Effect
YawGain/0.7 YawGain/0.4 Storq/0.2 SteerGain/1.0 d(sslip)/0.4 LataccGain/1.0 SteerPhase/0.4	YawRtRespTime/0.2 StMeanRespTime/0.6 YawPhase/0.4 YawRt/0.2 RollRtRespTime/0.2	Storq/0.6 d(storq)/0.2 d(storq)/0.4 YawRt/0.6 RollRtRespTime/0.6

Figure 2-25 – Metrics with highest levels of correlation to subjective measures – Crolla, Chen, Whitehead and Alstead (1998) [59]

In 2001, Crolla and Whitehead [60] wrote 'Reliable subjective assessment of vehicle handling by drivers – is it an elusive goal?'. The paper reviewed work from a number of authors and organisations on the evaluation of subjective assessments and in some cases their correlation with objective measurements. The main data that the paper focused on was work conducted with Leeds University and MIRA as explained in [59]. The purpose of this work was to aim to determine a function for each subjective parameter rating that related to one or more objective metrics. This would enable the use of virtual tuning to achieve a set of objective targets that would relate to high subjective ratings. The authors present a table showing the metrics used (Figure 2-26). The authors' conclusion to the hypothesis of the paper was that reliable assessment of vehicle handling still remains an elusive goal and 'no convincing evidence has yet been published in which subjective ratings are systematically and consistently linked to objective metrics'. However, they also note that car manufacturers are consistently able to produce cars with high customer satisfaction levels and therefore high subjective ratings, but the vehicle dynamics community has not been able to identify ways of articulating these skills and linking them to objective metrics.

Test	Description	Derived Metrics	Abbreviations
Steady state steering pad	33m radius, 0 to 6m/s² lateral acceleration clockwise and anti-clockwise.	d(hand wheel angle)/d(lateral acceleration) at ±2 and ±4 m/s d(front slip)/d(Lateral acceleration) at ±2 and ±4 m/s d(side slip)/d(Lateral acceleration) at ±2 and ±4 m/s d(Torque)/d(Lateral acceleration) at ±2 and ±4 m/s Roll angle at ±2 and ±4 m/s	d(hw)/0.2, /0.4 d(fslip)/0.2, /0.4 d(sslip)/0.2, /0.4 d(Storq)/0.2,/0.4 Roll angle/ 0.2, /0.4
J-Turns (Step steer input)	2 and 6 m/s² lateral acceleration clockwise and anti-clockwise.	Peak lateral acceleration response time Peak road wheel steer angle and response time Peak roll rate and response time Peak yaw rate and response time Peak steering torque and response time	LatacRespTime/0.2, /0.6 StMean/0.2, /0.6 StMeanRespTime/0.2, /0.6 RollRt/0.2, /0.6, RollRtRespTime/0.2, /0.6 YawRt/0.2, /0.6, YawRtRespTime/0.2, /0.6 Storq/0.2, /0.6, StorqRtRespTime/0.2, /0.6
Impulse (frequency response)	2 m/s² impulse inputs. Time histories transformed to frequency domain using handwheel angle as input	Lateral acceleration gain and phase at 0.4, 0.7 and 1.0 Hz Road wheel steer gain and phase at 0.4, 0.7 and 1.0 Hz Yaw rate gain and phase at 0.4, 0.7 and 1.0 Hz	LatacGain/0.4, /0.7, /1.0, LatacPhase/0.4, /0.7, /1.0 StMeanGain/0.4, /0.7, /1.0, StMeanPhase/0.4, /0.7, /1.0 YawGain/0.4, /0.7, /1.0, YawPhase/0.4, /0.7, /1.0

Figure 2-26 – Derived metrics for handling assessment – Crolla and Whitehead (2001) [60]

In 2002, Crolla and Whitehead, along with Ash and King [61] attempted to further define the links between subjective and objective measurements using neural networks. The investigation used the same data from the Leeds and MIRA test [59]. The authors noted that previous investigations including [59] had failed to find consistent links between subjective assessments and objective metrics using linear techniques, so the application of a non-linear neural network approach could lead to better correlation. Two different network types were formed; one with a single metric input and single subjective output and a second with two metrics used as inputs with a single subjective output. In the first method the neural network problem reduced to a simple non-linear regression analysis. In some cases the authors noted that their results were consistent with the findings of Mimuro et al (1990) [62], but in the case of the dual metric fitting network, no consistent results were found. The authors concluded that the methodology used in the paper was found to be a powerful tool in uncovering subjective-objective links where large amounts of noise are present and the links are not clearly defined by linear functions.

Heading	Subheading	Sub-Subheading	Question
Steady state Turning	Over smooth roads	Cornering behaviour	Progressive behaviour with decreasing lateral acceleration
Steady state Turning	Over smooth roads	Steering torque feedback	Indication of available grip
Steady state Turning	Over smooth roads	Steering torque feedback	Indication of magnitude of lateral acceleration
Steady state Turning	Over smooth roads	Steering torque feedback	Magnitude of torque levels- LOW lock/ HIGH lateral accel.
Steady state Turning	Over smooth roads	Steering torque feedback	Magnitude of torque levels- HIGH lock/ LOW lateral accel.
Steady state Turning	Over smooth roads	Steering torque feedback	Progression of handwheel torque levels
Steady state Turning	Over smooth roads	Steering torque feedback	Smoothness
Steady state Turning	Over smooth roads	Steering torque feedback	Symmetry
Steady state Turning	Over rough roads	Cornering behaviour	Ease with which a line is held
Steady state Turning	Over rough roads	Kickback on bumps	Kickback on bumps
Power change	Power on	Yaw response	Magnitude of response (state below whether over or under steer)
Power change	Power on	Yaw response	Progressiveness of yaw rate response
Power change	Power on	Yaw response	Yaw stability of vehicle at high lateral accel.
Power change	Power on	Steering torque feedback	Torque steer due to power change
Power change	Power off	Yaw response	Magnitude of response (state below whether over or under steer)
Power change	Power off	Yaw response	Yaw stability of vehicle at higher lateral accelerations
Sudden braking in a turn			Yaw rate response (state tendency to spin or plough below)
Sudden braking in a turn			Roll stability
Sudden braking in a turn			Wheel lift
Sudden braking in a turn			Wheel lock up
Transient cornering	Turn in response		Turn in response and precision on smooth surfaces (low lateral accel.)
Transient cornering	Turn in response		Turn in response and precision on smooth surfaces (medium lateral accel.)
Transient cornering	Turn in response		Turn in response and precision on smooth surfaces (higher lateral accel.)
Transient cornering	Turn in response		Body roll angle
Transient cornering	Turn in response		Body roll rate
Transient cornering	Steering torque feedback		Steering catch-up
Straight line directional stability	Constant throttle		Bump steer
Straight line directional stability	Constant throttle		Steer kickback
Straight line directional stability	Constant throttle		Over changing surface camber (state whether car wanders or pulls)
Straight line directional stability	Constant throttle		Over changing surface composition: ease with which a line is held
Straight line directional stability	Under acceleration		Torque steer
Straight line directional stability	Under acceleration		Tendency to pull to one side
Straight line directional stability	Under braking		Tendency to pull or weave
Obstacle avoidance	Single lane change	Trailing throttle	Turn in response
Obstacle avoidance	Single lane change	Trailing throttle	Recovery
Obstacle avoidance	Single lane change	Trailing throttle	Controllability
Obstacle avoidance	Single lane change	Trailing throttle	Limiting factor (state below whether stability, grip, steering ratio)
Obstacle avoidance	Single lane change	Balanced throttle	Turn in response
Obstacle avoidance	Single lane change	Balanced throttle	Recovery
Obstacle avoidance	Single lane change	Balanced throttle	Controllability
Obstacle avoidance	Balanced throttle		Limiting factor (state below whether stability, grip, steering ratio)
Obstacle avoidance			Double lane change
Response to steering impulse			Oscillation of vehicle
Response to steering impulse			Oscillation of handwheel
Response to steering impulse			Level of damping

Figure 2-27 – Driver subjective assessment questions – Crolla et al (2001/2002) [60], [61]

Referenced in both [60] and [61] is the work of Mimuro et al. In 1990, Mimuro, Ohsaki, Yasunaga and Satoh [62], published a paper on a 'Four parameter evaluation method of lateral transient response'. The method in the paper used four measureable metrics of car behaviour that can be obtained by fitting a 2 degree-of-freedom lateral bicycle model to car data. The four parameters also correspond to four subjective assessments to be carried out by test drivers. The metrics and subjective assessments are arranged into a rhombus shape. The authors note that 'the area of the rhombus denotes the vehicle handling potential and the distortion denotes the handling tendency'. The four metric parameters used and their relative subjective interpretations are shown in Figure 2-28 from [60], due to its increased clarity compared the to original version given in Mimuro et al. [62]. The steady state (DC) gain, natural frequency and damping ratio, all relate to the yaw response, whereas the phase delay relates to the lateral acceleration measured at the vehicle's centre of gravity. The authors carried out an investigation on 20 modern (in 1990) cars at 100 km/h and presented the results along with their averages and standard deviations on the rhombus shown in Figure 2-29. The phase delay axis is inverted, as a lower level of phase delay is perceived as good for performance. It is not possible to associate a numerical value with a subjective assessment directly, but the change in rhombus shape from metric values should produce a similar change in shape of subjective

assessments. Unfortunately no results are presented of subjective assessments of the changing speeds or parameters to determine how well these correlate with the measured metrics.

One advantage of this method is that each subjective assessment is linked only to a single objective metric and that with the rhombus it is easy to determine quickly where performance changes and vehicle characteristics have changed. In a subjective tuning sense, it could be useful to use relative measurements from a baseline vehicle rather than absolute values.

Metric	Subjective interpretation	Description
Steady state yaw rate gain	Heading easiness	The simple gain relationship between yaw rate output i.e. the amount of turning response for a given steer angle input
Natural frequency	Heading responsiveness	This is linked to the yaw rate response time in a transient manoeuvre – the higher the natural frequency, the shorter this response time
Damping ratio	Directional damping	Basically, high damping is linked with reducing the amount of overshoot and setting time following a transient input – however, if it were too high it would cause an undesirable, sluggish response
Phase delay of latac at 1 Hz	Following controllability	This is linked to responsiveness – again for a transient input, a small phase delay is linked to a feeling that the vehicle response tracks the steering demand input quickly

Figure 2-28 – Four metric parameters and their subjective interpretations – Mimuro, Ohsaki, Yasunaga and Satoh (1990) [62], reproduced in Crolla et al 2001 [60]

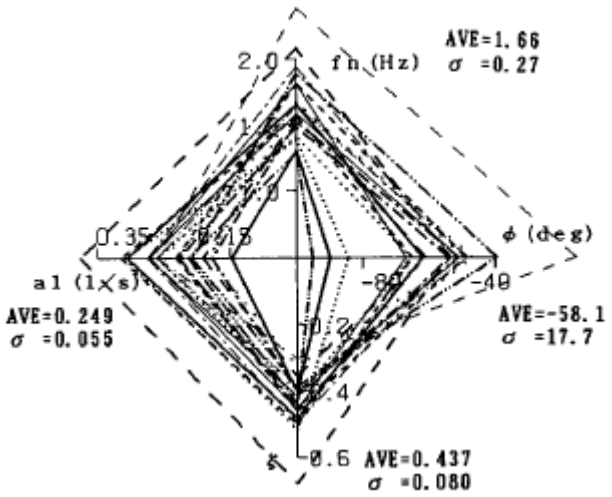

Figure 2-29 – Rhombus of parameters for 20 modern cars – Mimuro, Ohsaki, Yasunaga and Satoh (1990) [62]

In 2003, Fernandes and Okano [63] wrote a paper on 'Vehicle dynamics objective metrics'. The authors used a full car kinematic and dynamic ADAMS model of a vehicle, which had been validated with physical car data. Three different manoeuvres were used in the investigation, these were:

- Steering angle sine sweep from 0.2-3 Hz
- Constant radius turn (30m) with increasing velocity
- Power off in a curve

From each of the manoeuvres a number of performance metrics were determined. The authors used a matrix of vehicle parameters to note their effect on the metrics obtained from the three manoeuvres. The parameters varied were:

- Front anti-roll bar diameter
- Rear anti-roll bar diameter
- Longitudinal location of rear inboard upper lateral linkage
- Longitudinal location of rear inboard lower lateral linkage
- Axial and conical stiffness of trailing arm bush

The anti-roll bar stiffness changes were intended change the overall roll stiffness and roll stiffness distribution. The location of the lateral linkages would affect the rear roll steer, rear lateral force input to the chassis and the rear roll camber. The stiffness of the trailing arm bush would affect the rear steering compliance. Among other characteristics, the authors found that the yaw rate metrics from the 'power off in a curve' test were all dominated by the upper linkage location, with the lower linkage and anti-roll bars also having a fairly significant effect. Unlike the other parameters, the location of the suspension hard points is something that must be defined early on in a vehicle's design stage. The paper shows the advantages that can be made by using models to relate metrics to vehicle components early on. The authors note that the simulations have saved many hours of prototype construction, vehicle testing and evaluation.

In 2002, Norman [64] carried out a 'Multiple-bump road holding test' and produced a paper based on the findings. The investigation consisted of a number of constant speed constant radius steady-state tests in accordance with ISO 4138 [65]. Tests were carried out at different lateral accelerations and curvatures to achieve a range of bump frequencies, with all tests carried out both clockwise and counter-clockwise. A set of 3 trapezoidal bumps were driven over to excite the wheels of the vehicle. Norman calculated front axle, rear axle and net disturbances. Examples of two quite different responses are show in Figure 2-30. Norman notes that when the front axle hits the bumps there is a negative angle error, making the vehicle 'nose-out' and when the rear axle hits the bumps the angle error change is positive, making the vehicle 'nose-in'. The net angle error is the sum of the two axle disturbances. Figure 2-31 presents the front and rear axle disturbances versus bump frequency. Interestingly there were marked differences between the directions, especially for the rear axle disturbance. Norman notes that the maximum front, rear and net errors in term of magnitude and frequency can be

used to ‘interpret a vehicle’s multiple-bump road holding ability’. The author notes that ideally front and rear disturbances should be small and consistent through the frequency range. If the disturbances are equal front and rear then the vehicle would remain parallel to the original path but offset by a small amount. In an actual driving situation, this may result in the driver making adjustments after the front input which exacerbates the reaction of the rear axle, so it may actually be desirable to have a slightly larger disturbance at the front axle than the rear to counter this.

The paper is quite useful in pointing out that for good directional control of the car, the front and rear hub modes should be well damped, but also their relative differences should be minimised in order to provide a net heading angle error close to zero for a variety of frequency inputs. If this was not the case then the driver may have to correct the steering in a different direction for bumps of slightly different frequency, which would give the vehicle an unpredictable feel which is obviously undesirable.

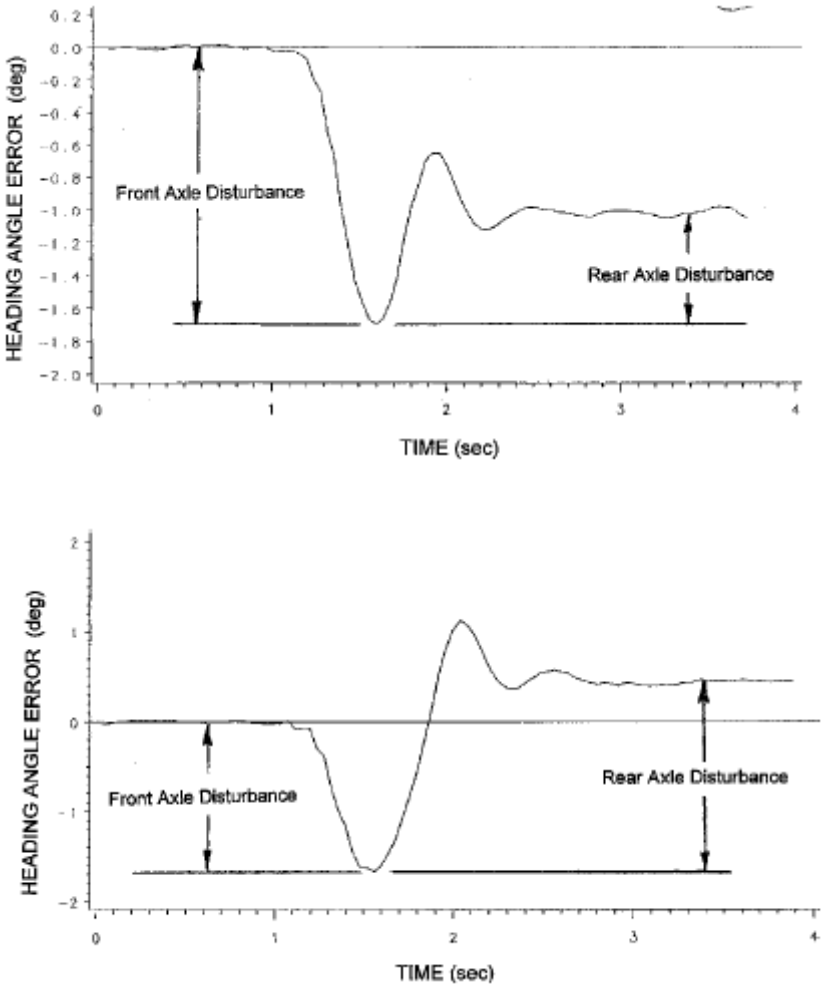

Figure 2-30 – Heading angle error – Norman (2002) [64]

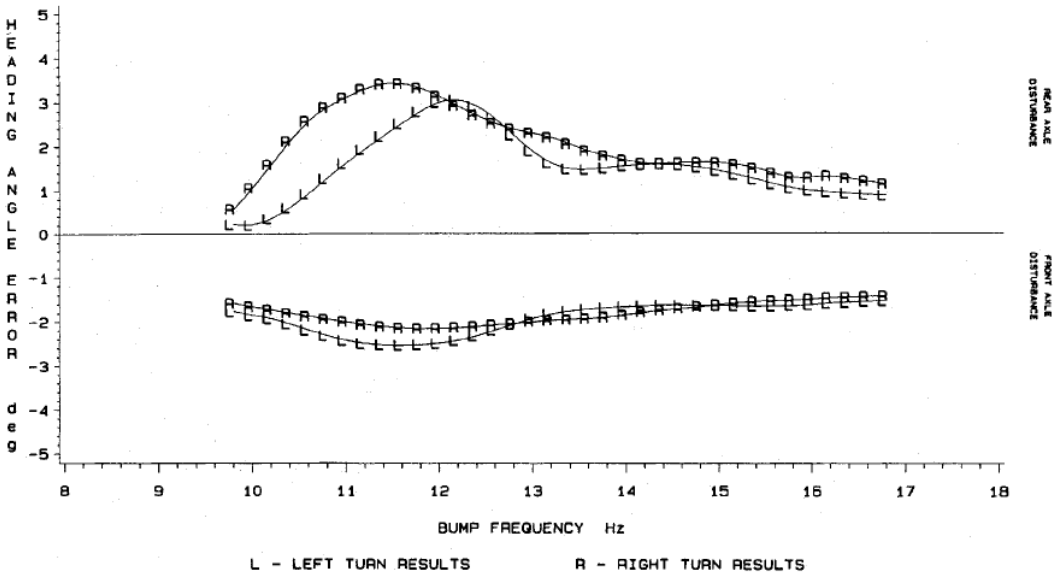

Figure 2-31 – Axle Disturbances – Norman (2002) [64]

3 – Road and Rig Inputs

This chapter of the thesis explains the inputs that the road surface can apply to a vehicle and ways in which this information can be manipulated and reproduced to be used as inputs to the vehicle from the four-post test rig.

The aim of the chapter is to produce a reliable, repeatable and efficient set of inputs that can be used to accurately determine the response of a vehicle as it would behave on the road surface.

Section 3.1– Road Spatial Characteristics, expands on the literature review of road inputs and presents different road spatial magnitudes and characteristics from reviewed literature for comparison.

Section 3.2 – Effect of Vehicle Speed, determines the effect that the forward speed of the vehicle has on a vehicle excited by road inputs, both in a magnitude and modal contribution sense.

Section 3.3 – Modal Rig Inputs, explains the use of modal inputs on the four-post rig so that these can be used to characterise the vehicle response separately for each modal input (heave, pitch, roll and warp).

Section 3.4 – An Efficient Rig Input, develops the modal rig inputs into a set of rig inputs that are efficient both in terms of test time and in terms of the information that can be extracted from them. This is achieved with the use of a constant peak velocity exponential chirp input, used in four different modes of input vibration.

Section 3.5 – Selection of Appropriate Amplitude, explains a way in which the appropriate amplitude of the efficient rig input can be chosen, so that responses obtained from the measured data and a road input would be most similar for a non-linear vehicle.

Section 3.6 – Road Input Construction from Spatial Characteristics and Drive Cycle, proposes two different methods in which representative time domain vehicle inputs can be created from spatial frequency characteristics and a forward speed drive cycle, to be used as inputs to simulation models and using the four-post rig.

Section 3.7– Collection of Road data and Basic Spatial Characteristic Estimation, explains the collection of road data using an instrumented vehicle on test drive routes in two different countries, and the basic estimation of the measured roads spatial frequency characteristics.

Body Acceleration Evaluations from Road Testing in Appendix 3, presents the findings of body acceleration PSDs from various roads during the testing explained in Section 3.7– Collection of Road data and Basic Spatial Characteristic Estimation.

3.1 – Road Spatial Characteristics

In the road surfaces section of the literature review of this thesis (Section 2.1– Road Surfaces) a number of papers were reviewed that presented information about the spatial frequency characteristics of road surfaces.

The papers generally presented plots of road displacement PSD verses the wavenumber (n – cycles/m). The papers also presented information about the roughness coefficients and exponents of different roads. Information was presented using two different spatial characteristic equations, a single gradient fit as in equation (3-1) and a dual gradient fit as in (3-2).

$$G_d(n) = G_d(n_0) \times \left(\frac{n}{n_0} \right)^{-w} \tag{3-1}$$

$$G_d(n) = Cn^{-w_1} \qquad 0 \le n \le n_0$$

$$G_d(n) = Cn^{-w_2} \qquad n_0 \le n \le \infty \tag{3-2}$$

Where:

G_d – Displacement PSD

C – Roughness coefficient ($Gd(n_0)$)

n - Wavenumber

w_1 – Low wavenumber gradient

w_2 – High wavenumber gradient

As well as the longitudinal spatial characteristics of roads, some papers also presented relationships between the left and right wheel paths by using a measure of coherence versus wavenumber. The main two different types were the use of isotropy presented by Robson [10] and the used of an exponential function presented by Bogsjo [16]. Figure 2-5 taken from Bogsjo [16] shows the coherence between the left and right wheel paths verses wavenumber for a selection of road surfaces using these two methods compared to measured road coherences.

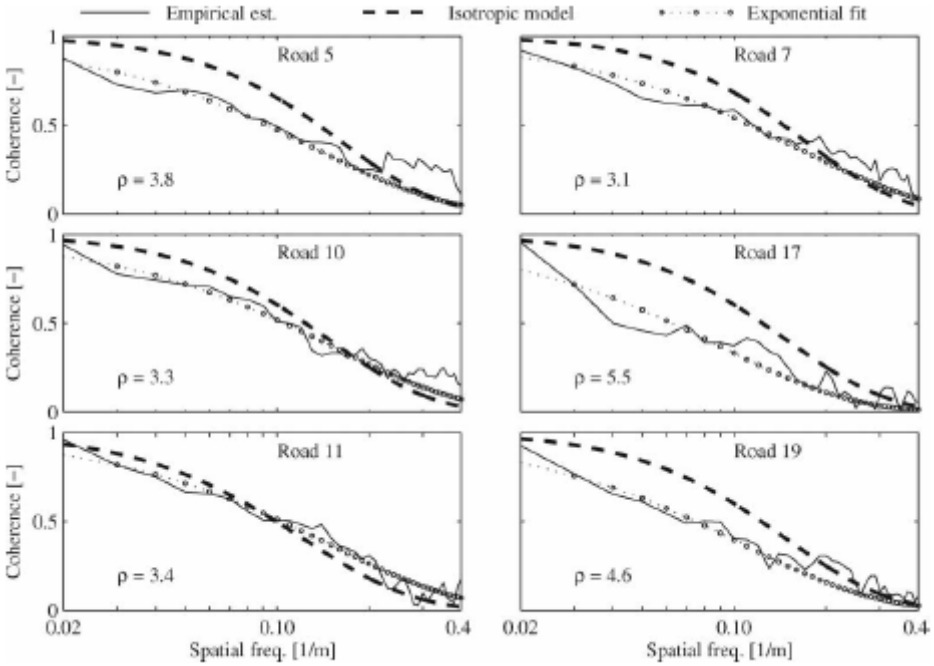

Figure 2-5 – Repeated from section 2 – Bogsjo [16]

Figure 3-1 compares road spatial frequency characteristics from ISO 8608 [4], a typical Swedish road presented in Andren [8], Motorway, Principal and Minor roads from Crolla, Firth and Horton [66] and 3 different roads of the 20 presented by Bogsjo [16].

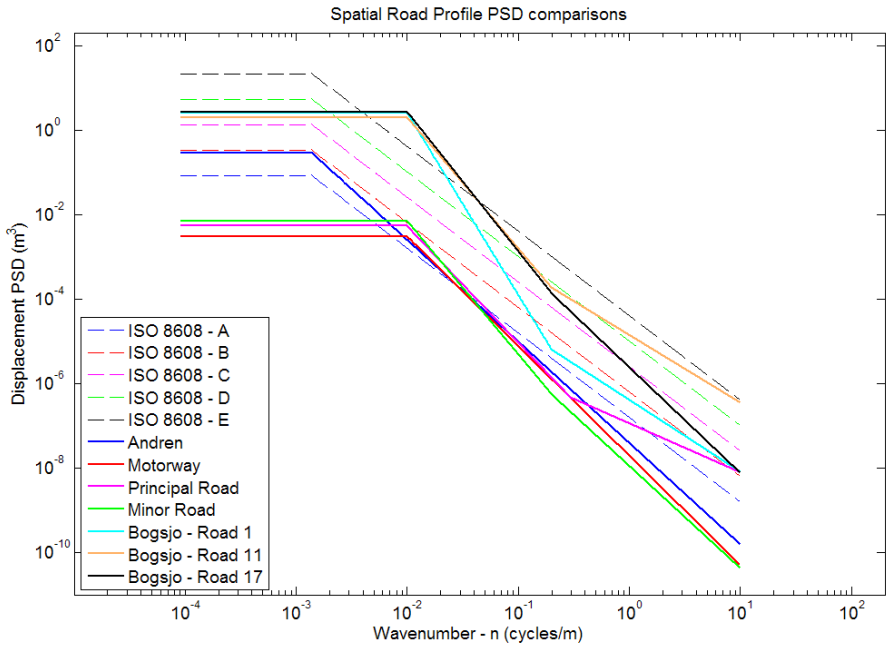

Figure 3-1 – Spatial Road Profile Comparisons

The PSDs from Figure 3-1 were used as inputs to fourth-order linear transfer functions of typical body acceleration and contact force responses used to represent a ¼ car at speeds of 15 and

30 m/s. Figure 3-2 compares the body acceleration output PSDs for some of the different road input PSDs from ISO 8608 [4], Andren [8], Crolla, Firth and Horton [66] and Bogsjo [16]. The body acceleration is linked to passenger discomfort, so the comparisons show how the magnitude and frequency distribution of discomfort would be expected to change between different roads. Figure 3-3 compares the tyre contact force output PSDs for the same input PSDs. The contact force is linked to the road holding ability of the vehicle.

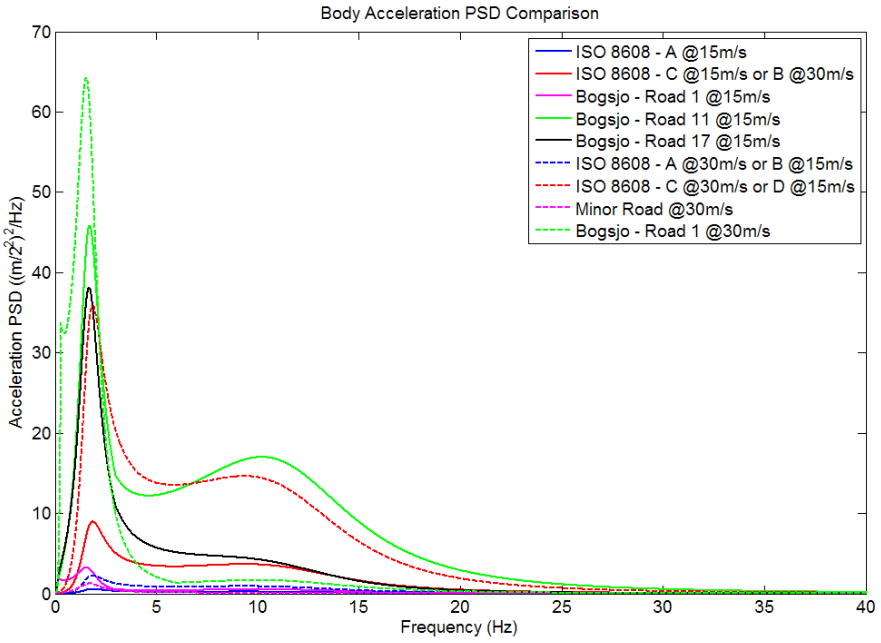

Figure 3-2 – Body Acceleration PSD Comparisons

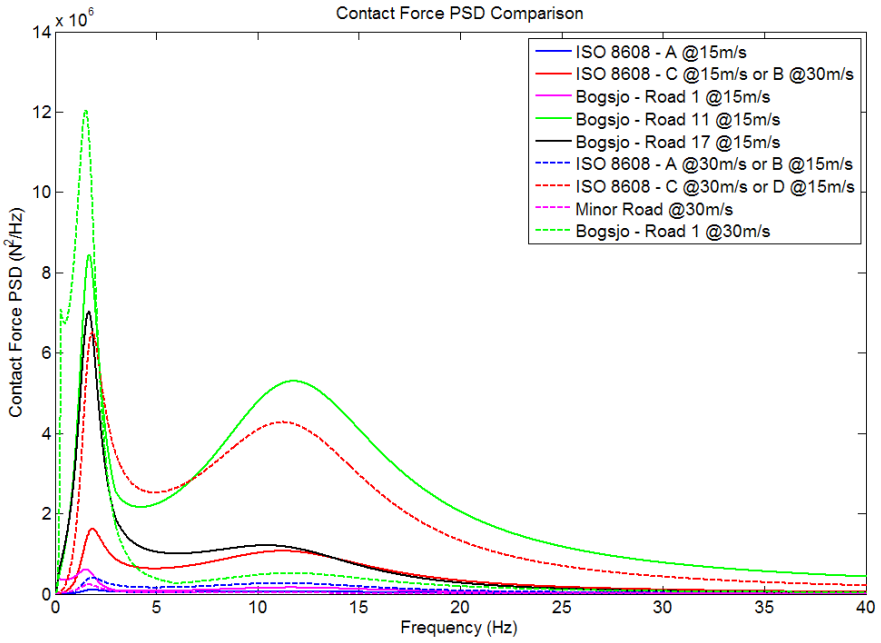

Figure 3-3 – Contact Force PSD Comparisons

Figure 3-2 and Figure 3-3 indicate the wide range of different output responses that a vehicle can experience on the road and how that tuning for just one example, such as Bogsjo [16] Road 1, could lead to a non-optimal response on other roads such as ISO 8608 [4] Road C. In this example when driving over Road 1 the passenger comfort and road holding could be improved by increased damping of the body mode natural frequency which occurs around 1.5 Hz. However, when driving the same vehicle over the ISO 8608 Road C road at the same speed, the increase in damping would cause the accelerations in the 5 to 10 Hz region to increase. From the BS 6481 [1] and ISO 8041 [26] standards we know that this region is very sensitive for passenger discomfort. The increase in damping would still improve the road holding though.

The exponents of the displacement PSDs compared in Figure 3-1 vary between 1.55 and 4.3. On average the best match for a single exponent would be around 2.4 which is consistent with Andren's [8] best fit for the entire Swedish road network. In ISO 8608 [4] all PSDs have an exponent of 2. This corresponds to a constant velocity PSD, which is theoretically equivalent to a white noise signal. This type of signal is easily converted to the correct displacement by integrating, as explained in Sayers [13]. This makes the input simple to implement in simulations and using the four-post rig.

When considering a vehicle travelling in a forward direction it is a common and a fairly valid assumption ([32], [10] ,[56]) that the rear wheels will encounter the same inputs as the front wheels, but lagged by a time constant based on the wheelbase and forward speed of the vehicle. Using this assumption, the inputs that the road surface can apply to the wheels of the vehicle can be characterised into four different types of modal excitation:

Heave – All four wheels of the vehicle are excited with the same input at the same time.

Pitch – The two rear wheel inputs are exited in anti-phase (180˚) with the front inputs, causing a rotation of the road surface about the longitudinal centre of the wheelbase.

Roll – The left and right inputs are excited in anti-phase, causing a rotation of the road surface about the lateral centre of the track.

Warp – Combines both pitch and roll instances, by the two diagonal wheel pairs being in anti-phase. This can be imagined as rolling of the road in opposite directions at each end of the car, or by pitching of the road in opposite directions on different sides of the car. The input is most likened to the single wheel input case.

In order to simplify the description of different possible road inputs, the normally rotational inputs applied to the vehicle by the road are considered in linear single-wheel terms. For example, a heave input with a 20 mm displacement would indicate that all four wheels were excited in phase at 20 mm amplitude. A roll input with a 20 mm displacement would indicate that left and right inputs each had 20 mm amplitudes, but 180° out-of-phase. When applied to the vehicle this would cause an angular rotation related to the level of displacement and track of the vehicle.

The heave and pitch inputs of the road are characterised by the spatial domain characteristics of the surface the forward speed and wheelbase. The roll and warp inputs are in addition characterised by these and the spatial frequency coherence of the road surface.

3.2 – Effect of Vehicle Speed

When using a spatial frequency road characteristic to define a road surface, the effect of increasing forward speed for a simple single wheel input can be applied by simply shifting the frequency range of interest towards lower wavenumbers. The conversion to the spatial domain from the frequency domain is done simply using equation (3-3).

$$f = nV \tag{3-3}$$

Where:

f – Frequency

n – Wavenumber

V – Forward Velocity

Increasing speed tends to increase the amplitude of the input at any frequency, as generally displacement decreases with increasing wavenumbers. For roads characterised by a single gradient, the amplitude at all points in the frequency domain is simply scaled as the speed is changed, as in Figure 3-2 where ISO 8608 [4] road A at 30 m/s is equal to road B at 15m/s. However when the road is characterised by two or more gradients (or a more complex function) the amplitude is no longer simply scaled identically across the frequency range, but changed in accordance with shifting along the wavenumber axis in the spatial frequency PSD. This causes different contributions in the frequency domain at different speeds. Figure 3-4 presents an example of the contact force PSDs of a vehicle with the same dynamic properties as in Figure 3-2 and Figure 3-3, travelling over a theoretical road surface with a steep low wavenumber exponent (2.4 below 0.3 cycles/m) and shallow high wavenumber exponent (1 above 0.3 cycles/m). The road PSD is quite similar to the principal road from Crolla, Firth and Horton [66], which has a low wavenumber exponent of 2.75 below 0.3 cycles/m and a high wavenumber exponent of 1.16 above 0.3 cycles/m. The theoretical road uses the shallower exponents in order to show the effect more clearly, but is well within the range of exponent values determined by Andren [8]. Figure 3-4 shows that in the 10 m/s case the hub mode peak at around 12.5Hz is dominant over the body mode peak at 1.8 Hz, but as speed is increased to 20 m/s the two modes have equal magnitudes and when further increased to 30 m/s the body mode is highly dominant over the hub mode. With this type of road profile vehicle responses tuned to behave well at low speeds, could potentially behave poorly at high speeds and vice-versa.

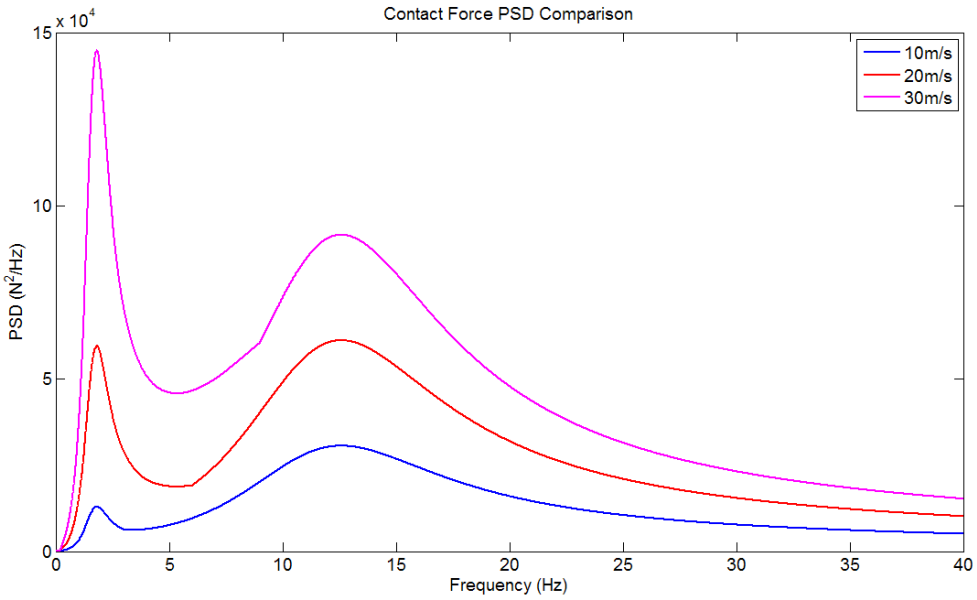

Figure 3-4 – Effect of Speed on Contact Force PSD for Dual Gradient Road Profile

As well as absolute amplitude, the speed of the vehicle also affects relative magnitude of vertical and roll excitations on a single axle. Sayers [13] work on the PSD functions of vertical and roll components of road roughness (Figure 3-5), found that at high wavenumbers there is almost no coherence between the left and right wheel paths, meaning that the averaged vertical input would be equal to the roll excitation of each wheel. At the low end of the spectral frequency range the situation is very different. In this case the coherence in the left and right wheelpaths is equal to 1. This means that there is no roll excitation and only pure vertical excitation for a single axle. These are the two extreme cases, but during the spatial frequency range of interest for a road car the coherence, and hence vertical and roll contributions, change significantly. As the vehicle speed affects the shift in the frequency range of interest along the spatial frequency range, then speed will have a major effect on relative magnitude of vertical and roll excitation of the vehicle.

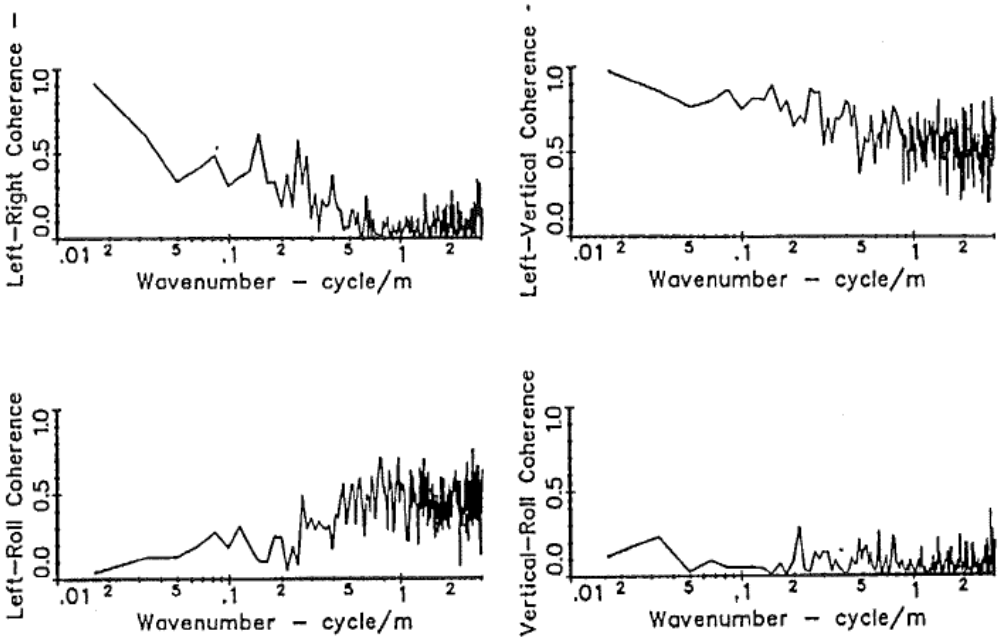

Figure 3-5 – Road Profile Coherence functions – Sayers (1986) [13]

The final effect of forward speed on the road surface inputs to a vehicle is known as wheelbase filtering. This characteristic is explained in Crolla [33] and Gillespie [11].

When a vehicle is travelling along a road at constant speed with identical left and right inputs, pure heave and pure pitch components appear at discrete frequencies due to the forward speed and wheelbase of the vehicle. In between these discrete frequencies the contributions of heave and pitch are combined. The situation can be defined in the frequency domain using equations (3-4), (3-5) and (3-6).

$$G_d \,\mathrm{Re}\,ar(f) = Gd(f) \times e^{-j2\pi f\left(\frac{l}{V}\right)}$$

(3-4)

$$G_d Heave(f) = 0.5\left(G_d(f) + \left(G_d(f) \times e^{-j2\pi f\left(\frac{l}{V}\right)}\right)\right)$$

(3-5)

$$G_d Pitch(f) = 0.5\left(G_d(f) - \left(G_d(f) \times e^{-j2\pi f\left(\frac{l}{V}\right)}\right)\right)$$

(3-6)

Where:

G_d - PSD of road input and front wheel input

G_dRear - PSD of rear wheel input

G_dHeave - PSD of heave input

G_dPitch - PSD of pitch input

l – Wheelbase

Figure 3-6 and Figure 3-7 present the heave and pitch contributions of road inputs created using equations (3-5) and (3-6) for forward speeds of 15 and 30 m/s respectively with a wheelbase of 2.635 m.

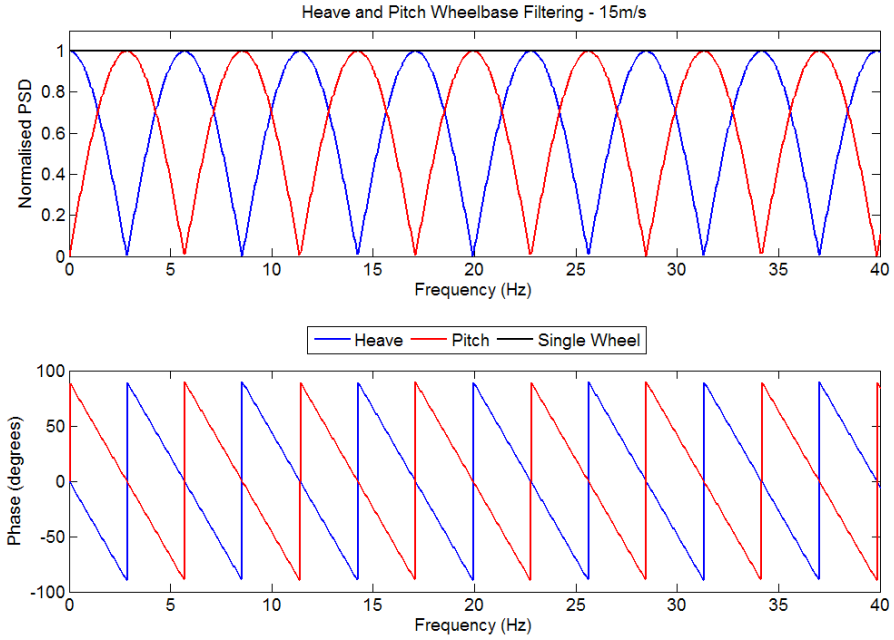

Figure 3-6 – Heave and Pitch Wheelbase filtering at 15m/s

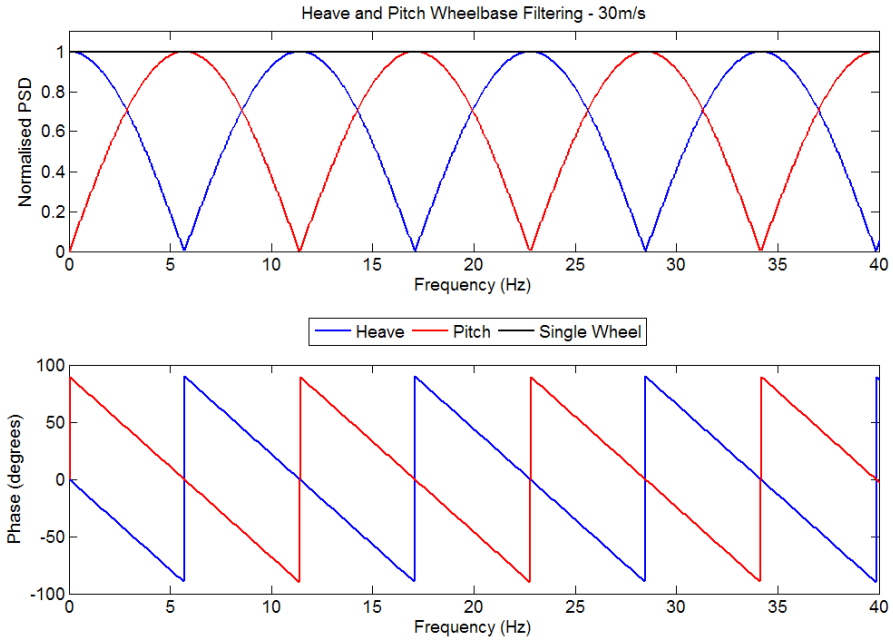

Figure 3-7 – Heave and Pitch Wheelbase Filtering at 30m/s

Comparison of Figure 3-6 and Figure 3-7 shows that at higher speeds there are fewer repetitions of the discrete heave and pitch frequencies in the 0 to 40 Hz range. This effect changes the contributions of the heave and pitch inputs to the overall response of the vehicle. For a car with poor pitch mode control travelling at 15 m/s, but a pitch mode that occurred at 6 Hz, the mode would not be excited, and hence the poor performance would not be noted. The same vehicle travelling at 30 m/s would excite the pitch mode at full amplitude leading to an undesirable response to the road inputs.

As with the heave and pitch wheelbase filtering, the same phenomenon occurs in roll and warp. The roll inputs are phased with heave and the warp inputs phased with pitch. However, due to the coherence in the left and right wheel paths, the relative magnitudes of the four modes change with frequency. As isotropy was not found to be a particularly reliable model of coherence by Robson [10] and Bogsjo [16], the exponential function defined by Bogsjo [16] can be used as a better model. Although this model is designed to be parametric, an average of analysed roads can be used to define the constant, ρ. In this thesis a value of 3.4 is used, as this best matched the constants for typical roads in Bogsjo [16].

The coherence defined by the exponential function is shown in equation (3-7).

$$\gamma(n) = e^{-\rho t_r n} \tag{3-7}$$

Where:

γ – Coherence

t_r – Track width

ρ – Coherence constant (3.4 used)

The coherence plot in Figure 3-8 was generated using equation (3-7) and also shows the 0.5 and 40 Hz spatial frequencies at 15 and 30 m/s to indicate what section of the coherence curve would be used at different speeds.

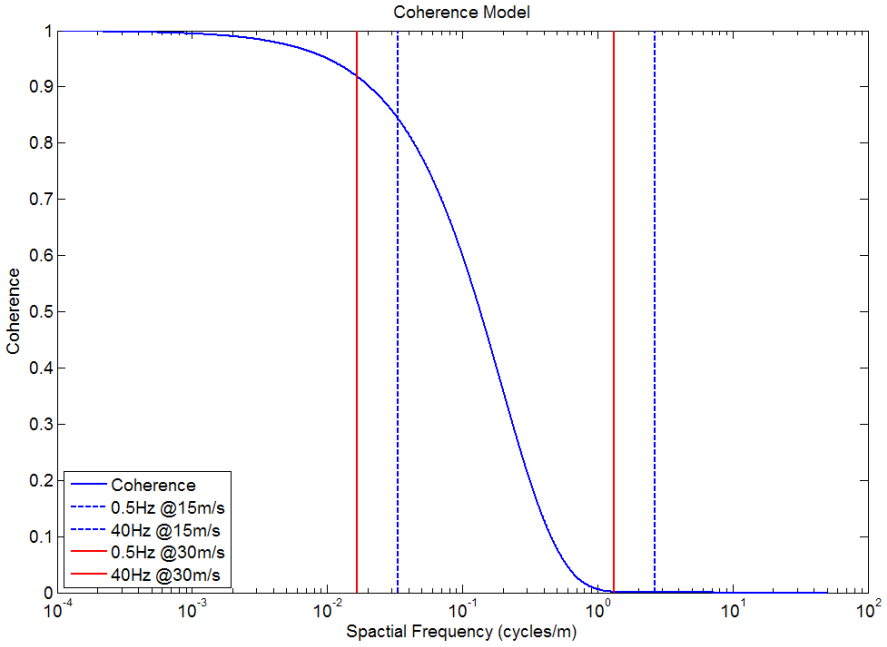

Figure 3-8 – Coherence using Bogsjo [16] model

If equation (3-7) is used to define the coherence between the left and right wheel paths, then the following points (as noted by Sayers [13]) are true.

- Coherence between the left wheel path and vertical input starts at 1 and reduces to 0.5
- Coherence between the left wheel path and linear roll input starts at zero and increases to 0.5.
- Coherence between single axle vertical and roll input is zero throughout the spatial frequency range.

With this information four modal input PSDs relating to the inputs that the road supplies to the vehicle can be constructed using equations (3-8) to (3-11).

$$G_d Heave(f) = \left(0.5 \left(G_d(f) + \left(G_d(f) \times e^{-j2\pi f\left(\frac{l}{V}\right)} \right) \right) \right) \times \left(\frac{\gamma(f)+1}{2} \right)$$

(3-8)

$$G_d Pitch(f) = \left(0.5 \left(G_d(f) - \left(G_d(f) \times e^{-j2\pi f\left(\frac{l}{V}\right)} \right) \right) \right) \times \left(\frac{\gamma(f)+1}{2} \right)$$

(3-9)

$$G_d Roll(f) = \left(0.5 \left(G_d(f) + \left(G_d(f) \times e^{-j2\pi f\left(\frac{l}{V}\right)} \right) \right) \right) \times \left(1 - \left(\frac{\gamma(f)+1}{2} \right) \right)$$

(3-10)

$$G_d Warp(f) = \left(0.5 \left(G_d(f) - \left(G_d(f) \times e^{-j2\pi f\left(\frac{l}{V}\right)} \right) \right) \right) \times \left(1 - \left(\frac{\gamma(f)+1}{2} \right) \right)$$

(3-11)

The plots in Figure 3-9 and Figure 3-10 were generated using equations (3-8) to (3-11) and show the Heave, Pitch, Roll and Warp contributions at 15 and 30 m/s respectively. In both cases heave is dominant over all other inputs at very low frequency and at high frequency all input modes have equal magnitudes and only the wheelbase filtering has an effect on the input contribution. In the 15m/s case the equalisation of magnitudes occurs around 15 Hz, while for the 30 m/s case this does not occur until around 25 Hz. This means that the relative roll and warp inputs compared to heave and pitch are smaller below 25 Hz in the 30 m/s compared to the 15 m/s case.

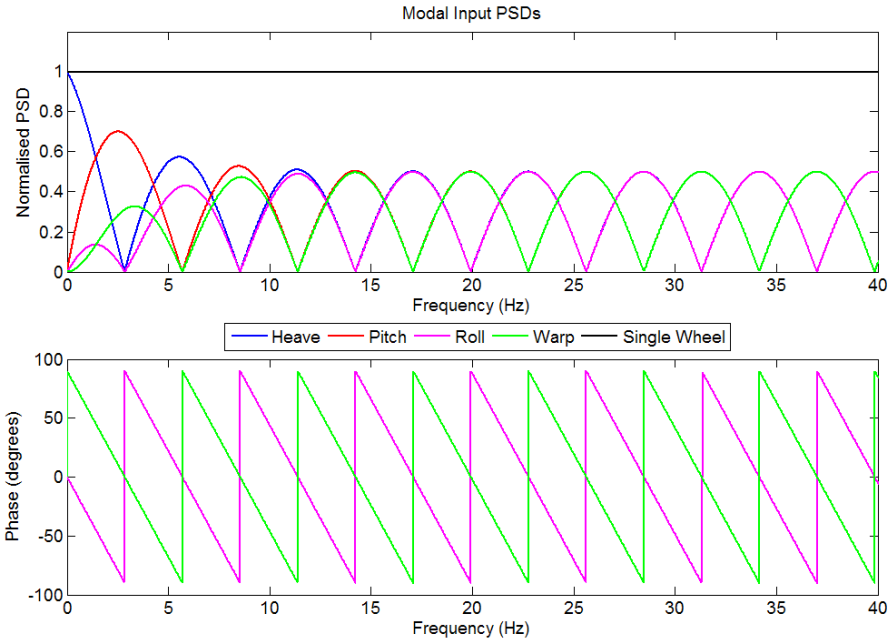

Figure 3-9 – Modal Input PSDs at 15m/s

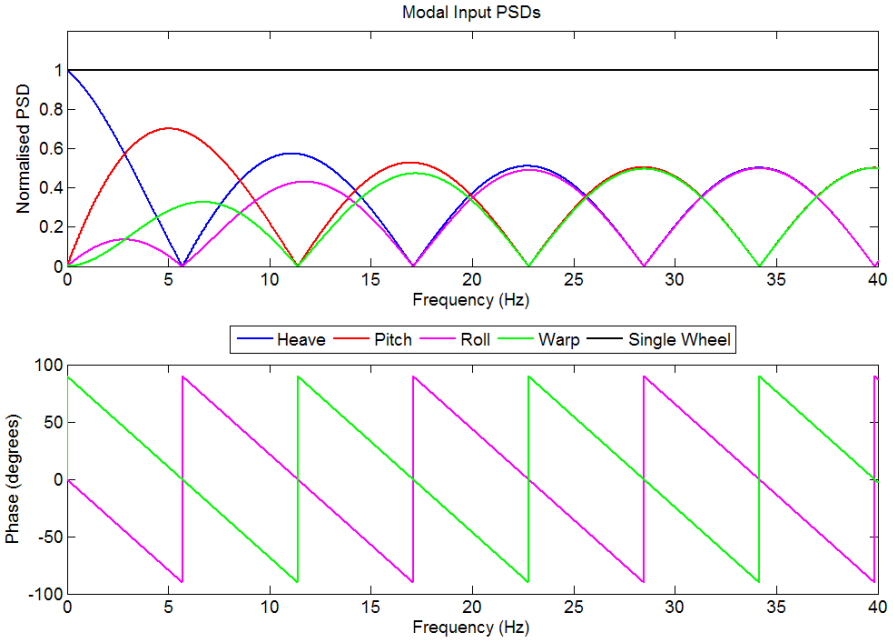

Figure 3-10 – Modal Input PSDs at 30m/s

3.3 – Modal Rig Inputs

Considering the contents of the previous two sections within this chapter, it is obvious that if a road surface input for a single road at a single constant speed were used to assess the performance of the vehicle, this would not be a good representation of the behaviour of the vehicle when excited by a different road surface at a different speed. This makes simple lag type inputs inappropriate for use in assessing general vehicle performance.

An alternative to road reconstruction type inputs is to test each of the modal inputs that the road can apply to the vehicle separately and calculate the modal response of the vehicle for each input. With this response information, the output of the vehicle to any combination of the modal road excitations can be determined in post processing, meaning that any number of different inputs and speed conditions could be calculated from a single test sequence. With a completely linear vehicle this would work equally well for any amplitude of input. For example a 50 mm input could be used across the frequency range 0 to 40 Hz. However, as real vehicle responses are non-linear, the amplitudes of these inputs and their change with frequency would need to be considered.

As was already discussed in section 3.1 – Road Spatial Characteristics, for a displacement PSD exponent of 2 the velocity input can be simulated by a white noise input, which can then be integrated to achieve the desired displacement. In this case a roughness coefficient of the road has to be chosen, along with a forward speed of the vehicle. This might indicate that the input is again restricted to being valid only for a certain road and forward speed, but this is not the case. Because the testing uses only one modal input at a time there is no effect of speed dependant wheelbase filtering. In addition, it was noted at the start of this chapter that forward speed simply scales the magnitude of a displacement PSD in the frequency domain when a single exponent is used. This then means that by testing a small range of inputs with constant velocity PSD across the frequency range of interest, responses would be generated that are valid for a number of different speeds and road roughness values using only a small amount of tests. For a non-linear vehicle the determination of the responses for different magnitude inputs would show how the vehicle would respond differently to either speed or road roughness factors.

When we consider that generally the roughest of roads are traversed at the lowest of speeds and vice-versa for the smoothest roads, the range of inputs required to characterise the vehicle over its general operating range is actually quite small. In addition, when tuning a vehicle it is often of little importance that the comfort and road holding be optimal for a very smooth road, as passengers are not sensitive to vibration at low levels of acceleration [1] and handling performance is not significantly affected when contact load variations are small [56]. This means that we can acquire all the response information required with a very small number of input amplitudes.

Figure 3-11 presents the characteristics of an integrated band-limited white noise input representative of an ISO 8608 [4] class A road, that would be used for simulation and rig inputs.

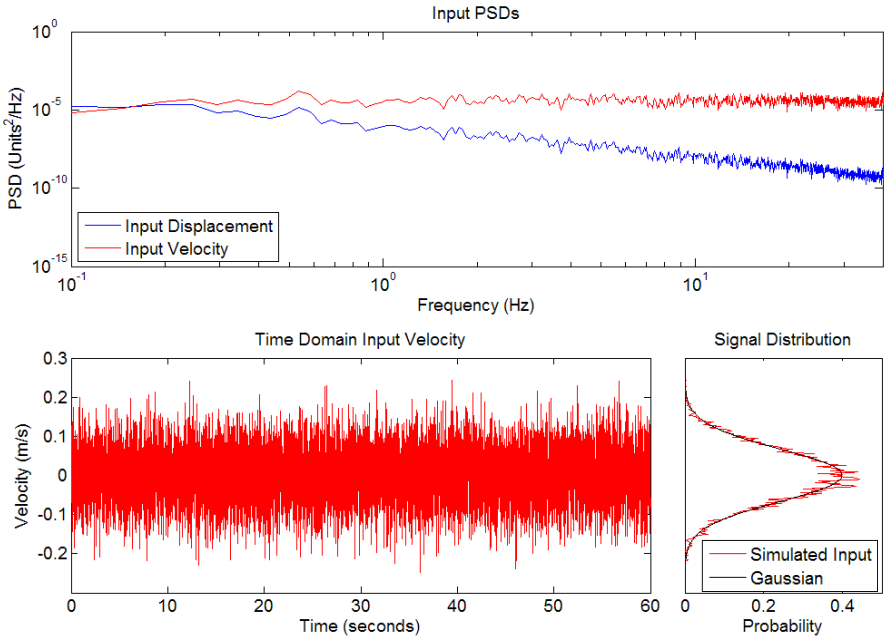

Figure 3-11 – Integrated white noise input properties

In order to calculate the vehicle response from the data acquired, FFTs (Fast Fourier Transforms) would be applied to the inputs and each desired output. From these the cross power spectral density of the output and input combination would be calculated and divided by the power spectral density of the input. This would create a complex response function in which both amplitude and phase information of the output with respect to the input would be contained. This can be achieved efficiently by using the 'tfestimate' function in MATLAB [67].

Using this method, responses can be determined quickly from relatively small amounts of data. For example a resolution in the frequency domain of 0.1 Hz would require only 10 seconds of data in the time domain. However, with only 10 seconds of data the signal distribution of a pseudo-random white noise input may not be as close to Gaussian as desired and transient start and end effects would mean that the complete 10 seconds of data could not be used for response calculation As the length of the data sample is increased the input and response estimates would improve.

The Fourier transform method effectively fits a number of discrete sine and cosine wave frequency components to a time domain signal. The result in the frequency domain is amplitude and phase values for each of the component waves. However, this means that any directionally non-linear behaviour of the vehicle is lost in the analysis. An example of the directional non-linear behaviour caused by a non-linear damper curve can be seen in Figure 3-12. This data is from the front suspension displacement of a Honda Civic tested on the four-post rig using a sine

sweep input. The directional non-linearity is caused by a damping charactistic that is heavily rebound biased.

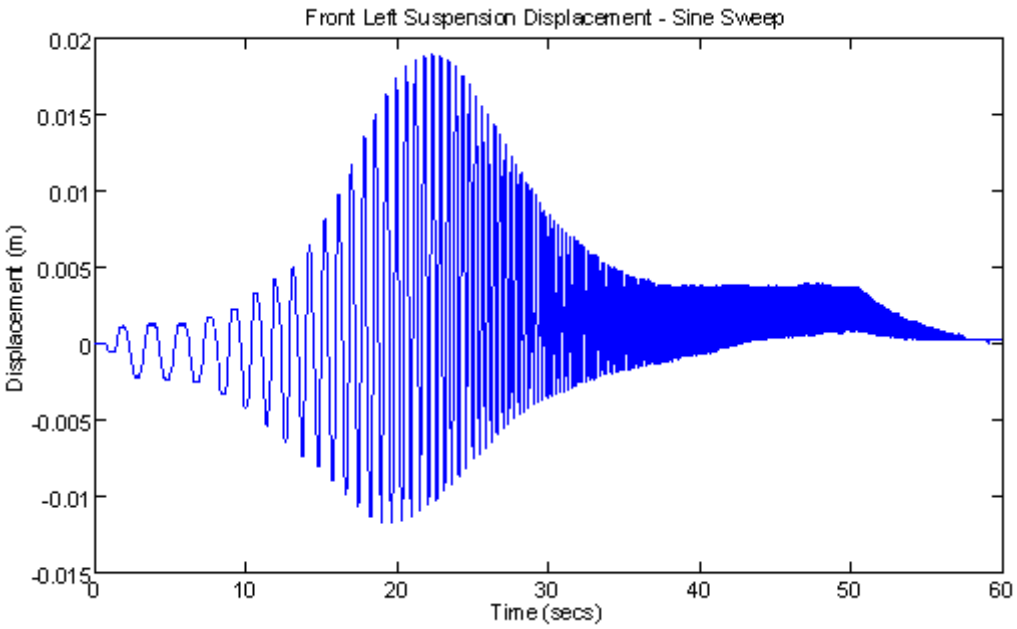

Figure 3-12 – Directional non-linearity cause by non-linear damper

Another input method that could be used to represent the same frequency spectrum is to create separate sine wave inputs at different frequencies all with the same velocity magnitude. Figure 3-13 presents the displacement of increasing frequency, constant peak velocity stepped sine inputs for use on a four-post rig. The input-output data at each discrete frequency tested can be used to determine the amplitude ratio and phase difference of the same signals. In addition the relative positive and negative amplitudes of the output can be used to assess the directional non-linearity of the response at each discrete frequency. Another advantage of sine wave data is that the spring stiffness and damper characteristics can be investigated in more detail. For example, the friction of the suspension system can be identified by looking at the suspension force when the suspension starts to move. Also the damper characteristics can be determined which can be of great value when benchmarking competitor vehicles for comparison purposes.

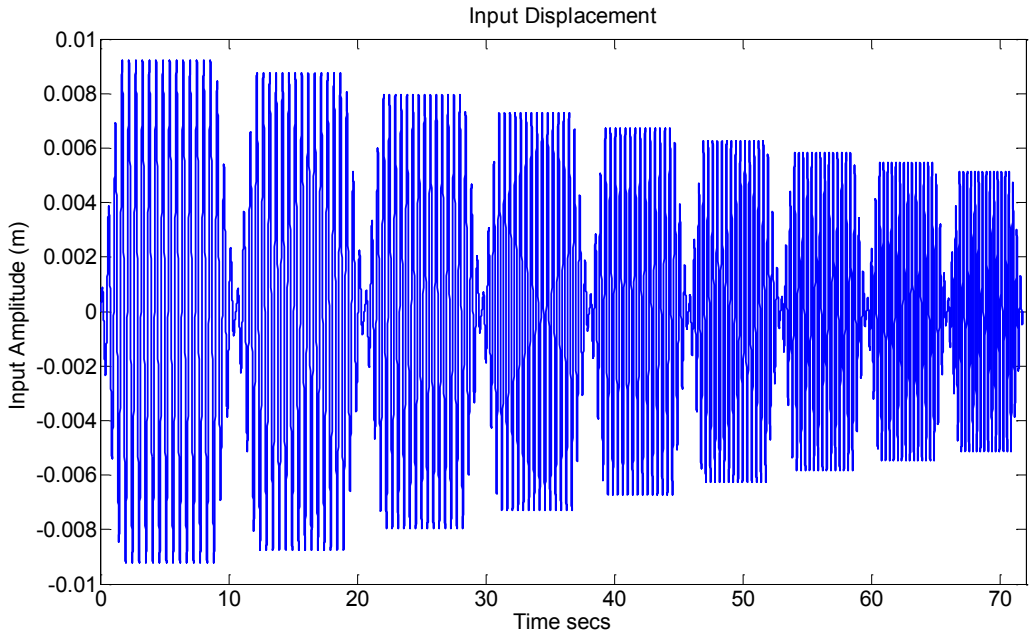

Figure 3-13 – Stepped sine inputs

However, one big disadvantage with this method is the amount of time taken to achieve the complete frequency range of interest with a suitable frequency resolution. It is important that the transients due to large accelerations at the start of the signal are overcome before the data is used to generate the actual response. This means that each frequency step may need to be a number of cycles long.

In order to overcome this problem a sine sweep or chirp signal can be used. In this type of signal the frequency increases with time, meaning that the input never covers a complete cycle at one discrete frequency. This can be analysed in the same way as the stepped sine input, but the test can be carried out much faster, as the undesirable transients only occur at the very start of the run. The limitation of the length of this signal is the rate at which the frequency is increased. By increasing the frequency too fast the number of cycles in any frequency range is reduced and hence the frequency resolution. This can also have the undesirable effects of altering the measured damping ratio and shifting the measured natural frequency. In the ISO 7626-2 [68] standard the maximum recommended rate for a linear chirp signal in Hz per minute is defined by equations (3-12) and (3-13).

$$a_{\max} = \frac{54 \times f_n^{\,2}}{Q^2} \tag{3-12}$$

$$Q = \frac{0.5}{\zeta}$$

(3-13)

Where

a_{max} – Sweep rate Hz/min

f_n – Estimated resonance frequency

Q – Estimated dynamic amplification (quality factor)

ζ - Estimated damping ratio

For a typical road car the lowest natural frequency would be expected to be around 1.2 Hz and the damping ratio a minimum of 0.3. Using equation (3-13), this would give a sweep rate of 28 Hz/min. So a frequency sweep from 0-30 Hz in 60 seconds would be slightly higher than the recommended rate. Figure 3-14 presents an example of a constant peak velocity linear chirp signal from 0-30 Hz over 30 seconds.

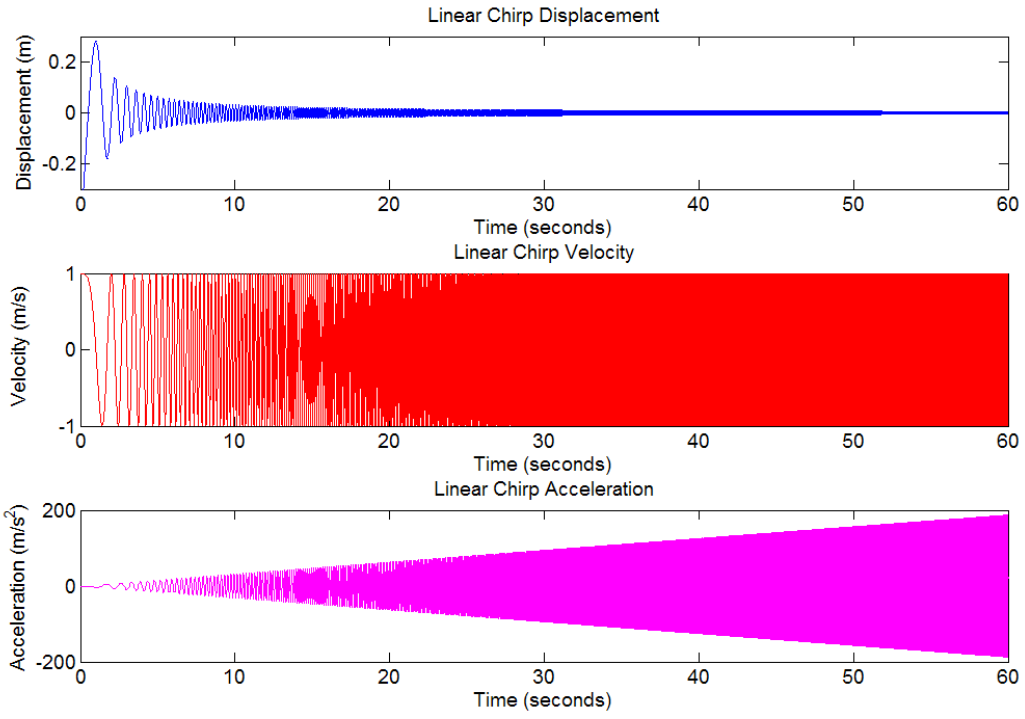

Figure 3-14 – Linear chirp signal – 0-30Hz over 60 seconds

3.4 – An Efficient Rig Input

Section 3.3 – Modal Rig Inputs, explained how a suitable linear chirp input signal from 0 to 30 Hz could be conducted with approximately a 60 second duration, according to ISO 7626-2 [68]. The limitation with this method is the frequency rate increase around the low frequency body modes to give the required accuracy. With 60 second duration the increase rate would be 0.5 Hz/s. In this case the change in frequency from 1 to 1.5 Hz would occur in just over one cycle. This single cycle is then required to provide all of the amplitude and phase information in the 1 to 1.5Hz region, despite only having a single peak and trough. Although this rate is suitable according to ISO 7626-2 [68], a slower frequency increase rate would provide increased accuracy of the vehicle response around the low frequency body modes, which could in turn impact on the accuracy of the parameter estimation. A slow frequency increase rate could produce sufficient information around these modes by having more low frequency cycles, but this is at the expense of a long run time. In addition the amount of cycles at higher frequencies is then more than is required to produce accurate responses.

In ISO 7626-2 [68] a maximum rate is also presented for a logarithmic frequency sweep (3-14). Gloth and Sinapius (2004) [69] carried out a critical review of the ISO 7626-2 [68] standard and a sweep rate investigation found that “no restrictions for the sine sweep rate are needed as long as proper data processing is applied to the time-domain data”.

In a logarithmic frequency sweep (sometimes called exponential chirp or geometric chirp) the frequency increase rate is dependent on the frequency at that point, so that the frequency increase between the start and end of each cycle is equal. This means that a frequency resolution rate can be chosen which is constant across the frequency range. The frequency calculation from time is given by equation (3-15) from [70].

$$S_{\max} = \frac{77.6 \times f_n}{Q^2} \tag{3-14}$$

Where

S_{max} = Maximum frequency sweep rate (Octaves/Min)

$$F(t) = f_0 k^t \tag{3-15}$$

$$k = e^{S_{Hz}}$$

(3-16)

Where:

f – Instantaneous frequency

f_o – Initial frequency

k – sweep rate constant

S_{Hz} – Frequency increase per cycle (Hz)

When creating the sine sweep in the time domain equation (3-17) from [70] must be used to generate the sine sweep signal.

$$x(t) = \sin\left(2\pi f_0 \frac{k^t - 1}{\ln(k)}\right)$$

(3-17)

When using an exponential chirp signal it is not sensible to start the sweep at zero frequency, as a large portion of the run would be needed just to reach the body mode natural frequencies, which typically lie between 1.2 and 2 Hz. Instead a lower frequency non-zero limit must be chosen. As all direct relationship responses (acceleration to acceleration, velocity to velocity, and so on) would be expected to be equal to 1 at 0 Hz, the sine sweep can be initiated at a slightly higher frequency, but low enough that we would still able to determine the rise of amplitude ratio preceding the natural frequency. For a lowest expected natural frequency of 1.2 Hz, an appropriate number for the starting frequency would be 0.5 Hz. In order to determine the maximum frequency of the sweep, the response of the vehicle and limitations of the rig have to be considered. For the Multimatic four-post rig the maximum suggested input frequency of the rig is 40 Hz. Generally the frequency range associated with ride and handling is up to 25 or 30 Hz [39]. Due to the properties of the exponential frequency sweep, the difference in input signal length between an input that stops to 30 Hz and one that stops at 40 Hz is small compared to the overall signal length. In this case it was decided that an upper frequency limit of 40Hz would be used to provide data in the 30 to 40Hz frequency region that may be of interest.

If the limits of the sweep are set at 0.5 and 40Hz and the frequency increase per cycle set at 0.1 Hz, then a complete sweep could be achieved in 43.8 seconds.

It was observed in section 3.3 – Modal Rig Inputs, that transients will occur at the start of a sine wave input, because of the finite time required to accelerate to a non-zero velocity value. This

high magnitude acceleration excites the vehicle being tested and starts a transient oscillation. If the data during the transient were to be used in the calculation of response data, then errors would occur. In order to avoid this situation a fade can be applied to the start of the signal, so that the input displacement, velocity and acceleration are all zero at the first time step, and the signal is gradually increased to the desired signal amplitude. Using the 'Profile Generator' of the Multimatic Dynosoft software [71] described in section 4.1.2 - Data Acquisition System, the fade applied is a sine step to the desired velocity of the signal which is a cosine wave. By applying the fade to the velocity, the mean displacement of the signal after the fade period is offset from the original displacement zero. The only way to stop this would be to create the desired input outside of Dynosoft and import it as a '.TRK' file, which can be read by the Dynosoft software. The loading of these files when changing between rig inputs was found to take considerably longer than using the profile creator generated inputs. The small offset was tolerated for this reason, as well as the fact that the displacement offset has no significant effect on the response of the vehicle and can be easily removed during post-processing.

Because of the fade applied to the input signal, some of the frequency sweep would not be at full amplitude, and hence it is necessary to have constant frequency excitation at the lowest input frequency until the end of the fade. In the case of the rig input used in this thesis the fade length was chosen to be 2 seconds, one complete cycle of the 0.5 Hz starting frequency. An additional two 0.5 Hz cycles were also added before the start of the sine sweep. These were in place so that additional information could be obtained from the sine sweep that related to approximately steady-state conditions. For example, in the warp test the front and rear roll stiffness values could be obtained and during the start of the roll test the vehicle's centre of gravity height could be estimated.

When designing the rig input for the project, one of the objectives was that a single input should be no more than 60 seconds long, in order to keep complete test time for a vehicle to a reasonable length. With 3 cycles at 0.5 Hz, 6 seconds of the length of the input were already determined. In order to stick to the 60 second objective the sine sweep from 0.5 to 40 Hz was made 54 seconds long, giving a frequency increase rate of around 0.08Hz per cycle.

Based on the information given in this chapter, the input used for the majority of rig tests was a constant peak velocity exponential chirp with the following parameters:

- Test Length – 60 seconds.
- Frequency Range – 0.5-40 Hz.
- Initial constant frequency cycles – 3 at 0.5 Hz
- Fade length – 2 seconds

An example of the displacement, velocity and acceleration of this signal in the time domain is shown in Figure 3-15.

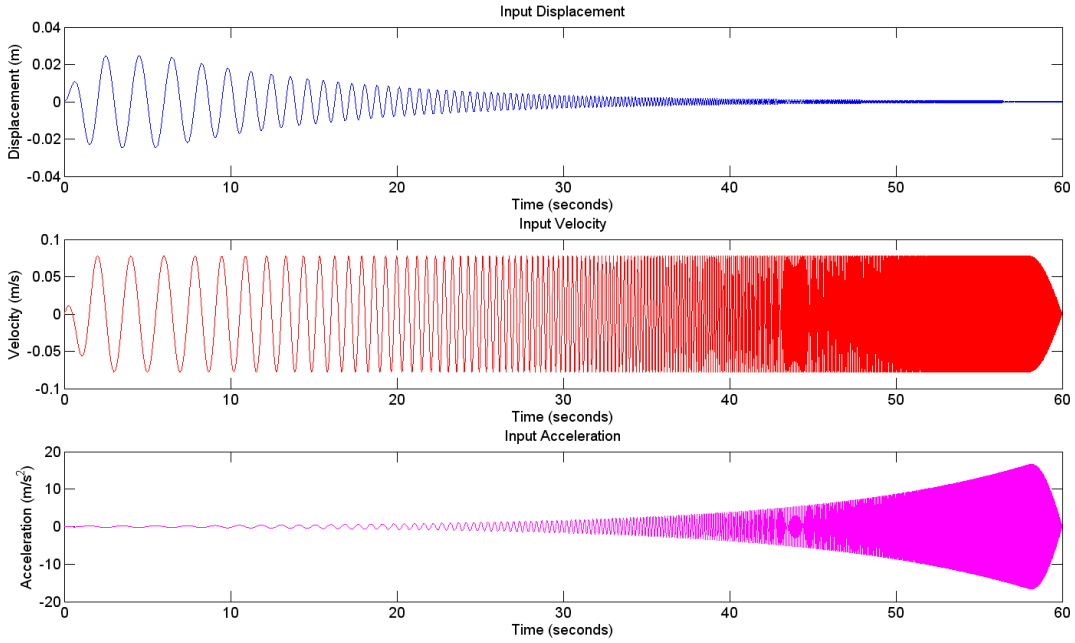

Figure 3-15 – Constant Peak Velocity Exponential Sine Sweep

3.5 – Selection of Appropriate Amplitude

Once the time domain characteristics of the frequency sweep had been determined, the final factor that is required is to define the magnitude of the constant peak velocity for the input.

It was explained earlier in section 3.1 – Road Spatial Characteristics and 3.2 – Effect of Vehicle Speed, that the PSD is dependent on the road roughness and forward speed of the vehicle. However, in order to determine the sine sweep amplitude for the same operating conditions, an appropriate conversion is required from the PSD. This ensures responses acquired by either sine sweep or integrated white noise inputs are comparable for a non-linear vehicle.

The PSD defines the content of the signal within infinitely small frequency bands. In order to determine the magnitude of a single sine wave component over a small frequency range, the PSD can be converted to a sine wave amplitude using the method explained graphically in Figure 3-16 and in equations (3-18) to (3-20).

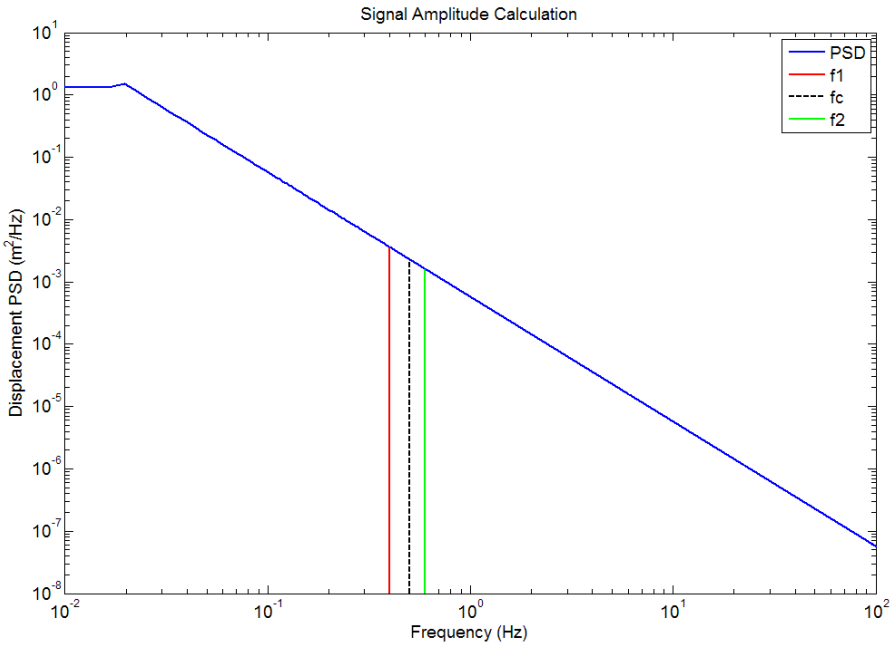

Figure 3-16 – Signal Amplitude from PSD calculation

$$x_{Amp} = \sqrt{2} \times \sqrt{\int_{f_1}^{f_2} PSD(f)df} \qquad \textbf{(3-18)}$$

Or more approximately

$$x_{Amp} = \sqrt{2} \times \sqrt{PSD(f_c) \times (f_2 - f_1)}$$

(3-19)

Then

$$x(t) = x_{Amp} \sin(2\pi f_c t)$$

(3-20)

Initially it would appear that in the case of the swept sine input the correct amplitude could be achieved by using the same frequency resolution as that of the swept sine signal (0.08 Hz/cycle). However, this generates two problems. Firstly, the amplitude of the sine sweep becomes dependent on the sweep rate. Slower sweep rates would have smaller amplitudes, as the size of the integrated frequency range would be smaller than for fast sweep rates. Secondly, in the random road case, all frequencies would be expected to be excited at the same time, but in the sine sweep frequencies are excited separately. This causes the overall level of the signal to be much smaller than the random road case.

The first problem can be dealt with when we consider that the velocity PSD and sine sweep peak velocity is known to be constant across the frequency range. In this case the amplitude can be calculated for the complete frequency range of interest (0.5 to 40Hz) using equation (3-18).

In order to determine the appropriate signal amplitude an investigation was carried out using a two-degree-of-freedom quarter car model in Simulink with a non-linear function used to represent the damper characteristic. An example of the damper characteristic used is presented in Figure 3-17, where the damper is modelled using equation (3-21).

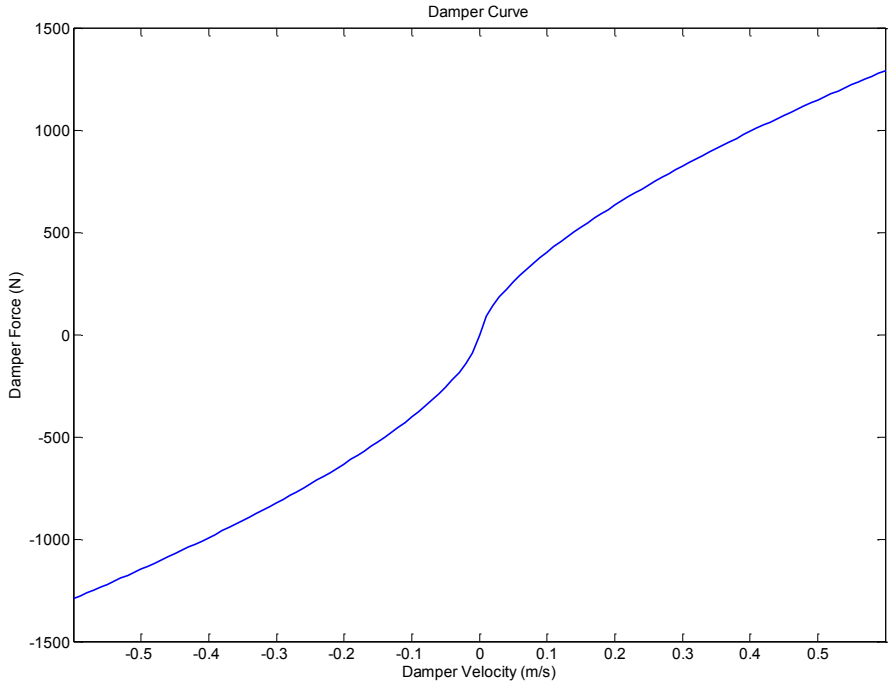

Figure 3-17 – Non-linear damper characteristic

$$F(V) = C\left|V^{0.65}\right| \times sign(V)$$

(3-21)

Where:

F – Damper Force

V – Damper Velocity

The model was simulated using two different types of input. The first, was an integrated white noise signal with PSD that was equal to the class B road from ISO 8608 [4] at 30 m/s. The second, was a selection of different amplitude constant peak velocity sine sweeps. In both cases the response of the vehicle was analysed using the 'tfestimate' function in MATLAB [67]. Figure 3-18 shows an example sprung mass response calculated from the different inputs.

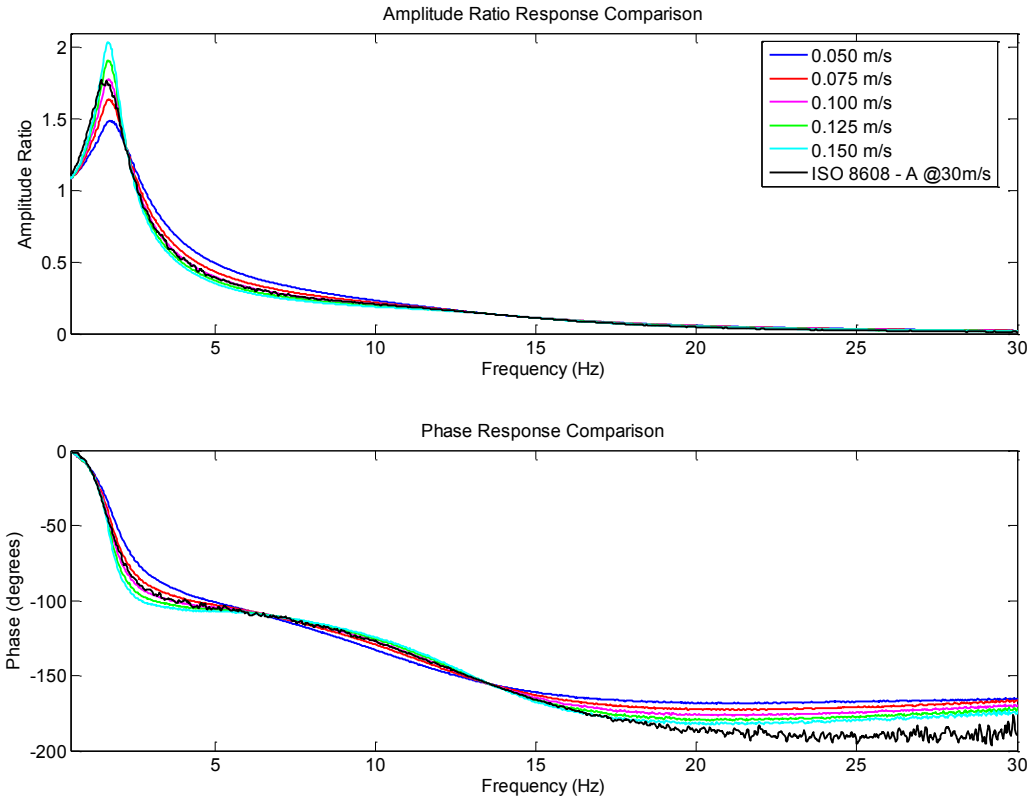

Figure 3-18 – Non-linear Model Response Comparison

A scaling factor was determined which related the magnitude of the velocity PSD integrated over the frequency range of interest (0.5-40Hz) to a constant velocity sine sweep amplitude that would produce a response with minimum least square error to the response derived from the integrated white noise input. The most suitable scaling factor was found to be equal to 1.156 times the RMS from the velocity PSD, as shown in equation (3-22).

$$\dot{X}_{Amp} = 1.156 \int_{0.5}^{40} PSD(f)df \qquad \textbf{(3-22)}$$

3.6 – Road Input Construction from Spatial Characteristics and Drive Cycle

Sections 3.1– Road Spatial Characteristics and 3.2 – Effect of Vehicle Speed have explained the way in which the vehicle is excited by the road surface. In these sections forward speeds of 15 and 30m/s were used as examples to show the amplitudes and modal contributions at the corresponding speeds. In real vehicles there are cases where constant or near constant speeds are common, such as motorway driving, or driving within low speed limits. However, there are also considerable cases where cars are required to brake, corner and accelerate along the length of a road. In this case the forward velocity changes significantly within the duration of the road. This means that the amplitude and phasing effects due to speed are no longer constant across the frequency range. Creation of modal PSD inputs for a non-constant speed cycle could produce important information about the response to typical modal PSD inputs across the frequency range.

There were two main objectives when creating this type of input:

1. Creation of time domain input that could be used as rig input to vehicle.
2. Generation of modal input PSD contributions for complete drive cycle.

In order to generate the spatial domain input two considerations had to be made:

1. Single track spatial frequency PSD characteristics.
2. Left and right wheel path coherence.

For simplicity the spatial frequency PSD characteristics used were taken from the B (good) and C (average) class roads from the ISO 8608 [4] standard.

To define the coherence between wheel paths equation (3-7) from Bogsjo [16] was used with a ρ value of 3.4 and a vehicle track width of 1.5m.

As well as the spatial domain input, a speed cycle must be defined in order to convert from the spatial domain to the time domain. For European emission compliance vehicles must complete emissions tests for the MVEG-A (Figure 3-19) drive cycle [72], whist measuring fuel usage and exhaust emissions so that various parameters about the vehicle's fuel consumption and emissions can be presented to the general public. This speed cycle consists of four repetitions of the ECE-15 (urban) driving cycle and a single EUDC (Extra-Urban Driving Cycle). Honda engineers noted that the EUDC part was more representative of the speed range of typical subjective assessments than the complete MVEG-A cycle, so this part of the driving cycle was used for the work in this thesis.

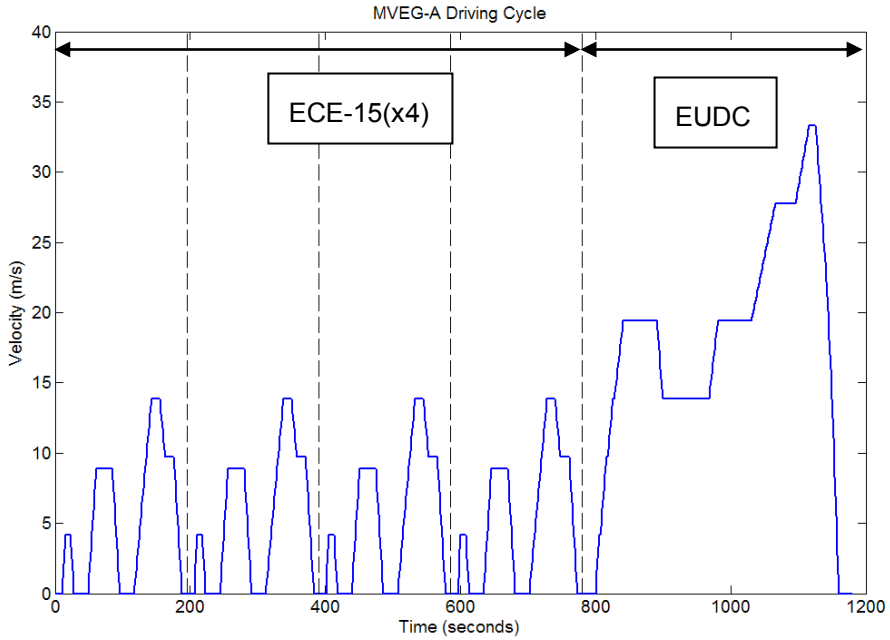

Figure 3-19 – MVEG-A Drive Cycle

In order to create the spatial domain inputs the inverse FFT method was used. Initially the spatial frequency displacement PSD must be converted to the correct magnitude and phase information included to create a two-sided FFT. This can then be converted from the spatial frequency to the spatial domain by carrying out an inverse FFT.

The process to create the spatial domain signals for both wheel paths is defined in the flowchart below.

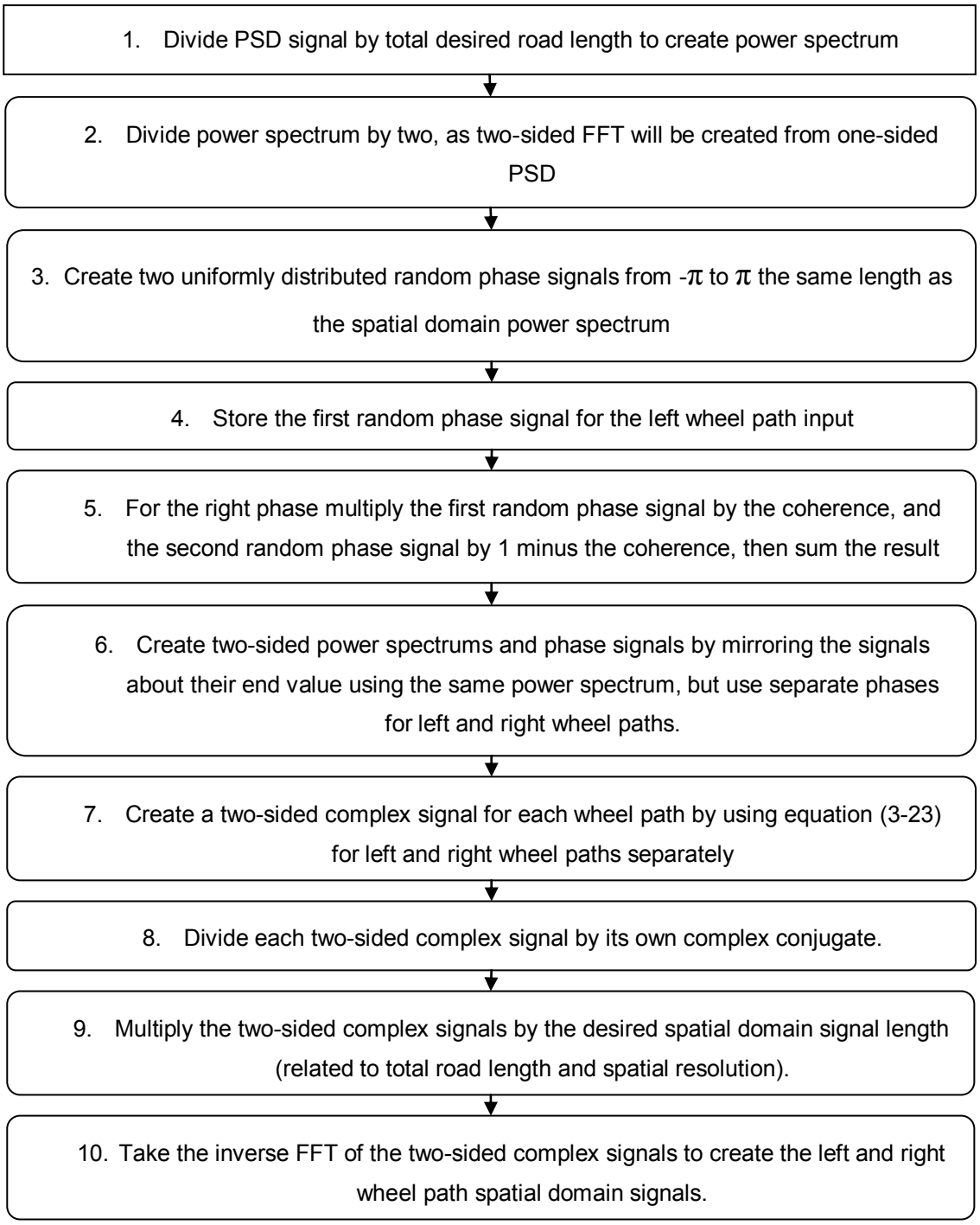
1. Divide PSD signal by total desired road length to create power spectrum
2. Divide power spectrum by two, as two-sided FFT will be created from one-sided PSD
3. Create two uniformly distributed random phase signals from -π to π the same length as the spatial domain power spectrum
4. Store the first random phase signal for the left wheel path input
5. For the right phase multiply the first random phase signal by the coherence, and the second random phase signal by 1 minus the coherence, then sum the result
6. Create two-sided power spectrums and phase signals by mirroring the signals about their end value using the same power spectrum, but use separate phases for left and right wheel paths.
7. Create a two-sided complex signal for each wheel path by using equation (3-23) for left and right wheel paths separately
8. Divide each two-sided complex signal by its own complex conjugate.
9. Multiply the two-sided complex signals by the desired spatial domain signal length (related to total road length and spatial resolution).
10. Take the inverse FFT of the two-sided complex signals to create the left and right wheel path spatial domain signals.

$$Z = \mathrm{Re}^{j\theta}$$

(3-23)

Where:

Z – Complex Signal

R – Signal Magnitude

θ – Signal Phase (radians)

Using this method the accuracy of each single wheel input to the desired PSD is very good. However, the accuracy of the measured coherence compared to the desired coherence is not particularly good, as show in Figure 3-20. Similar problems were noted by Cebon and Newland [20].

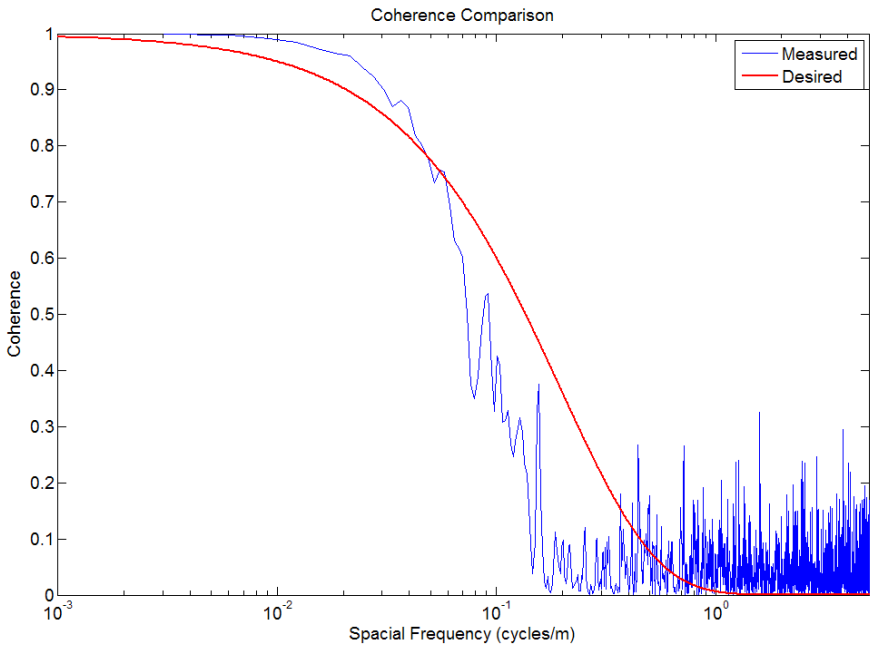

Figure 3-20 – Desired and Measure Coherence using inverse FFT method

In an attempt to improve the coherence accuracy, an individual harmonic component summation method was used. However, this was found to provide very similar coherence and took many times longer to create the signal than using the inverse FFT method.

From the construction of the time domain inputs for the complete drive cycle the relationship between the four input modes and a single wheel road input can be calculated from the relevant PSDs. The relationship generated using the EUDC drive cycle [72], Bogsjo [16] coherence model and the spatial domain conversion process explained in the flow chart above is presented in Figure 3-21.

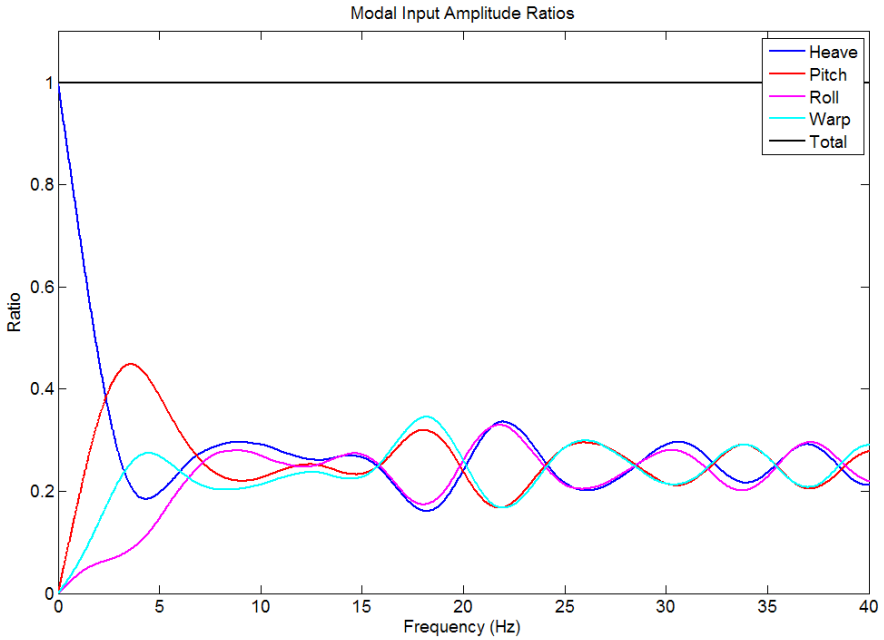

Figure 3-21 – Modal Input Amplitude Ratios for EUDC Drive Cycle

The modal input ratios show that at very low frequency the heave input is dominant over all other modes. As the frequency increases towards 4 Hz, the pitch, roll and warp inputs start to increase. The increase in pitch input and drop in heave input at around 4 Hz is due to the wheelbase filtering effects. This is also the cause of the increased warp input in comparison to roll at the same frequency. As the frequency further increases the relative magnitude of all inputs becomes similar overall, but with the wheelbase filtering effects still present. This relationship highlights the relative importance of the different modal responses in the 0 to 7 Hz frequency range. The roll input is the lowest in this region, with the warp being larger than roll but smaller than pitch, and heave being the largest overall.

With this information modal frequency weightings can be produced that can be used to weight the relative importance of each modal response across the frequency range.

3.7 – Collection of Road data and Basic Spatial Characteristic Estimation

Two sets of subjective assessment tests were carried out with Honda R&D Europe using a Civic as the test car for the purpose of this thesis. The first set of tests were carried out using a driving route around the Honda Swindon factory in the UK. The second set were carried out on a driving route around the Honda R&D facility in Offenbach, Germany. These routes were typical routes the Honda test drivers use for subjective assessment.

In addition to the subjective assessments, an Oxford Technical Solutions Inertial Measurement Unit (IMU) [73] was fitted to the vehicle along with a National Instruments LabView data logger and accelerometers that were connected to the rear uprights, seat base and seat surface.

The IMU device was used to measure the GPS location of the vehicle, as well as other measurements, such as; roll, pitch, yaw, lateral acceleration and side slip angle. The IMU unit used is a high precision device designed specifically for automotive testing.

The National Instruments data logger was used primarily to measure the accelerations of the two rear suspension hubs in order to assess the road surface roughness characteristics and compare to the ISO 8608 [4] standard and other published road profiles. Additionally the seat rail acceleration was measured for comparison and it was intended to use a ‘sit-pad’ seat accelerometer assess the seat transmissibility with a real passenger. However, issues with this sensor meant the data was unreliable.

For confidentiality reasons the exact location or names of the roads travelled on have not been presented, but examples of the GPS signals from an original point of reference have been shown in Figure 3-22, Figure 3-23 and Figure 3-24. The Offenbach data was separated into two separate runs, due to resetting of the IMU during the route.

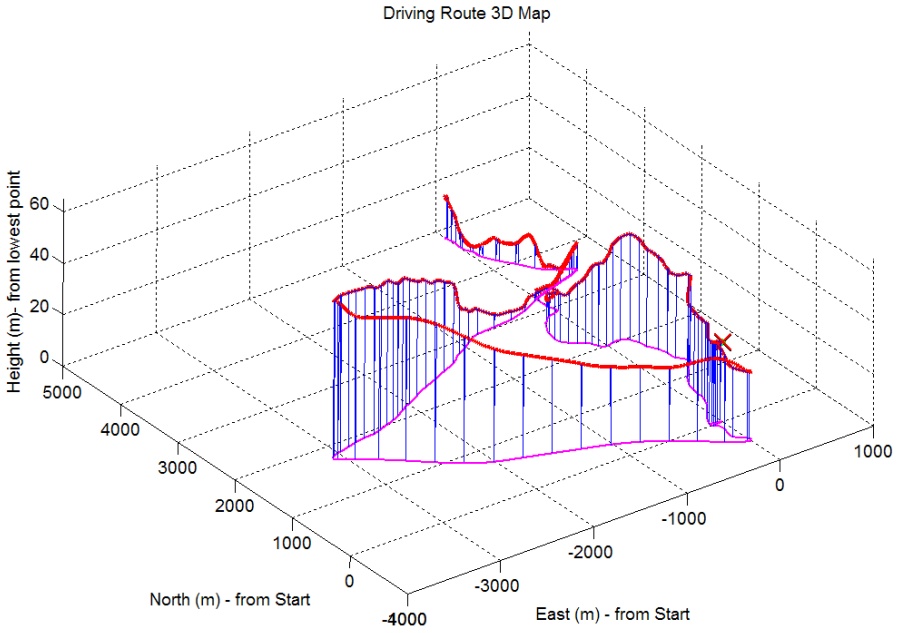

Figure 3-22 – Swindon Driving Route

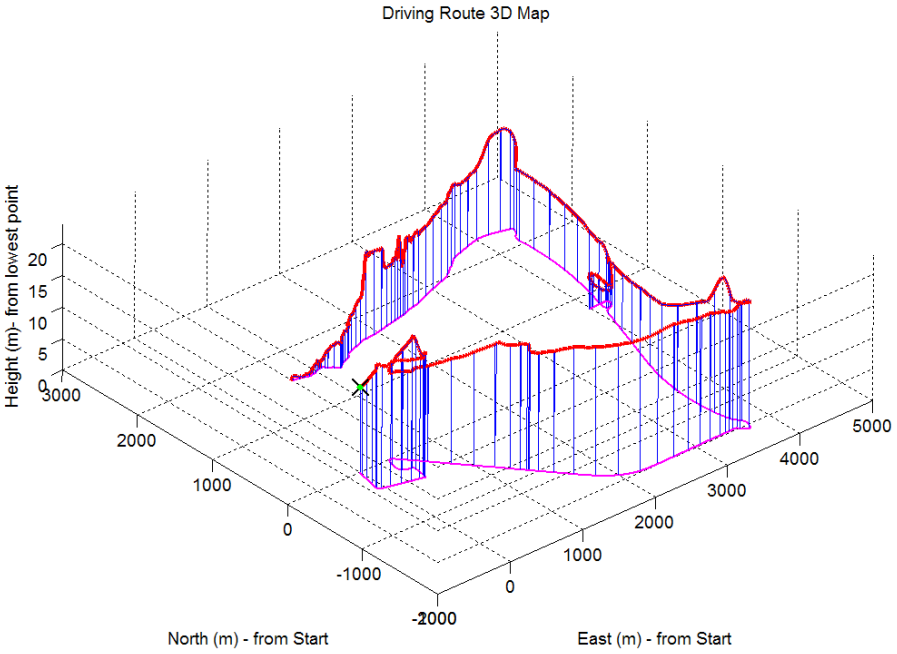

Figure 3-23 – Offenbach Driving Route – Part 1

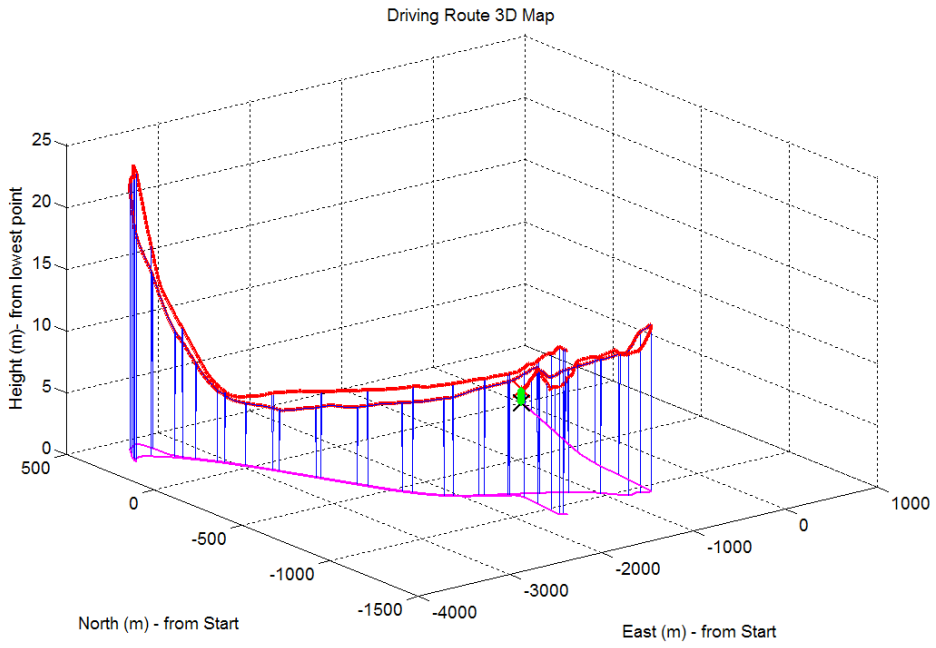

Figure 3-24 – Offenbach Driving Route – Part 2

The driving routes were also separated into different road sections based on their traversed speed and road type so that assessment of different parts of the route could be carried out.

The placement of the two accelerometers on the rear hubs was chosen specifically as the frequency response for the rear unsprung mass was known to be far more linear than the front from previous four-post testing. This allows more accurate measurement of the road characteristics over a wider range of amplitudes. In addition, both accelerometers were placed at one end of the car so that coherence in the left and right wheel paths could be estimated.

In order to estimate the road surface characteristics from the hub accelerometer data, a four-post rig test derived transfer function was used to represent the hub acceleration to road acceleration relationship. The hub acceleration response was obtained for the baseline vehicle during the objective test described in section 7.3 - Validation of Comfort and Performance Index with Subjective-Objective Test. The measured hub acceleration response from the four-post test was curve fitted using a 4^{th} order linear transfer function, as shown in Figure 3-25. This transfer function provided the hub acceleration for a given road acceleration. In the road calculation case the inverse transfer function was required to determine the road acceleration from the hub acceleration data. The transfer function was inverted and an additional 80Hz low-pass filter transfer function used to ensure the transfer function was stable. The final transfer function response used is shown in Figure 3-26.

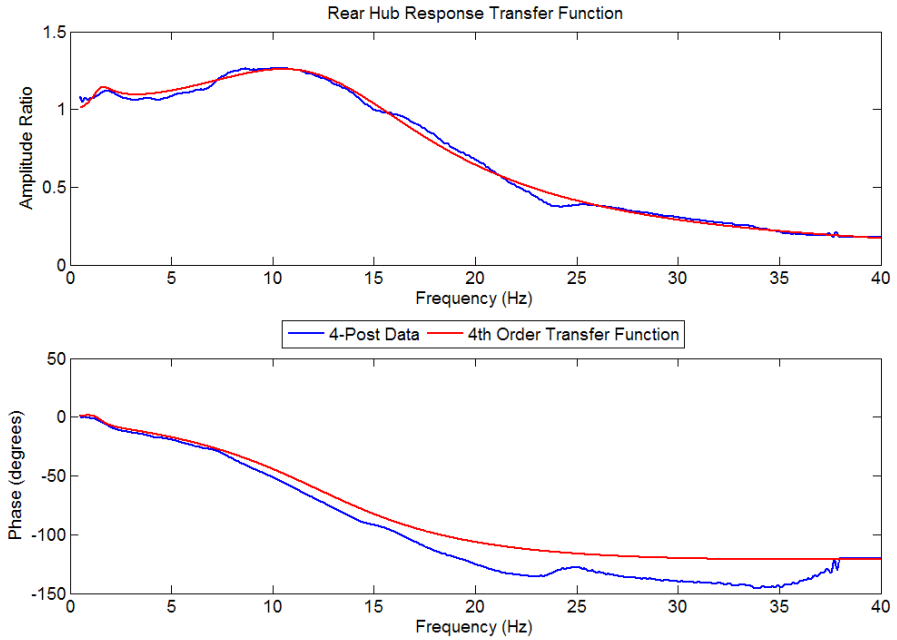

Figure 3-25 – 4th Order Transfer Function Approximation of Rig Data

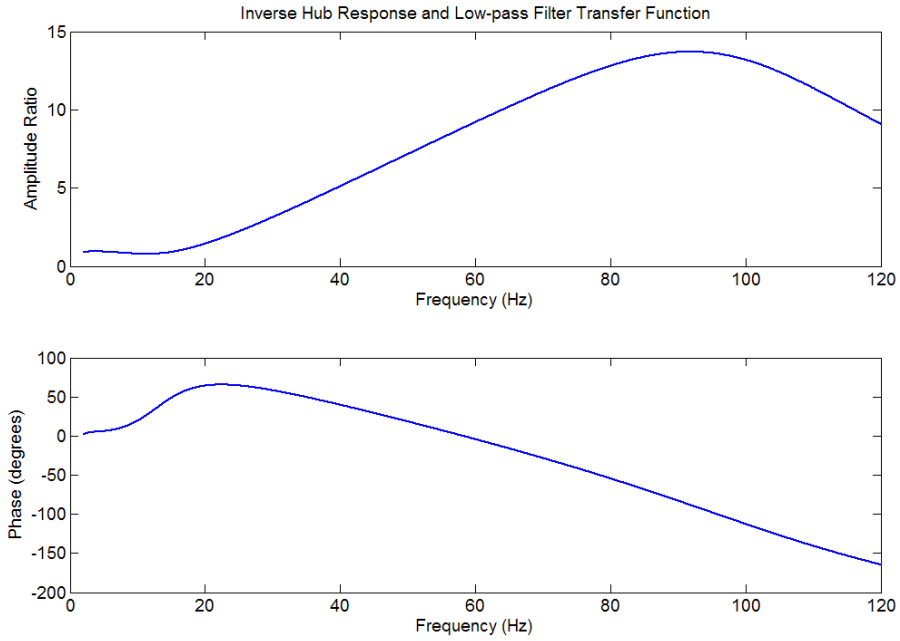

Figure 3-26 – Inverse Hub Response Transfer Function and Low-pass Filter

Applying the transfer function to the measured hub acceleration data allowed an estimate of road acceleration to be made. This was then integrated twice in order to produce a road displacement in the time domain. In order to convert to the spatial domain the forward velocity measured by the IMU was integrated to give road distance from the original starting point of the data.

The spatial frequency displacement PSDs were then calculated for various road sections from the two routes. In order to characterise each section of road a single gradient road profile fit was applied to the road displacement PSD using a least square error minimisation. This was done within a limited wavenumber range between 1Hz at an 'Upper Speed' value and 15 Hz at 'Lower Speed' value. The upper and lower speeds were defined as speeds one standard deviation from the mean of the forward velocity for the road section. The 15 Hz limitation was chosen because after this point the hub response decays significantly and a small error in the response could produce a road amplitude estimate with a significantly different amplitude from the actual road, whereas the hub acceleration response between 1 and 15 Hz was known to be between 0.77 and 1 from Figure 3-25. Figure 3-27 presents comparisons of some roads and their single gradient fits, whilst Figure 3-28 compares the calculated road profile fits in comparison to the ISO 8608 [4] standard classes of road.

Table 3-1 presents the roughness, exponent and class values for all analysed sections of road and overall Swindon, Offenbach Part 1 and Offenbach Part 2 routes.

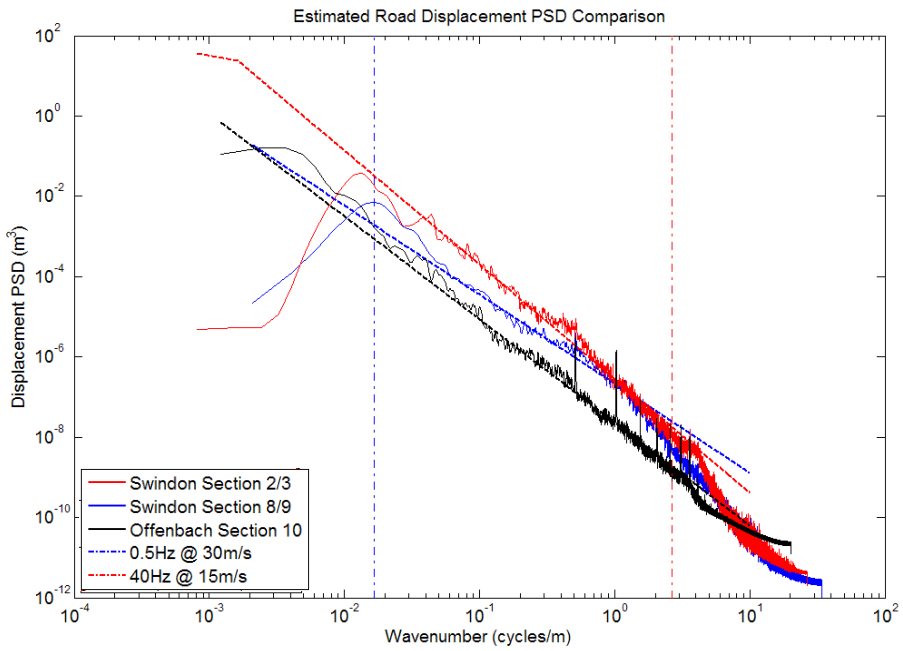

Figure 3-27 – Estimated Road Displacement PSDs

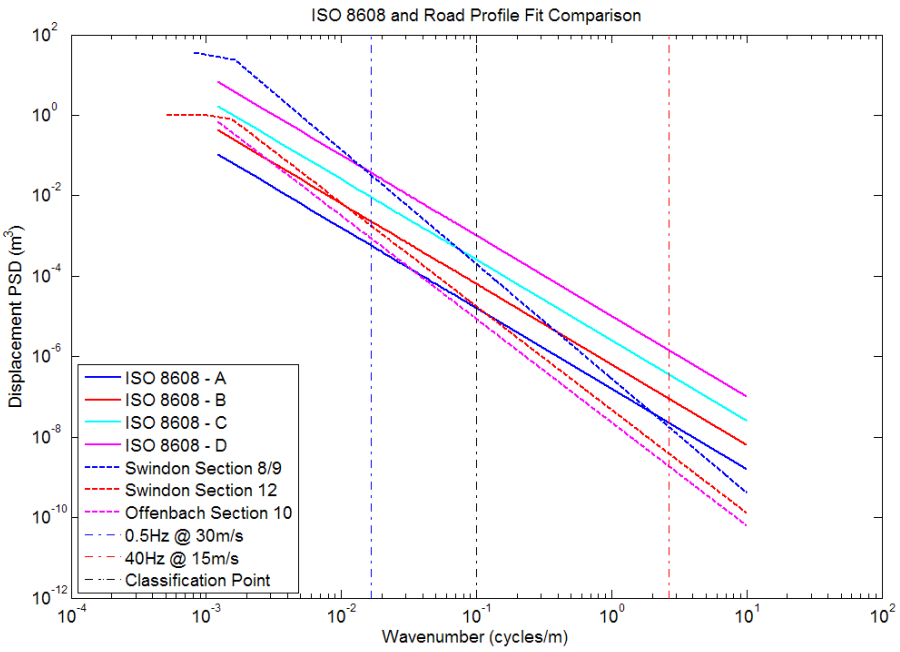

Figure 3-28 – Comparison of ISO 8608 [4] Road Profiles and Road Profile Fits

Swindon			
Section/s	Roughness - C (m^2)	Exponent - w	Class
2 and 3	3.65E-05	2.21	B
4	1.94E-04	2.38	C
5 and 6	1.04E-04	2.6	B
7	1.01E-04	2.62	B
8 and 9	2.00E-04	2.84	C
11	1.54E-04	2.93	C
12	1.86E-05	2.56	A
σ	7.16E-05	0.248	-
Overall	1.31E-04	2.67	C
Offenbach - Part 1			
2	4.57E-05	2.7	B
3	3.78E-05	2.48	B
4	2.69E-05	2.7	A
5	2.38E-05	2.84	A
7	1.63E-05	2.38	A
8	8.28E-05	2.8	B
σ	2.39E-05	0.182	-
Overall	5.00E-05	2.5	B
Offenbach - Part 2			
9	4.43E-05	2.71	B
10	8.64E-06	2.57	A
11	6.08E-05	2.51	B
12	1.46E-05	2.51	A
13	3.38E-05	2.8	B
σ	2.14E-05	0.130	-
Overall	1.97E-05	2.54	A

Table 3-1 – Road Roughness and Exponent Fits

The results show some interesting characteristics. The Swindon roads have a much higher standard deviation of roughness and exponent than the Offenbach roads, as well as being rougher in general. The fact that the Offenbach roads have a lower standard deviation indicates that it would be easier to find a compromise setup that worked well on all sections of the Offenbach route, compared to the Swindon route.

All roads have an exponent larger than 2, with 2.67 being the overall value for the Swindon route and 2.52 being the average value for the two complete Offenbach routes.

Coherence analysis of Swindon section 12 showed a similar coherence to the exponential fit used in the creation of the drive cycle road input. Due to the low frequency limitation of the hub accelerometers (approximately 1 Hz), the coherence could not be estimated for wavelengths longer than 20 m. The coherence is also affected at frequencies above 80 Hz, due to the transfer function used to estimate the road acceleration from hub acceleration.

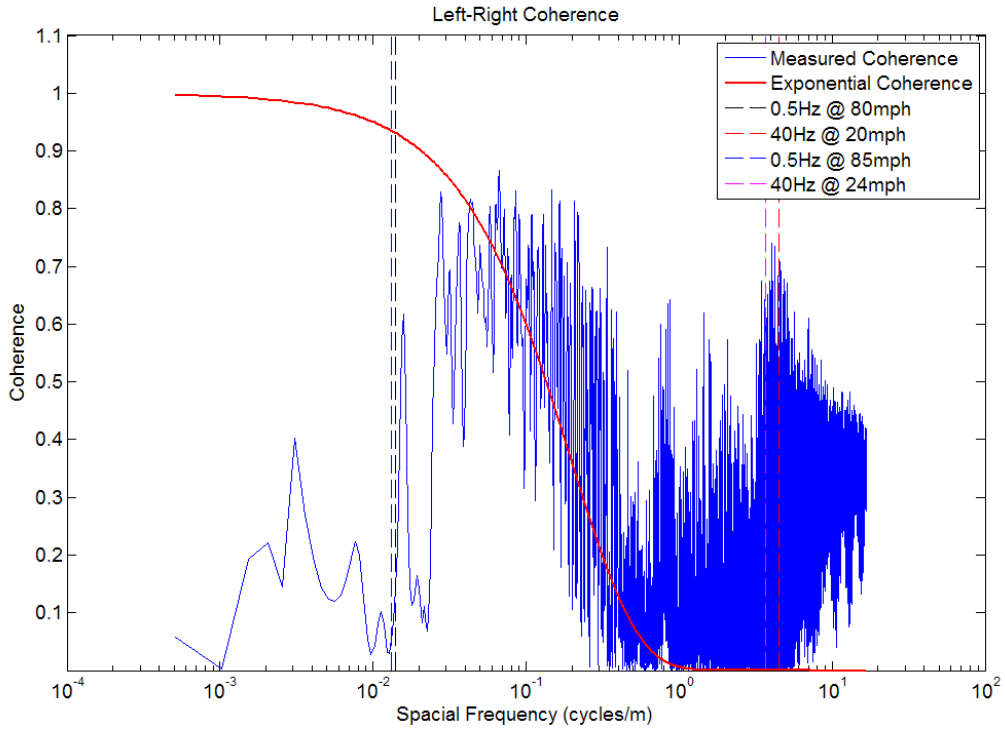

Figure 3-29 – Measured Coherence from Swindon Section 12

4 - Four-post Rig Experimental Operation

This chapter describes the experimental operation of the Multimatic Four-post Rig used in this PhD. The chapter initially explains the functions of the rig and its mechanical construction in 4.1.1- Mechanical System, as well as the data acquisition system in 4.1.2- Data Acquisition System and calibration in 4.1.3 - Calibration.

The organisation of the output data files from the rig and the run lists recorded during testing are explained in section 4.2.1 - Organisation of Data Files. The signal processing that is applied to the output data in order to create vehicle responses for the parameter determination is described in detail.

One of the aims of this project was to create a testing technique that would be consistent and repeatable for Honda to use in the future. The process of the test method used in the project is explained in section 4.3 - Testing Procedure.

A General User Interface is used to run a MATLAB code in order to acquire required parameters from the rig output data. The need and use of this interface is described in section 4.3.3 - Parameter Estimation General User Interface.

The limitations of the Four-post Rig method of vehicle testing is explained in section 4.4 - Four-Post Rig Method Limitations.

4.1 - Multimatic Four- Post Rig

The four-post Rig at Oxford Brookes University was designed, built and installed by Multimatic Incorporated. It was calibrated and commissioned for use in August 2008. The primary use of the rig is for the testing and analysis of road cars and race cars within the 0.5 to 40 Hz road input frequency range. This is the frequency range associated with the ride and handling area of vehicle dynamics.

4.1.1 - Mechanical System

The Multimatic Four-post Rig consists of three main groups of components, these are;

1. Four Servo Hydraulically Controlled Actuators
2. Two 200 Bar Hydraulic Fluid Supply Pumps
3. Control box and rig user PC

Figure 4-1 to Figure 4-3 show the general layout of the rig.

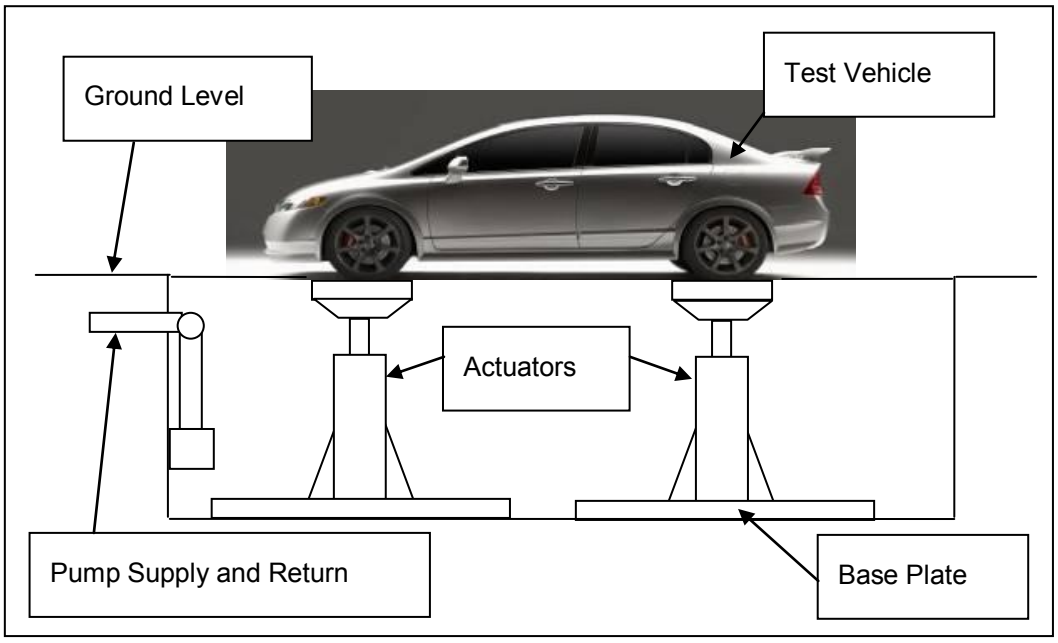

Figure 4-1 – Rig Layout

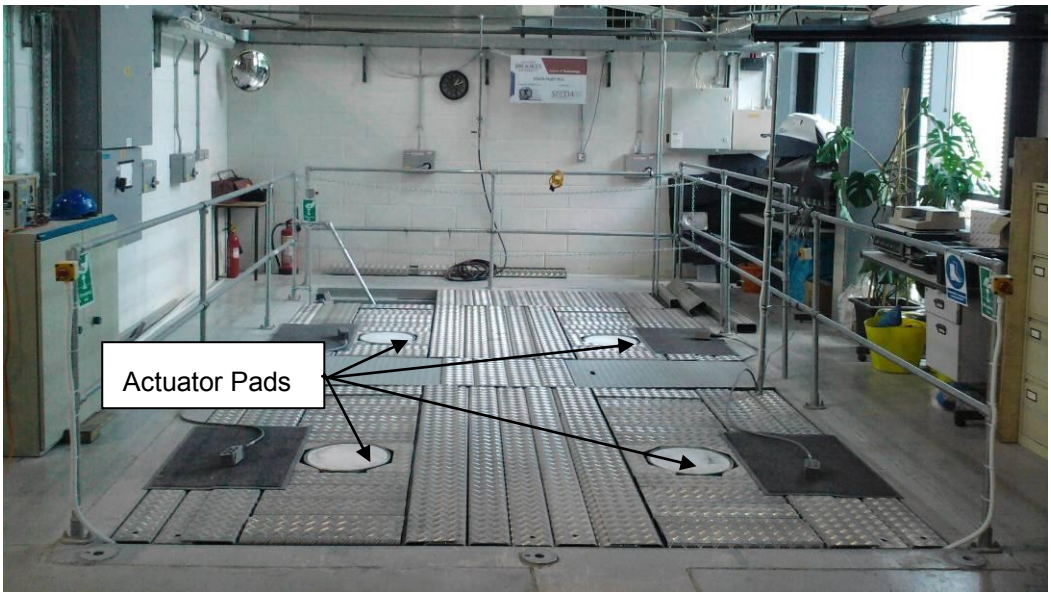

Figure 4-2 – Four-post Rig - Top View

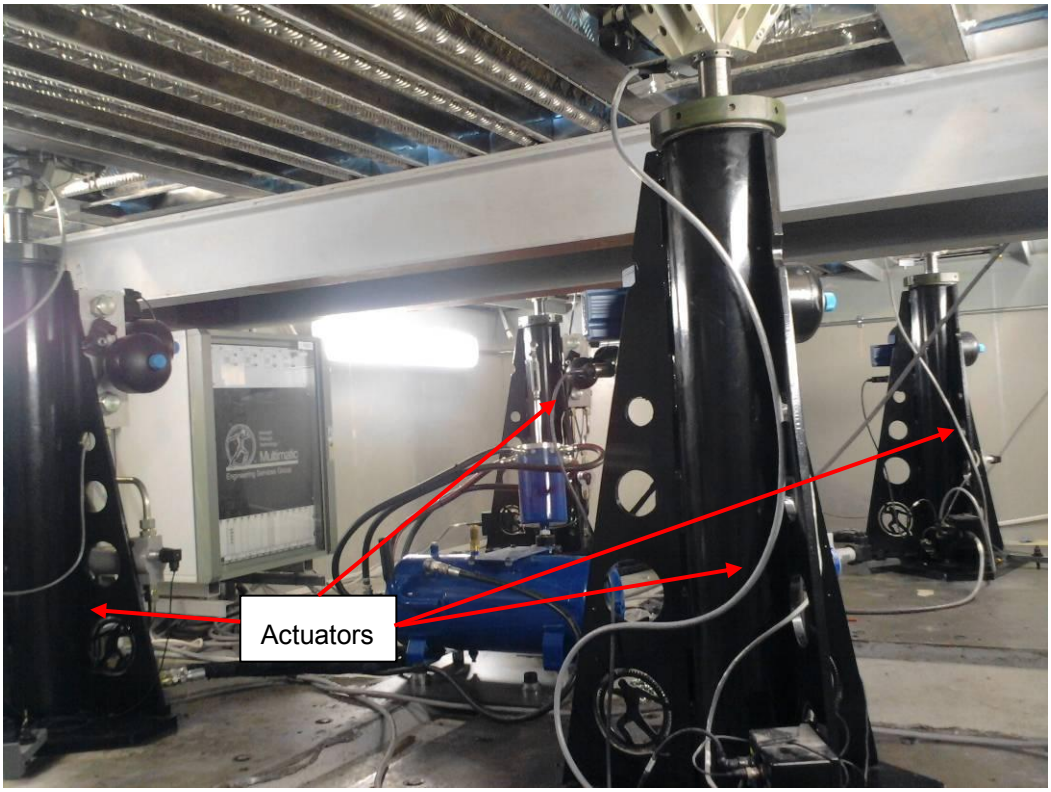

Figure 4-3 – Four-post Rig – Lower View

The four actuators are used to supply controlled displacements to the four road wheels of a vehicle. Each of the actuators is bolted down to a 25 mm thick steel plate which is bonded to a concrete seismic mass. The purpose of the seismic mass is to reduce the effects of external and base vibration on the experimental results and to minimise the effect of the rig vibration on other experiments in the building. The actuators can be moved around the four separate steel plates so that vehicles of different dimensions can be tested.

Each of the actuators is fitted with a Moog D661 Servo Valve. The position of the spool in the valve body is determined by an electrical current. The position of the spool determines the flow of hydraulic fluid from the high pressure supply port to either of the valve outputs. The hydraulic fluid flow produces a pressure differential across the actuator piston which forces the rod of the actuator in the desired direction. Figure 4-4 shows an example layout of the valve and actuator. A schematic of the servo-jet type D661 [74] valve is shown in Figure 4-5. The step response time of the servo valve is dependant on the stroke of the spool, for 100 percent spool displacement the step response is 10 ms (100 Hz). Multimatic suggest that input signals supplied to the rig should not exceed 40 Hz, as the rig may not be able to reproduce the signal accurately above this.

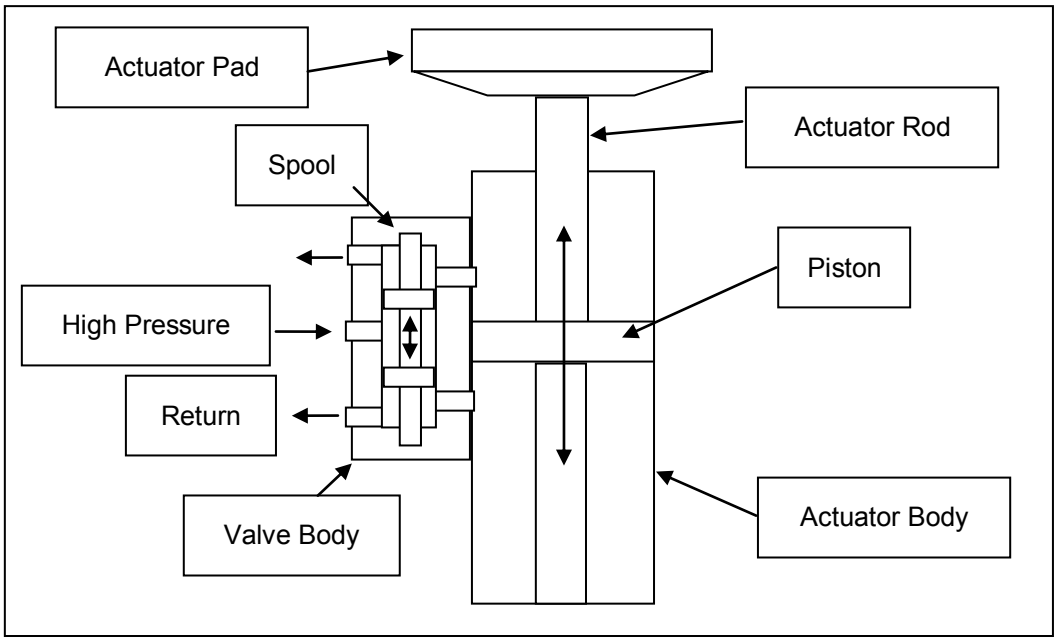

Figure 4-4– Actuator and Servo-Hydraulic Valve Schematic

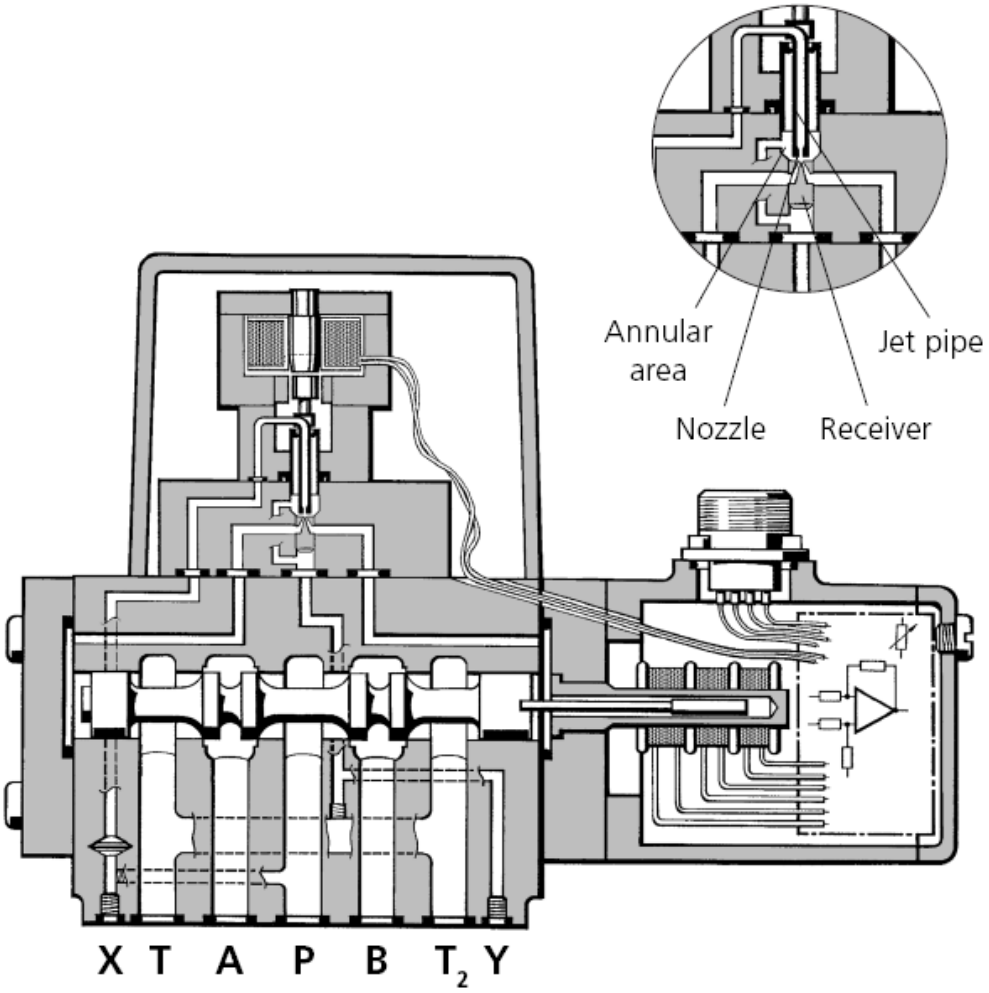

Figure 4-5 – Moog D661 Servo-jet Value Schematic [74]

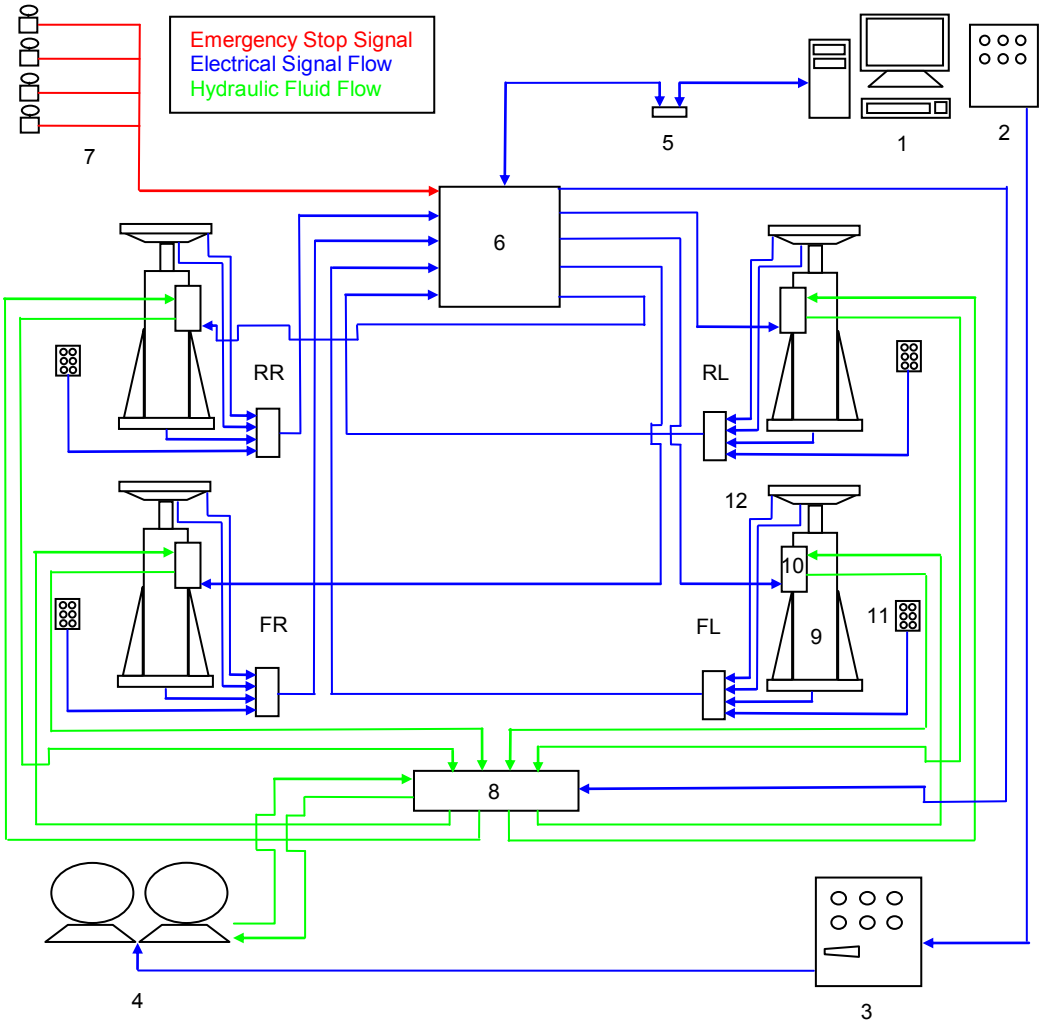

Figure 4-6 – Four-post Rig Electrical and Fluid Flow Schematic

1. Control PC
2. Remote Pump Control Box
3. Main Pump Control Box
4. Hydraulic Pumps x 2
5. PC to DSP, USB to Ethernet Connector
6. DSP Rig Control Unit
7. Emergency Stops x 4
8. Pump to Rig Manifold Block
9. Corner Actuator x 4
10. Moog Servo Valve x 4
11. 6 Channel Connector Box x 4
12. Actuator Pad (Pad Acc and CPL Signals) x 4

The actuators have a maximum stroke of 168 mm and a maximum velocity of 3 m/s. As well as the Moog valve there are an additional set of valves that are used as safety locks. When the valves are closed, hydraulic fluid either side of the piston is 'locked' in place, stopping the actuator from moving even if the Moog valve spool is open. These locks are used to hold the actuator ram position for safety reasons and will stop movement of the actuators within 10ms in the event of a system failure or emergency stop.

On top of each actuator rod is a wheel pan that is the contact point with the vehicle's tyres. Within the actuator pad are a number of sensors that will be discussed in section 3.1.2- Data Acquisition System. Each of the actuators is fitted with a separate particle filter that filters the high pressure fluid before it reaches the Moog valve. Flexible supply and return lines transport the hydraulic fluid to and from each of the actuators. These supply and return lines terminate at a manifold block located at the front of the pit. The main supply and return hard-lines are connected to the manifold block and the hydraulic pumps and reservoir are located in an external pump room. Figure 4-6 shows a schematic of the four-post rig electrical and hydraulic flows around the system.

The two pumps are variable angle swashplate pumps and are each powered by a 45kW electric motor requiring a 415 volts, 3 phase supply. Each pump can supply 210 bar pressure and 100 l/min flow rate. With both pumps running a flow rate of 200 l/min can be achieved. The pump control box is used to turn on and off the pumps while in the pump room. This also contains an emergency stop and a number of warning lights that show if the system is not functioning as it should. There is a secondary pump control box located next to the four-post rig which can also be used to stop and start the pumps. For the majority of tests only one of the pumps is required, as a flow rate of more than 100 l/min is not necessary, the exception is for large velocity inputs such as curb inputs, where the pressure drop is too large with only one pump. The two pump control units are shown in Figure 4-7 and Figure 4-8.

Figure 4-7 – Pump Room Control Box

Figure 4-8– Four-post Rig Pump Control Box

4.1.2 - Data Acquisition System

It was noted in section 3.1.1 - Mechanical System, that the position of the actuators is determined by the position of the servo-hydraulic valve spool, which is in turn determined by the current to the valve. This current varies between +/-10 mA and its signal comes from the digital signal processer based controller. This controller is located within the four-post rig pit and is connected to each of the actuators as well as the control PC. The control PC is windows based and runs Multimatic's Dynosoft software [71]. This program is used to control the rig, as well as view and store output data. Figure 4-9 shows the main run screen of the Dynosoft software.

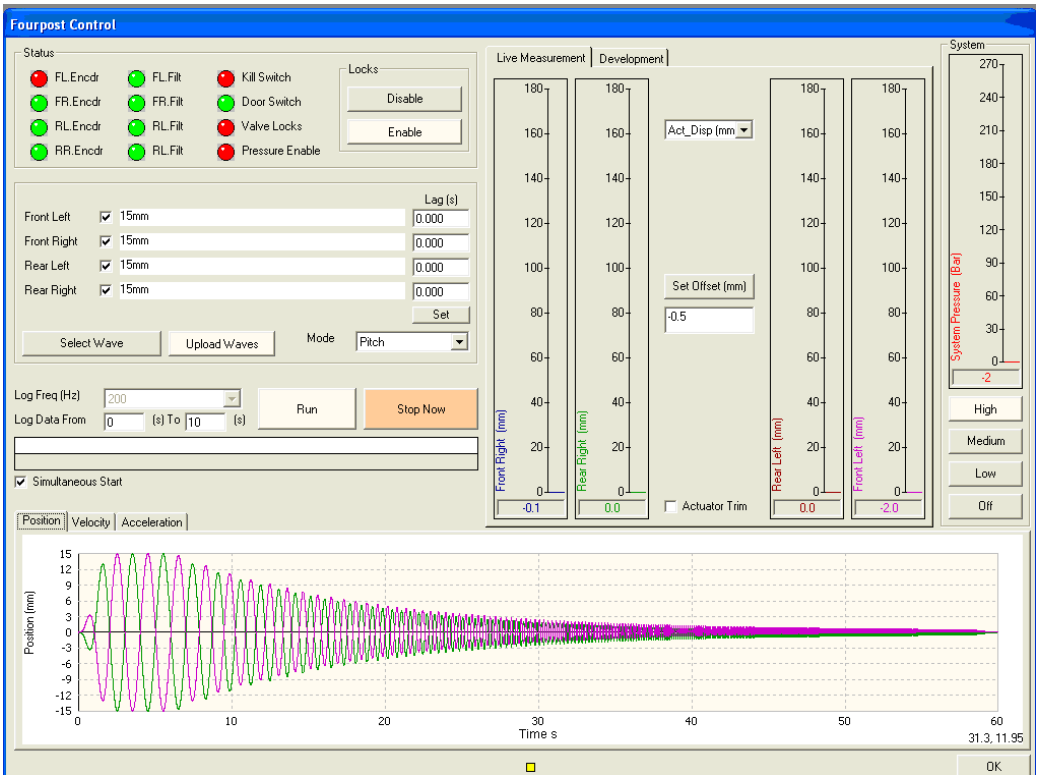

Figure 4-9– Dynosoft Run Screen

The 'Choose Profile' button links to a 'Profile Creator' window shown in Figure 4-10.

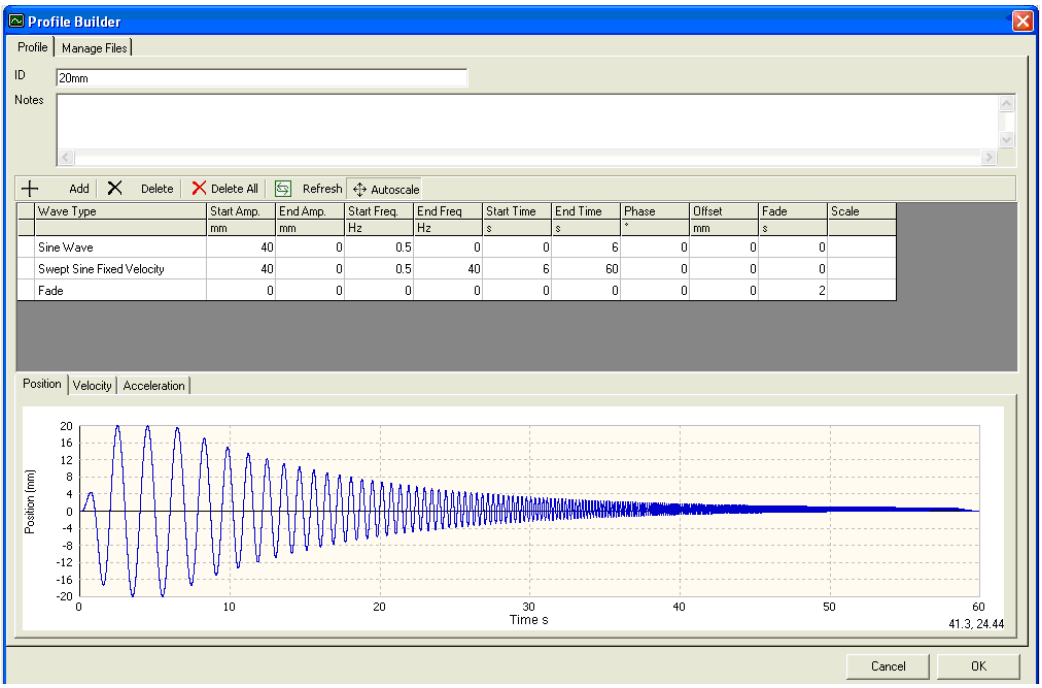

Figure 4-10 – Profile Creator Window

The profile creator is in essence a 'function editor' allowing the user to create a desired input displacement waveform. Many different standard signals can be created, such as:

- Square Waves
- Saw tooth Waves
- Sinusoidal and Swept Sinusoidal Waves

In addition 'Track Data' can be imported from an external file in the correct format. This allows any input desired to be created.

The displacement of the actuators is measured using linear Hall Effect encoders. The absolute position of the actuator is determined by the digital signal from the encoder that is positioned inside the actuator ram. The encoders are Newall SHG AM units that supply a different digital signal for all positions and can determine position to an accuracy of 20 μm. The controller uses the desired and measured positions of the actuator's encoders to determine an error based on Proportional Integral Derivative (PID) control theory. The controller also uses a modelled current signal based on a tuned theoretical model of the Moog valve.

This modelled signal and the PID error are used to determine the actual current that is supplied to the valve.

As well as the position encoder, each actuator is fitted with two other measurement devices that are important to the rig analysis, these are;

- Pad Accelerometer
- Pad Load Cells

The actuator pad is attached to the actuator rod via a screw thread that enables the height of the pads to be adjusted during the original commissioning of the rig. This is to ensure that when the actuators are at zero displacement all pads are level. The actuator pads consist of three main parts;

- Upper Pad
- Lower Pad
- PTFE Pad

Figure 4-11 shows one of the actuator pads fitted to an actuator.

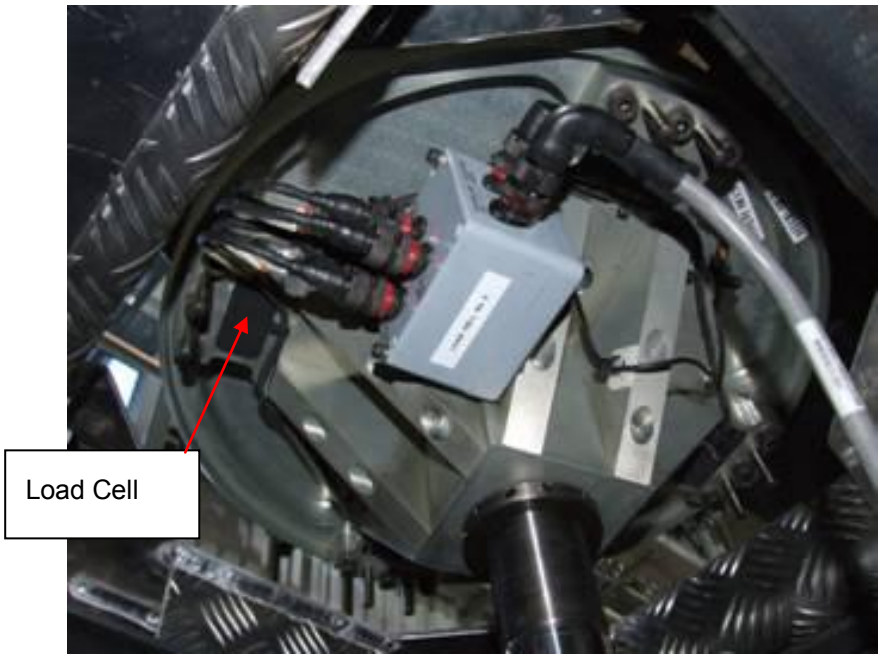

Figure 4-11– Actuator Pad

The pad accelerometer is connected to the upper pad, which is connected to the lower pad via four strain gauged supports that act as load cells. The PTFE pad is located on top of the upper pad, but is not connected. Its purpose is to produce a low friction surface between the vehicle tyres and pad surface, so that the tyre is free to scrub in a similar way to a rotating wheel. The low friction also reduces the side forces on the actuator ram and bearings compared to direct contact between the tyre and upper pad. In the longitudinal direction, freedom of wheelbase change is assured by the free rotation of the vehicle's wheels

The pad accelerometers are single axis IC Sensors 3021 Piezoresistive accelerometers with a +/-10 g range, with a working frequency of 0-400 Hz. The strain gauge arrangement is a one-off design by Multimatic. Four strain gauges per pad are used so that any offset load on the pad would result in the same measured vertical load as if the load was in the centre of the pad. If only one unit was fitted then an offset force would cause a bending moment on the load cell, which would affect its load reading. Within the pad unit the four load cell signals are summed to provide just one vertical load output.

As well as sensors fitted to the actuators there are also sensors fitted to the test vehicle at each of the 4 corners. This are;

- Body Accelerometer
- Hub Accelerometer
- Strut Displacement Sting Potentiometer

As with the other sensors, these were supplied by Multimatic when the rig was commissioned.

Both body and hub accelerometers are Silicon Designs SDI 2210(Figure 4-12) +/-10 g capacitive type accelerometers that respond to both DC and AC accelerations in a single axis.

Figure 4-12 – SDI 2210 Accelerometer

The body accelerometers are fitted to a stiff part of the vehicle body, ideally very close to a point vertically above the wheel centre. An ideal place to position them is the strut turret where spring and dampers are bolted to the chassis. However, this is not always possible due to plastic interior trim or carpet. Figure 4-13 and Figure 4-14 show examples of the body accelerometers fitted to the front and rear of a Honda Civic.

Figure 4-13 – Rear Body Accelerometer Position

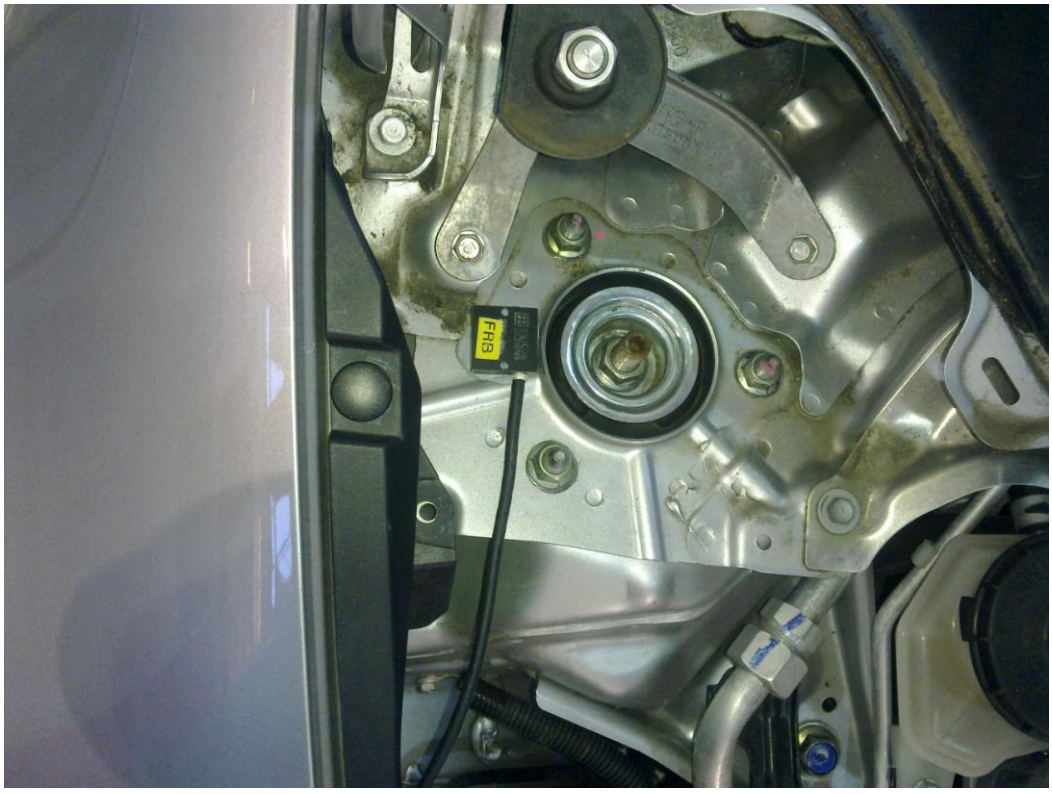

Figure 4-14 – Front Body Accelerometer Position

The hub accelerometers are fitted to the lower inside surface of the wheel rim, as close as possible to a vertical point above the contact centre of the tyre. An example of a hub accelerometer fitted to a Honda Civic is show in Figure 4-15.

Figure 4-15 – Hub Accelerometer Position

In some cases, seat and floor accelerometers are used in addition to the four body accelerometers. Again these are Silicon Design 2210s. The floor accelerometer is placed on the outer seat rail of the front right seat (Figure 4-16) and the seat accelerometer is located on top of the driver seat ballast bag of the front right seat (Figure 4-17).

Figure 4-16 – Floor Accelerometer Position

Figure 4-17 – Seat Accelerometer Position

All accelerometers are attached to the vehicle using ‘Blu-tac’. This provides a highly mouldable mounting that enables the accelerometers to be fitted without damaging the vehicle and without the need to remove components from the vehicle. Once attached to the vehicle with ‘Blu-tac’,

the accelerometers positions are subtly adjusted in accordance with a ‘Bulls-eye’ type spirit level, which allows the users incrementing the vehicle to visually determine when the accelerometer body is perpendicular to the earth’s gravitational force. If it is not possible to place the body accelerometers at a point vertically above the centre of the tyre’s contact patch, then their positions with reference to the front axle centre line in longitudinal and lateral axis are measured and recorded in the ‘Run List’.

The strut displacement string potentiometer is fitted to a 1” square section steel tube that is attached to the test vehicle’s wheel rim using heavy duty cable ties, as shown in Figure 4-18 . The opposing end of the string is then attached to the body of the vehicle using a suction pad and adhesive tape. The strut displacement string converts the linear extension of the string into rotational displacement of a potentiometer. Depending on the position of the rotary potentiometer the voltage output varies, so that the displacement of the string can be defined. The string potentiometers used are Celesco SP1-12 (Figure 4-18).

Figure 4-18 – Celesco SP1-12 String Potentiometer

This sensor arrangement means that no modification or damage of the vehicle has to take place to measure the vehicle response. It is also very fast and simple to apply and remove.

For each of the four corners of the vehicle a ‘Corner Box’ is used that the sensors are connected to, which are in turn connected to the digital signal processor. As well as the two accelerometers and string pot channels, there is also a spare DC channel, spare AC channel and a thermocouple input. When floor and seat accelerometers are used, these are connected to the spare DC channels on the front right and rear right ‘Corner Boxes’. Figure 4-19 shows an example of a ‘Corner Box’.

Figure 4-19 – Corner Box

4.1.3 - Calibration

Initial calibration of the four-post rig was carried out when the rig was commissioned in August 2008. This calibration was carried out by Multimatic technicians and a certificate of calibration presented. Since the initial calibration, annual calibrations have been performed by Multimatic technicians.

In addition to manufacturer calibration, the accelerometers and encoders are regularly cross calibrated. This is done by fixing the body and hub accelerometers at each corner to the relevant actuator pads with the PTFE pads removed. An excitation wave is then executed and the acceleration signals of the body, hub and pad accelerometers are compared to double differentiated encoder signal in the Dynosoft software. If the difference between any accelerometer and the encoder output is more than 1% RMS then the calibration of that accelerometer is changed so that the difference is removed on re-calibration.

The strut displacement string pots are also calibrated regularly. This is achieved by using a set of vernier callipers to measure the displacement of the string and the Dynosoft software to measure the voltage. The calibration of the sensor is then calculated from the linear gradient of displacement with respect to voltage.

An investigation was carried out to determine the effective mass of the upper part of the actuator pad and the PTFE pad. The mass of the upper part of the pad and pad accelerometer signal are used in conjunction with the actuator load cell signals to create a contact patch load that represents the force between the tyre and the PTFE pad. This is done within the Dynosoft software and is required because the upper part of the pad acts on the load cells when it accelerates, meaning that the measured force is not purely due to the vehicle accelerating, but also the upper pad. In the Dynosoft software the mass value of the upper pad (including PTFE pad) was 7.2 kg. By direct measurement the PTFE pad weighed 1.5 kg.

To confirm the mass used within the software, tests were conducted both with and without the PTFE mass in place. The inputs used were sine waves at 5, 15 and 30 Hz. Using the Dynosoft software the load cell forces and pad accelerations were compared. By taking the gradient of the force with respect to acceleration, the mass could be obtained according to Newton's second law of motion (4-1)

$$F = ma \tag{4-1}$$

Where;

F – Force of the loadcell

m – Mass

a – Acceleration of the pad

Figure 4-20 shows an example of the force gradient with no PTFE pad fitted and a 5 Hz sine wave input.

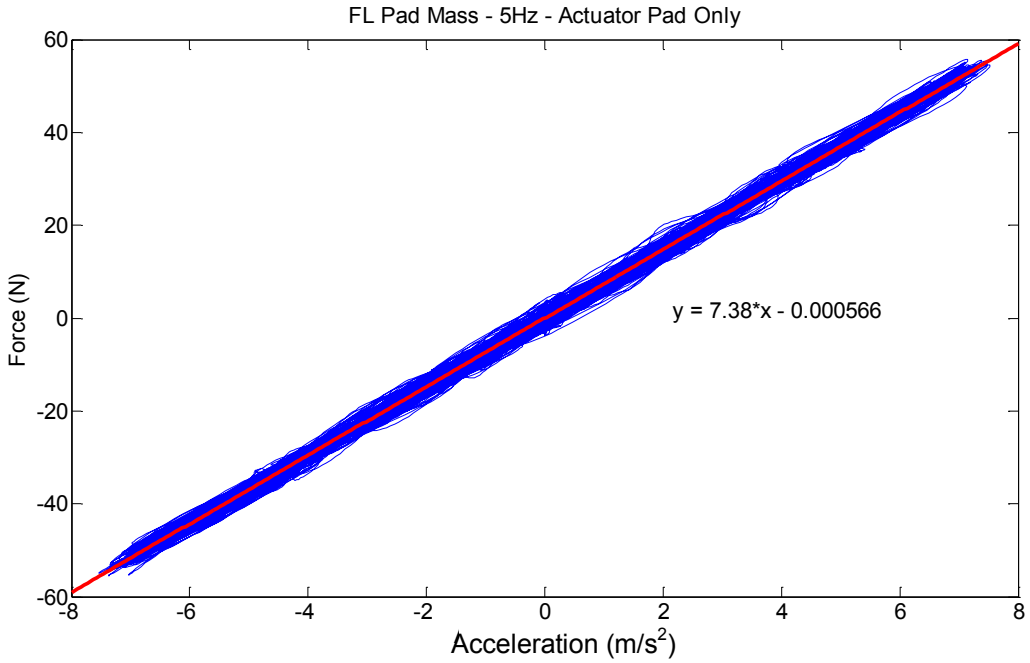

Figure 4-20 – Upper Pad Mass – 5Hz – Actuator Pad Only

Without the PTFE pad in place the mass was calculated to be 7.38 kg. This was consistent to within 0.04 kg at all three test frequencies. In order to test with the PTFE pad in place, a small amount of double sided adhesive tape was used to secure the PTFE pad to the upper pad. The three test frequencies were all repeated three times so that an average mass could be calculated. The values rounded to 100 grams were found to vary between 8.9 and 9 kg depending on the actuator and PTFE pad used. As the PTFE pads are often removed and fitted to different actuators when they are replaced a value of 9 kg was taken for all four corners. The obtained value of upper pad mass was 1.8 kg larger than that the default value within the Dynosoft software. At high levels of pad acceleration this could cause quite large errors in the contact force signal.

A comparison was carried out to compare the contact force response of a Honda Civic with both 7.2 and 9.0 kg upper pad masses used to calculate the contact patch force from the actuator force and pad acceleration. The peak error of the lower mass was found to provide a contact

force 14% larger than the 9.0 kg mass at 30 Hz. The difference between 8.9 and 9 kg mass would cause only a 0.78% error at 30 Hz, which was deemed acceptable. Figure 4-21 shows the contact force error for the 7.2 kg mass across the frequency range.

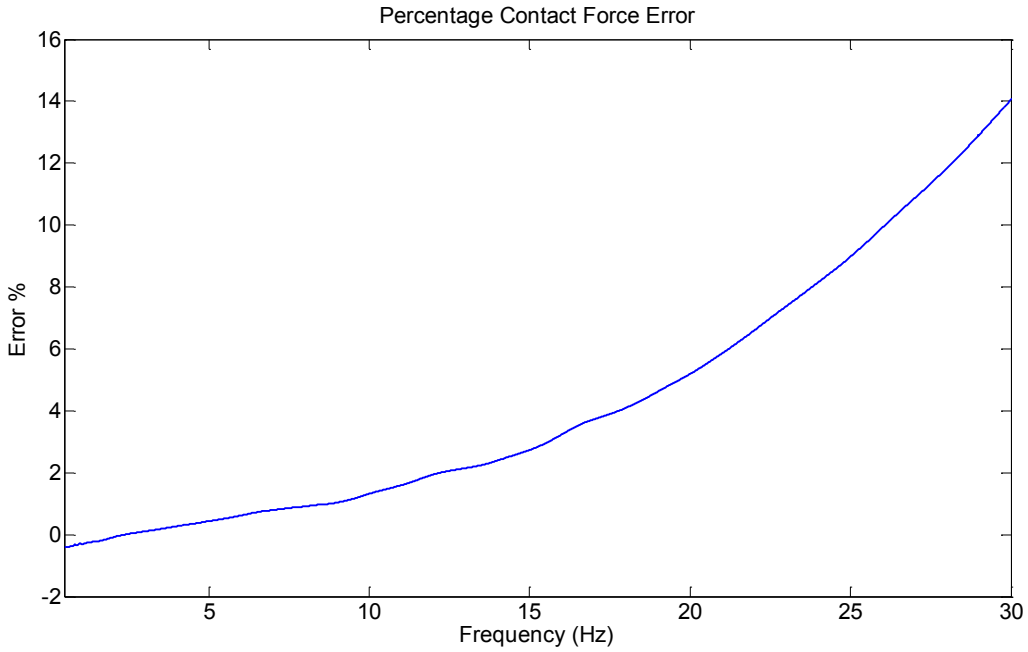

Figure 4-21– Percentage Contact Force Error with 7.2 kg Upper Pad Mass

4.2 - Data Management

4.2.1 - Organisation of Data Files

One of the main purposes of this project was to create a test and analysis technique that could be used to benchmark different vehicles and set-ups. This means that over time a huge amount of data would be acquired. The data needs to be organised in such a way that it is always easy to access and to make sure that 'like for like' comparisons are being made when benchmarking. This will help to make the benchmarking process efficient and accurate.

This section of the thesis details the organisation of the data files from the four-post rig and vehicle model so that efficient comparisons can be made between different vehicles and set-ups.

Within the Dynosoft software there are two different methods of saving the rig data. The standard method is to save the series of runs in a DMX file which is named according to a user input for 'Test Name'. However, this DMX file is encrypted and can only be read by Multimatic software. The Dynosoft software is quite limited in its data processing abilities, so it is necessary to import the raw data into another software package such as MATLAB. In order to do this, the data from a series of runs is saved in '.txt' format with each individual run having its own file. This also allows the method to be adapted to other similar multi-post rigs with ease, as it is very likely that '.txt' or '.csv' exports would be available. A feature in Dynosoft allows this to be done in one action by selecting to save a set of tests with a '1File/1Run' option. This saves the data to '.txt' files that are named according to the 'Test Name' and their run number. The maximum number of runs allowed per test file in the Dynosoft software is 15. It may be required that more than 15 runs are used for one vehicle or set-up so individual runs are also named with a 'Part' number. An example of an output file name is shown below.

'C:\Rig Data\Honda_Civic _Test_29_10_10\Honda_Civic _Test_29_10_10_Part_1_Run_6.txt'

In this format each file for each different vehicle or set-up can be easily distinguished and accessed. To accompany each test a 'Run List' is created in Excel. This run list contains information about each run number and other details about the specification of the vehicle.

Run No.	Mode	Wave	Amplitude (mm)	Notes	Part No.
1	Heave	Const.	30	Warm-up	Part 1
2	Heave	CPV	25	Shakedown - All signals OK	
3	Heave	CPV	25	First Test -Set-up 1	
4	Pitch	CPV	20		
5	Roll	CPV	15		
6	Warp	CPV	15		
7	Heave	Track Input	Scale 1	EUDC Drive Cycle - Good Road	

Table 4-1 – Run List Example

Table 4-1 is a typical run list for a single part. The 'Part No.' and 'Run No.' in this table match that of the saved '.txt' file saved using Dynosoft.

The run list details the mode in which the rig has been run for each test, the type of input wave and the amplitude of the wave. In the constant peak velocity (CPV) input case the amplitude only actually relates to the displacement amplitude at 0.5 Hz.

As well as the actual list of runs the run list contains information about the vehicle being tested.

Wheelbase	2.5	m	**Front Tyre Pressure:**		32	PSI		
Front Track	1.6	m	**Rear Tyre Pressure:**		35	PSI		
Rear Track	1.4	m						
Track Ratio	**0.875**							
Corner Weights	**FL**	**FR**	**RL**	**RR**	**Total**	**% Front**	**% Cross**	**% Left**
Car Only	400	400	250	250	1300	61.54	50.00	50.00
Car + Driver Ballast (Optional)	420	420	270	270	1380	60.87	50.00	50.00
Car + Total Ballast (Optional)	0	0	0	0	0	#DIV/0!	#DIV/0!	#DIV/0!
Driver Mass on Seat - Only required if seat accelerometers fitted								
55	kg							
Unsprung Mass - Set to zero if unknown								
Front Unsprung Mass	30	kg						
Rear Unsprung Mass	0	kg						
Installation Ratios								
IR_FL	1.00	Gives Wheel displacement from pot						
IR_FR	1.00							
IR_RL	1.00							
IR_RR	1.00							
Body Accelerometer Locations - Not required if approximately over wheel pad centre lines								
Front Acc Lat Distance Apart	1200	mm	0.600	(m) From lateral centre line				
Rear Acc Lat Distance Apart	0	mm	0.000	(m) From lateral centre line				
Front Acc Long Pos(+ve Rwd)	50	mm	From Front Axle CL			From CofG	0.928	m
Rear Acc Long Pos(-ve Fwd)	0	mm	From Rear Axle CL			From CofG	1.522	m
Seat Accelerometer Locations - Only required if seat accelerometers fitted								
Floor Acc Lat Pos (+ve Left)	250	mm	From lateral centre line					
Seat Acc Lat Pos (+ve Left)	300	mm	From lateral centre line					
Floor Acc Long Dist (+ve Rwd)	900	mm	From front axle centre line					
Seat Acc Long Dist (+ve Rwd)	800	mm	From front axle centre line					
Front Top Mount Type								
Single Path								
Rear Top Mount Type								
Dual Path								

Table 4-2 – Vehicle Information Example

Table 4-2 shows the details of the vehicle information part of the run list. Information about the wheelbase and track dimensions of the vehicle are required for analysis and modelling of the vehicle. The track ratio is the ratio of rear track width divided by front track width. This is required for vehicles where the front and rear tracks are not the same, as using the same amplitude inputs for front and rear in roll would cause a partial warp input which is not equivalent to rolling the vehicle about a flat ground plane. Instead the rear input amplitude is multiplied by this ratio to create a pure roll input. The ratio may also be used for warp, although its significance is reduced.

Tyre pressures are of importance as they can have a significant effect on the ride and handling behaviour of the vehicle. The tyre pressures noted are only the initial setup tyre pressures. In some cases it may be desired to investigate the effect of tyre pressure,the tyre pressure would then be written in the notes section next to the relevant run or on a separate set-up sheet that is referenced by the run list.

The corner weights section of the run list describes the weight distribution of the vehicle, which is again very important to the ride and especially handing of the vehicle. Each individual corner weight is input separately using the values measured for the static vehicle after shakedown in Dynosoft. These are then used to create information about the total mass and front, diagonal and left weight distributions. The values are normally recorded for vehicle only with its fuel contents and then again with the specified passenger ballast.

If a test has been conducted on the vehicle previously and the unsprung mass is known with confidence, this can be stated in the vehicle information part of the run list. The purpose of this is to speed up the analysis procedure, as the method of extracting the unsprung mass value from the vehicle data is the most time consuming part of the parameter determination.

The installation ratios refer to the ratio between movement of the suspension displacement string potentiometer and the vertical displacement of the wheel. The ideal way to fit the string potentiometers is shown in Figure 4-18. However, this may not be possible in all vehicles due to the wheels and wheel arch design. In this case it may be necessary to mount the string potentiometer in a way that its movement is not equal to the vertical wheel movement. In this case a linear ratio between the two would be determined and noted in the run list. This ratio can be used within the rig analysis program to compensate for the positioning of the string potentiometer and produce results in terms of vertical wheel coordinates.

When no inputs are entered into the body accelerometer locations part of the run list, the body accelerometers are assumed to be located vertically over the wheel pad centre lines. The locations of the accelerometers are used when determining pitch and roll accelerations of the vehicle from the vertical accelerations of the individual accelerometers. If it is not possible to locate the accelerometers securely at a point over the wheel pad centres then the positional information of the accelerometers is required to calculate accurate pitch and roll accelerations of the vehicle body.

The seat accelerometer locations are used much in the same way as the body accelerometer locations, but in this case there is no default location, so the information must be included.

Secure and reliable storage of the data set from a complete set of tests was achieved by storing the ‘Run List’ spreadsheet together with all of the individual data files containing data from each period of vibrational input, together in one folder having an appropriate name. In this way all the general data relating to the entire test is available in the run list together with the dynamic data recorded for each input waveform.

4.2.2 - Signal Processing

It was noted in section 4.2.1 - Organisation of Data Files, that the output files used from the Dynosoft software are in '.txt' format. Within the file is a 'Time' column stating the data acquisition time in seconds. After this point the columns are separated into FL, FR, RL, RR and SYS. These indicate the grouping of the signals into their relative corners. The signals contained within each of the corner groups depend upon the calibration file used within Dynosoft. Typically they would consist of the signals;

- Act_Force
- Temp
- Pad_Acc
- Hub_Acc
- Body_Acc
- Strut_Disp
- Act_Disp
- CPL (Contact Patch Load)

In order to perform analysis on the rig data the contents of the '.txt' file is imported into MATLAB. This is done using the 'dlmread' command to extract the signal data and 'textscan' to extract the relevant headers. This produces separate arrays of each individual signal. As the unit system output from Dynosoft can be changed, the measurement units are extracted for each column using 'textscan' and converted to SI units where required.

The following section describes the signal processing relating to a constant peak velocity sine sweep only. This input is the most common input used within the project to characterise the vehicle's dynamic behaviour.

Once the data has been extracted from the '.txt' file the signal processing procedure can take place. During the majority of tests carried out for this project, only the four body accelerometers were fitted to the car body and not the floor or seat accelerometers. However it is still desired that the data collected at any point within the project can be compared in every sense except the floor and seat accelerations. For this reason if the seat and floor acceleration headers do not appear in the '.txt' file, then false signals are created with a value of zero across the time range.

The output signals from the '.txt' file are raw measurements with no zeroing within Dynosoft taken into account. This means that the zeroing of signals needs to be done in the signal processing.

For all of the acceleration signals a simple mean is taken of the entire run and that value removed from the signal to give zero mean.

The Act_Disp, Act_Force and Strut_Disp signals are all offset by their initial value. The fluctuation of Act_Force is only around 0.1kg when the vehicle is static, and the static values of actuator force are already recorded in the run list. The Strut_Disp signals offset can vary significantly during a run, even if the amplitude of the wave is relatively small. This is due to both friction of the suspension system and non-linearity of the damping characteristics. For this reason taking the first value of the signal as the offset is the most convenient method.

At this point the Strut_Disp signals are multiplied by the individual installation ratio values, to compensate for the difference between the sting potentiometer and vertical wheel movement.

The suspension velocity for each Strut_Disp signal is calculated using the central difference method of differentiation shown in equation (4-2). This is used rather than standard numerical differentiation to avoid phase shifting of the calculated velocity by one data sample step.

$$\dot{x}(n) = \frac{x(n+1) - x(n-1)}{t(n+1) - t(n-1)}$$

(4-2)

Where:

x - Displacement Signal

$\dot{x}$ - Velocity Signal

t – Time

The next set of signals created are the CPL signals. It was explained in section 4.1.3 - Calibration, that the CPL signals are created within Dynosoft using the Act_Force and Pad_Acc signals. A calibration investigation found that the 7.2 kg pad mass used in the Multimatic calculation was incorrect and that the actual pad mass was between 8.9 and 9.0 kg. For this reason a new set of CPL signals are created within signal processing using the original Act_Force and Pad_Acc signals and the value of 9kg determined in the calibration.

All of the signals are then filtered using a realisation of an analogue 5th order chebychev filter with a low-pass cut-off frequency of 35 Hz. This is implemented within MATLAB using the 'filtfilt' command which filters the signal in the forward direction and then the backward direction. This has the effect of doubling the filter order and removing the phase lag introduced when using a single filter direction. The form of the filter transfer function is show in equation (4-3) below.

$$H(s) = \frac{B(s)}{A(s)} = \frac{b(1)s^n + b(2)s^{n-1} + \cdots + b(n+1)}{s^n + a(2)s^{n-1} + \cdots + a(n+1)}$$

(4-3)

The purpose of the filter is to reduce the high frequency noise on all of the signals. This is especially true for the Pad_Acc signals that were found to include a large amount of noise compared to other signals.

It has already been stated in this chapter that the most common input used in this project was the constant peak velocity swept sine. The complete form of input is explained in section 3.4 – An Efficient Rig Input. The signal processing procedure includes a method to determine the frequency and amplitude properties of the swept sine.

As the desired input form is known, but not necessarily its frequency or length properties (defined in the 'Profile Editor'), some signal processing is used to determine the variables that fit the equation for the desired input.

The Act_Disp signal measured by the encoder is the input signal with the least noise and highest accuracy. For this reason this signal is used to determine the frequency increase rate. The frequency is determined by finding an accurate time value for each zero crossing. One problem with the input signal created by the Dynosoft software is that it uses a sine pulse fade at the start of the run. This has a positive effect in reducing the length of transients at the start of the test, but by multiplying the original velocity cosine wave by a sine step, the mean displacement sine wave shifts during the fade. This means that the displacement amplitude of the input no longer coincides with the static actuator height. This problem can be overcome by simply filtering the signal with a high-pass chebychev filter with a lower cut-off than the initial start frequency of the input.

With the signal symmetrical about zero, the cycle length can be determined using the times at which the signal crosses zero. This process is done in two stages. Firstly any index positions in the array where the signal is precisely zero are recorded. For a real system there is unlikely to be any values that are zero to a sufficiently high number of decimal places. The next stage multiplies each value in the array by its preceding value. All results that are less than one show that a zero crossing has taken place between the two data points. The time at the index position before the crossing occurs could be used to determine a rough crossing time at low frequency,

but this may not produce accurate estimates when the sampling rate is only a few multiples of the exciting frequency. To achieve a better estimate of crossing time, the amplitudes of the two values either side of the zero crossing can be used. For angles below 15° a sine wave is close to linear. So assuming linearity, a very accurate zero crossing time can be calculated using the ratio of the two amplitudes either side of the zero crossing, multiplying that ratio to the sampling step size and adding the time at the index before the crossing occurs. A graphical representation of the method is shown below in Figure 4-22, along with equation (4-4).

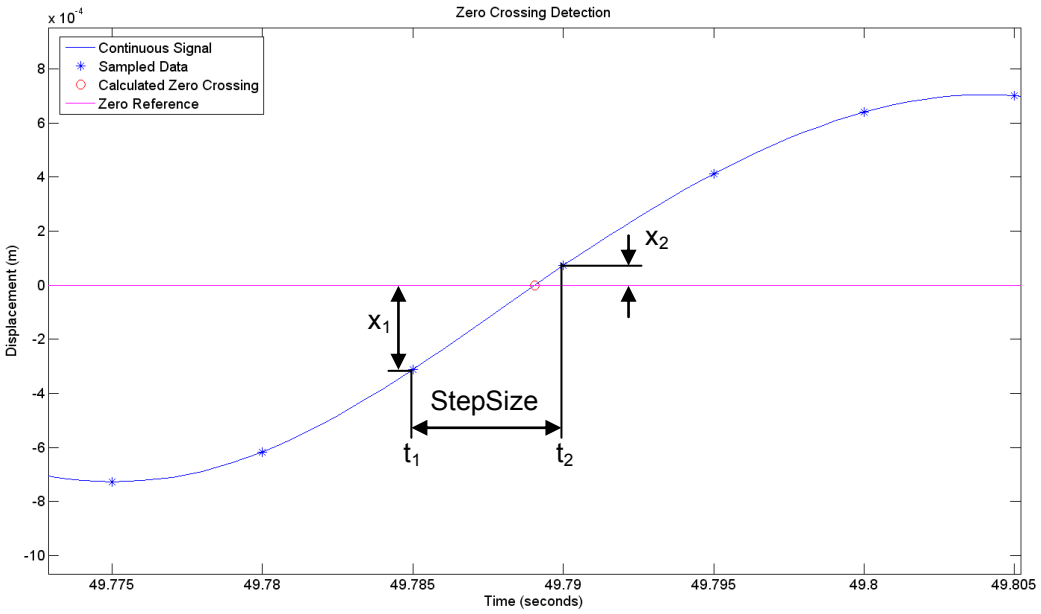

Figure 4-22 – Zero crossing calculation

$$t_{cross} = t_1 + \left[\left(\frac{|x_1|}{|x_1| + |x_2|} \right) \times StepSize \right] \quad \textbf{(4-4)}$$

Where:

t_{cross} – Zero crossing time

t_1 – Time pre zero crossing

t_2 – Time post zero crossing

x_1 – Amplitude pre zero crossing

x_2 – Amplitude post zero crossing

Having calculated accurate times for all of the crossings in the Act_Disp signal the half cycle length can be calculated by determining the difference between each of the crossing times. The frequency for each cycle can then be determined by taking the inverse of twice the half cycle length. The frequency sweep rate constant k, can then be determined using equation (4-5).

$$k = \left(\frac{f(t_1)}{f(t_2)} \right)^{\frac{1}{t_2 - t_1}}$$

(4-5)

Where:

k - Sweep Rate Constant

f – Instantaneous Frequency

t_1 – Time at first data point (close to start of run)

t_2 – Time at second data point (close to end of run)

The only remaining parameter required to calculate the instantaneous frequency at any point during the run is then f_0 which can be calculated simply using the first two zero crossing times.

To calculate the peak velocity required for the input the RMS of the Act_Vel signal is calculated and multiplied by √2. The desired displacement, velocity and acceleration signals can then be created and compared to the measured signals as shown in Figure 4-23.

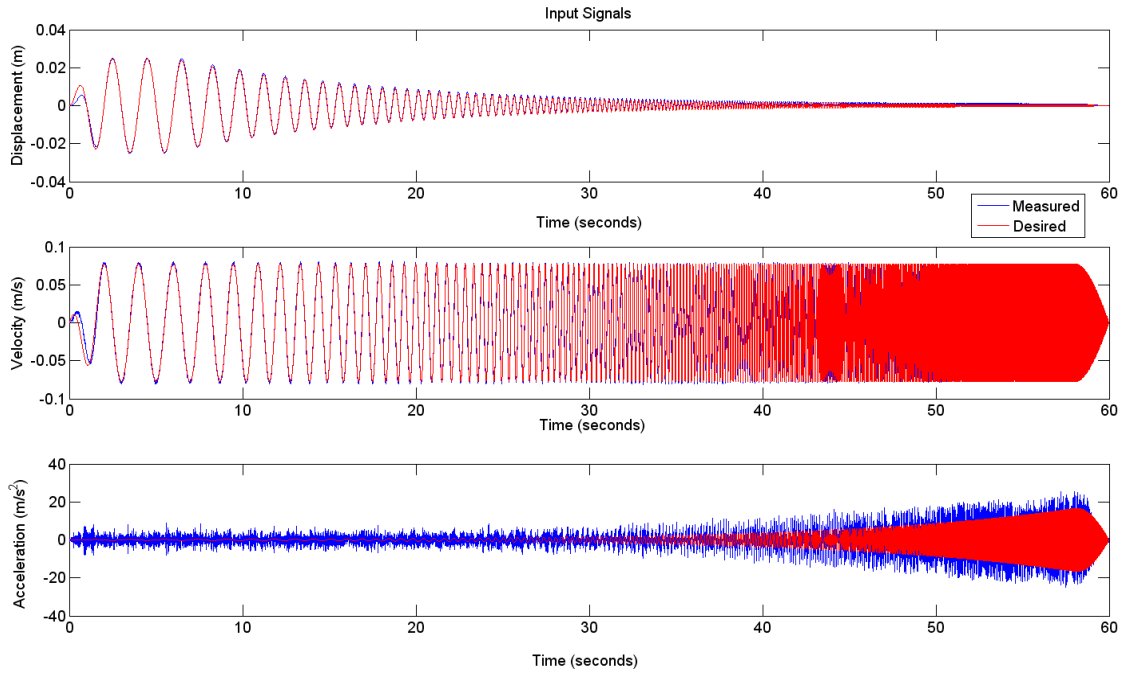

Figure 4-23 – Desired and Measured Signal Comparison

In Figure 4-23, the desired and measured displacement and velocity signals are quite consistent. However, the acceleration signals are significantly different early in the run (low frequency). The measured signal contains a large amount of high acceleration peaks and in some cases it is difficult to see any correlation to the desired signal. Originally the signal was thought to be heavily contaminated with noise, but after some investigation it was found that the pad was actually accelerating in this way, due to the actuator valves and control system.

The control system of the four-post rig uses the encoder measurement of actuator ram displacement as its signal to evaluate and alter the current signal to the Moog valve on the actuators. This control system operates at 2000 Hz, additionally the Moog valve has its own control system based on the control current and spool position. The valves used are able to provide a flow rate that can move the rams at a maximum velocity of 3 m/s. The large port size required to achieve this, makes it difficult for the spool valve to be able to achieve the small changes in fluid flow rate that are required for a low frequency, low amplitude input. For this reason, the larger the desired input velocity, and hence fluid flow rate, the lower error between desired and achieved pad acceleration at low frequency (<3 Hz). An example of this can be seen by looking at Figure 4-24 and Figure 4-25.

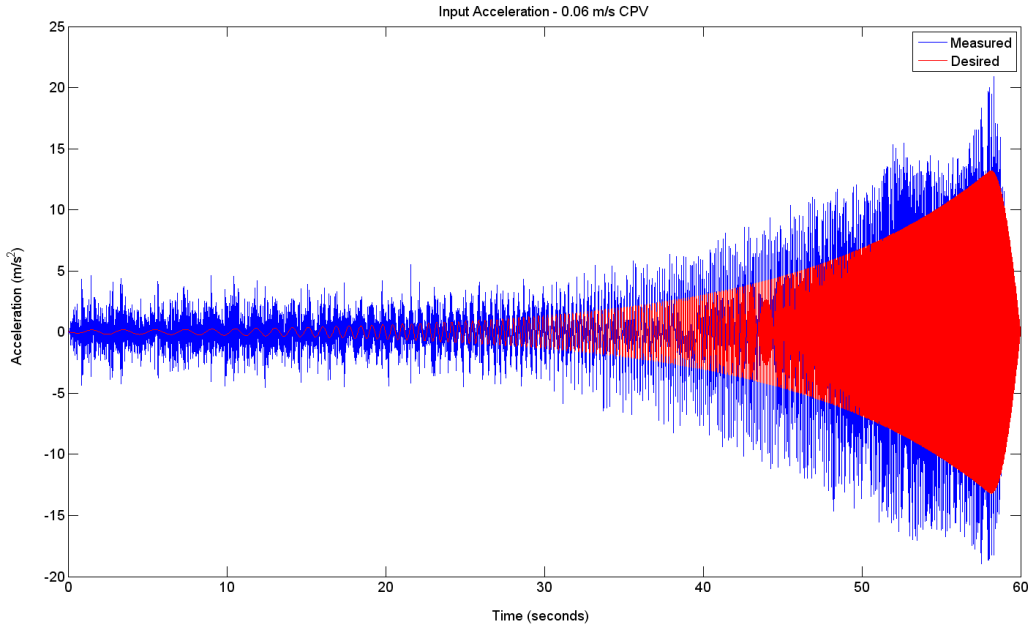

Figure 4-24 – Input Acceleration Comparison - 0.06 m/s CPV Input

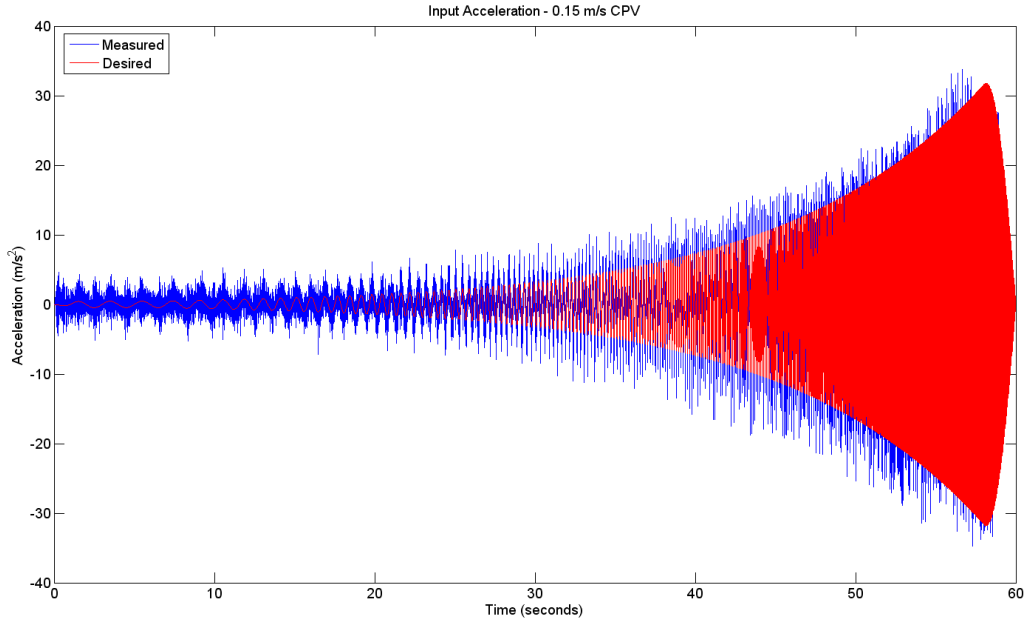

Figure 4-25 - Input Acceleration Comparison - 0.15 m/s CPV Input

When using a sine sweep it is desirable that only one frequency component be excited at a time, so that the response with respect that that input frequency at its specified amplitude can be obtained with confidence. Due to the low natural frequency of the body modes (generally 1.5-2 Hz) the higher frequency acceleration components have very little effect on the body acceleration signals measured on the rig. However, the unsprung mass, which has a much

higher natural frequency, is affected at low frequency. If the frequency responses were calculated using a Fourier transform method then this would be less of a problem. However, when using a Fourier transform method other problems may occur and certain information is lost. The method used in this project to estimate the response of the vehicle uses the signal envelopes of the input and output waves across the frequency range. This method will be explained in more detail later in this section. If the input and output signals contain information at anything but the desired input frequency, then the response will be estimated with a certain amount of error.

In order to ensure that only information at the correct frequency is used to determine the response, a low pass filter can be used. The fact that the input frequency is continuously changing makes sufficient filtering more difficult than a constant frequency input. One method would be to set up a number of different low pass filters that filter a certain range of data. However by doing this, the data point at the end of one range may not be the same as the data point at the start of the next range. Also it means that data is filtered unequally within each range, which could have an effect on the obtained frequency response. A second and more appropriate way to filter the data with respect to its desired frequency is to use a non time-dependent step size with a fixed amount of data points per cycle. To the knowledge of the author the method used here to achieve this type of filtering is original to this thesis.

The frequency increase rate is defined by equation (3-15). In the fixed points per cycle data we would like to determine the points in time for a linear frequency increase. A typical sine sweep may have a frequency increase rate per cycle of 0.1 Hz. If 40 data points are desired to represent each cycle, then a frequency step size of 2.5e-005 Hz is required. For each of these points in the frequency domain the related time domain value can be calculated using equation (4-6).

$$t = \frac{\ln\left(\frac{f}{f_0}\right)}{\ln(k)} \qquad \textbf{(4-6)}$$

Where:

f – Frequency at desired points

f_0 – Frequency at t(0)

k – Sweep rate constant

t – Time at desired points

ln – Natural Logarithm

Using the points in the time domain calculated from equation (4-6) a new signal equally spaced in the frequency domain can be created by interpolating between data points of the original data. The type of interpolation used in this case is a cubic spline method. Depending on the original signal sampling rate, the frequency and the amount of desired points per cycle, this may (and often does) result in areas where the signal has been interpolated to a higher sample rate than the original data. As the input is sinusoidal and our expected output is sinusoidal then using the cubic interpolation can supply an improved sinusoidal fit to data which may only contain 5-6 points per cycle originally. When using the envelopes of the signals to create the response this can be a benefit as it ensures that data points are present close to the peak and trough of each wave. An example of original and interpolated signals is shown in Figure 4-26.

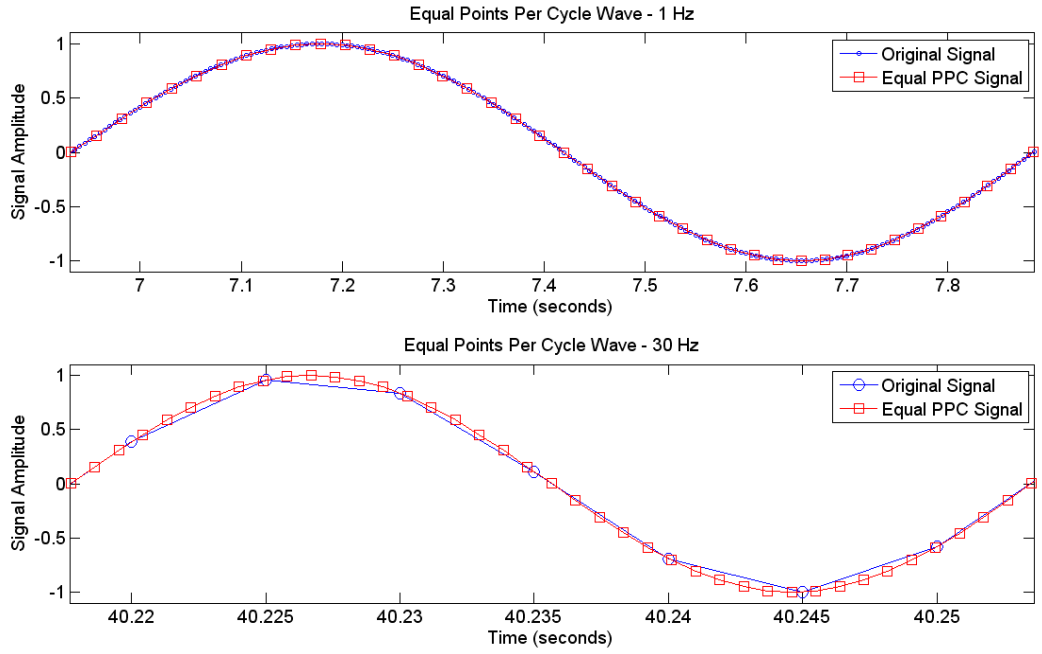

Figure 4-26 – Equal Points per Cycle Signals

By creating the equal data points per cycle signal, the relationship between input frequency and sampling frequency is fixed across the frequency range. This means that the use of a single transfer function low pass filter will have the same effect with relation to input frequency for any cycle.

The aim of this filtering technique is to be able to create both a linear estimate of the vehicle response, and an estimate of the response showing directional non-linearity about the initial conditions across the frequency range. The linear response estimate creates very similar results to those extracted using Fourier analysis and is used for characterising the vehicle response, extracting linear parameters and comparing to linear modelling results. The non-linearity is used

when looking at characteristics that may affect the vehicle behaviour in a way that a Fourier transform method would be unable to do. In order to get an adequate linear response estimate the signals must be heavily filtered to significantly reduce the amplitude of any undesired frequency components. In the non-linear case the filter cut-off must be set to a higher frequency to ensure that the signal is not linearised significantly by the filtering, but still enough to reduce high frequency components caused by the input acceleration.

For both the significantly filtered and relatively unfiltered signals the next part of the signal processing procedure is used to determine the envelope of the signals. This is done in several stages.

The first stage involves using the zero crossing detection method explained earlier in the chapter to determine the start of each cycle. The second stage involves determining the minimum and maximum signal values from the start of each cycle to the start of the next cycle. From the minimum and maximum values for each cycle, a mean value is calculated. In the case of the signal used to create a linearised response of the vehicle the mean value is used as an offset to redistribute the signal so that it is symmetrical about zero and calculate the relevant linear amplitude of the sine wave. In the case of the signal used to determine non-linearity characteristics of the vehicle the mean is one of the parameters measured.

The last part of the signal processing carried out on individual linearised signals is to once again determine zero crossing values for the newly distributed signal. The zero crossing method used is as explained in Figure 4-22. This provides a very good estimate of the zero crossing time of the linearised signal.

The same signal processing technique is used on all signals extracted from the rig data. Once the signals are filtered to provide linearised amplitude and zero crossing times, as well as a non-linear peak, trough and mean values, responses can be created by determining the relative amplitude and phase of the signals with respect to the input acceleration signal.

To determine the amplitude ratio of a signal with respect to input acceleration, the amplitude of the signal is simply divided by the amplitude of the input acceleration signal corresponding to that corner of the vehicle. To determine the phase of the signal with respect to the input acceleration signal, the difference in time between the crossing of signal and the crossing of the input acceleration signal is calculated and multiplied by the input frequency at the time of the input acceleration zero crossing. This value is then multiplied by 2π to produce the phase difference between the two signals in radians.

With the amplitude ratio and phase information calculated for the signal the complex exponential response can be calculated using equation (4-7):

$$Z = \mathrm{Re}^{j\theta}$$

(4-7)

Where:

Z – Complex Response

R – Amplitude Ratio

e – Exponential Function

j – Imaginary Unit

θ – Phase Angle

Once all of the output signals in the form of complex exponential responses with respect to their relative input accelerations have been calculated, averaging of signals or calculation of other responses with respect to other signals can be carried out very easily. This makes the same signal processing technique applicable in all of the input modes, as rotational responses can be easily and efficiently calculated from two linear responses with known distances between accelerometers.

Responses can also be converted to acquire a response that is no longer with respect to input acceleration, but could be with respect to input displacement or velocity. This can be done without having to recalculate the response through the whole signal processing technique described, just using omega arithmetic, as in Mercer [75]. This makes the creation of this signal both efficient and consistent with the original measurement.

An example of where this may be required is in the extraction of the tyre dynamic stiffness with respect to frequency.

From the original signal processing, a response is created for the contact patch load with respect to input acceleration, and the hub acceleration with respect to input acceleration. To calculate the tyre displacement response, which is required to determine the dynamic tyre stiffness, the tyre acceleration response can be calculated simply by subtracting 1 from the hub acceleration response. The tyre acceleration response can then be converted from to tyre displacement response using equation (4-8).

$$\frac{Z_0 - Z_1}{\ddot{Z}_0} = \left(\frac{\ddot{Z}_0 - \ddot{Z}_1}{\ddot{Z}_0}\right) \times \left(\frac{-1}{\omega^2}\right)$$

(4-8)

Where:

Z_0 – Input Displacement

Z_1 – Hub Displacement

ω – Angular Frequency

Once the tyre displacement with respect to input acceleration response has been obtained, the tyre stiffness response can be calculated simply by dividing the contact force response by the tyre displacement response. An example of the output can be seen in Figure 4-27.

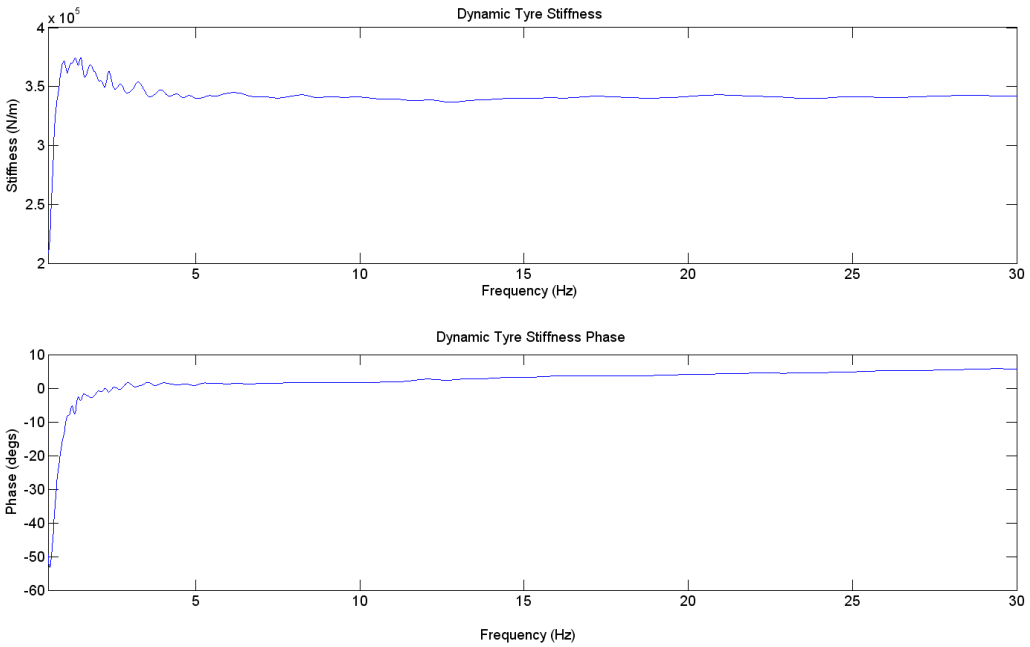

Figure 4-27 – Dynamic Tyre Stiffness Example

Once all of the required responses have been calculated the signal processing stage is complete and the estimation of parameters can take place. The explanation of the parameter estimation method can be found in section 5 - Estimation of Vehicle Parameters.

4.3 - Testing Procedure

This section details a typical test procedure used to acquire parameters and vehicle characteristics from a four-post rig test of a vehicle.

4.3.1 – Rig and Vehicle Setup

In order for a vehicle to be tested on the rig, the locations of the four actuators need to be positioned so that the actuator pads are approximately in line with the four contact patch centres of the vehicle. Prior to a rig test, dimensions such as the wheelbase and front and rear track widths are measured so that the actuators can be positioned before the vehicle arrives at the test facility.

Before the vehicle can be rolled onto the rig the hydraulic system and control PC need to be started in order to carry out a rig warm-up, calibration checks and actuator force zeroing.

The warm-up run has an amplitude of 30 mm, is run in heave and is a constant frequency sine wave. The input is designed specifically for efficient warming and circulation of the hydraulic fluid within the four-post rig system, to ensure that tests after this point are repeatable.

Calibration checks (if not recently done) are then carried out on the SD2010 body and hub accelerometers using the method described in section 4.1.3 - Calibration.

Once the rig has been warmed-up and calibration checks have been conducted, the Act_Force signals are zeroed with only the mass of the PTFE pad on the actuator pads. This is to ensure that the force measured when the vehicle is on the rig is purely due to the vehicle.

When the rig is activated and ready for use the vehicle to be tested can then be rolled onto the rig, ensuring that the centre of each road wheel is approximately over the centre of each actuator pad.

To determine the four corner weights of the vehicle on its own the Act_Force signals are viewed and recorded in the run list. It should also be noted approximately how much fuel is in the vehicle, and any other vehicle based masses that are likely to change during normal operation of a vehicle.

4.3.1.1 - Passenger Ballast

In order to ensure that the mass and weight distribution of the test vehicle is the same as would be expected on the road, passenger ballast is fitted.

The ballast was designed to be around 70 kg per person, to be representative of the average European adult. In order to organise the mass into realistic locations of the human body masses, a multi-body dynamics model of the human body was consulted. This was done with the use of the paper 'Analysis of Human Body Response to Vibration Using Multi-body Dynamics Model' by Teng, Cheng, and Peng [76].

Figure 4-28 shows a figure of the multi-body dynamic model presented in the paper.

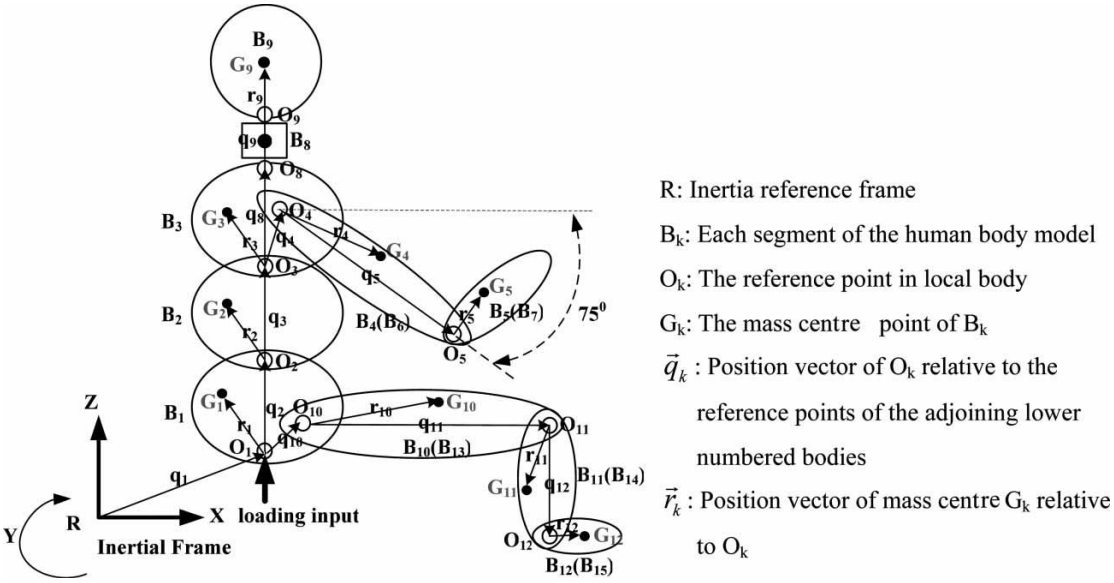

Figure 4-28 – Human Multi-Body Dynamics Model - Teng, Cheng, and Peng [76]

The body consists of 10 segments each with an associated mass. These masses are presented in Table 4-1.

No.	Name	Mass	% Total Mass
1	Head	4.5	5.93
2	Neck	1.22	1.61
3	Chest	17.52	23.08
4	Middle Torso	2.22	2.92
5	Pelvis	20.16	26.55
6	Upper Leg x 2	12.44	16.39
7	Lower Leg x 2	6.56	8.64
8	Foot x 2	2.5	3.29
9	Upper Arm x 2	4.18	5.51
10	Forearm x 2	4.62	6.09
Total		75.92	

Table 4-3 – Body Segment Masses

In the case of this model, the total mass was larger than the desired mass of 70kg, so values were scaled using the percentage mass values.

Sandbags are used to represent the occupants in the vehicle, as it is a much lower cost alternative to a manikin type model, and is easier to manoeuvre in and out of the vehicle. If each segment of the body were divided into individual sandbags then it would be difficult to fit all of the segments to the seat and floor in a secure way, and would be less representative of the human body as there would be no connection between the segments. By grouping certain masses the number of sand bags could be reduced to five to represent five major areas of the body. However, none of the bags should be too heavy that one person cannot lift the bag into the front seat of the vehicle without straining. For this reason the maximum bag mass was limited to 18 kg. The grouping resulted in the flowing distribution of mass resulting in a total mass of 71 kg per occupant.

1. Upper legs – 10 kg
2. Feet and lower legs – 10 kg
3. Proportion of pelvis – 15 kg
4. Proportion of pelvis, middle torso, chest and arms – 18 kg
5. Proportion of chest, neck, head and arms – 18 kg

The sandbags are positioned in a way that is representative of the multi-body dynamic model in Figure 4-28. A diagram of the sandbag layout is shown in Figure 4-29 and a picture of the sandbags located in a real vehicle is shown in Figure 4-30.

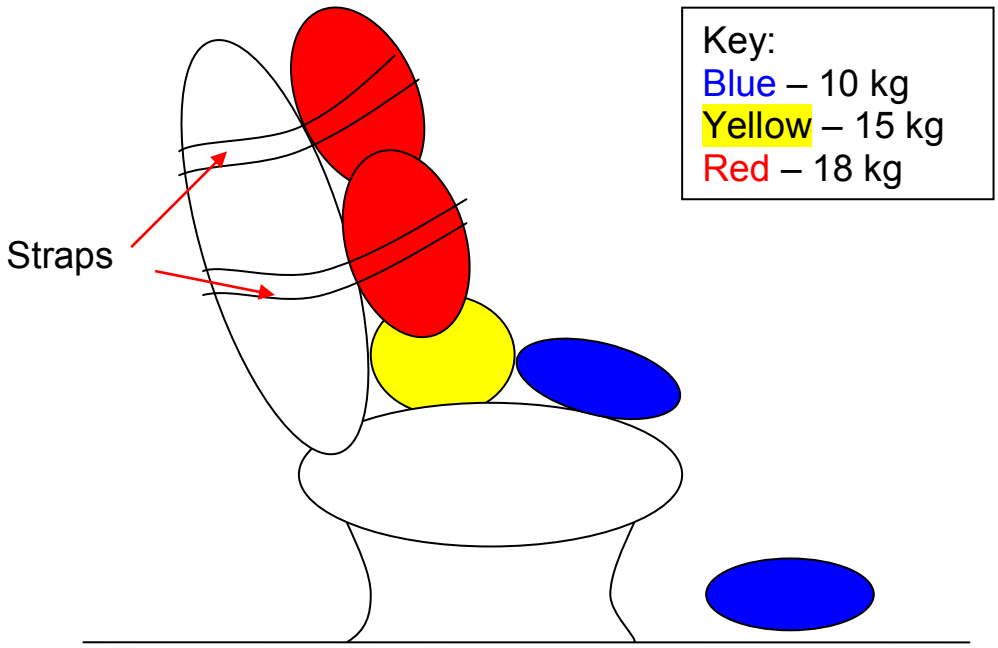

Figure 4-29 – Ballast Sandbag Layout

Figure 4-30 – Ballast Sandbags Fitted

For the majority of testing ballast is fitted for the driver and front passenger. Obviously it is also possible to test with different occupant masses and different numbers of occupants located in the different seats, or even with a boot full of luggage. Once the ballast has been fitted, the 'Act Force' signals are recoded to determine the total mass and weight distribution of the vehicle in the 'Ballast Fitted' condition.

Once the ballast has been fitted, sensors can be attached to the vehicle using the methods shown in section 4.1.2 - Data Acquisition System. At this point testing of the vehicle can commence.

4.3.2 – Testing the Vehicle

With the vehicle fitted to the rig and instrumented the first test to be carried out is the 'Shakedown' test. This is a word commonly used in industry for a period of testing, usually to determine any faults with a system. In this case the shakedown is a 78.5 mm/s constant peak velocity sine wave input. The purpose of the shakedown run is check that all of the measurement devices fitted to the test vehicle and rig are working as desired, so that confidence can be gained to test a number of runs without individually checking the data in the Dynosoft software after each run. A secondary purpose of the shakedown run is to settle the vehicle into an equilibrium position before the first data set used for analysis is recorded. Due to friction in the vehicle's suspension it may be the case that if the vehicle has been 'jacked-up' or sat for a long time then the suspension position may not be the same at the start of this run as the end. If this data were to be used for analysis, then it may give the illusion that this would occur for every repeated run, when this is unlikely to be the case. Once the run is complete the results are viewed. Each of the signals from the sensors fitted to the test vehicle are inspected to check that the output is within the expected range.

If problems are found during the first shakedown run, then these problems are resolved and another shakedown run carried out. The shakedown runs should be recorded within the run list, so that the run list run numbers correspond to the Dynosoft run numbers.

At this point it is possible to start the part of the rig test of which the data will be analysed.

Typically a full set of runs consists of constant peak velocity inputs with the following modal and amplitude characteristics:

- Heave – 78.5 mm/s
- Heave – 94.25 mm/s
- Heave – 125.7 mm/s
- Heave – 157.1 mm/s
- Pitch – 94.25 mm/s
- Pitch – 125.7 mm/s
- Roll – 62.8 mm/s
- Roll – 78.5 mm/s
- Warp – 62.8 mm/s
- Warp – 75.5 mm/s

As each of the inputs take 60 seconds a complete set of runs takes a minimum of 10 minutes. However, during tuning of a vehicle some multiple amplitude tests can be omitted to save time, reducing the testing time to a minimum of 4 minutes.

By testing more than one amplitude in each mode the non-linearity of the vehicle response in each mode can be determined. Most of the information about non-linearity is obtained from the heave runs, hence a wider range of input amplitudes are used.

During the test, the 'Run List' is updated with the input mode and amplitude of each input, along with any notes thought necessary.

Once a full set of runs have been completed the run files are saved.

With the rig data saved as individual runs the data can then be analysed using the program created in MATLAB through the use of the 'Parameter Estimation General User Interface'.

4.3.3 - Parameter Estimation General User Interface

The purpose of the general user interface for the parameter estimation method is to allow for quick and efficient selection of the runs to be processed and to allow the user to input information that is required within the parameter estimation procedure.

The signal processing and parameter estimation procedure is carried out using code constructed in MATLAB using the process explained in section 4.2.2 - Signal Processing and section 5.2 - Parameter Estimation Method, respectively. Construction of a code is necessary, as the signal processing and parameter estimation processes contain a large amount of operations. If all of these operations were to be conducted manually on each occasion the process would take an extremely long time and there would be large room for human error. By constructing the code, the same analysis can be run in exactly the same way for each test, allowing direct and accurate comparisons to be made. The code also processes the data many times faster than could be done if each operation was carried out by the user. It is possible to input the required test parameters and test data directly into the code. However, this is not ideal if this is being done regularly, or by someone who is not familiar with the code.

In order to overcome this problem a general user interface (GUI) was created for users of the code to use without having to access the code itself. The GUI was created within MATLAB and is linked directly to the signal processing and parameter estimation code. The GUI is designed to be used by the author and personnel at Honda R&D Europe for an interim period. It is intended that once the engineers at Honda have built up experience testing with the rig and GUI, that a new signal processing and parameter estimation code and GUI will be created professionally for Honda based on the work and existing code from this project.

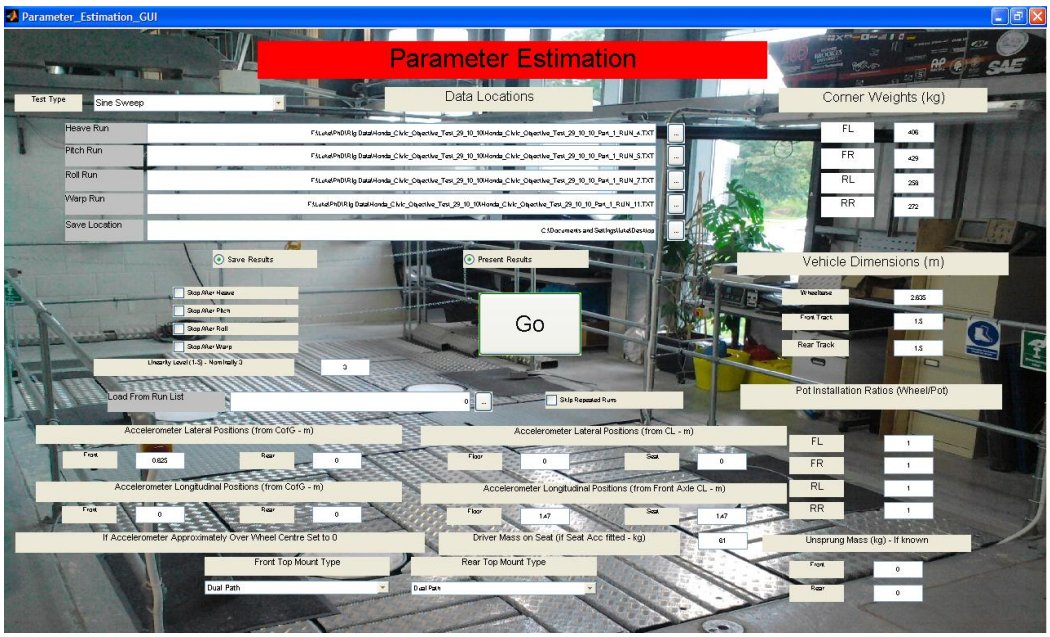

Figure 4-31 – Parameter Estimation GUI

The parameter estimation GUI is shown in Figure 4-31. Parameters such as the corner weights, vehicle dimensions, suspension potentiometer installation ratios and accelerometer positions are loaded directly from the values in the 'Run List' explained in section 4.2.1 - Organisation of Data Files. To select the data to be analysed the user can either directly type in the data location and name for each of the input modes and save location folder, or browsers by the side of the text boxes can be used to select the file locations, as shown in Figure 4-32.

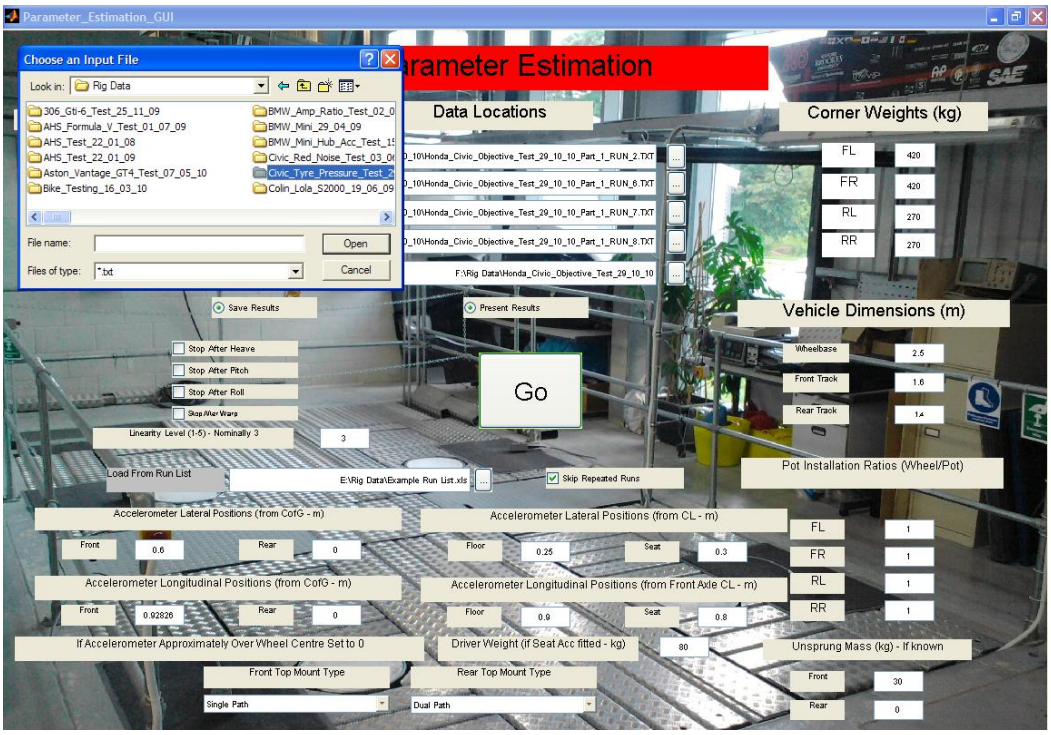

Figure 4-32 – File location browser

Other options on the GUI are the ability to skip repeated runs. In the case of a normal rig test a variety of heave amplitudes may be used to asses the non-linearity whilst only one or two roll runs used. It is not desirable to re-analyse these roll runs each time if the same data is used, so data from these runs is simply loaded from the existing saved data to save time. Other options are the 'Stop After …' check boxes. These can be ticked only one at a time and stop the signal processing and parameter estimation code once the desired run has been completed. This is used if the user wants to look in more depth at the details of the rig data, for example the filtered time domain outputs. These would not normally be exported in the saved data set, as they are not used directly to compare different vehicles or set-ups. There are also check boxes to determine if the data analysed is to be saved and whether results plots are desired once the signal processing and parameter estimation code is complete.

On pressing the 'Go' button the parameters entered into the GUI are saved and signal processing and parameter estimation code is executed. The output from the code is a list of estimated parameters, measured responses and performance and comfort index measures from each of the four data sets saved in the desired location. If the plotting of results has been

requested a number of plots showing the vehicle response and measured parameters are presented.

For the benchmarking case this point marks the end of the test and the vehicle can be de-instrumented and removed from the rig. In the case of a vehicle to be tested with different suspension components the vehicle is de-instrumented to the required state (String Potentiometers and Hub Accelerometers removed if wheels are to be removed) before the components are changed. After changing the required components the vehicle is then re-instrumented and re-tested using the inputs described in 4.3.2 – Testing the Vehicle.

4.3.4 - Analysed Data Comparison

Whether the test being conducted is for benchmarking purposes or for tuning of a single vehicle, it is desirable that the response results of different runs are compared as well as the comfort and performance index values. In order to make this process very simple an 'Analysis Comparison GUI' is used to select the runs to be compared. The GUI is simply used to determine which runs are compared, with a maximum of four per input mode allowed.

Once the runs have been selected the results that were obtained and saved during the signal processing and parameter estimation are loaded and plotted so that comparisons can be made.

The user can select the results to be plotted from a list including:

- Body Acceleration Responses
- Upright Acceleration Response
- Contact Force Responses
- Comfort Responses

An example of the Analysis Comparison GUI is shown in Figure 4-33.

Figure 4-33 – Analysis Comparison GUI

With the results plotted the user can compare the response results of the different vehicles or set-ups to obtain a better understanding than simply using the performance and comfort index values. For example two very different vehicles could have the same comfort index with very different responses. If one of the vehicles had a lightly damped body mode (<20% critical) and

the other had a moderately highly damped body mode (~50% critical) then their overall comfort index in Heave may be very similar, whereas the ‘feel’ of the vehicle would be very different in each case. It is also useful to compare the response results for the same vehicle set-up with different input amplitudes to note the non-linearity of the vehicle.

4.3.5 - Simulation Model Parameter Sweeps

In the case where a rig test is being used to tune a single vehicle, tuning of the vehicle can be assisted with the use of simulation model sweeps to minimise the amount of physical component changes and physical tests that take place.

The simulation model used for this is explained in section 6 - Vehicle Model. As with the parameter estimation and analysis comparisons, the running of the simulation model is carried out through the use of a GUI. An example of the Simulation Model GUI is show in Figure 4-34.

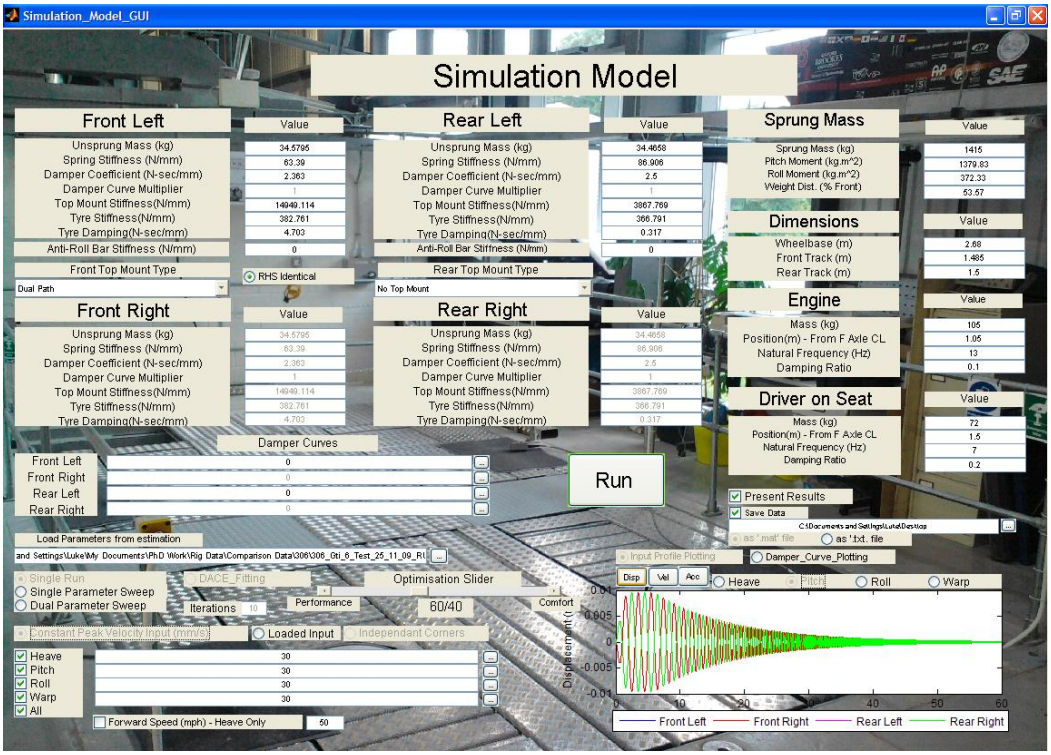

Figure 4-34 – Simulation Model GUI

The Simulation Model GUI has many different options and parameters that can be changed (70+) in order to allow it to be used in a variety of ways for a large variation of vehicles.

In the single vehicle tuning case the input used in the simulation is matched to the desired input of the vehicle on the rig. The original parameters are selected by loading the estimated parameters from the parameter estimation of the vehicle on the rig. In most cases this results in the model being completely linear, but there is also the option of loading damper curves directly from the analysed data or damper dynamometer test or even a simulated damper curve using a damper model. In this case the overall magnitude of the damper force can be altered, but the shape remains the same. This is of use when the engineer has decided on a certain damping characteristic to give a certain 'feel' to the vehicle handling, but the optimum magnitude of the damping required is not known.

The first step carried out in the simulation model is to run a set of tests with the same input as the rig and the original estimated parameters. The output data is then saved as a '.txt' file and the results analysed using the Parameter Estimation GUI and compared to the actual rig responses using the Analysis Comparison GUI. At this stage it can be established whether or not the simulation is a suitable representation of the real vehicle. In some cases simple modelling of the engine's vertical vibration on its mountings, or the driver on the seat may be necessary to provide a better simulation.

Once an adequate simulation has been achieved, tuning of the simulation model can take place. There are two main options for this; the first is to use a single parameter sweep and the second a dual parameter sweep. In both cases the selected parameter/s are swept through values from their input 'Min' to 'Max' values through the selected number of iterations. In the case of the dual parameter sweep the number of iterations may actually be larger than the user input, as the sweep matrix must be square.

For each of the iterations the comfort and performance index values are calculated in the same way as in the parameter estimation program. The outputs from the simulation are three plots showing the effect on comfort index, performance index and comfort/performance compromise due to the parameter/s. The compromise factor is determined using the 'Optimisation Slider'. The user can select the whether the vehicle is to be performance biased, comfort biased or anywhere in between. This output for the compromise index is only to be used as an indication, as it is very difficult to determine the relative importance of comfort and performance. Examples of the comfort, performance and compromise plots for a dual parameter sweep are shown in Figure 4-35 to Figure 4-37.

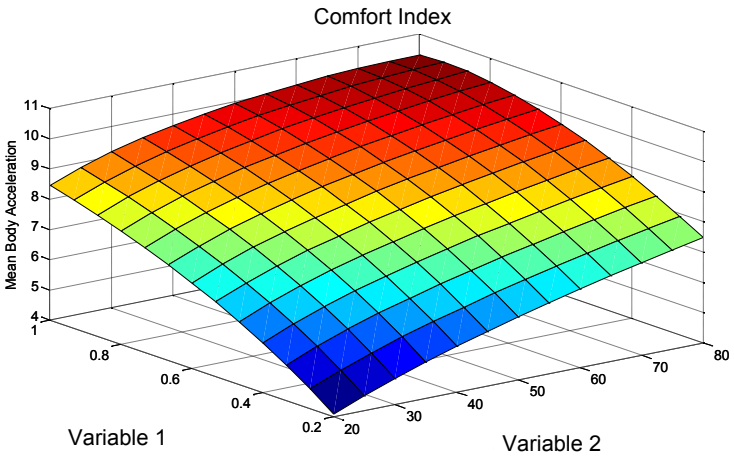

Figure 4-35 – Comfort Index - Dual Parameter Sweep

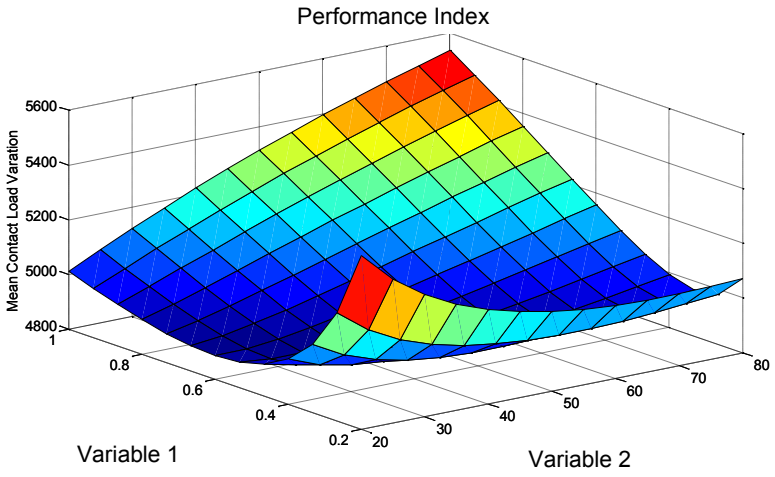

Figure 4-36 – Performance Index – Dual Parameter Sweep

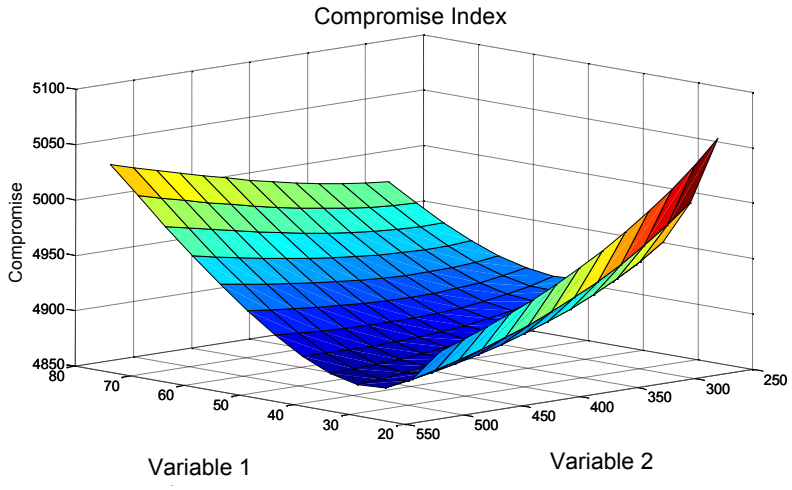

Figure 4-37 – Compromise – Dual Parameter Sweep

The results from the simulation model can be used to determine the component parameters most likely to provide the desired comfort and performance index values. This way the number of physical tests to be carried out on the vehicle and the number of components required is dramatically reduced.

4.4 - Four-Post Rig Method Limitations

The four-post rig is a very useful tool for analysing the response of a vehicle to road inputs, but like any method of testing there are limitations to its use and accuracy compared to a vehicle driving over an actual road surface.

One of the main factors in which the rig is different to the vehicle travelling on a real road is the rotation of the tyres. This has an effect in more than one way. This section explains the differences between the effects seen from rotating and non-rotating wheels in three areas;

- Tyre Stiffness
- Wheel/Tyre Imbalance
- Roll Response

4.4.1 – Tyre Stiffness

Figure 4-38 below shows an example of tyre stiffness change with speed. As the speed of rotation is increased so is the stiffness. This implies that the tyre stiffness experienced during a rig test is lower than it would be on the road. One way to improve this would be to increase the tyre pressure used when testing to simulate a higher stiffness. However, this would require knowledge of the tyres fitted to each vehicle tested on the rig.

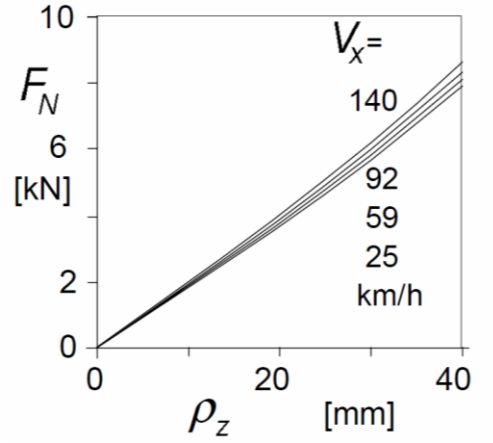

Figure 4-38 – Tyre Deflection and Growth with Speed – Pacejka [58] p464

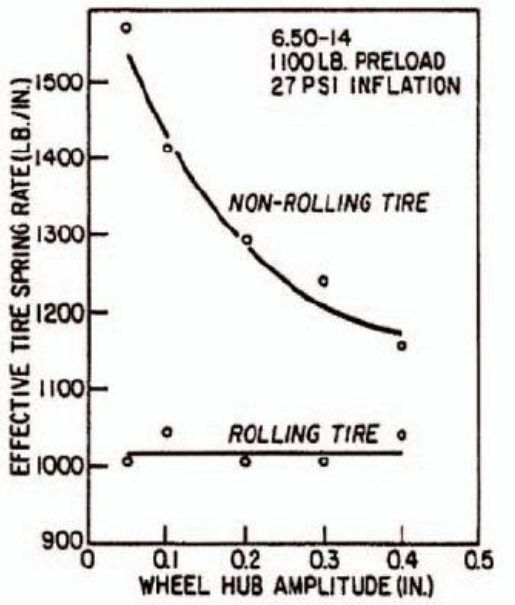

Figure 4-39 – Tyre Stiffness Non-linearity – The Pneumatic Tire [77] p368

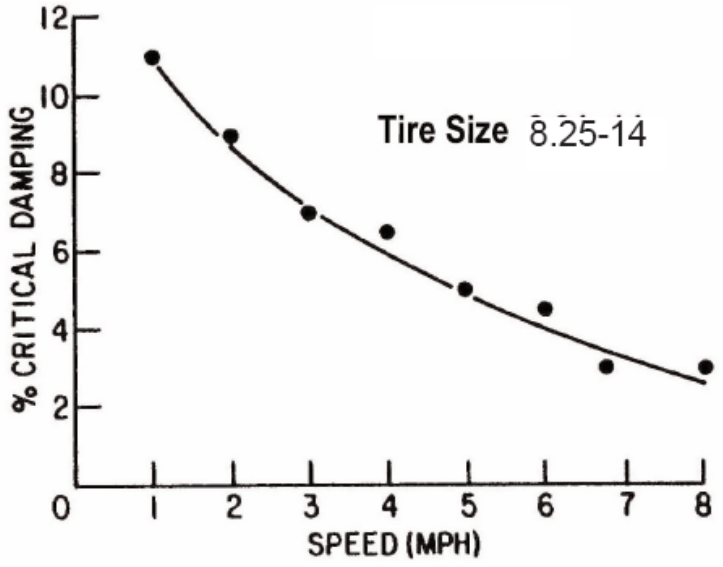

Figure 4-40 – Tyre Damping Speed Dependency – The Pneumatic Tire [77] p368

Figure 4-39 and Figure 4-40 show tyre stiffness amplitude non-linearity and damping speed dependency taken from The Pneumatic Tire by Gent and Walter [77]. The differences between the rolling and non-rolling tyre are quite significant. With the rolling tyre the stiffness remains approximately constant with increasing deflection. In the case of the non-rotating tyre, the stiffness reduces by around 25% (between 1.5 and 8.9 mm of tyre deflection), but still remains 15% larger than the rotating tyre.

The critical damping percentage in Figure 4-40 changes significantly over a small speed range, reducing as speed is increased. This indicates that the damping ratio of tyre related modes for a non-rotating tyre will be increased.

One quote in The Pneumatic Tyre [77] states 'Most investigators believe these changes in spring rate and damping are the result of the tire footprint constraint being relaxed as the tire begins to rotate'. By using the PTFE pad the level of friction between the tyre and ground interface is significantly reduced. This means that the constraint of the footprint is reduced, so the non-rotating effects to stiffness and damping should also be reduced. Figure 4-41 shows the extracted dynamic tyre stiffness from a series of increasing amplitude tests on the four-post rig. It is clear to see that the stiffness does indeed reduce with increasing amplitude as seen in Figure 4-39. In this case the stiffness was found to reduce by 8.5%, from 1.57 to 3.63 mm tyre deflection, showing that although the PTFE pad reduces the friction level, it does not allow the tyre to be independent of amplitude.

It is clear that it is not possible to simply simulate the true behaviour of a rotating tyre during a four-post test. However, if all vehicles are tested using the same conditions and inputs then it is still valid to compare the relative responses of the vehicles for benchmarking purposes.

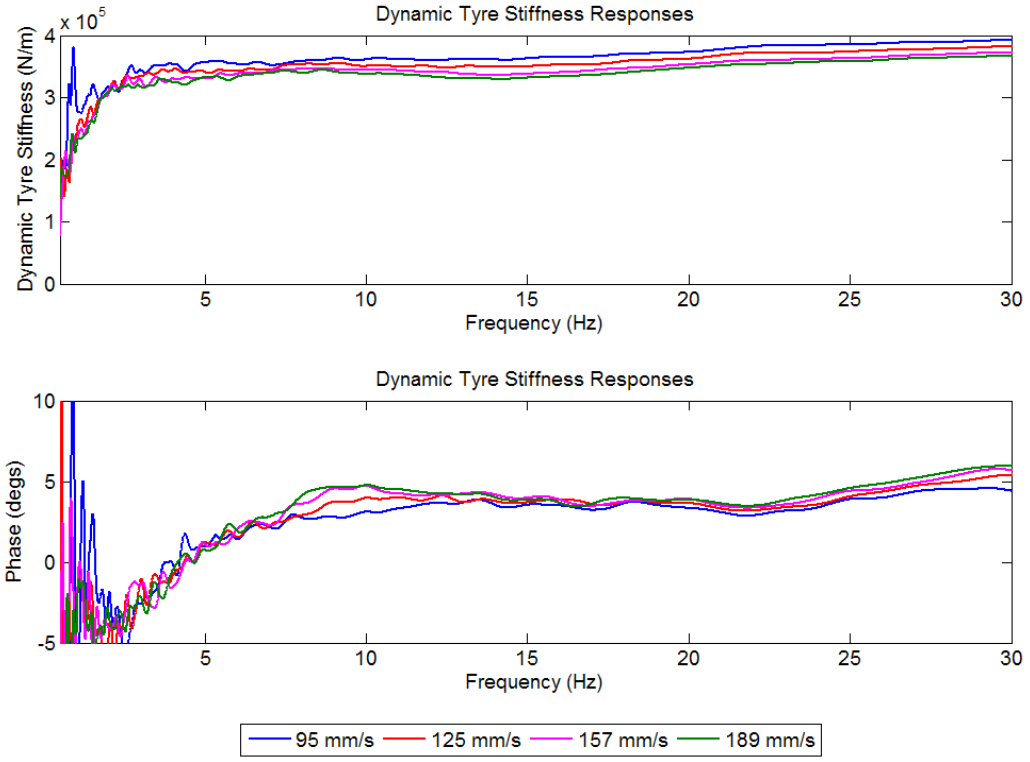

Figure 4-41 – Tyre Dynamic Stiffness Amplitude Dependence

4.4.2 – Wheel/Tyre Imbalance

With a rotating wheel, any slight imbalance of the wheel and tyre will cause an unbalanced centripetal force on the wheel mounting. Once resolved into the vertical wheel axis, this force causes acceleration of the unsprung mass and in-turn sprung mass. When the rotational speed of the wheel is close to the unsprung mass natural frequency then the magnitude of the sprung mass acceleration could become large and very uncomfortable for the vehicle occupants. In addition with large acceleration of the unsprung mass the contact patch force variation would also be large, causing a loss of available grip.

When a vehicle is tested on the rig and the wheels are not rotating the significance of this situation is not measured. However, using parameters acquired from the parameter estimation, the response of the sprung mass to this type of excitation and the forward speed at which it will occur can be estimated. Figure 4-42 shows an example of a two-degree-of-freedom eccentric base excitation system representing a single corner unsprung and sprung mass.

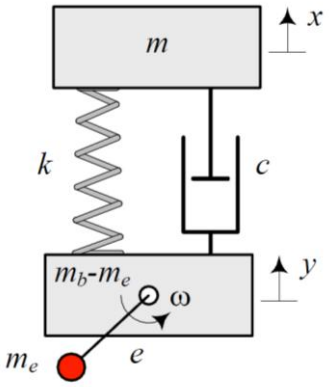

Figure 4-42 – Eccentric Base Excitation Model – Vehicle Dynamics Theory and Application [78] p 775.

Where:

m – Sprung Mass

m_b – Unsprung Mass

m_e – Unbalanced Mass

e – Distance between m_e and rotation centre

k – Spring Stiffness

c – Damping Coefficient

ω – Angular Velocity

4.4.3 – Roll Response

The most significant difference caused by the non-rotating wheels is the response of the vehicle in roll. During a roll input from the rig, in order for the vehicle to move laterally the tyres must deform laterally or the lateral forces at the contact patch must overcome the friction between the tyre and the actuator pad. However, in the rotating wheel case of a vehicle on a real road, for the same amount of lateral displacement a considerable longitudinal displacement would have taken place, so the lateral deflection of the tyre for the same input would be much smaller. In addition the lateral force generated at the tyre would be much smaller. The difference between the two cases makes the roll response of the vehicle on the rig much more sensitive to lateral tyre stiffness and the friction level. For the majority of tests a PTFE pad is placed on top of the actuator pad in order to reduce the friction between the tyre and actuator pad, but there is still enough friction to enable significant lateral tyre deflection in roll. An investigation was carried out to determine the sensitivity of the vehicle response to the friction levels between the tyre and actuator pad.

4.4.3.1 - Roll Response Investigation

In order to determine the effect of friction on the roll response of a vehicle tested on the four-post rig, a test was proposed where the vehicle was excited using two different constant peak velocity sine sweep inputs with two different friction conditions. The first friction condition was with the normal PTFE pads in place, and the second was with some low-friction plastic sheeting placed between the vehicle's tyres and the PTFE pads. The plastic sheeting was folded into a quarter of its original size to ensure that there was as little friction as possible. Figure 4-43 and Figure 4-44 present the contact force roll torque to rotational input acceleration response at the front and rear of a 5-Door Honda Civic tested at two different amplitudes in both normal friction and reduced friction cases.

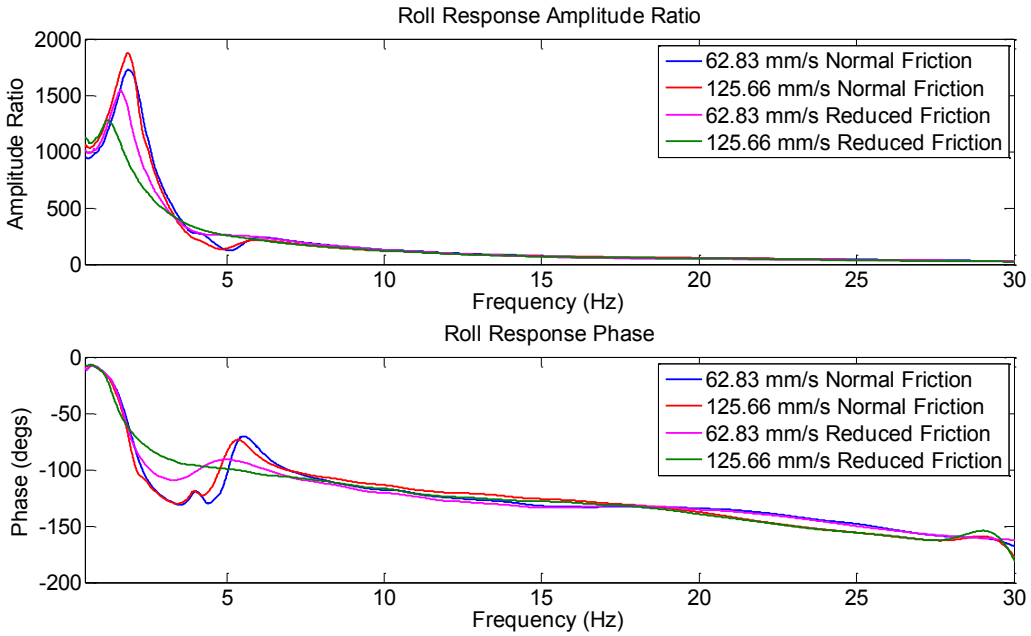

Figure 4-43 – Front Contact Force Roll Response

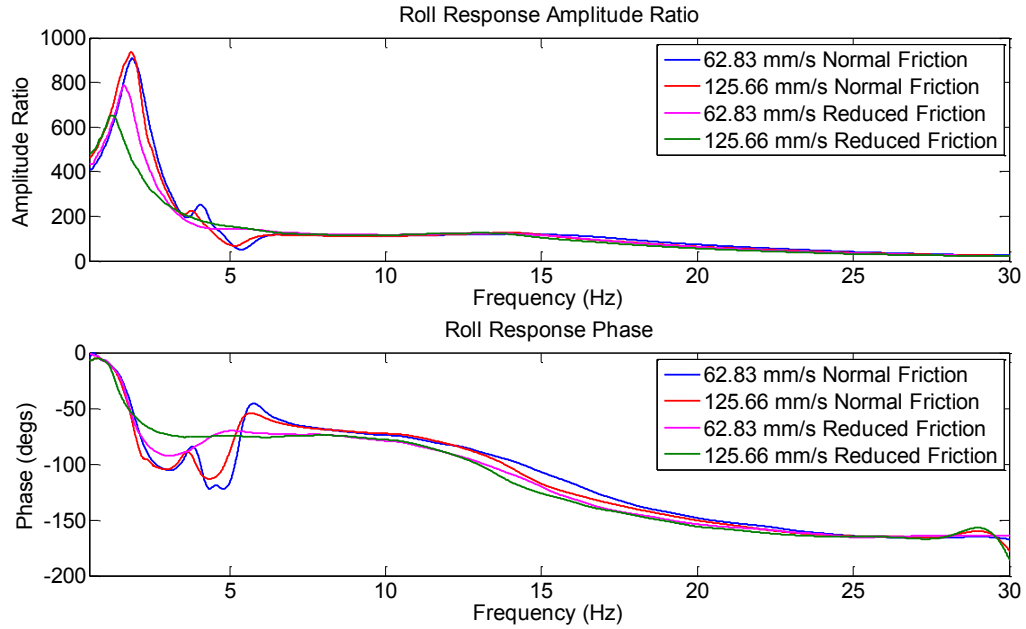

Figure 4-44 – Rear Contact Force Roll Response

The contact force roll responses in Figure 4-43 and Figure 4-44 show that significant differences arise by changing the friction level between the tyre and actuator, and in the low friction case also by changing the input amplitude.

In the normal friction case there is a slight increase in peak amplitude caused by a slight decrease in damping ratio. This is due to the digressive nature of the damper curves, especially

at the front of the vehicle. In the normal friction case there is significant lateral deflection of the tyre, but very little movement of the contact patch with respect to the actuator pad. With reduced friction, the amplitude of the mode is reduced significantly, along with a decrease in natural frequency. The response can also be seen to behave much more like a two degree-of-freedom fourth order system in the high amplitude low-friction case. The yaw acceleration magnitude of the vehicle on the rig was also significantly reduced in the low-friction case due to the roll-yaw coupling present with significant lateral tyre deflection. The cause of the increased sensitivity of the system to amplitude in the low friction case is due to that fact that there is no longer significant lateral tyre deflection, but there is significant lateral displacement between the tyre and actuator pad. This makes the system much more non-linear, as the friction is a constant force that is overcome at a certain level, whereas the lateral tyre stiffness is almost linear.

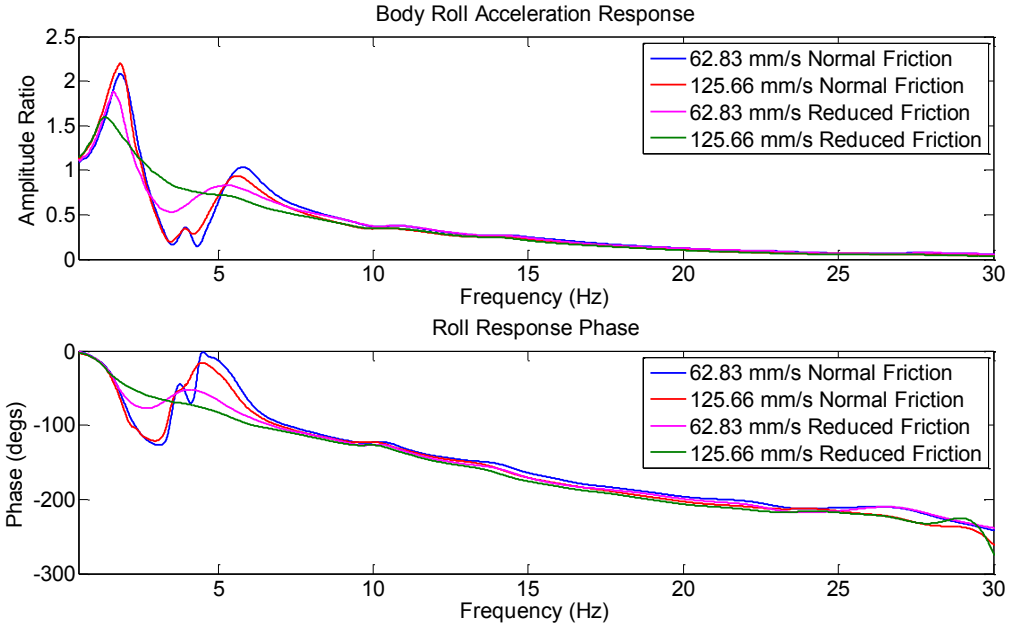

Figure 4-45 – Body Roll Acceleration Response

The body acceleration response in Figure 4-45 shows a similar trend to the contact force response in terms of the changes due to friction level and input amplitude. However, the relative amplitudes of the first and second peaks (high friction case) are much more similar in amplitude than in the contact force responses. As the majority of the contact force is due to the rotational acceleration of the body it would initially appear that the sprung mass moment of inertia in roll changes with frequency. Figure 4-46 and Figure 4-47 show the estimated front and rear roll inertias for the two friction cases and input amplitudes.

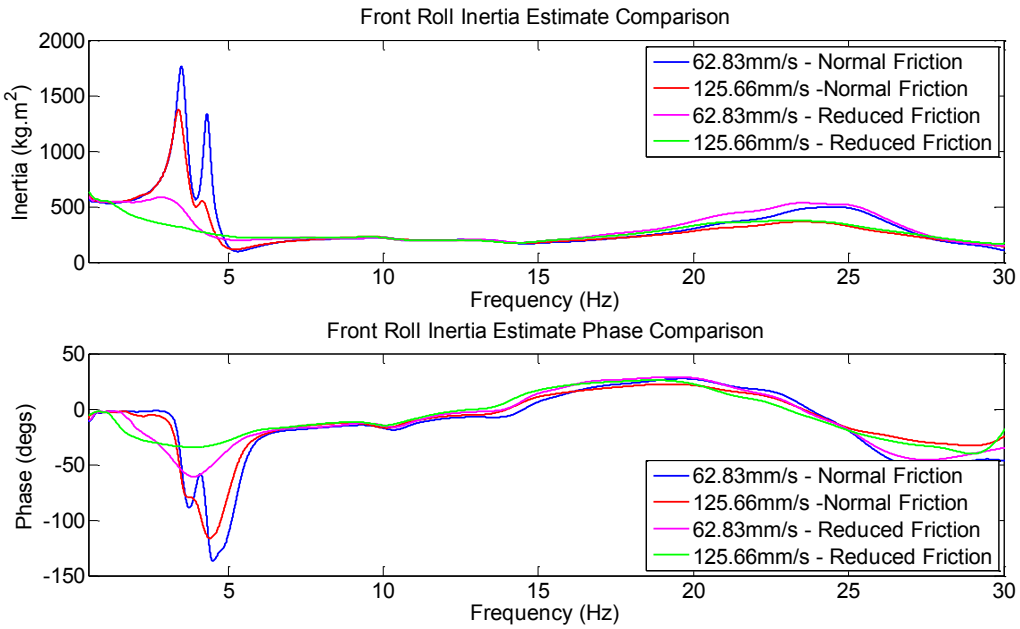

Figure 4-46 – Front Roll Inertia Estimate

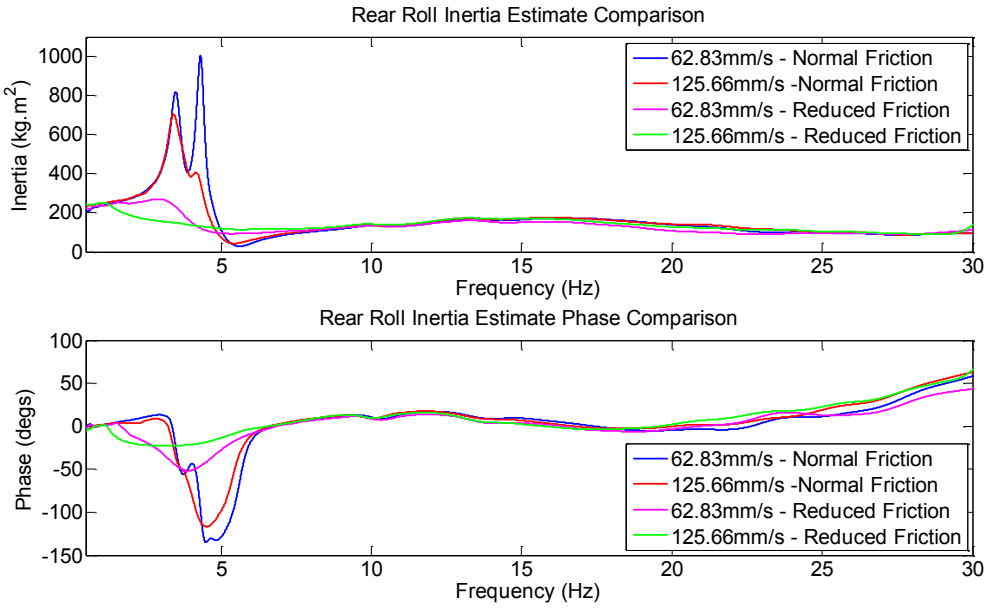

Figure 4-47 – Rear Roll Inertia Estimate

The roll inertia estimates are consistent between all runs at the start frequency (0.5 Hz) and between 7.5 to 17 Hz. However, in all cases the estimated roll inertia at the start frequency is considerably larger than in the 7-17 Hz range, especially at the front of the vehicle. This effect is caused by the rolling of the vehicle about a different vertical height dependant upon the input frequency, when the calculation assumes that the sprung mass always rotates around its CofG. Results displaying the migration of the roll centre height with frequency are shown in Figure 4-48 and Figure 4-49.

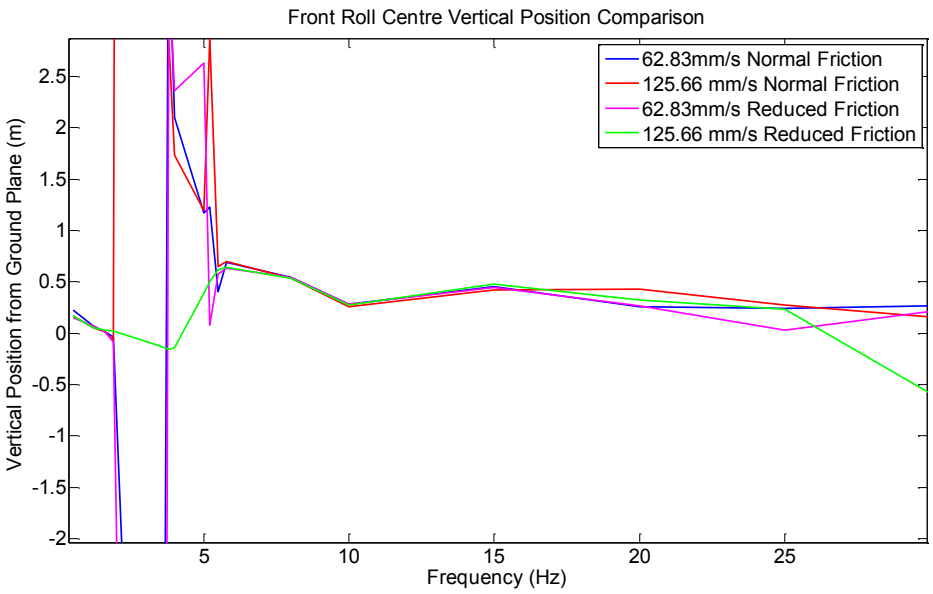

Figure 4-48 – Front Roll Centre Height

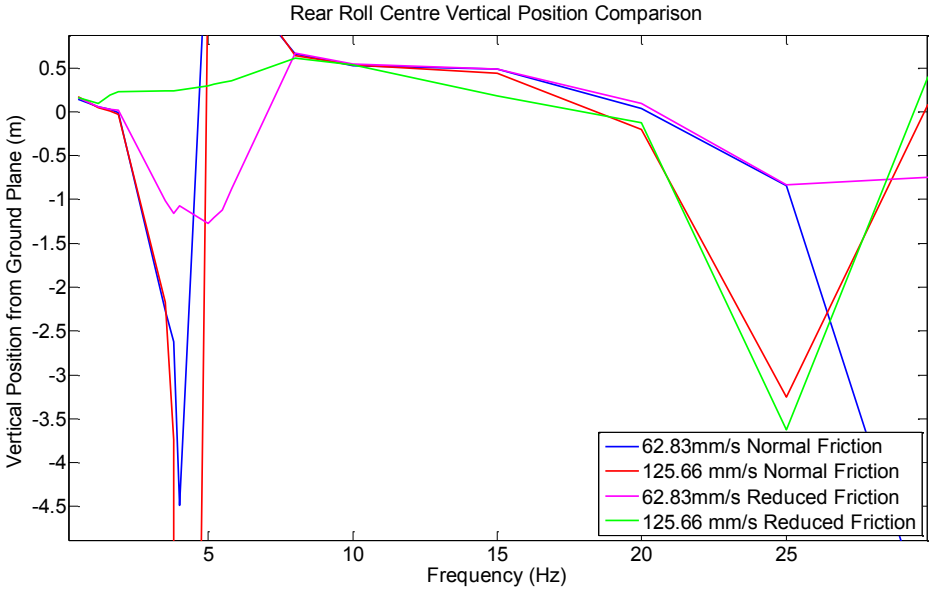

Figure 4-49 – Rear Roll Centre Height

The roll centre height was calculated by fitting accelerometers measuring both vertical and lateral accelerations at four positions on the vehicle body and calculating the resulting velocity vectors to determine the instant centre of rotation. The positioning of the accelerometers is show in Figure 4-50, whilst an example calculated roll centre is shown in Figure 4-51.

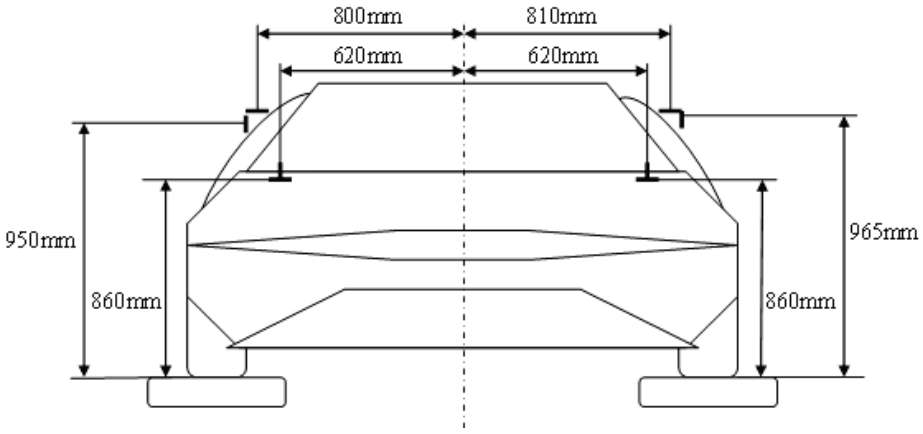

Figure 4-50 – Roll Response Investigation Accelerometer Positions

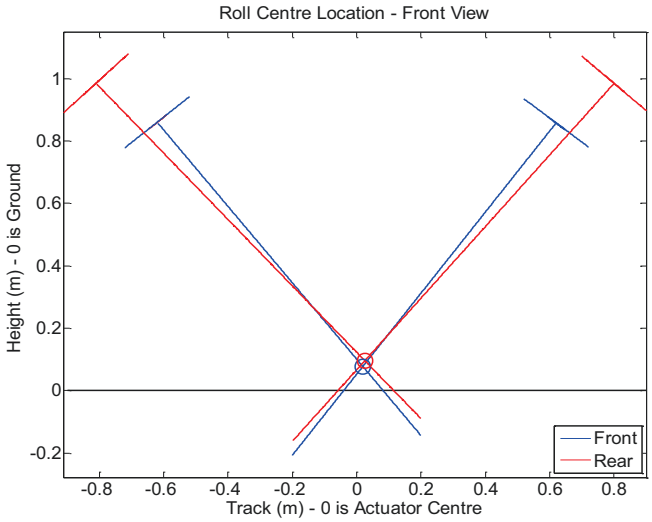

Figure 4-51 – Roll Centre Calculation

The results in Figure 4-48 and Figure 4-49, show that in all cases the roll centre can be seen to start at a height very close to the ground input plane, but by 7.5 Hz the height of the roll centre moves to a point close to the CofG height of the sprung mass (~0.64m). With the standard seven-degree-of-freedom model the sprung mass is forced to rotate around its CofG which can seen to not be the case when testing on the rig below 7.5 Hz.

In order to gain a better understanding of the effect of forward speed on the roll response, a test was carried out in ADAMS using a full kinematic and dynamic model of a vehicle and the same input used in when testing on the rig. The masses and dimensions of the vehicle were representative of the Honda Civic tested on the rig, as were the effective vertical spring stiffnesses, damping coefficients and roll stiffnesses. The tyre models used were PAC2002 tyre models using coefficients from a 235/60 R16 Tyre. Although the suspension layout was different to the Civic, the front and rear roll centre locations were matched to kinematics and compliance rig data supplied by Honda. The response of this model was not intended to exactly replicate

the vehicle on the rig, but to asses the changes in response with forward speed. Figure 4-52 shows and example of the ADAMS model used and Figure 4-53 shows the roll response for forward velocities of 0, 5, 10 and 25 m/s.

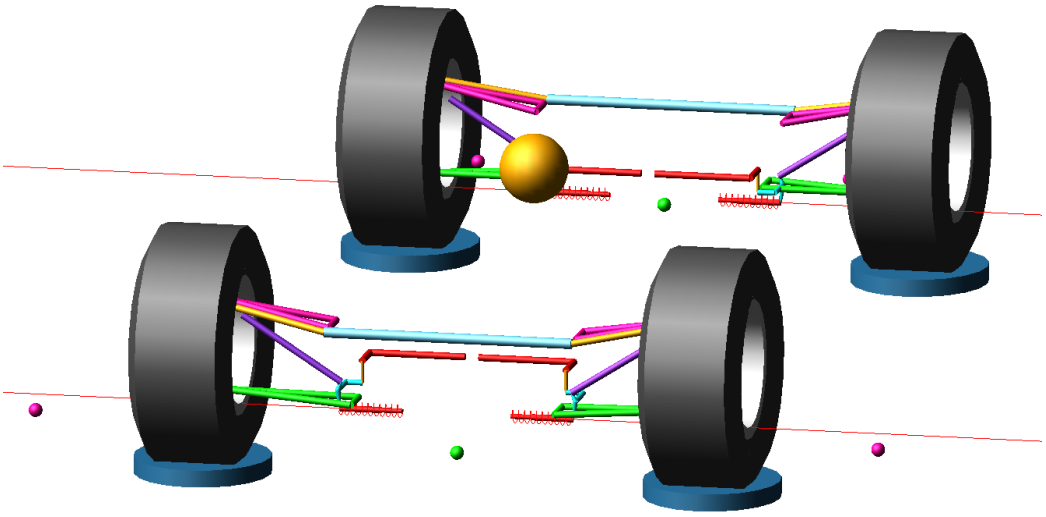

Figure 4-52 – Full Car ADAMS Model

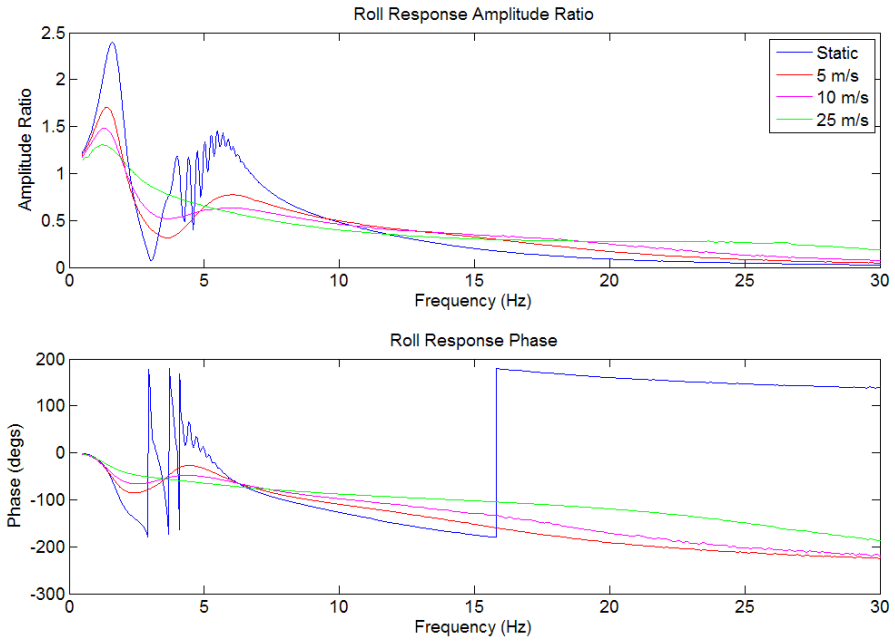

Figure 4-53 – FL Contact Force Comparison with Forward Speed

The roll response comparison shows that the contact force response changes significantly due to the forward speed of the vehicle. In the static condition the result is not completely smooth due to problems with running the tyre model at zero forward speed. Even with low forward speed of 5 m/s the response peak is reduced significantly, this peak decreases even further as the speed is increased. The roll responses produced by the ADAMS model for the 5 m/s and 25

m/s cases are quite similar to the normal friction and the low friction, high amplitude test cases from the rig test. The reason behind this change in roll response with speed in the ADAMS model is due to the slip angle generated by the lateral displacement of the contact patch. In the static case there is no longitudinal velocity, so even a small lateral velocity generates a large slip angle, which in-turn produces a lateral force and lateral deflection of the tyre. As the speed is increased, for the same amount of lateral velocity, the longitudinal velocity is increased. This reduces the slip angle, lateral force and lateral deflection. By doing this the roll response of the vehicle is much less sensitive to the lateral stiffness of the tyre and the roll response of the body about the roll centre and hence the damping ratio becomes larger.

This effect makes the roll response of the vehicle on the four-post rig difficult to apply comfort and performance weightings to, as the response on an actual road when travelling at normal speeds is likely to be very different. However, the information gained from the roll response of the vehicle on the four-post rig can be used to simulate the response of the vehicle due to a vehicle model without the inclusion of tyre modelling.

5 - Estimation of Vehicle Parameters

One of the main aims of this work is to enable vehicle optimisation through simulation. In order to simulate the dynamic behaviour of the vehicle accurately it is necessary to obtain accurate values of the vehicle parameters used in the model (Table 5-1). One way to obtain such parameters would be to measure a number of static and dynamic parameters for each component through disassembly of the vehicle, another would be to simply use design values from the manufacturer. Neither of these is satisfactory. In the first case, disassembly is time consuming and parameters so determined may not accurately reflect the installed values. In the second, the values are simply not generally available. This means that to enable an accurate simulation, all parameters required within the model must be acquired through either analysis of the four-post rig test data in the case of dynamic parameters, or through simple dimension measures, such as wheelbase and track for static parameters.

This chapter details the estimation of the parameters required for the simulation of a vehicle suspension and its subsequent optimisation. The process is problematic and a short review is made of the many methods that were attempted before a robust technique was developed.

From the literature review in section 2.6 – Parameter Determination, most of the methods relating to parameter determination of vehicle parameters are carried out by minimising the mean error between the response or output of the simulated system and the measured system, accepting the parameters that arise. A difficulty with these methods is that the parameters so obtained may not actually represent the best estimate for individual parameters themselves, rather that set of parameters which for the case in question produces the closest overall response. This cannot be then extended to optimisation since it is not necessarily the case that the modified parameters suggested through optimisation would result in exactly the improvements suggested. To avoid this problem the parameter estimation technique developed within this project aims to determine each parameter as individually as possible. The methods developed for the determination of vehicle parameters by these means is a new and original contribution to the field.

5.1 - Required Parameters

In order to simulate the response of the vehicle on the four-post test rig simplified to a 7-degree-of-freedom system, 20 different parameters are required (Table 5-1). When estimating parameters, symmetry about the longitudinal axis of the vehicle is assumed.

Parameter Symbol/s	Parameter Description	Units
M_2	Sprung Mass	kg
J_{2p}	Sprung Mass Pitch Moment of Inertia	$kg.m^2$
J_{2r}	Sprung Mass Roll Moment of Inertia	$kg.m^2$
FL_{m1}, FR_{m1}	Front Unsprung Mass	kg
RL_{m1}, RR_{m1}	Rear Unsprung Mass	kg
l	Wheelbase	m
F_t	Front Track	m
R_t	Rear Track	m
a	Distance from front axle to CofG	m
b	Distance from rear axle to CofG	m
FL_{ks}, FR_{ks}	Front Spring Stiffness	N/m
RL_{ks}, RR_{ks}	Rear Spring Stiffness	N/m
FL_{kt}, FR_{kt}	Front Tyre Stiffness	N/m
RL_{kt}, RR_{kt}	Rear Tyre Stiffness	N/m
FL_{ktm}, FR_{ktm}	Front Top Mount Stiffness	N/m
RL_{ktm}, RR_{ktm}	Rear Top Mount Stiffness	N/m
F_{ksr}	Front Anti-roll Stiffness	N/m
R_{ksr}	Rear Anti-roll Stiffness	N/m
FL_C, FR_C	Front Damping Coefficient	N-sec/m
RL_C, RR_C	Rear Damping Coefficient	N-sec/m

Table 5-1 – Required Parameters for 7-DoF Model

Some of these parameters can be determined by simple measurement of the vehicle, such as:

- l
- F_t
- R_t

By measuring the static mass of the vehicle on the actuator pads the lengths *a* and *b* can be approximated using equations (5-1) and (5-2).

$$b = \frac{Wd_F}{l} \tag{5-1}$$

$$a = l - b$$

(5-2)

Where:

Wd_f – Proportion of mass carried by the front wheels

These equations determine the lengths *a* and *b* relative to the weight distribution of the entire vehicle. Depending on the unsprung mass at the front and rear of the vehicle these lengths could be different for the sprung mass only and require recalculating once the unsprung masses have been determined.

All other parameters require estimation from dynamic analysis of the vehicle. As explained in section 4.1.2 - Data Acquisition System, there are a limited amount of sensors fitted to the vehicle, which provide information about the force, displacement and acceleration. Figure 5-1 shows a reminder of the available measurements at each corner of the vehicle.

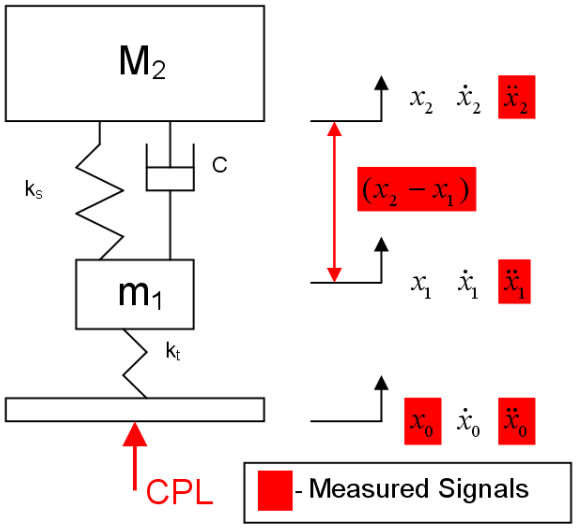

Figure 5-1 – Four-post Rig Measured Signals

5.2 - Parameter Estimation Method

This section of the thesis describes the final chosen parameter estimation methods implemented within the Parameter Estimation GUI MATLAB code used when analysing vehicle results from four-post rig testing. The methods were chosen based on robustness and computation time as well as accuracy.

The majority of parameter estimations are carried out using data from a heave sine sweep excitation, unless explicitly stated that data is from one of the other modal inputs.

5.2.1 – Tyre Stiffness Estimation

The tyre stiffness is the first parameter that can be estimated from the sine sweep rig data, as it requires no other parameters to be determined previously. Equation (5-3) can be used to calculate the tyre stiffness.

$$k_t = \frac{F_1}{x_0 - x_1} \tag{5-3}$$

Where:

F_1 – Contact Patch Load

x_0 – Rig Actuator Displacement

x_1 – Hub Displacement

As the hub displacement is not directly measured it must first be calculated from the hub acceleration. In the time domain this can be done by double integration of the hub acceleration signal. The hub displacement can then be subtracted from the actuator displacement signal to produce the tyre displacement. An example of the calculated tyre displacement and measured contact force signals are shown in Figure 5-2.

For the first 20 seconds of the test the estimation of tyre displacement is not consistent with the measured tyre force. This is due to very low acceleration levels at low frequency being overpowered by the much higher frequency (and higher acceleration) vibrations caused by the high frequency adjustment of the actuator's hydraulic control valve, as explained in 4.2.2 - Signal Processing. This high frequency content is filtered before the signal is integrated. The frequency reached by 20 seconds is 1.5 Hz, close to body mode natural frequency. After this point the tyre displacement signal is appropriate to use for stiffness estimation.

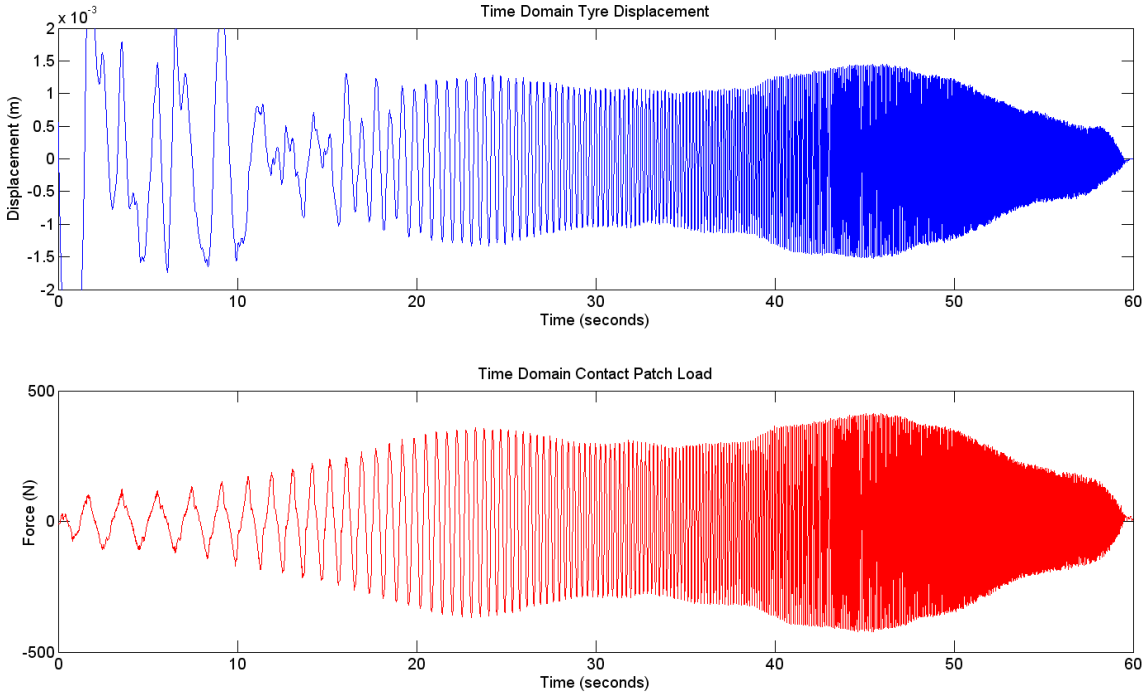

Figure 5-2 – Time Domain Tyre Displacement and Contact Patch Load

In order to calculate the stiffness from the two signals in Figure 5-2, the gradient of contact force against displacement can be fitted with a 1st order polynomial function. This can be carried out for the complete run, or if individual cycles are separated the stiffness can be evaluated at each cycle to note its changes over the frequency range.

The same calculation can also be carried out in the frequency domain. In the signal processing method explained in section 4.2.2- Signal Processing, responses were created for each of the measured signals with respect to their relevant corner input acceleration. The response of hub acceleration with respect to input acceleration can be used to calculate the response of tyre displacement to input acceleration simply by subtracting 1 and dividing by $-\omega^2$. As the contact force response is with respect to the same input acceleration the use of the responses in equation (5-3), simply cancels the input accelerations to produce the dynamic tyre stiffness. An example of tyre stiffness estimates using the time and frequency domain methods is shown in Figure 5-3.

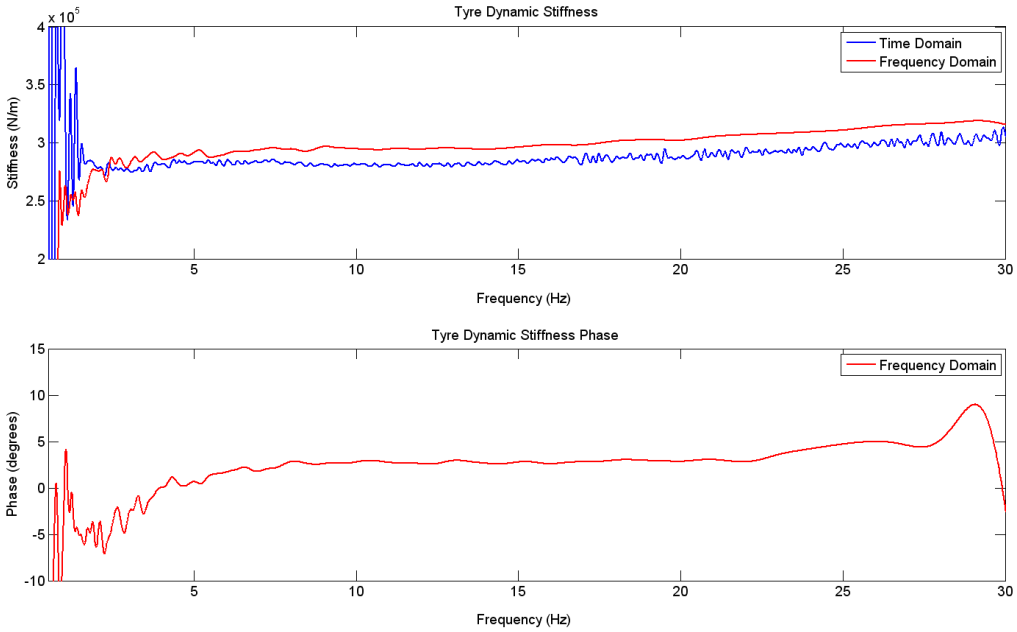

Figure 5-3 – Time and Frequency Domain Tyre Stiffness Estimates

The estimated tyre stiffness using time and frequency domain methods is fairly flat across the 3-30 Hz frequency range, with a very low phase angle of approximately 2.5° over the 3-30 Hz range, indicating that it is suitable to model the tyre as a simple spring. The estimate of tyre stiffness is ultimately estimated from the mean of frequency domain method in the 5-20 Hz range, as well as an estimate of tyre damping coefficient from the same frequency range. Within the script both methods are analysed and the estimates over the frequency range can be produced as a result for the engineer to analyse and compare.

The tyre stiffness estimation is carried out separately for each of the 4 tyres with left and right results averaged to produce front and rear stiffness values k_{tf} and k_{tr}.

5.2.2 – Unsprung Mass Estimation

The estimation of unsprung mass from four-post rig data was found to be the most challenging part of the project, with many different methods attempted, as explained in section 5.3 - Unsprung Mass Estimation Method Review. However, the unsprung mass estimation is essential for the accurate estimation of other vehicle parameters, due to the fact that all suspension component parameters and inertias are calculated from suspension forces, which are calculated from two measured signals and the estimated unsprung mass.

This section presents two unsprung mass estimation methods used within the Parameter Estimation GUI MATLAB code, as well as a rough estimate unsprung mass check that can be used by the engineer to determine if the main estimated unsprung mass is highly inaccurate.

5.2.2.1 – Unsprung Mass Estimation Check

In order to obtain a rough estimate of unsprung mass some simple manipulation of the equations of motion of the 2DoF quarter-car or 4DoF half-car systems can be used. For simplicity the 2DoF equations are used in this case, but the situation is valid for both systems.

In the 2DoF system, normalisation of the body acceleration by the hub acceleration produces a 1DoF sprung mass response function. The same operation on the contact force produces the sprung mass force with respect to the hub acceleration, with an added offset of unsprung mass, as can be seen in equation (5-4).

$$\frac{k_t(x_0 - x_1)}{\ddot{x}_1} = \frac{M_2\ddot{x}_2}{\ddot{x}_1} + m_1 \tag{5-4}$$

The ideal situation would be that zero body acceleration coincided with a large hub acceleration and large contact force. This way all the contact force would be due to acceleration of the unsprung mass, and there would be a high signal-to-noise ratio. Even if the zero body acceleration does not occur a large ratio of hub acceleration to body acceleration is desirable for the estimation of the constant unsprung mass offset. Applying this method in the time domain would cause problems due to dividing by very small numbers, as the hub acceleration signal passes through zero. For this reason and others the equation is implemented in the frequency domain from the calculated responses of the signals with respect to input acceleration.

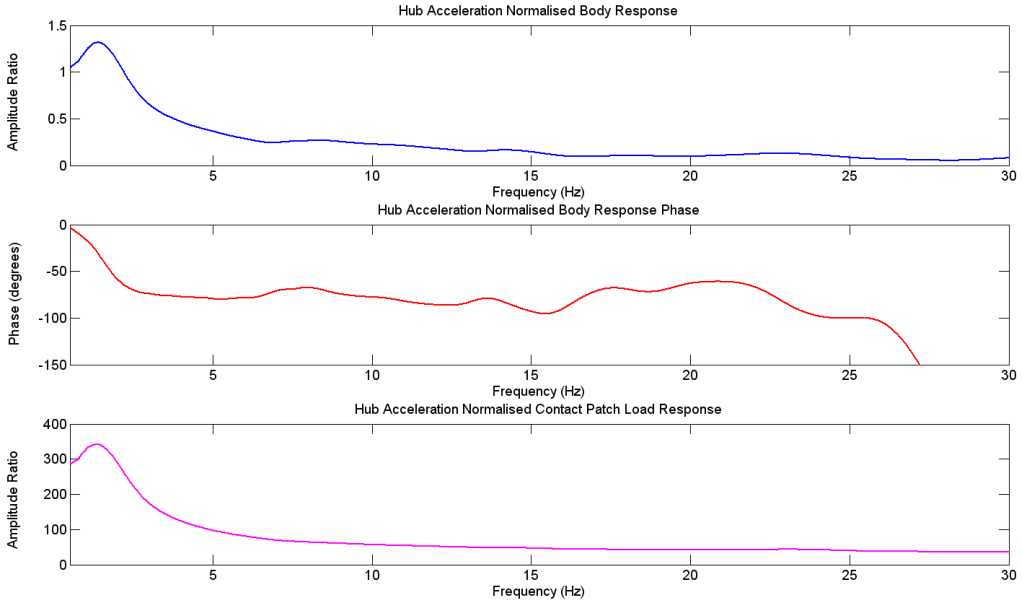

Figure 5-4 – Hub Acceleration Normalised Responses

The plots in Figure 5-4 show the responses of the hub acceleration normalised body acceleration and contact force. For this particular case, the amplitude ratio of body acceleration is lower than 10% in the 17-23 Hz range, along with a phase close to 90°. For this condition a large majority of the hub acceleration normalised contact force, would be expected to be due to the unsprung mass. For this particular case the unsprung mass evaluated in the 17-23 Hz range was found to be 42.5 kg, with a range of 1.26 kg. This method is not applicable when high damping is present and the phase angle between the body acceleration and hub acceleration does not reach 90°.

5.2.2.2 – Unsprung Mass Estimation using Time Domain Zeros and Peaks

The zeros and peaks method in the time domain uses the contact force, hub acceleration and body acceleration signals at each corner of the vehicle to attempt to find data points where it is suitable to estimate the unsprung mass. Considering equation (5-5) which can be used to determine the contact patch force of the 2DoF model, if the acceleration of the sprung mass is zero, then all of the contact force will be due to acceleration of the unsprung mass. As the two accelerations and contact patch force are measured, then the equation can be rearranged to calculate unsprung mass.

$$F_1 = M_2 \cancelto{0}{\ddot{x}_2} + m_1 \ddot{x}_1 \qquad \textbf{(5-5)}$$

For a simulated system we could expect the unsprung mass result to be correct for each instance that the body acceleration crossed zero. However, as the real vehicle system is more complicated than the 2DoF model and there will be some error in the measured signals, the problem has to be designed to be robust in its estimation from real vehicle data.

Considering the real vehicle system, the ideal occasion to estimate the unsprung mass is when the body acceleration is zero and the hub acceleration and contact force are at their peak within a cycle. In the case where hub acceleration and body acceleration are at 90° to each other then this will be true. However, finding data points at which the phase is exactly 90° may not be possible for many systems. In order for the method to work a tolerance must be applied to the locations of the body acceleration zeros and the peaks of contact patch force and hub acceleration. In circumstances where the error is less than the tolerance, the unsprung mass can be assessed. By only assessing the unsprung mass at values where the hub acceleration and contact patch forces are close to their peaks, the signal-to-noise ratio is large, so the estimates are less likely to be corrupted with electrical noise.

The procedure for this method is presented in the flow chart below:

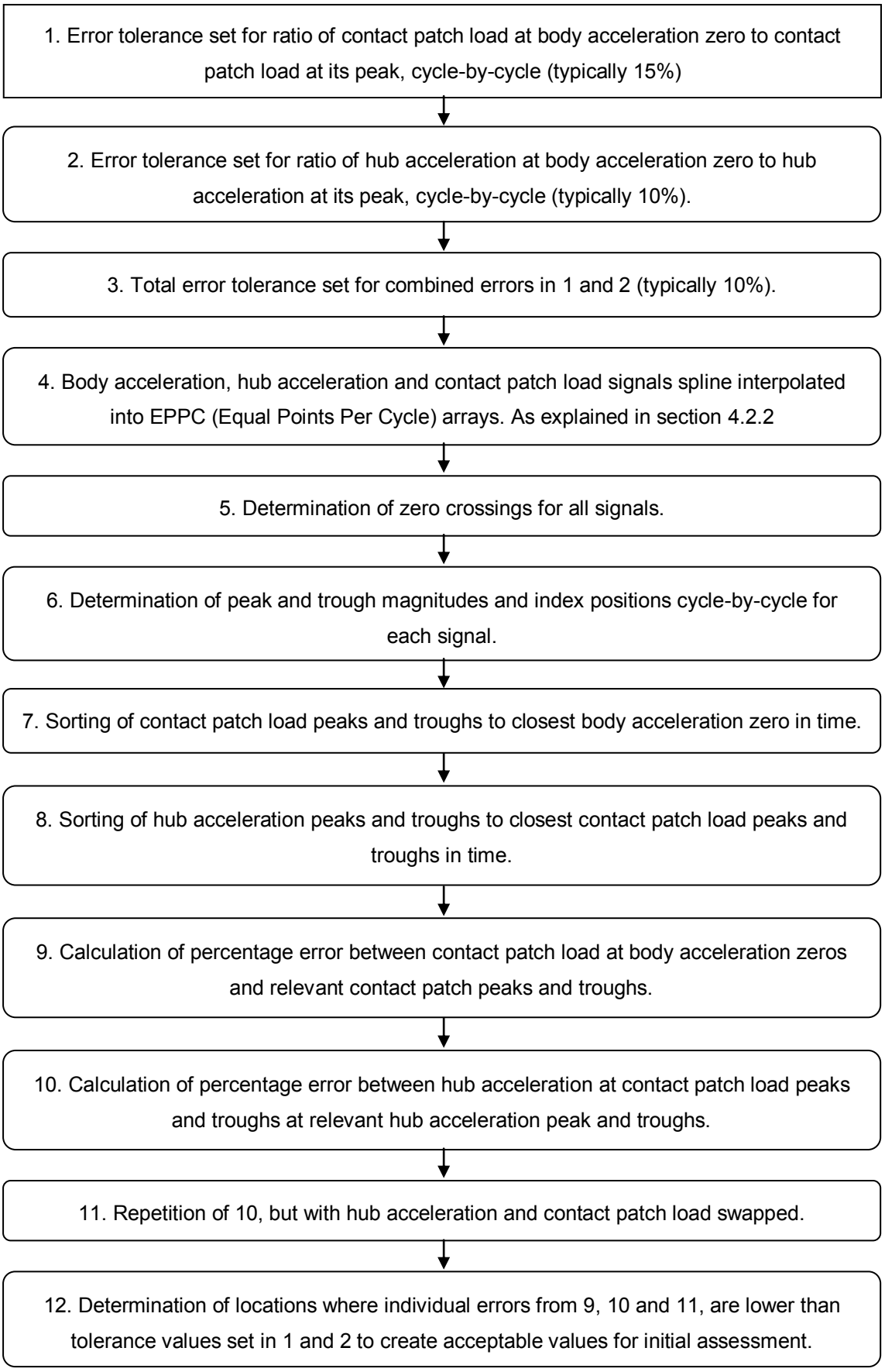
1. Error tolerance set for ratio of contact patch load at body acceleration zero to contact patch load at its peak, cycle-by-cycle (typically 15%)
2. Error tolerance set for ratio of hub acceleration at body acceleration zero to hub acceleration at its peak, cycle-by-cycle (typically 10%).
3. Total error tolerance set for combined errors in 1 and 2 (typically 10%).
4. Body acceleration, hub acceleration and contact patch load signals spline interpolated into EPPC (Equal Points Per Cycle) arrays. As explained in section 4.2.2
5. Determination of zero crossings for all signals.
6. Determination of peak and trough magnitudes and index positions cycle-by-cycle for each signal.
7. Sorting of contact patch load peaks and troughs to closest body acceleration zero in time.
8. Sorting of hub acceleration peaks and troughs to closest contact patch load peaks and troughs in time.
9. Calculation of percentage error between contact patch load at body acceleration zeros and relevant contact patch peaks and troughs.
10. Calculation of percentage error between hub acceleration at contact patch load peaks and troughs at relevant hub acceleration peak and troughs.
11. Repetition of 10, but with hub acceleration and contact patch load swapped.
12. Determination of locations where individual errors from 9, 10 and 11, are lower than tolerance values set in 1 and 2 to create acceptable values for initial assessment.

13. Calculation of unsprung mass estimates from contact patch load at acceptable hub acceleration peaks and troughs to create ‘under’ estimates, as estimate will be equal to or smaller than actual unsprung mass.

14. Calculation of unsprung mass estimates from hub acceleration at acceptable contact patch load peaks and troughs to create ‘over’ estimates, as estimate will be equal to or larger than actual unsprung mass.

15. Scaling-up of ‘under’ estimates by error factor between contact patch load at peak and estimate position. Scaling-down of ‘over’ estimates by error factor between hub acceleration at peak and estimate position.

16. Averaging of under and over estimates for peaks and troughs to create estimates for each acceptable peak and trough.

17. Calculation of summed, mean and total error from under and over estimates for each peak and trough.

18. Determination of peak and trough estimates within allowable total error set in 3.

19. For each peak and trough estimate within total tolerance a numerator and denominator is calculated. The numerator is the estimated value multiplied by a linear weighting function from 1 to 5. Where values at maximum allowable error are multiplied by 1 and values at no error are multiplied by 5. The denominator value uses the weighting function directly.

20. Estimates are created from all peak instances by using the peak numerator and denominator to create a weighted mean estimate based on the expected error. This is repeated for troughs.

21. Estimates are also calculated using both peaks and trough numerators and denominators to create an overall weighted mean estimate.

22. If no estimates are possible within the error tolerances defined in 1, 2 and 3, then an estimate of 0 is returned.

This procedure is carried out separately for each road wheel of the vehicle. Generally estimates are averages left to right to produce front and rear estimates of unsprung mass. However, if one of the left or right results are zero and the other not, then this is used as the estimate.

Although this method has many steps and is fairly complicated, it is computationally quite fast, requiring only 1 or 2 seconds in MATLAB on a computer with 3 GHz Intel processor and 2 GB of RAM. The method has the benefit of being able to determine if the estimate will be an under or over estimate of unsprung mass and also being able to predict the level of error of the individual and overall estimates. This way the engineer can note how accurate the estimate is likely to be and have varying degrees of confidence in the parameter estimates accordingly.

A disadvantage with this method is that it will not always produce results if the estimates are not within the allowed tolerances. This may be the case with high levels of damping where contact patch load and hub acceleration signals do not come close to being in-phase.

Figure 5-5 to Figure 5-8 present results from some parts of the estimation process graphically.

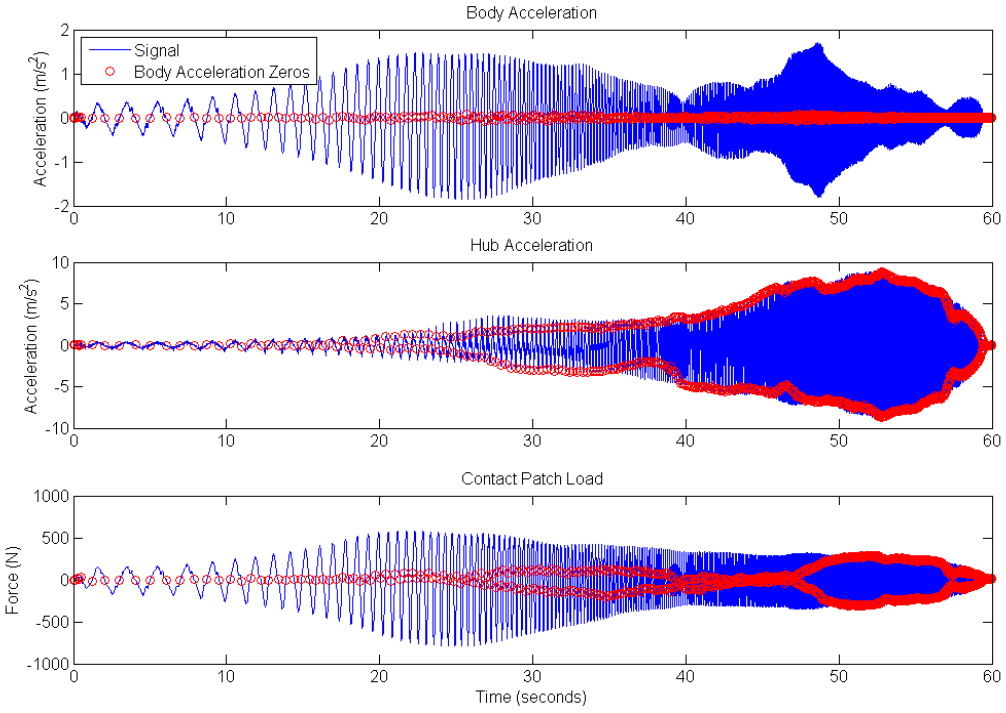

Figure 5-5 – Body Acceleration Zeros

Figure 5-5 presents the body acceleration, hub acceleration and contact patch load signals for one corner of the car, with the time of the body acceleration zeros plotted for each signal. From around 40 seconds the body acceleration zeros occur close to the peaks and troughs of the hub acceleration signal. However, it is not until between 50 and 57 seconds that the contact patch load peaks and troughs also coincide with the body acceleration zeros. It is at this point in the run that the unsprung mass can be estimated.

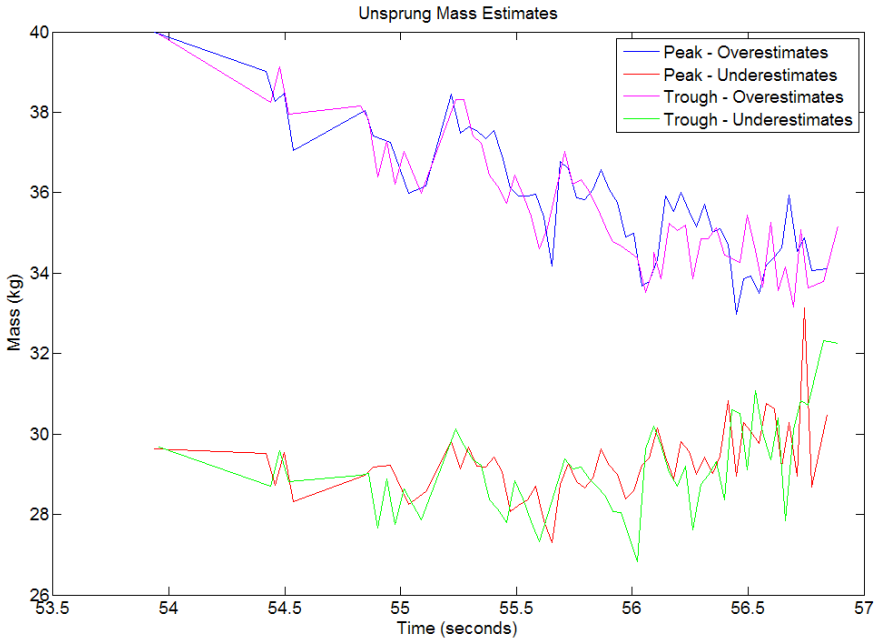

Figure 5-6 – Unsprung Mass over and underestimates

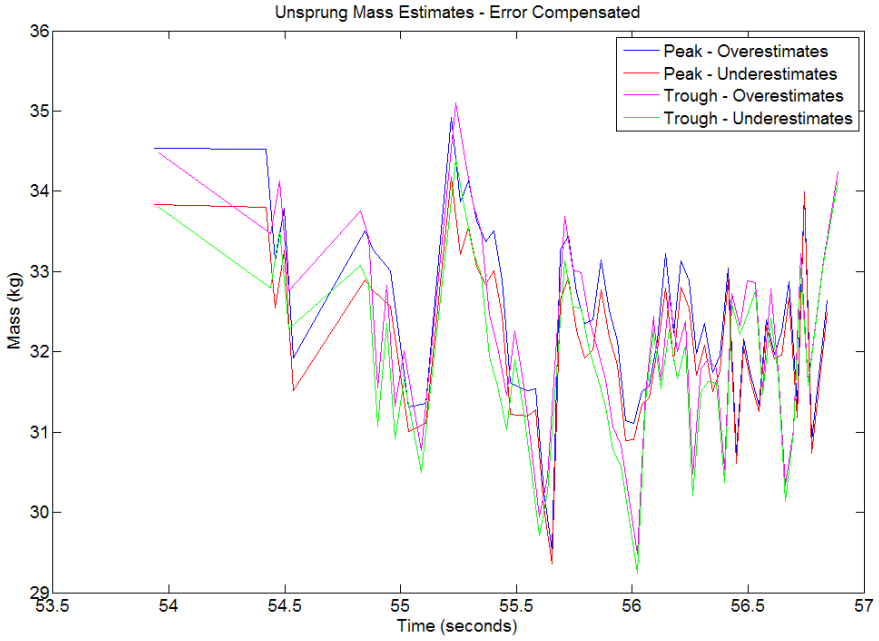

Figure 5-7 – Error compensated under and overestimates of unsprung mass

Figure 5-6 presents the under and overestimates from the peaks and troughs within the allowable tolerances set in operations 2 and 3. These estimates are then scaled up or down depending on their error to produce error compensated estimates as shown in Figure 5-7.

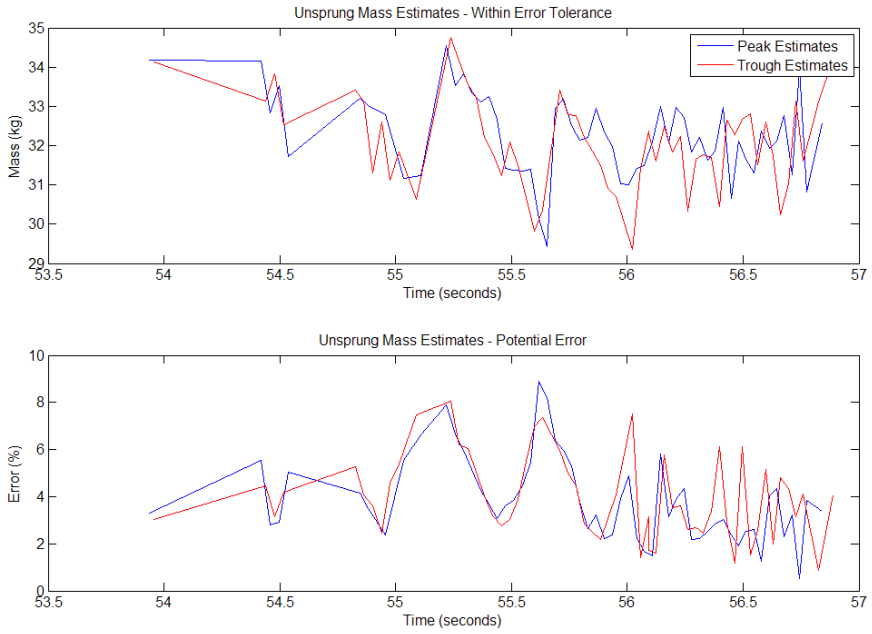

Figure 5-8 – Peak and trough unsprung mass estimates within error tolerance

The under and overestimates are averaged to produce peak and trough estimates (Figure 5-8). However, if the sum of their errors is larger than the tolerance set in 3, then they will be excluded from the final estimation of unsprung mass.

5.2.2.3 – Unsprung Mass Estimation using Dual Wave Simulation

If the method explained in the previous section is unable to provide estimates of unsprung mass, then a second method is used. This method uses the acquired vehicle responses from signal processing of four-post rig data and then simulates the response of the vehicle when excited by two combined sinusoidal inputs whose frequency and amplitude are varied. The properties of the input waves are adjusted in an attempt to achieve the situation in which body acceleration, suspension displacement and suspension velocity are all zero at the same instance. If the real vehicle were to behave like a 2DoF or 4DoF model then zero body acceleration would have to be zero, if both suspension force and velocity were zero, but at the real vehicle is not as simple as the models, then all 3 are retained for robustness. An example of the situation at which unsprung mass is evaluated is shown in Figure 5-9.

During four-post testing of the vehicle it was found that the situation where body acceleration, suspension displacement and suspension velocity were simultaneously zero could be achieved by using an input of two different sine sweeps superimposed and that results estimates of unsprung mass using this input were adequate. However the time requirement to create the condition was substantial. This method is discussed in section 5.3 - Unsprung Mass Estimation Method Review.

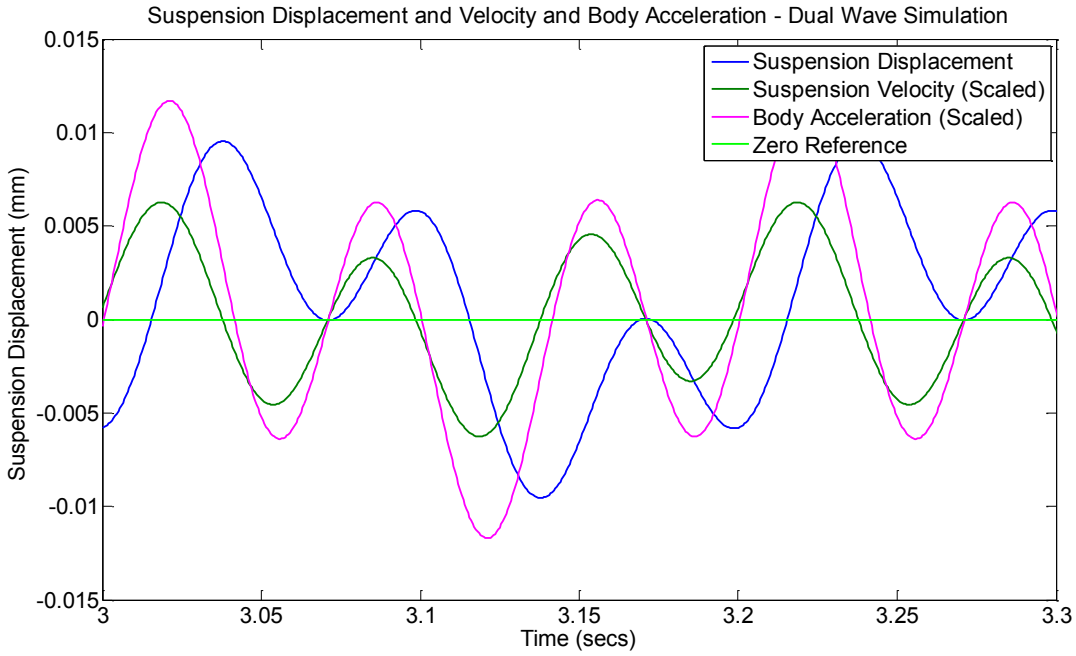

Figure 5-9 – Body Acceleration, Suspension Displacement and Suspension Velocity Simultaneous Zero

In order to measure the approximate error of assessing the unsprung mass at any one point a method was used that relied on initial approximate estimates of the sprung mass, suspension stiffness and damping. The approximate sprung mass comes from the assumption that the

unsprung mass will account for approximately 13% of the total mass of the vehicle. Then using this value to calculate a rough suspension force, initial suspension stiffness and damping coefficients are estimated using the methods presented in 5.2.3 – Spring Stiffness and Damping Coefficient Estimates. The error index then works by weighting the values of body acceleration, suspension displacement and suspension velocity by their relative mass, stiffness and damping coefficient to provide an error that can be used to asses how accurate the estimate of unsprung mass taken at that point in time would be.

Firstly, for each dual wave input a scaling factor is used that factors the maximum contact force by 0.1, so that an error value of 1 would mean that the force error due to the required signal would be 10%. This error value is then split into 3 (for the 3 different signals) and for each signal a scaling factor is produced based on the mass, stiffness or damping coefficient. The magnitudes of the signals are multiplied by their respective scaling factors to produce individual errors, which are summed to provide the overall error index. The process is explained in equations (5-6) to (5-13).

$$ScaleErr_{Total} = (\max|CPL|) \times 0.1 \tag{5-6}$$

$$Scale_{Disp} = \left(\frac{0.3 ScaleErr_{Total}}{ks_{Initial}} \right)^{-1} \tag{5-7}$$

$$Scale_{Vel} = \left(\frac{0.3 ScaleErr_{Total}}{C_{Initial}} \right)^{-1} \tag{5-8}$$

$$Scale_{Acc} = \left(\frac{0.3 ScaleErr_{Total}}{M_{2\,Initial}} \right)^{-1} \tag{5-9}$$

$$Err_{Disp} = |x_1 - x_2| \times Scale_{Disp} \tag{5-10}$$

$$Err_{Vel} = \left|\dot{x}_1 - \dot{x}_2\right| \times Scale_{Vel}$$

(5-11)

$$Err_{Acc} = \left|\ddot{x}_2\right| \times Scale_{Acc}$$

(5-12)

$$Err_{Tot} = Err_{Disp} + Err_{Vel} + Err_{Acc}$$

(5-13)

Where:

$ScaleErr_{Total}$ – Total Error Scaling Factor

$Scale_{Disp}$ – Suspension Displacement Scaling Factor

$Scale_{Vel}$ – Suspension Velocity Scaling Factor

$Scale_{Acc}$ – Body Acceleration Scaling Factor

$ks_{Initial}$ – Initial Spring Stiffness Estimate

$C_{Initial}$ – Initial Damping Coefficient Estimate

$M_{2Initial}$ – Initial Sprung Mass Estimate

Err_{Disp} – Error due to Suspension Displacement

Err_{Vel} – Error due to Suspension Velocity

Err_{Acc} – Error due to Body Acceleration

Err_{Total} – Total Error

For each dual wave input the unsprung mass is estimated at the point where Err_{Total} is at is minimum. To determine the lowest Err_{Total} and estimate the unsprung mass with the highest accuracy, a variety of dual wave inputs are used. The input consists of a low and high frequency sinusoid, where the higher frequency has a fixed relationship to the lower frequency, but the lower frequency and relative amplitudes of the two inputs are adjusted in each iteration. The method uses 3 iterative stages. The first is a wide range of frequency and relative amplitudes. From the minimum error values in this step the search is refined. This is then repeated for a second time to further refine the search range. The minimum error value from this final search is

used to estimate unsprung mass. For each stage a 15x15 matrix of the two input parameters is simulated in order to measure the predicted error and estimate the unsprung mass.

Figure 5-10 to Figure 5-12 show examples of the error index values and unsprung mass estimates for the 3 iterations of the procedure.

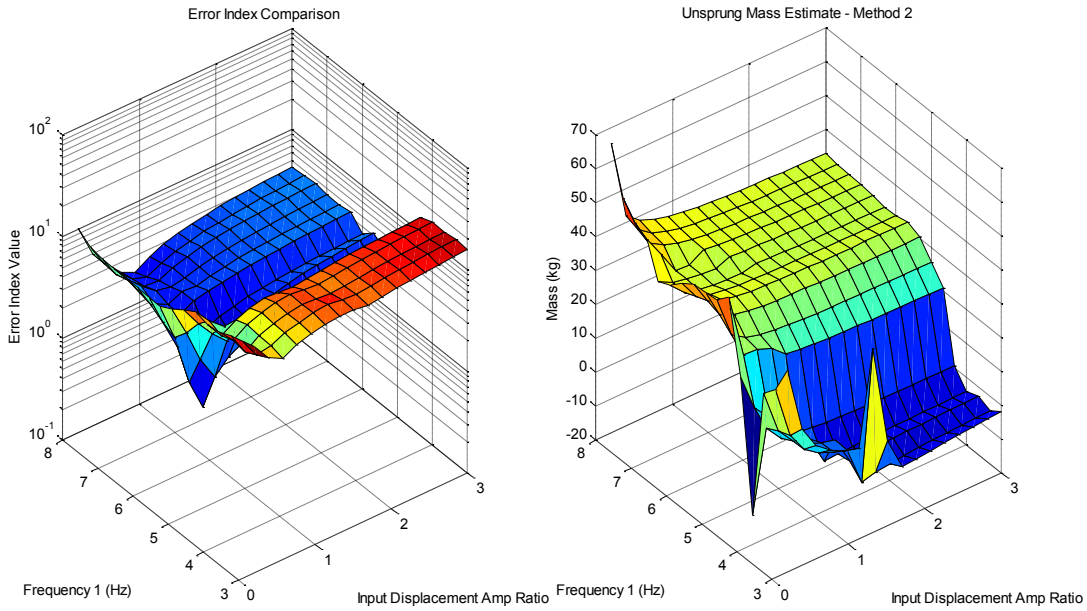

Figure 5-10 – Error Index and Estimated Unsprung Mass – Initial Iteration

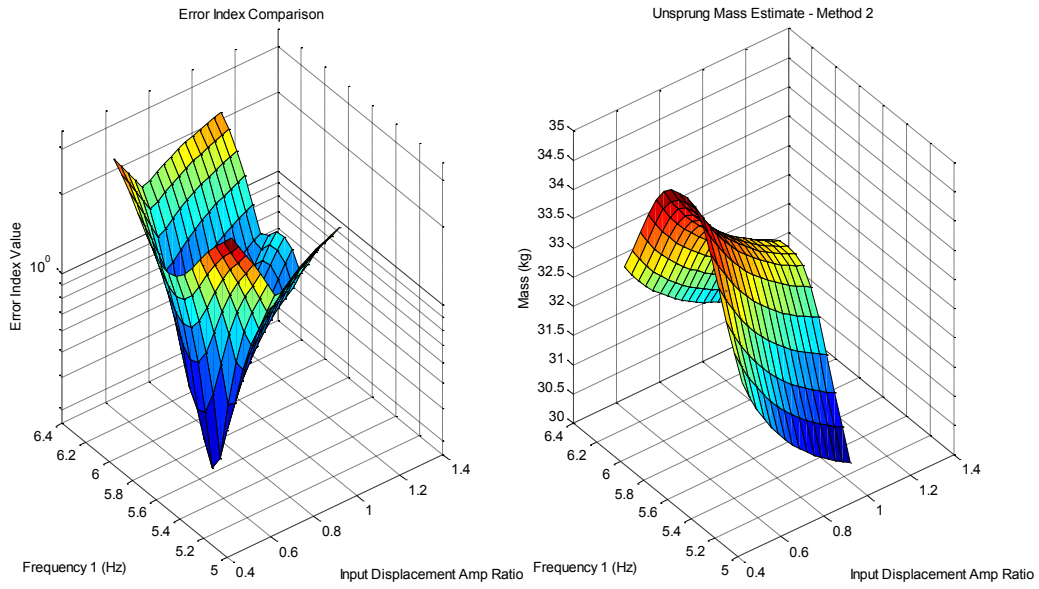

Figure 5-11 – Error Index and Estimated Unsprung Mass – Refined Search 1

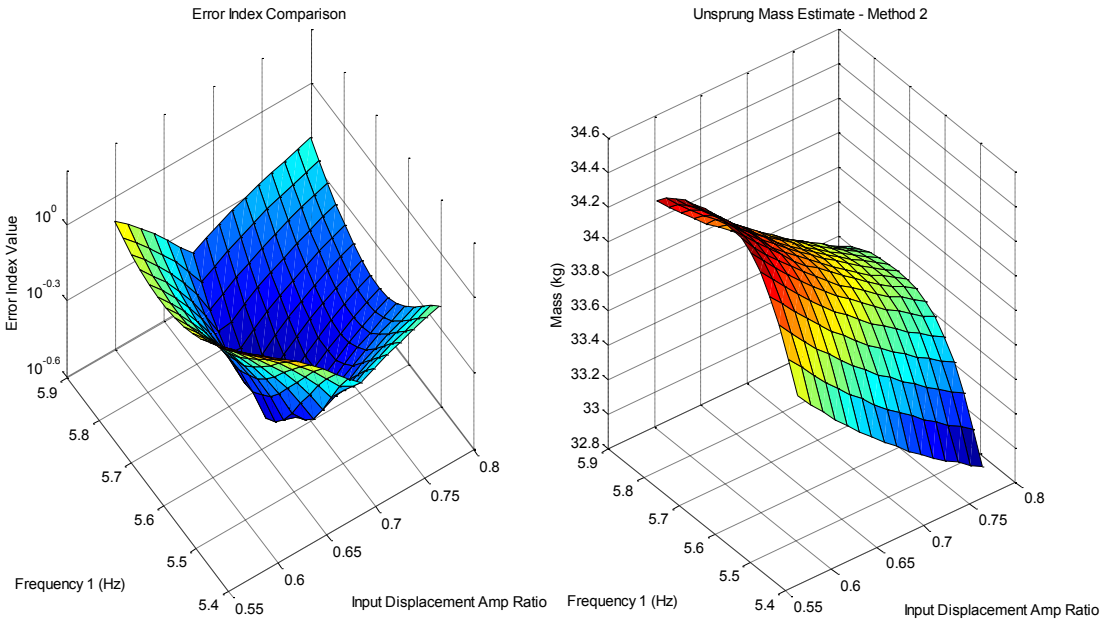

Figure 5-12 – Error Index and Estimated Unsprung Mass – Refined Search 2

The advantage of this method over the time domain method is that an unsprung mass result can always be created by manipulation of the two input waves. However, this comes with the disadvantage of increased computation time, typically 30 seconds using the same computer as the time domain method. The method is also sensitive to inaccuracies in the calculated responses, as these are used both to quantify the error and estimate the unsprung mass. For these reasons this method is only carried out if it is not possible to calculate the unsprung mass from the time domain method with the defined tolerances.

As with the time domain method, a predicted error is provided with the unsprung mass estimate to allow the engineer to be aware of how accurate the unsprung mass estimation is likely to be.

5.2.3 – Spring Stiffness and Damping Coefficient Estimates

Once the front and rear unsprung mass values have been estimated the suspension forces can be calculated by removing the unsprung inertial forces from the contact patch loads.

The suspension forces can then be used to estimate linear spring stiffness and damping coefficient values. These estimates are based on the assumption that the top mount is infinitely stiff. For some race cars the resulting errors are acceptably small and useful models without top-mount compliance can be developed. However, for any vehicle with appreciable top mount compliance, the resulting errors are not acceptable. The next section details how the spring stiffness, damping coefficient and top-mount stiffness can be determined from measurements in the time domain. The method presented requires an initial estimate of the spring and damper values in order to converge and the main purpose of this section is to present the method by which these initial estimates are prepared.

All of these measurements use the suspension displacement directly from the string potentiometer and velocity differentiated from this with respect to time, although integration and double integration of difference between body and hub acceleraions could be used to determine velocity and displacement respectively.

As with the time domain tyre stiffness calculation, the suspension stiffness and damping coefficient calculations are carried out for each cycle of the sine sweep, so that changes can be noted over the frequency range.

For each cycle, three different calculations are made. Firstly, the spring stiffness is estimated from the forces at maximum and minimum suspension displacement within the cycle. Secondly, a 1st order polynomial is fitted to the force-displacement curve to describe the dynamic stiffness of the suspension. Thirdly, the energy dissipated over the cycle is calculated from integration of force with respect to displacement.

Using the calculated energy, displacement amplitude and centre frequency for the cycle, an estimation can be made of the linear damping coefficient using equation (5-14). This method ensures the total energy dissipated by the linear damping coefficient is the same as the non-linear damper characteristic for the displacement amplitude of the cycle. Another method of extracting a linear coefficient from a non-linear damper characteristic is simply to fit a 1st order polynomial to the measured force-velocity characteristic. However, for large differences in bump and rebound characteristics the method in equation (5-14) was found to be more suitable.

$$C = \frac{E}{\pi \times A^2 \times (2\pi f)} \qquad \textbf{(5-14)}$$

Where:

E – Energy dissipated within cycle

A – Suspension displacement amplitude

f – Frequency

Figure 5-13 and Figure 5-14 present examples of the spring stiffness and damping coefficient calculated throughout the frequency range. The plots show that for both parameters the estimate is not accurate at all points in the frequency range. At very low frequency (<1 Hz), where friction is the dominant suspension force, both estimates are poor. At higher frequencies where the displacements are very small, the string potentiometer is unable to measure the suspension displacement accurately. The spring stiffness estimate can be seen to remain fairly constant in the 1.3 to 4 Hz region, before being less reliable at increased frequencies. In order to estimate a single value of spring stiffness using this method, an estimate is made from the average spring stiffness from the body mode natural frequency to 1 Hz above.

The damping coefficient estimate is more consistent than the spring stiffness estimate for the majority of the frequency range, but is still affected by the friction at low frequency and the limitations of the string potentiometer. In order to estimate a single value of damping coefficient using this method, the values in the range of 1Hz above to 4Hz above the body mode natural frequency are averaged.

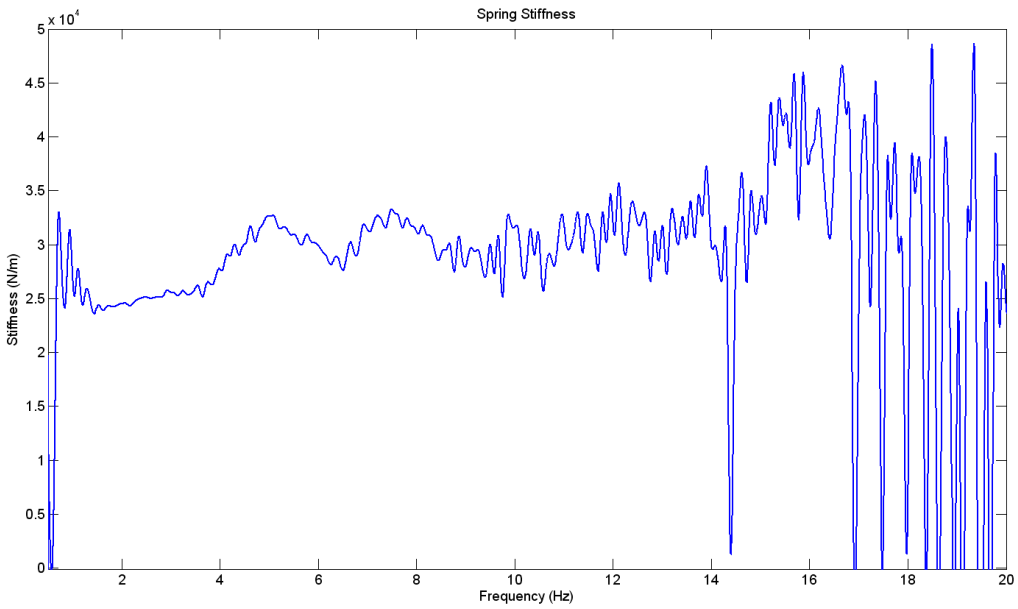

Figure 5-13 – Cycle-by-cycle Time Domain Spring Stiffness Estimation

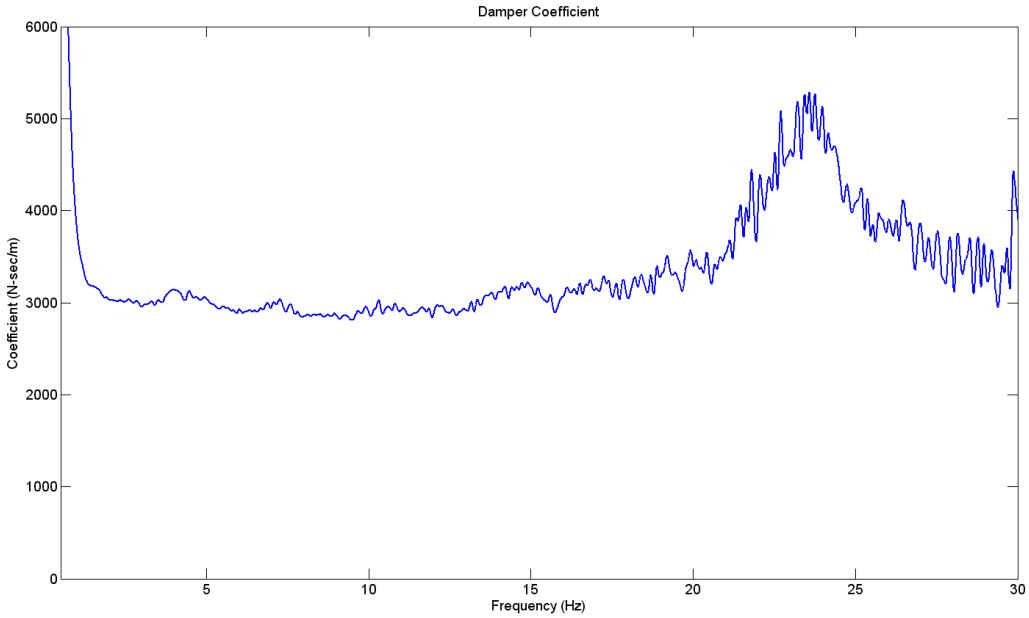

Figure 5-14 – Cycle-by-cycle Time Domain Damping Coefficient Estimation

During this part of the parameter estimation procedure, the force-displacement and force-velocity characteristics of the damper are presented to the engineer. In order to separate the spring and damping forces, the spring force is calculated from the estimated spring stiffness value and the suspension displacement. The damper force is then calculated by removing the spring force from the total suspension force. Figure 5-15 and Figure 5-16 present examples of force-displacement and force-velocity characteristics around the body mode natural frequency.

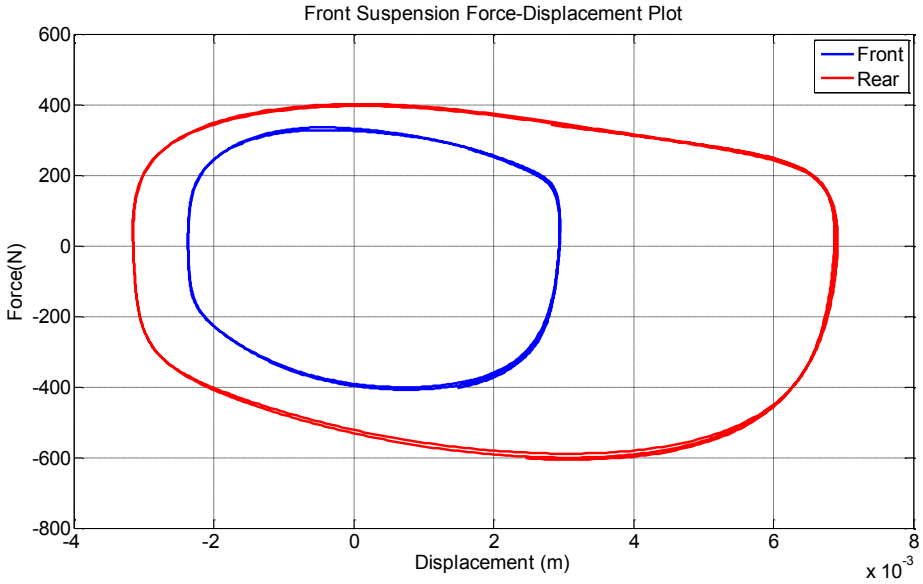

Figure 5-15 – Force-Displacement Damper Characteristic

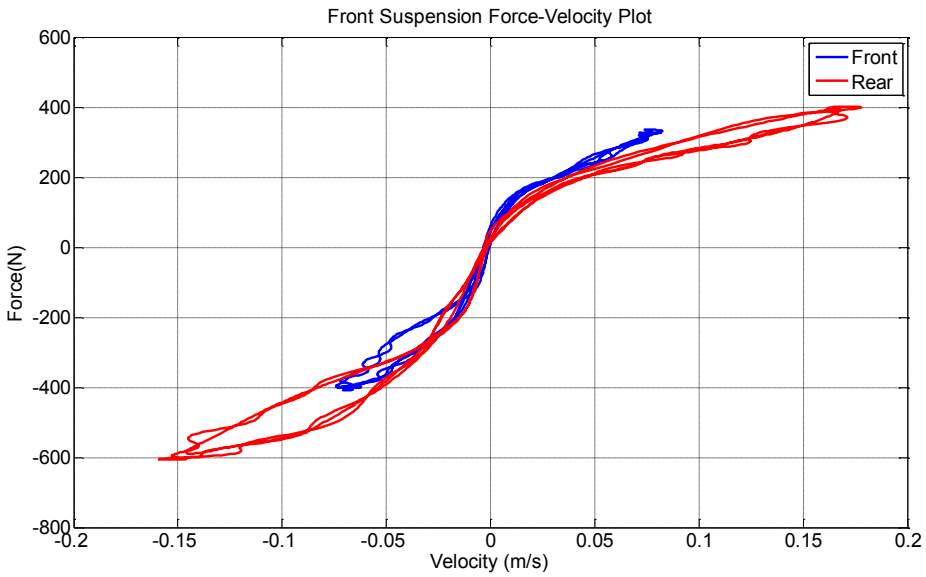

Figure 5-16 – Force-Velocity Damper Characteristic

The phenomenon of 'clipping' is shown in Figure 5-17 below. In this case the frequency of the displacement is sufficiently low that friction results in the spring-damper coming to a complete rest at the bottom and top of the stroke. This effect rapidly becomes negligibly small with frequency and it was not necessary to include it in the model in order to obtain good agreement between model and experiment.

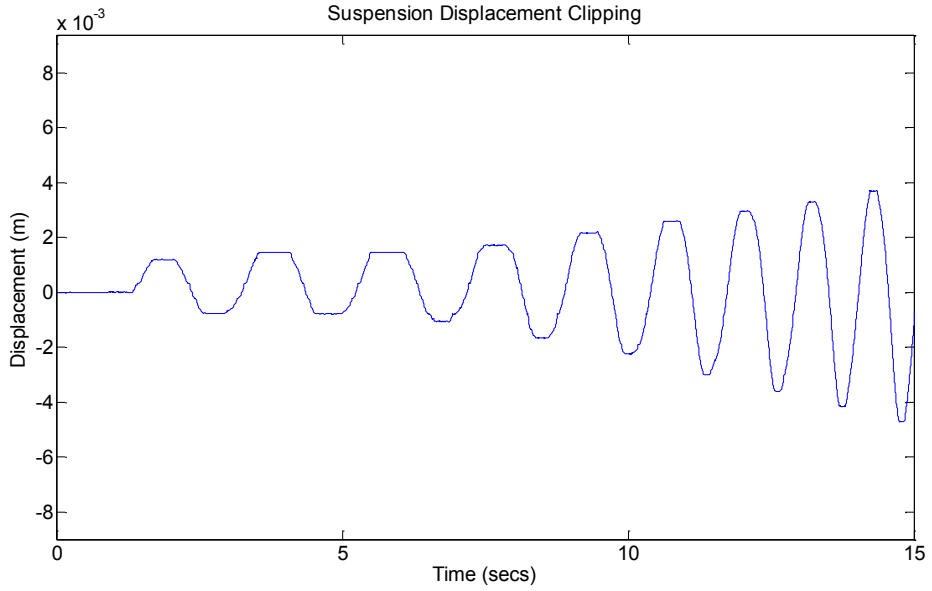

Figure 5-17 – Suspension Displacement Clipping due to Friction

The time domain spring stiffness and damping coefficient estimates are stored during the parameter estimation process, their main use being to define starting values in the dual wave unsprung mass estimation and the frequency domain suspension parameter estimation.

5.2.4 –Suspension Parameter Estimation in the Frequency Domain

In cases where a top mount component is included within the suspension system, the estimation of the spring stiffness, damping coefficient and top mount stiffness together becomes very difficult in the time domain, so a frequency domain approach is more easily used.

The suspension force response in the frequency domain can be divided by the suspension displacement response in order to create a dynamic stiffness with both real and imaginary components. In the simple spring damper case the real part represents the spring stiffness and the imaginary part represents the damping coefficient multiplied by ω. However, in the more complex cases with top mounts included this is no longer the case. In this case the dynamic stiffness magnitude and phase can be used to describe the system. The magnitude is related to the combined springing and damping effects and the phase can be used to determine the relative levels of springing and damping. For example a phase angle of 0˚would indicate that the complete dynamic stiffness would be due to the spring, whist an angle of 90˚ would indicate that the force was in phase with velocity and hence due to the damper.

It is possible to calculate the suspension displacement frequency response either directly from the string potentiometer signal and input acceleration signal, or from the body and hub accelerometer signals with a division by $-\omega^2$. However, when using the string potentiometer signal some problems may be encountered at higher frequencies where displacements are small, increasing the apparent stiffness. Examples of this behaviour can be seen in Figure 5-18, where the dynamic stiffness estimated from the string potentiometer and accelerometers is compared. The same figure also compares the dynamic stiffness magnitude using the time domain method.

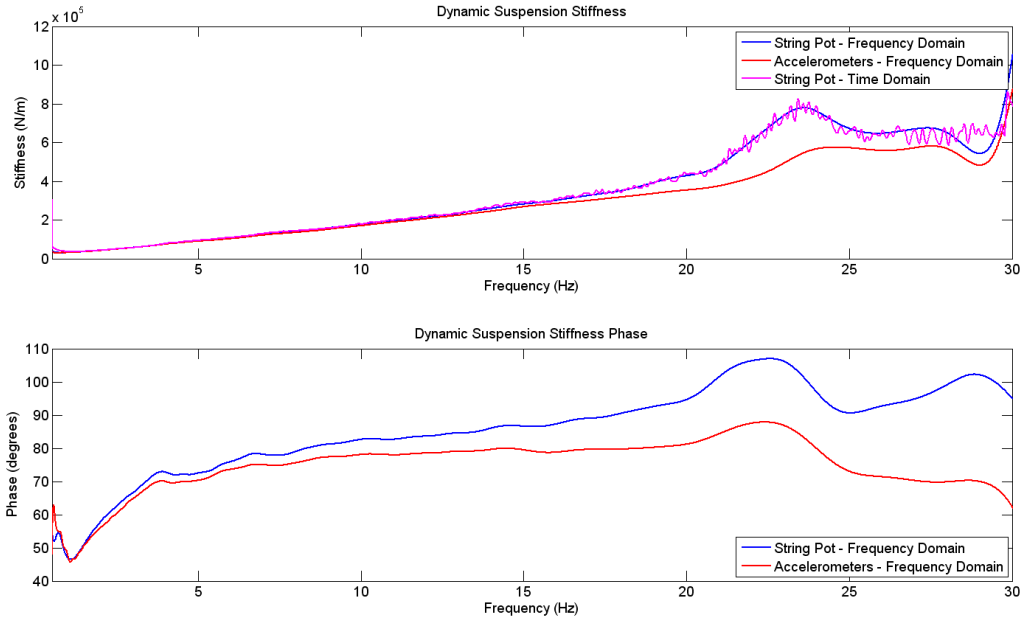

Figure 5-18 – Dynamic Suspension Stiffness Response Comparison

The technique used to determine the 3 suspension parameters is the 'fminsearch' function in MATLAB. This function uses the simplex search method which is a non-linear unconstrained optimisation. This method is used as it is easy to apply weightings to the error, so that error is minimised over a particular range. For example, if all the data from 0 to 30 Hz were used the estimate in the critical areas would be compromised by behaviour at high and low frequencies. By applying a weighting window the error in the 1.5 to 15 Hz region can be weighted with more significance, allowing a better estimate of the general characteristic of the suspension system.

An example of the system equation for the 'dual-path' type suspension is shown in equation (6-12) (Duplicated from section 6.3.2 - Suspension System Layout)

$$k_{dyn} = \left(k_s + \left(\frac{1}{jC\omega} + \frac{1}{k_{tm}} \right)^{-1} \right) \quad \textbf{(6-12)}$$

Where:

k_{dyn} – Dynamic Stiffness

k_s – Spring Stiffness

k_{tm} – Top Mount Stiffness

C – Damping Coefficient

j – Imaginary Unit

In order to solve for the best fitting parameters, the suspension equation is modelled within the 'fminsearch' function. The difference between the modelled and measured responses is then weighted and the RMS calculated to produce an error value for the function to minimise. The error is calculated individually for the real and imaginary parts and then summed to give a total error. The 'fminsearch' function then searches for the 3 parameter values that minimise the error between the measured and modelled suspension characteristic until either the maximum limit of iterations has been reached, or the defined error tolerance is reached. In order to find a solution quickly, all 3 parameters are defined with initial values. The spring stiffness and damping coefficient values are defined by the initial time domain estimates and the top mount stiffness is given a default value of 800 kN/m. The time required to solve for minimum error can vary significantly depending on how well the provided equation describes the measured dynamic stiffness and the initial values. Typical solving times range between 0.5 and 30 seconds for a 3GHz Intel processor with 2 GB of RAM.

Examples of the measured and estimated dynamic stiffness characteristics are shown in Figure 5-19 and Figure 5-20. In both cases the characteristic in the main frequency range of interest 1.5-15 Hz is well matched between the measured and estimated suspension system characteristic. The example in Figure 5-19, has low amounts of friction and high top mount stiffness, making the suspension behave almost like the pure spring-damper system. The example in Figure 5-20, has more friction, as can be seen by the high phase angle at very low frequency. The phase can also be seen to reduce at higher frequency, due to the effects of a low stiffness top mount in relation to the damping level.

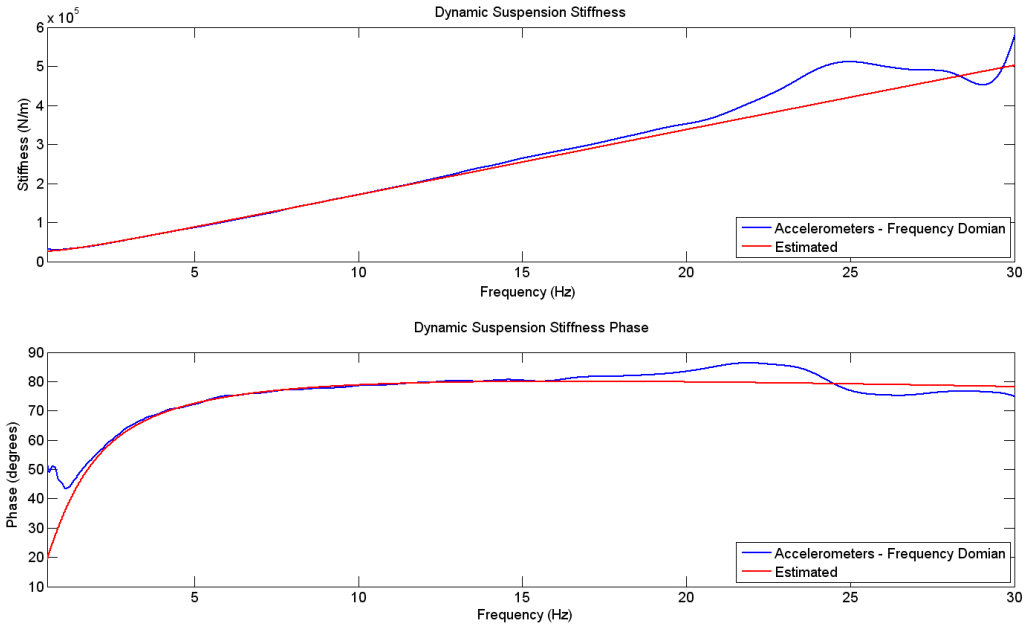

Figure 5-19 – Estimated Dynamic Stiffness – Low Friction, High Top Mount Stiffness

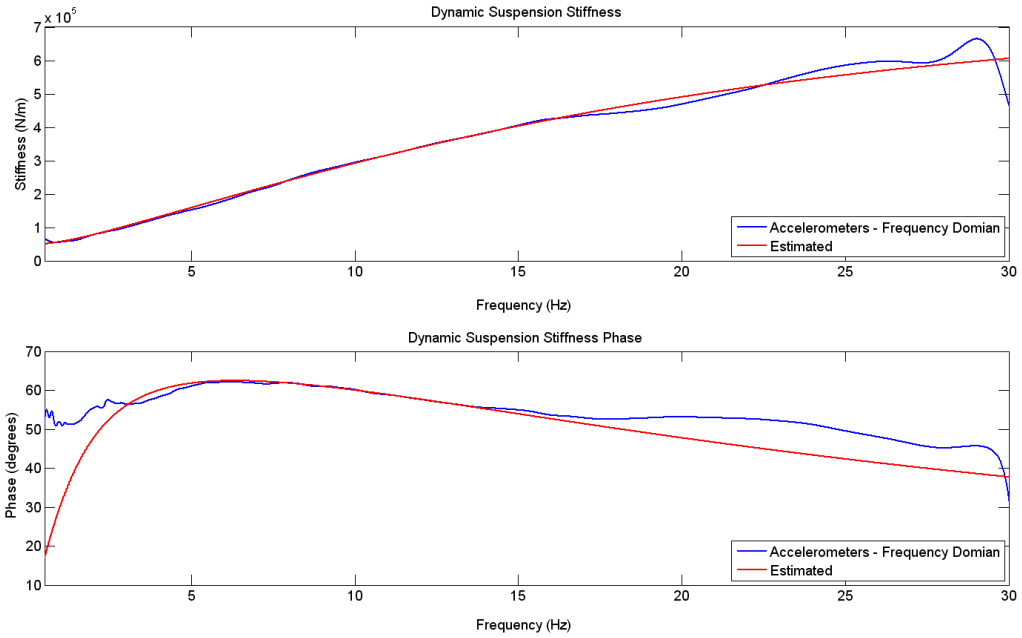

Figure 5-20 – Estimated Dynamic Stiffness – High Friction, Low Top Mount Stiffness

5.2.5 - Sprung Mass and Moments of Inertia Estimations

5.2.5.1 - Sprung Mass Estimation

There are two ways in which the sprung mass of the vehicle can be estimated. The first simply involves subtracting of the estimated unsprung masses from the total mass to produce a sprung mass value and the sprung mass weight distribution. Although this produces a number that can be used in simulation of the vehicle, it is not as useful as estimating the sprung mass across the frequency range.

In order to produce an apparent sprung mass response, the total suspension force can simply be divided by the vertical acceleration at the CofG calculated from the body acceleration responses in pure heave. Alternatively the front and rear apparent masses can be determined separately by using the front suspension force divided the front body acceleration and the same at the rear. This means that any pitching of the sprung mass will have an influence of the apparent mass at each end of the vehicle. An example of the front and rear apparent sprung mass is presented in Figure 5-21.

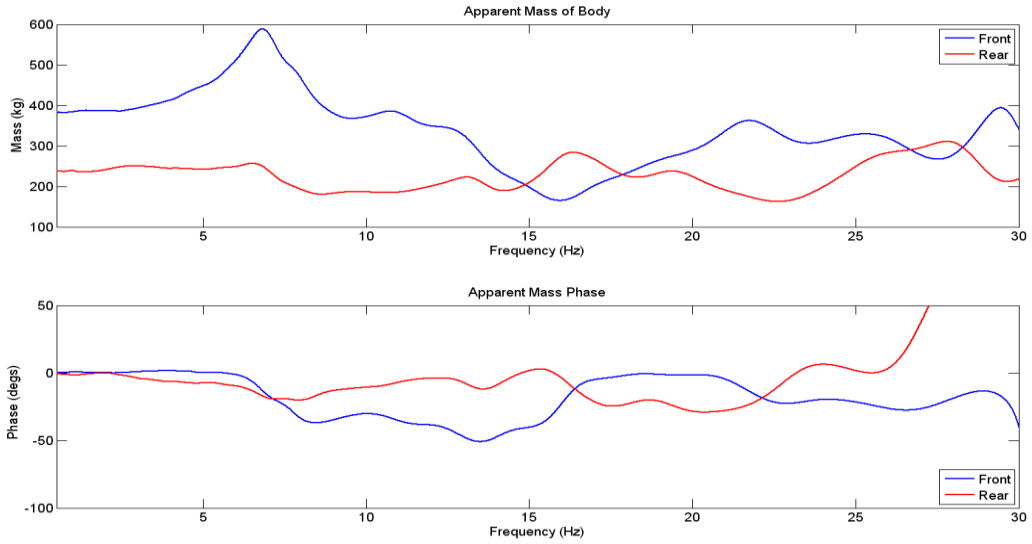

Figure 5-21 – Front and Rear Apparent Sprung Mass

At very low frequency the apparent sprung mass is equal to the mass estimated from the total mass minus the unsprung mass at each end of the vehicle. However, as the frequency increases the front apparent sprung mass (and to a much smaller extent the rear), increases and decreases, along with a significant phase change. This indicates that some part of the vehicle attached to the sprung mass goes through resonance at approximately 7 Hz. As the change in apparent mass is so significant at the front compared to the rear, this would indicate that the component is close to the front axle, for example the engine.

Although only a single value of sprung mass is estimated within the parameter estimation, the apparent mass response is presented to the engineer for further analysis. The apparent sprung mass can be a very useful tool in allowing the engineer to note the poor dynamic properties of various components attached to the sprung mass that can have a significant effect on both comfort and handling.

5.2.5.2 – Pitch Moment of Inertia

In order to estimate the pitch moment of inertia, data from the pitch mode sine sweep is used. In this case the pitch acceleration would be expected to be largest and hence the signal-to-noise ratio large.

Estimation can be carried out in both time and frequency domains. The time domain method involves calculating the rotational torque applied to the sprung mass by the suspension and determining the gradient between the torque and rotational acceleration of the sprung mass. The estimate is best made at the pitch mode natural frequency. It is this result that is output from the parameter estimation technique as the pitch moment of inertia. An example of the pitch moment of inertia calculated in the time domain is presented in Figure 5-22.

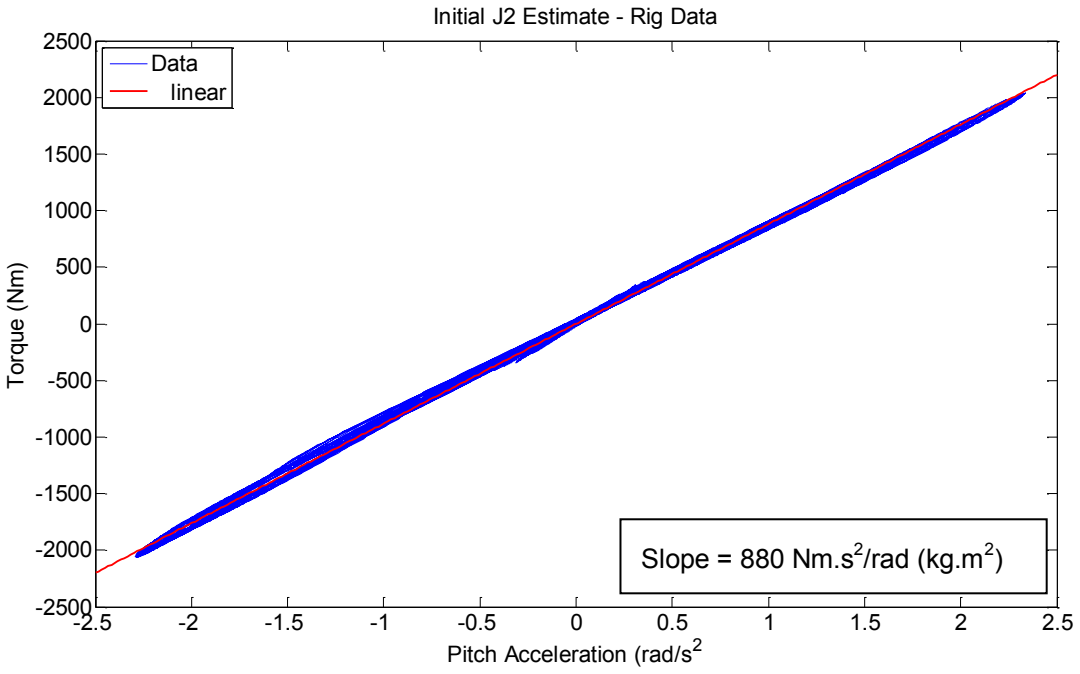

Figure 5-22 – Time Domain Pitch Moment of Inertia Estimation

The pitch moment of inertia can also be determined in the frequency domain by dividing the calculated pitch torque response by the calculated rotational pitch acceleration response. As with the apparent sprung mass this apparent moment of inertia would be expected to change with the vibration of components attached to the sprung mass. An example of apparent pitch moment of inertia is presented in Figure 5-23.

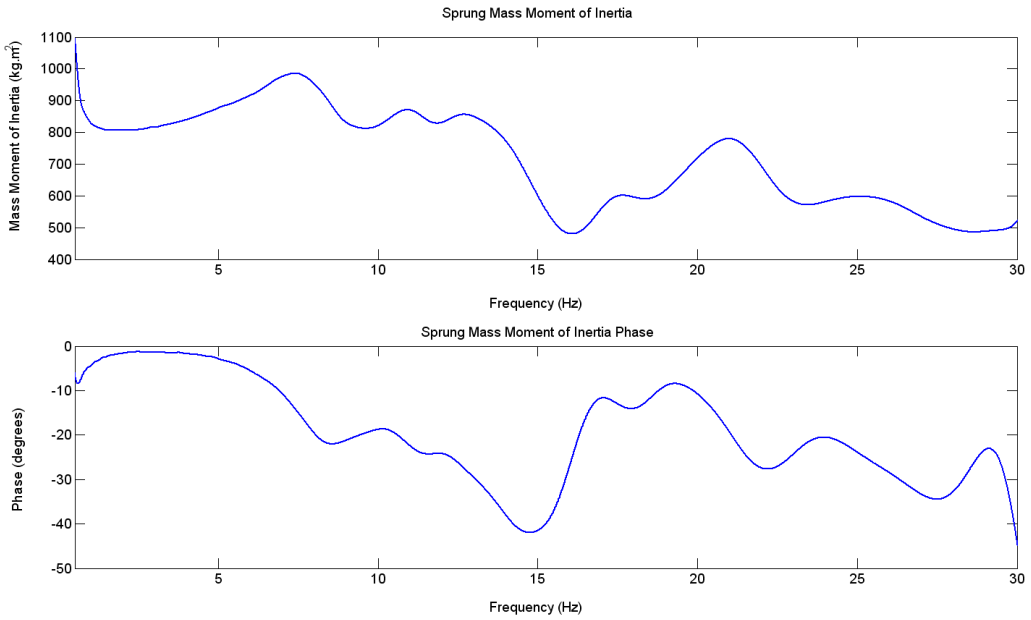

Figure 5-23 – Apparent Pitch Moment of Inertia

The apparent moment of inertia at very low frequency can be seen to be large and is not in phase with acceleration. This is due to the friction in the wheel bearings and brakes causing the vehicle to pitch about the ground plane, rather than rotate the wheels, and allow rotation about the vehicle's CofG. Once the friction has been overcome the apparent pitch moment of inertia is very similar to the value that would be obtained from the time domain method. As the frequency continues to increase, similar effects to the apparent sprung mass can be seen.

5.2.5.3 - Roll Moments of Inertia Estimation

The roll moment of inertia values are best calculated in the frequency domain, due to the complex nature of the roll response when testing on four-post rig. Roll moments of inertia are calculated from the roll mode sine sweep test.

The roll response of the vehicle on the rig generally produces two modes attributed to the sprung mass as explained in section 4.4.3. It was noted that just after the second natural frequency the sprung mass rotates around its CofG. At this point in the frequency range, the roll moment of inertia relating to the sprung mass can be estimated using the roll torque and roll acceleration frequency responses.

It was also noted that at very low frequency the vehicle was forced to roll around the ground plane. In this case the inertia about the contact patch relates to the roll inertia and the distance between the ground plane and the vehicle's CofG height using parallel axis theorem. The equation used to estimate the CofG height is shown in equation (5-15).

$$h = \sqrt{\frac{J_{\varphi(Ground)} - J_{\varphi 2} - 2\left(m_{1f} \times \left(\frac{t_f}{2}\right)^2\right) - 2\left(m_{1r} \times \left(\frac{t_r}{2}\right)^2\right)}{M_T}}$$

(5-15)

Where:

h – Complete vehicle CofG height

M_T – Total mass of vehicle

$J_{\varphi(Ground)}$ – Total vehicle moment of inertia about ground plane at 0.5 Hz

$J_{\varphi 2}$ – Sprung mass moment of inertia

m_{1f} – Front unsprung mass

m_{1r} – Rear Unsprung mass

t_f – Front track

t_r – Rear track

Two major assumptions are made within this estimation. Firstly, it is assumed that the vehicle rotates directly around the contact patch with no suspension or tyre deflection. Secondly, the unsprung masses are assumed to be point masses located at the wheel centres.

This estimation is not designed to be highly accurate, but instead provide an indication of the CofG height of the vehicle for comparison with other vehicles.

5.2.6 – Roll Stiffness Estimation

The roll stiffness estimation is the most simple of all the estimations carried out from four-post rig data. The estimation is made from the initial constant frequency part of the warp mode sine sweep.

The linear roll stiffness is equivalent to equation (5-16).

$$k_r = \frac{F_{1L} - F_{1R}}{(x_{1L} - x_{2L}) - (x_{1R} - x_{2R})} \quad \textbf{(5-16)}$$

Where:

k_r – Roll stiffness

F_{1L} – Left contact patch load

F_{1R} – Right contact patch load

x_{1L} – Left hub displacement

x_{2L} – Left body displacement

x_{1R} – Right hub displacement

x_{2R} – Right body displacement

The string potentiometers are used to determine the x_1-x_2 displacements, as calculating the displacements from the accelerometer signals would be inaccurate at the low levels of acceleration.

The linear roll stiffness is determined separately front and rear using the gradient of force to displacement. The total roll stiffness is determined by summing of the front and rear. Both the total roll stiffness and front to rear roll stiffness distribution are of great use to an engineer when tuning a vehicle, so knowledge of these parameters is important. An example of estimated roll stiffness is presented in Figure 5-24.

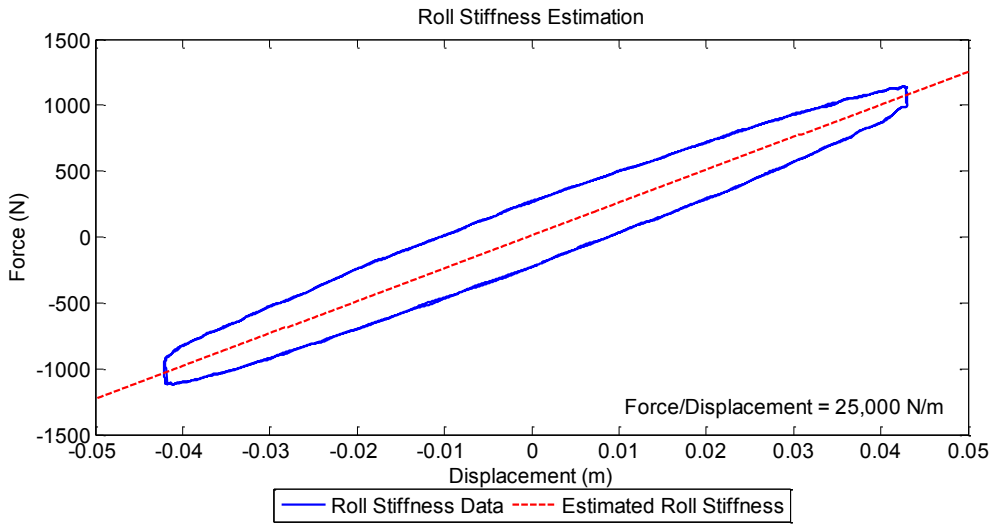

Figure 5-24 – Roll Stiffness Estimation

5.2.7 - Unsprung Mass Estimation Validation

In order to validate the estimation of unsprung mass using the methods described in section 5.2.2.2 – Unsprung Mass Estimation and 5.2.2.3 – Unsprung Mass Estimation using Dual Wave Simulation, a test was conducted using a Honda Civic provided by Honda on the four-post rig. The test was conducted using various amplitude sine sweep heave inputs, and analysed using 3 different methods:

1. Dual Wave Simulation - With offset compensation.
2. Dual Wave Simulation – Without offset compensation.
3. Peak and Trough Time Domain Method

The with and without offset compensation relate to compensating the force with the suspension displacement offset experienced due to non-linear damping characteristics.

The four-post tests were carried out with the vehicle in two different test conditions. One test was carried out with 16” wheels fitted, whilst the second was carried out with 17” wheels, which were statically measured to be 3.6 kg heavier than the 16” equivalents. If the change in estimated unsprung masses matches this static change, then the method would be validated. Table 5-2 presents the estimated unsprung mass values for the two cases with different magnitude sine sweeps. The front left unsprung mass has been omitted from the table, as a damaged accelerometer during the test meant that the front left hub acceleration could not be measured.

	Input Velocity (mm/s)						
Unsprung Mass(kg)	16"	125	157	17"	125	157	173
Front Simulated Dual Wave - With Offset Compensation		40.99	42.12		41.83	45.40	44.92
Front Simulated Dual Wave - Without Offset Compensation		38.30	37.37		35.13	39.64	38.74
FR Peaks and Troughs		NA	37.12		41.03	41.17	40.90
Rear Simulated Dual Wave - With Offset Compensation		35.26	36.89		40.19	40.57	42.92
Rear Simulated Dual Wave - Without Offset Compensation		36.50	37.64		41.81	40.57	43.61
RL Peaks and Troughs		36.91	36.67		38.28	37.92	38.06
RR Peaks and Troughs		39.04	38.60		39.26	40.02	39.24

Table 5-2 – 16” and 17” Wheel Unsprung Mass Estimations

The results presented in Table 5-2, show that at the front there are noticeable differences between the two dual wave simulation estimation methods. This is due to the large magnitude of suspension pull-down caused by a heavily rebound biased damper characteristic. The method 2 estimate at the front is not possible in the lowest amplitude 16” wheel case, but for other measurements is generally most similar to the dual wave input without offset compensation. The method 2 estimation is the most consistent with changing amplitude, with a range of less than 0.3 kg. In this case the change in unsprung mass between the single 16”

value and the averaged 17” value was 3.91 kg, 0.31 kg larger than the statically measured difference.

For the rear estimates, the difference between the two dual wave simulation methods was much smaller due to the quite linear characteristic of the rear dampers fitted to the vehicle. In both 16” and 17” wheel cases the rear left unsprung mass calculated from peaks and troughs was lighter than the rear right. The appearance of the rear suspension beam was symmetrical, but the fact that the left and right wheels are highly coupled by the beam means that the beam dynamics affect the left to right distribution of force and acceleration. The difference in 16” and 17” wheel unsprung mass was representative of the measured change mass in all but the rear right wheel case using method 2, where values were only approximately 0.7 kg different.

The measurement of static unsprung mass was also carried out on the vehicle with the 17” wheels fitted. The vehicle was lowered onto axle stands whist on the four-post rig. At the front the anti-roll bar was disconnected to avoid any coupling between the left and right suspensions. The top mount securing nuts where then loosened and the wheel pads lowered until the strut top just came out of contact with the suspension turret. This way it would be known that none of the sprung mass force would be fed through the spring damper unit into the unsprung mass and measured on the wheel pad load cell, although the complete damper would be included in the unsprung mass measurement, rather than just the lower portion. In this case it was still possible that the wishbone bushes could apply a load to either increase of decrease the apparent unsprung mass. The unsprung mass was lifted by hand and dropped, allowing the unsprung mass to settle at static equilibrium. At the rear, the springs and dampers were removed from the suspension system. The wheel pads were lifted so that the distance between the wheel and wheel arch was the same as the static ride height condition. Again the wheels were lifted by hand and dropped to reach static equilibrium. The springs and dampers were also placed on the wheel pad, so that the combined load would be measured. Due to the stiffness of the rear suspension beam the difference between left and right wheel loads was very sensitive to the height of the wheel pad in relation to the vehicle, causing different unsprung masses to be estimated left and right. The values measured in this process are presented in Table 5-3.

Static Unsprung Mass (kg)		
	Left	Right
Front	38.3	38.6
Rear	43.3	41.0

Table 5-3 – Statically Measured Unsprung Mass – 17” Wheels

The front unsprung mass measured statically was found to be around 3kg lighter than the estimated mass using the peak and trough method. It was known that the wishbone bushes would be reacting some of the unsprung mass force in the statically measured condition, making the unsprung mass appear lighter than reality, although the actual magnitude could not be measured. At the rear the difference in left to right measured unsprung mass could be

accounted to the stiffness of the suspension beam, although the statically measured average mass was 3.36 kg more than the average estimated mass using the peak and trough method. Again, although the actual magnitude is unknown the estimated mass would be expected to be smaller than the statically measured mass. This due to the fact that when the unsprung mass is in motion, it is forced to rotate about the beam pivot, which is a 0.5 m in front of the wheel centre. Due to the mass of the beam itself, the mass centre of the complete unsprung mass would be expected to be between the wheel centre and beam pivot, causing the unsprung mass moment of inertia about the beam pivot to be measured using the peak and trough method, rather than the static unsprung mass. Also, as with the front suspension the top portion of the damper is included within the unsprung mass measurement, when in reality it belongs to the sprung mass.

The investigation has shown that to validate the estimated unsprung mass to an overall unsprung mass value is a difficult task, as the static unsprung mass may not directly relate to its dynamic effects on the vehicle. By using two different wheel sizes with a known difference the validation becomes simpler. In this case, although complete accuracy was not achieved, the dual wave simulation method without displacement compensation and the peak and trough method were found to provide good agreement with the value of changed mass. In particular the front peak and trough method provided consistent unsprung mass estimates with only a 0.3kg error between the statically measured and estimated difference between the two wheel sizes.

In order to assess the effect of inaccurate unsprung mass estimation on other estimated parameters, a spring rate was estimated from four-post date with significantly different levels of unsprung mass used to estimate the suspension force, with the assumption that 40 kgs was an accurate representation of the actual unsprung mass (Table 5-4).

Unsprung Mass (kg)	Spring Rate Estimate (N/mm)
30	43.49
40	42.93
50	46.85

Table 5-4 – Effect of Unsprung Mass on Estimated Spring Rate

The estimated spring rate for an unsprung mass 10 kg lower than the accurate value was only 0.56 N/mm (1.3%) larger than the spring rate with the accurate mass, whilst the overestimate by 10 kg produced a much larger overestimate of 3.92 N/mm (9.1%) for the spring rate. The change in estimate is non-linear due to the phasing of the body and upright accelerations. The result indicates that it is more desirable for the unsprung mass estimation to be an underestimate, rather than an overestimate.

The effect of unsprung mass estimation was also considered in terms of simulation of the hub mode natural frequency and its effect on contact load variation. The case was considered where

a 40 kg unsprung mass was used along with a 43 N/mm spring stiffness, 350 N/mm tyre stiffness and 2.2 N-sec/mm damping coefficient to define the natural frequency and damping ratio using equations (5-17) and (5-18).

In addition the effect on input acceleration normalised contact load variation was calculated using equation (5-19) the results are presented in Table 5-5. In this case all other parameters remained equal, which would not necessarily be the case if the unsprung mass was estimated incorrectly.

$$\omega_n = \sqrt{\frac{k_s + k_t}{m_1}}$$

(5-17)

$$\zeta = \frac{C}{2m_1\omega_n}$$

(5-18)

$$\frac{F_1}{\ddot{x}_0}(\omega_n) = m_1\left(\sqrt{1+\frac{1}{4\zeta^2}}\right)$$

(5-19)

Where:

ω_n – Undamped Natural Frequency

ζ - Damping Ratio

k_s – Spring Stiffness

k_t – Tyre Stiffness

C – Damping Coefficient

m_1 – Unsprung Mass

F_1 – Contact Patch Load

$\ddot{x}_0$ – Input Acceleration

m1	ω_n(f)	ζ	$F_1 / \ddot{x}_0$ (Wn)	Error(%)
35	16.86	0.30	68.60	-16.79
40	15.78	0.28	82.44	0.00
45	14.87	0.26	97.08	17.75

Table 5-5 – Effect of Estimated Unsprung Mass on Simulated Hub Mode Contact Load Variation

The results in Table 5-5, show that the simulated hub mode contribution to contact force is significantly affected by estimated unsprung mass, even more than the obvious effect of the mass change (+/-12.5%). Potentially the optimal tuning of an estimated vehicle in simulation could lead to a non-optimal solution in the real vehicle case if attention is not paid to the correlation between the simulated and measured contact load variations around the hub mode natural frequency. When using the simulation model from estimated parameters it is important for the user to compare measured and simulated results to gauge how accurately the real vehicle responses have been recreated. This will indicate how reliable the performance and comfort index changes with various parameter changes would be.

5.3 - Unsprung Mass Estimation Method Review

The accurate estimation of unsprung mass from rig data proved a difficult task, with many different methods attempted before deciding upon the final process. Methods that worked with 100% accuracy in simulations were found to provide poor estimates with real data.

Initial investigations were carried out in simulation and used equations derived from the 2DoF and 4DoF model equations of motion to calculate unsprung mass from other signals and known masses. The 2DoF equation is presented in equation (5-20) with the front and rear equations for the 4DoF model presented in equations (5-21) and (5-22) respectively.

$$m_1 = \frac{-M_T \ddot{x}_2 + F_1}{\ddot{x}_1 - \ddot{x}_2}$$

(5-20)

Where:

m_1 – Unsprung Mass

M_T – Total Corner Mass

F_1 – Contact Patch Load

$\ddot{x}_2$ - Body Acceleration

$\ddot{x}_1$ - Hub Acceleration

$$m_{1f} = \frac{-M_{Tf} \ddot{x}_{2v} - \left(\frac{J_2 \ddot{\theta}_2}{a+b} \right) + F_{1f}}{(\ddot{x}_{1f} - \ddot{x}_{2v})}$$

(5-21)

$$m_{1r} = \frac{-M_{Tr} \ddot{x}_{2v} + \left(\frac{J_2 \ddot{\theta}_2}{a+b} \right) + F_{1r}}{(\ddot{x}_{1r} - \ddot{x}_{2v})}$$

(5-22)

Where:

m_{1f} – Front Unsprung Mass

m_{1r} – Rear Unsprung Mass

M_{Tf} – Total Mass on Front Axle

M_{Tr} – Total Mass on Rear Axle

F_{1f} – Front Contact Load

F_{1r} – Rear Contact Load

$\ddot{x}_{2v}$ - Vertical CofG Body Acceleration

$\ddot{\theta}_2$ - Pitch Rotational Body Acceleration

$\ddot{x}_{1f}$ - Front Hub Acceleration

$\ddot{x}_{1r}$ - Rear Hub Acceleration

In simulation, both the methods were found to work with 100% accuracy. However, when the equations were applied to real four-post rig data the results were far from ideal, as shown in Figure 5-25 and Figure 5-26.

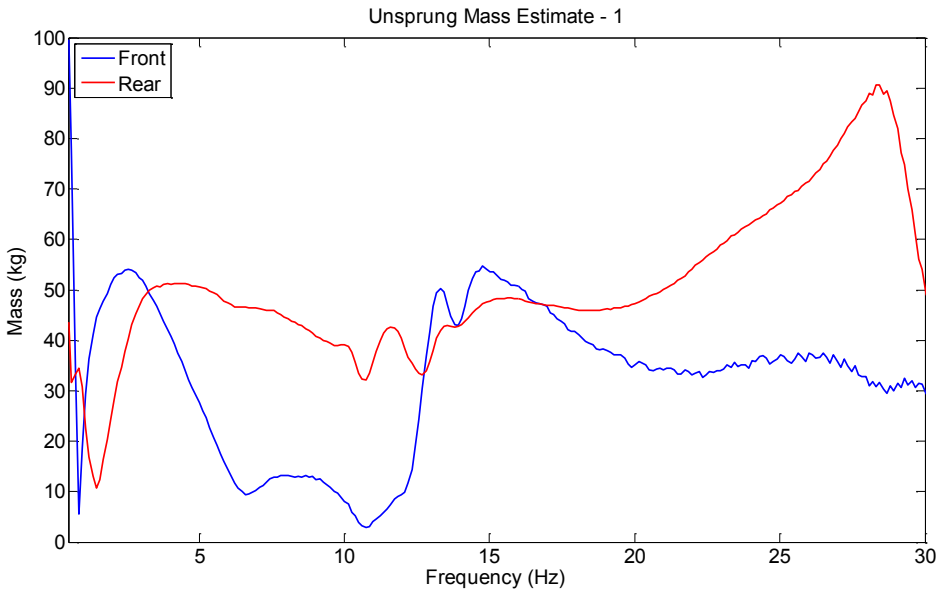

Figure 5-25 – 2DoF Unsprung Mass Estimate - Rig Data

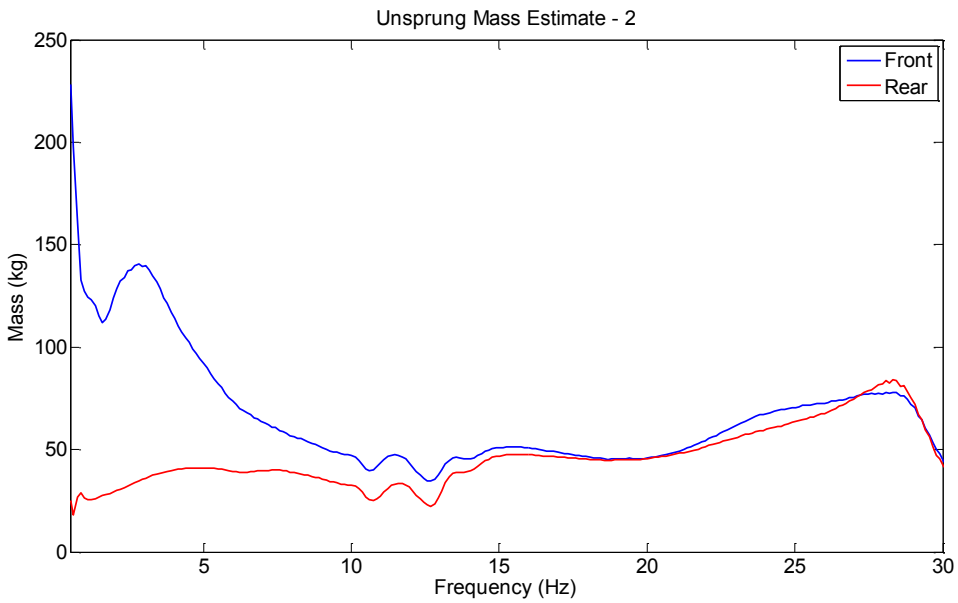

Figure 5-26 – 4DoF Unsprung Mass Estimate – Rig Data

Other tested methods involved using the equations of motion of the 4DoF system with the measured acceleration signals and sweeping through values of sprung to unsprung mass ratio and pitch moments of inertia to determine M_2 and J_2 values (Figure 5-27). These would be defined as the mass and inertia where the minimum error occurred between rig measured contact forces and recalculated contact forces using the measured acceleration signals and swept mass values. The same approach would then be used to determine the relative front and rear unsprung masses (Figure 5-28).

When using this method it was found that there was quite low sensitivity to error when sweeping the ratio of sprung to unsprung mass. This was caused by the dominance of the body mode on contact patch load responses and the fact that the phase of the body and hub accelerations were similar at the body mode natural frequency.

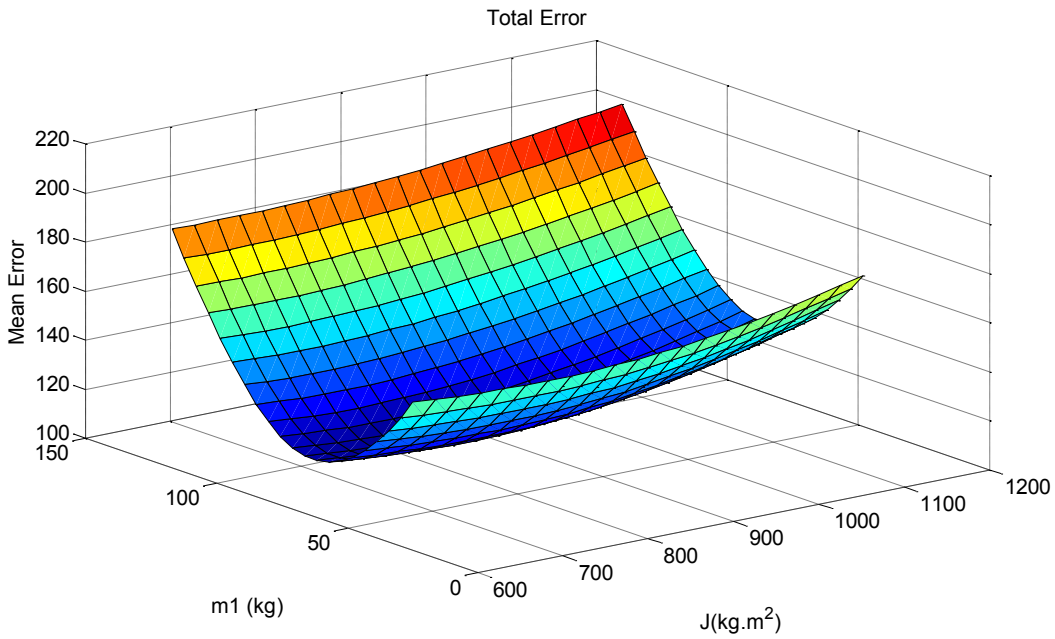

Figure 5-27 - Mean Contact Load Error – Rig Data

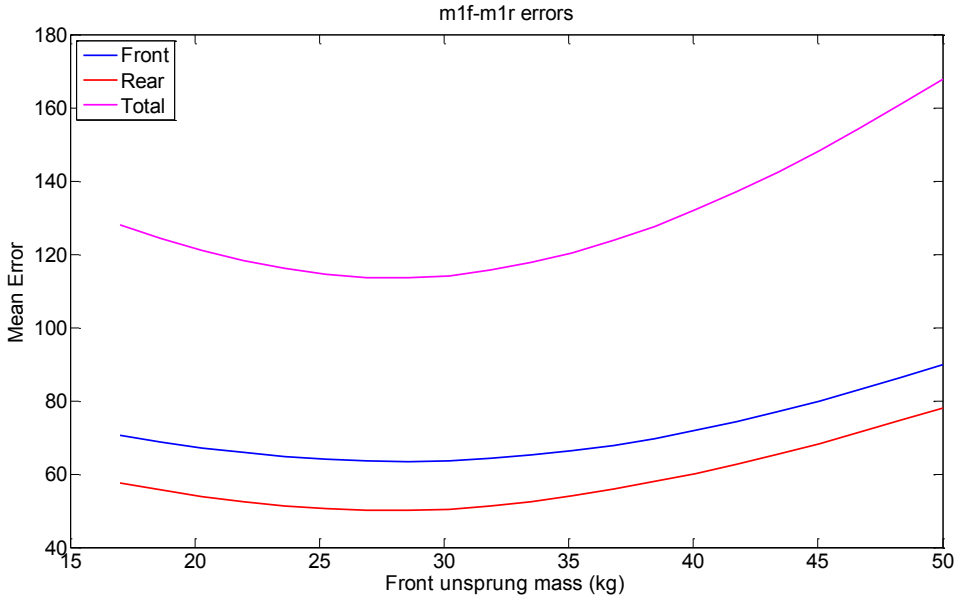

Figure 5-28 – Mean Contact Load Errors in m_{1f} and m_{1r} Estimation – Rig Data

Further methods focussed on creating a situation where the force in the contact patch would be purely due to the acceleration of the unsprung mass. Initial investigations attempted to use a step input, but the four-post rig was unable to provide the desired step signal (Figure 5-29).

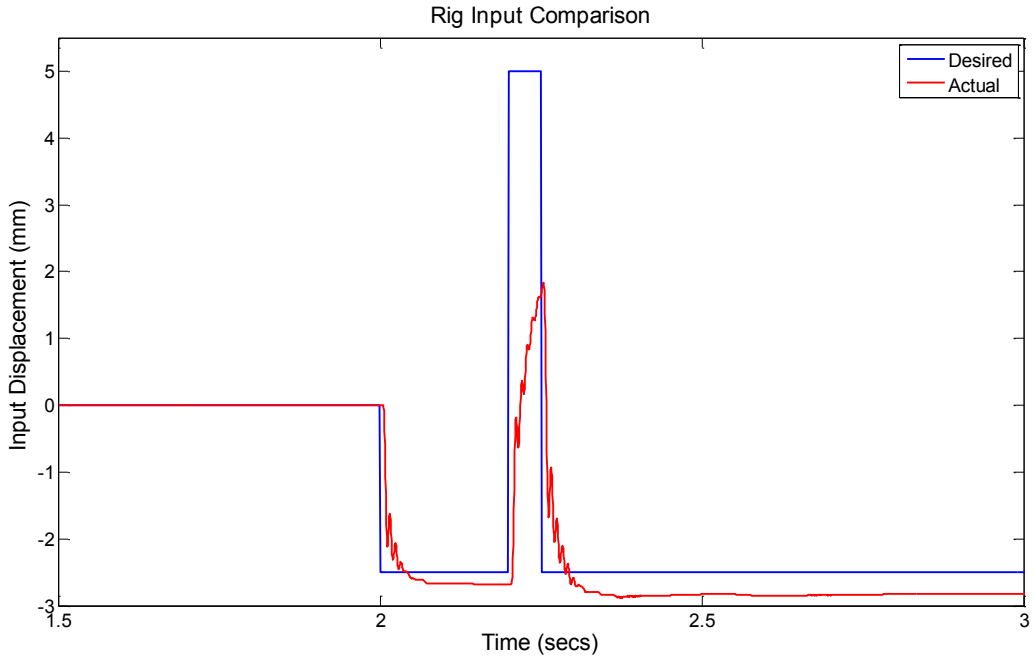

Figure 5-29 - Step Input Comparison

As it was not possible to use a step input, other inputs were used in an attempt to create this situation. The most successful of the inputs was the dual wave swept sine. This method involved using constant peak velocity swept sines of different velocity magnitudes and different frequency ranges superimposed. Assessment of the unsprung mass estimation error was then conducted using a method very similar to the error weighting explained in section 5.2.2.3 – Unsprung Mass Estimation using Dual Wave Simulation (Figure 5-30). Using this method is was possible to determine some instances where the unsprung mass could be estimated with reasonable accuracy. However, the amount of time taken to tune the input for a specific vehicle response, so that the unsprung mass could be estimated was substantial, so the final method simulated the dual wave input using the response results acquired during modal testing, rather than having to actually supply the input to the real vehicle.

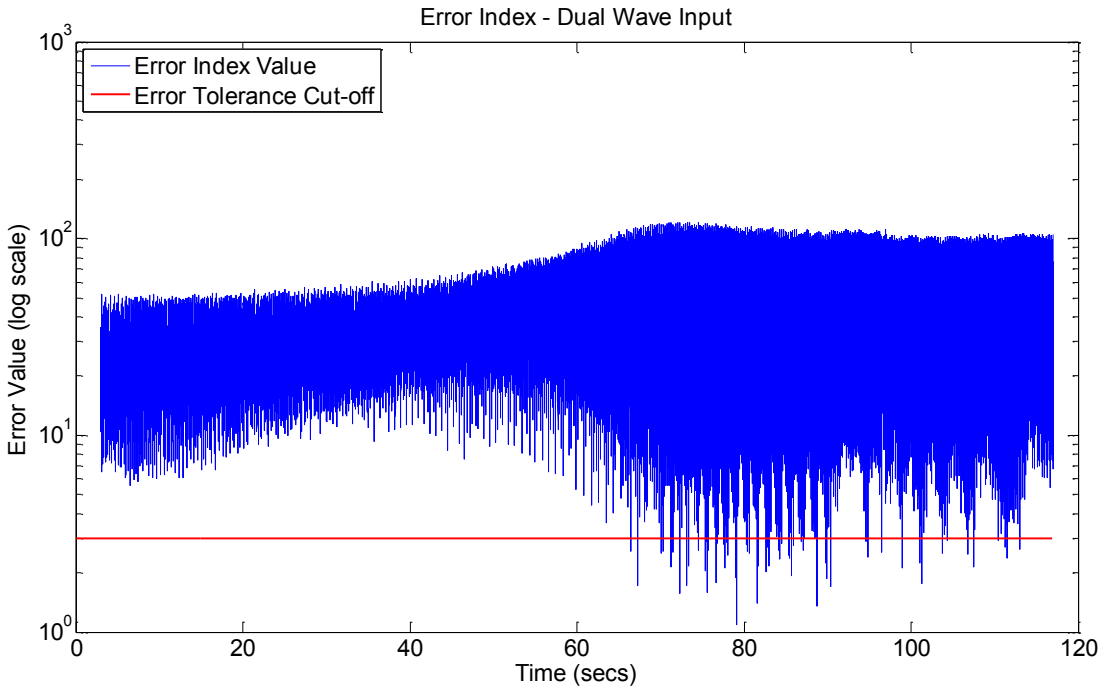

Figure 5-30 - Error Index for Dual Wave Input

5.4 - Parameter Estimation Discussion

The parameter estimation method explained in this chapter is a new and original contribution to the estimation of vehicle parameters from multi-post rig data. The estimation method of unsprung mass is also by itself new and original for both implementation methods explained in section 5.2.2 – Unsprung Mass Estimation.

The method is designed to estimate each parameter as independently as possible. By doing this the output is not simply a best fit of the available parameters by minimising output signal error from an approximated model of the real system. The reasoning behind this approach is due to the fact that the parameters will be used within a simulation model of the vehicle in which all parameters can be altered to note the effect on various output responses and performance indices. If an output error minimisation technique was used to establish all parameters from only a small amount of output signals, the output response could match well for that single condition, even if the estimated parameters were incorrect, due to low sensitivity of one or more parameters. However, if one of the parameters were altered on both the real car and simulation, the incorrectly estimated parameters that were insensitive for the first case, could cause large errors between the simulation and real vehicle in the second case.

An example of this would be the estimation of parameters from the contact force for a well damped hub mode natural frequency. In this case the contact load signal would be dominated by the acceleration of the sprung mass and unsprung mass would have very little effect. This means that the unsprung mass could be estimated at a wide range of values with very little effect on the error between measured and estimated output signals. If these parameters were then used in a simulation where the damping was reduced significantly, the location and magnitude of the hub mode natural frequency, and its effect on contact force, could be very different to that of the real vehicle with the same damping change. When carrying out optimisations and parameter sweeps, it is vital that the model responds in the same way to a parameter change as the real vehicle, otherwise the optimisation of parameters is invalid.

A second reason for using this type of method is that the engineer using the rig will be able to note unexpected behaviour in the estimates of the model that would indicate areas where the model and real vehicle were significantly different and where the model may need improving to model the real vehicle behaviour more accurately. The unexpected behaviour could also be used to identify parameters that cause the vehicle to behave in an undesirable way that would be difficult to establish in normal vehicle running conditions, such as poorly controlled drivetrain mountings.

An advantage of this method is that if a new suspension system were required to be estimated, this could be easily implemented within the code, without rewriting of complex matrices (as in an inverse matrix method), or rewriting of the complete error minimisation algorithm for all parameters. The vehicle simulation model designed for this project is also built in this way, so

that it is possible to change the suspension system within the model, with minimal modification of its interacting components. The same is also true for the modelling of additional components on the sprung mass, such as passengers on seats, or the engine on its mountings. Currently 3 different suspension systems are modelled within the code and vehicle model. These are explained in section 6.3.2 - Suspension System Layout.

6 - Vehicle Models

In this chapter of the thesis the vehicle models used for simulation are discussed. Section 6.1.1 – Determination of Modelling Software, explains the choice of modelling software tool to be used, using a simple two-degree-of-freedom model to compare the 3 different modelling tools on speed of construction, speed of simulation and room for error. The considerations relating to the sophistication of model used are explained in 6.1.2 - Model Complexity.

Section 6.2 - 8 Degree-of-freedom Model, describes the model used for simulation of the vehicle on the four-post rig, which is created in Simulink. Section 6.2.1 – Engine and Passenger Vibration Modelling, explains the requirement for simulation of masses connected to the sprung mass for accurate correlation to the real vehicle and the ability to reduce the model to 7-degrees-of-freedom if this is not required.

Section 6.3 - Modelling Suspension System Features, explains the modelling of non-linear dampers and their effect on the model response, as well as different types of suspension systems that are required to be modelled if accurate correlation is to be achieved.

6.4 – Full Car Modelling, details a full car lateral model that was used in the creation of the performance index and also includes details of the 'Magic Formula' tyre model which the model utilises to generate tyre forces.

6.1 - Determination of Modelling Method and Complexity

In published literature many different models are used to describe the behaviour of a vehicle suspension system. These range from very simple single degree-of-freedom systems as shown in [80] (pp. 61), to very complicated kinematic and dynamic models with many degrees-of-freedom and complex non-linearity as in [35] and [56]. The purpose of the model to be used in this project is to allow the user to determine the sensitivity of various suspension parameters to the ride and handling behaviour of the vehicle. In order to fulfil its purpose the model must be accurate enough that it will react to a parameter change in the same manner as the real vehicle, but it is not required to be able to calculate specifics such as, the maximum cornering speed of the vehicle or steering response time for each parameter.

A second requirement of the model is that all of the parameters in the basic model must be determined using data acquired from four-post rig testing of the vehicle or simple dimension measurements, without dismantling of any part of the vehicle. This excludes a model with detailed parameters of the tyre's lateral and longitudinal parameters, or factors such as aerodynamics.

Finally, as the purpose of the simulation model when tuning a vehicle is to evaluate many different parameter values much faster than could be carried out by physical testing, the time taken for the parameters to be changed and the model to be run should be as low as possible.

These requirements mean that the model used should ideally be quite a simple system, and that the method should allow simple modification in order to simulate different vehicles.

6.1.1 – Determination of Modelling Software

In order to determine which modelling software would be most suitable for the project, an investigation was carried out that simulated a simple two degree-of-freedom model using three different methods:

- ADAMS Multi-body Code
- MATLAB/Simulink
- Excel Spread Sheet Analytical Model

In order to determine which type of model is most suitable, the three modelling methods were assessed on:

- Construction Time
- Margin for Human Error
- Computation Time

The two-degree-of-freedom model is very commonly used in vehicle suspension simulation and tuning and when used for suspension simulation is commonly referred to as the quarter-car model. The system consists of a large mass representing the sprung mass of the vehicle, a small mass representing the unsprung mass, with a spring and viscous damper linking the two masses and a spring linking the unsprung mass to the ground, to act as the tyre. An example of this model is shown in Figure 6-1, with the equations of motion for the system in equations (6-1) and (6-2).

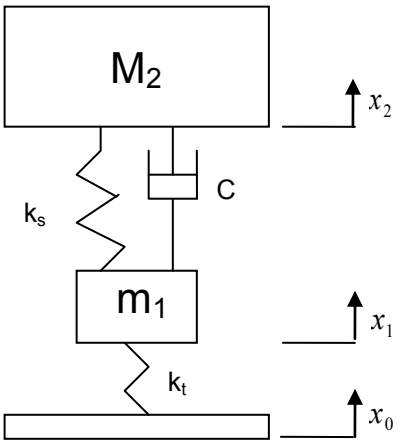

Figure 6-1 – Two-degree-of-freedom System

Where:

M_2 – Sprung Mass

m_1 – Unsprung Mass

k_s – Spring Stiffness

k_t – Tyre Stiffness

C – Damper Coefficient

$$0 = -M_2\ddot{x}_2 + k_s(x_1 - x_2) + C(\dot{x}_1 - \dot{x}_2)$$

(6-1)

$$0 = -m_1\ddot{x}_1 + k_t(x_0 - x_1) - k_s(x_1 - x_2) - C(\dot{x}_1 - \dot{x}_2)$$

(6-2)

From the investigation it was determined the Simulink method was most appropriate, as the execution time was many times faster than the ADAMS model and the construction was much faster than and less prone to error than the analytical Excel model, which had the fastest execution time.

Using Simulink also has advantages in other areas. As the Simulink model is time domain based it is very simple to include non-linear elements, such as non-linear damping characteristics and friction. To simulate these using the Excel spreadsheet would require more complex equations.

6.1.2 - Model Complexity

When designing the vehicle model, the more similar the response of the model is to the real vehicle behaviour, the better the tuning ability and confidence in the model. However, to achieve increased coherence the vehicle model complexity must be increased.

Although increasing the complexity has the advantage of making the model more accurate, it also has many disadvantages. One obvious disadvantage is the amount of time that the model would take to run. Figure 6-2 and Figure 6-3 show two plots taken from Harty, The Myth of Accuracy (2001) [79]. The first plot shows how the expected accuracy of a model related to its duration of calculation, whereas the second plot shows an example of the papers author's representation of usefulness with respect to accuracy and the 'myth' that the relationship is linear.

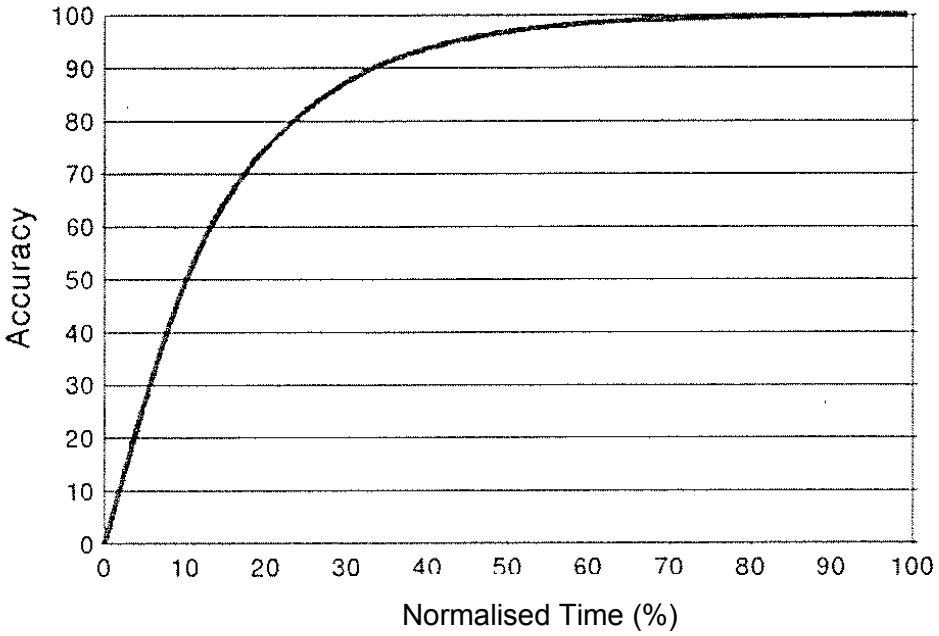

Figure 6-2 – The Cost of Accuracy – The Myth of Accuracy (2001) [79]

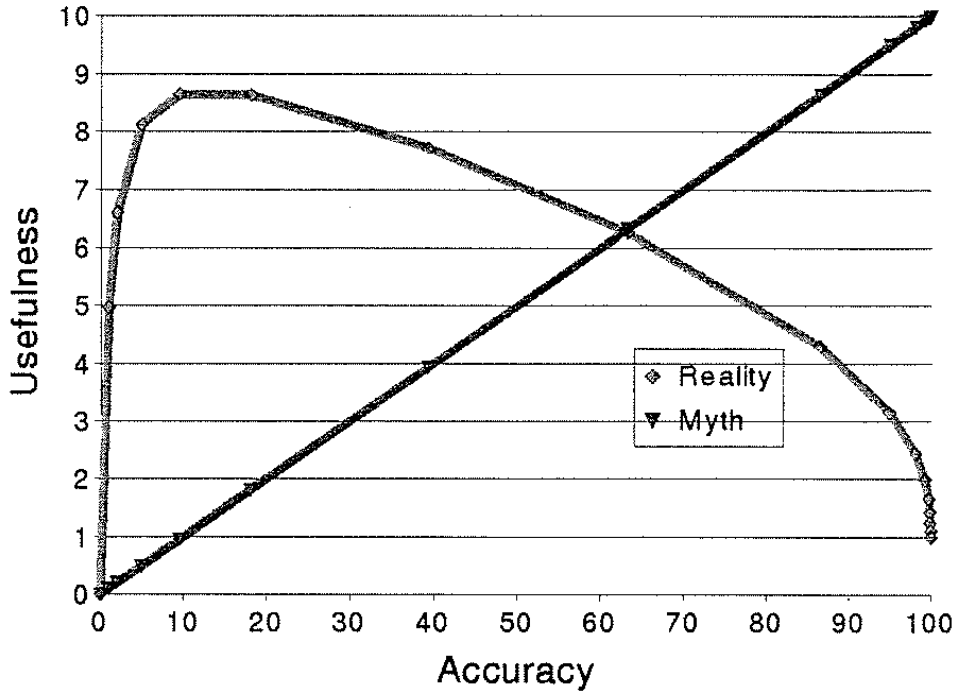

Figure 6-3 – Usefulness vs. Accuracy – The Myth of Accuracy (2001) [79]

As the vehicle model is to be used for tuning of the real vehicle, the model should be as useful as possible for this task. This means that it would not be worthwhile to increase accuracy from 95% to 100%, by taking double the amount of time.

A similar trend also relates to the number of component parameters used in the simulation and the accuracy. A requirement of the testing technique is that all parameters are estimated from four-post rig data or simple dimension measurements. As the number of component parameters increase, the parameter estimation task becomes increasingly complex and time consuming.

In addition, increasing the number of component parameters can cause problems when the vehicle model is intended to be generic for any road car. For example, if the model were to include the kinematics relating to the rear suspension. In the case of a 2007 Honda Civic, the rear wheels are located on a common axle that rotates about a point forward of the rear wheels. In the case of a 2004 Honda Civic, the rear wheels are located on independent links and the uprights to rotate around a point defined by their lateral linkages. This would mean that the two different vehicles would require different models and different parameter estimation methods, which is not desirable. The vehicle model needs to be simple enough that it can model the typical range of vehicle suspension systems without major adjustment of the model or parameter estimation method. This eliminates the use of any models with kinematic suspension effects, as the variation in types of suspension linkage systems fitted to modern day vehicles is large.

In order to determine a suitable complexity of model, 2 DoF (quarter-car), 4 DoF (half-car), 7 DoF (full-car) and 8 DoF (full car with additional mass) dynamic models of the vehicle were constructed in Simulink and compared on their ability to model the response of a vehicle on the four-post rig and road surface and execution time.

The 2 DoF model, as explained in section 6.1.1 – Determination of Modelling Software, solved a time domain simulation of the 60 second rig input described in section 3.4 – An Efficient Rig Input, within 2 seconds. However, the model is very limited in its ability to model the real behaviour of the vehicle on the four-post rig, as the model response is the same regardless of the modal input applied to the vehicle. Thompson [32], noted that if the front and rear of a vehicle are elastically and inertially decoupled then the vehicle will only respond vertically to vertical inputs (heave) and rotationally to rotational inputs (pitch), in which case the heave and pitch behaviour of the vehicle can be modelled using point mass 2 DoF models at the front and rear of the vehicle. However, Thompson also notes that it is not normally applicable to the majority of vehicles, due to the coupling between front and rear system. In this case, to model the heave and pitch behaviour of a vehicle, the model must be extended to a 4 DoF system in which the sprung mass has both vertical and rotational degrees-of-freedom.

The 4 DoF constructed in Simulink was found to solve the same input within 2.5 seconds. The 4 DoF model was found to be considerably more useful than the 2 DoF model because of its ability to model heave and pitch behaviour of the vehicle, including effects caused by the phenomenon of wheelbase filtering explained in section 3.2 – Effect of Vehicle Speed.

Increasing model complexity to the 7 DoF was achieved by allowing the sprung mass a roll degree-of-freedom and inclusion of unsprung masses at each corner. This model allows all rig and road modal inputs to be simulated. The 7 DoF model constructed in Simulink solved in just over 4 seconds. Comparison of the roll behaviour from four-post rig data and the vehicle model found significant differences due the unexpected roll behaviour of the vehicle on the rig, as investigated in section 4.4.3.1 - Roll Response Investigation. However, the 7 DoF model was still deemed more useful than the 4 DoF model due to its ability to model the effects of warp inputs and the fact that the roll response from the model was expected to reflect the roll response of the vehicle on the road at speeds above 10 m/s with more accuracy than the four-post test data (section 4.4.3.1 - Roll Response Investigation). Extension from the 7 DoF to 8 DoF model was achieved by the addition of a single mass connected by a spring-damper to the sprung mass, the purpose of this was to model the dynamic behaviour of the engine on its mounting, as four-post testing of vehicles had found that components not rigidly mounted to the sprung mass could have a significant influence of the apparent sprung mass of the vehicle across the frequency range, as explained in section 5.2.5.1 - Sprung Mass Estimation. The addition of this mass was found to have very little effect on execution time of the model (less than 0.2 seconds) and the modelling feature could be easily omitted by setting the mass to zero. Due to these factors the 8 DoF model offered an increase in usefulness.

6.2 - 8 Degree-of-freedom Model

From investigation of various level of complexity dynamic models (2 DoF, 4 DoF, 7 DoF and 8 DoF), the 8 DoF model was found to be the most 'useful' for modelling the dynamic behaviour of a vehicle on the four-post rig and road surface. An example of the 8 DoF model constructed for use in the thesis is shown in Figure 6-4 along with the equations of motion of the system in equations (6-3) to (6-10).

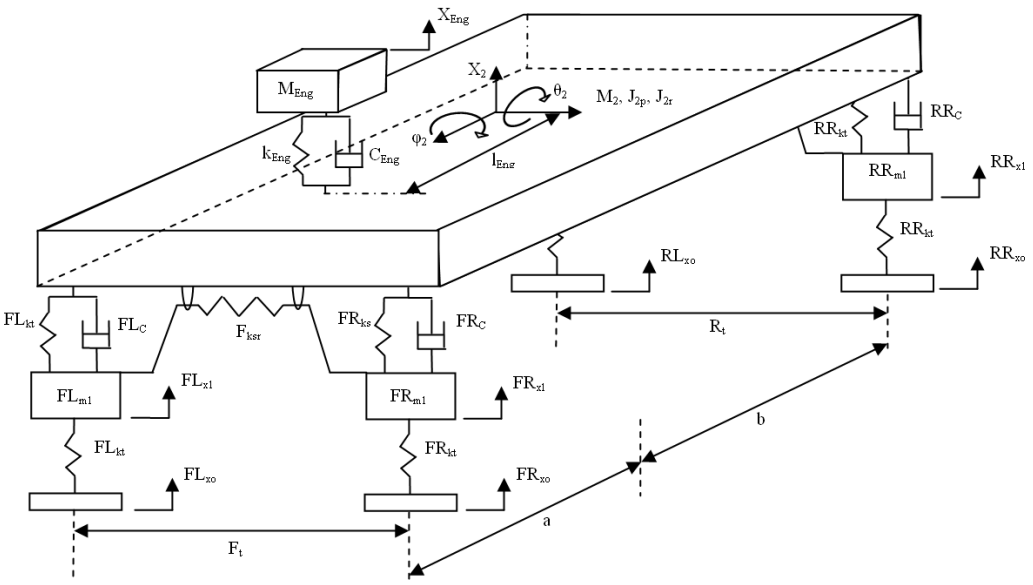

Figure 6-4 – 8 DoF Vehicle Model

Where:

M_2 – Sprung Mass

J_{2p} – Sprung Mass Pitch Moment of Inertia

J_{2r} – Sprung Mass Roll Moment of Inertia

FL,FR,RL,RR_{m1} – Unsprung Masses

FL,FR,RL,RR_{ks} – Spring Stiffness's

FL,FR,RL,RR_{kt} – Tyre Stiffness's

FL,FR,RL,RR_C – Damping Coefficients

F_{ksr} – Front Roll Stiffness

R_{ksr} – Rear Roll Stiffness

F_t – Front Track

R_t – Rear Track

a - Distance from front wheel centre to sprung mass CofG

b - Distance from rear wheel centre to sprung mass CofG

FL,FR,RL,RR_{x0} – Input Displacements

FL,FR,RL,RR_{x1} – Unsprung Mass Displacements

X_2 – Sprung Mass Displacement

θ_2 – Sprung Mass Pitch Angle

φ_2 – Sprung Mass Roll Angle

M_{Eng} – Engine Mass

k_{Eng} – Engine Mounting Stiffness

C_{Eng} – Engine Mounting Damping

l_{Eng} – Forward Distance of Engine Mass and Sprung Mass CofG

$$0 = -M_{Eng}\ddot{x}_{Eng} + k_{Eng}((x_2 + l_{Eng}\theta) - x_{Eng}) + C_{Eng}((\dot{x}_2 + l_{Eng}\dot{\theta}) - \dot{x}_{Eng})$$

(6-3)

$$\begin{aligned}0 = {} & -M_2\ddot{x}_2 + FL_{ks}(FL_{x1} - (x_2 + a\theta_2 + F_t\frac{\varphi_2}{2})) + FL_C(FL_{\dot{x}1} - (\dot{x}_2 + a\dot{\theta}_2 + F_t\frac{\dot{\varphi}_2}{2})) \\ & + FR_{ks}(FR_{x1} - (x_2 + a\theta_2 - F_t\frac{\varphi_2}{2})) + FR_C(FR_{\dot{x}1} - (\dot{x}_2 + a\dot{\theta}_2 - F_t\frac{\dot{\varphi}_2}{2})) \\ & + RL_{ks}(RL_{x1} - (x_2 - b\theta_2 + R_t\frac{\varphi_2}{2})) + RL_C(RL_{\dot{x}1} - (\dot{x}_2 - b\dot{\theta}_2 + R_t\frac{\dot{\varphi}_2}{2})) \\ & + RR_{ks}(RR_{x1} - (x_2 - b\theta_2 - R_t\frac{\varphi_2}{2})) + RR_C(RR_{\dot{x}1} - (\dot{x}_2 - b\dot{\theta}_2 - R_t\frac{\dot{\varphi}_2}{2})) \\ & - k_{Eng}((x_2 + l_{Eng}\theta) - x_{Eng}) - C_{Eng}((\dot{x}_2 + l_{Eng}\dot{\theta}) - \dot{x}_{Eng})\end{aligned}$$

(6-4)

$$0 = -J_{2p}\ddot{\theta}_2 + a\left(FL_{ks}(FL_{x1} - (x_2 + a\theta_2 + F_t\frac{\varphi_2}{2})) + FL_C(FL_{\dot{x}1} - (\dot{x}_2 + a\dot{\theta}_2 + F_t\frac{\dot{\varphi}_2}{2}))\right)$$
$$+ a\left(FR_{ks}(FR_{x1} - (x_2 + a\theta_2 - F_t\frac{\varphi_2}{2})) + FR_C(FR_{\dot{x}1} - (\dot{x}_2 + a\dot{\theta}_2 - F_t\frac{\dot{\varphi}_2}{2}))\right)$$
$$- b\left(RL_{ks}(RL_{x1} - (x_2 - b\theta_2 + R_t\frac{\varphi_2}{2})) + RL_C(RL_{\dot{x}1} - (\dot{x}_2 - b\dot{\theta}_2 + R_t\frac{\dot{\varphi}_2}{2}))\right)$$
$$- b\left(RR_{ks}(RR_{x1} - (x_2 - b\theta_2 - R_t\frac{\varphi_2}{2})) + RR_C(RR_{\dot{x}1} - (\dot{x}_2 - b\dot{\theta}_2 - R_t\frac{\dot{\varphi}_2}{2}))\right)$$
$$- l_{Eng}\left(k_{Eng}((x_2 + l_{Eng}\theta) - x_{Eng}) + C_{Eng}((\dot{x}_2 + l_{Eng}\dot{\theta}) - \dot{x}_{Eng})\right)$$

(6-5)

$$0 = -J_{2r}\ddot{\varphi}_2 + 0.5F_t\left(FL_{ks}(FL_{x1} - (x_2 + a\theta_2 + F_t\frac{\varphi_2}{2})) + FL_C(FL_{\dot{x}1} - (\dot{x}_2 + a\dot{\theta}_2 + F_t\frac{\dot{\varphi}_2}{2}))\right)$$
$$- 0.5F_t\left(FR_{ks}(FR_{x1} - (x_2 + a\theta_2 - F_t\frac{\varphi_2}{2})) + FR_C(FR_{\dot{x}1} - (\dot{x}_2 + a\dot{\theta}_2 - F_t\frac{\dot{\varphi}_2}{2}))\right)$$
$$+ 0.5R_t\left(RL_{ks}(RL_{x1} - (x_2 - b\theta_2 + R_t\frac{\varphi_2}{2})) + RL_C(RL_{\dot{x}1} - (\dot{x}_2 - b\dot{\theta}_2 + R_t\frac{\dot{\varphi}_2}{2}))\right)$$
$$- 0.5R_t\left(RR_{ks}(RR_{x1} - (x_2 - b\theta_2 - R_t\frac{\varphi_2}{2})) + RR_C(RR_{\dot{x}1} - (\dot{x}_2 - b\dot{\theta}_2 - R_t\frac{\dot{\varphi}_2}{2}))\right)$$
$$+ F_tF_{ksr}\left((FL_{x1} - F_t\frac{\varphi_2}{2}) - (FR_{x1} + Ft\frac{\varphi_2}{2})\right) + R_tR_{ksr}\left((RL_{x1} - R_t\frac{\varphi_2}{2}) - (RR_{x1} + Rt\frac{\varphi_2}{2})\right)$$

(6-6)

$$0 = -FL_{m1}FL\ddot{x}_1 + FL_{kt}(FL_{x0} - FL_{x1}) - FL_{ks}(FL_{x1} - (x_2 + a\theta_2 + F_t\frac{\varphi_2}{2}))$$
$$- FL_C(FL_{\dot{x}1} - (\dot{x}_2 + a\dot{\theta}_2 + F_t\frac{\dot{\varphi}_2}{2})) - 0.5F_{ksr}\left((FL_{x1} - F_t\frac{\varphi_2}{2}) - (FR_{x1} + F_t\frac{\varphi_2}{2})\right)$$

(6-7)

$$0 = -FR_{m1}FR\ddot{x}_1 + FR_{kt}(FR_{x0} - FR_{x1}) - FR_{ks}(FR_{x1} - (x_2 + a\theta_2 - F_t\frac{\varphi_2}{2}))$$
$$- FR_C(FR_{\dot{x}1} - (\dot{x}_2 + a\dot{\theta}_2 - F_t\frac{\dot{\varphi}_2}{2})) + 0.5F_{ksr}\left((FL_{x1} - F_t\frac{\varphi_2}{2}) - (FR_{x1} + F_t\frac{\varphi_2}{2})\right)$$

(6-8)

$$0 = -RL_{m1} RL\ddot{x}_1 + RL_{kt}(RL_{x0} - RL_{x1}) - RL_{ks}(RL_{x1} - (x_2 - b\theta_2 + R_t \frac{\varphi_2}{2}))$$
$$- RL_C(RL_{\dot{x}1} - (\dot{x}_2 - b\dot{\theta}_2 + R_t \frac{\dot{\varphi}_2}{2})) - 0.5R_{ksr}\left((RL_{x1} - R_t \frac{\varphi_2}{2}) - (RR_{x1} + R_t \frac{\varphi_2}{2})\right)$$

(6-9)

$$0 = -RR_{m1} RR\ddot{x}_1 + RR_{kt}(RR_{x0} - RR_{x1}) - RR_{ks}(RR_{x1} - (x_2 - b\theta_2 - R_t \frac{\varphi_2}{2}))$$
$$- RR_C(RR_{\dot{x}1} - (\dot{x}_2 - b\dot{\theta}_2 - R_t \frac{\dot{\varphi}_2}{2})) + 0.5R_{ksr}\left((RL_{x1} - R_t \frac{\varphi_2}{2}) - (RR_{x1} + R_t \frac{\varphi_2}{2})\right)$$

(6-10)

The 8 DoF model consists of four unsprung masses, a single sprung mass, and an engine mass. The unsprung masses and engine each have a single vertical degree-of-freedom and the sprung mass has a vertical degree-of-freedom, a rotational degree-of-freedom in pitch and a rotational degree-of-freedom in roll. The model includes suspension stiffness and damping at each corner of the vehicle, with a simple spring to represent the tyre. In addition anti-roll bars are fitted at the front and rear of the model and supply a force based on the difference in suspension displacements on the left and right hand sides.

With this type of model, all four input modes that are applied to the vehicle by the four-post rig during a test can be applied to the vehicle model. Although the additional mass connected to the sprung mass is named as the engine, it could easily be used to simulate the response of passengers on their seats instead. In cases where seat accelerometers are fitted, the response of the passenger on the seat can be determined during the parameter estimation procedure and simulated within the model to note the effect of parameters on absolute passenger acceleration including the seat dynamics. The engine mounting and seat properties are modelled using a simple spring and damper in parallel. In reality the engines mount (hydromount) and seat dynamics (foam and seat cover) would be expected to be more complicated than this, but using this simple arrangement allows the main characteristics to be simulated with minimal parameters. If the seat accelerometers were not fitted during a test and modelling of the engine is not desired then the mass value can be set to zero and the model reduces to a 7 DoF system.

An example of the 8 DoF Simulink model is shown in Figure 6-5.

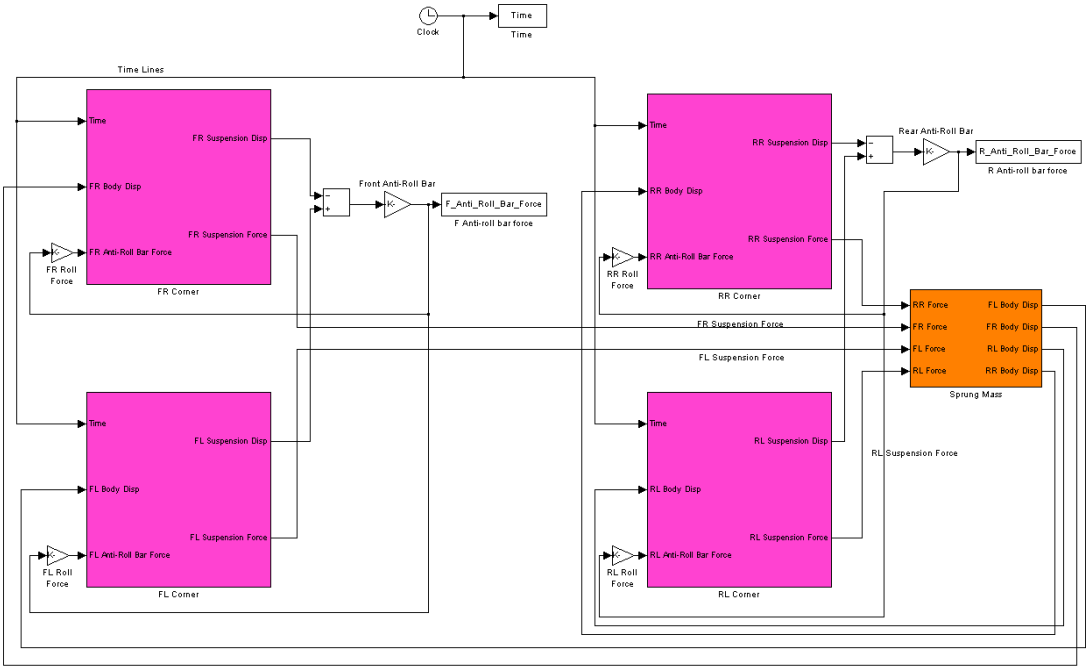

Figure 6-5 – 8 DoF Simulink Model

As the Simulink model is time domain based, any input can be used. This means that once the vehicle parameters have been estimated, if desired, the vehicle could be simulated for a wide range of inputs much faster than a physical test. For example, a whole drive cycle route could be simulated at more than 10 times real-time.

Although the 8 DoF model can be used to simulate the roll response of a vehicle, the difference between the roll response extracted from the four-post rig test and the vehicle model can be large. Section 4.4.3 - Four-Post Rig Method Limitations – Roll Response, showed that when a vehicle is rolled on the rig the roll response is different to that of a vehicle with rotating wheels. This means that parameters estimated from a four-post rig test of the vehicle in roll and applied to the Simulink model, will not provide a response that matches rig data. However, the response from rig data is also dissimilar to the case where the wheels are rotating. The response from the 8 DoF is more similar to the vehicle on the road travelling above 10 m/s, but still does not include factors due to the lateral displacement of the CofG, or the rotation of the sprung and unsprung masses about any axis than their own CofG.

In order to simulate the roll response of the vehicle on the four-post rig a further degree of complexity is required for the sprung mass, lateral motion. An additional two degrees of freedom are required to describe each of the unsprung masses motion, a lateral motion and a rotational motion about their CofG in the longitudinal direction. This model also requires parameters such as the CofG heights, roll centre heights and lateral tyre stiffnesses for simulation of the model. An example of a possible roll model to improve the correlation between four-post rig data and simulated roll response is shown in Figure 6-6.

The task of estimating the roll centre heights and lateral tyre stiffness would be difficult using the four-post rig, as lateral forces and lateral displacements or accelerations are not measured. As the response of the vehicle on the four-post rig does not match the response of the vehicle with rotating tyres, to build the more complex model to match the rig response would reduce the usefulness of the model.

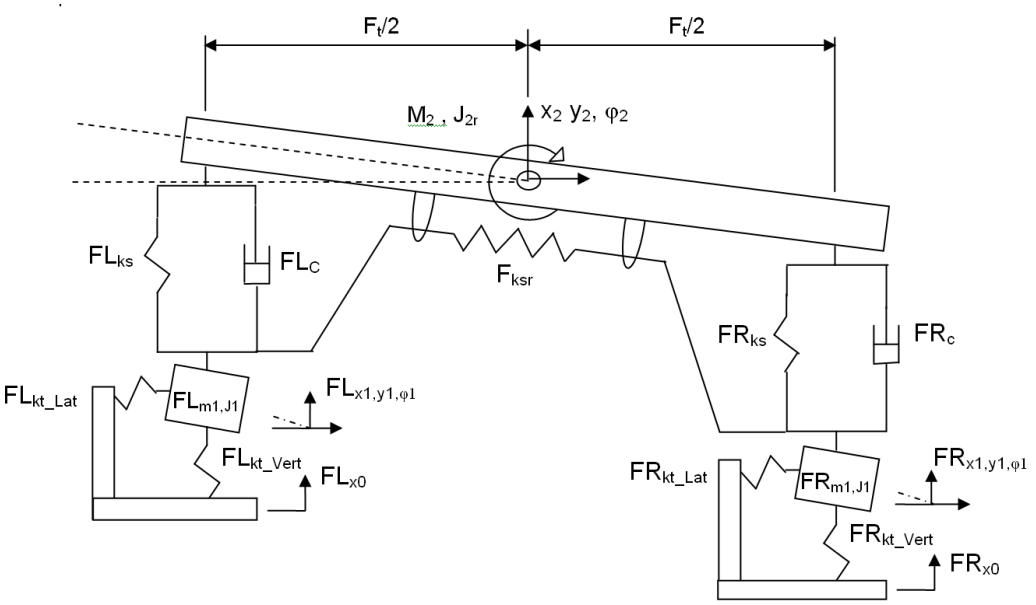

Figure 6-6 – Roll Model with Lateral Compliance

Where:

FL,FR$_{kt\_Lat}$ – Lateral Tyre Stiffness

FL,FR$_{kt\_Vert}$ – Vertical Tyre Stiffness

FL,FR$_{y1}$ – Unsprung Mass Lateral Displacements

FL,FR$_{\varphi 1}$ – Unsprung Mass Roll Angle

y_2 – Sprung Mass Lateral Displacement

6.2.1 – Engine and Passenger Vibration Modelling

When the sprung mass is modelled as a single solid component (as in the 7 DoF model), the assumption is made that every component attached to the vehicle body infinitely stiff and all components are attached rigidly, including the engine, passengers, exhaust, and so on. It is obvious that in the real world this will not be the case. The engine and exhaust are attached to the vehicle body using flexible mountings and the passengers are supported by the seats. It is likely that the some of natural frequencies of these systems will be within the 0.5 to 40 Hz frequency range tested on the rig. If the responses of these objects are poorly controlled then they could have a significant effect on the response of the sprung mass, which in turn has an effect on the contact force response.

Fairly simple models exist where the vertical response of the engine and passengers are simulated as additional single degree-of-freedom systems attached to the vehicle body. However, complex models also exist where the biodynamics of the human body is considered [81], as shown in Figure 6-7.

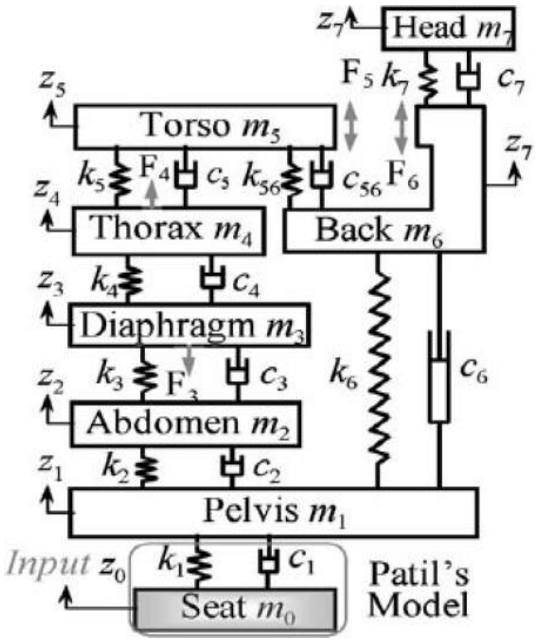

Figure 6-7 – Seven-degree-of-freedom Biodynamic Model – Patil (1977) [81]

It is not the intention of this testing technique to be able to establish absolute levels of discomfort of the passengers to a high degree of accuracy. The intention is to provide a technique that will enable the engineer analysing the data to asses the relative difference in discomfort between different setups or different vehicles. In order to model the complex biodynamic system shown in Figure 6-7 a number of very difficult to acquire parameters would have to be estimated. The increase in accuracy of the comfort assessment would be outweighed by the increased complexity of the model and hence the usefulness of the model would decrease.

Figure 6-8 shows an example of the front apparent sprung mass of a Honda Civic tested on the four-post rig and simulation using Simulink model in its 7 DoF arrangement.

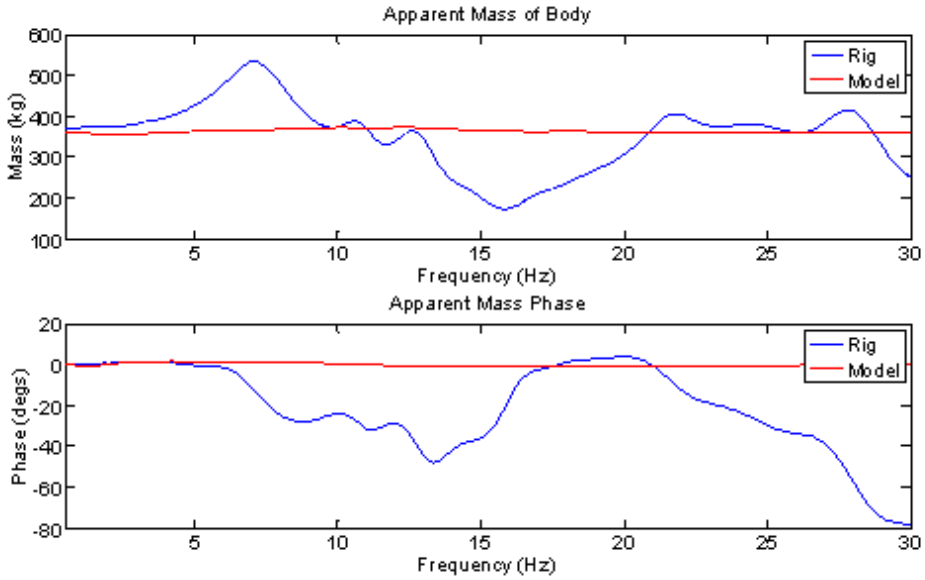

Figure 6-8 – Front Apparent Mass Comparison - Rig Data and 7-DoF Simulink

At very low frequency the values for the rig data and Simulink model both indicate a mass of ~380kg per corner. Across the frequency range the Simulink model's apparent mass can be seen to vary slightly. This is due to slight pitching of the vehicle. In the case of the measured rig data, there is a significant variation in apparent mass, from a maximum of 540 kg to a minimum of 180 kg. The changes in apparent mass are accompanied by a relative phase change in the suspension force and body acceleration. This indicates that the changes in mass are due to the response of objects connected to the sprung mass. At around 6-8 Hz, there is a large increase in mass of almost 160kg and a 30° phase change. The shape of the mode indicates that the damping ratio is not excessively small, so to cause a mass change as large as 160kg, the mass of the object must be significant. This indicates that the response is due to either the engine, or passengers.

In an attempt to replicate the apparent mass of the vehicle tested on the four-post rig the model was used in the 8 DoF configuration. With no measurement of engine acceleration, unknown engine mass, unknown accurate engine CofG position and not even knowing if the apparent mass change was due to engine vibration this was a difficult task and not one that would be simple to implement in a parameter estimation technique (modelling of passenger ballast with accelerometers fitted would be far simpler). In order to match the response, guesses were made at the initial parameters and these were then tuned to provide and appropriate response. Figure 6-9 shows the apparent mass comparison using the eight-degree-of-freedom model.

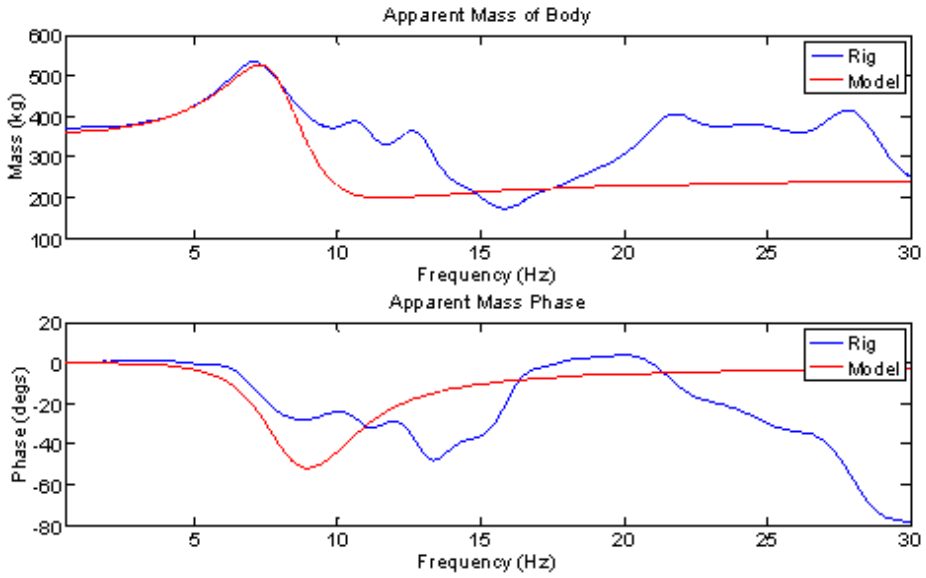

Figure 6-9 - Front Apparent Mass Comparison - Rig Data and 8-DoF Simulink

By modelling the engine degree-of-freedom the accuracy of the simulated apparent mass has improved significantly, especially in the 2-8 Hz range. This would provide a better estimation of body acceleration in that range, which would in-turn improve the estimation of discomfort. However, in the 10-12 Hz and 22-28 Hz ranges the original model performed better. It is obvious from the measured apparent mass that modelling one additional degree-of-freedom is not sufficient to provide a highly accurate simulation of apparent mass, and hence body acceleration. However, it is also not suitable to add many more degrees of freedom to the system for which it is not possible to efficiently extract parameters for from rig data, and that are likely to change significantly in mass, position and mounting properties for different vehicles. For this reason only one additional mass with a single degree-of-freedom was added to the 7 DoF model. The use of this mass is not restricted to modelling of the engine, it could also be used to model any other component desired

6.3 - Modelling Suspension System Features

This section of the thesis details the modelling of suspension system features that are not included within the standard 8 DoF model. In some cases these features can have a large effect on the response of the vehicle and without them tuning of the vehicle in simulation may not provide consistent results with the same tuning applied to the real vehicle.

6.3.1 - Non-linear Dampers

For the previous models explained in this chapter, a linear damping coefficient has been used to express the force across the damper with respect to its velocity. Figure 6-10 shows the force-displacement and force-velocity characteristics of a two different dampers. One linear and a second with a typically non-linear damper curve, both dissipating the same amount of energy for a 20 mm displacement sine wave at 1.5 Hz. The non-linear damper has an almost linear coefficient for negative velocities, which is 43% larger than the linear damper. At positive velocities below 40 mm/s the damping force of the non-linear damper is larger than that of the linear damper, but the characteristic is very digressive, so by 150mm/s the non-linear damping force is only 60% of the linear damper. Figure 6-11 shows body acceleration response for a two-degree-of-freedom suspension model using both the linear and non-linear damper characteristics, where the constant peak velocity sine sweep input amplitude was tuned to provide a suspension displacement of +/-20mm at the body mode natural frequency of 1.5 Hz.

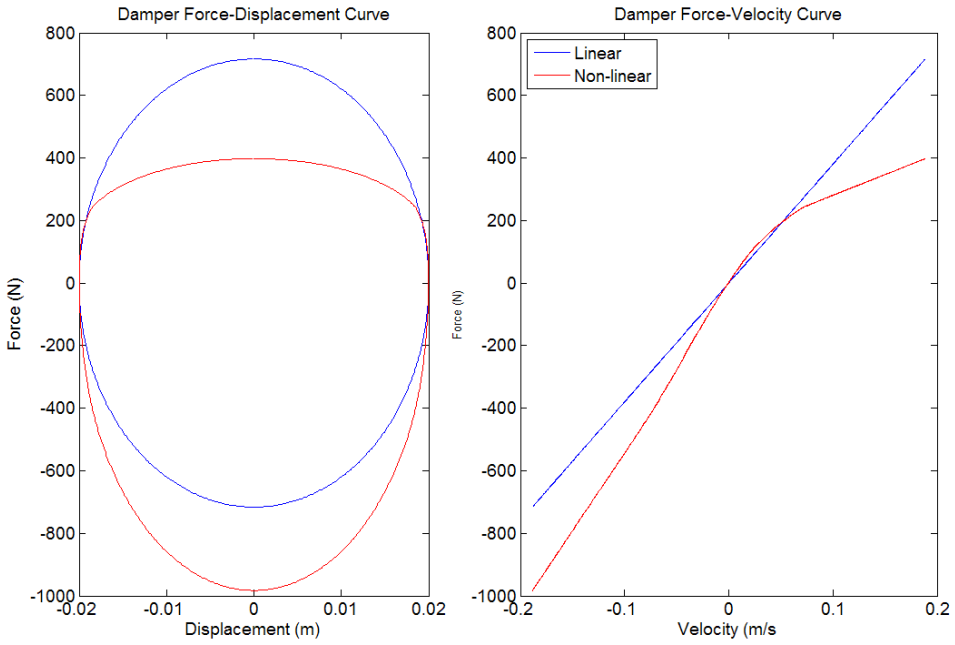

Figure 6-10 – Damper Curve Comparison

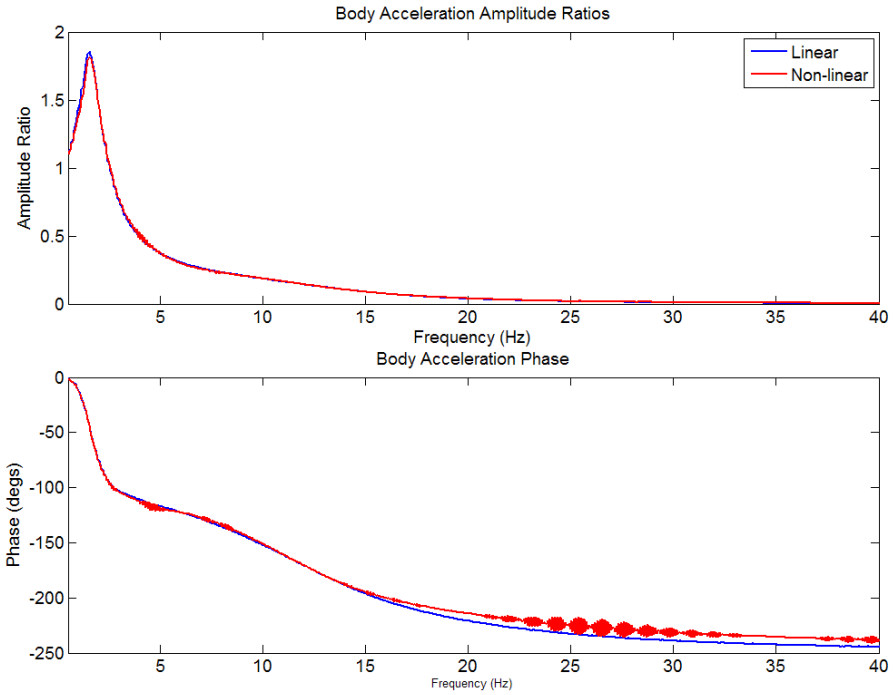

Figure 6-11 – Body Acceleration Response Comparison

Comparing the body acceleration response of both dampers (Figure 6-11) showed very little difference between the linear and non-linear damping response.

In order to compare the transient response of the model using both damper characteristics, a pothole type input taken from [66] pp. 12 (which the author notes was used by Jaguar at MIRA) was modelled and traversed at a forward speed of 15 m/s. The input is shown in Figure 6-12.

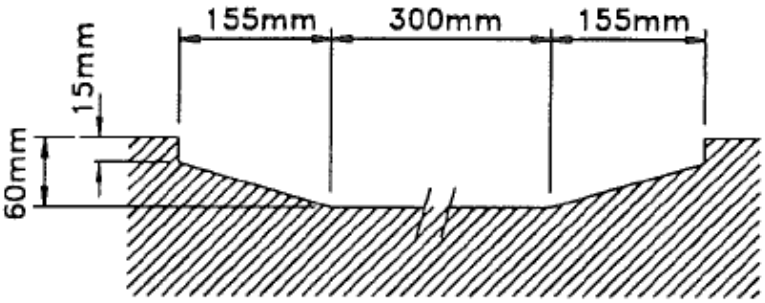

Figure 6-12 – Pothole Input – Crolla et al. [66] pp. 12

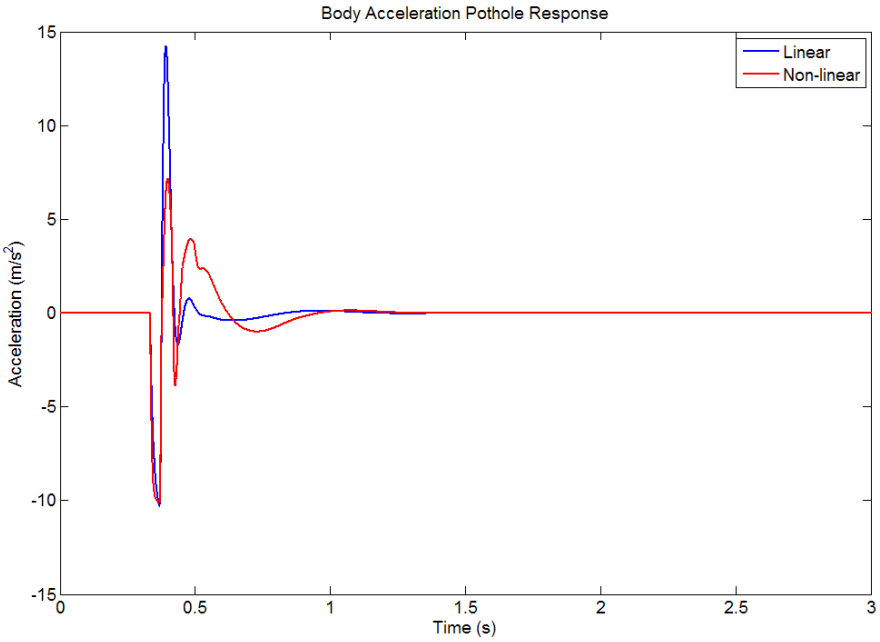

Figure 6-13 – Transient Response to Pothole Input Comparison

The response of the model to the pothole input can be seen to be significantly different for the two different damper characteristics. The linear damper has both a higher peak (double) and peak-to-peak body acceleration than the non-linear damper, which would cause a higher level of peak discomfort to the passengers.

For road cars it is normal practice to use a non-linear damper with a digressive characteristic on the compression side of the damper. This digressive characteristic ensures that peak body accelerations are not excessive due to impulse-type inputs such as pot holes, but for lower amplitude inputs in the random roughness range the suspension displacement range, and contact force control is sufficient. Looking back at Figure 6-10 the non-linear damper can be seen to be digressive in compression, but not in extension. In the case of a downwards pulse input, when the damper force is large enough the tyre will lose contact with the road, and the sprung mass will only accelerate downwards due to gravity and the force due to downwards motion of the unsprung mass, so the acceleration is limited to around -9.81 m/s^2, this makes the digressive blow-off unnecessary in extension.

The asymmetrical damper characteristic also has an effect on the suspension displacement in both the sine sweep and pothole input case. By having more damping force on the rebound side of the damper the point of zero suspension displacement must be shifted to offset the zero suspension force in accordance with the body acceleration. In the case where there is a higher level of damping in extension than compression, this shortens the length of the suspension, reducing the available suspension working space. Figure 6-14 shows an example of the suspension displacement signal measured during the rig test of a vehicle with a similar damping characteristic as the non-linear damper shown in Figure 6-10.

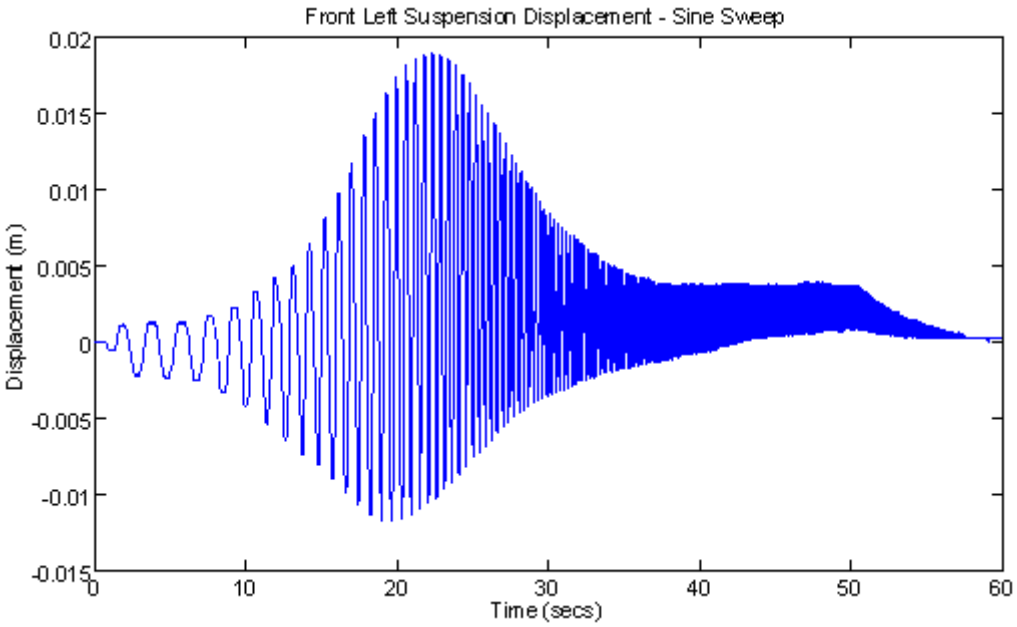

Figure 6-14 – Suspension Displacement of Rebound Biased Damper

The shape of the suspension displacement sine wave can be seen to be very non-linear over the length of the frequency sweep, especially around 18 to 30 seconds, where the suspension displacement is large.

Another use of non-linear damping characteristics in the tuning of road cars is to control the transient roll behaviour of the vehicle due to driver inputs. The damping required to adequately control the roll velocity of the body during the initial stages of heavy cornering is likely to be larger than the damping requirement to provide sufficient contact force control, suspension displacement control and comfort levels from road roughness. This means that a compromise has to be made. As the velocities involved with roll control of the vehicle are relatively low, then a larger coefficient in the first portion of the force-velocity characteristic is common, whilst the digressive characteristic provides more adequate damping for the comfort of the vehicle at larger velocity levels. For this case it is also beneficial to have a higher level of damping in extension than compression, as this will reduce the initial jacking of vehicle caused by the position of the roll centre height relative to the ground plane.

From the information in this section, it is obvious that the non-linear characteristic of the damper plays a significant part in the behaviour of a vehicle. For this reason it is desirable to be able to model the response of the Simulink model due to a non-linear damping characteristic. However, there are also many different forms that the damping characteristic could take, so it would prove a difficult task to use the simulation model to determine the ideal shape of curve, as attempted in Eberhard *et al*. [82].

To overcome this problem the majority of tuning work in simulation can be carried out with a simple linear damper, to determine the levels of damping required to suit the vehicle. Once

tuning with a linear damping coefficient has been completed the non-linear damper can be included in the simulation. In order to do this the engineer can design a particular shape of damper curve that is known to provide a desirable 'feel' of vehicle. The magnitude of the damping force can then be tuned to determine the damping levels required with the desired curve. In addition, different curve designs can be assessed by the engineer using the simulation model. However, the optimisation cannot separate differences in performance index due to the shape or magnitude of the damping characteristic only their combined effect.

In order to improve the simulation of vehicles tested on the four-post rig, damper characteristics extracted directly from the rig data can also be used within the vehicle simulation model.

To implement the non-linear damping characteristic into the vehicle simulation a lookup table is used in the place of the normal gain block used to define the damping coefficient. In the case where a linear damping coefficient is to be used a simple lookup table is created using the linear coefficient.

6.3.2 - Suspension System Layout

Typically the suspension systems modelled in the majority of vehicle models ([32], [36] and [39]), consist of a spring and damper connected in parallel between the sprung and unsprung masses, as has been shown in all of the previous models in the section of the thesis. However, for real vehicles it is not commonly the case that both spring and damper are connected rigidly to the sprung mass. The connection of the damper is almost always in series with a flexible bushing called a top mount. In some cases the spring is also connected to the sprung mass through the top mount. These types of suspension are called 'single-path' and 'dual-path' respectively. An analysis of the 'dual-path' type of suspension system was carried out by Gallagher and Volterra [53]. The authors showed mathematically that by using this type of suspension the maximum amplitude of the impulse response could be reduced by as much as 30% compared to the system where the spring and damper were connected rigidly to the sprung mass. As the impulse response is similar to that of a pot hole type input, this is obviously an important factor in reducing the discomfort felt by the passengers due to such inputs. As well as having an influence on the impulse response of the suspension, the top mount will also have an effect on the frequency response, by changing the dynamic stiffness with respect to frequency. Figure 6-15 and Figure 6-16 show examples of the single-path and dual-path type suspension layouts, with their dynamic stiffness equations shown in equations (6-11) and (6-12) respectively.

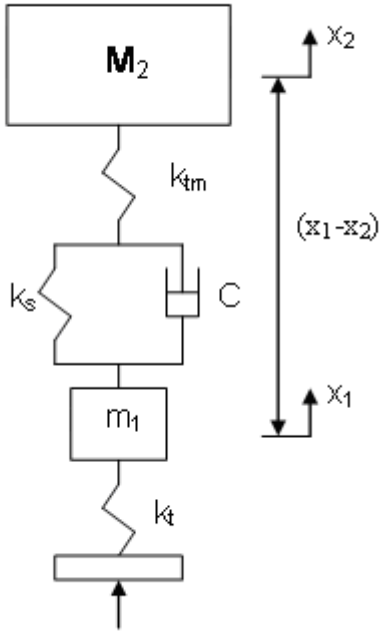

Figure 6-15 – Single-path Suspension Layout (Model 1)

$$k_{dyn} = \left(\frac{1}{k_s + jC\omega} + \frac{1}{k_{tm}} \right)^{-1}$$

(6-11)

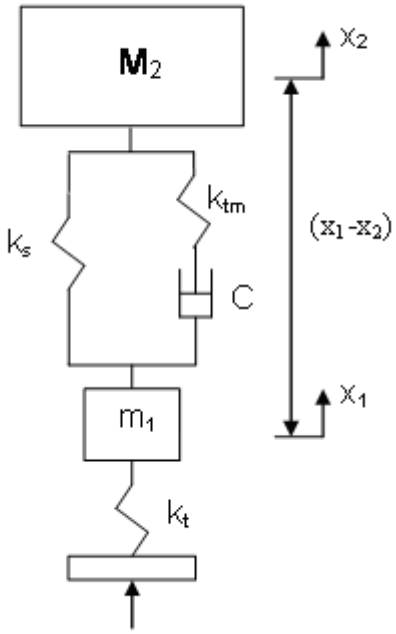

Figure 6-16 – Dual-path Suspension Layout (Model 2)

$$k_{dyn} = \left(k_s + \left(\frac{1}{jC\omega} + \frac{1}{k_{tm}} \right)^{-1} \right)$$

(6-12)

Where:

k_{dyn} – Dynamic Stiffness

k_s – Spring Stiffness

k_{tm} – Top Mount Stiffness

C_s – Damper Coefficient

j – Imaginary unit

Figure 6-17 compares the dynamic stiffness response of three different top mount stiffness values (Table 6-1) using the single-path and dual path cases.

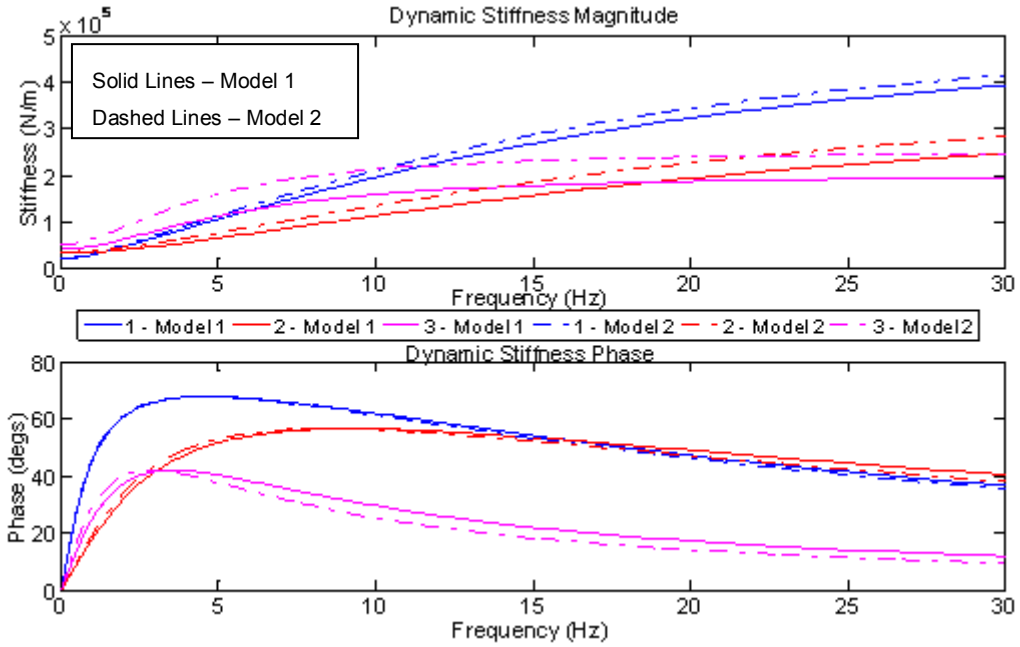

Figure 6-17 – Dynamic Stiffness Models Comparison

	Case 1	Case 2	Case 3
ks	20,000	35,000	50,000
ktm	500,000	350,000	200,000
C	3500	2000	5000

Table 6-1 – Dynamic Stiffness Parameters

Figure 6-17 shows that the top mount stiffness has a significant effect on the dynamic stiffness of the suspension system. The dynamic stiffness magnitude shows the overall stiffness of the suspension system with frequency, whereas the phase shows the phase of the force with reference to displacement. In order to control the unsprung mass it is important that the damping is sufficiently high around the hub mode natural frequency. With reduced top mount stiffness the magnitude of dynamic stiffness is reduced, but more vitally the phase of the dynamic stiffness is also reduced at higher frequencies, decreasing the damping of the hub mode. In some cases this can be quite significant. If a hub mode is poorly controlled due to a low stiffness top mount, then the engineer might seek to improve this by increasing the damper coefficient. In some cases this will actually reduce the damping of the hub mode and will also increase the damping present in the 4-10 Hz range, which has a direct effect on the discomfort felt by the passengers. Figure 6-18 shows the unsprung mass response for a system without a top mount, a dual-path system with a 400 N/mm top mount and the same system with the damping coefficient increased by 20%. Figure 6-19 shows the weighted body acceleration PSDs of the three different setups for a road surface with a constant velocity PSD.

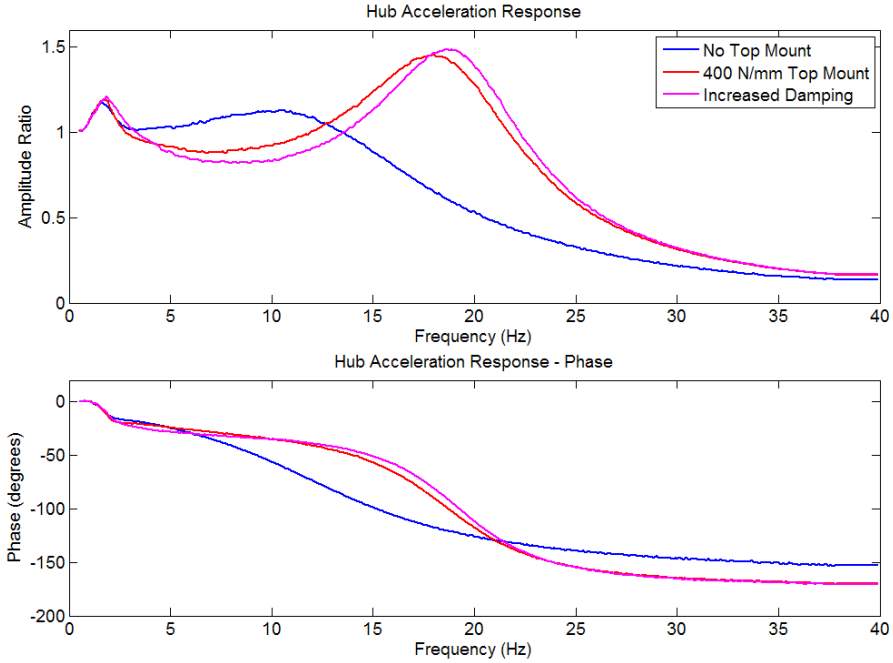

Figure 6-18 – Hub Acceleration Response

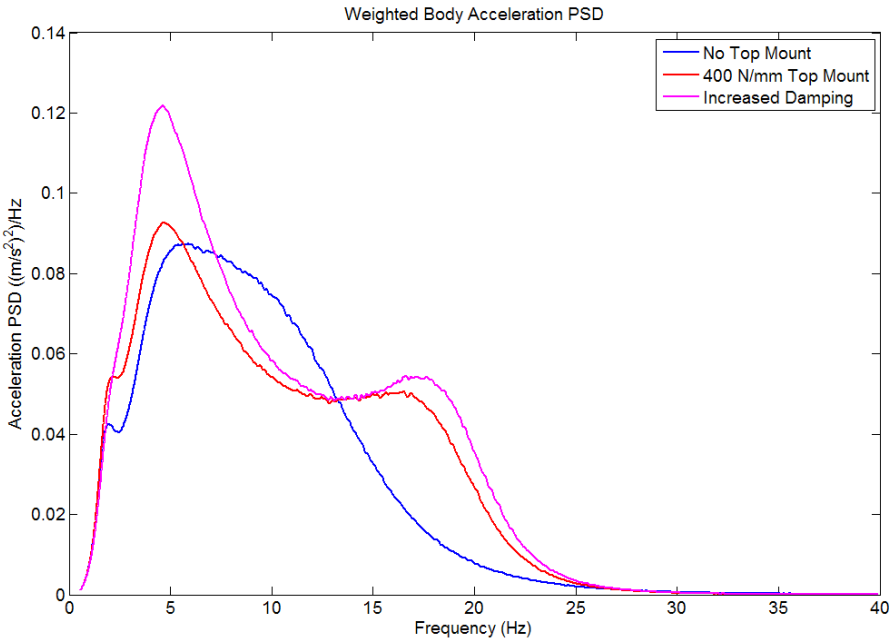

Figure 6-19 – Weighted Body Acceleration Response

It is clear that the modelling of the correct suspension system is vital to ensure that the top mount stiffness is tuned as a suspension component and not neglected, as its influence can be significant. As it is quite common for vehicles to have either single-path or dual-path tyre suspension systems then it is also a requirement that both can be modelled within the same vehicle model.

There are two main ways in which these systems could be modelled. The first is to add a small mass between the top mount and its connection to the damper in the dual-path system, or in the single-path system between the spring and damper and top mount. However, this would involve adding and an additional four-degrees-of-freedom to the vehicle model, and the inclusion of a small mass may provide a very stiff system that is difficult for Simulink to solve. The second method is to replace the spring and damper in original model with a transfer function that represents the dynamic stiffness of the desired suspension system. However, this means that a non-linear damper characteristic can no longer be used. As it may be desirable to model both a non-linear damper and a less than infinite top mount stiffness within the same model another method must be found.

The method used to solve this problem was to use both a transfer function and the non-linear damper characteristic within the same model by using a linearised damping coefficient within the transfer function and a fully non-linear damper look-up table. In order to do this an additional displacement is used to define the displacement at the point of the top mount connection to the rest of the suspension system. This point is described as $x_{1.5}$ and an example of the single-path system with including $x_{1.5}$ can be seen in Figure 6-20.

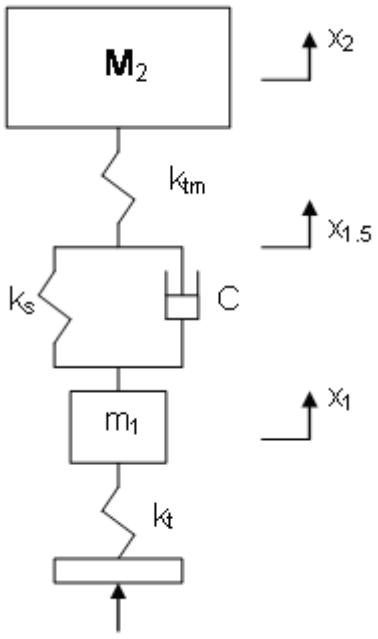

Figure 6-20 – Dual-path System with additional $x_{1.5}$ displacement

In this system the force in the spring and damper must be equal to the force in the top mount, as shown in equation (6-13).

$$k_s(x_1 - x_{1.5}) + C(\dot{x}_1 - \dot{x}_{1.5}) = k_{tm}(x_{1.5} - x_2) \quad \textbf{(6-13)}$$

By taking a Laplace Transform of equation (6-13) and expanding,

$$CX_1 s - CX_{1.5} s + k_s X_1 - k_s X_{1.5} = k_{tm} X_{1.5} - k_{tm} X_2$$

(6-14)

Combining $X_{1.5}$ terms and taking X_1 terms the right,

$$X_{1.5}(Cs + k_s + k_{tm}) = k_{tm} X_2 + X_1(Cs + k_s)$$

(6-15)

Resolving for $X_{1.5}$ and separating X_1 and X_2 terms

$$X_{1.5} = \left(\frac{k_{tm}}{Cs + k_s + k_{tm}} \right) X_2 + \left(\frac{Cs + k_s}{Cs + k_s + k_{tm}} \right) X_1$$

(6-16)

By implementing equation (6-16) within the Simulink model the displacement of $x_{1.5}$ can be acquired, which can then be used to calculate the force due to spring displacement and the suspension velocity to be used in a damper look-up table.

In the dual-path case the same theory is applied but the resulting equation is shown in equation (6-17).

$$X_{1.5} = \left(\frac{k_{tm}}{Cs + k_s + k_{tm}} \right) X_2 + \left(\frac{Cs}{Cs + k_s + k_{tm}} \right) X_1$$

(6-17)

In this case the spring displacement is calculated using x_1 and x_2, whereas the damper velocity is calculated by differentiation of (x_1-$x_{1.5}$)

By using a variety of gain blocks that can be switched depending on the type of suspension system used, single-path, dual-path and no top mount systems can be simulated within one vehicle model.

6.4 – Full Car Modelling

In order to investigate the effect of load variations on vehicle handling so that various aspects of the performance index could be created, a full car lateral model was created in Simulink. The model is explained in detail in section 6.4.2– Full Car Lateral Vehicle Model, whilst the tyre modelling in particular is explained in section 6.4.1 - Tyre Modelling.

6.4.1 - Tyre Modelling

Although the vertical tyre models used in most vibration simulations consist typically of a simple spring or spring-damper, the interactions of the tyre with the road are far from simple and far from linear. There are many different tyre models that exist that allow simulation of the forces and torques at the contact patch including analytical models such as Dugoff et al. (1970) [83], thermo-mechanical tyre models such as Michelin's TaMeTirE (2007) [84] and finite element tyre models as used in [85]. Probably the most popular of the tyre models used in relatively simple simulations in research and the automotive industry is the 'Magic Formula' tyre model [57]. The model is a semi-empirical model which uses a large number of constants (150+) to model the longitudinal, lateral and combined force generation characteristics of a tyre. Generally these constants are determined by fitting the model to tyre test rig data from a number of different running conditions. Figure 6-21 shows a comparison between the model and measured data taken from Pacejka's 'Tyre and Vehicle Dynamics' book [58].

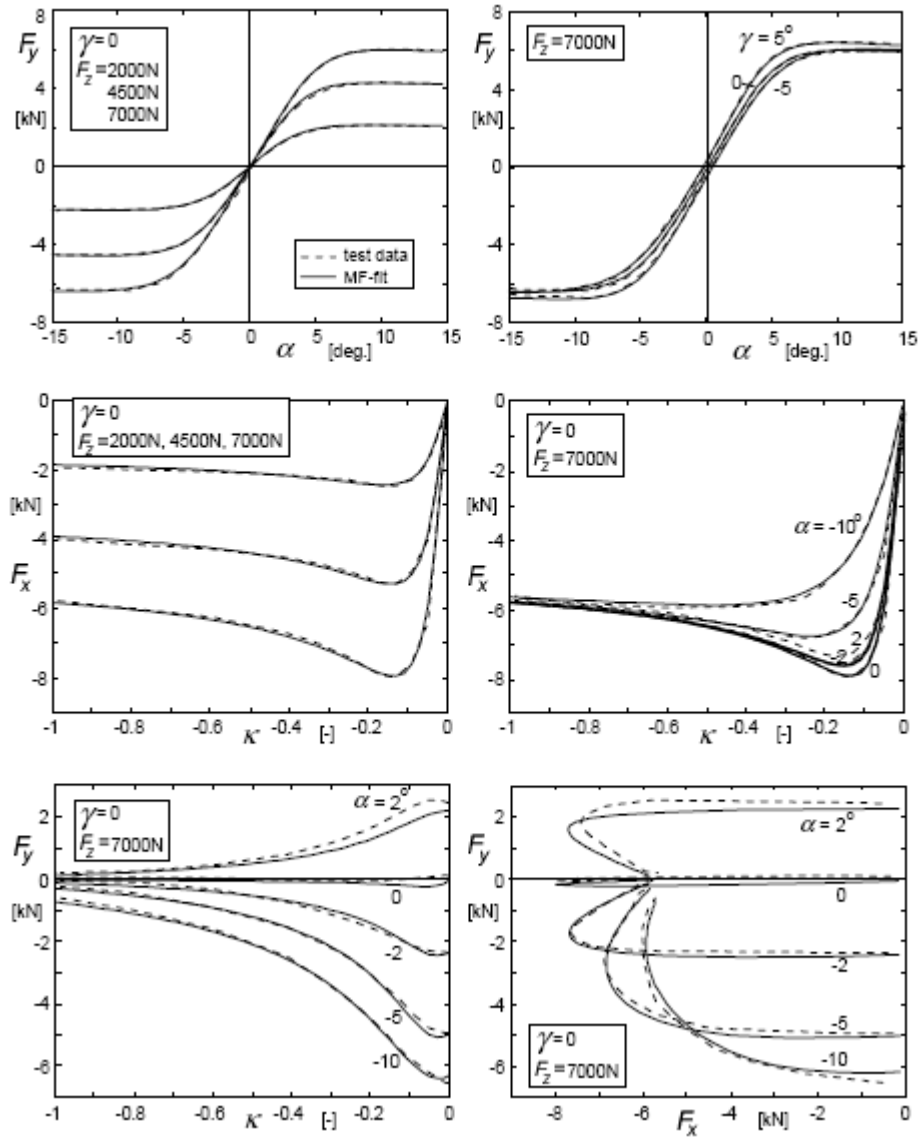

Figure 6-21 - Comparison of tyre data (dotted lines) and magic tyre fits (solid lines) – Pacejka [58] pp. 210

The basic shape fitting of the 'Magic Formula' model is explained briefly in section 2.7 – Vehicle Modelling. For more details of the equations used to define the force characteristics Pacejka [58] should be consulted.

The inputs to the tyre model are as follows:

- F_z – Vertical Force
- α – Slip Angle
- κ – Longitudinal Slip (Slip Ratio)
- γ – Camber

With the outputs

- F_y – Lateral Force
- F_x – Longitudinal Force
- M_z – Aligning Moment

The simplest form of slip angle is defined using equation (6-18) and explained graphically in Figure 6-22.

$$\alpha = -a\tan\left(\frac{V_y}{V_x}\right) \tag{6-18}$$

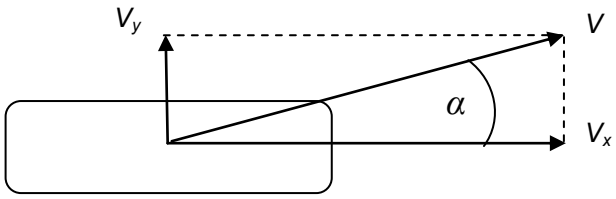

Figure 6-22 – Slip Angle Definition

Where:

V_y – Lateral velocity at wheel centre

V_x – Longitudinal velocity at wheel centre

V – Velocity magnitude at wheel centre

The simple slip ratio is defined using equation (6-19) and shown graphically in Figure 6-23

$$\kappa = -\frac{V_{sx}}{V_x} \tag{6-19}$$

Where,

$$V_{sx} = V_x - (\Omega \times r_e)$$

(6-20)

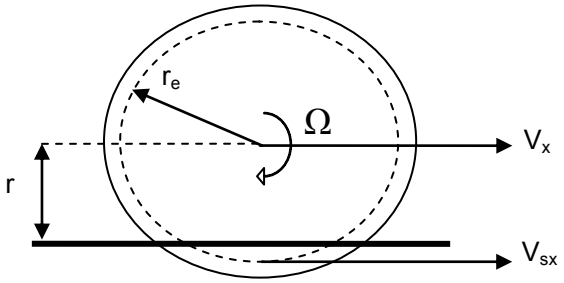

Figure 6-23 – Slip Ratio Definition

Where:

V_{sx} – Slip velocity

r_e – Effective rolling radius

r – Loaded radius

Ω – Angular wheel speed

As well as steady-state tyre characteristics, an adaption to the model using a 'relaxation length' allows transient modelling of the tyre due the fast slip angle and changes and vertical load vibrations. An example of the lateral tyre forces generated at a range of frequencies for the same slip angle and load variation is shown in Figure 6-24.

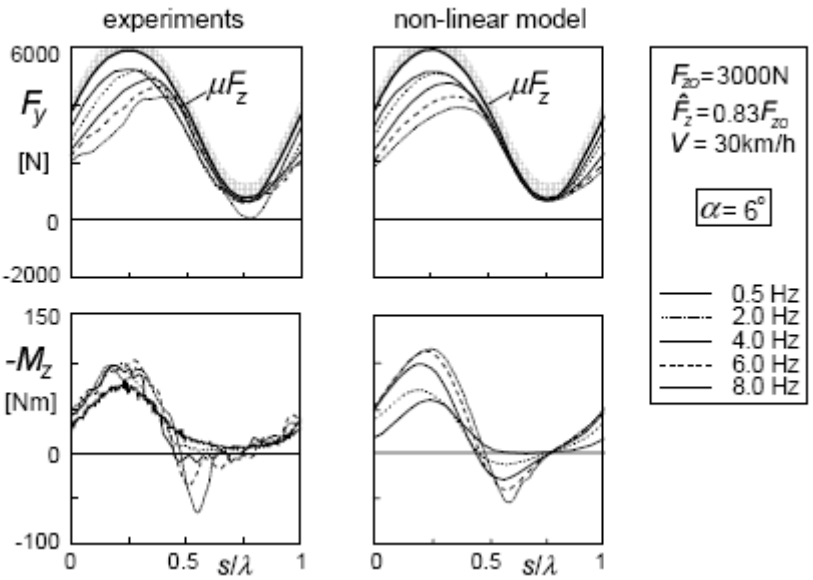

Figure 6-24 - Dynamic vertical load effects on lateral force generation – Pacejka [58] pp. 374

The equations from the 'Magic Formula' tyre model were reproduced from Pacejka [58] to create a tyre model in a MATLAB S-function that could be run in Simulink. Rather than using the tyre parameters from Pacejka a set of tyre parameters from the ADAMS/Tire help document [86] for a 235/60 R16 tyre. These parameters were used as it was the only case where a complete set of parameters required to model the tyre including transients could be obtained.

6.4.2 – Full Car Lateral Vehicle Model

The full car lateral model used in simulations within this thesis was a 6 degree-of-freedom model (Figure 6-25), with the vehicle body having yaw and lateral degrees of freedom, but using a forced speed in the longitudinal direction. Each of the wheels had a rotational degree-of-freedom and were coupled to the 'Magic Formula' model S-function as explained in the previous section.

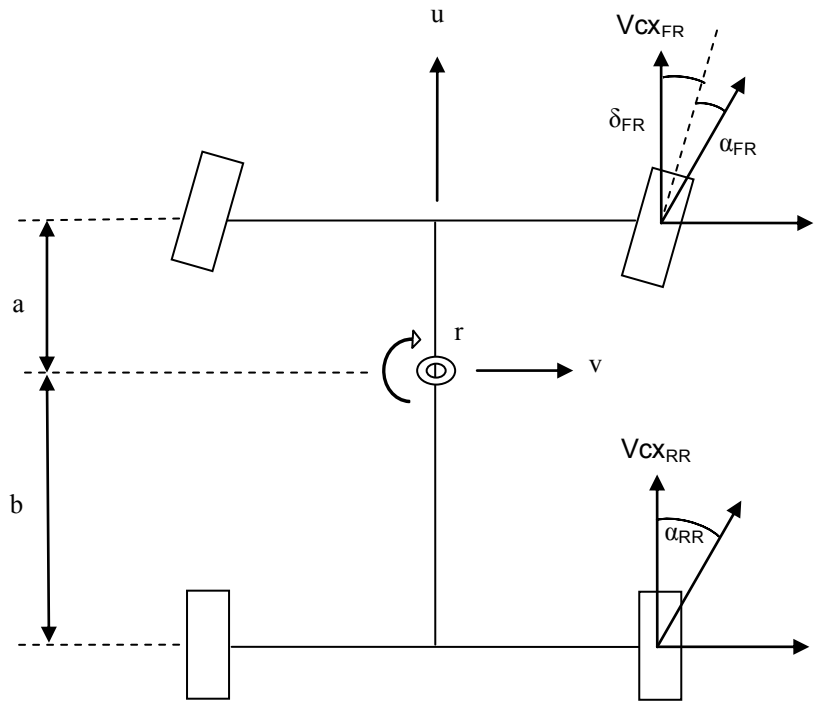

Figure 6-25 – Full Car Lateral Vehicle Model Definitions

The weight transfer due to lateral acceleration was modelled using front and rear roll centre heights and weight distribution, as well as the relative front and rear roll stiffness distribution. The model itself had no vertical degrees-of-freedom, but vertical loads could be applied at the four contact patches from the 8 degree-of-freedom four-post model. In addition a time dependant lateral force scalar could be applied to each of the contact patches.

To control the steering of the vehicle, two different options were modelled. In the first case the steering could be forced to a predefined angle. In the second case a curvature could be defined and the steering model defined by Rill in [55] used to control the steer velocity.

The lateral and yaw equations of motion of the vehicle model are given in equations (6-21) and (6-22).

$$M(\dot{v} - ur) = Fy_{FL} + Fy_{FR} + Fy_{RL} + Fy_{RR}$$

(6-21)

$$J\dot{r} = a(Fy_{FL} + Fy_{FR}) - b(Fy_{RL} + Fy_{RR})$$

(6-22)

Where:

M – Vehicle Mass

J – Vehicle Yaw Moment of Inertia

Fy_{FL}, Fy_{FR}, Fy_{RL}, Fy_{RR} – Tyre Lateral Forces

a – Longitudinal Distance from Front Axle to CofG

b – Longitudinal Distance from Rear Axle to CofG

v – Lateral Velocity of CofG

r – Yaw Velocity

For each tyre the lateral force is defined using equation (6-23).

$$Fy = \lambda_{Fy} \times (MagicFormula(Fz, Vcx, \alpha))$$

(6-23)

Where:

Fz – Vertical Force

Vcx – Longitudinal Velocity at Wheel Centre

α – Slip Angle

λ_{Fy} – Lateral Force Scaling Factor

Longitudinal velocities at each wheel are calculated using equations (6-24) and (6-25), with slip angles at each wheel calculated using equations (6-26) to (6-29). Small angle approximations are used throughout.

$$Vcx_{FL}, Vcx_{RL} = u + \left(\frac{F_t}{2} r \right)$$

(6-24)

$$Vcx_{FR}, Vcx_{RR} = u - \left(\frac{R_t}{2} r \right)$$

(6-25)

Where:

F_t – Front Track

R_t – Rear Track

$$\alpha_{FL} = \left(\frac{v + ar}{Vcx_{FL}} \right) - \delta_{FL}$$

(6-26)

$$\alpha_{FR} = \left(\frac{v + ar}{Vcx_{FR}} \right) - \delta_{FR}$$

(6-27)

Where:

δ_{FL} – Front Left Road Wheel Steering Angle

δ_{FR} – Front Right Road Wheel Steering Angle

$$\alpha_{RL} = \left(\frac{v - br}{Vcx_{RL}} \right)$$

(6-28)

$$\alpha_{RR} = \left(\frac{v - br}{Vcx_{RR}} \right)$$

(6-29)

Road wheel steering angles are calculated using equations (6-30) and (6-31).

$$\delta_{FL} = \delta_{HW} \left(\frac{1}{R_{Ack}} \right) \quad \delta_{HW} \geq 0$$

$$\delta_{FL} = \delta_{HW} \left(R_{Ack} \right) \quad \delta_{HW} < 0$$

(6-30)

$$\delta_{FR} = \delta_{HW} \left(R_{Ack} \right) \quad \delta_{HW} \geq 0$$

$$\delta_{FR} = \delta_{HW} \left(\frac{1}{R_{Ack}} \right) \quad \delta_{HW} < 0$$

(6-31)

Where:

δ_{HW} – Hand Wheel Steering Angle (no steering ratio)

R_{Ack} – Ackermann Steering Ratio

In the case where the steering is open-loop, the hand wheel angle is directly controlled from an external variable. In the path following (closed-loop) control mode, the steering angular velocity is determined using equation (6-32) and integrated.

$$\dot{\delta}_{HW} = (\rho_{Des} - \rho_{Act}) K \times u$$

(6-32)

Where:

ρ_{Des} – Desired Curvature

ρ_{Act} – Actual Curvature

K – Steering Gain

The vertical loads on the tyres are a combination of static mass, weight transfer and artificially added load variation, as in equations (6-33) to (6-36).

$$Fz_{FL} = M\left(\frac{b}{a+b}\right) + WT_F + CPL_{FL}$$

(6-33)

$$Fz_{FR} = M\left(\frac{b}{a+b}\right) - WT_F + CPL_{FR}$$

(6-34)

$$Fz_{RL} = M\left(\frac{a}{a+b}\right) + WT_R + CPL_{RL}$$

(6-35)

$$Fz_{RR} = M\left(\frac{a}{a+b}\right) - WT_R + CPL_{RR}$$

(6-36)

Where:

WT_F – Front Weight Transfer

WT_R – Rear Weight Transfer

CPL_{FL}, CPL_{FR}, CPL_{RL}, CPL_{RR} – Artificially Added Load Variation

The front and rear weight transfers are calculated using equations (6-37) and (6-38).

$$WT_F = \frac{RC_F\left(\frac{b(M(\dot{v}-ur))}{a+b}\right) + \left(\frac{F_{ksr}(M \times RC_{CofG})}{(F_{ksr}+R_{ksr})}\right)}{F_T}$$

(6-37)

$$WT_R = \frac{RC_R\left(\frac{a(M(\dot{v}-ur))}{a+b}\right)+\left(\frac{R_{ksr}(M\times RC_{CofG})}{(F_{ksr}+R_{ksr})}\right)}{R_T}$$

(6-38)

Where:

RC_F – Front Roll Centre Height

RC_R – Rear Roll Centre Height

RC_{CofG} – Roll Axis Height at CofG

F_{ksr} – Front Roll Stiffness

R_{ksr} – Rear Roll Stiffness

For this method to be valid the lateral acceleration was constrained so that it was not possible to have negative load on one wheel due to weight transfer. In addition, the tyre models were constrained so that negative load due to contact load variation caused Fy to be zero, rather than negative.

For investigations carried out within the thesis, all parameters were set to be representative of a 2007 5-Door Honda Civic.

In order to tune the closed-loop steering model a test was carried out to determine the appropriate gain (K), to ensure that the driver model would not apply steering corrections at a higher frequency than a driver would be likely to do. Initially an open-loop swept sine steering input was used to determine the yaw velocity frequency response of the vehicle at 20 m/s. The closed-loop mode was then used to follow a swept sine curvature for a variety of steering K values, again at 20 m/s. The curvature was defined so that the magnitude of the steering input at 0.05 Hz was the same as the open-loop case. The results are shown in Figure 6-26 below.

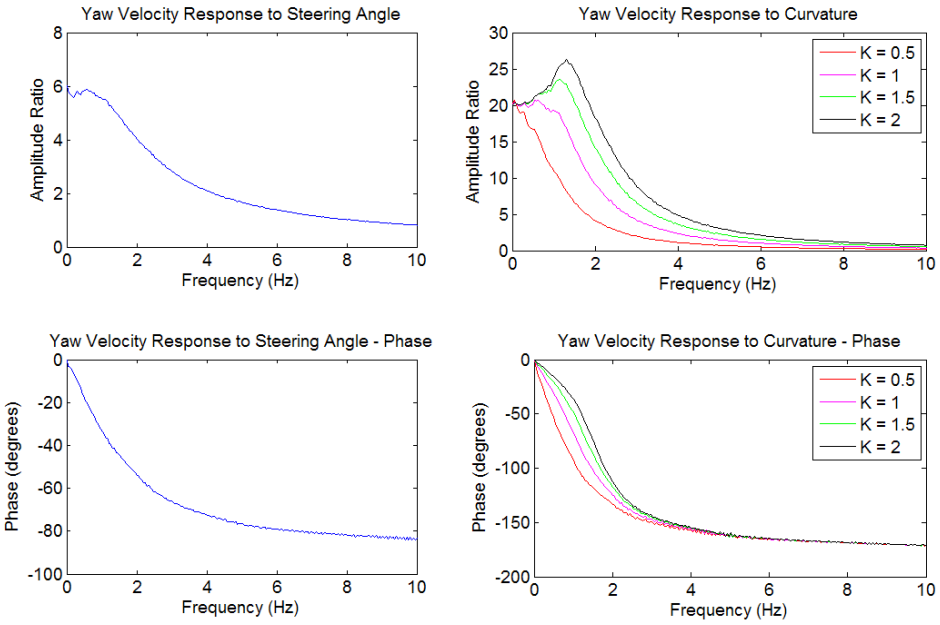

Figure 6-26 – Yaw Velocity Response to Steering Angle and Curvature

The steering model gain results (Figure 6-26) show that in cases where the steering gain was high, the driver model would correct at frequencies where the steering input was significantly out-of-phase with the yaw velocity, causing a higher than steady-state yaw response to curvature. In reality it is unlikely that a non-professional driver would steer in the opposite direction to the direction in which the car should travel to correct its path, as it is counter intuitive. With a gain of 1, the steering behaviour response is similar to that of the vehicles yaw response. This is a more realistic case for the simple driver model, even though it might still control the vehicle to a higher frequency than the non-professional driver would be able to do.

6.5 – Parameter Estimation and Vehicle Model Validation

In order to validate the vehicle model and parameter estimation technique a test was carried out using a 2007 Honda Civic with a variety of different components from different models to create 18 different set-ups. As the parameters of the components were unknown the process would validate both the simulation model and the parameter estimation technique, as if either were incorrect the response would be inaccurate.

For each set-up a set of Heave, Pitch, Roll and Warp constant peak velocity sine sweeps were carried out at a variety of amplitudes. For each set-up the vehicle parameters were estimated and the vehicle model in its seven degree-of-freedom state used to simulate the vehicle response due to the identical inputs as the rig. (Note: At this point in the project no accelerometers were available to measure seat and floor acceleration). Responses were then created using the same signal processing method as the rig data, as to avoid any possible differences due to signal processing.

Table 6-2 shows the suspension components used for each of the 18 set-ups.

Set-up No.	Front				Rear		
	Wheels (Inches)	Springs	Dampers	Anti-roll Bar (mm)	Springs	Dampers	Pre-load Tube (mm)
1	16	Std	Std	23	Std	Std	41
2	17	Std	Std	23	Std	Std	41
3	17	Std	Std	23	1.8 5 Dr	Std	41
4	17	Std	Std	23	1.8 5 Dr	Type R	41
5	17	Std	Std	23	2.2 D	Type R	41
6	17	Std	Std	23	2.2 D	1.8 5 Dr	41
7	17	Std	1.8 5 Dr	23	2.2 D	1.8 5 Dr	41
8	17	1.8 5 Dr	1.8 5 Dr	23	2.2 D	1.8 5 Dr	41
9	17	1.8 5 Dr	2.2 D	23	2.2 D	1.8 5 Dr	41
10	17	1.8 5 Dr	2.2 D	23	2.2 D	Type R	41
11	17	1.8 5 Dr	2.2 D	23	Std	Type R	41
12	17	1.8 5 Dr	2.2 D	0	Std	Type R	41
13	17	1.8 5 Dr	2.2 D	24	Std	Type R	41
14	17	1.8 5 Dr	2.2 D	24	Std	1.8 5 Dr	41
15	17	1.8 5 Dr	Std	24	Std	1.8 5 Dr	41
16	17	1.8 5 Dr	Std	24	Std	Type R	41
17	17	1.8 5 Dr	Std	24	Std	Type R	39
18	17	1.8 5 Dr	Std	24	Std	Type R	43

Table 6-2 – 2007 Honda Civic Setup Table

The first set-up tested was with the Civic in the same set-up as it arrived at Oxford Brookes. The parameters estimated using the parameter estimation program are shown below in Table 6-3.

Set-up Number		1
Unsprung Mass (kg)	Front	38.47
	Rear	38.1
Sprung Mass (kg)		1150
Inertia (kg.m^2)	Pitch	1612
	Roll	330
Spring Rate (N/mm)	Front	51.7
	Rear	22.89
Damper Coefficient (N-sec/mm)	Front	3.662
	Rear	2.452
Top Mount Stiffness (N/mm)	Front	1059
	Rear	1857
Tyre Stiffness (N/mm)	Front	248
	Rear	226
Roll Stiffness (N/mm)	Front	69.8
	Rear	24.6

Table 6-3 – Set-up 1 Estimated Parameters

Once the parameters had been estimated the parameter values were put into the Simulink model, which was run in Heave, Pitch, Roll and Warp input modes. The results from this were exported to a '.txt' file in exactly the same format as the files exported by the Multimatic four-post rig program. The data was then used in the parameter estimation as if it were real rig data. The parameter estimation correctly identified all of the simulation model input parameters to within 1.5% accuracy. Then the output responses from the model were compared to that of the rig data. Figure 6-27 presents the front body acceleration response comparison.

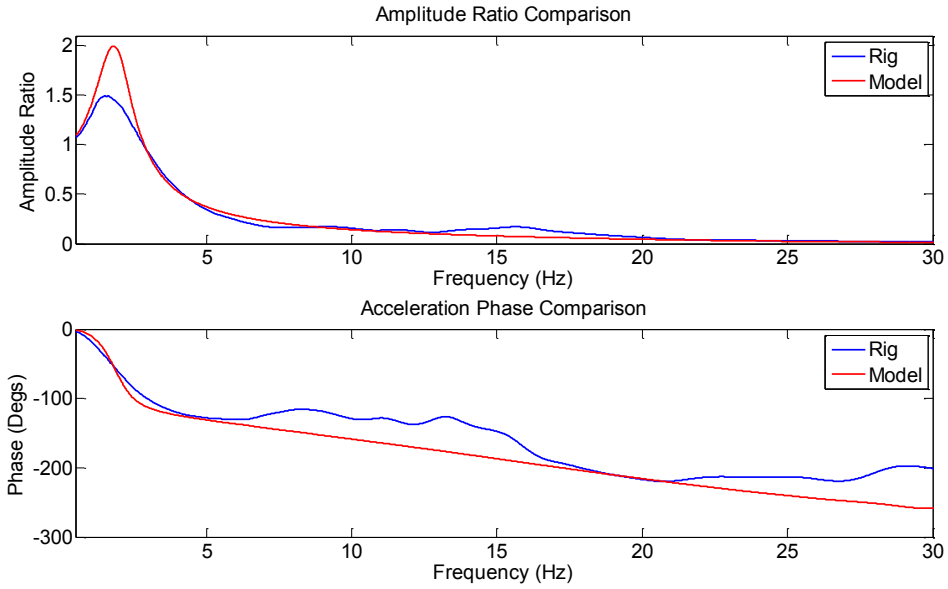

Figure 6-27 – Front Body Acceleration Response Comparison – Set-up 1

The correlation of the front body acceleration response does not show a promising start for the model estimation. The damping ratio of the body mode is much too low, resulting in much higher peak acceleration. Figure 6-28 shows the same comparison at the rear of the Civic.

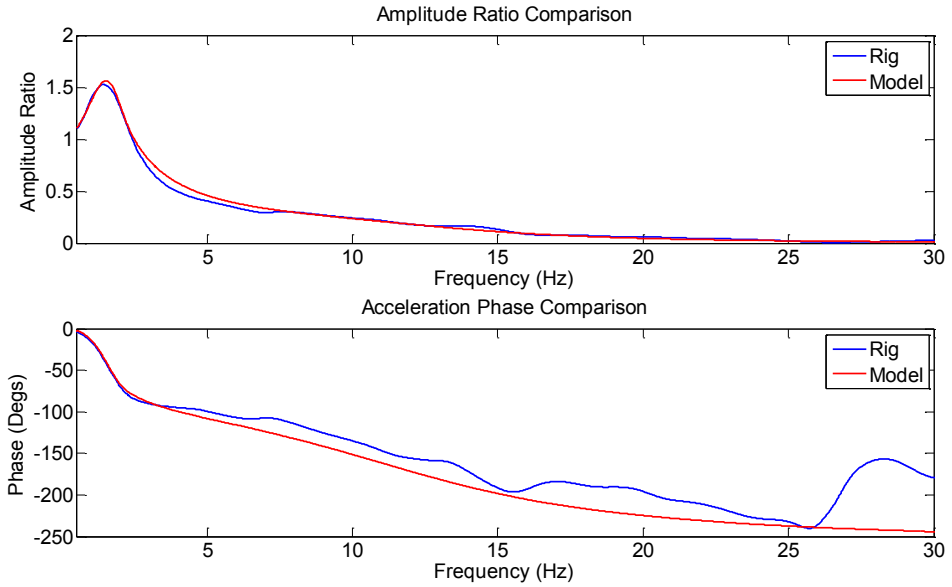

Figure 6-28- Rear Body Acceleration Response Comparison – Set-up 1

The rear body acceleration model response at low frequency is much more similar to the rig response. This indicates that the rear suspension parameters are sufficiently accurate. The inaccuracies at higher frequency are due to vibrations occurring within the body of the vehicle that are not modelled in the vehicle model. One of the most significant differences between the rig and model result was the front apparent mass shown in Figure 6-29.

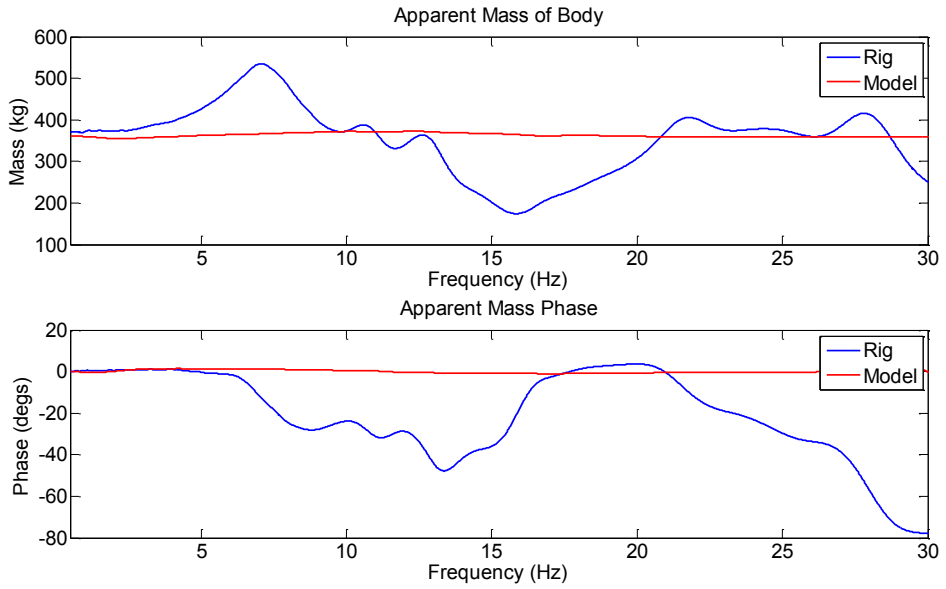

Figure 6-29 – Front Apparent Mass Comparison – Set-up 1

The front apparent mass rig response changes significantly over the frequency range, indicating parts fitted to the sprung mass of the vehicle going into resonance. This effect was described in section 6.2.1 – Engine and Passenger Vibration Modelling, and the simulated apparent sprung mass response was improved by modelling the response of the engine on its mountings (Figure 6-30). The engine modelling was only carried out for this example and not used in the rest of the model simulations.

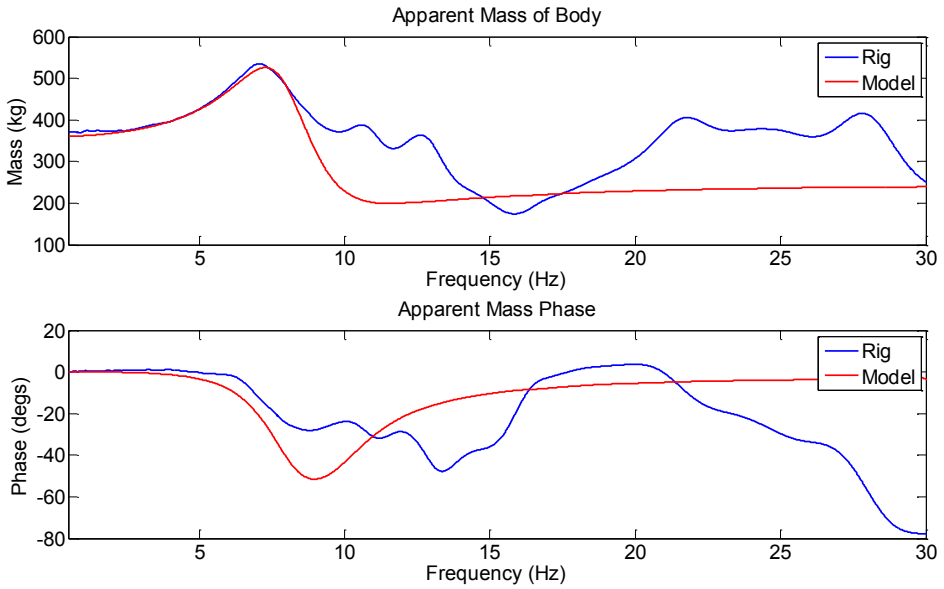

Figure 6-30 – Apparent Mass Comparison with Modelled Engine Response

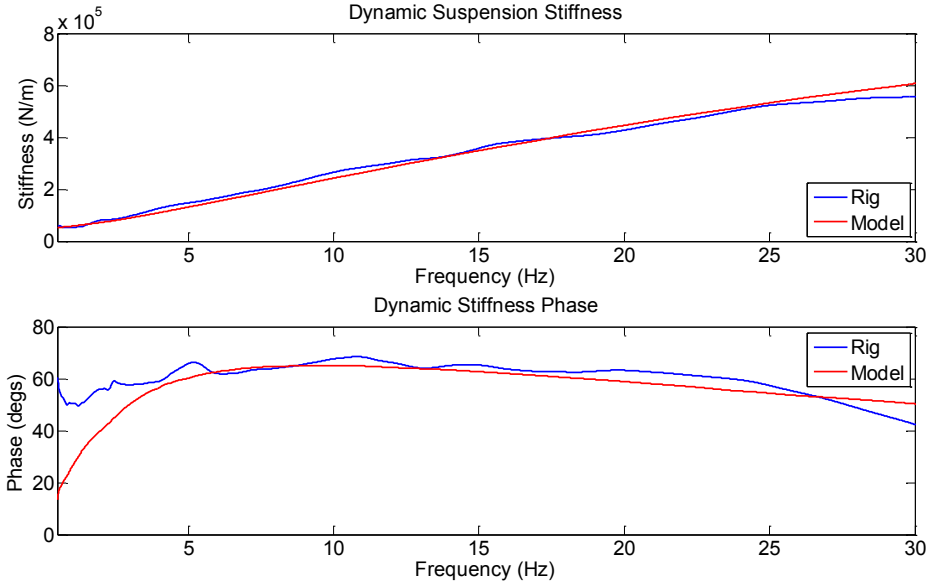

Figure 6-31 – Front Dynamic Stiffness Comparison – Set-up 1

Comparison of the front dynamic stiffness for the rig and model shows very different phase angles around the location of the body mode (1.7 Hz). The rig data shows a large phase angle of around 54° at the body mode, whereas the modelled phase is only 37°. This means that the damping present in the model was much lower than that of the real vehicle. However, over the rest of the frequency range the phase and magnitude of the rig data and model match quite well.

There are a few different reasons why the damping in the rig data may be so high. At very low frequency there is some damping due to the friction, but at the body mode where suspension displacement and velocity are large its effect should be small. The digressive nature of the front damper curve will also have an effect on the damping coefficient across the frequency range. However, areas where the velocity is high the damping coefficient should be lowest. This is the opposite effect being seen in the rig phase response in Figure 6-31. One other factor that may cause increased damping is bump stop contact. It is known that the Civic uses the bump stops a large amount due to its very low suspension working space in the front suspension. The bumpstop will have its own stiffness and damping characteristics, but the fact that it is not in contact for the complete cycle means that the dynamic stiffness is a combination of the traditional suspension system and the bumpstop. In order to improve the accuracy of the modelled response around the body mode, the dynamic stiffness estimator was tuned so that it would work out the most accurate parameters for a small portion of data around the body mode (1-4 Hz). From this new front suspension parameters were identified, so that the body mode could be modelled more accurately. Figure 6-32 shows the measured and estimated dynamic stiffness for the 1-4 Hz tuned parameters.

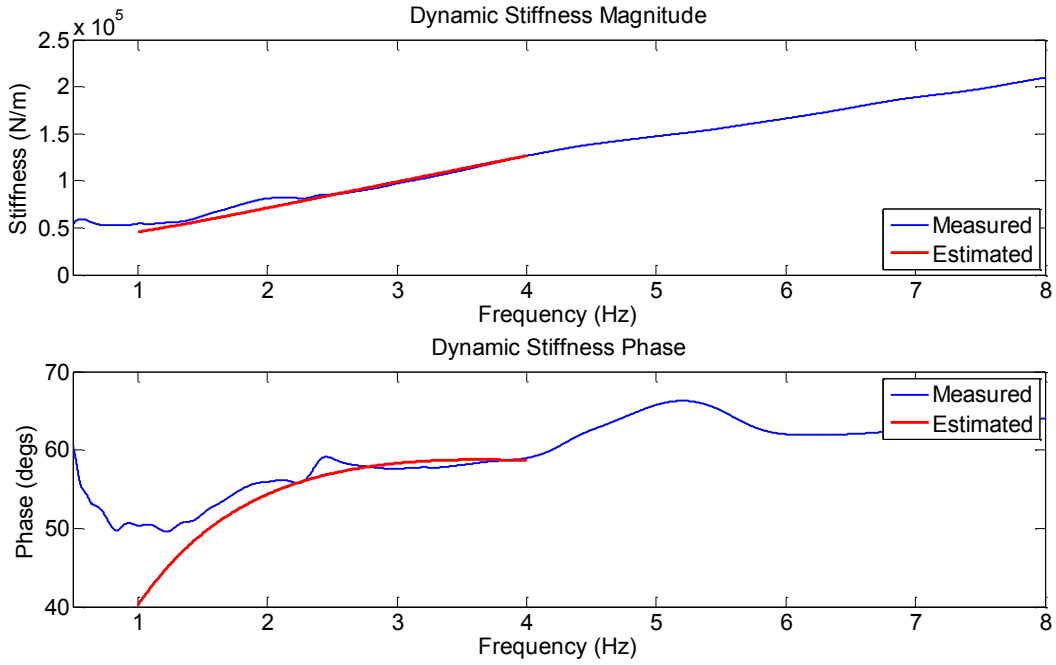

Figure 6-32 – Dynamic Stiffness Comparison – Set-up 1, 1-4Hz

The parameters estimated using this part of the data were:

k_s – 32.581 N/mm

k_{tm} – 384.54 N/mm

C – 4.708 N-sec/mm

These values were then input into the vehicle model so that the responses could be compared to the rig data. Figure 6-33 to Figure 6-42 show the comparisons between the rig and modelled data with the new parameters.

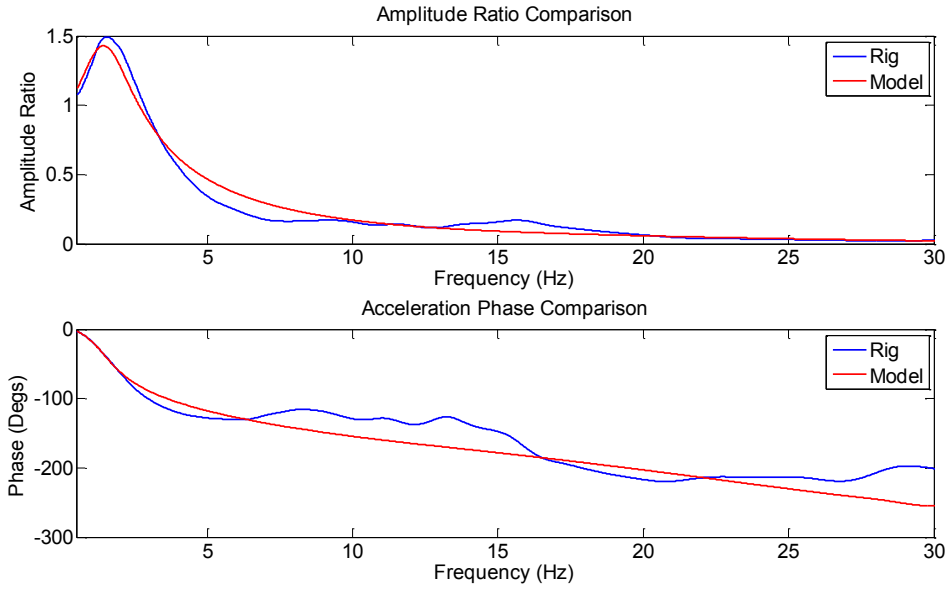

Figure 6-33 – Front Body Acceleration Response – Set-up 1, Amended

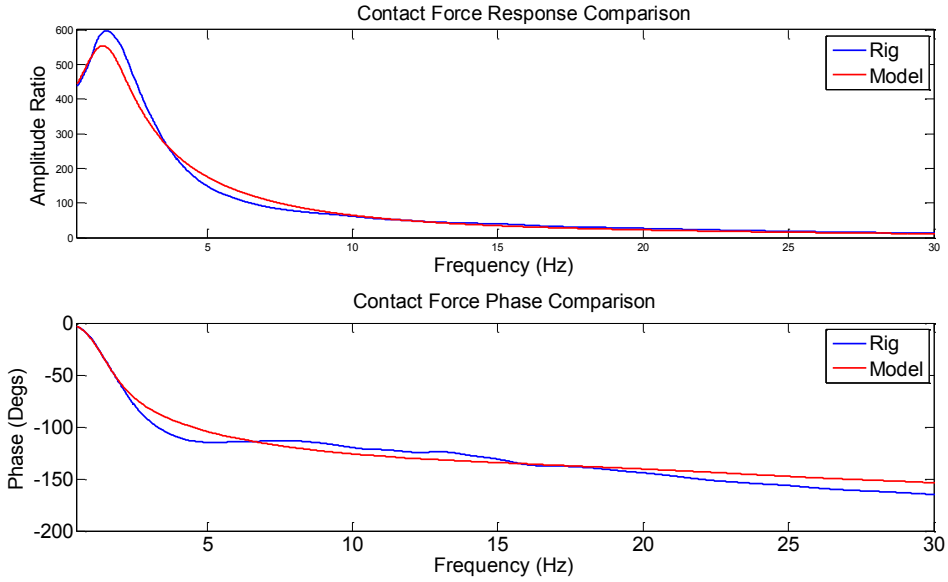

Figure 6-34 – Front Contact Force Response – Set-up 1, Amended

The front body acceleration response plot in Figure 6-33 shows much improved correlation with the new suspension parameters, the same is true of the contact force responses shown in Figure 6-34.

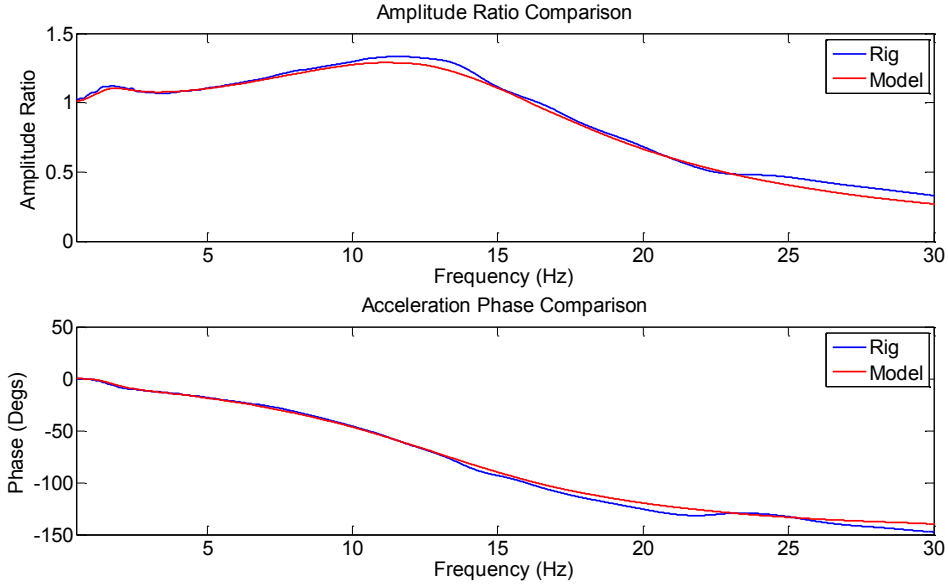

Figure 6-35 – Rear Hub Acceleration Response – Set-up 1, Amended

The rear hub acceleration (Figure 6-35) has good correlation between the rig and model responses.

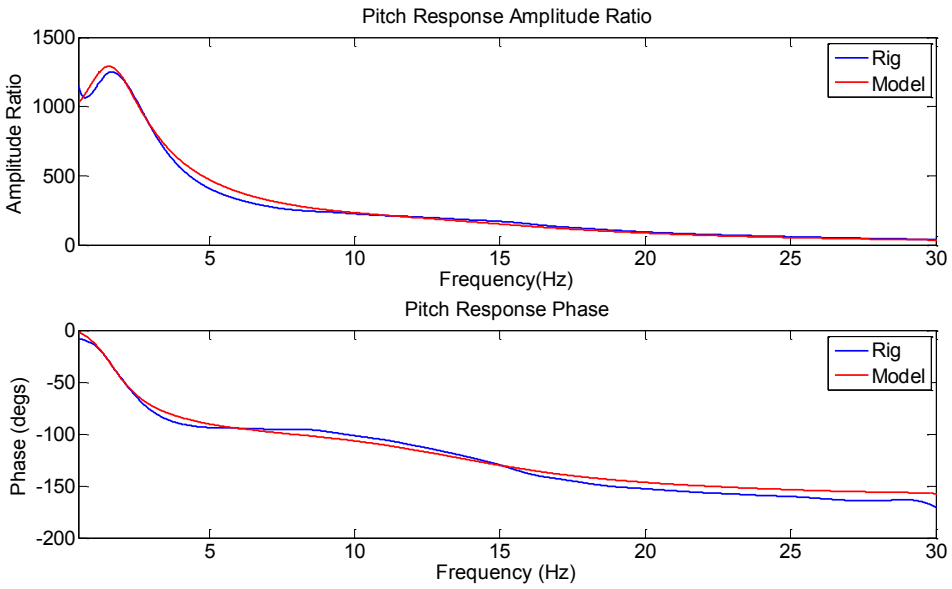

Figure 6-36 – Contact Force Pitch Response – Set-up 1, Amended

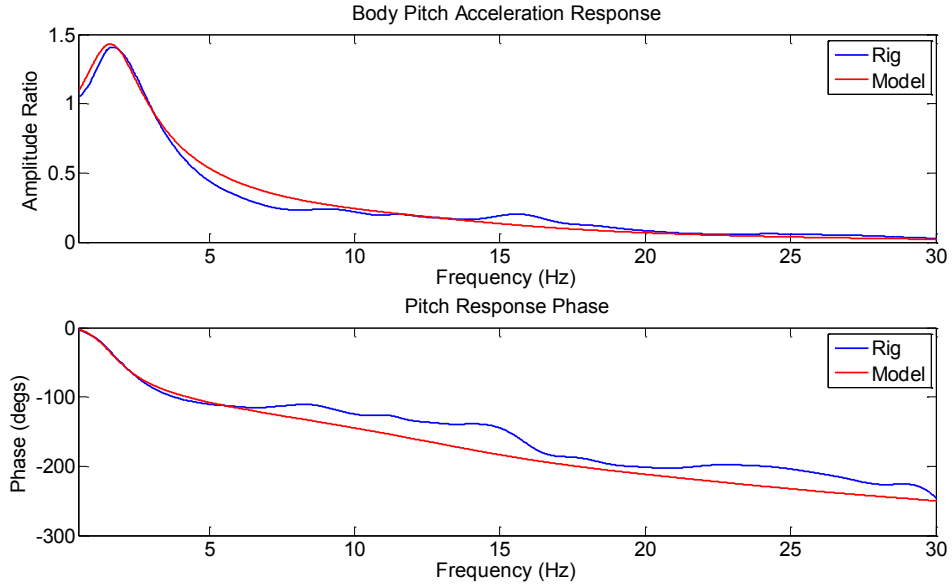

Figure 6-37 – Pitch Body Acceleration Response – Set-up 1, Amended

The pitch contact force and body acceleration responses show fair correlation, but again there are discrepancies at higher frequency due to the fact that the real vehicle is far more complicated than the 7 degree-of-freedom system modelled.

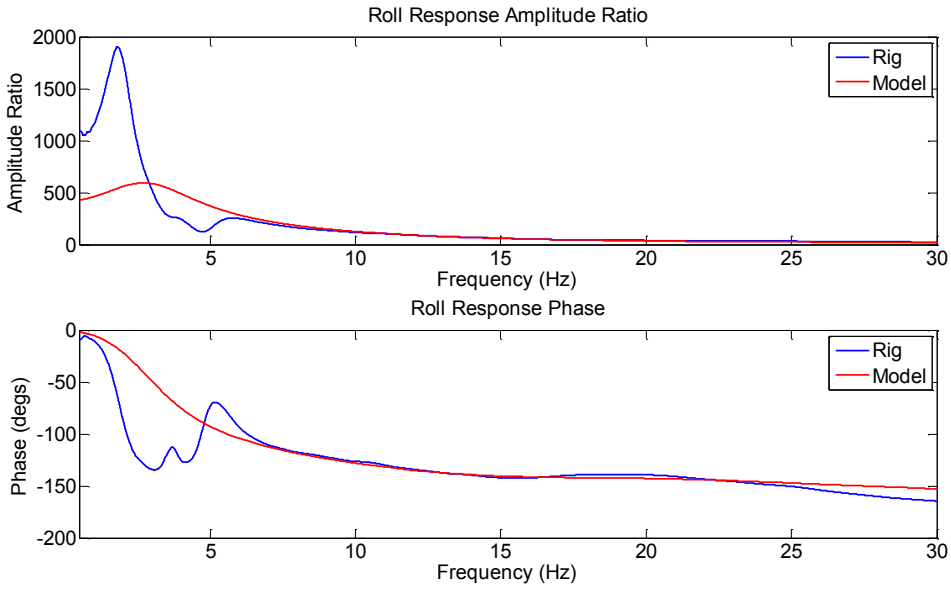

Figure 6-38 – Front Roll Contact Force Response - Set-up 1, Amended

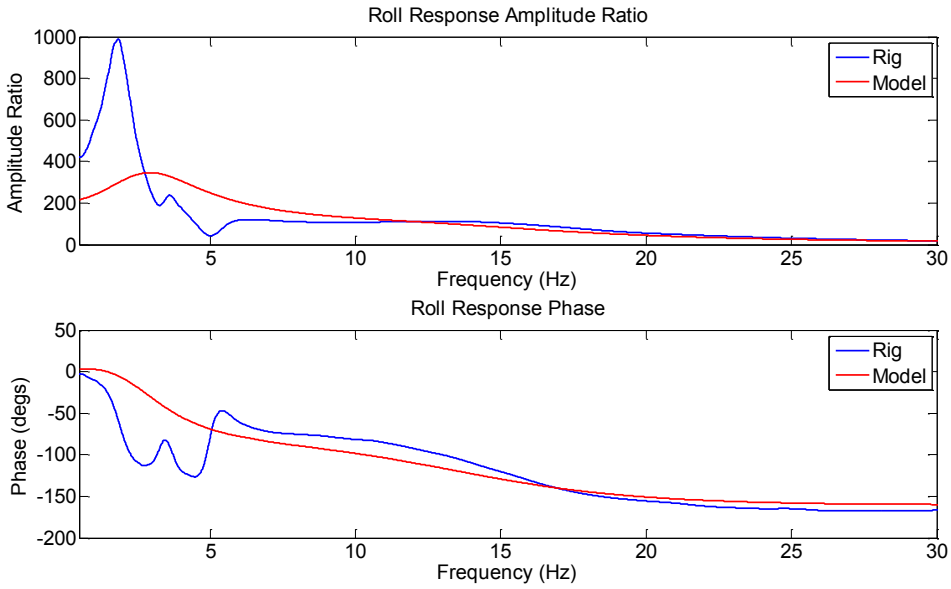

Figure 6-39 – Rear Roll Contact Force Response - Set-up 1, Amended

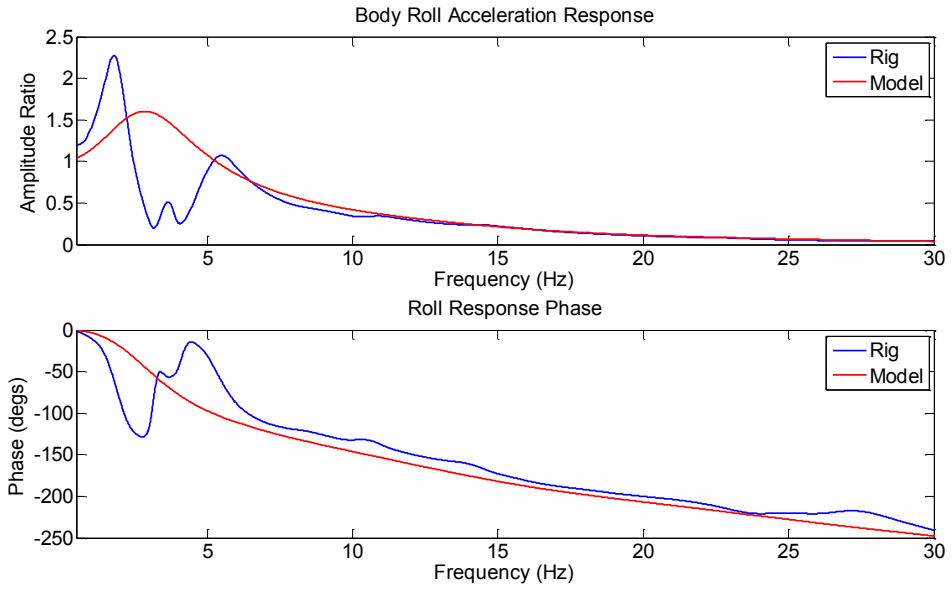

Figure 6-40 – Roll Acceleration Response - Set-up 1, Amended

The roll responses in Figure 6-37 to Figure 6-39 show significant differences between the rig and model. This problem was addressed previously in section 4.4.3 – Roll Response.

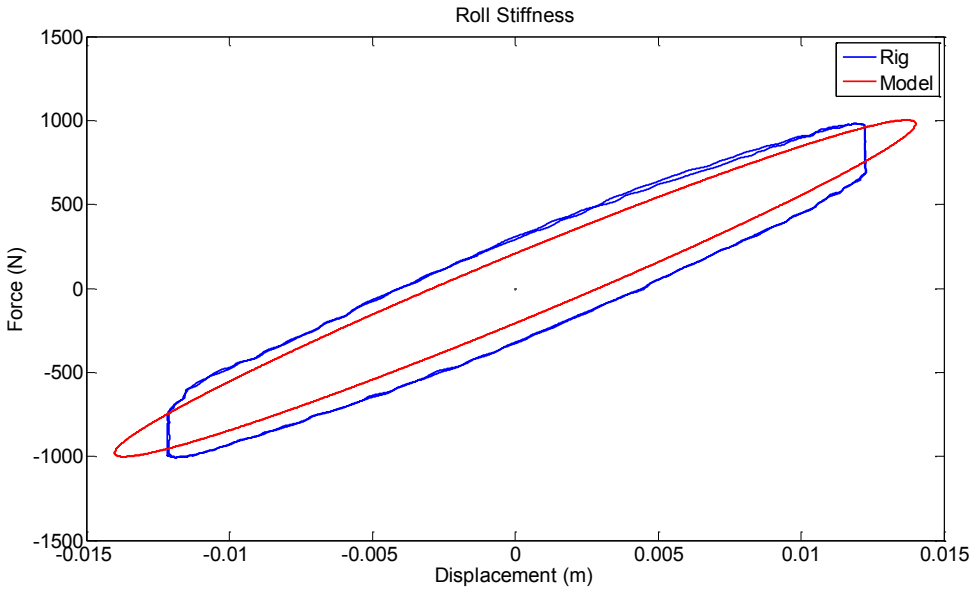

Figure 6-41 – Front Roll Stiffness – Set-up 1, Amended

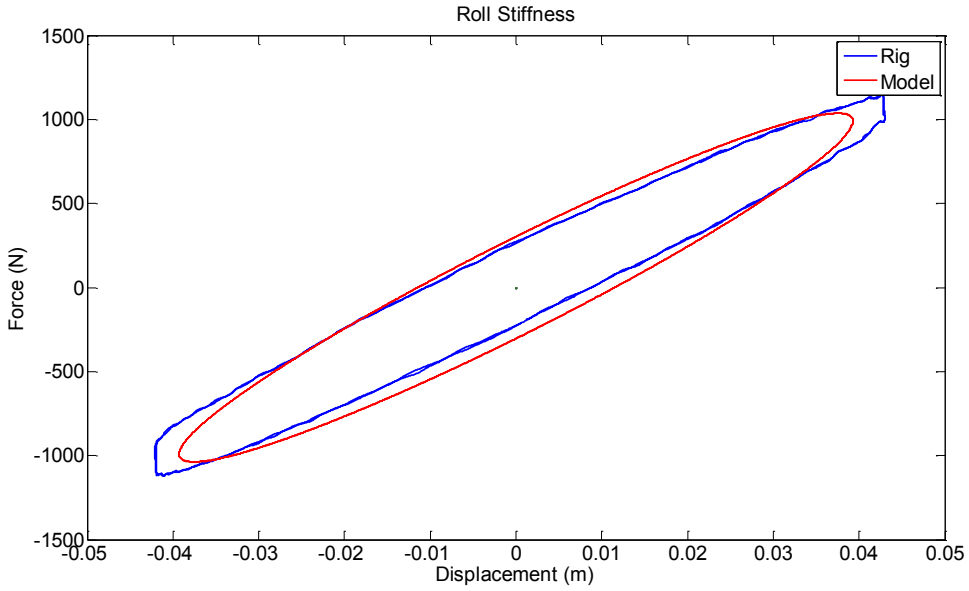

Figure 6-42 – Rear Roll Stiffness – Set-up 1, Amended

The roll stiffness plots for the front and rear suspensions show good correlation between the rig and model data for stiffness. Both the front and rear rig data shows quite a large amount of friction present, which is not modelled in the vehicle model.

The first set-up change made to the Civic was to fit 17" wheels and tyres. Table 6-4 shows the parameters estimated using the parameter estimation for this set-up.

Set-up Number		1	2
Unsprung Mass (kg)	Front	38.47	42.7
	Rear	38.1	41.6
Sprung Mass (kg)		1150	1149
Inertia (kg.m^2)	Pitch	1612	1607
	Roll	330	342.5
Spring Rate (N/mm)	Front	51.7	49.7
	Rear	22.89	23.13
Damper Coefficient (N-sec/mm)	Front	3.662	4.28
	Rear	2.452	2.639
Top Mount Stiffness (N/mm)	Front	1059	969
	Rear	1857	1503
Tyre Stiffness (N/mm)	Front	248	314
	Rear	226	304
Roll Stiffness (N/mm)	Front	69.8	70.4
	Rear	24.6	24.6

Table 6-4 – Parameter Estimation Results Set-up 2

The two parameters expected to change by fitting the 17" wheels and tyres were the unsprung masses and tyre stiffnesses. Both of these increased in the expected way, indicating that the parameter estimation worked well.

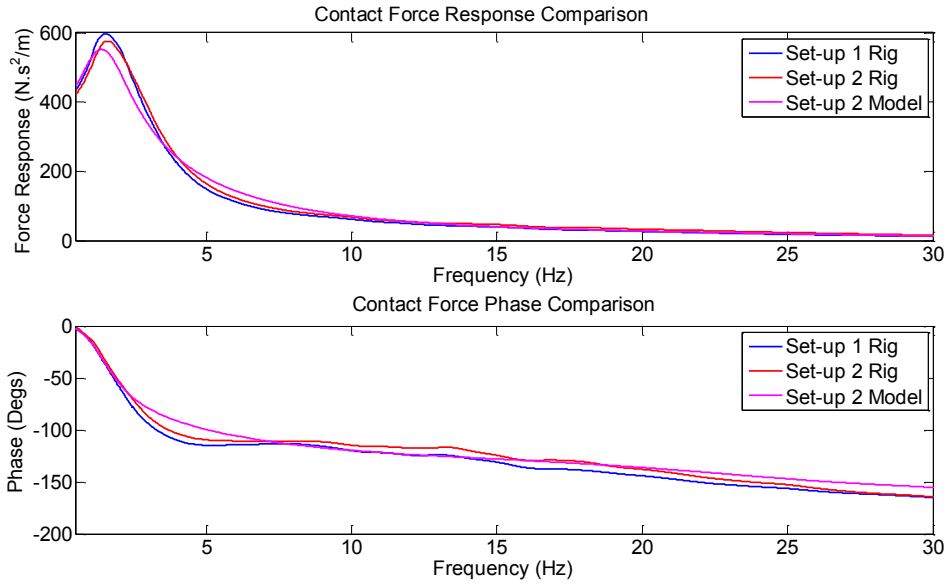

Figure 6-43 – Front Contact Force Response Comparison – Set-up 2

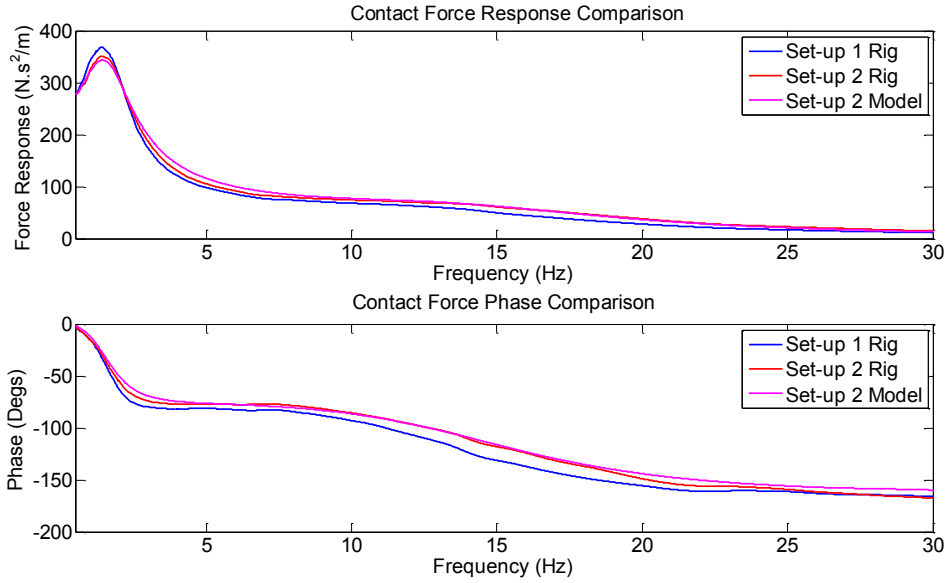

Figure 6-44 – Rear Contact Force Response Comparison – Set-up 2

The contact force response comparisons (Figure 6-43 and Figure 6-44) show that in both front and rear cases the contact force peak at the body mode was reduced for set-up 2 compared to set-up 1. Again the modelled front contact force is quite accurate, but not as accurate as the rear modelled contact force, which is accurate around the body mode natural frequency and has near perfect amplitude and phase between 8 and 18 Hz.

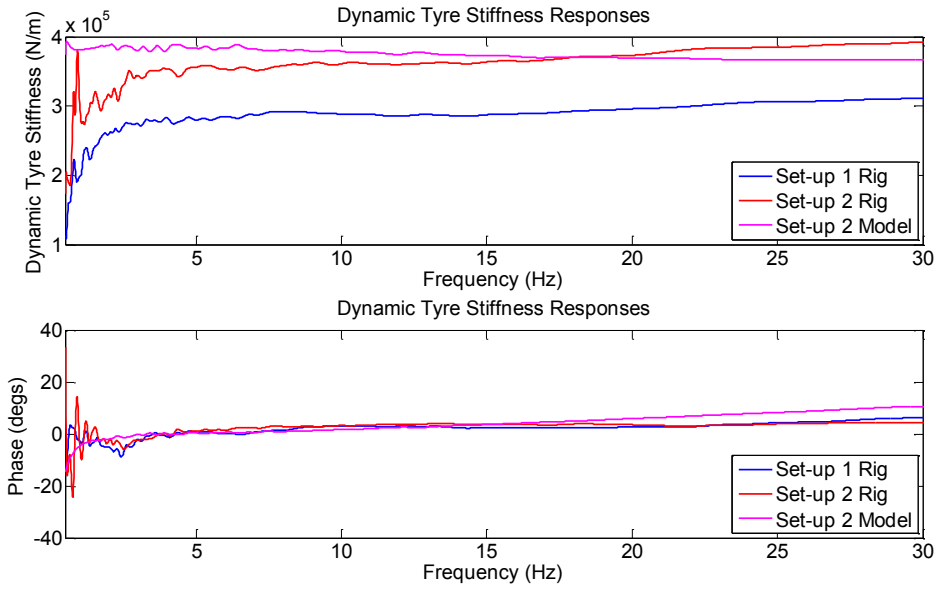

Figure 6-45 – Rear Dynamic Tyre Stiffness Comparison – Set-up 2

The rear dynamic tyre stiffnesses (Figure 6-45) show that the rear tyres fitted to the 17" wheels are around 80 N/mm stiffer than the tyres fitted to the 16" wheels. The dynamic tyre stiffness estimation below 5 Hz was poor due to low acceleration levels which are used to calculate the displacement. Although the tyre stiffness in rig data can be seen to increase with frequency, the tyre stiffness in the model is constant across the frequency range.

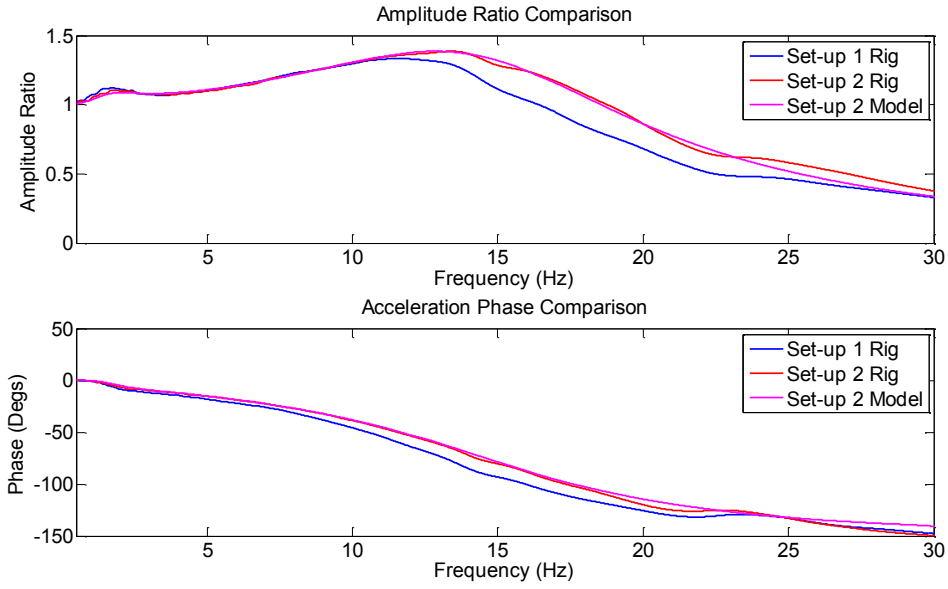

Figure 6-46 – Rear Hub Acceleration Response Comparison – Set-up 2

As the tyre stiffness was increased by fitting the 17" wheels it was expected that the natural frequency of the hub modes would increase and their damping ratio decrease. Figure 6-46 shows that as expected the peak response of the rear hub acceleration was increased by fitting

stiffer tyres and making no other adjustments. This change is reflected well in the model response.

For set-up 3 the rear springs were changed for 1.8 5Dr items, with only a small difference noted in dynamic stiffness. For set-up 4 the rear dampers were replaced with Type R specification dampers and the set-up 3 springs remained. The parameters estimation found that the rear damping had increased from 2.571 to 3.542 N-sec/mm due to this change.

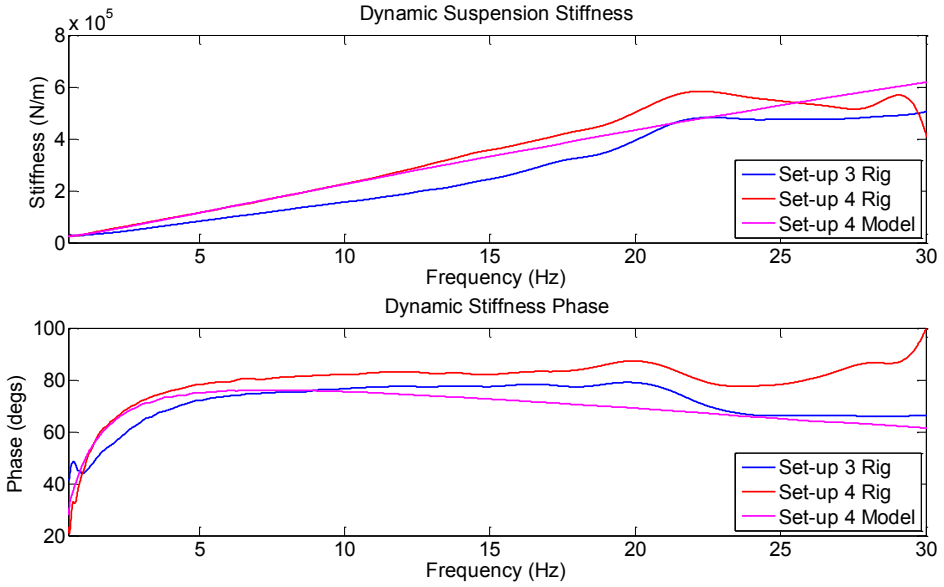

Figure 6-47 – Rear Dynamic Stiffness Comparison – Set-up 4

The dynamic stiffness comparison in Figure 6-47 shows a large increase in the magnitude and phase of the dynamic stiffness for Set-up 4 compared to Set-up 3, indicating increased damping. The modelled Set-up 4 response correlates well at low frequency, but correlation becomes poor higher frequencies.

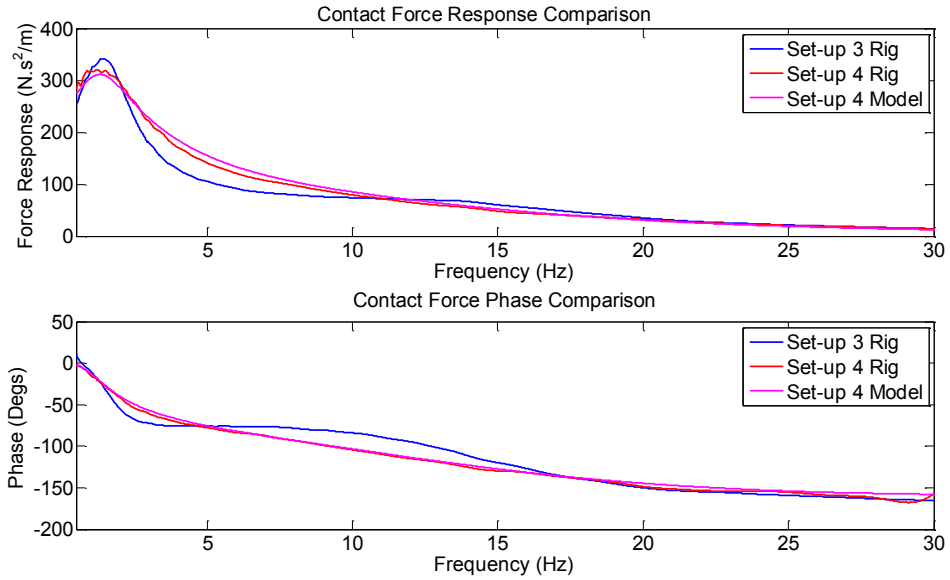

Figure 6-48 – Rear Contact Force Response Comparison – Set-up 4

The rear contact force response (Figure 6-48) shows that with the Type R rear dampers fitted the damping of the body mode is much larger. This results in less contact force change at the body mode and hub mode, but a higher level of amplitude between the two. The modelled response is quite accurate across the frequency range. The same is true for the rear hub acieration response in Figure 6-49.

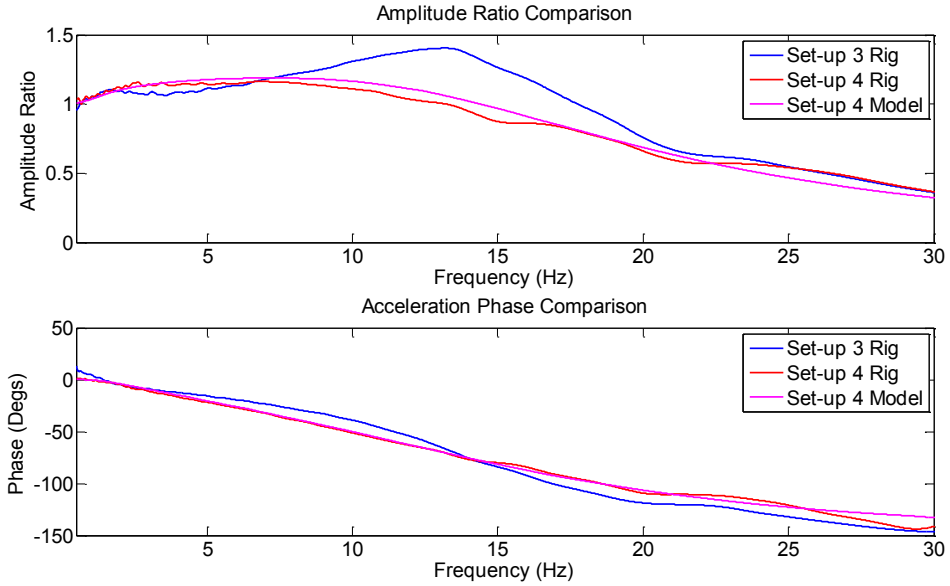

Figure 6-49 – Rear Hub Acceleration Response Comparison – Set-up 4

Set-up 5 changed the rear springs to the 2.2D specification with minimal effect on any of the parameters or responses. For Set-up 6 the 1.8 5Dr rear dampers were fitted to the vehicle with the same rear springs as Set-up 5.

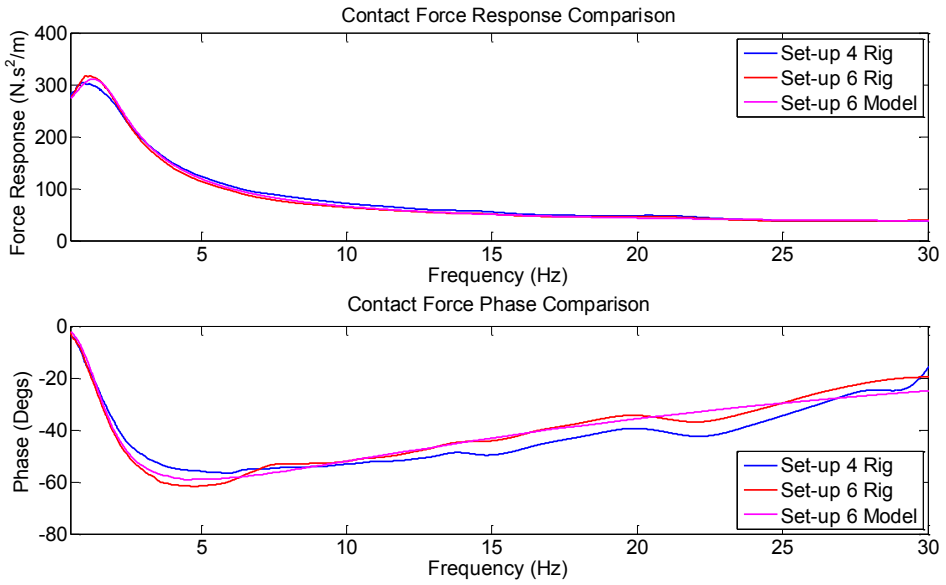

Figure 6-50 – Rear Contact Force/Hub Acc Response Comparison – Set-up 6

The hub acceleration normalised contact force in Figure 6-50 shows that by fitting the rear 1.8 5 Dr dampers the body mode damping was reduced slightly, but not as significantly as if the standard dampers were fitted. The model shows good correlation to the rig data for almost the whole frequency range.

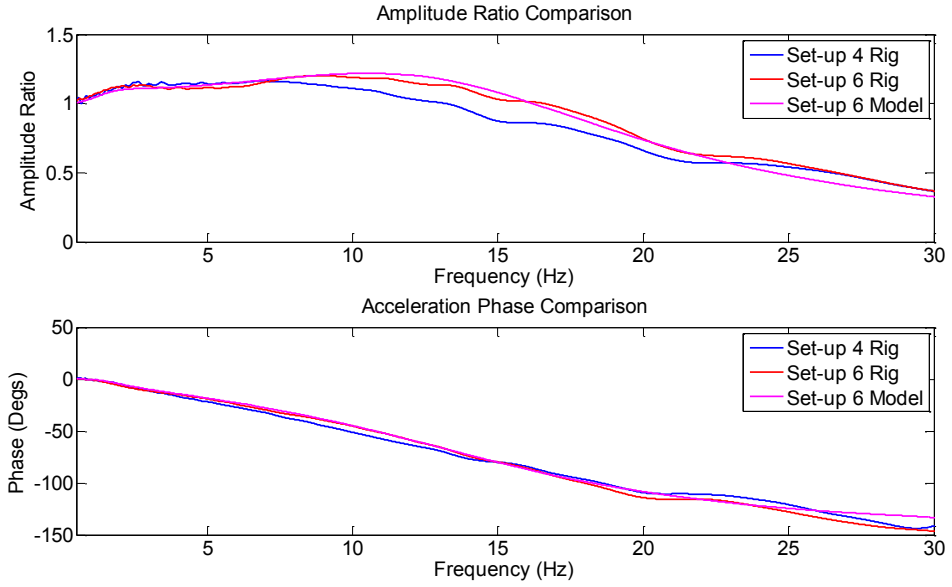

Figure 6-51 – Rear Hub Acceleration Response Comparison – Set-up 6

The rear hub acceleration response in Figure 6-51 shows an increase in amplitude at the hub mode due to the reduced damping of the 1.8 5Dr dampers. This is also well modelled using the estimated parameters.

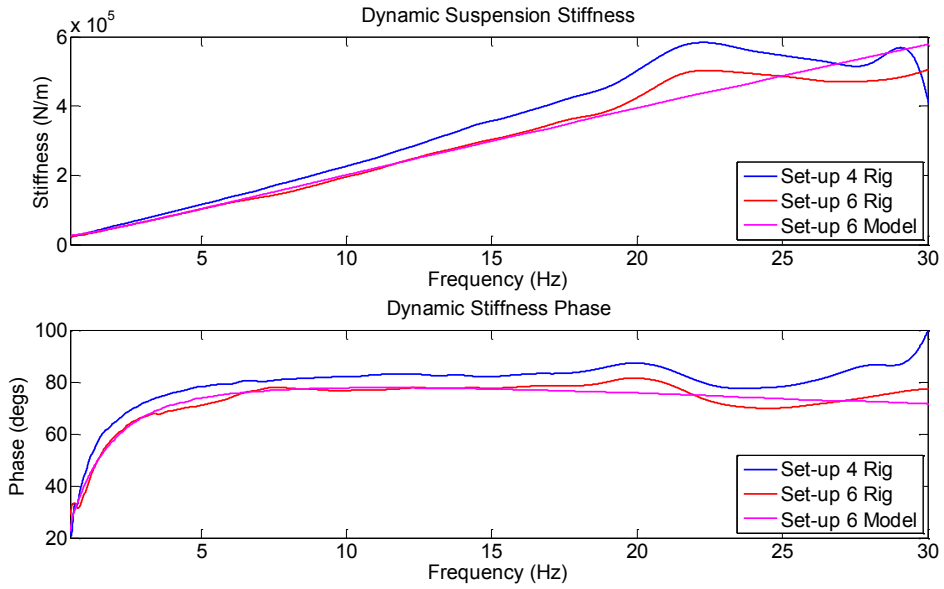

Figure 6-52 – Rear Dynamic Suspension Stiffness Comparison – Set-up 6

The dynamic stiffness (Figure 6-52) magnitude and phase have both been reduced by fitting the 1.8 5Dr rear dampers. Again the modelled dynamic stiffness accurately represents the measured dynamic stiffness. Between 3 and 6 Hz, there is a small change in the trend of the dynamic stiffness phase of the set-up 6 rig data. This was thought to be due to non-linearity in the damper. Figure 6-53 shows the measured rear damper curve from set-up 6 which has a slightly digressive characteristic in both bump and rebound with a slightly rebound biased coefficient.

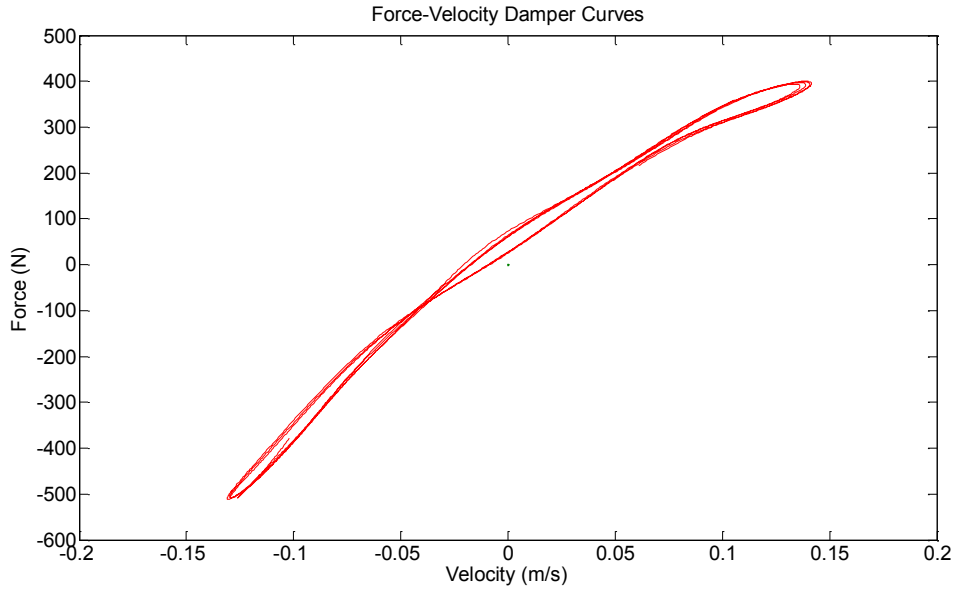

Figure 6-53 – Rear Damper Curve – Set-up 6

Set-up 7 involved fitting 1.8 5Dr front dampers with the standard springs, with the rear set-up remaining the same as Set-up 6. The estimated front damper coefficient increased from 3.44 to 4.51 N-sec/mm due to this change.

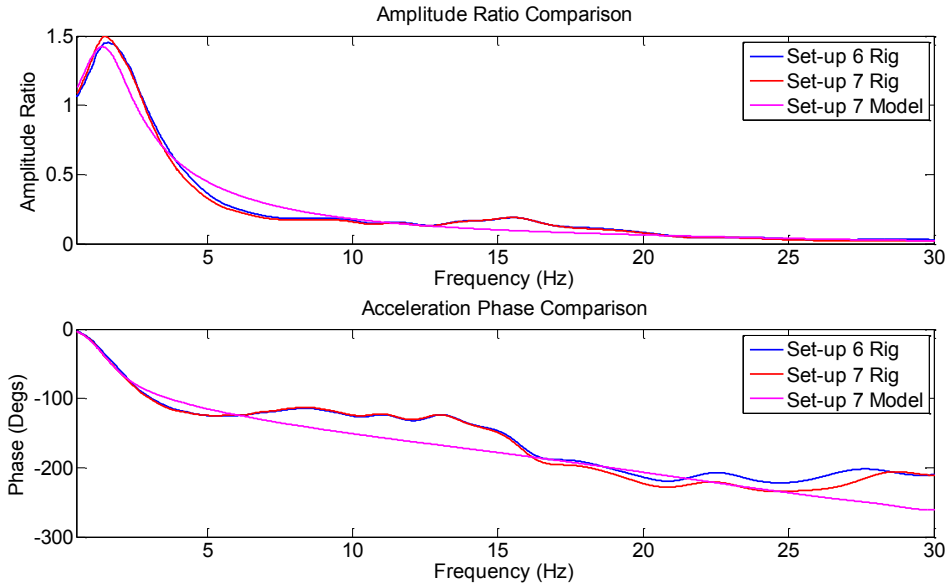

Figure 6-54 – Front Body Acceleration Response Comparison – Set-up 7

Although the estimated damping was increased for set-up 7, the body acceleration response in Figure 6-54 shows very little difference, with just a slight increase in the peak amplitude ratio. In this case the model response is not a particularly good match for rig data.

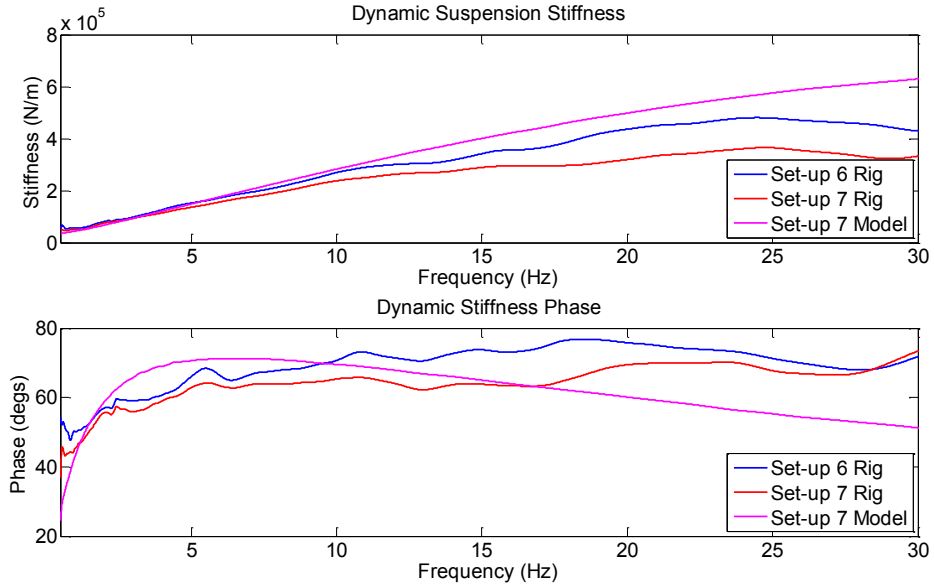

Figure 6-55 – Front Dynamic Stiffness Comparison – Set-up 7

The front dynamic stiffness (Figure 6-55) explains why the hub mode of set-up 7 is modelled inaccurately. The amount of damping present in the 2 to 10Hz range is much larger for the model than that of the real vehicle.

Set-up 8 involved fitting the 1.8 5Dr front springs to the vehicle, with all other suspension parts remaining the same. Investigation of the results found that the response of the vehicle was almost identical to Set-up 7. Set-up 9 used the 2.2 D front dampers with all other parameters remaining the same. In this case the front damping coefficient estimate further increased to 6.14 N-sec/mm and the estimated spring stiffness increased by 2.5 N/mm.

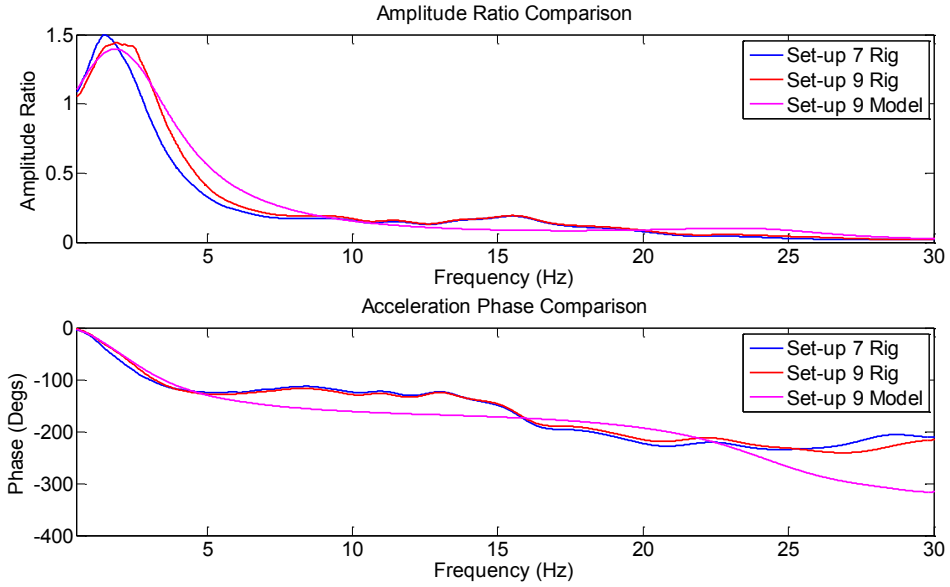

Figure 6-56 – Front Body Acceleration Response Comparison – Set-up 9

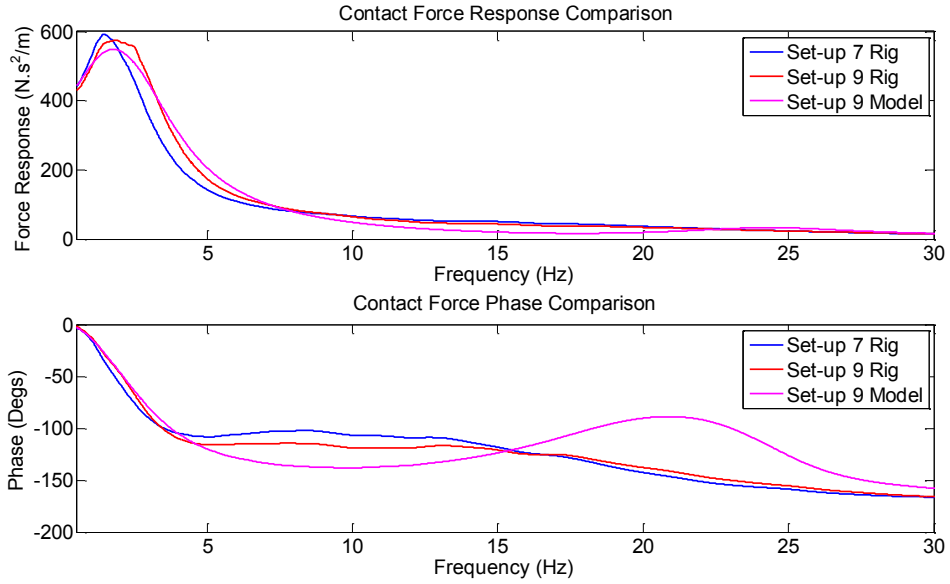

Figure 6-57 – Front Contact Force Response Comparison – Set-up 9

The body acceleration and contact force responses in Figure 6-56 and Figure 6-57 show that with the 2.2 D front dampers fitted the peak response was slightly reduced, and the body mode natural frequency increased. At low frequency the model response can be seen to have a quite similar shape to the Set-up 9 rig data. However, at high frequency the correlation is very poor. It can also be seen that the peak of the responses for Set-up 9 seems to be flattened off compared to the expected mode shape. This is thought to be due to a significant amount of bumpstop contact.

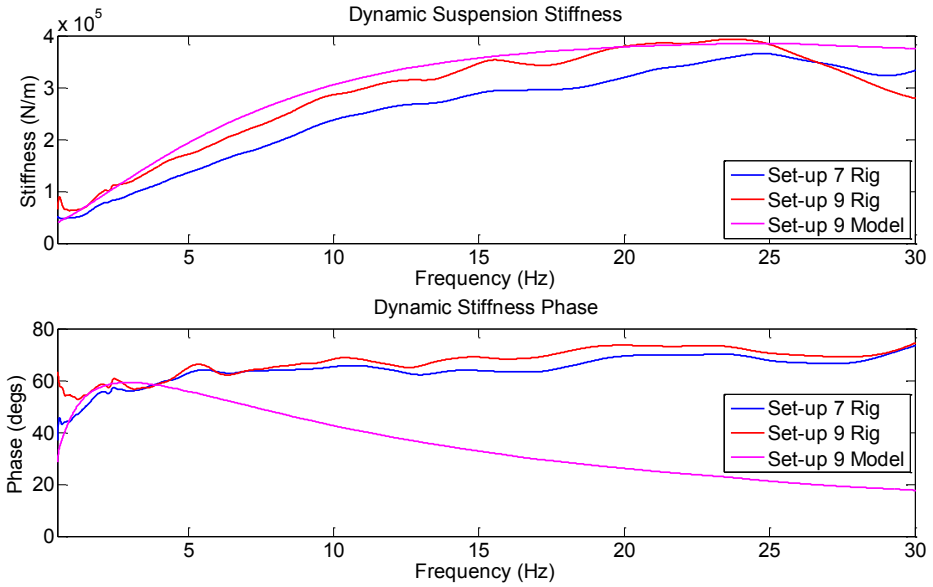

Figure 6-58 – Front Dynamic Stiffness Comparison – Set-up 9

Figure 6-58 shows the front dynamic stiffnesses for Set-ups 7 and 9. It can be seen that by fitting the 2.2 D dampers the damping has been increased quite significantly. As the front dynamic stiffness model was only tuned between 1 and 4 Hz, the accuracy at high frequency can be seen to be poor for the phase. Figure 6-59 shows the force displacement damper curves for Set-ups 7 and 9.

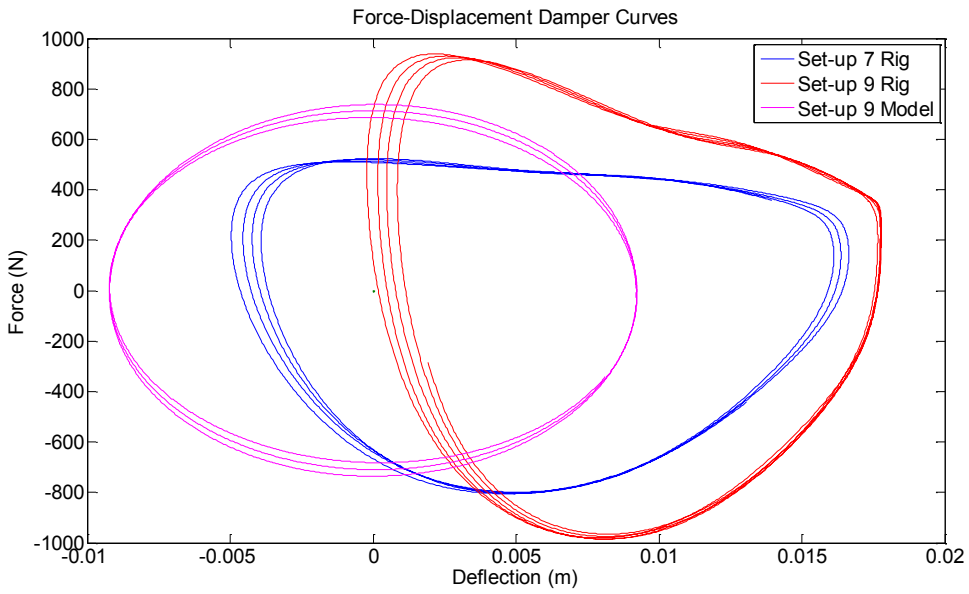

Figure 6-59 – Front Damper Curve Comparison – Set-up 9

The fact that the Set-up 9 Rig damper curve is at an angle (Figure 6-59) shows that the gradient was incorrectly estimated during the parameter estimation. The reason for this was down to the amount of bumpstop contact present during the run. The front damper curves indicate that there was a much higher rebound coefficient than bump coefficient. This would cause the suspension to pull-down during the run, meaning that the bumpstop contact would be very large during the test, as would be the case on the road.

For Set-up 10 the Type R rear dampers were fitted, whist all other components remained the same. Set-up 11 used the standard rear springs with the Type R dampers. In both cases estimated parameters and hence model responses, were very similar to the first time that the components were fitted. For Set-up 12 the front anti-roll bar drop links were removed so that the anti-roll bar would become ineffective. In addition, in Set-up 13 the 24mm front anti-roll bar was fitted. By removing the anti-roll bar stiffness the roll stiffness was reduced from 70.5 to 30 N/mm for a double wheel input and then increased to 76.5 N/mm by fitting the 24mm anti-roll bar. In all cases the simulated roll stiffness matched that of the rig.

For Set-up 14 the 1.8 5Dr rear dampers were re-fitted. As with Set-ups 10 and 11, the estimated damping coefficient was very similar to the previous time that these dampers were fitted in Set-up 6.

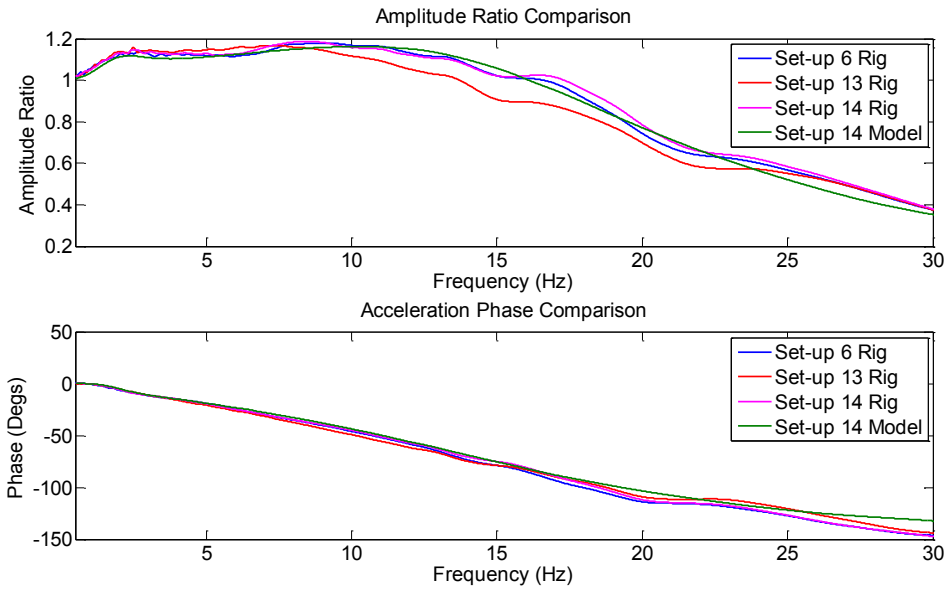

Figure 6-60 – Rear Hub Acceleration Response Comparison – Set-up 14

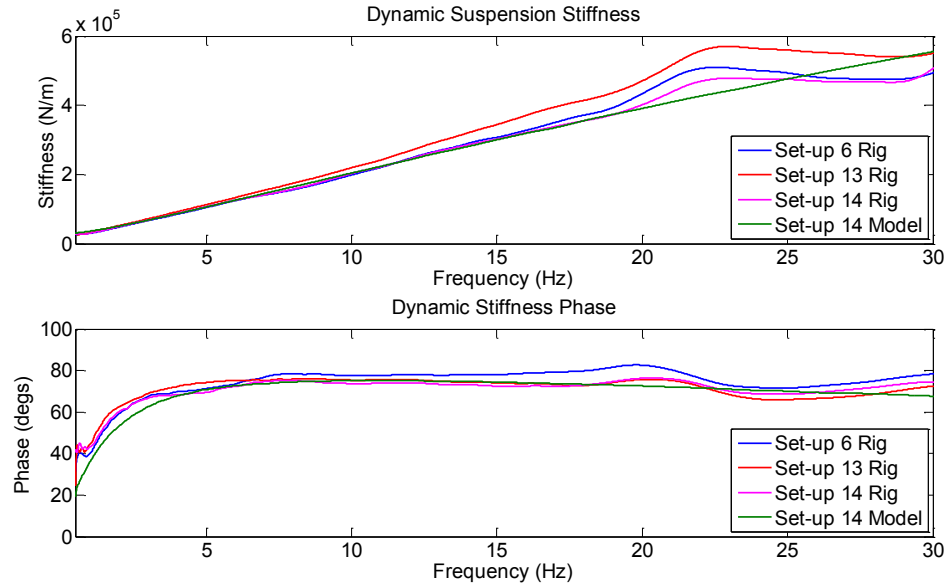

Figure 6-61 – Rear Dynamic Suspension Stiffness Comparison – Set-up 14

Figure 6-60 and Figure 6-61 compare the hub response and dynamic stiffness responses for Set-ups 6, 13 and 14 with the model result of Set-up 14 also presented. The responses show good correlation both between Set-ups 6 and 14 rig data and the Set-up 14 model. They also show that the damping is higher in Set-up 13 with the Type R rear dampers fitted and that this results in a more highly damped hub mode. Set-up 15 was a return to the standard front dampers, where the estimated parameters and model response were found to match in a very similar way to the last set-up where these items were fitted. For Set-ups 16 to 18 an attempt was made to change the top mount stiffness characteristic of the real car and analyse the effect

on the hub mode response. Unfortunately the changes made to the stiffness were too small to capture a significant difference in the dynamic stiffness or hub mode response.

6.5.1 Parameter Estimation and Model Validation Discussion

The validation exercise in section 6.5 – Parameter Estimation and Vehicle Model Validation, showed that in most cases the technique was able to estimate the vehicle parameters and produce a similar response to the physical test using the vehicle model with the estimated parameter values. The main exception to this was in roll excitation, where the rig and simulation results were significantly different (Figure 6-40). This result was expected, as the behaviour of the vehicle in roll on the rig had been investigated in section 4.4.3.1 - Roll Response Investigation and the model created in section 6.26.2 - 8 Degree-of-freedom Model, was not sufficiently complex to simulate this behaviour. Initially the front body acceleration response from the model had poor correlation to the physical test (Figure 6-27) due to the front dynamic stiffness parameter estimation having lower damping around the body mode natural frequency than the real vehicle. This was resolved by adjusting the frequency range in which the dynamic stiffness parameters were estimated, producing a much more satisfactory correlation, as shown in Figure 6-33. The requirement to tune the dynamic stiffness estimation frequency range highlighted the difficulty in modelling the highly non-linear system with a linear model. The rear correlation between the model and physical test responses was good throughout (Figure 6-46), partially because the rear damping characteristic was more linear than the front and there was no bumpstop contact at the rear. The large variation in front apparent mass across the frequency range (Figure 6-30) indicated that results could be improved when simulating the engine and/or passenger responses to vertical vibration.

The validation exercise highlighted that a ‘sanity check’ of the correlation between measured and simulated responses should be carried out by the engineer before any tuning of parameters. In some cases is may be necessary to change the frequency range over which the dynamic stiffness parameters are identified, or may be vital to model the engine response. If the model is not an accurate representation of the vehicle before tuning with the model takes place, then the results produced could cause the engineer to take the wrong tuning direction. An example of this would be if a front damping coefficient sweep were carried out on the initial Set-up 1 parameters. In this case the model would suggest that to improve the contact force variation the damper coefficient should be increased significantly. However, the response of the real vehicle was actually quite well damped so the decrease in contact force variation would soon be outweighed by a decrease in comfort.

The validation exercise effectively validated the parameter estimation and vehicle model simultaneously and found the results to be satisfactory in all but the roll mode of excitation.

7 - Performance and Comfort Optimisation

This chapter of the thesis describes the derivation and application of the performance and comfort indices used to define the characteristic of a vehicle from four-post rig testing.

Section 7.1 - Comfort Index, describes the creation of the comfort responses through the use of frequency weighting functions and road surface modal weightings. The responses are used to produce a comfort index relating to the passenger comfort rating of the vehicle. In addition an assessment is made of the seat's ability to isolate the driver from accelerations measured at the vehicle body.

The comfort weighting functions, and the use of these to assess discomfort is not novel and has been used in much other literature. The particular comfort index explained in this section, although not particularly complex, is a new and original contribution to the generalised assessment of comfort in vehicles tested on multi-post shaker rigs, or using vehicle simulation.

Section 7.2 - Performance Index, describes the method used to define the suspension performance of a vehicle tested on the four-post rig. Tyre modelling is carried out in order to investigate how the vertical load variations on the wheels caused by road inputs affect the forces generated within the tyre. A lateral dynamics model, coupled with a tyre model is used to analyse the effect of vertical load variations on the steady-state and transient performance of a vehicle. A set of performance indices are created based on the anticipated effect of the four-post rig measured ride behaviour on the vehicle handling, as well as an overall performance index.

The creation and use of the specific performance index is a new and original contribution to the assessment of ride performance on handling. The method goes someway towards bridging the large gap between simple RMS contact load variation and full vehicle model handling manoeuvre performance indices.

Section 7.3 - Validation of Comfort and Performance Index with Subjective-Objective Test, describes the use of four-post objective tests and subjective driver assessments to attempt to validate the performance and comfort indices with drivers comments of the relative performance and comfort of 4 different vehicle setups.

7.1 - Comfort Index

7.1.1 – Frequency Weighting of Modal Body Acceleration Responses

From the literature review of discomfort in vehicles in section 2.2 – Human Discomfort, the vast majority of literature concurs that acceleration is the primary cause of discomfort. The ISO 2631 [26] and BS 6841 [1] standards provide frequency weighting functions that can be used to quantify human discomfort when applied to simulated or measured whole-body accelerations of passengers in the seated position. These weightings are well used in literature and the automotive industry, and therefore have credibility to be used in the comfort index in this thesis.

Figure 7-1 presents the BS 6841 [1] frequency weighting functions for vertical, pitch rotation and roll rotation accelerations at the seat surface and vertical acceleration at the feet. These are created from weightings W_b for vertical accelerations and W_e for rotational accelerations, with scaling factors applied for pitch, roll and feet accelerations.

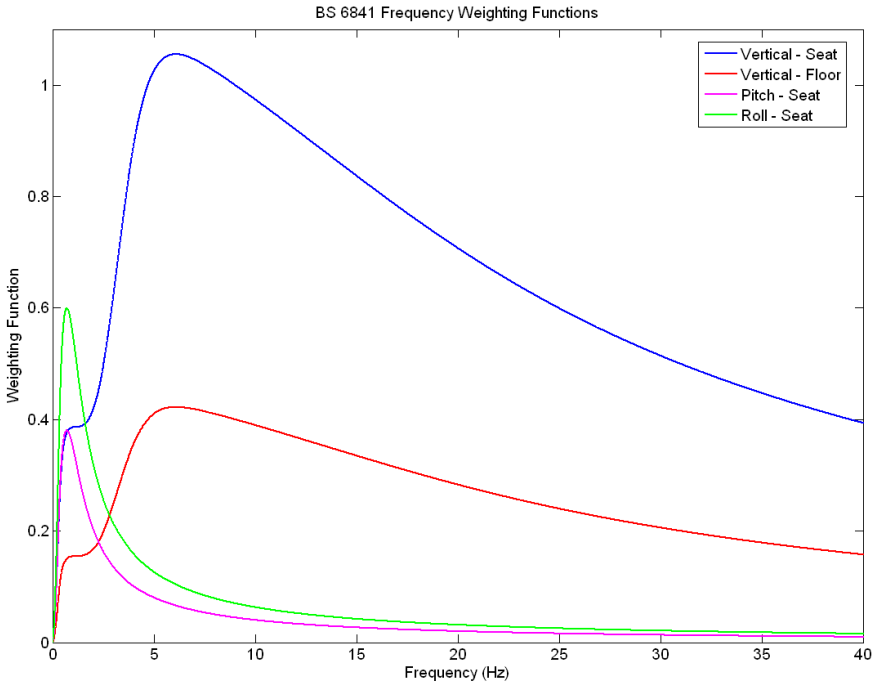

Figure 7-1 – BS 6841 Frequency Weighting Functions

The weighting functions show that pitch and roll accelerations are considered to be most uncomfortable at approximately 0.8 Hz, with roll being more uncomfortable than pitch. The vertical weighting function is quite different to that of the rotational ones and peaks at 6 Hz, with the high frequency accelerations being much more significant than in the rotational cases.

To convert the body acceleration responses into comfort responses the vertical and rotational response functions from four-post testing or simulation of a vehicle can simply be multiplied by the relevant frequency weighting functions. An example of the heave comfort response from a four-post test can be seen in Figure 7-2.

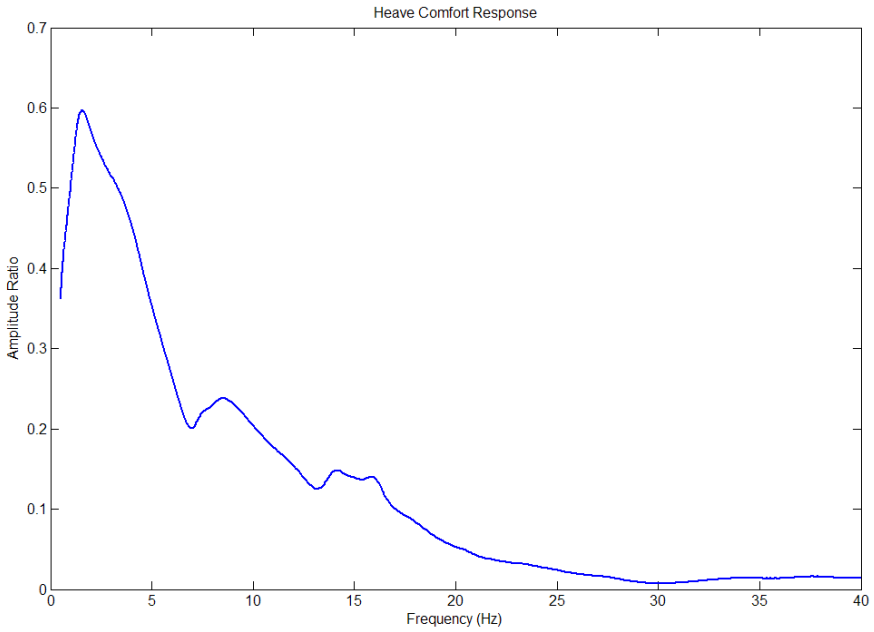

Figure 7-2 – Example Heave Comfort Response

These responses represent the discomfort of passengers due to a constant acceleration input of 1 m/s^2 at the road surface. As the road input used on the rig is approximated to a constant peak velocity, to calculate the discomfort of passengers across the frequency range for the rig input used this response needs to be multiplied by jω, or ω, if only the magnitude is required. The weighted response squared can also be multiplied by the road acceleration PSD corresponding to a constant forward vehicle speed and constant velocity PSD road surface. This is done for each of the road excitation modes to produce information about the level and frequency distribution of discomfort for each mode. Examples from 4 vehicles tested on the Oxford Brookes University four-post rig using the test and analysis methods explained in 4.3 - Testing Procedure can be seen in Figure 7-3.

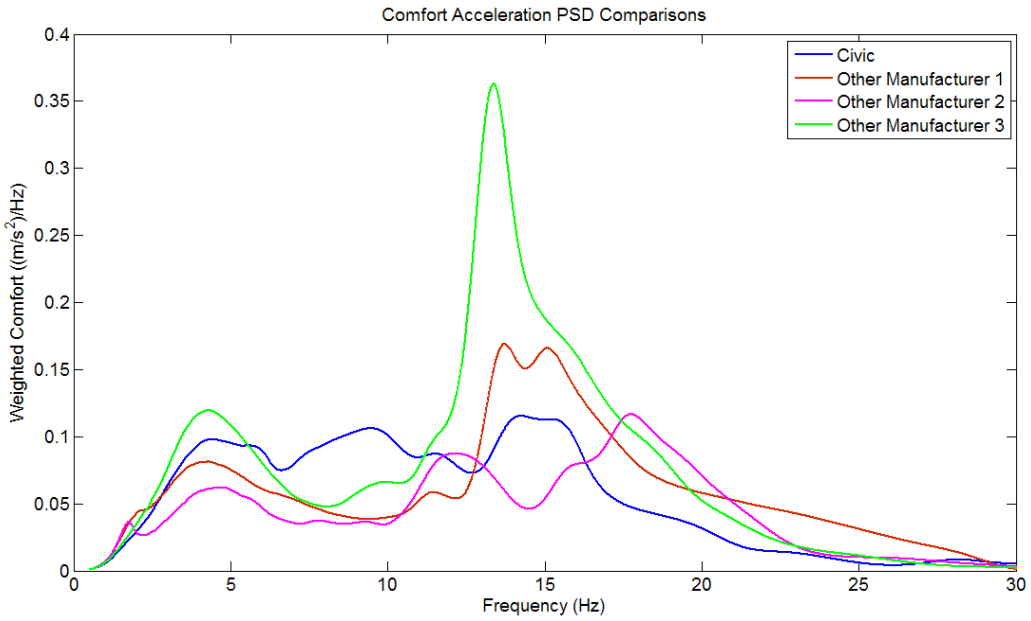

Figure 7-3 – Comfort Acceleration PSD Comparison for Civic and 3 other Vehicles

The first set of comfort indices can be derived at this point. The comfort indices are created by calculating the RMS of the comfort response in the heave (seat and floor), pitch and roll cases for each of the modal inputs. In accordance with the BS 6841 standard [1], the summations of these multiple measurements are created by taking the root sum of squares of the RMS values. In the case of heave, pitch and roll at the seat, again in accordance with BS 6841 [1], if any individual RMS is less than 25% of the maximum, then it is omitted from the equation. For a well decoupled vehicle it would be expected that only the weighted RMS values in the same direction as the input mode would be retained.

Two cases are considered for these comfort indices. Firstly, the case where seat and floor accelerometers are used with the relevant scaling factors for weighting. Secondly, the case where the seat and floor accelerations are not used, but the sprung mass acceleration at the CofG is used with the W_b acceleration weighting and a scaling factor of 1.

These two cases are used for two main reasons. Firstly, it may not always be possible to use floor and seat accelerometers, due to sensor or data acquisition channel restraints. Secondly, it can be useful to decouple the seat acceleration from the total discomfort to focus on the comfort index relationship with suspension parameter changes. This is also of use when benchmarking, as a competitor's vehicle may have poorer suspension control, but a seat with better isolation properties or vice-versa and an overall result would not provide the required detail to differentiate between these circumstances.

7.1.2 - Modal Contributions of Discomfort

When tuning a vehicle suspension or analysing different tested vehicles, if all comfort indices in all input modes change in the same direction between the different cases, it is easy to determine which is better or worse. However, in many circumstances this will not be case, and some of the indices will decrease as others increase. In this case the engineer will have to make a decision on which setup or vehicle is better. In order to assist this decision a second set of comfort indices are produced that include the expected modal contributions of the road input.

The modal contributions for the ISO 8608 [4] 'Class B' road with the EUDC driving cycle [72] were presented in section 3.6 – Road Input Construction from Spatial Characteristics and Drive Cycle. This information can be used to weight the modal discomfort responses across the frequency range in order to achieve a more representative combined comfort response than simply combining the 4 modal cases with the constant peak velocity approximation. To make the modal distributions more generic, the repetitions in the 14 to 40 Hz region were smoothed, so that equal contributions from each input mode were achieved. The result is shown in Figure 7-4 below.

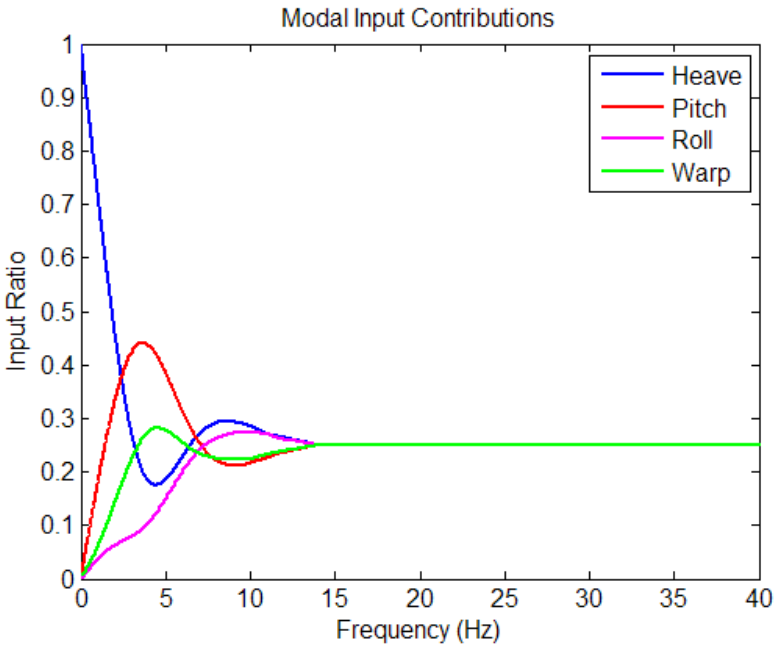

Figure 7-4 – Smoothed Modal Contributions

Using the modal contributions and a single wheel acceleration PSD representative of the of EUDC drive cycle [72] on an ISO 8608 [4] B road, the comfort responses can be used to create modal and combined discomfort PSDs for a typical road surface and a typical drive cycle. These can be used by the engineer to have a more clear representation of the expected discomfort from a vehicle. If the assumptions are made that the road is Gaussian and the vehicle response linear, then the PSDs can be used to generate modal and combined comfort index RMS values.

These values should relate to similar values on the scales presented by Griffin [25] (Figure 2-11). This way, as well as benchmarking different vehicles and setups, an overall comfort index that relates to overall discomfort can be obtained. As before, comfort indices are created both with and without the seat.

Use of the modal weighting has some obvious advantages, but it also has some disadvantages. One issue is that the weighting functions relate to the particular road at a particular set of speeds. If there were a particularly badly controlled mode at a point with very little weighting, then potentially this could be missed. For this reason it is always good to use both the modal weighted and non-modal weighted discomfort responses. A second disadvantage is that the road characterisation and drive cycle used may not be particularly representative of the route that the test drivers use for subjective evaluation. In this case the optimal vehicle setup for comfort would be different in each case and setups that appear worse from rig data may actually be better for the subjective driver assessment.

This problem could be overcome by carrying out a road characterisation, as in 3.7 – Collection of Road data and Basic Spatial Characteristic Estimation, and using a speed trace from the same route to create new modal weightings and acceleration PSD based on the findings. This then produces a new problem relating to the relevance of the subjective driver assessment route and speed trace, to general use of the vehicle by the actual owners.

7.1.3 - SEAT Assessment

The vibrational response of the passenger on the seat can have a large effect on passenger discomfort. Ideally the seat would reduce the level of discomfort that the passengers experienced compared to direct transmission of acceleration from the floor to the seated passenger. In some cases where seat design is poor, however, the response of the passenger on the seat may dominate the discomfort levels experienced by the passengers. In other cases the response of the passenger on the seat may be very close to 1 across the frequency range, meaning that the suspension control dominates the response. During a four-post rig test it is unlikely that seat tuning would take place, but it is very useful to be able to characterise the response of the passenger on the seat and produce an estimate of how much the seat characteristics increase or decrease the passenger comfort.

The response of the passenger on the seat can be determined by dividing the seat accelerometer response by the floor accelerometer response. An example of the seat acceleration response for a four-post test carried out on a Honda Civic can be seen in Figure 7-5. In the four-post rig tests used in this thesis ballast was used to represent the passengers on the seat as explained in section 4.3.1.1- Passenger Ballast, the use of real passengers would require ethical approval. It is also much more consistent to use the ballast rather than different passengers who may have different responses themselves.

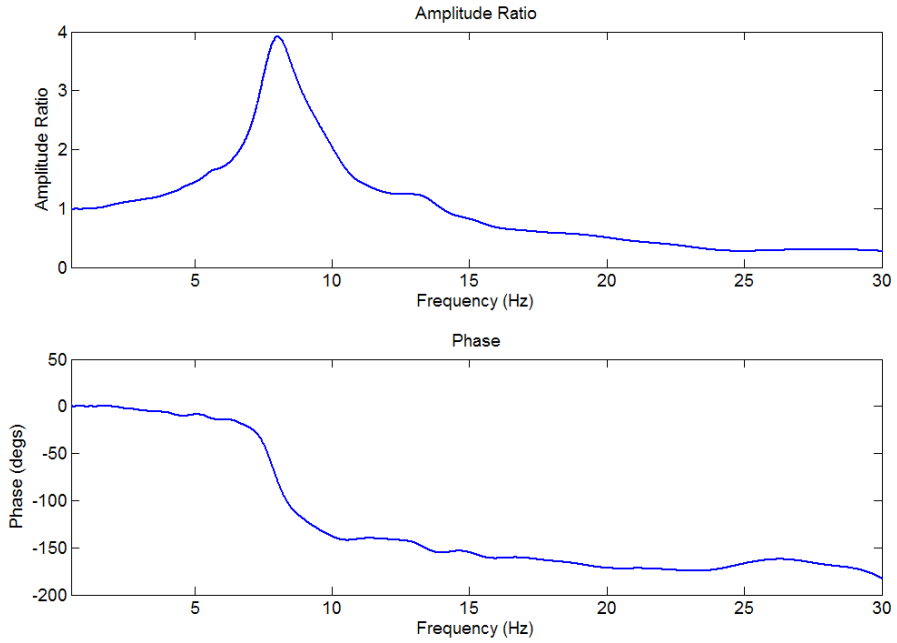

Figure 7-5 – Response of passenger ballast on seat

The BS EN 30326-1 standard [87] provides a method of quantifying the seat transmissibility in a single number called SEAT (Seat Effective Amplitude Transmissibility). The method uses the W_k frequency weighting from the ISO 2631 [26] standard to weight the acceleration of the vibration

platform and the seat surface. The RMS values of these weighted accelerations are then used in equation (7-1) to define SEAT.

$$SEAT = \frac{a_W s}{a_W p}$$

(7-1)

Where:

$a_w s$ = Weighted seat acceleration RMS

$a_W p$ = Weighted platform acceleration RMS

The W_k weighting in ISO 2631 [26] is very similar to the W_b weighting in BS 6841 [1]. As the BS 6841 weightings are already used in the comfort index, the SEAT value is calculated from the W_b weighted seat and floor RMS values created from the rig input velocity normalised responses explained in section 7.1.1 – Frequency Weighting of Modal Body Acceleration Responses.

7.2 - Performance Index

The majority of the performance or road holding measures reviewed in the literature simply use the RMS of contact load variation as a measure of the suspension performance (e.g. [34] and [37]). A paper by Fukushima et al. [36] used a load fluctuation rate defined as a ratio of the RMS load variation to static load, and a ground contact rate which measures the percentage of time that the tyre is in contact with the road surface. The load fluctuation rate is useful as it normalises the performance of the suspension to vehicle mass. This allows cars of different masses to be compared more easily, as for the same acceleration response a heavy vehicle would have a larger load fluctuation rate, but not necessarily perform any worse. The ground contact rate could also be quite useful. However, it requires a distance based road surface to be defined as well as a tyre radius which may or may not be deformable.

From this level of performance index, there is a large jump to the performance indices used during subjective testing and full vehicle modelling with handling manoeuvres, as described by Gobbi et al.[38] and Fernandes et al. [63]. These types of investigation clearly allow more subtle and accurate tuning of the vehicle suspension in order to achieve the desired characteristics. However, they require a large amount of information about the vehicle and its tyres. For assessment from four-post rig testing it is not possible to acquire all of these parameters, so full vehicle simulation could not be carried out without large assumptions being made for the unidentifiable parameters required.

The performance index created for use in this thesis aims to bridge the gap between the very simple RMS contact load variation performance indices and the full vehicle model handling manoeuvre performance indices.

7.2.1 – Static Loss

Within the 'Magic Formula' tyre model, the cornering stiffness ($C_{F\alpha}$) defines the initial gradient of the lateral force to slip angle relationship. The cornering stiffness changes with the vertical load applied to the tyre in a non-linear manner, an example of a cornering stiffness curve using the Magic Formula tyre model and coefficients explained in section 6.4.1- Tyre Modelling, is shown in Figure 7-6.

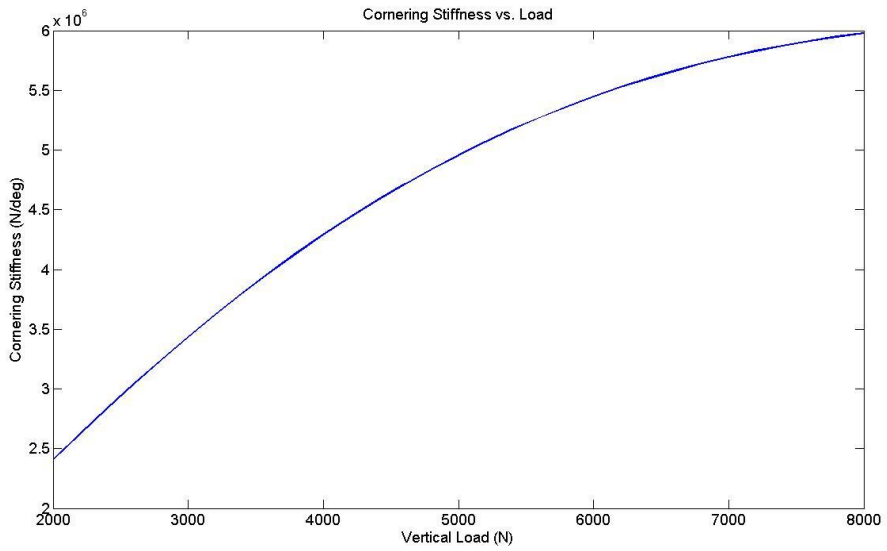

Figure 7-6 – Effect of vertical load on cornering stiffness

When cornering, the vehicle will experience load transfer from one side of the vehicle to the other, due to the CofG of the vehicle being above the ground plane. This load transfer increases the vertical force on the outer wheels and decreases the vertical force on the inner wheels. Due to the convex nature of the cornering stiffness characteristic, the average cornering stiffness is lower than in the straight line condition, so the ability to generate lateral force is reduced. This is one of the main reasons why sports cars manufactures strive to minimise the CofG height.

When we consider variations in the vertical force of a single wheel the same effect occurs. For a sinusoidal force variation the average lateral force potential is reduced compared to a static force with the same mean. Pacejka [58] calls this reduction 'static loss'. An example of this is shown graphically in Figure 7-7. The dynamic characteristics of the Pacejka model are discussed in section 7.2.2 – Dynamic Loss.

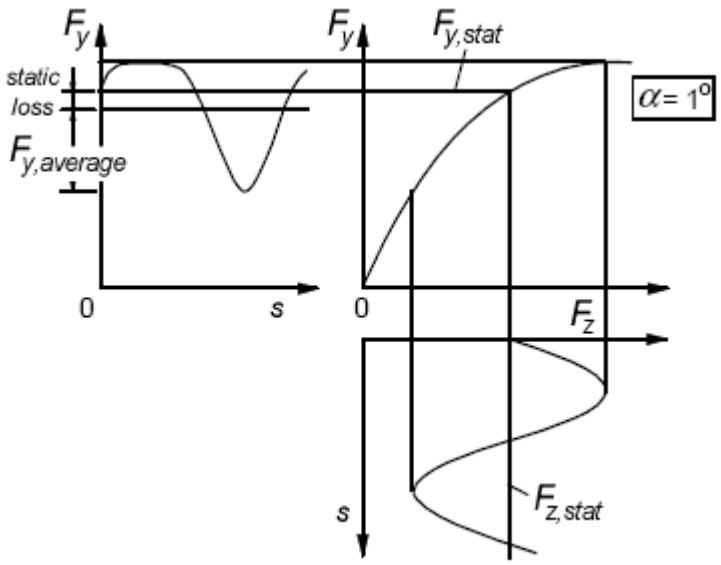

Figure 7-7 – Graphical representation of static loss – Pacejka [58] page 368

The cornering stiffness characteristic shows that the higher the level of load variation the higher the static loss. Using the cornering stiffness curve to determine the static loss is only appropriate at low slip angles, where the gradient of lateral force versus slip angle is linear. Figure 7-8 presents the static loss for multiple levels normalised load variation, different slip angles and 3 different normal loads. The relationship is non-linear for all parameters.

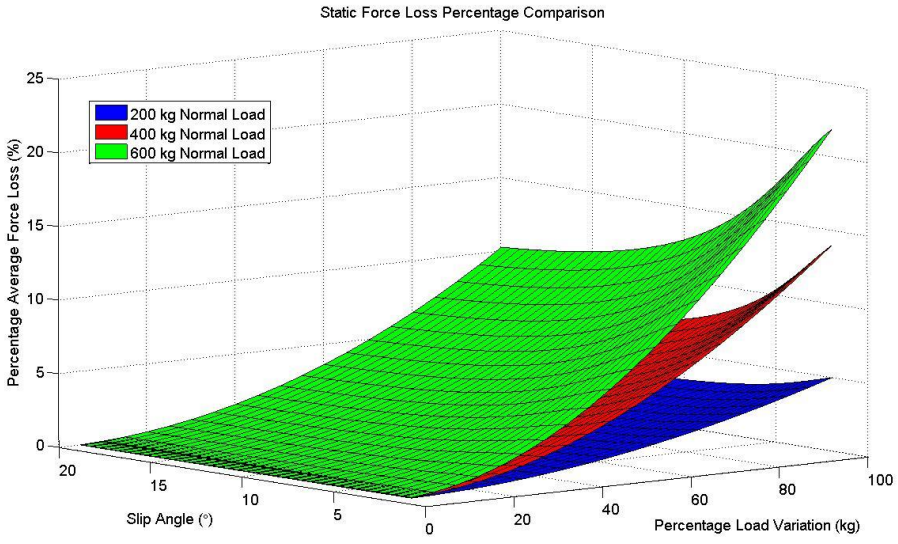

Figure 7-8 – Effect of load variation, slip angle and normal load on static loss

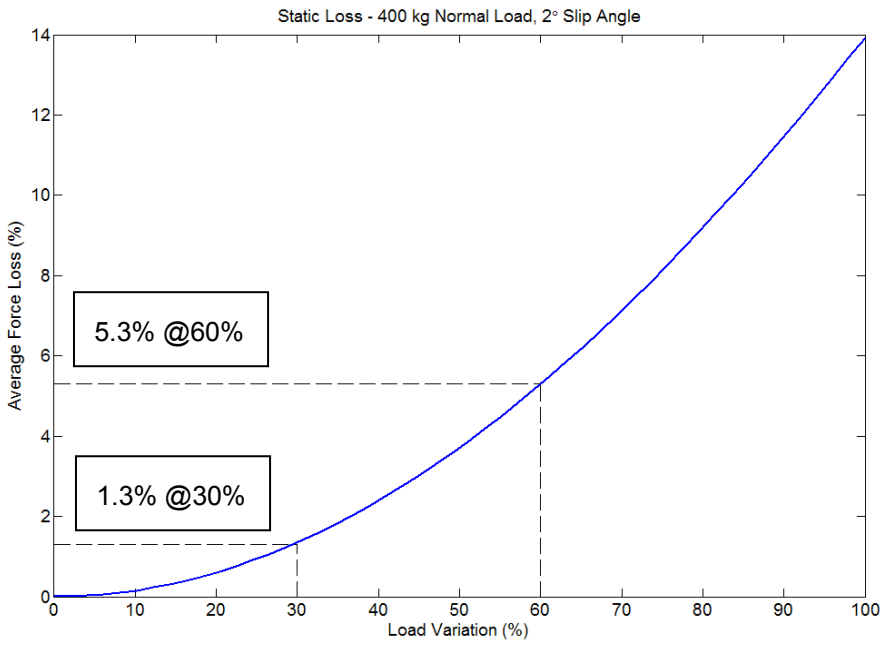

Figure 7-9 – Static loss characteristic 400 kg normal load and 2° slip angle

A section from Figure 7-8 is presented in Figure 7-9. At 30% vertical load variation, the lateral force loss is only a quarter of the loss at 60% vertical load variation. If a simple RMS were used then the 60% variation case would only be considered to have twice the average force loss of the 30% case.

In order for the performance index to represent this effect the non-linearity present in the static loss should be used within the weighting of the contact load variation of the tyres. The problem that arises is that it is not suitable to use the properties from one specific tyre for all cases. It is also not possible to acquire tyre parameters for all tyres fitted to vehicles tested on the rig. If enough tyre data or magic formula coefficients for specific tyres were available then it may be possible to create generalised static loss characteristics based on the tyre size and measured vertical stiffness from the four-post rig data.

One characteristic that it is important to capture is the fact that variations on a lightly loaded tyre are much less significant in terms of static lateral force loss than a highly loaded tyre. For front wheel drive cars with high proportions of weight on the front axle, the same percentage load variation for both front and rear wheels would actually cause a higher static loss at the front of the car than the rear. This would in turn change the handling balance of the car as the road roughness, and hence load variation, was increased.

In order to facilitate the use of the tyre properties to create a static loss performance index it was decided that the characteristics would be scaled by tyre width, although other parameters of the tyres would be expected to have a significant influence on the characteristic as well. In order to do this a second set of magic formula coefficients were used.

In this case the coefficients were taken from Pacejka [58] and represented a 205/60 R15 tyre. Comparison of the static loss characteristics at 2° slip angle is presented in Figure 7-10. A scaling factor that was equal to the ratio of widths to the power of 2.5, was acceptable to determine the static loss of the 205/60 R15 tyre from the 235/60 R16 tyre data with a mean error of less than 1.6% of the static loss using the 235/60 R16 tyre coefficients (Figure 7-11). A slip angle of 2 degrees was chosen as the reference, as this angle would be commonly reached during normal driving conditions and in cases with higher slip angles the magnitude of the force loss follows a similar characteristic, although the magnitude is reduced (Figure 7-8).

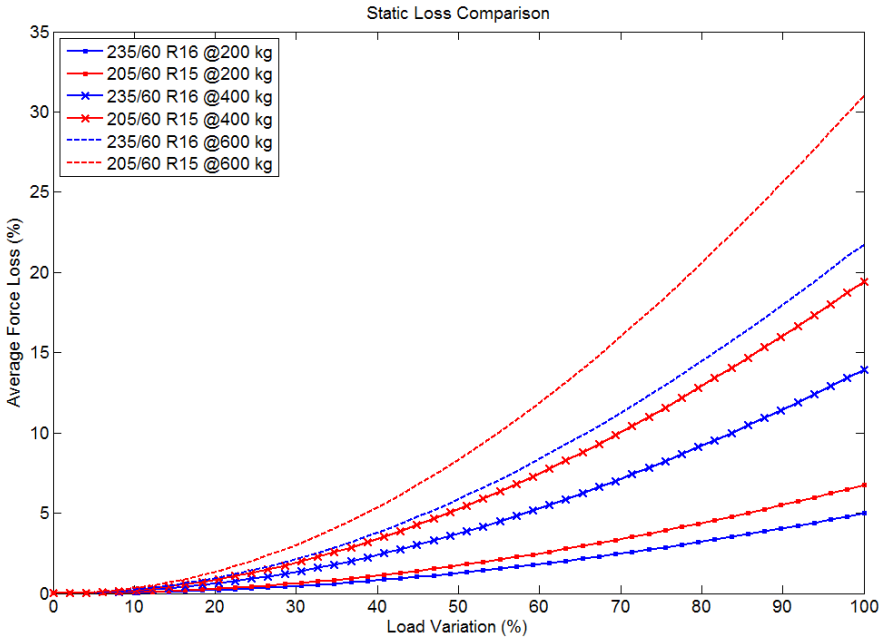

Figure 7-10 – Comparison of 235/60 R16 and 205/60 R15 static loss

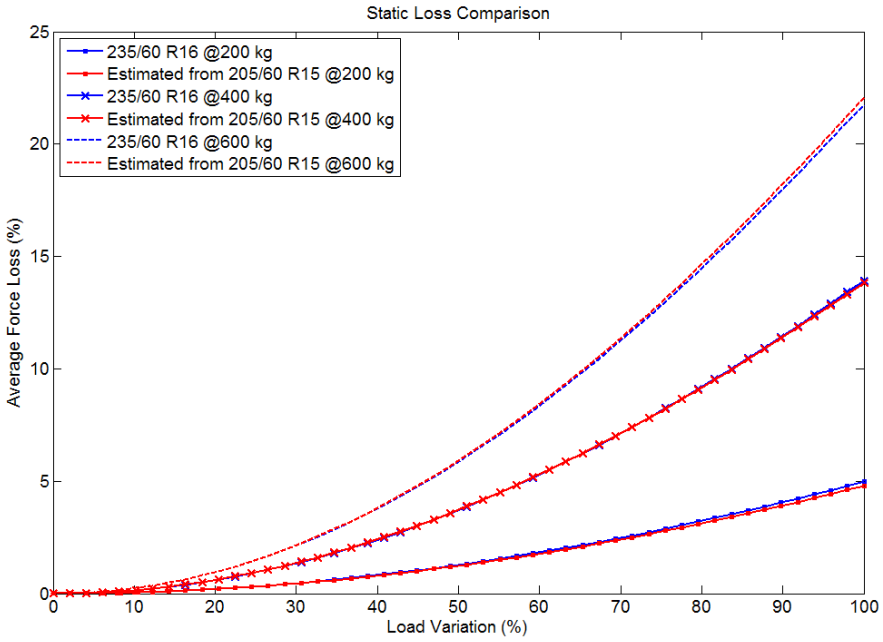

Figure 7-11 – Comparison of 235/60 R16 static loss and static loss estimated from 205/60 R15 tyre and width scaling factor

In order to define a level of static loss from any four-post test data an equation must be defined that uses the parameters:

- Tyre width
- Normal load
- Load variation percentage

Tyre width would be used straight from the manufactures size reference on the tyre. The normal load on the tyre can be measured statically and load variation percentage can be calculated as a response function by normalising the contact patch load response by the static load and multiplying by 100.

$$F_{y\,Loss\_Static\_400} = -2.43\times10^{-6}\times A_{Fz}{}^{3} + 1.67\times10^{-3}\times A_{Fz}{}^{2} - 3.14\times10^{-3}\times A_{Fz}$$

(7-2)

$$F_{zStatic\_Factor} = -6.90\times10^{-12}\times F_{zStatic}{}^{3} + 7.15\times10^{-8}\times F_{zStatic}{}^{2} + 9.97\times10^{-5}\times F_{zStatic} - 7.62\times10^{-2}$$

(7-3)

$$F_{y\,Loss\_Static} = \frac{F_{yLoss\_Static\_400} \times F_{zStatic\_Factor}}{\left(\frac{T_W}{235}\right)^{2.5}}$$

(7-4)

Where:

$F_{yLoss\ Static}$ – Average lateral force loss (%)

A_{Fz} – Amplitude of normalised load variation sine wave (%)

$F_{zStatic}$ – Static vertical tyre force (N)

T_w – Width of tyre (mm)

$F_{yLoss\ Static\_400}$ – $F_{yLoss\ Static}$ for 400kg Normal Load

$F_{zStatic\_Factor}$ – Multiplication factor for normal loads

Due to the non-linear nature of the static loss, it is not possible to simply add the RMS static loss calculated from the modal weighted PSDs to create an RMS static loss for the complete road excitation (as is done for the comfort index). To create the static loss for the complete road excitation the modal contact load variations must be combined to create a complete load variation PSD and the RMS calculated from this can then be used to calculate the expected static loss.

7.2.2 – Dynamic Loss

As well as the static loss of lateral force due to variations of load along the non-linear cornering stiffness curve, Pacejka [58] also describes a dynamic loss due to the lateral dynamics of the tyre.

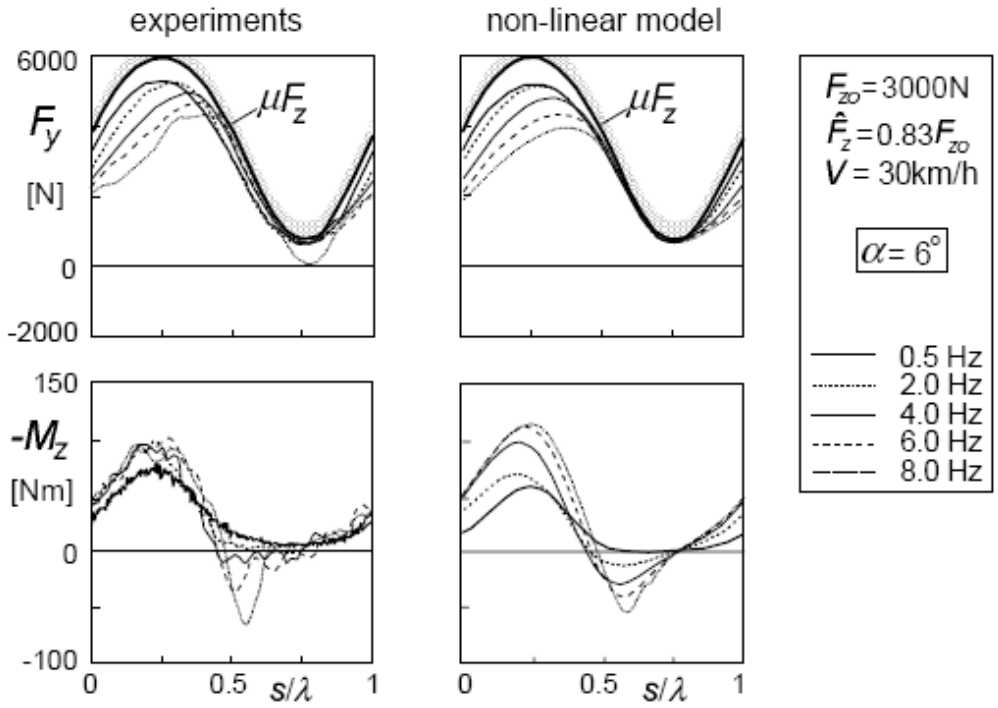

Figure 7-12 – Variation in Lateral Force During Vertical Force Variation. Pacejka [58] p374

In this case a load dependent 'relaxation length' parameter is used to control the dynamic characteristic of the tyre. Figure 7-12 shows that as the frequency of load variation increases, so does the lag between the lateral force generation and vertical load. However, as μFz defines the absolute limit of lateral force generation, the lag is not simply a phase shift of lateral force. This effect causes a significantly larger net grip loss than the static loss at higher frequencies. Figure 7-13 shows the effect of frequency and slip angle on the dynamic loss of lateral force at 400kg normal load with 60% load variation.

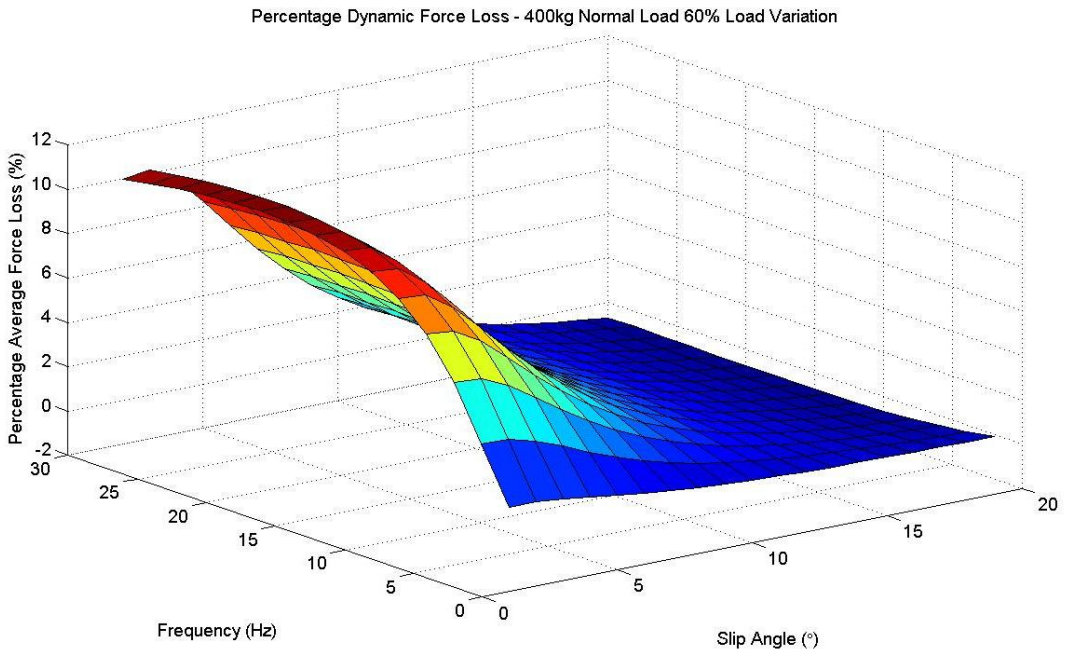

Figure 7-13 – Effect of Frequency and Slip Angle on Dynamic Loss

In order to simplify the application of the dynamic loss, again a slip angle of 2° was chosen for the creation of factors to be used within the performance index. The decision was made that the static loss equation would be used for this purpose, with the A_{Fz} parameter being replaced by a dynamic equivalent. This term is created from the original A_{Fz} term weighted using a transfer function, whose numerator and denominators are dependant on the static tyre force. As this relationship is also non-linear with load variation a power term was added, but only to be applied once the frequency weighted load variations from each excitation mode were added together. One benefit of using a transfer function is that the method can also be applied in the time domain. This gives the engineer the ability to simulate the vehicle travelling over a particular road surface and still capture the frequency dependant tyre losses in the performance index.

The first step in the process of creating the appropriate transfer functions was to determine the A_{Fz} scaling factor in order that the result from the static loss equation was equal to the total loss. This was carried out across the 0-40 Hz frequency range for the normal load range from 200 to 600 kg, with a fixed load variation of 50%. As there was also a non-linear load variation dependency, an appropriate power term was determined using the 400 kg normal load case. Figure 7-14 presents the scaling factors determined using this method.

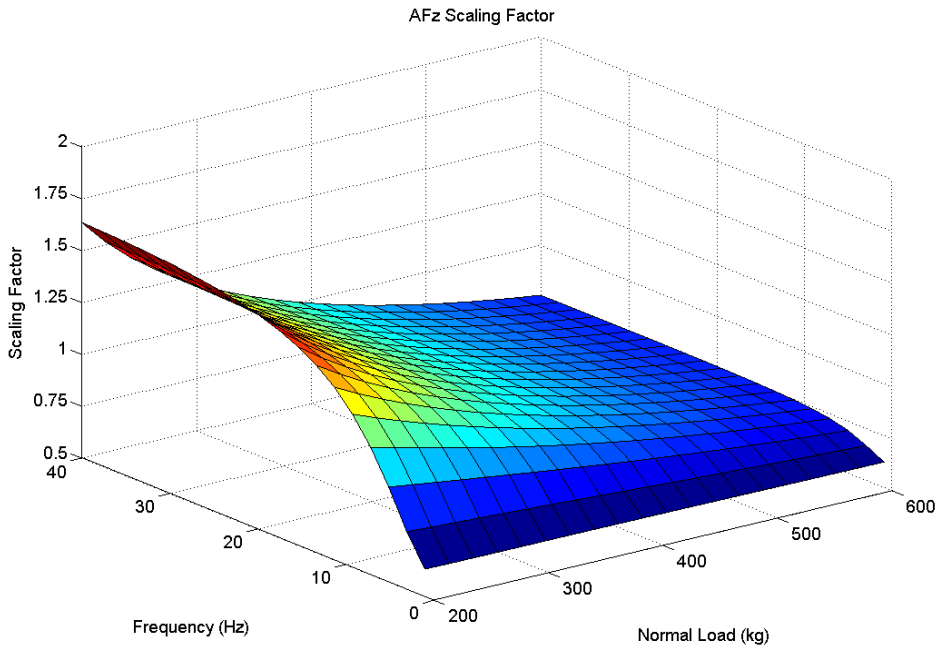

Figure 7-14 – A_{Fz} Scaling Factor with Normal Load and Frequency

A 2nd order transfer function was fitted to the scaling factor for each of the normal load conditions in a least square errors sense. In order to change the transfer function that is used the appropriate numerators and denominators are used relating to the normal load of the tyre. The variation in these values (Figure 7-15) is quite non-linear, this means that the most appropriate way to implement the correct coefficients is to use a lookup table and interpolate between points loads that are not present (this was also tested for intermediate loads and found to provide accurate results). Due to the fact that the desired transfer function has no imaginary value, the second numerator and denominator terms can be omitted.

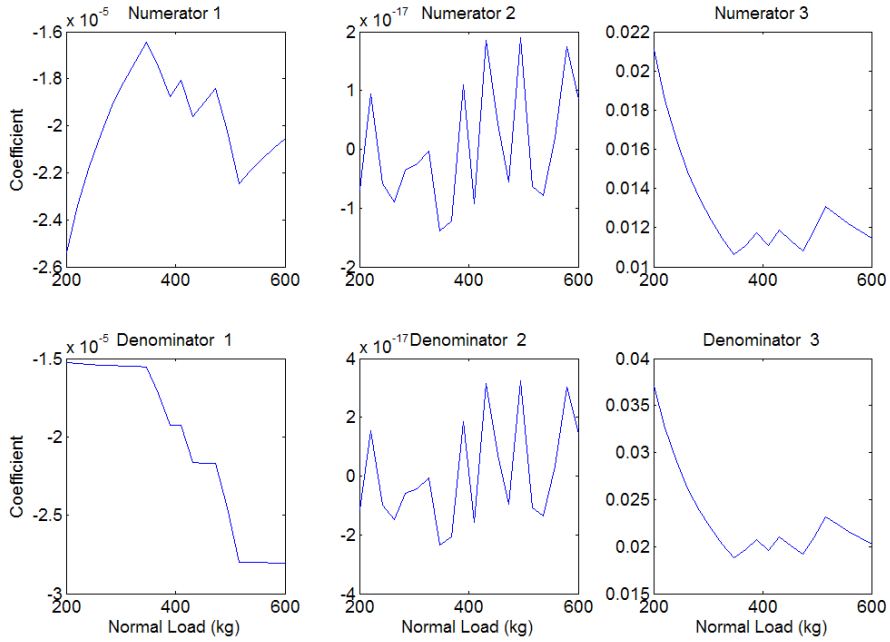

Figure 7-15 – A_{Fz} Frequency Weighting Numerators and Denominators for different Normal Loads

$$A_{FzDynamic} = \left(A_{Fz}(\omega) \times \frac{n1(F_{ZStatic})s^2 + n3(F_{zStatic})}{d1(F_{ZStatic})s^2 + d3(F_{zStatic})} \right)^{1.17} \quad \textbf{(7-5)}$$

Where:

$A_{FzDynamic}$ – Dynamic Equivalent of A_{Fz}

n - Normal Load Numerator Coefficients

d - Normal Load Denominator Coefficients

s - $j\omega$

Figure 7-16 and Figure 7-17 compare the total (combined static and dynamic loss) from the 'Magic Formula' model and created using equation (7-5) and equations (7-2) to (7-4) with A_{Fz} replaced with A_{Fz} dynamic.

In order to ensure that the result is sufficiently accurate around the levels of load variation expected to be experienced on the real road, some compromise has to be made in the accuracy of the total loss for higher load variations.

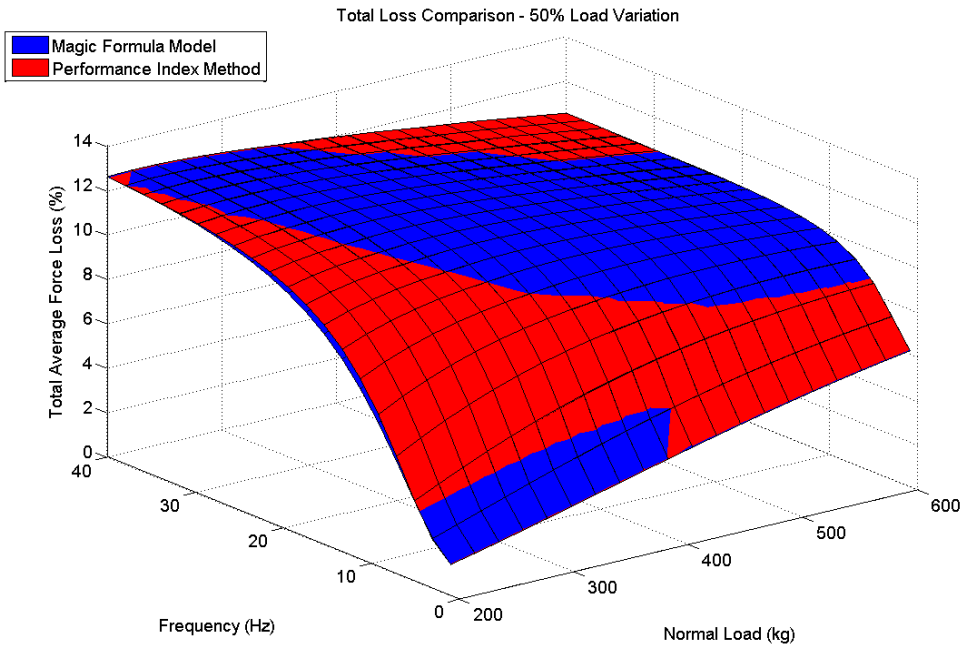

Figure 7-16 – Total Loss Comparison between Magic Formula Model and Performance Index Coefficients – 50% Load Variation

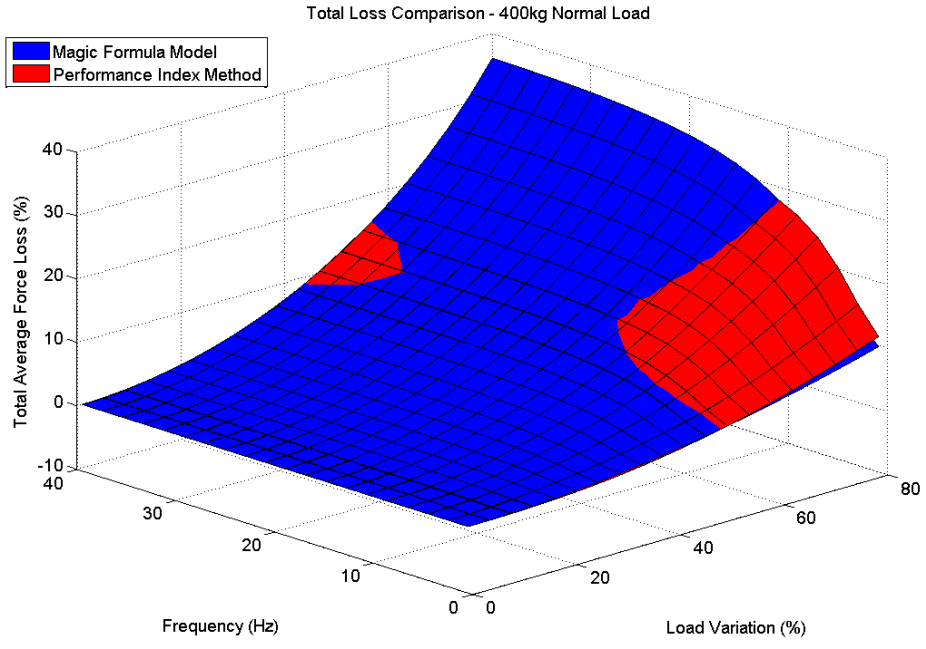

Figure 7-17 – Total Loss Comparison between Magic Formula Model and Performance Index Coefficients – 400kg Normal Load

In order to apply the method using the measured responses from rig data the first step required is to apply the dynamic loss transfer function to the static load normalised contact load variation. This is carried out for each excitation mode separately using equation (7-6).

$$F_{Z\_Norm\_Dynamic}(\omega) = F_{Z\_Norm}(\omega) \times \frac{n1(F_{ZStatic})s^2 + n3(F_{zStatic})}{d1(F_{ZStatic})s^2 + d3(F_{zStatic})}$$

(7-6)

Where:

F_{Z_Norm} – Normalised Load Variation Response (%)

$F_{Z\_Norm\_Dynamic}$ – Dynamic Loss Weighted F_{z_Norm}

The $F_{Z\_Norm\_Dynamic}$ response squared is then multiplied by the relevant modal input acceleration PSD relating to the ISO 8608 [4] B road and EUDC drive cycle [72]. The resultant PSD for each of the 4 modes is then summed to create a combined PSD.

The time domain RMS of the combined PSD is then used in equation (7-7) to provide a single sine wave amplitude to be used in the static loss equation (7-2), where A_{Fz} is given by (7-7).

$$A_{Fz} = \left(RMS\left(F_{Z\_Norm\_Dynamic\_Combined}\right) \times \sqrt{2}\right)^{1.17}$$

(7-7)

Where:

$F_{z\_Norm\_Dynamic\_Combined}$ – Combined normalised load variation

Equations (7-2) to (7-4) are used with the new A_{Fz} but the resultant is now F_{yLoss_Total} rather than F_{yLoss_Static}.

This process is carried out for both front and rear axle load variations and the values are then used to determine two of the performance indices. The 'Total Grip Loss' performance index value is determined by the summing of front and rear F_{yLoss_Total} values, whilst the 'Balance Change' performance index value is determined by subtracting the rear F_{yLoss_Total} from the front.

The 'Total Grip Loss' and 'Balance Change' performance indices define how the steady-state behaviour of the vehicle would be expected to vary over a moderately rough surface in comparison to a completely smooth surface. Ideally the absolute magnitude of the two numbers would be as small as possible, so that the driver of the vehicle could be confident that the

vehicle would react the same regardless of the road surface. However, this is not likely to be achievable. The balance change performance index is more important and more useful than the overall grip performance index, as it lets the engineer know how the steady-state balance would be expected to change with a moderately rough road. If the number is positive then the vehicle would be expected to have a more under-steering balance than on a smooth road, if the number is negative then the vehicle would be expected to have a more neutral or over-steering balance (depending on the initial balance of vehicle). The latter case is less desirable as the vehicle is more difficult to control for the non-professional driver and the vehicle can become unstable. An example of a vehicle with an under steering balance for a smooth road that changes to an over steering balance on rougher roads was demonstrated by Mashadi and Crolla (2005) [56].

7.2.3 - Vehicle Behaviour

Although the steady-state balance change of a vehicle over rough roads is of importance to the engineer, it is not the only parameter that should be considered when tuning the performance part of the suspension system. Another important consideration is the requirement of the driver to adjust the wheel during cornering. A paper that investigates the effect of suspension damping on the driver requirement over rough road surfaces was described by Rill (1986) [55].

Ideally the suspension system would have the properties that as the road roughness increases, the driver would not need to make any steering corrections to maintain the same path. However, this would not be possible with conventional passive suspension and steering systems, but when tuning for performance the requirement should be minimised.

7.2.3.1 – Effect of Load Variation on Driver Steering Requirement

To investigate the lateral dynamics of the vehicle the model explained in section 6.4.2– Full Car Lateral Vehicle Model, was used. Initially the model was used with a set of constant speed, constant radius turns to determine the effect of load variation on under steer gradient and other parameters such as lateral acceleration and yaw velocity, in a similar manner to Mashadi and Crolla's investigation in [56]. In this first investigation the front and rear load variations were applied with different phasing from 0 (pure heave) to 180 (pure pitch) and the standard deviations of various vehicle states obtained across the frequency range (Figure 7-18).

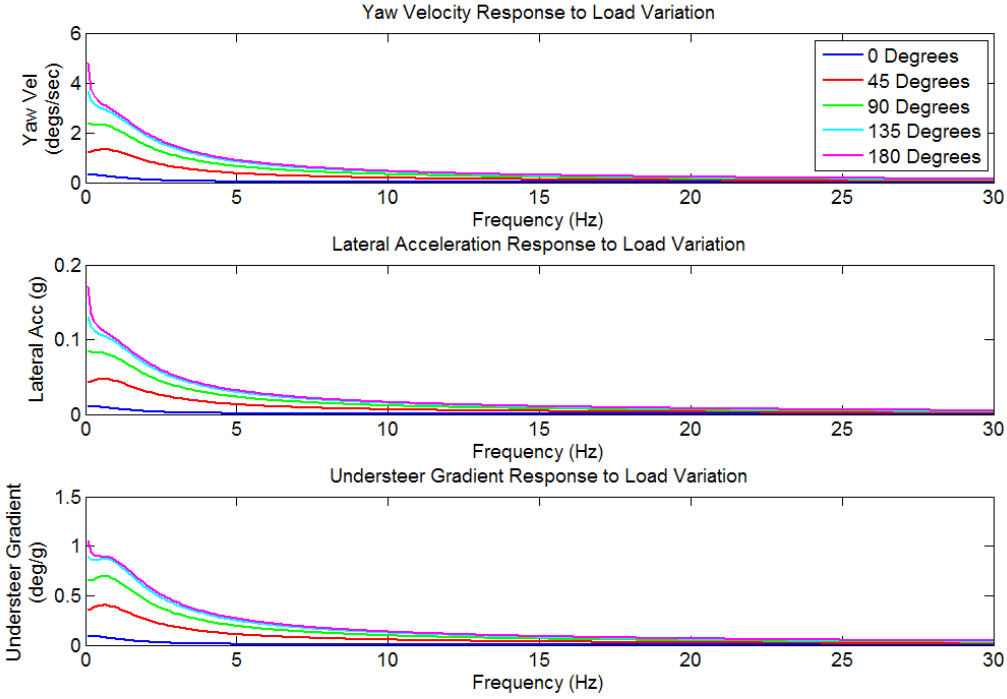

Figure 7-18 – Frequency Response of Vehicle States due to Load Variation

This method produced weighting functions that were heavily biased to low frequency variations in load and also included the dynamic and static loss effects of the tyres. The reason for the very low frequency bias was due to the fact that the vehicle would travel a long way off the intended path with a fixed steering angle and the longer the vehicle was travelling along the wrong curvature the bigger the error. In reality the driver would have only had to make very small and very slow corrections at these frequencies. To improve the relevance of the weighting functions created with the model, the steering model used by Rill [55] was employed.

To produce a more suitable set of weighting functions, no load variation was applied to the four wheels, but lateral force scalars were used to vary the lateral force at all 4 tyres using a 0.1 to 50 Hz band-limited white noise signal with an RMS of 20%. The forward speed input was the EUDC driving cycle [72] and the intended path for the vehicle to follow was constant radius turn of 140 m. Combined, these provided a range of lateral acceleration magnitudes up to 7.85 m/s^2 (0.8g). The investigation was carried out for all 4 road input modes individually so that driver requirement frequency responses could be determined for each excitation mode. As opposed to just using the full car model parameters relating to the Civic, a range of +/- 15% vehicle mass, yaw mass moment of inertia and roll stiffness balance were analysed, as well as a change from 63 to 50% front weight distribution. By taking the mean response from each of these set-ups the frequency response would be appropriate for a much wider range of vehicles, rather than being limited to the response of the Civic. For each of the averaged responses a 2nd order transfer function was fitted to the magnitude of the response. Again, by using a transfer function the method can be used in both time and frequency domains. Figure 7-19 presents and example of the steer velocity response to lateral force variations in pure pitch.

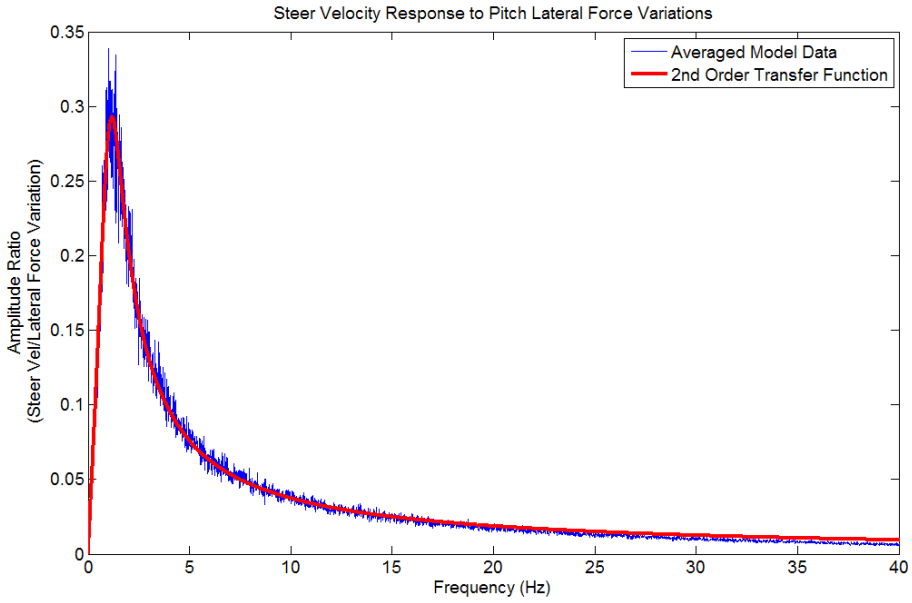

Figure 7-19 – Pitch Steer Velocity Response Transfer Function Fitting

The steering velocity responses for all four excitation modes are shown in Figure 7-20 below.

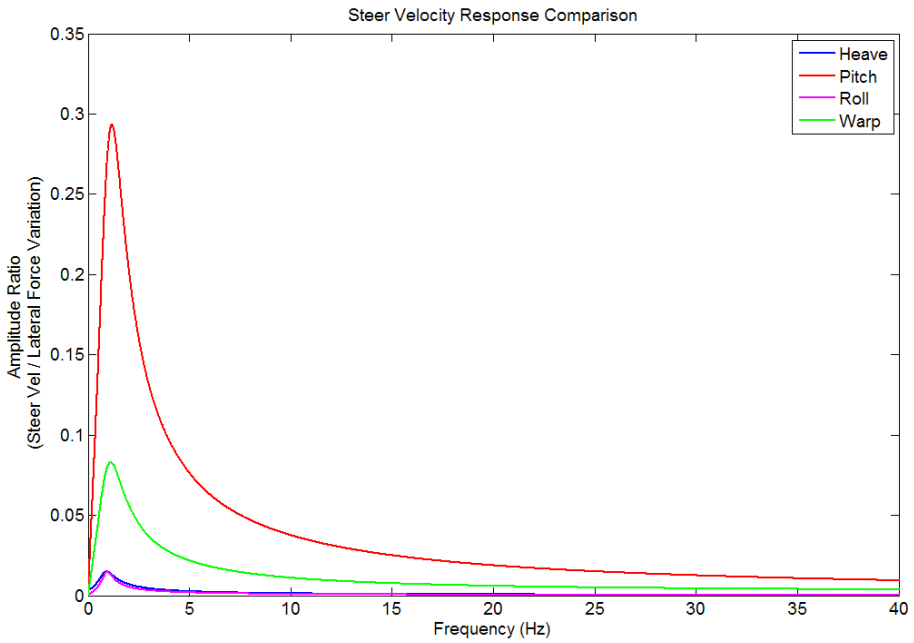

Figure 7-20 – Steering Velocity Response to Lateral Force Variation Comparison

The steering velocity response comparison (Figure 7-20) clearly shows that lateral force variation in pitch is dominant for the driver's steering velocity requirement to maintain a desired path. The second largest mode is warp, with heave and roll responses being similar in peak magnitude to each other, but considerably less significant than pitch and warp. The result is quite intuitive considering how the lateral force variation (ultimately due to vertical force variation) occurs in each case. In heave the lateral force on all 4 tyres is reduced in magnitude at the same time and same level. This results in a variation of total grip which requires only a small correction by the driver. In roll the total grip scalar remains the same, as the tyres on the left and right sides of the vehicle are at different vertical loads (due to load transfer) the effect of grip loss has a different effect on the each side of the car, so again a small correction is required by the driver. In the pitch case the front tyres gain lateral force, whilst the rear tyres lose lateral force and vice-versa. In this case the grip balance of the vehicle is being changed significantly, requiring the driver to apply more steering while the front lateral force is low, and conversely apply less steering when the rear lateral force is low, when compared to steady-state conditions. In warp the front left-rear right and front right-rear left lateral forces are scaled out of phase. This provides a combination of the pitch and roll cases. Considering the vehicle in a turn, as the outside front lateral force is increased the outside rear lateral force is reduced. On its own this would require a reduction in steering by the driver. However, at the same point, the front inside lateral force is reduced and the rear inside lateral force increased, which on its own would require an increase in steering by the driver, which provides some cancellation of the net driver requirement compared to the pure pitch case.

If the variation of lateral force at the front and rear of the vehicle is in-phase, but not identical, then there would be expected to be an increased driver requirement compared to the pure in-phase lateral force scaling. An example is shown in Figure 7-21 where the scaling of lateral force variation was 20% higher on the front axle and 20% lower the rear compared to pure heave.

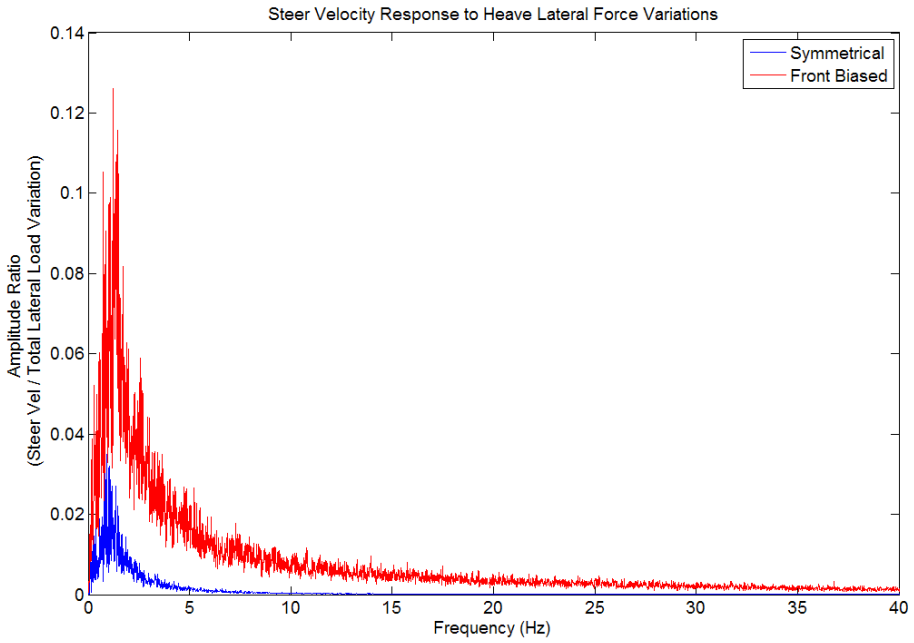

Figure 7-21 – Effect of Front Biased Heave on Steer Velocity Response

Due to this effect, it is important to calculate all the variations of lateral force for heave, pitch, roll and warp within each excitation mode.

In order to calculate the lateral force variation for a given vertical force variation, a similar approach is used as the dynamic loss frequency weighting, with a transfer function whose coefficients are based on the normal load of the tyres being applied to the normalised load variation response. The transfer function coefficients are presented in Figure 7-22 and their resultant lateral force variation maps can be seen in Figure 7-23 and Figure 7-24. Equation (7-8) is used to acquire the lateral force variation from the static load and normalised load variation response. Again the second terms of the numerator and denominator can be omitted.

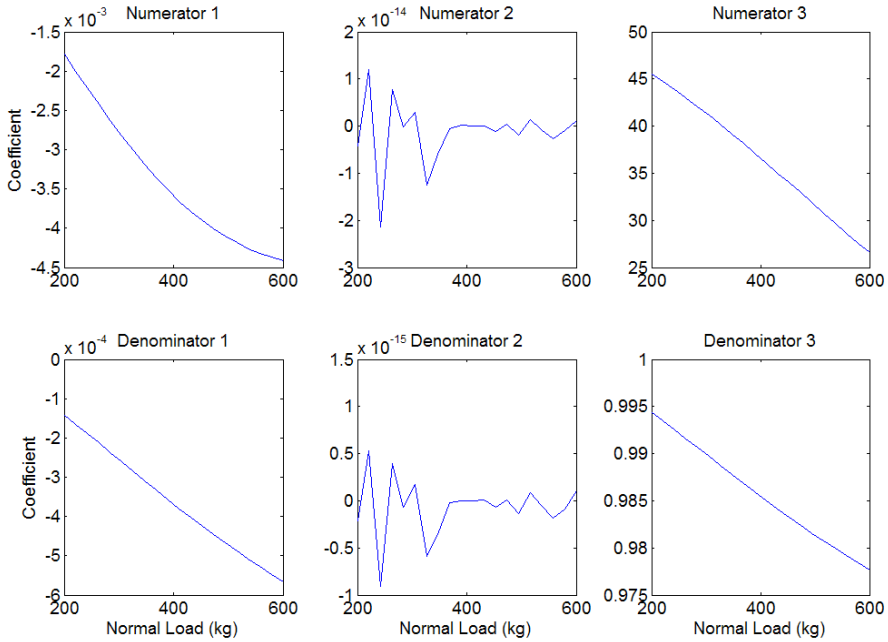

Figure 7-22 – Lateral Force Variation Transfer Function Coefficients for Different Normal Loads

$$F_{y\_Var}(\omega) = 0.02\left(F_{Z\_Norm}(\omega) \times \frac{n1(F_{ZStatic})s^2 + n3(F_{zStatic})}{d1(F_{ZStatic})s^2 + d3(F_{zStatic})} \right)$$

(7-8)

Where:

$F_{y\_}Var$ – Variation in lateral force (%)

n – Lateral Force Variation Numerator Coefficients

d – Lateral Force Variation Denominator Coefficients

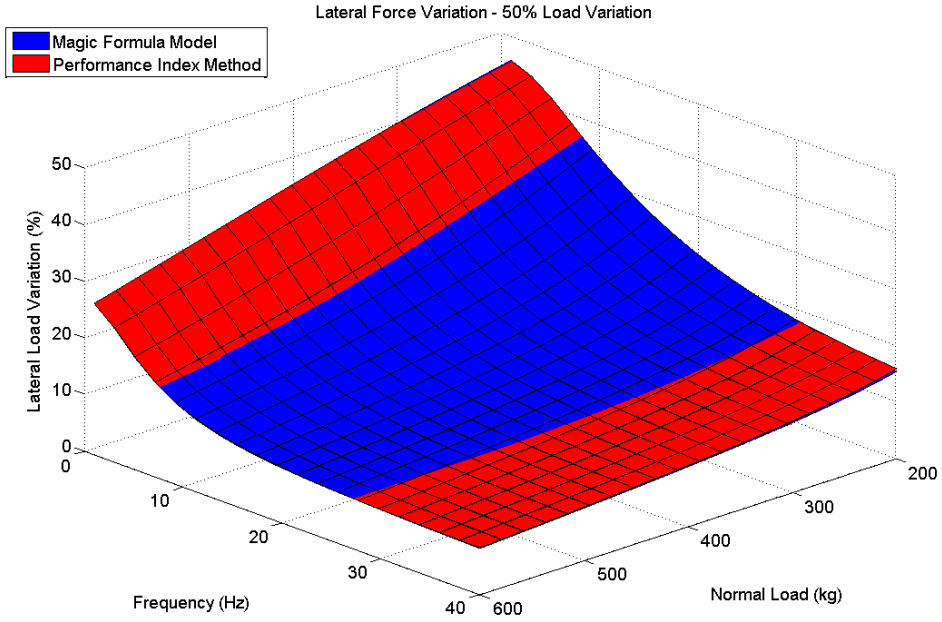

Figure 7-23 – Lateral Force Variation Comparison between Magic Formula Model and Performance Index Coefficients – 50% Load Variation

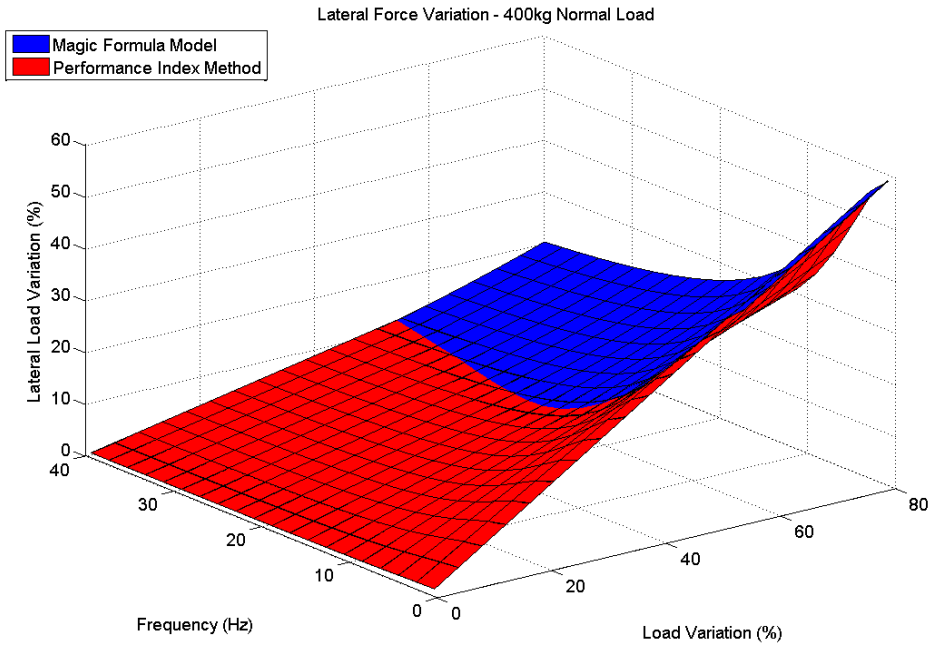

Figure 7-24 - Lateral Force Variation Comparison between Magic Formula Model and Performance Index Coefficients – 400kg Normal Load

For a single modal excitation the F_{y_Var} responses are calculated for each wheel of the vehicle. Equations (7-9) to (7-16) are then used to determine the required steering velocity response for each of the modal responses for a single modal input excitation. This is carried out for all 4 modal input excitations. Equations (7-17) to (7-20) are used to determine the steer velocity requirements for each of the road input modes by multiplying by the relevant model input

acceleration PSDs (as with the grip loss performance indices) and combined to produce a single steering velocity requirement for the EUDC cycle [72] on the ISO 8608 [4] B road surface (equation (7-21)). The time domain RMS calculated from the combined PSD is used as the 'Driver Requirement' performance index value.

$$F_{y\_Heave}(\omega) = \left| \frac{F_{y\_Var\_FL}(\omega) + F_{y\_Var\_FR}(\omega) + F_{y\_Var\_RL}(\omega) + F_{y\_Var\_RR}(\omega)}{4} \right|$$

(7-9)

$$F_{y\_Pitch}(\omega) = \left| \frac{\left(F_{y\_Var\_FL}(\omega) + F_{y\_Var\_FR}(\omega)\right) - \left(F_{y\_Var\_RL}(\omega) + F_{y\_Var\_RR}(\omega)\right)}{4} \right|$$

(7-10)

$$F_{y\_Roll}(\omega) = \left| \frac{\left(F_{y\_Var\_FL}(\omega) - F_{y\_Var\_FR}(\omega)\right) + \left(F_{y\_Var\_RL}(\omega) - F_{y\_Var\_RR}(\omega)\right)}{4} \right|$$

(7-11)

$$F_{y\_Warp}(\omega) = \left| \frac{\left(F_{y\_Var\_FL}(\omega) + F_{y\_Var\_RR}(\omega)\right) - \left(F_{y\_Var\_FR}(\omega) + F_{y\_Var\_RL}(\omega)\right)}{4} \right|$$

(7-12)

Where:

$F_{y\_Var\_FL,FR,RL,RR}$ – Lateral Load Variation Frequency Responses

F_{y_Heave} – Heave Lateral Load Variation Frequency Response

F_{y_Pitch} – Pitch Lateral Load Variation Frequency Response

F_{y_Roll} – Roll Lateral Load Variation Frequency Response

F_{y_Warp} – Warp Lateral Load Variation Frequency Response

$$V_{Steer\_Heave}(\omega) = F_{y\_Heave}(\omega) \times \frac{n1_{Heave}s^2 + n2_{Heave}s + n3_{Heave}}{d1_{Heave}s^2 + d2_{Heave}s + d3_{Heave}}$$

(7-13)

$$V_{Steer\_Pitch}(\omega) = F_{y\_Pitch}(\omega) \times \frac{n1_{Pitch}s^2 + n2_{Pitch}s + n3_{Pitch}}{d1_{Pitch}s^2 + d2_{Pitch}s + d3_{Pitch}}$$

(7-14)

$$V_{Steer\_Roll}(\omega) = F_{y\_Roll}(\omega) \times \frac{n1_{Roll}s^2 + n2_{Roll}s + n3_{Roll}}{d1_{Roll}s^2 + d2_{Roll}s + d3_{Roll}}$$

(7-15)

$$V_{Steer\_Warp}(\omega) = F_{y\_Warp}(\omega) \times \frac{n1_{Warp}s^2 + n2_{Warp}s + n3_{Warp}}{d1_{Warp}s^2 + d2_{Warp}s + d3_{Warp}}$$

(7-16)

Where:

V_{Steer_Heave} – Steering Velocity Requirement Response due to Heave Lateral Force Variation

V_{Steer_Pitch} – Steering Velocity Requirement Response due to Pitch Lateral Force Variation

V_{Steer_Roll} – Steering Velocity Requirement Response due to Roll Lateral Force Variation

V_{Steer_Warp} – Steering Velocity Requirement Response due to Warp Lateral Force Variation

n – Numerators for Steer Velocity Transfer Functions

d – Denominators for Steer Velocity Transfer Functions

$$V_{Steer\_Combined\_Heave}(\omega) = G_{A\_Heave}\left(V_{Steer\_Heave}(\omega) + V_{Steer\_Pitch}(\omega) + V_{Steer\_Roll}(\omega) + V_{Steer\_Warp}(\omega)\right)^2$$

(7-17)

$$V_{Steer\_Combined\_Pitch}(\omega) = G_{A\_Pitch}\left(V_{Steer\_Heave}(\omega) + V_{Steer\_Pitch}(\omega) + V_{Steer\_Roll}(\omega) + V_{Steer\_Warp}(\omega)\right)^2$$

(7-18)

$$V_{Steer\_Combined\_Roll}(\omega) = G_{A\_Roll}\left(V_{Steer\_Heave}(\omega) + V_{Steer\_Pitch}(\omega) + V_{Steer\_Roll}(\omega) + V_{Steer\_Warp}(\omega)\right)^2$$

(7-19)

$$V_{Steer\_Combined\_Warp}(\omega) = G_{A\_Warp}\left(V_{Steer\_Heave}(\omega) + V_{Steer\_Pitch}(\omega) + V_{Steer\_Roll}(\omega) + V_{Steer\_Warp}(\omega)\right)^2$$

(7-20)

$$V_{Steer\_Combined}(\omega) = V_{Steer\_Combined\_Heave}(\omega) + V_{Steer\_Combined\_Pitch}(\omega) + V_{Steer\_Combined\_Roll}(\omega) + V_{Steer\_Combined\_Warp}(\omega)$$

(7-21)

Where:

$V_{Steer\_Combined\_Heave}$ – Steer Velocity Requirement PSD due to Heave Input

$V_{Steer\_Combined\_Pitch}$ – Steer Velocity Requirement PSD due to Pitch Input

$V_{Steer\_Combined\_Roll}$ – Steer Velocity Requirement PSD due to Roll Input

$V_{Steer\_Combined\_Warp}$ – Steer Velocity Requirement PSD due to Warp Input

$V_{Steer\_Combined}$ – Steer Velocity Requirement PSD for Complete Road Input

G_{A_Heave} – Input Acceleration PSD Heave Input for EUDC Drive Cycle on ISO B Road.

G_{A_Pitch} – Input Acceleration PSD Pitch Input for EUDC Drive Cycle on ISO B Road.

G_{A_Roll} – Input Acceleration PSD Roll Input for EUDC Drive Cycle on ISO B Road.

G_{A_Warp} – Input Acceleration PSD Warp Input for EUDC Drive Cycle on ISO B Road.

The relative importance of the 'Total Grip Loss', 'Grip Balance' and 'Driver Requirement' index values to the driver's perceived 'Performance' of a vehicle is something that is very difficult to establish with simulation, or a small amount of subjective testing. For this reason the initial scaling factors have been set to 1, but it is the intention that Honda engineers would tune the relative importance of these indices based on subjective driver assessments for a range of vehicles or set-ups where the performance index values were also measured.

7.2.4 - Suspension Displacement

As an additional measure of vehicle performance the expected RMS suspension displacement at the front and rear suspensions from the ISO 8608 [4] B road and the EUDC drive cycle [72] is reported. The intention of this metric is to allow the engineer to determine how much of the available suspension range the vehicle is using, so that they can anticipate how often the vehicle is likely to come into contact with the bump stops and droop limitation of the suspension.

In the design stage of a vehicle this metric could also be used to help determine how much allowable suspension travel the vehicle should have for optimum performance and comfort behaviour, and the effects of limiting suspension displacement.

This metric is required as simulation of very softly sprung vehicle will generally produce both favourable comfort and performance index values, but at the expense of a large amount of suspension displacement. If these settings are applied to a real vehicle with suspension displacement limitations, then the comfort and performance perception of the vehicle will be poor, as the vehicle will commonly come into contact with the bumpstops and possibly droop limitations.

In order to calculate the suspension displacement for a given road and drive cycle equation (7-22) is used.

$$xSus_{F\_Heave\_PSD}(\omega) = G_{A\_Heave}(xSus_{F\_Heave}(\omega))^2$$

(7-22)

Where:

$xSus_{F\_Heave\_PSD}$ - PSD of front suspension displacement

$xSus_{F\_Heave\_}$ – Frequency Response of front suspension displacement with respect to input acceleration

This calculation is repeated for both front and rear suspensions for all 4 modal inputs. In the case of roll and warp, front and rear displacements correspond to the difference in left and right displacements divided by 2.

From the combined suspension displacement PSDs the RMS values for a Gaussian input are determined.

7.3 - Validation of Comfort and Performance Index with Subjective-Objective Test

In order to validate the comfort and performance indices to subjective driver ratings, a subjective-objective test was carried out in November 2010. Both subjective and objective parts of the test were carried out using the same 2007 5-door Honda Civic with 4 different suspension setups that were consistent for each test. Objective measurements were carried out by the author, using the Oxford Brookes University four-post rig and the test and analysis methods described in this thesis. The subjective parts of the test were carried out using Honda test drivers around Honda's subjective evaluation routes in Swindon and Offenbach, as previously described in section 3.7 – Collection of Road data and Basic Spatial Characteristic Estimation. The subjective assessment questionnaires were not Honda's usual questionnaires, but instead questionnaires developed for this thesis as explained in section 7.3.2 - Subjective Test Results. The data collected from both objective and subjective tests, was purely for use in this thesis, including on car measurements from the subjective routes explained in section 3.7 – Collection of Road data and Basic Spatial Characteristic Estimation.

The 3 main objectives of these tests were:

1. Obtain response results to create performance and comfort index values for Honda Civic with 4 different setups.

2. Carry out subjective assessments for the same 4 setups, on both UK and German roads.

3. Determine the correlation between the objective measurements from four-post rig testing and subjective assessments by test drivers.

The setups used in the investigation are shown in Table 7-1.

Set-up No.		Front			Rear		
	Wheels (Inches)	Springs	Dampers	Anti-roll Bar (mm)	Springs	Dampers	Pre-load Tube (mm)
1	16	Std	Std	23	Std	Std	41
2	17	Std	Std	23	2.2 D	Type R	39
3	17	1.8 5 Dr	2.2 D	23	2.2 D	1.8 5 Dr	43
4	16	Std	1.8 5 Dr	23	1.8 5 Dr	Std	41

Table 7-1 – Civic Setup Combinations

7.3.1 – Four-post rig results

In this section the results from the four-post rig testing of the 4 setups in Table 7-1 are compared and their comfort and performance index values presented.

7.3.1.1 - Comfort Index

Figure 7-25 presents the weighted body accelerations at the seat surface and floor for a pure heave input over a constant velocity PSD road surface. The results show a significant influence of the seat on the level and frequency distribution of discomfort. Setups 2 and 3 show an increased level of discomfort over the entire frequency range compared to the baseline and setup 4, with setup 2 being the most uncomfortable for the majority of the frequency range and setup 4 being very similar to setup 1 for the majority of the frequency range.

Figure 7-26 shows the measured seat transmissibility for the 4 different setups. The transmissibility can be seen to shift in frequency slightly due to the non-linear nature of the seat dynamics. In general the SEAT value was around 140%. This indicates that in the 0.5-30 Hz frequency range it would be around 40% more uncomfortable to sit on the seat than the floor, this is obviously an undesirable seat characteristic to have.

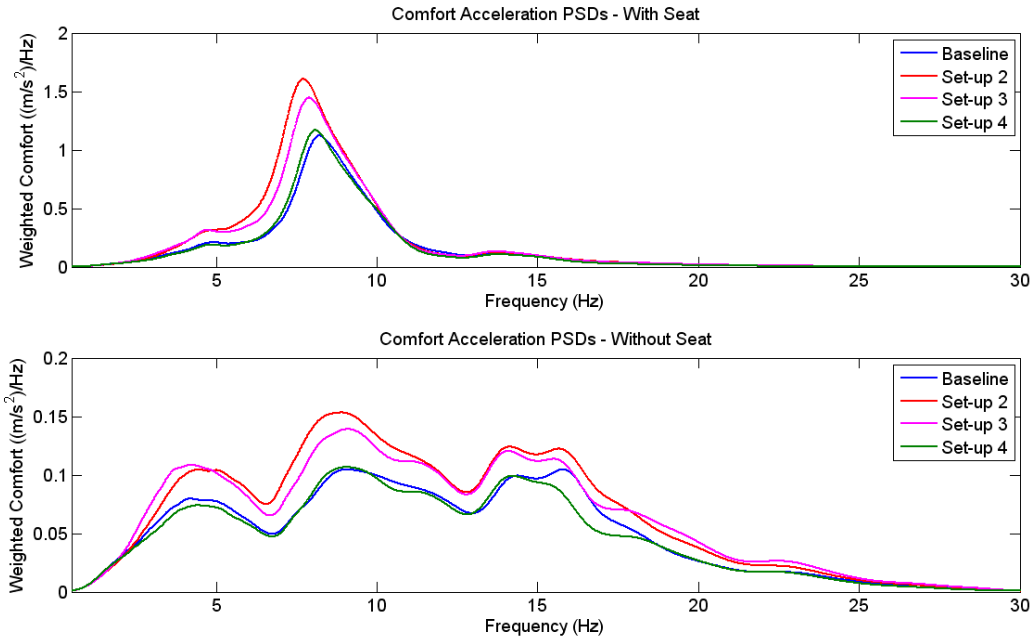

Figure 7-25 - Weighted Body Accelerations with and without seat – Heave

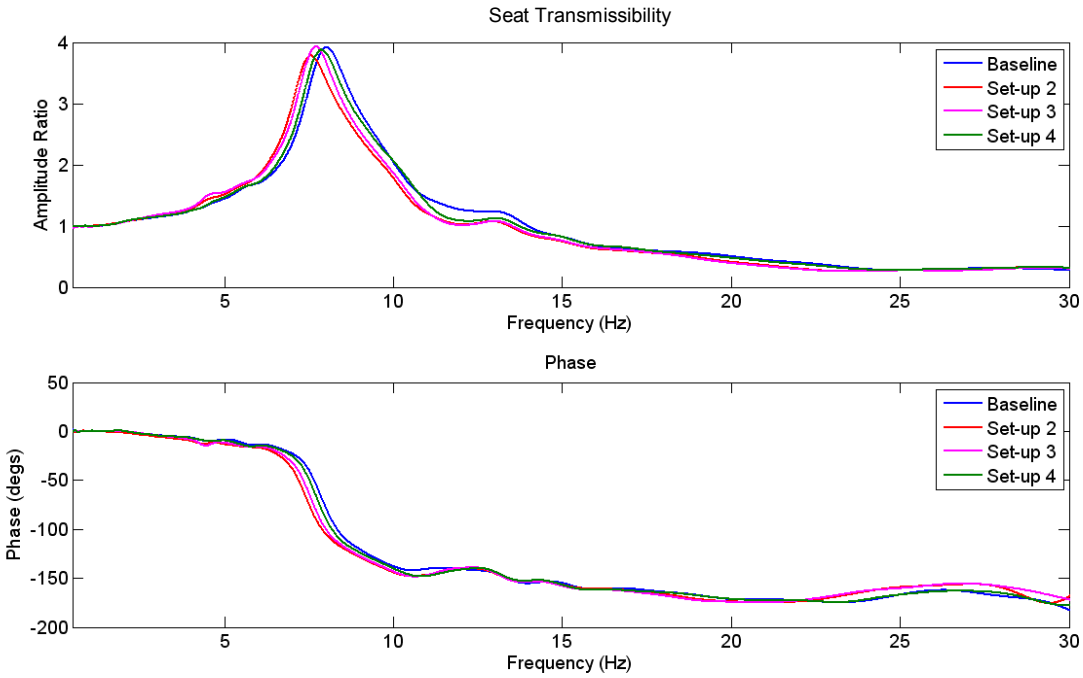

Figure 7-26 – Seat Transmissibility

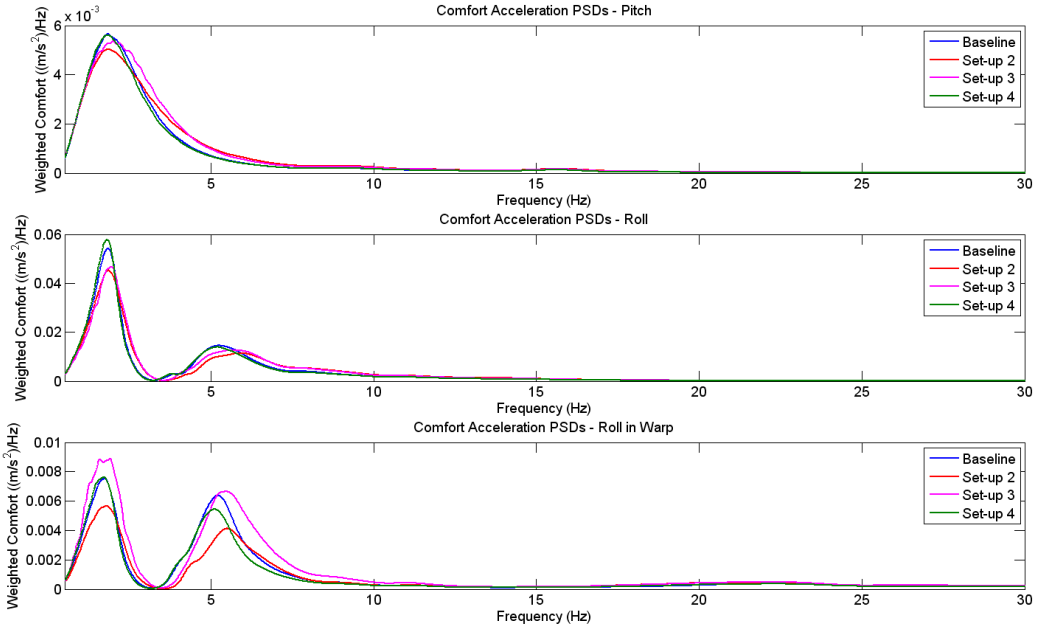

Figure 7-27 – Weighted Body Accelerations – Pitch, Roll and Roll in Warp

Figure 7-27 presents the weighted body acceleration PSDs in pure pitch, pure roll and roll in pure warp. Together with the heave PSDs these are weighted using the relevant model weightings from the EUDC drive cycle [72] and summed to produce a combined weighted body acceleration (Figure 7-28).

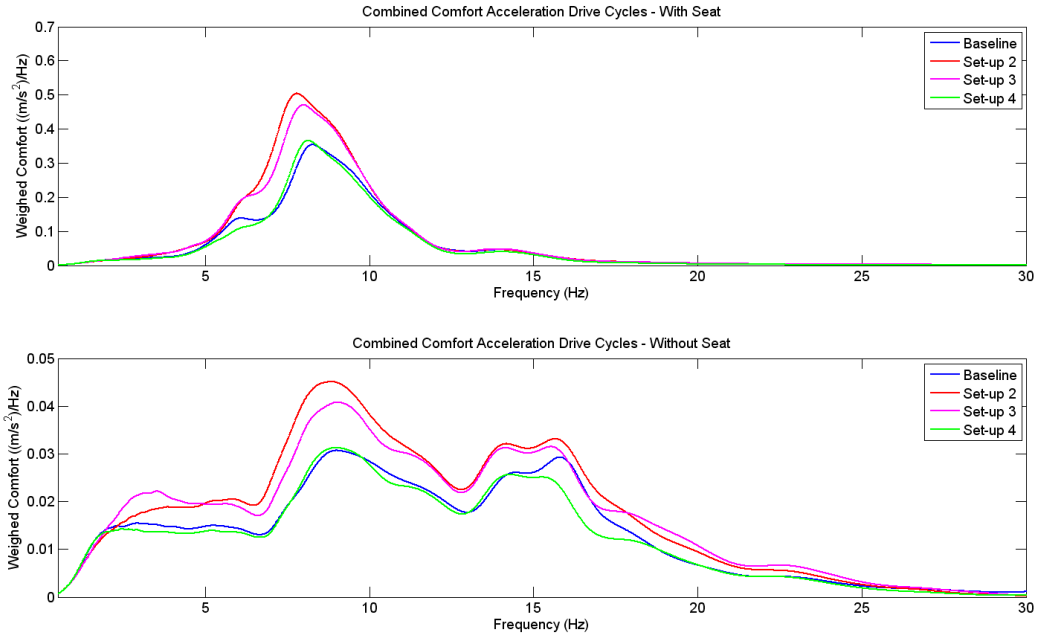

Figure 7-28 – Combined Weighted Body Acceleration PSDs

Rather than using one measure for total comfort, the comfort assessment was separated into:

- Low Frequency Heave
- Low Frequency Pitch
- Low Frequency Roll
- Vibration and Harshness

In the objective test case the cut-off for low frequency was set at 5 Hz, and anything beyond this point in any axis would be considered vibration and harshness.

Table 7-2 presents the individual and combined comfort index values for the 4 different setups tested, while Figure 7-29 compares setups 2 to 3 in comparison to the baseline.

	Comfort Index Measures				
Set-up	Low Frequency Heave	Low Frequency Pitch	Low Frequency Roll	Vibration and Harshness	C.I.
1	0.4539	0.1145	0.2603	1.1157	1.2376
2	0.4963	0.1154	0.2505	1.2919	1.4112
3	0.5208	0.1197	0.2561	1.2601	1.3925
4	0.4374	0.1130	0.2644	1.0852	1.2048

Table 7-2 – Objective Comfort Index Results

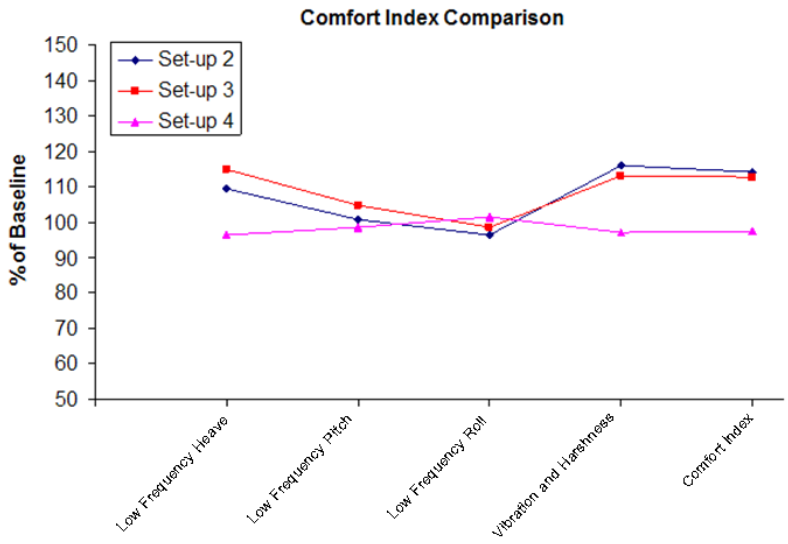

Figure 7-29 – Comfort Index Relative to Baseline

The comfort index comparison results in Figure 7-29 show that overall setup 4 would be considered 2.65% more comfortable than the baseline, only being less comfortable in low frequency roll. Setups 2 and 3 would both be considered around 13% less comfortable than the baseline, although both slightly more comfortable in low frequency roll.

7.3.1.2 – Performance Index

Figure 7-30 and Figure 7-31 present the normalised contact force PSDs for the baseline setup, weighted using the modal EUDC drive cycle weighting functions and their combined contact load variations. The two responses show quite different shapes, with the front having the highest load variation at around 2.5 Hz and the rear having the highest load variation around 15Hz.

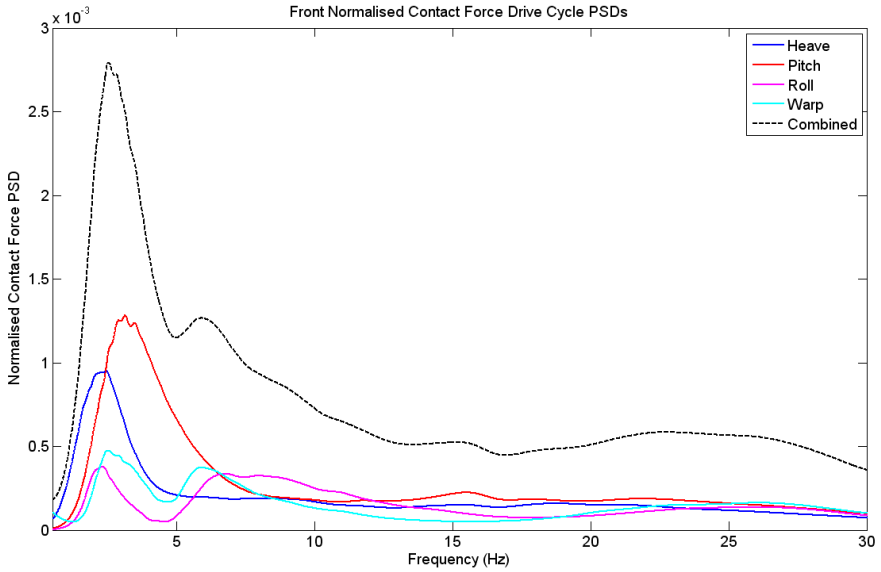

Figure 7-30 – Front Normalised Contact Force Contributions – Baseline

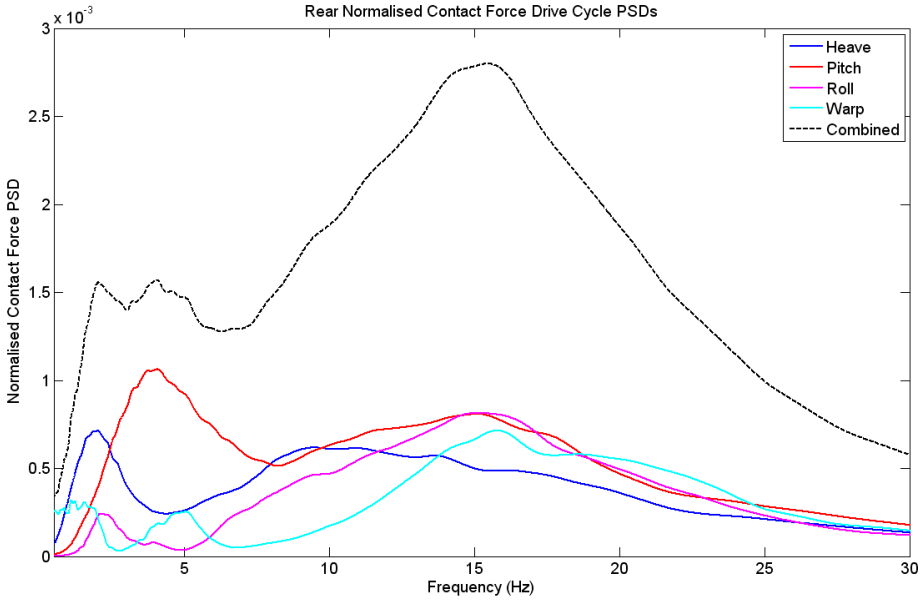

Figure 7-31 – Rear Normalised Contact Force Contributions – Baseline

The driver steering velocity requirement PSD contributions for the baseline setup are shown in Figure 7-32. The pitch contribution is highly dominant, mainly due to the fact that the required steering velocity response to lateral force variations in pitch has a much larger magnitudes than the other modes.

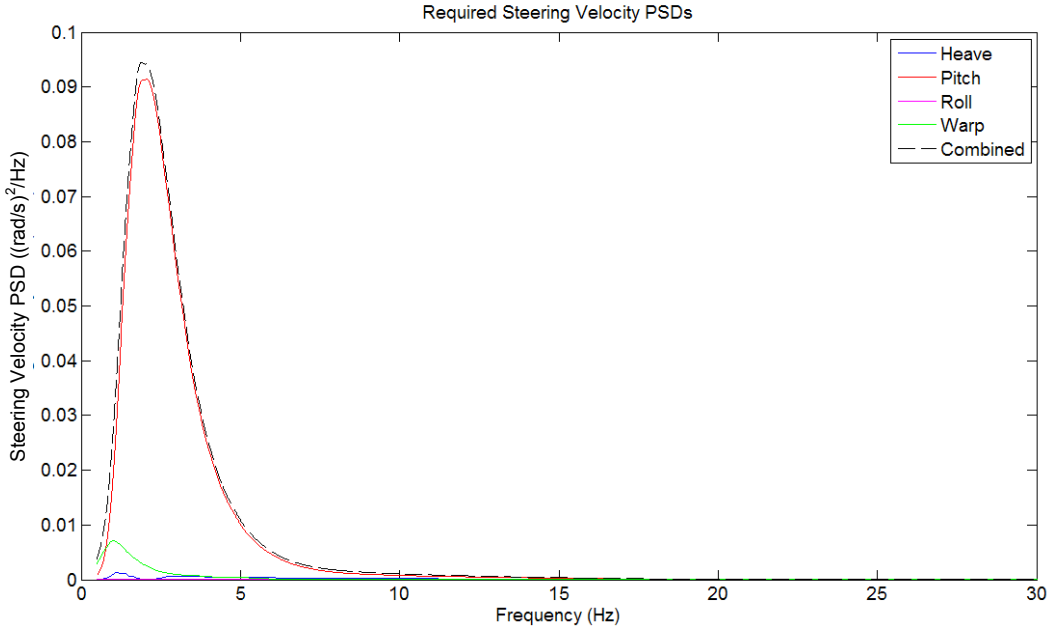

Figure 7-32 – Steering Velocity PSD Contributions - Baseline

Comparisons of the 4 combined contact load variations for the 4 different setups are presented in Figure 7-33 and Figure 7-34, with the steering velocity requirement PSDs shown in Figure 7-35. The front results show similar load variations for setups 1, 2 and 4, but an increased level of load variation for setup 3. Setup 3 also has the highest peak and RMS steering velocity requirement, whilst setup 2 has less than 3, but more than 1 and 4.

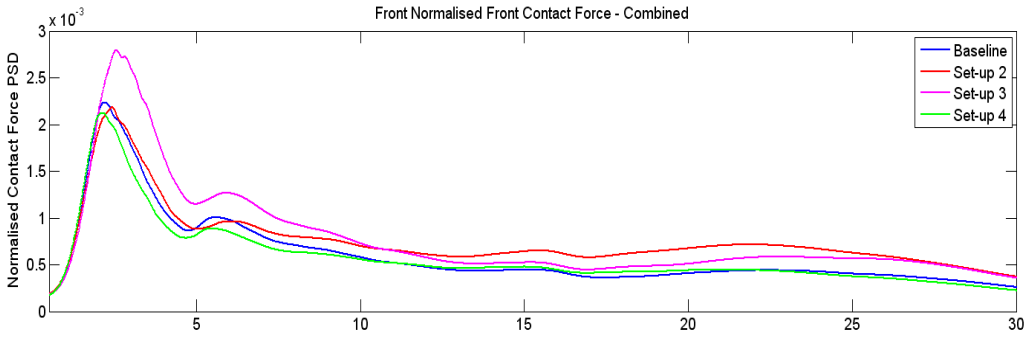

Figure 7-33 – Combined Normalised Contact Force – Front

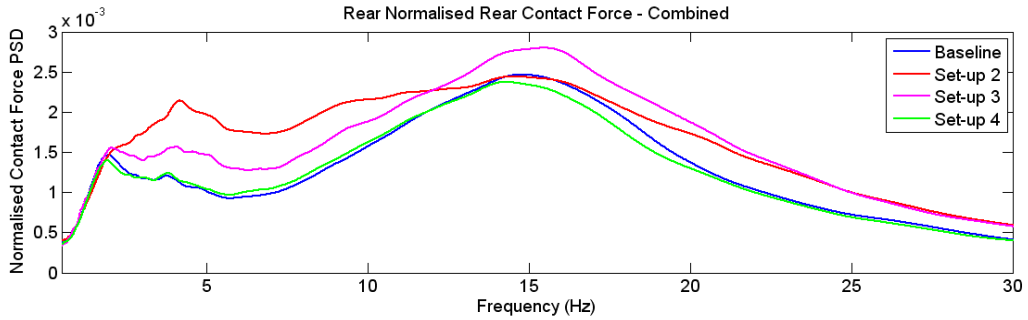

Figure 7-34 – Combined Normalised Contact Force – Rear

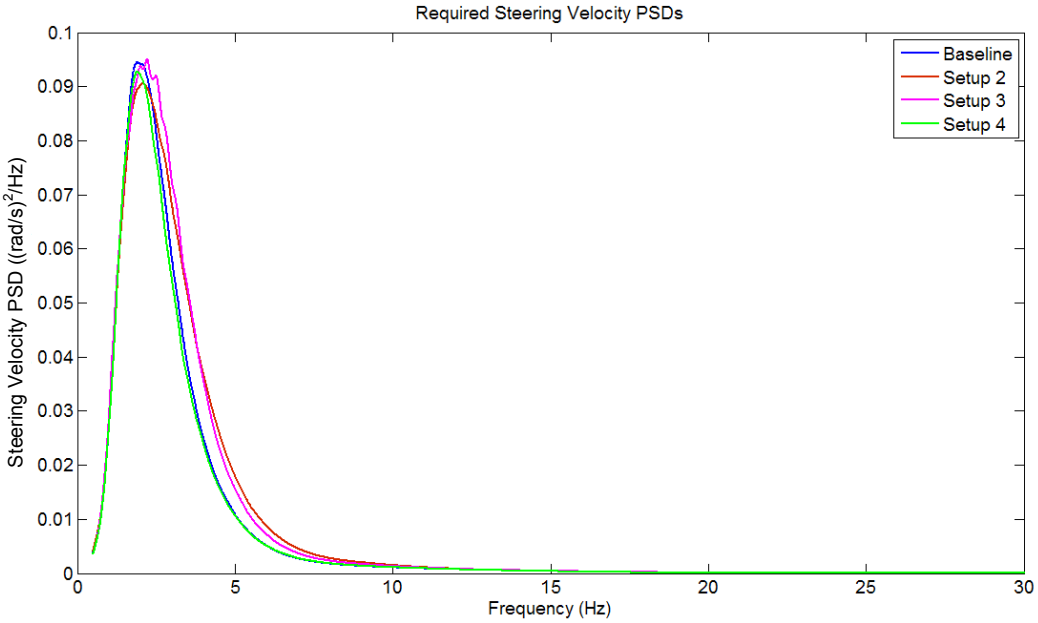

Figure 7-35 – Combined Steer Velocity PSDs

In the performance objective assessment, the overall performance index is split into 3 different measures; total grip loss, balance change and driver requirement to allow the driver to assess different aspects of the vehicles handling that can be compared to objective results. Setup 4 was found to provide a slight improvement of all 3 performance indices than the baseline. Setups 2 and 3 were worse than the baseline in all cases and similar to each other in performance index values, even though the characteristics of the front and rear load variations, and steer velocity PSDs were quite different.

	Performance Index Measures			
Set-up	Total Grip Loss	Balance Change	Driver Requirement	P.I.
1	3.2447	-1.5484	0.4839	5.2770
2	4.1791	-1.8468	0.5168	6.5427
3	4.1872	-1.8824	0.5188	6.5884
4	3.1316	-1.5035	0.4748	5.1099

Table 7-3 – Objective Performance Index Results

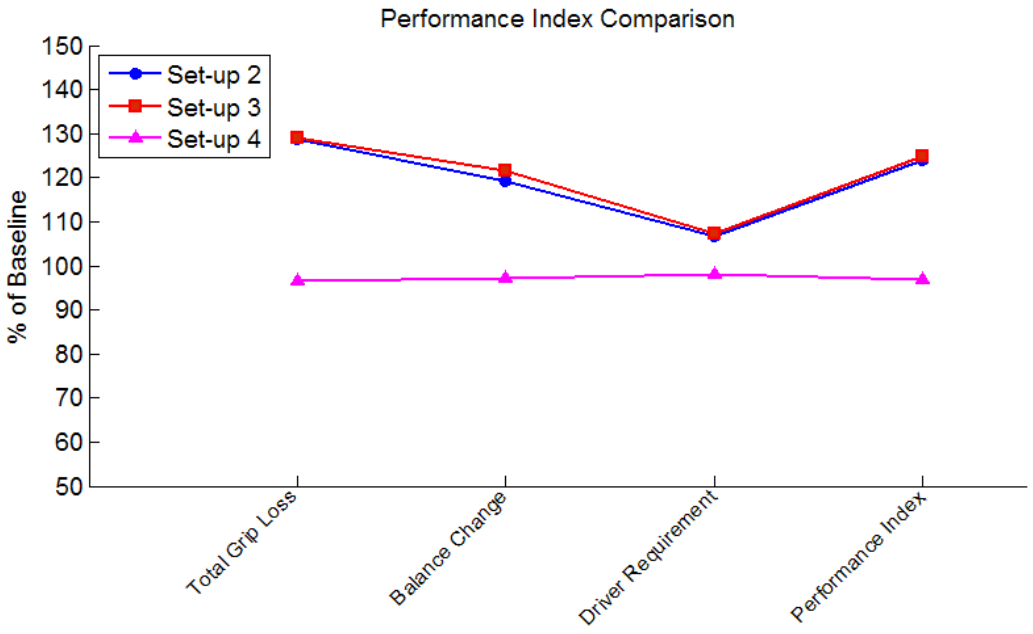

Figure 7-36 – Performance Index Relative to Baseline

7.3.1.3 – Suspension Displacement

Figure 7-37 presents the front and rear suspension displacement modal contribution PSDs for the baseline setup on the ISO 8608 [4] 'Good' road and EUDC drive cycle [72]. For the front suspension the majority of the suspension displacement is due to heave motion, with pitch being the second most significant contributor. At the rear, heave and pitch have similar relationships, but at low frequency the warp motion dominates. This is due to the relative roll stiffness of the front and rear suspensions. The front roll stiffness is much larger than the rear roll stiffness. In a low frequency warp input case the front suspension has little movement, so the body rolls with the input from the road, as the input from the road is in anti-phase at the rear, this results in a much higher level of suspension displacement.

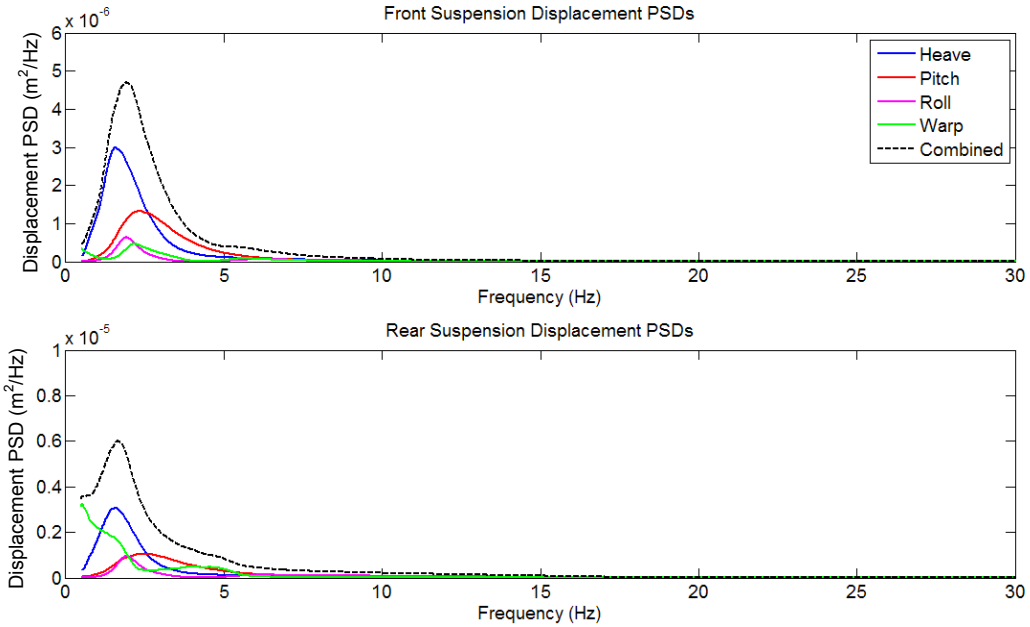

Figure 7-37 – Suspension Displacement Contributions – Baseline

The front and rear RMS suspension displacements for the 4 setups tested are presented in Table 7-4.

	Supension Displacement	
Set-up	Front	Rear
1	3.2582	3.9598
2	3.3331	3.6918
3	3.0776	3.9233
4	3.4336	3.9998

Table 7-4 – RMS Suspension Displacements (mm)

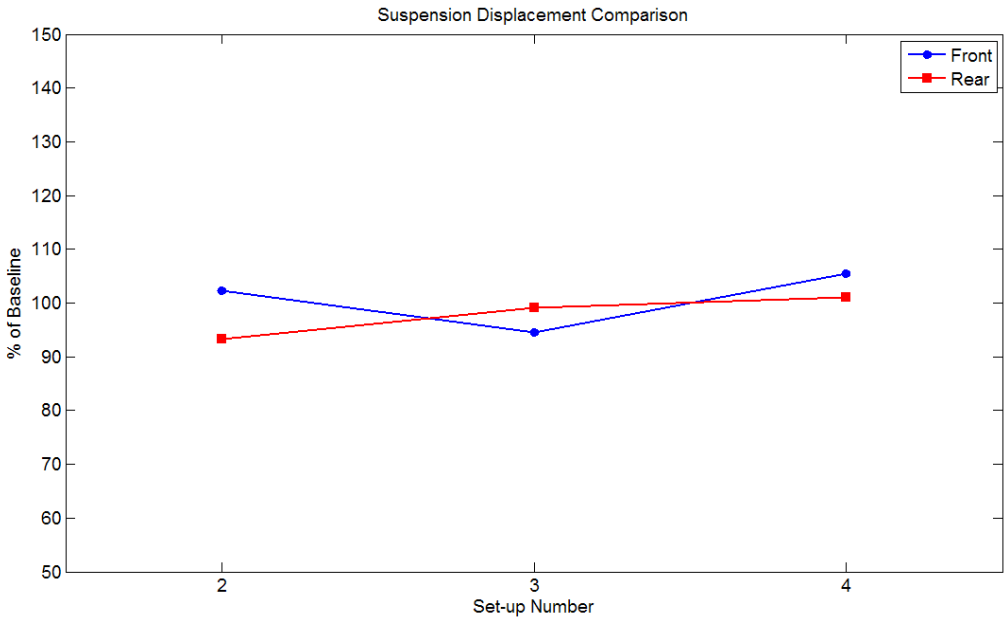

Figure 7-38 – RMS Suspension Displacement Comparison

7.3.2 - Subjective Test Results

As previously explained in this chapter, subjective assessments were carried out on drive routes around Honda facilities in Swindon, UK and Offenbach, Germany. For each of the setups 3 drivers drove the vehicle and then completed a subjective assessment form at the end of each drive. The drivers were not told any of the changes that were made to the vehicle setups to avoid prior knowledge of component changes affecting the subjective driver ratings. In ideal circumstances a much larger group of test drivers would have been used and the drivers would have been identical for the tests in each location. However, due to time and personnel constraints it was only possible to use 3 drivers in each case, 2 of whom where the same and a different 3rd driver in each case for Swindon or Offenbach.

Ideally the drivers would have used their standard subjective assessment questionnaire to assess each setup, but as the work was to be published then this was not possible. Instead a subjective questionnaire was devised using information from literature.

The subjective driver assessment of the vehicle setups was split into two methods, one for the baseline vehicle and another to compare the other 3 setups to the baseline. The reason for splitting the subjective assessment like this was due to the use of this method in studies in literature with large experience in subjective-objective correlation in road vehicles [59], [60]. However, it is also interesting to know how the drivers assess the baseline vehicle globally compared to other vehicles they had driven previously.

As explained in section 7.3.1.1- Comfort Index, the comfort assessment was split in to low and high frequency regions, in order to establish a clearer picture of the driver's assessment of the vehicle behaviour. In the comfort index the cut-off between low and high frequency was set at 5Hz. In reality the drivers were asked to separate high and low frequency using Honda's normal understanding of primary and secondary vibrations.

For the subjective performance assessment, literature on the subject was investigated. It was decided that Mimuro's [62] 4 parameter assessment method would be used, as it had been found to provide a good overall indication of the vehicle performance and included vital performance measures included in more extensive subjective questionnaires [59].

The objective metrics and their relative subjective metrics and questions are presented in Table 7-5 , for the initial assessment and Table 7-6 for assessment relative to baseline.

Objective Metric	Subjective Metric	Subjective Question
Steady-state yaw velocity gain	Steady-state balance	How does the relationship between steady-state rotation of the vehicle and steering wheel angle feel?
Natural frequency of yaw velocity	Heading responsiveness	How does the response of heading angle to steering input feel?
Damping ratio of yaw velocity response	Directional damping	How does the amount of heading angle over shoot feel? How do you rate the steering requirement to maintain a path?
Phase-delay of lateral acceleration response at 1Hz	Delay of lateral acceleration build-up	How good do you think the lag between the heading angle and lateral acceleration is?

Table 7-5 – Objective and Subjective Metrics with Subjective Questions for Baseline Subjective Assessment

Objective Metric	Subjective Metric	Subjective Question
Steady-state yaw velocity gain	Steady-state understeer	How much understeer is there compared to the baseline?
Natural frequency of yaw velocity	Heading responsiveness	How fast is the response of vehicle heading angle with steering input, compared to the baseline?
Damping ratio of yaw velocity response	Directional damping	How much overshoot from steering input is there compared to the baseline? How much steering adjustment is required when cornering compared to baseline? More overshoot and required steering means less damping.
Phase-delay of lateral acceleration response at 1Hz	Delay of lateral acceleration build-up	How much difference in lag is there between the yawing of the car and lateral acceleration compared to the baseline?

Table 7-6 – Objective and Subjective Metrics with Subjective Questions for Assessment Relative to Baseline

At the start of each subjective assessment test day, each of the drivers was given an assessment sheet. On one side of the sheet was the assessment for the baseline vehicle and on the other side the assessment for setups 2 to 4 compared to the baseline. Assessments for setups 2 to 4 were all to be entered on the same piece of paper, with different symbols used to identify the different setups. By doing this the test drivers could easily indentify how they had rated the previous setups as well as the baseline.

For initial assessment of the baseline the drivers were told to record their feeling for each of the comfort and performance metrics on a continuous scale from ‘Excellent’ to ‘Very Poor’, with indications of the positions of ‘Good’, ‘Fair’ and ‘Poor’. The drivers were also provided space to write ‘Comfort Comments’ and ‘Performance Comments’. An example of the baseline assessment sheet is presented in Figure 7-39.

For assessment of setups 2 to 4 compared to the baseline the drivers were again asked to record their feelings on a continuous scale, but this time from ‘Much Less Than’ to ‘Much More Than’. Space was provided for performance and comfort comments for each of the setups. An example of the setup comparison assessment sheet is presented in Figure 7-40.

Copies of the completed subjective test assessment sheets are presented in Appendix 2.

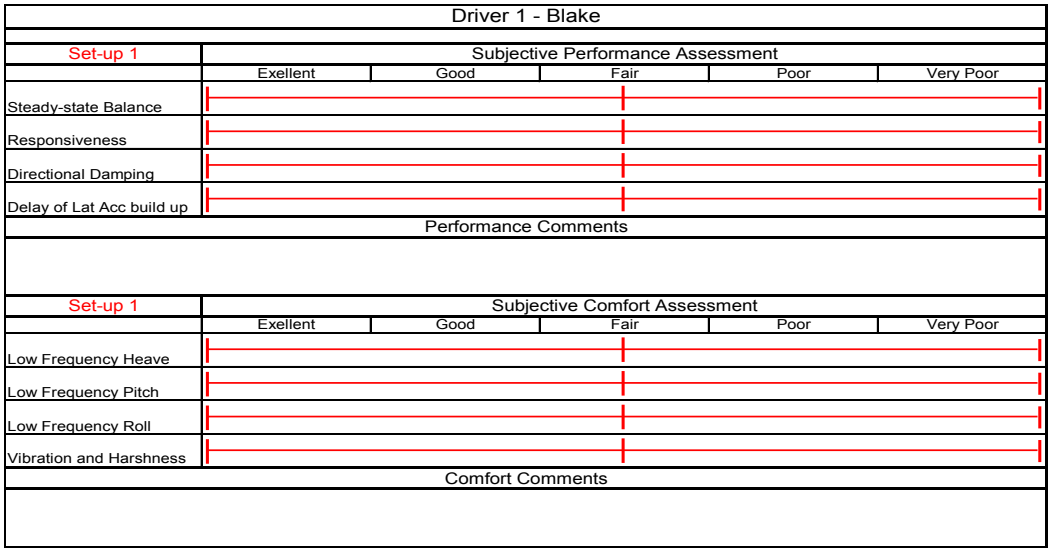

Figure 7-39 – Initial Vehicle Subjective Assessment Sheet

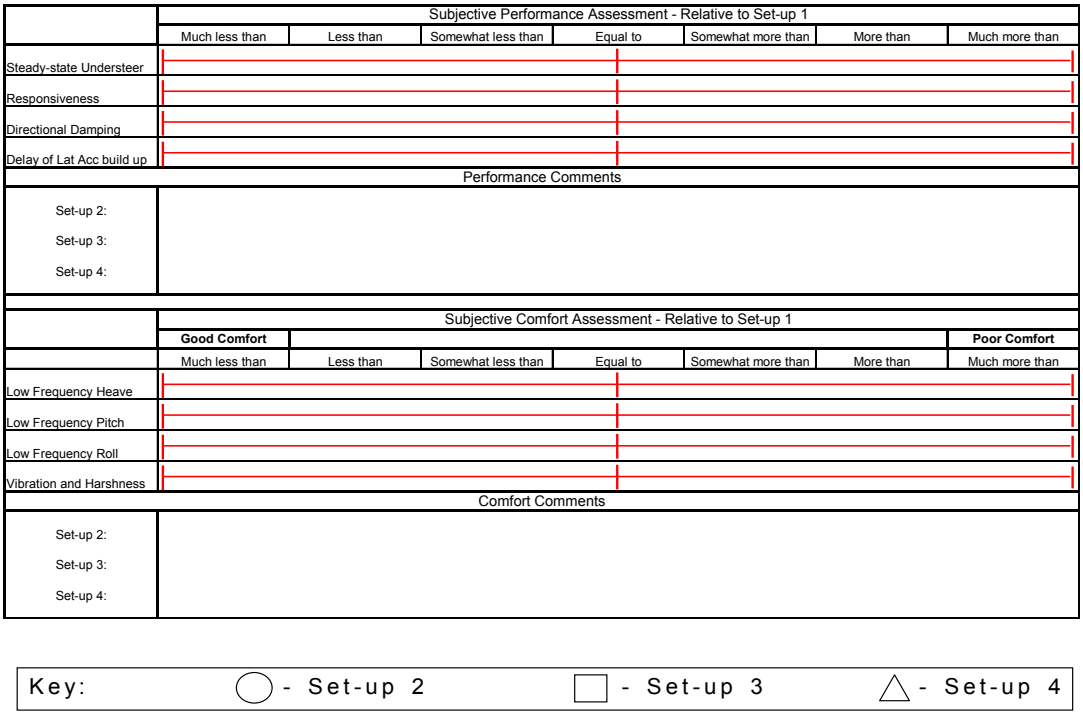

Figure 7-40 – Setup Comparison Subjective Assessment Sheet

7.3.2.1 - Subjective Comfort Results

In order to analyse the subjective assessment results and compare to the objective results, the positions of the markers on the continuous scales were measured and recorded as a value between 1 and 100. Results for the initial assessment of the baseline in Swindon and Offenbach are presented in Figure 7-41 and Figure 7-42 respectively.

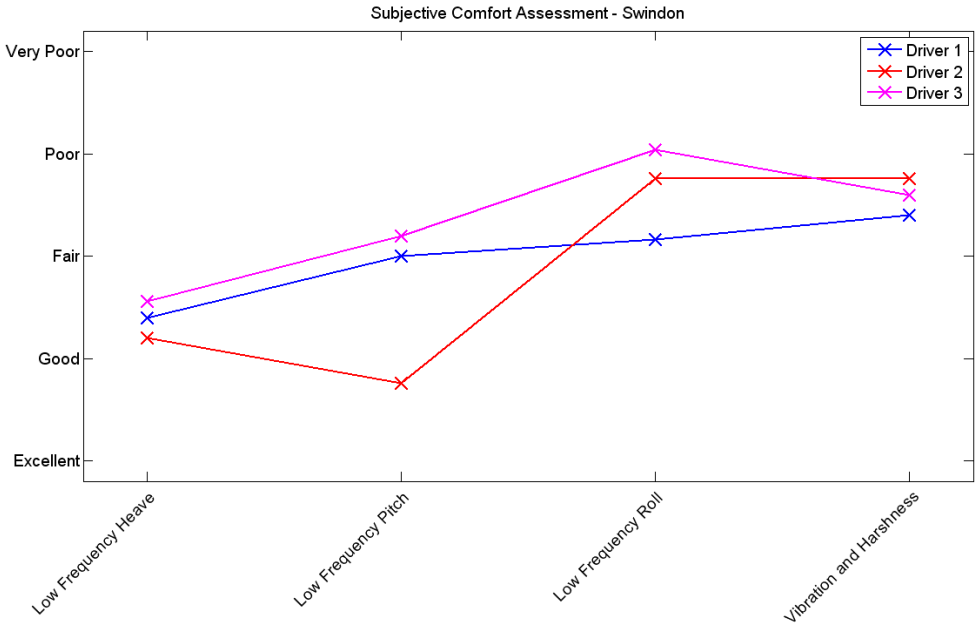

Figure 7-41 – Initial Subjective Comfort Assessment – Swindon

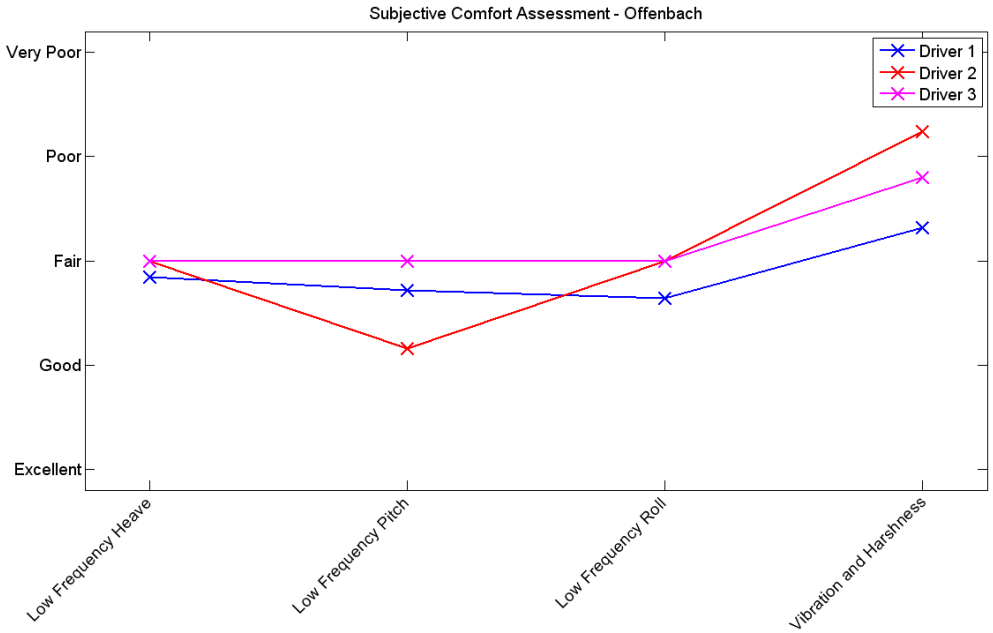

Figure 7-42 – Initial Subjective Comfort Assessment – Offenbach

For both Swindon and Offenbach the 3 driver's assessment of low frequency heave were quite consistent. For Swindon the assessment was around half way between 'Good' and 'Fair', whilst for Offenbach the assessment was much closer to 'Fair'. For the 'Low Frequency Pitch' metric, both drivers 1 and 3 where fairly consistent in their assessment for both test locations, whilst driver 2 rated the metric closer to 'Good' for both occasions. Interestingly it was drivers 1 and 3 who remained the same through both tests, whilst driver 2 was different each time. For 'Low Frequency Roll' the assessments were quite different for the two locations. For Swindon, drivers 1 and 2 rated the metric close to 'Poor', with driver 3 rating as 'Fair'. For Offenbach the assessment of all drivers reduced in level, but most significantly for driver 1. The IMU measurements from the Swindon and Offenbach drive routes in Appendix 3 - Body Acceleration Evaluations from Road Testing, showed significantly lower levels of low frequency roll for Offenbach compared to Swindon. It would appear that this is also notable in the driver's assessment of the baseline vehicle. For the 'Vibration and Harshness' metric all drivers rated the baseline vehicle worse than 'Fair' in both test locations, although there was a much larger spread of assessments for Offenbach.

In order to present the results from setups 1 to 3 in comparison with the baseline the average of the 3 driver's ratings were used as the defining value, whilst error bars were also used to indicate the range of the 3 driver's ratings for each subjective metric. The comfort assessments relative to the baseline setup are presented in Figure 7-43 and Figure 7-44 for Swindon and Offenbach respectively.

On occasions where the range of driver ratings are low, the average value can be used with confidence to determine the overall subjective change relative to baseline. However, where the range is large, little confidence can be had in the average rating.

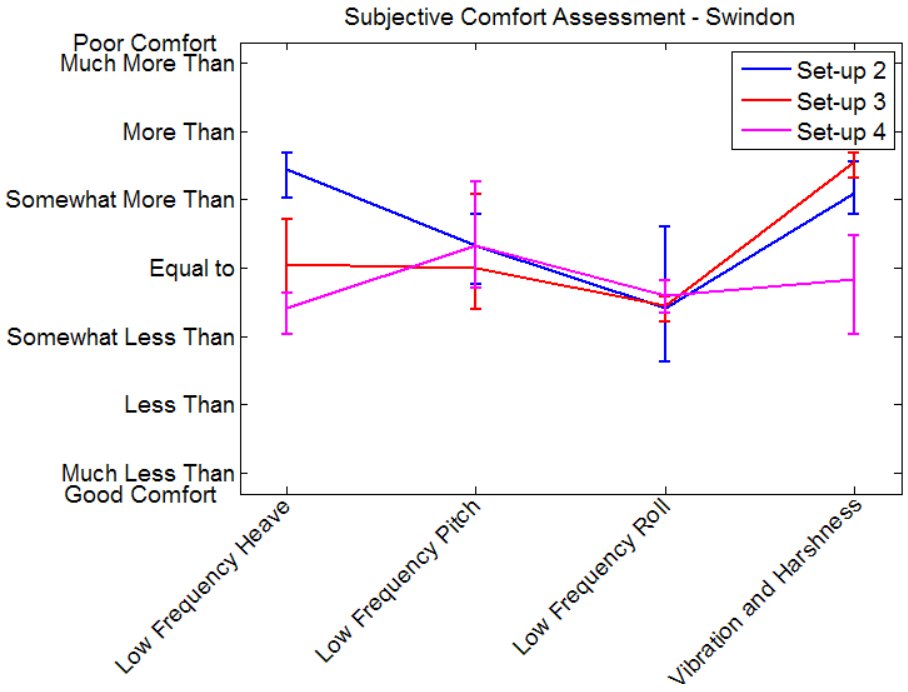

Figure 7-43 – Subjective Comfort Assessment Relative to Baseline – Swindon

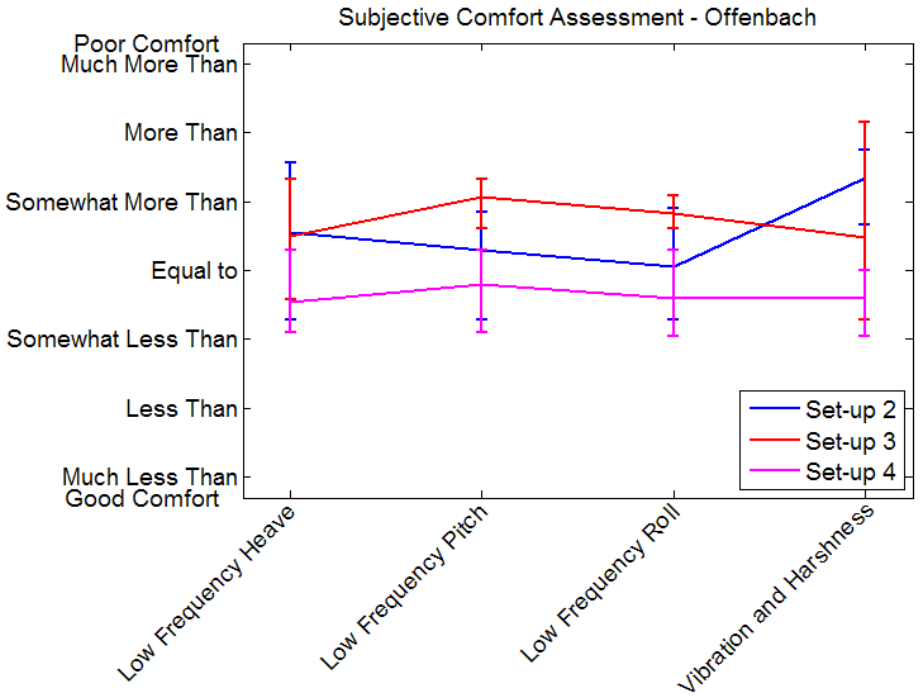

Figure 7-44 – Subjective Comfort Assessment Relative to Baseline – Offenbach

Comments on the Swindon and Offenbach comfort assessment relative to baseline:

Low Frequency Heave

- Mean Swindon assessment for setup 2 was between 'More Than' and 'Somewhat More Than', with a reasonably small range.
- Offenbach had a mean closer to the original set-up, but with much larger difference between driver assessments.
- Setup 3 Swindon results were equal to the baseline, but with larger range than setup 2.
- Offenbach assessment was similar to setup 2, again with large range.
- Setup 4 Swindon and Offenbach results were quite consistent with an assessment slightly lower than the baseline. The range was also quite low, indicating good reliability of character change.

Low Frequency Pitch

- Setup 2 assessments were similar for Swindon and Offenbach with a moderate range between drivers and comfort slightly worse than the baseline.
- Setup 3 results were quite different between Swindon and Offenbach with Offenbach assessments being 'Somewhat More Than' the baseline and Swindon equal to baseline. In the Offenbach case the differences between drivers was lower, indicating a more reliable assessment.
- Setup 4 results were opposite sides of the baseline for Swindon and Offenbach, with both having large ranges between driver assessments.

Low Frequency Roll

- Swindon assessments were quite similar for setups 2 and 3, with the response being better than the baseline. Setup 4 was only slightly better than baseline. For setups 3 and 4 there was good agreement between the 3 drivers, with a large range between assessments for setup 1.
- For Offenbach, assessment was quite different, both for individual setups and in relation to Swindon assessments. Setup 3 was found to be somewhat more uncomfortable, with quite low variation between drivers.

Vibration and Harshness

- Assessment for Swindon shows that setup 2 and 3 were between ‘Somewhat More Than’ and ‘More Than’ compared to the baseline with a reasonably low range between drivers. Setup 4 was very close to baseline, but with quite a large variation in driver assessment.
- For Offenbach, again setups 2 and 3 were found to be more uncomfortable than the baseline, but to differing degrees, with setup 2 being the worst.
- Setup 4 was assessed to be better than baseline and better than Swindon, with a moderate range between drivers.

In order to easily identify how much confidence could be placed on each average result, each subjective metric was assigned with a ‘Good’, ‘Fair’ or ‘Poor’ correlation rating. To achieve this, the range between driver assessments was averaged for each parameter over setups 2 to 3. In cases where the average range was less than one interval (e.g. from ‘Equal To’ to ‘Somewhat More Than’), the correlation would be rated ‘Good’. For a range between 1 and 2 intervals the correlation would be rated ‘Fair’ and for ranges larger than 2 intervals the correlation would be rated ‘Poor’. This was carried out separately for Swindon and Offenbach, as not all the drivers were the same in both cases. Additionally correlation was measured between mean results from Swindon and Offenbach for each subjective metric. In this case the same assignments were used, but the tolerances changed so that only differences of half one interval would be rated ‘Good’ and more than one and a half intervals rated ‘Poor’. The results of these correlations are presented in Table 7-7.

Subjective Driver Assessment Correlation - Comfort				
	Low Frequency Heave	Low Frequency Pitch	Low Frequency Roll	Vibration and Harshness
Swindon	Good - O	Fair - Δ	Good - O	Good - O
Offenbach	Fair - Δ	Fair - Δ	Fair - Δ	Fair - Δ
Mean Correlation Between Tests	Good - O	Good - O	Fair - Δ	Good - O

Table 7-7 – Subjective Assessment Correlation – Comfort

The results presented in Table 7-7 show that in general the subjective results from Swindon had better consistency between drivers, indicating that the mean subjective assessment results are more reliable than the ones obtained from the Offenbach test. However, ‘Good’ to ‘Fair’ correlation was also obtained between the mean results from both tests.

7.3.2.2 – Subjective Performance Results

The subjective performance results were processed in the same way as the comfort results to allow ease of comparison. The subjective assessments for the baseline setup for Swindon and Offenbach are presented in Figure 7-45 and Figure 7-46 respectively.

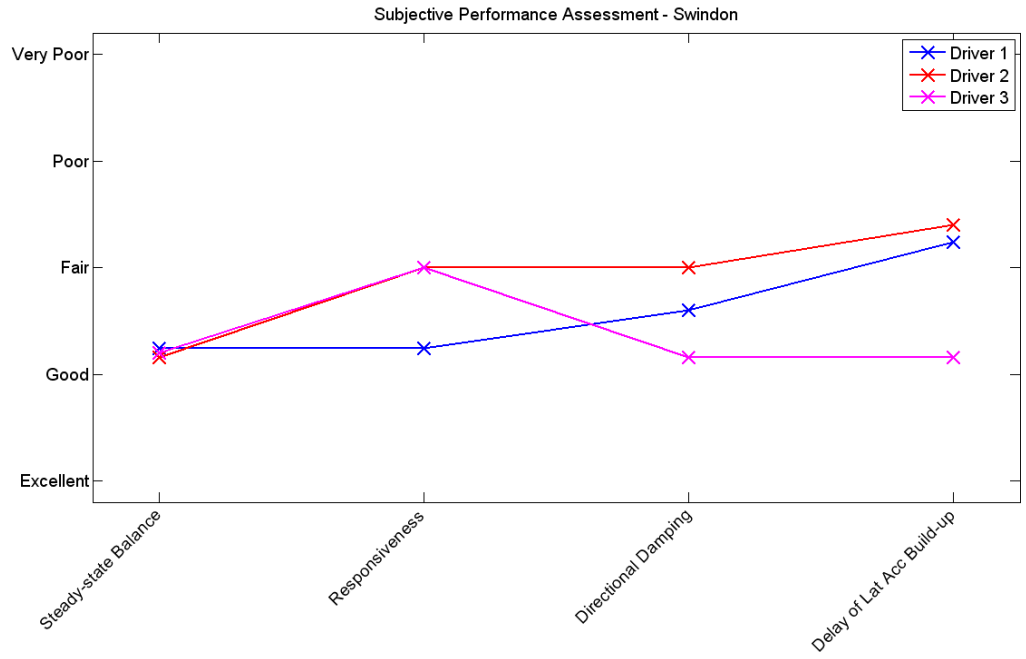

Figure 7-45 – Initial Subjective Performance Assessment – Swindon

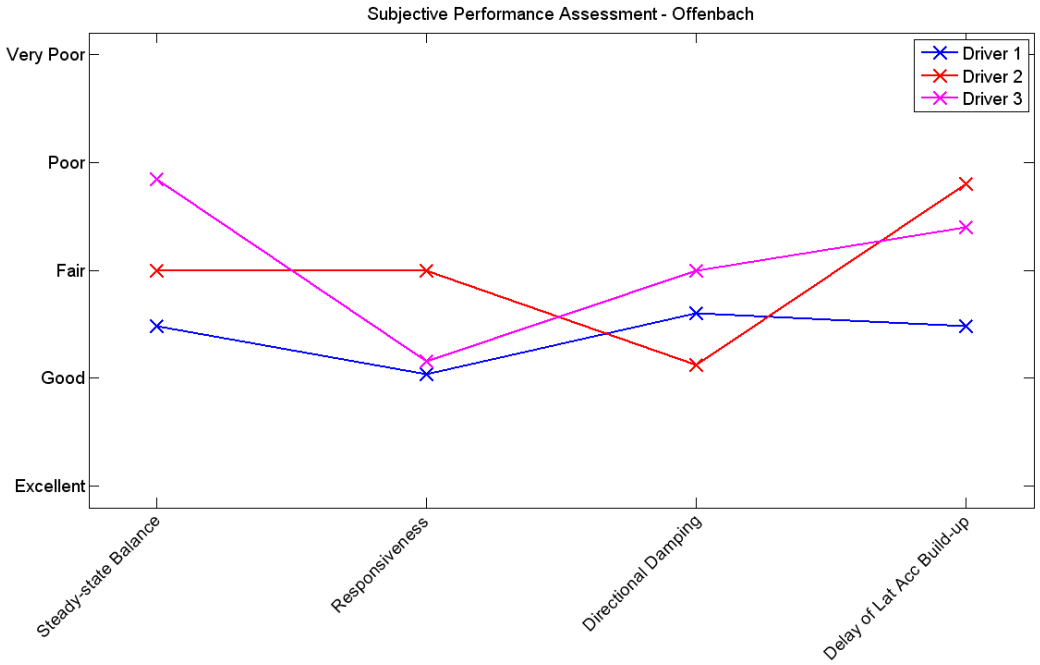

Figure 7-46 – Initial Subjective Performance Assessment – Offenbach

The ‘Steady-state Balance’ results for Swindon and Offenbach are quite startlingly different in terms of the driver assessment range. For Swindon all 3 drivers assess the ‘Steady-state Balance’ close to ‘Good’ and very similar to each other. For Offenbach driver 1’s assessment was quite similar, but driver 3 rated the metric close to ‘Poor’. For the ‘Responsiveness’ subjective metric drive 1 again rated similarly for Swindon and Offenbach, close to ‘Good’. However, again driver 3 rated quite differently with a rating of ‘Fair’ for Swindon and closer to ‘Good’ for Offenbach. Driver 2 rated close to ‘Fair’ both times, although the driver was not actually the same. For ‘Directional Damping’, again driver 1 was consistent in the rating for Swindon and Offenbach, with a rating about halfway between ‘Good’ and ‘Fair’. The driver 2 and 3 ratings were inverse for Swindon and Offenbach, with driver 3 rating ‘Good’ in Swindon and ‘Fair’ in Offenbach and driver 2 doing the opposite. For the lateral acceleration delay, results were quite inconsistent, both between different drivers and Swindon and Offenbach.

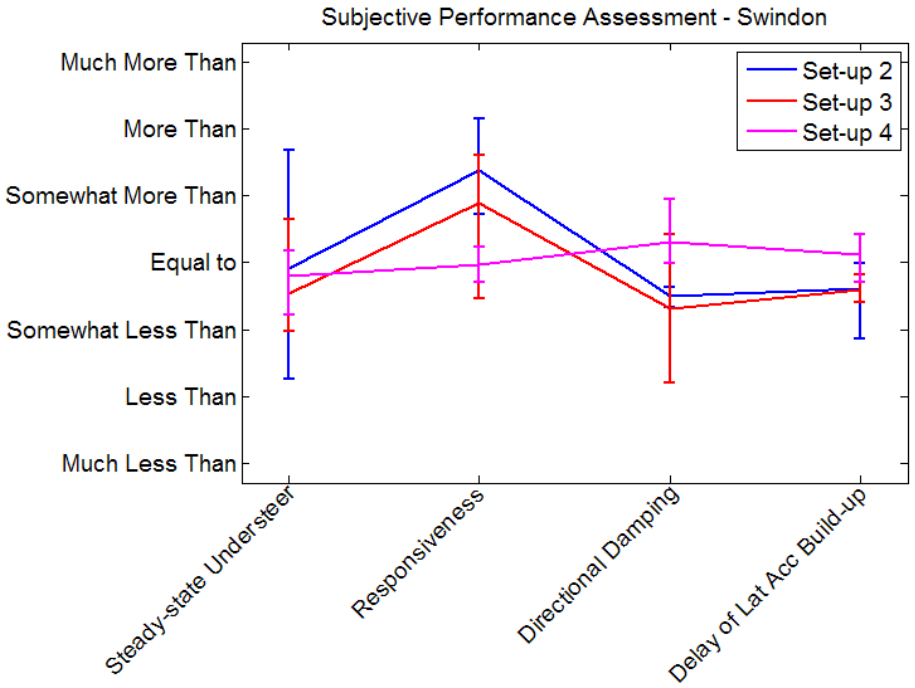

Figure 7-47 - Subjective Performance Assessment Relative to Baseline – Swindon

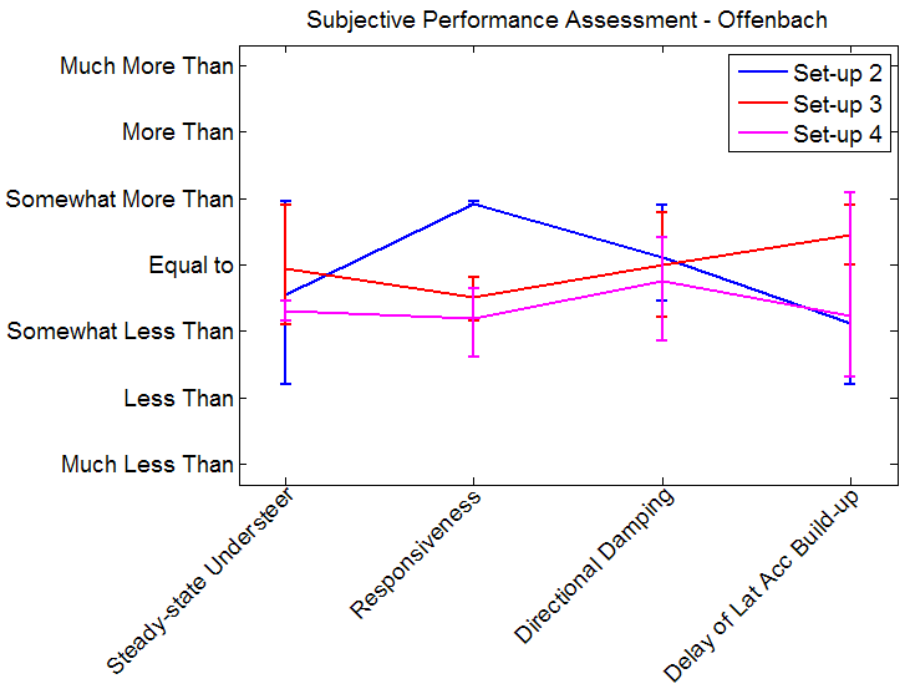

Figure 7-48 - Subjective Performance Assessment Relative to Baseline – Offenbach

Comments on the Swindon and Offenbach assessment of performance relative to the baseline (Figure 7-47 and Figure 7-48):

Steady-state Understeer

- Swindon mean assessment for setup 2 was equal to baseline, but the range of driver assessment was very large, almost from 'More Than' to 'Less Than', so assessment is unreliable.
- Setup 3 mean assessment was 'slightly less' understeer than the baseline, but again with a fairly large variation between drivers. Setup 4 was similar to baseline, with the lowest range between drivers.
- For Offenbach, again drivers range was large for setup 2 making the result unreliable. Setup 3 was assessed as 'Equal To' with a similar range to Swindon.
- Setup 4 was assessed close to 'Somewhat Less Than' with only a small difference between drivers.

Responsiveness

- Assessment from Swindon showed increased response for setup 2, as did Offenbach assessment with almost exactly the same assessment made by all drivers.
- For setup 3, Swindon and Offenbach assessments were opposite sides of the baseline. There was a large difference between drivers for Swindon and much smaller range for Offenbach.
- Mean Swindon assessment for setup 4 was very close to baseline, whereas Offenbach assessment was close to 'Somewhat Less Than'. The range between drivers was larger for Offenbach than Swindon.

Directional Damping

- Assessment of setup 2 in Swindon was found to be half way between 'Somewhat Less Than' and 'Equal To', with very similar assessments for all drivers.
- Setup 3 mean assessment was similar to setup 2, but the driver's range was large. Setup 3 mean assessment was close to baseline, but again large driver range.
- All Offenbach 'Directional Damping' mean assessments were close to baseline, but all with large range between drivers.

Lat Acc Delay

- Assessment for Swindon shows setups 2 and 3 to be slightly less than baseline, with a medium range for setup 2 and small range for setup 3. Setup 4 was rated as 'Equal To', again with a small range.
- Offenbach assessments had much bigger range in all cases, but means showed similar trend for setup 2 and different trends for 2 and 4.

Subjective Driver Assessment Correlation - Performance				
	U/S Balance	Responsiveness	Directional Damping	Lat Acc Delay
Swindon	Poor - X	Fair - Δ	Fair - Δ	Good - O
Offenbach	Fair - Δ	Good - O	Fair - Δ	Fair - Δ
Mean Correlation Between Tests	Good - O	Fair - Δ	Good - O	Good - O

Table 7-8 – Subjective Assessment Correlation – Performance

The driver assessment correlation ratings in Table 7-8 shows that there was ‘Poor’ correlation between the drivers assessment of the understeer balance change of the vehicle between setups for Swindon and ‘Fair’ for Offenbach. The ‘Responsiveness’ assessment had ‘Fair’ correlation for Swindon and ‘Good’ correlation for ‘Offenbach’. The ‘Direction Damping’ assessment had ‘Fair’ correlation between drivers for both locations, whist the ‘Lat Acc Delay’ metric correlation was ‘Good’ for Swindon and ‘Fair’ for Offenbach.

Comparison of the mean ratings from the Swindon and Offenbach tests showed on average ‘Good’ correlation, although individually some of the results were poorly correlated between tests, such as the ‘Responsiveness’ for setup 3.

Considering that there were only two cases of ‘Good’ correlation between drivers over the whole performance assessment and that these were not for the same test route, or even same parameter. It shows how difficult it is to rely on a small group subjective driver test to optimise the performance of a vehicle.

7.3.3 – Subjective-Objective Correlation

The main aim of the subjective-objective test was to determine the correlation between the objective comfort and performance index obtained through four-post rig testing and the subjective assessment of the test drivers from driving the actual vehicle. For comfort the four measures from four-post rig data are the same metrics the drivers were asked to assess, so these can be compared directly. For performance the four-post rig derived measured is not compared directly to the metrics that the drivers were asked to assess. In this case Table 7-9 explains the relationship between the objective measures from the four-post rig and the subjective driver metrics.

Subjective Metric	Objective Metric
Steady-state Understeer	Balance Change
Responsiveness	Total Grip Loss
Directional Damping	Driver Requirement
Lat Acc Delay	No Equivalent - Not used

Table 7-9 – Subjective Metrics and Objective Equivalents

The link between the change in steady-state understeer and balance change from grip loss front and rear is an obvious link, but the other two parameter equivalents in Table 7-9 are less obvious. Responsiveness is linked to total grip loss, as the loss of total grip occurs to effectively lower cornering stiffness (as well as absolute grip level). By lowering the cornering stiffness of the tyres, the yaw natural frequency is reduced and therefore the driver's perception of responsiveness would also be expected to reduce as the vehicle would take longer to react to driver inputs. Driver requirement is linked to directional damping, as a vehicle that requires a lot of input from the driver to maintain on a certain path would be considered to have low directional damping and high directional damping would remove the necessity to adjust the path of the vehicle. In order to ease comparison between subjective assessments and the objective performance measures, the performance index results as they would be expected to change the vehicle behaviour are presented in Figure 7-49.

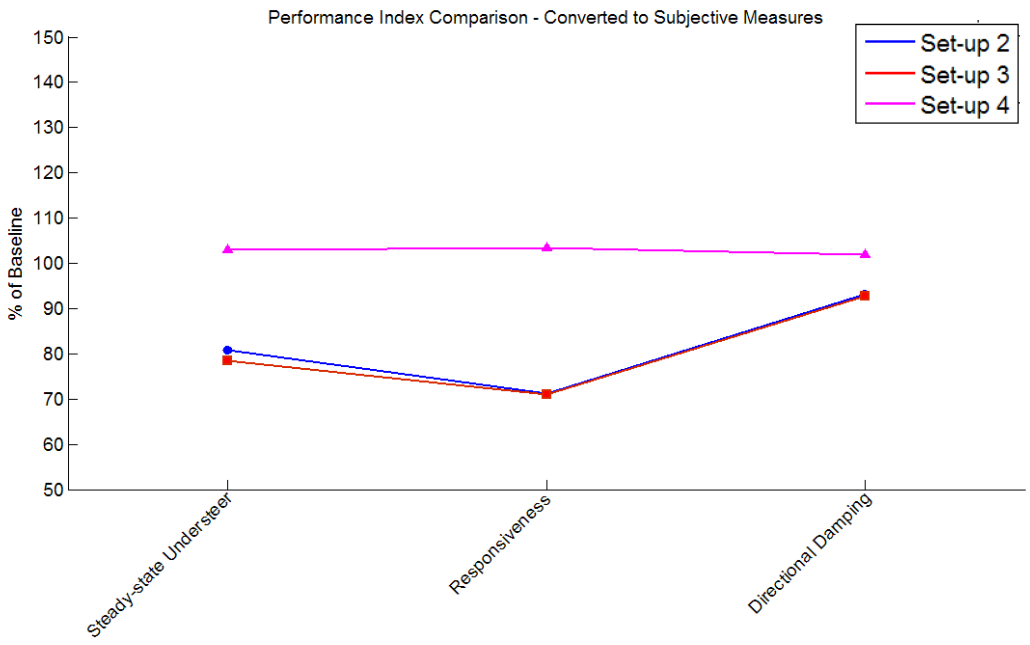

Figure 7-49 – Performance Index Values Converted to Relative Subjective Measures

Comparison of the objective and subjective comfort results can be achieved by viewing the comfort index comparison in Figure 7-29 and the subjective comfort assessment comparisons in Figure 7-43 and Figure 7-44.

Comments on the subjective-objective correlation of comfort measures:

- 'Low Frequency Heave' correlation for setups 2 and 4 is quite high, but not very good for Set-up 3.
- 'Low Frequency Pitch' correlation not very high for setup 2, but fair for 3 and 4.
- 'Low Frequency Roll' between setups shows same characteristic, but not same magnitude. However, driver assessment range was large for this parameter.
- Vibration and Harshness correlation is quite good. Especially when comparing to Swindon subjective assessments.

In order to summarise the subjective-objective correlation, mean driver ratings were compared for each subjective-objective measure for both test locations separately. As the measures were not on the same scale it was not possible to compare directly, but intelligent decisions were made based on the direction and magnitude of the change relative to the baseline setup, as well as subjective assessment range in order to determine if the correlation was considered 'Good', 'Fair' or 'Poor'. This summary is presented in Table 7-10.

Subjective/Objective Correlation - Comfort				
	Low Frequency Heave	Low Frequency Pitch	Low Frequency Roll	Vibration and Harshness
Swindon	Fair - Δ	Poor - X	Good - O	Good - O
Offenbach	Fair - Δ	Fair - Δ	Poor - X	Fair - Δ

Table 7-10 – Subjective-Objective Correlation – Comfort

Comparison of the objective and subjective performance results can be achieved by viewing the performance index comparisons in Figure 7-36 and Figure 7-49 as well as the subjective performance assessment comparisons in Figure 7-47 and Figure 7-48.

Comments on the subjective-objective correlation of performance measures:

- 'Responsiveness' correlation is 'Poor', as setups 2 and 3 were assessed more responsive than baseline in Swindon, but objective measure rates with 30% more total grip loss (different tyres).
- Fair correlation to 'Understeer Balance' in Swindon and 'Poor' for Offenbach but large range in driver assessments for both cases.
- 'Driver Requirement' correlation is 'Good' for Swindon assessment, but 'Poor' for Offenbach, where assessment was very different to Swindon.
-

Subjective/Objective Correlation - Performance			
	Steady-state US	Responsiveness	Directional Damping
Swindon	Fair - Δ	Poor - X	Good - O
Offenbach	Poor - X	Poor - X	Poor - X

Table 7-11 – Subjective-Objective Correlation – Performance

7.4 – Optimisation

The optimisation method used for this project is relatively simple and the focus of the optimisation is simply to note the effect of vehicle parameter changes on the performance and comfort index values. The suspension displacement index can also be used, but more as a limitation factor.

The use of the Simulation Model GUI to undertake model parameter sweeps was explained in 4.3.5 - Simulation Model Parameter Sweeps. The results from these sweeps show the effect of one or two model parameters on the Performance Index, Comfort Index and Compromise Index. The Compromise Index is the summation of the Comfort and Performance Index values with a scalar applied to each. The level of the relative scalars is determined by the 'Optimisation Slider' position on the GUI. This allows the engineer to decide what type of character the vehicle will have and then rely on the Compromise Index to choose suspension parameters to test. Currently in the slider's centre position a scalar of 4 is used on the Comfort Index prior to a scalar of 0.5 being used on both Performance and Comfort Index. The second scalar is then altered between 0 and 1 for each of the indices depending on the position of the slider. In the high performance case a scalar of 1 is used on Performance Index and a scalar of 0 on the Comfort index. The scalar of 4 is a preliminary value from a small amount of testing and it is proposed that this would be changed by Honda if required.

From the optimisation results the engineer can determine the most suitable parameters for the vehicle, and can also determine how sensitive the performance and comfort of the vehicle is to certain parameters.

The intention of this optimisation technique is not to completely remove the use of four-post testing and subjective testing after the base vehicle has been tested, but more to find a small number of component parameters to test, so that a finalised setup can be determined in a much shorter amount of time with a lower expenditure.

7.5 – Performance and Comfort Indices Discussion

The comfort index derived in section 7.1 - Comfort Index uses the well established BS 6841 standard [1] frequency weighting functions to convert measured body acceleration responses into comfort responses. A new and original method is then used to transform the responses into PSDs from which the comfort index values are obtained. The method uses single wheel PSD and modal contribution frequency weightings representative of a vehicle travelling over an ISO 8608 [4] class B road surface with a vehicle speed determined by the EUDC drive cycle [72].

The performance index derived in section 7.2 - Performance Index, is an original piece of work and aims to bridge the gap between simple RMS contact load variations and performance measures from full car models undertaking driving manoeuvres. The performance index uses the static force normalised variations of contact force along with aspects of Pacejka's Magic Formula tyre model [58] to estimate a percentage lateral tyre force loss due to vertical vibrations of various magnitudes (7.2.1– Static Loss) and frequencies (and 7.2.2– Dynamic Loss). By doing this for the front and rear axles of the vehicle, both total grip loss and balance can be evaluated. In addition, an estimation of lateral force variation is used along with a generic steering velocity response to lateral force in order to estimate the level of driver requirement to maintain a constant path (7.2.3.1– Effect of Load Variation on Driver Steering Requirement). The total tyre loss, balance change and driver requirement are combined to produce a single performance index. As with the comfort index, the results are produced using the vehicle responses and the same specific modal input PSDs. The performance and comfort index calculations can be used in both time and frequency domains. This allows their values to be calculated based on measured responses and a road surface PSD or directly from a 'road replay' type input that could be used to indentify vehicles comfort and performance characteristics over more specific input inputs.

In order to validate the performance and comfort indices, objective and subjective tests were carried out using a Honda Civic as the test car (7.3 - Validation of Comfort and Performance Index with Subjective-Objective Test). From the subjective test in section 7.3.2 - Subjective Test Results, it was found that there were often large variations in the assessments of different drivers for the same vehicle set-up and even large variations between a single driver's assessment of a single set-up on the two different drive routes. This highlighted the difficulty in using a small number of subjective driver assessments for vehicle set-up optimisation.

The correlation between the subjective assessments and objective measures was analysed in 7.3.3 – Subjective-Objective Correlation. Results for the comfort correlation were fair to good overall but generally better for the Swindon assessment than Offenbach. However, the performance correlation was overall between poor and fair with Offenbach results all poor. The results for the responsiveness assessment were almost opposite to the total grip measure that it was intended to be related to. This was most probably caused by the fact that set-ups 2 and 3 used different sized wheels with lower profile tyres than set-ups 1 and 4. These tyres would be

expected to produce a more responsive feel due to their higher cornering stiffness. However, this would not have been reflected in the objective performance index as it only accounts for changes in the responsiveness due to changes in the vertical load variation.

Overall it cannot be said that the performance index derived in this project correlated to subjective driver assessments. However, this does not mean that the performance index itself is of no value and not able to reflect the change in behaviour in the vehicle due to contact patch load responses in different circumstances, as there were often large variations in subjective assessments between drivers. Other much larger subjective-objective investigations have found similar issues. Crolla, Chen, Whitehead and Alstead [59] carried out an investigation with 8 professional test drivers and 49 subjective questions and found that for most of the questions the result could be 'confidently' (95% confidence level) on the 'better' or 'worse' line of the baseline setup. In the same paper the authors stated that it was important that the vehicle parameter changes resulted in sufficiently different levels of performance that the drivers could perceive the differences subjectively. The setup changes made during the subjective-objective test in this project were relatively small, due to the available components being limited to components from different models of the Honda Civic. In fact the largest effect on subjective assessments was the change of wheels and tyres, of which the difference in lateral tyre behaviour was not modelled in the performance index. Figure 7-50 presents the normalised contact force PSDs for the Honda Civic baseline setup and 3 different manufacturers' vehicles in similar car classes (all 3 or 5 door hatchbacks). The changes in normalised contact force PSDs are far larger than for the 4 different setups used in the subjective-objective test, which can be seen in Figure 7-33 and Figure 7-34.

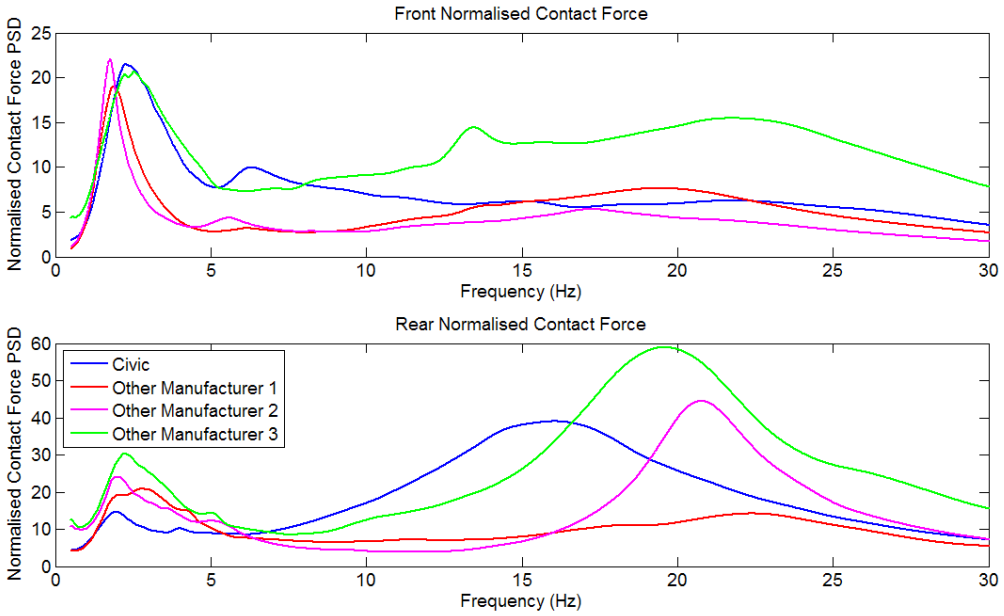

Figure 7-50 – Normalised contact force comparisons – Civic vs. other manufacturers

8 – Conclusions

In chapter 1 – Introduction the desire of Honda to have a method of testing and assessing vehicle performance using a four-post test rig was explained. There were three main aims for this method, these were:

1. Creation of a four-post rig testing technique and vehicle parameter estimation method.
2. Creation of a method of quantifying 'Performance' and 'Comfort' of a vehicle from four-post test measurements.
3. Creation of a model and simulation tool capable of allowing the engineer to optimise the vehicle suspension for 'best performance', 'best comfort' or a defined 'best compromise'.

From the work presented in this thesis, it has been shown that the objectives of the project to produce a four-post testing technique suitable for the analysis and tuning of vehicles has been achieved.

More specifically:

1) The inputs that the road supplies to a vehicle have been investigated from literature and the findings used to create a set of modal rig inputs suitable for characterising the response of a vehicle, as well as a set of novel specific road characteristic and speed cycle generated modal PSDs used to weight the vehicle responses and create an overall output of various vehicle measures.

2) Analysis of road spatial characteristics from an instrumented vehicle driving on Honda's specified routes found typically a higher amplitude gradient with frequency than the ISO 8608 [4] standard, as well as a larger standard deviation between the characteristics of the UK roads and German roads tested.

3) An 8 degree-of-freedom model of a vehicle on the four-post rig was developed with the ability to model different suspension layouts, non-linear dampers and engine vibration, or the driver on the seat.

4) A novel parameter estimation technique was created that was found to be suitably accurate to allow a 7 degree-of-freedom model to simulate the measured vehicle responses with satisfactory accuracy with the exception of the roll mode which was found to behave unexpectedly.

5) It was determined that the roll behaviour of the vehicle on the four-post rig is highly dependent on the friction level between the tyres and actuator pads and with simulation using a full-car ADAMS model, a similar effect to reducing this friction was found by increasing vehicle speed.

6) A comfort index was created using the BS 6841 [1] discomfort weighting functions and the input PSDs described in 1) above.

7) A novel performance index was created using the vertical force fluctuations in the contact patch to determine total tyre grip loss using both static and dynamic factors from Pacejka [58]. The total tyre grip loss was used to create a vehicle grip loss and balance change due to road inputs. The vertical force variations were also weighted using a steering velocity response to determine a driver requirement measure.

8) An objective-subjective validation exercise found fair to good correlation between objective and subjective comfort measures. However, the correlation between objective and subjective performance measures was poor.

9) The level of variation in subjective driver assessments was surprisingly large, in particular for performance assessments, highlighting the difficulty in using small group subjective assessments to optimise a vehicle set-up.

10) A set of three general user interfaces were created to run parameter estimation, analysis comparison and simulation model MATLAB codes to allow the user to carry out four-post tests and optimisation efficiently.

The method created allows characterisation of the comfort and handling performance of a vehicle within 30-40 minutes of arriving at the test facility, as well as estimation of parameters suitable to model the vehicle. The method requires no disassembly of any parts of the vehicle and attachment of the sensors will cause no damage. In the benchmarking case the method can provide the users with important information about the responses of competitor's cars, as well as the parameters which cause the vehicle to respond in this way. In the tuning case re-characterisation of vehicle after setup changes can be carried out within 10 minutes for full characterisation, or as low as 4 minutes for single amplitudes in each mode. Simulated setup changes can be carried out far faster than physical tests with the simulation model sweeps of vehicle parameters. This allows the user to determine the setup direction and significantly reduce the amount of physical component tests required.

9 – Future Work

This chapter of the thesis describes additional work that the author believes would enhance the value of this research project.

Variable Friction Roll Response

For future development of the four-post rig testing technique, it would be recommended that a controlled friction device would be fitted between the tyres and actuator pads during testing, as well as a device for measuring the lateral forces and displacements. By doing this, multiple roll tests with different friction levels could be carried out to determine the effect on roll response. Through further modelling these could be related to different forward speeds of the vehicle, to give the engineer the knowledge of how the roll response of the vehicle would be expected to change over the speed range. In addition, this would allow the calculation of further vehicle parameters such as lateral tyre stiffness, force-based roll centre heights and yaw mass moment of inertia. The ability to calculate these additional parameters would allow the use of a more complex vehicle model that could more accurately model the roll response of the vehicle on the four-post rig and in low-speed driving conditions.

Increased relevance of modal input PSDs

In future it would be recommended that instead of using the input PSD from the ISO 8608 [4] 'Class B' road roughness model and the EUDC speed profile [72] to create frequency domain modal input PSDs, data more specific to Honda, such as the road profile and speed profiles measured during the subjective tests, could be used when creating performance and comfort index values. Using this method, the drive route could be split up into individual parts and performance and comfort index values for each part could be reported. The output PSDs generated for specific parts of the route could also help engineers to understand why comfort or performance is particularly poor over specific parts of the route. The results in Appendix 3 - Body Acceleration Evaluations from Road Testing, show considerably different comfort weighted acceleration PSDs for different sections of road from the subjective assessment drive routes. By applying this method the comfort and performance index values would become more specific to Honda's driver assessment conditions.

Performance index with improved representation of the overall handing performance

For future development of the performance index, it would be suggested that performance measures relating to the general performance of the vehicle were also included, rather than just how vertical load variation would be expected to change the performance characteristics of the car. These would include measures such as:

- vehicle mass to tyre size ratio
- centre of gravity height
- overall roll stiffness
- roll stiffness distribution
- roll damping
- pitch damping.

These measures would be expected to change the driver's perception of vehicle performance and could be measured using the four-post rig.

Larger subjective-objective correlation exercise

For improved understanding of the correlation between subjective assessments and the indices derived in this project, it is recommended that a much larger subjective and objective correlation exercise would be carried out. This would involve more test drivers, more setups and greater vehicle changes, as the exercise undertaken for this project used a very small driver group with only minor set-up changes to the vehicle as explained in section 7.5 – Performance and Comfort Indices Discussion.

More sophisticated optimisation of vehicle parameters

For future development of the model and optimisation technique there are two main areas in which the method could be improved. Firstly, the current run-time of approximately 4 seconds is not particularly long for a single evaluation. However, if many different parameters of the model were to be tuned at a relatively high resolution to optimise a vehicle set-up, then the overall computing time could be quite long. To improve this, a two-stage optimisation process could be adopted using two different modelling methods. For initial sweeping of parameters the vehicle responses could be determined using analytical transfer functions in a similar way to the Excel spreadsheet used in section 6.1.1– Determination of Modelling Software. This type of model would run many times faster than the Simulink model simulation of the four-post sine sweep.

However, it would require transfer functions to be determined for each of the outputs used within the comfort and performance index functions, which would take time and would need to be validated to ensure no errors had been made in the derivation of the transfer functions. Once the preliminary optimisation using the transfer functions had been completed a more in depth optimisation would then be carried out using the model as it currently exists where non-linear aspects of the model could be tuned. For any investigation of time domain inputs or modelling of special suspension features or characteristics the current Simulink model would still be used.

The second aspect of the optimisation that could be developed further is to use a better approach to global optimisation of the vehicle parameters. Using the current method, where a maximum of two parameters can be varied simultaneously the user is required to think carefully about the effect that tuning some parameters might have on the optimum values of other parameters. For example the optimum damping coefficient for one spring stiffness is unlikely to be the optimum damping for a different spring stiffness. If front and rear springs were tuned simultaneously with damping held constant and then front and rear damping tuned using the previously determined optimum springs then the solution would be unlikely to be globally optimal. A method of improving the quality of the optimisation would be to incorporate a method similar to Georgiou et. al. (2007) [37] and Gobbi et. al. (1999) [38], where multi-dimensional, multi-objective optimisations were carried out to determine a set of pareto-optimal parameter value sets. In using this type of method many different solutions of parameter sets would be determined that would be optimal in a sense that from moving from one parameter set to another one or more of the performance measures would decrease whilst others increased and in no cases would all of the performance measures decrease and be non-optimal, as could occur in the normal tuning case. Gobbi et al. (1999) [38], compared the final production specification of a vehicle to one of the pareto-optimal parameter sets for the same vehicle and found an improvement over all performance indices of 6.6% on average and 16.7% maximum, with not one index being better for the production vehicle than the pareto-optimal solution, determining that the production specification vehicle was not optimally tuned for any of its performance indices. Using this method the engineers can also easily determine the parameters required for different levels of comfort and performance compromise, but always ensuring that the set-up is globally optimal for their chosen compromise. As there are many variable parameters to the vehicle model and each would be expected to change the optimal relationship of each other, a huge amount of simulations would have to be run to determine the pareto-optimal solution set, which would take a considerable amount of time even using the transfer function modelling solution. If this method were to be employed then a neural network and genetic algorithm method would need to be employed as in Gobbi et al. (1999) [38], in order to reach a solution quickly. This would be a significant amount of work to add to the project, but it is thought that the value that this would add to the optimisation method would be considerable.

References

[1] – British Standards Institution, 1987, *BS6841:1987 Measurement and Evaluation of Human Exposure to Whole-body Mechanical Vibration and Repeated Shock*, London: BSI

[2] - Sayers, M.W., Karamihas, S.M. (1998), *The Little Book of Profiling – Basic Information about Measuring and Interpreting Road Profiles*, University of Michigan Transportation Research Institute.

[3] – Imine, H., Delanne, Y. and Sirdi, N.K.M. (2006), Road Profile Input Estimation in Vehicle Dynamics Simulation, *Vehicle System Dynamics* 44, No.4, pp.285-303.

[4] – British Standards Institution, 1996, *Mechanical vibration – Road surface profiles – Reporting of measured data BS 7853:1996 ISO 8608:1995*, London: BSI.

[5] – Rouillard, V., Bruscella, B. and Sek, M.A. (2000), Classification of Road Surface Profiles, *Journal of Transportation Engineering* 126, pp. 41-45.

[6] – Sayers, M.W. (1995), On the Calculation of International Roughness Index from Longitudinal Road Profile, *Transportation Research Record* 1501, pp. 1-12.

[7] – Kropac, O. and Mucka, P. (2005), Be Careful When Using the International Roughness Index as an Indicator of Road Unevenness, *Journal of Sound and Vibration* 287, pp. 989-1003.

[8] – Andrén, P. (2006), Power Spectral Density Approximations of Longitudinal Road Profiles, *International Journal of Vehicle Design* 40, (3), pp. 2-14.

[9] – Hassan, S.A. and Lashine, O.S. (2002), Identification of Road Surface Qualities for Linear and Non-linear Vehicle Modelling, *Proceedings of SPIE - The International Society for Optical Engineering* 4753 I, pp. 318-323.

[10] – Robson, J.D. (1979), Road Surface Description and Vehicle Response, *International Journal of Vehicle Design*, 1 (1), pp. 25-35.

[11] – Gillespie, T.D. (1992), *Fundamentals of Vehicle Dynamics* (1), Warrendale: SAE International, pp. 168-172.

[12] – Kamash, K.M.A. and Robson, J.D. (1978), Application of Isotropy in Road Surface Modelling, *Journal of Sound and Vibration*, 57 (1), pp. 89-100.

[13] – Sayers, M.W. (1986), Characteristic Power Spectral Density Functions for Vertical and Roll Components of Road Roughness, *American Society of Mechanical Engineers, Applied Mechanics Division,* 80, pp. 113-129.

[14] – Robson, J.D. (1978), The Role of the Parkhilovskii Model in Road Description, *Vehicle System Dynamics* 7, pp. 153-162.

[15] – Rill, G. (1984), The Influence of Correlated Random Road Excitation Process on Vehicle Vibration, *8th IAVSD Symposium on the Dynamics of Vehicles on Roads and Railway Tracks*, pp. 449-459.

[16] – Bogsjo, K. (2008), Coherence of Road Roughness in Left and Right Wheel-path, *Vehicle System Dynamics* 46, Supplement 1, pp. 599-609.

[17] – Mucka, P. (2004), Road Waviness and the Dynamic Tyre Force, *International Journal of Vehicle Design* 36, Nos. 2/3, pp. 216-232.

[18] – Kropac, O. and Mucha, P. (2007), Effect of Obstacles in the Road Profile on the Dynamic Response of a Vehicle, *Proceedings of the Institution of Mechanical Engineers, Part D: Journal of Automobile Engineering*, March 1, 2008, 222 (3), pp. 353-370.

[19] – Rouillard, V., Sek, M.A. and Bruscella, B. (2001), Simulation of Road Surface Profiles, *Journal of Transportation Engineering* 127, pp. 247-253.

[20] – Cebon, D. and Newland, D.E. (1984), The Artificial Generation of Road Surface Topography by the Inverse FFT Method, *8th IAVSD Symposium on the Dynamics of Vehicles on Roads and on Railway Tracks*, pp. 29-42.

[21] – Kushiro, I., Yasuda, E. and Doi, S. (2004), An Analysis of Pitch and Bounce Motion, Requiring High Performance of Ride Comfort, *Vehicle Systems Dynamics Supplement*, 41, pp. 83-92.

[22] – Ebe, K. and Griffin, M.J. (2000), Quantitative Models of Seat Discomfort Including Static and Dynamic Factors, *Ergonomics*, 43, pp. 771-790.

[23] – Ebe, K. and Griffin, M.J. (2000), Quantitative Prediction of Overall Seat Discomfort, *Ergonomics*, 43, pp. 791-806.

[24] – Leatherwood, J.D., Dempsey, T.K. and Clevenson, S.A. (1980), Design Tool for Estimating Passenger Ride Discomfort Within Complex Ride Environments, *Human Factors* 22, No. 3, pp. 291-312.

[25] – Griffin, M.J. (1986), Evaluation of Vibration with Respect to Human Response, *Society of Automotive Engineers*, 860047, pp. 11-34.

[26] – International Standards Office, 1997, *ISO 2631-1:1997 (E) Mechanical Vibration and Shock – Evaluation of Human Exposure to Whole-body Vibration*, Geneva: ISO

[27] – Griffin, M.J. (2007), Discomfort from Feeling Vehicle Vibration, *Vehicle System Dynamics* 45, no. 7-8, pp. 679-698.

[28] – Giacomin J. and Hacaambwa T.M. (2001), Performance of ISO 2631 and BS 6481 Comfort Criteria for Evaluating Automobile Road Vibrations. Available at: http://www.perceptionenhancement.com/papers/gh2001poi.pdf

[Last accessed 14th January 2012]

[29] – Jang, H.-K. and Griffin, M.J. (2000), Effect of Phase, Frequency, Magnitude and Posture on Discomfort Associated with Differential Vertical Vibration at the Seat and Feet, *Journal of Sound and Vibration* 229, no. 2, pp. 273-286.

[30] – Liang, C.-C and Chiang C.F. (2006), A Study on Biodynamic Models of Seated Human Subjects Exposed to Vertical Vibration, *International Journal of Industrial Ergonomics* 36, pp. 869-890.

[31] – Barak, P. (1991), Magic Numbers in Design of Suspensions for Passenger Cars, *SAE Passenger Car Meeting and Exposition*, SAE paper 911921, Vol. 100, Section 6, pp. 1698-1733.

[32] – Thompson A.G. (1973), Quadratic Performance Indices and Optimum Suspension Design, *Proc. Instn Mech Engrs*, 187, pp.129-139.

[33] – Crolla, D.A. and King, R.P. (1999), Olley's 'Flat Ride' Revisited, *Vehicle System Dynamics Supplement* 33, pp. 762-774.

[34] – Thompson, A.G. (1983), Suspension Design for Optimum Road-Holding, *SAE Technical Paper Series*, SAE paper 830663.

[35] – Vilela, D. and Tamai, E.H. (2003), Ride Comfort Suspension Optimisation With Simulation Tools, *International Conference On Modelling Identification and Control*, 22, pp. 136-140.

[36] – Fukushima N., Hidaka K. and Iwata K. (1983) Optimum Characteristics of Automotive Shock Absorbers under Various Driving Conditions and Road Surfaces, *JSAE Review*, March, pp. 62–69.

[37] – Georgiou, G., Verros, G. and Natsiavas, S. (2007), Multi-Objective Optimization of Quarter-Car Models with a Passive or Semi-Active Suspension System, *Vehicle System Dynamics* 45, pp. 77-92.

[38] – Gobbi, M., Mastinu, G. and Doniselli, C. (1999), Optimising a Car Chassis, *Vehicle System Dynamics* 32, pp. 149-170.

[39] – Vanhees, G. and Maes, M. (2002), Vehicle Suspension Characterisation By Using Road Simulation on a 4-Poster Test Rig, *Proceedings of the 2002 International Conference on Noise and Vibration Engineering*, pp. 63-70.

[40] – Nuti A.C., Garzeri F.J. and Orives R.A. (2002), Damper Analysis Using Energy Method, *SAE Technical Paper Series*, 2002-01-3536

[41] – Nuti A.C., Garzeri F.J. and Orives R.A. (2002), Head Toss x Roll Behaviour – Difficult Compromise*, SAE Technical Paper Series,* 2002-01-3537

[42] – Kowalczyk, H.R. (2002), Damper Tuning with the use of a seven post shaker rig, SAE Technical Paper Series, 2002-01-0804.

[43] – Kelly, J.E., Kowalczyk, H.R. and Oral, H.A. (2002), Track Simulation and Vehicle Characterization with 7 Post Testing, *Proceedings of the 2002 SAE Motorsports Engineering Conference and Exhibition*, 2002-01-3307.

[44] – White, M. (2007), *Multimatic Technical Centre, Vehicle Dynamics Expo 2007*, Suspension Measurements and Characteristics –What Learning Can Be Shared Between Road and Race Cars,

http://www.vehicledynamics-expousa.com/07_conf/pdfs/day_1/white.pdf

[Last accessed 9th October 2011]

[45] – Haney, P. (2001), Ohlins 7-Post Shaker Rig in North Carolina, *Inside Racing Technology, Discussions of Racing Technical Topics*, http://insideracingtechnology.com/o7postshkr.htm, http://insideracingtechnology.com/oshkrtest.htm, http://insideracingtechnology.com/oshkrdata.htm, http://insideracingtechnology.com/oshkrq%26a.htm

[Last accessed 9th October 2011]

[46] – Miller, A. (2002), Testing a Formula SAE Racecar on a Seven-poster Vehicle Dynamics Simulator, SAE Technical Paper 2002-01-3309.

[47] – Brueck, D.M. and Ward, E.D, (1977), A Simplified Method for the Identification of Vehicle Suspension Parameters, SAE Technical Paper 770884.

[48] – Boggs, C., Ahmadian, M. and Southward, S. (2009), Application of System Identification for Efficient Suspension Turning in High-Performance Vehicles: Quarter-Car Study, *SAE International Journal of Passenger Cars – Mechanical* Systems, Volume 1, Issue 1, 2008-01-2962, pp. 1298 – 1310.

[49] – Boggs, C., Ahmadian, M. and Southward, S. (2009), Application of System Identification for Efficient Suspension Tuning in High-Performance Vehicles: Full-Car Model Study, *SAE International Journal of Passenger Cars – Mechanical Systems*, Volume 2, Issue 1, 2009-01-0433, pp. 622-635.

[50] – Thite, A.N., Banvidi, S., Ibicek, T. and Bennett, L. (2011), Suspension Parameter Estimation in the Frequency Domain Using a Matrix Inversion Approach, *Vehicle System Dynamics* 49, Issue 12, pp. 1803-1822.

[51] – Yi, K. and Hedrick, K. (1993), Observer Based Identification of Nonlinear Vehicle Suspension Parameters, *Proceedings of the 1993 American Control Conference*, pp. 711-715.

[52] – Dixon, A., Franco-Jorge, M. and Webb, M. (2002), Integrated Vehicle Corner Modelling for Ride and Handling Development, *Proceedings of the 2002 International Conference on Noise and Vibration Engineering*, pp. 1117-1121.

[53] – Gallagher, J. and Volterra, E. (1952), A Mathematical Analysis of the Relaxation Type of Vehicle Suspension, *Journal of Applied Mechanics* 74, pp. 389-396.

[54] – Kasprzak, J.L. and Floyd, R.S. (1994), Use of Simulation to Tune Race Car Dampers, *Proceedings of the 1994 SAE Motorsports Engineering Conference and Exhibition*, SAE 942504, pp. 171-178.

[55] – Rill, G. (1986), Steady State Cornering on Uneven Roadways, *SAE Technical Paper Series* 860575.

[56] – Mashadi, B. and Crolla, D.A. (2005), Influence of Ride Motions on the Handling Behaviour of a Passenger Vehicle, *Journal of Automobile Engineering*, Part D, IMechE, Vol. 219, No D9, pp. 1047-1058.

[57] – Pacejka, H.B. and Bakker, E. (1993), Magic Formula Tyre Model, *Vehicle System Dynamics* 21, Supplement, Tyre Models for Vehicle Dynamics Analysis, pp. 1-18.

[58] – Pacejka, H.B. (2005), *Tyre and Vehicle Dynamics*, Oxford: Butterworth-Heinemann.

[59] – Crolla, D.A., Chen, D.C., Whitehead, J.P. and Alstead, C.J. (1998), Vehicle Handling Assessment Using a Combined Subjective-Objective Approach, *Proceedings of the 1998 SAE International Congress & Exposition,* SAE Technical Paper 980226, pp. 61-71.

[60] – Crolla, D.A. and Whitehead, J.P. (2001), Reliable Subjective Assessment of Vehicle Handling by Drivers – Is it an Elusive Goal?, *American Society of Mechanical Engineers*, *Design Engineering Division* 112, pp. 95-105.

[61] – King, R.P. Crolla, D.A., Ash, H.A.S. and Whitehead, J.P. (2002), Identification of Subjective-Objective Vehicle Handling Links Using Neural Networks for the Foresight Vehicle, SAE paper 2002-01-1126.

[62] – Mimuro, T., Ohsaki, M., Yasunaga, H. and Satoh, K. (1990), Four Parameter Evaluation Method of Lateral Transient Response, SAE paper 901734.

[63] – Fernandes, C. and Okano, F.J. (2003), Vehicle Dynamics Objective Metrics, SAE paper 2003-01-3631.

[64] – Norman, K.D. (2002), Multiple-Bump Roadholding Test: Description and Metric Interpretation, *Proceedings of the Institution of Mechanical Engineers. Part D: Journal of Automotive Engineering* 216 (4). pp. 251-258.

[65] – British Standards Institution, 2004. *BS ISO 4138: 2004 Passenger Cars – Steady-State Circular Driving Behaviour – Open-Loop Test Methods*. London: BSI.

[66] – Crolla, D.A., Firth, G. and Horton D., An Introduction to Vehicle Dynamics, Department of Mechanical Engineering, University of Leeds., unpublished.

[67] – Mathworks, Documentation Centre, tfestimate,

http://www.mathworks.co.uk/help/signal/ref/tfestimate.html

[Last accessed 7th October 2012]

[68] – British Standards Institution, 1990*, BS 6897-2:1990, ISO 7626-2:1990, Method for Experimental Determination of Mechanical Mobility –Part 2*. BSI: London.

[69] – Gloth G. and Sinapius M. (2004), Analysis of Swept-Sine Runs During Modal Identification, *Mechanical Systems and Signal Processing* 18 (6), pp. 1421-1441.

[70] – Wikipedia, Chirp, http://en.wikipedia.org/wiki/Chirp

[Last accessed 8th October 2012]

[71] – Multimatic Technical Centre Europe (2008), Dynosoft MX User Manual

[72] – DieselNet, Emission Test Cycles: ECE -15 + EUDC/ NEDC.

http://www.dieselnet.com/standards/cycles/ece_eudc.php

[Last accessed 1st October 2011].

[73] – Oxford Technical Solutions (2008), RT User Manual

[74] – MOOG, D661 Highresponse Series, General Technical Data

[75] – Mercer C. A. (2006), *Acceleration, Velocity and Displacement Sprectra – Omega Arithmatic,* Prosig, http://signalprocessing.prosig.com/OmegaArithmetic.pdf

[76] - Teng T.L., Chang F.A. and Peng C.P. (2006), Analysis of Human Body Response to Vibration using Multi-body Dynamics Method, *Proceedings of the Institution of Mechanical Engineers, Part K: Journal of Multi-body Dynamics* 222 (3), pp. 191-202.

[77] – Gent A. N. and Walter J. D. (2005), *The Pneumatic Tyre*, Washington DC: NHTSA

[78] – Jazar R. N. (2008), *Vehicle Dynamics: Theory and Application*, New York: Springer.

[79] – Harty D. (2001), The Myth of Accuracy, *Journal of the Engineering Integrity Society* 9 pp. 22-28.

[80] – Dixon, J.C. (1999), Chapter 2, *The Shock Absorber Handbook*, Warrendale, PA: Society of Automotive Engineers, Inc. p 61.

[81] – Patil, M.K Patil, M.K., Palanichamy, M.S., Ghista, D.N. (1977), Dynamic response of human body seated on a tractor and effectiveness of suspension systems. *SAE Paper 770932*, pp. 755−792.

[82] – Eberhard, P., Piram, U. and Bestle, D. (1999), Optimization of Damping Characteristics in Vehicle Dynamics, *Engineering Optimization* 31, pp. 435-455.

[83] – Dugoff H., Fancher P. and Segel. L (1970), An Analysis of Tire Traction Properties and Their Influence on Vehicle Dynamic Performance, SAE Technical Paper 700377.

[84] – Fevrier P. and Fandard G (2007), A new Thermal and Mechanical Tire Model for Handling Simulation, *VDI Berichte* (2014), pp. 261-275.

[85] – Lee C., Kim J., Hallquist J., Zhang Y. and Farahani A. (1997), Validation of a FEA Tire Model for Vehicle Dynamic Analysis and Full Vehicle Real Time Proving Ground Simulations, SAE Technical Paper 971100.

[86] – MSC Software (2010), ADAMS/Tire Help,

http://simcompanion.mscsoftware.com/infocenter/index?page=content&id=DOC9364&cat=MD_2010&actp=LIST

[Last accessed 18th February 2012]

[87] – British Standards Institution, 1994, *BS EN 30326-1:1994*, *Mechanical Vibration – Laboratory Method for Evaluating Seat Vibration – Part 1: Basic Requirements*. BSI: London.

Appendix 2

Subjective driver assessment sheets

Swindon

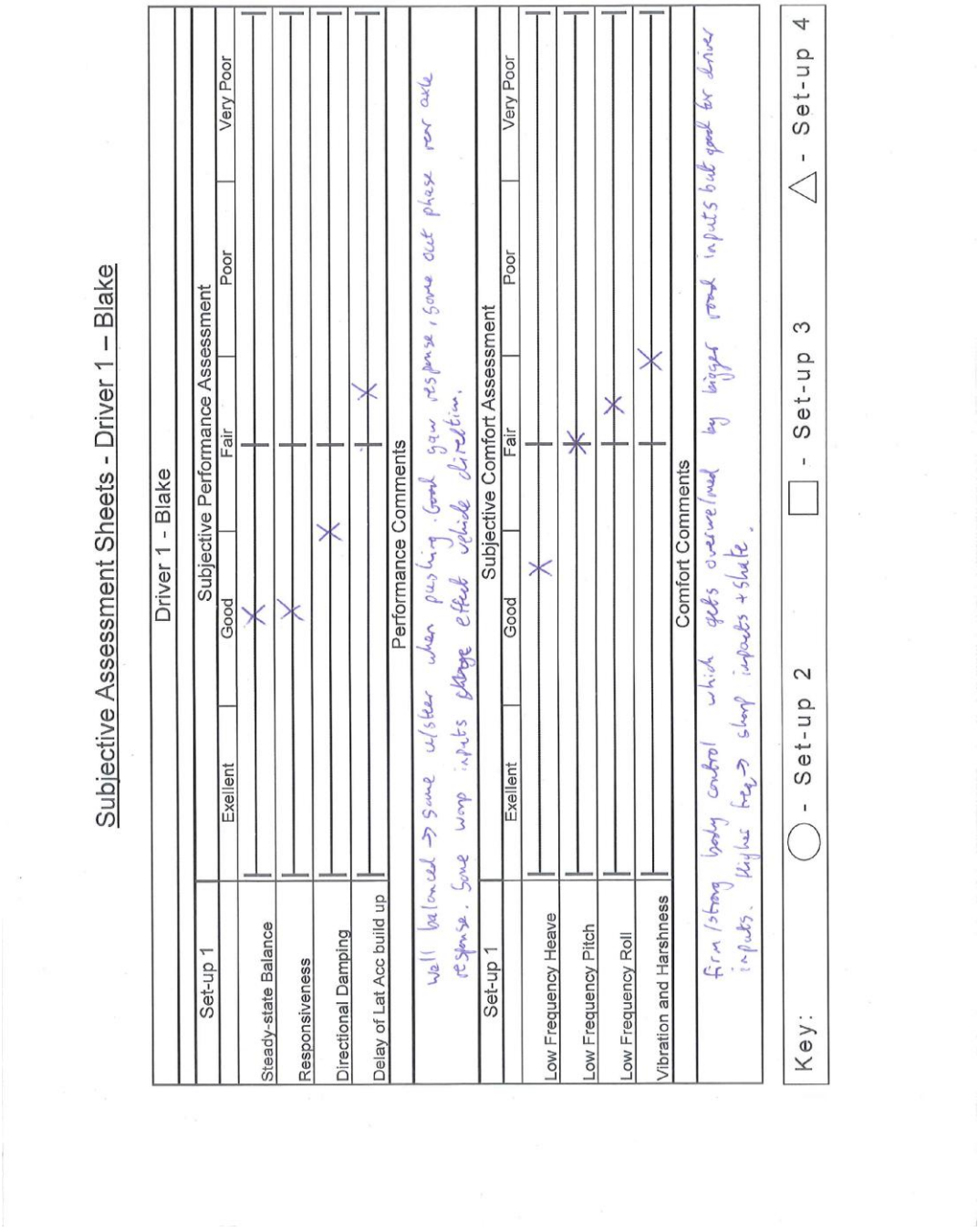

Subjective Assessment Sheets - Driver 1 – Blake

Driver 1 - Blake

Subjective Performance Assessment

Set-up 1	Exellent	Good	Fair	Poor	Very Poor
Steady-state Balance		X			
Responsiveness		X			
Directional Damping			X		
Delay of Lat Acc build up				X	

Performance Comments

Well balanced → some understeer when pushing. Good yaw response, some wet phase rear axle response. Some wasp inputs perhaps effect vehicle direction.

Subjective Comfort Assessment

Set-up 1	Exellent	Good	Fair	Poor	Very Poor
Low Frequency Heave		X			
Low Frequency Pitch			*		
Low Frequency Roll			X		
Vibration and Harshness			X		

Comfort Comments

Firm/strong body control which gets overcome/rewd by bigger road inputs but good for driver inputs. Keyhole type steering inputs + shake.

Key: ◯ - Set-up 2 □ - Set-up 3 △ - Set-up 4

Driver 1 Baseline Subjective Assessment - Swindon

x = setup 2.
□ = setup 3
△ = setup 4

Subjective Assessment Sheets - Driver 1 – Blake

	Subjective Performance Assessment - Relative to Set-up 1						
	Much less than	Less than	Somewhat less than	Equal to	Somewhat more than	More than	Much more than
Steady-state Understeer				△	□	X	
Responsiveness				□ △	~~□~~	X	
Directional Damping			X		□	△	
Delay of Lat Acc build up			X	□ △	~~□~~		

Performance Comments

Set-up 2: → More u/steer but quicker yaw response. Vehicle feels like crabs more, steer torque compliance/delay.

Set-up 3: → Less responsiveness, slower yaw ⇒ lat acc delay more similar to yaw.

Set-up 4: → More yaw delay + less u/steer. Slower to respond + gain levels down (need more steer angle).

	Subjective Comfort Assessment - Relative to Set-up 1						
	Good Comfort						**Poor Comfort**
	Much less than	Less than	Somewhat less than	Equal to	Somewhat more than	More than	Much more than
Low Frequency Heave			□	△		X	
Low Frequency Pitch			□	△	X		
Low Frequency Roll		□	△		X		
Vibration and Harshness				△	□	X	

Comfort Comments

Set-up 2: → Firmer spring mass with more Heave disturbance. More shake/harshness worse. Starting to collapse at front on turn. Roll stiffness up but roll damping/control worse.

Set-up 3: → More spring mass movement roll/heave/pitch → less accel. + control. More shake.

Set-up 4: → Less spring mass movement than 3 & and better controlled, lowest vibration levels.

AM → PM → Increasing amount of grip + reduction u/steer levels, car less nervous.

Subjective Assessment Sheets - Driver 2 – Chris

Driver 2 - ~~Blake~~ Chris

Set-up 1	Subjective Performance Assessment				
	Exellent	Good	Fair	Poor	Very Poor
Steady-state Balance		X			
Responsiveness			X		
Directional Damping		X			
Delay of Lat Acc build up		X			

Performance Comments

BALANCE DIFFICULT TO JUDGE BECAUSE OF SLIPPERY SURFACE, BUT NEUTRAL WITH SLIGHT YAW DELAY ON CORNER TURN-IN (GOOD THROUGHOUT SPEEDING & BODY MOTION) YAW STABILITY GOOD (MARRED BY ROLL-ROCK?) DELAY OK - INCLUDING LANE CHANGE

Set-up 1	Subjective Comfort Assessment				
	Exellent	Good	Fair	Poor	Very Poor
Low Frequency Heave			X		
Low Frequency Pitch				X	
Low Frequency Roll					X
Vibration and Harshness				X	

Comfort Comments

HEAVE SLIGHTLY REBOUND-BIASED - GETS ~~WORSE~~ BETTER DOWN PITCHES @ SLOW SPEED (THROUGHOUT TURN) ROLL-ROCK VERY PRONOUNCED INPUTS HARSH & SHARP.

Key: ○ - Set-up 2 □ - Set-up 3 △ - Set-up 4

Driver 2 Baseline Subjective Assessment - Swindon

① - VERY WET & COLD - SLIPPERY
② → DRYING OUT
③ → DRYING OUT
④ → ALMOST DRY

GRIP ① = ② ≪ ③ ≤ ④

2 - ○
3 - □
4 - △

Subjective Assessment Sheets - Driver 2 – Chris

	Subjective Performance Assessment - Relative to Set-up 1						
	Much less than	Less than	Somewhat less than	Equal to	Somewhat more than	More than	Much more than
Steady-state Understeer			□ △	○			
Responsiveness					△	○	□
Directional Damping			□ ○	△			
Delay of Lat Acc build up				□ ○	△		

Performance Comments	
Set-up 2:	REDUCED YAW RESPONSE / DELAY ON TURN-IN. YAW STABILITY ON STRAIGHT SLIGHTLY WORSE
Set-up 3:	MUCH MORE GRIP (DRY SURFACE), BUT ALSO PERCEIVED REDUCED [44.9] USTEER - RR SLIDE ON LIFT-OFF.
Set-up 4:	RESPONSIVENESS MUCH IMPROVED, ALTHOUGH RR AXLE NOW STRUGGLES SLIGHTLY TO KEEP UP. YAW STABILITY WORSE ON BLUNSDON RD (BUMPY) SOFTER IN RESPONSE COMPARED TO ABOVE BUT WELL BALANCED - TREE FR AXLE MATCHES RR AXLE RESPONSE - GOES WELL WITH THE SOFTER BODY CONTROL

	Subjective Comfort Assessment - Relative to Set-up 1						
	Good Comfort						Poor Comfort
	Much less than	Less than	Somewhat less than	Equal to	Somewhat more than	More than	Much more than
Low Frequency Heave			~~○~~	△	□	○	
Low Frequency Pitch				○ △	~~○~~	□	
Low Frequency Roll			○	□ △		~~○~~	
Vibration and Harshness			~~○~~		△	○	□

Comfort Comments	
Set-up 2:	END OF BUMP TRAVEL MORE ABRUPT. PITCH SLIGHTLY IMPROVED (LOW SPEED) & ~~MUCH~~ LESS ROLL-ROCK, MAKES LESS CONTROLLED, SHAKEY (ESP. RR AXLE)
Set-up 3:	FIRMER FR AXLE - IMPROVED HEAVE CONTROL (ESPECIALLY ON LARGER BUMP). LOW SPEED PITCHING SIMILAR TO PREVIOUS SETTINGS, BUT OUT-OF-TOWN PITCH RESPONSE WORSE. HIGHER FREQUENCY MUCH HARDER FEEL. BUT BETTER CONTROL THAN SU 2 - LESS SHAKE.
Set-up 4:	GENERALLY SOFTER OVERALL THAN ABOVE. BETTER HEAVE BALANCE (NOT AS FORCED IN REBOUND) PITCH SIMILAR TO SU3 SLIGHTLY LESS ROLL-ROCK - ESPECIALLY THROUGH TOWN (LOW SPEED) QUITE WOODEN & SHAKY, ESP. RR.

Driver 3 Baseline Subjective Assessment - Swindon

Set-up 1 - Reference - Slightly more responsive, but very similar in general.

2 = ○
3 = □
4 = △

Subjective Assessment Sheets - Driver 3 – John

	Subjective Performance Assessment - Relative to Set-up 1					
	Much less than	Less than	Somewhat less than	Equal to	Somewhat more than	More than	Much more than
Steady-state Understeer		○	□	△			
Responsiveness			△			□	○
Directional Damping		□		○	△		
Delay of Lat Acc build up			□	○	△		

Performance Comments	
Set-up 2:	→ Very small steering input when loaded, more response, slightly nervous feeling.
Set-up 3:	→ Feels like heavier steering effort
Set-up 4:	→ Less sporty, Sluggish. Desirable steering response, unresponsive.

	Subjective Comfort Assessment - Relative to Set-up 1						
	Good Comfort						Poor Comfort
	Much less than	Less than	Somewhat less than	Equal to	Somewhat more than	More than	Much more than
Low Frequency Heave			△		□	○	
Low Frequency Pitch				□		○ △	
Low Frequency Roll			○	□ △			
Vibration and Harshness			△		◇	□	

Comfort Comments	
Set-up 2:	→ Slightly higher frequency vertical, bouncy, lack of shake.
Set-up 3:	→ Feels like rebound is held, very little movements, more vibration through road surface
Set-up 4:	→ Feels like more of a comfort setting. More suitable for 5 Door Family Car.

Set-up 1 : Slightly Wider, Very wet but not raining } Low Wind, No significant bump change

2 - Bump similar
3 - Dry
4 - Dry

Driver 3 Setup Comparison Subjective Assessments - Swindon

Offenbach

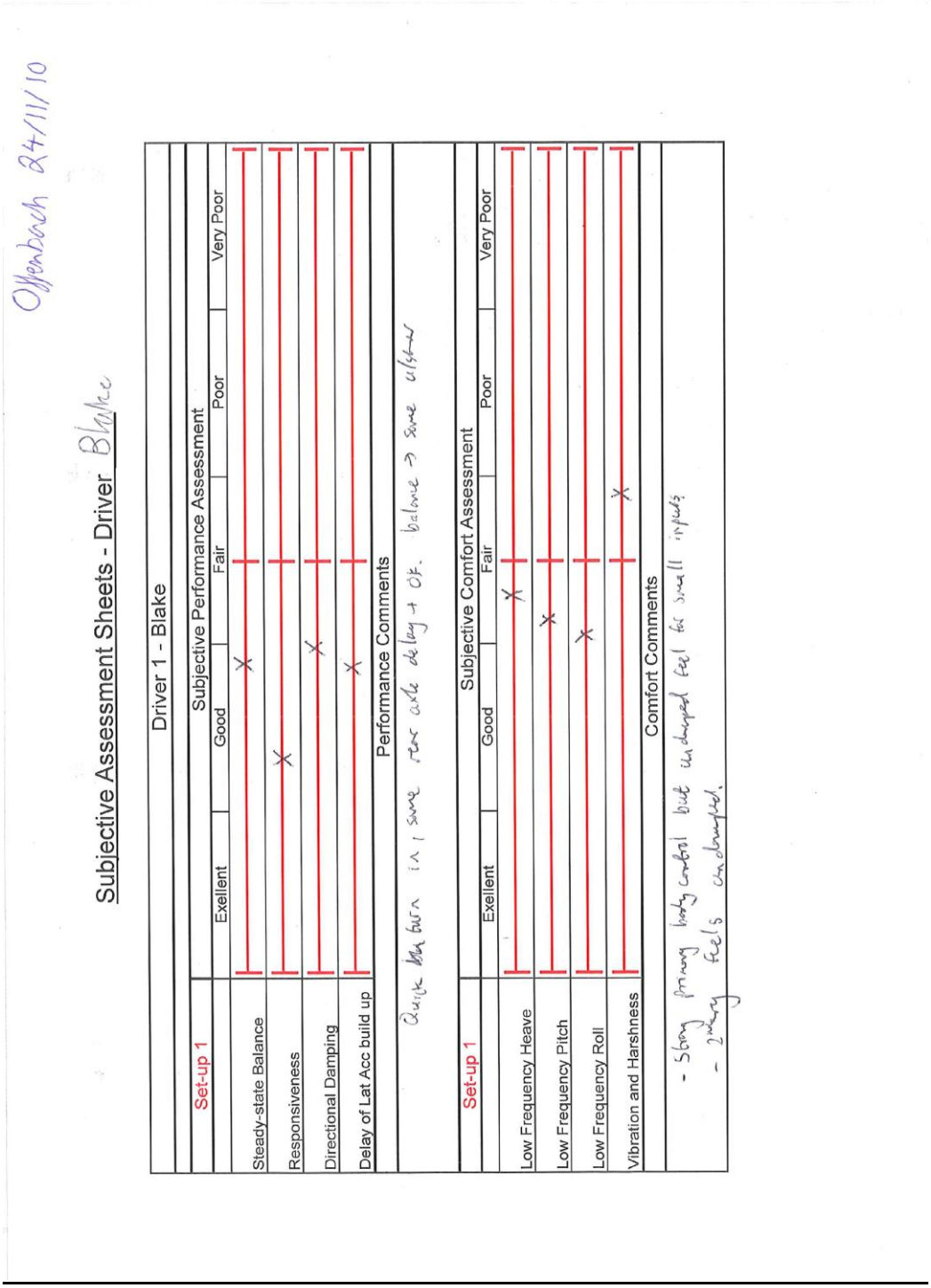

Driver 1 Baseline Subjective Assessment - Offenbach

Subjective Assessment Sheets - Driver

Subjective Performance Assessment - Relative to Set-up 1

	Much less than	Less than	Somewhat less than	Equal to	Somewhat more than	More than	Much more than
Steady-state Understeer			△	□	⊘		
Responsiveness			△	□	○		
Directional Damping			○	▯	△		
Delay of Lat Acc build up				◇	□	△	

Performance Comments

Set-up 2:	faster response to steering inputs but lower grip.
Set-up 3:	More similar to stock in terms of weight, + more yaw delay than setup 1
Set-up 4:	More delay than other.

Subjective Comfort Assessment - Relative to Set-up 1

	Good Comfort						Poor Comfort
	Much less than	Less than	Somewhat less than	Equal to	Somewhat more than	More than	Much more than
Low Frequency Heave			○	△	▯		
Low Frequency Pitch			○	△	▯		
Low Frequency Roll			○	△	▯		
Vibration and Harshness			▯	◇	○		

Comfort Comments

Set-up 2:	Tighter body control, but more secondary vibration.
Set-up 3:	More primary motion but less harsh secondary.
Set-up 4:	Softer primary somewhat between 2 + 3 but more than stock.

Key: ◯ - Set-up 2 ▯ - Set-up 3 △ - Set-up 4

Driver 1 Setup Comparison Subjective Assessments- Offenbach

Driver 2 Baseline Subjective Assessment - Offenbach

Subjective Assessment Sheets - Driver

S. Suzuki

	Subjective Performance Assessment - Relative to Set-up 1					
	Much less than	Less than	Somewhat less than	Equal to	Somewhat more than	More than	Much more than
Steady-state Understeer		○	△ □				
Responsiveness			△		○		
Directional Damping				△	□ ○		
Delay of Lat Acc build up			○ △	□			

Performance Comments

Set-up 2: Increase Fr/Rr response - and less understeer and rear delay. better damping

Set-up 3: Front axle delay. Not linear.

Set-up 4: Fr/Rr balance is good. little bit bigger roll bit less understeer.

	Subjective Comfort Assessment - Relative to Set-up 1						
	Good Comfort						Poor Comfort
	Much less than	Less than	Somewhat less than	Equal to	Somewhat more than	More than	Much more than
Low Frequency Heave			△		○	□	
Low Frequency Pitch			△		◇	□	
Low Frequency Roll			△		○	□	
Vibration and Harshness			△		○	□	

Comfort Comments

Set-up 2: less structural direction - and more hard stable. bit busy feel. body motion is more quicker

Set-up 3: More less stroke feel. Also more harsh.

Set-up 4: Good comfort direction. less harshfeel.

Key: ○ - Set-up 2 □ - Set-up 3 △ - Set-up 4

Driver 2 Setup Comparison Subjective Assessments - Offenbach

Subjective Assessment Sheets - Driver

Driver 1 - Blake Brown

Set-up 1	Subjective Performance Assessment				
	Exellent	Good	Fair	Poor	Very Poor
Steady-state Balance			6		
Responsiveness			6		
Directional Damping		6			
Delay of Lat Acc build up			6		
Performance Comments					

Set-up 1	Subjective Comfort Assessment				
	Exellent	Good	Fair	Poor	Very Poor
Low Frequency Heave			6		
Low Frequency Pitch		6			
Low Frequency Roll			6		
Vibration and Harshness				6	
Comfort Comments					

Driver 3 Baseline Subjective Assessment - Offenbach

Driver 3 Setup Comparison Subjective Assessments - Offenbach

Appendix 3

Body Acceleration Evaluations from Road Testing

Section 3.7– Collection of Road data and Basic Spatial Characteristic Estimation, detailed tests carried out on Swindon and Offenbach driving routes for the collection of rear hub acceleration for use in road characterisation. In the same investigation an IMU device was fitted to the vehicle along with an accelerometer on the driver's seat rail recorded using a national instruments logger. Using the measured seat rail acceleration and the vertical, roll and pitch accelerations measured by IMU, assessment could be made of the driver discomfort for various parts of the driving routes.

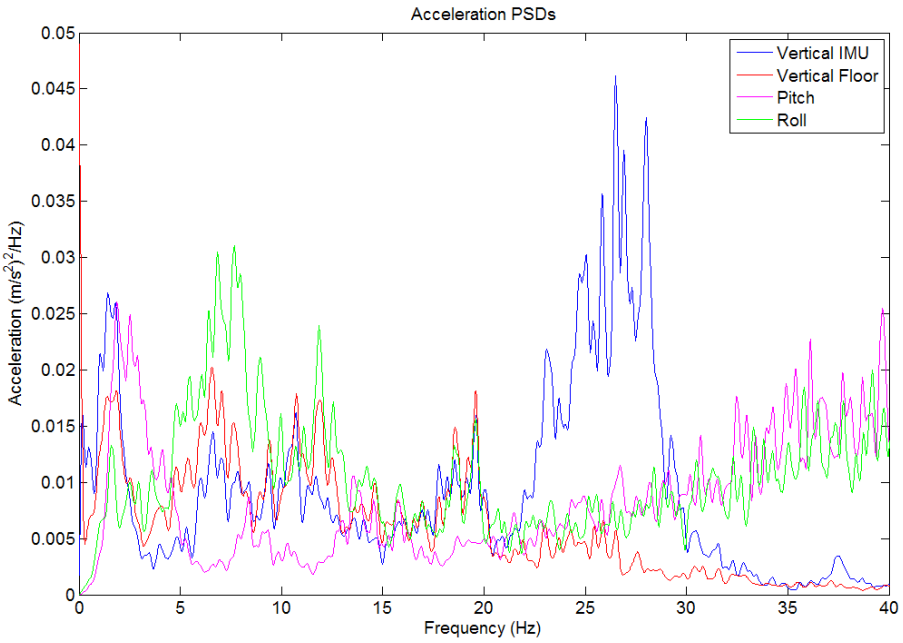

Figure 0-1 – Un-weighted Body Acceleration – Swindon Section 2/3

Figure 0-1 presents the un-weighted acceleration measured at the floor (using the seat rail accelerometer) and the vertical roll and pitch accelerations from the IMU. Evidence of the wheelbase filtering effect explained in section 3.2 – Effect of Vehicle Speed, can be seen at frequencies up to 13Hz. A large amount of pitch acceleration is present between 1.6 and 2.9Hz and a large amount of roll acceleration present between 6 and 8Hz, where as the vertical body acceleration is quite consistent up to 13Hz when it is excited by the road input. The difference between the vertical IMU and vertical floor accelerations below 20 Hz is due to the locations of the two accelerometer units and the vertical acceleration caused by pitch and roll. The floor accelerometer was placed on the seat rail of the drivers seat, whist the IMU was mounted on a pole between the floor and roof in the between the front and rear seats in the centre of the car. The large vertical IMU accelerations around 27Hz are thought to be due to a structure mode caused by the floor, roof and IMU mounting system.

The same accelerations weighted using the BS6841 [1] weighting functions are presented in Figure 0-2. In this case the vertical acceleration becomes dominant in terms of comfort and is worst in the 5-12Hz range. Figure 0-3 presents the weighted vertical acceleration surface along the length and width of the car with reference the IMU position. The lowest acceleration is experienced at a point 0.5m ahead of the IMU, approximately in-line with the centre of the driver and front passenger seats. The highest level of discomfort would be experienced in the outer rear passenger seats. From the speed histogram in Figure 0-4 it can be seen that the speed during this section was fairly well distributed with a bias towards higher speeds, although 30% of the time was spent between 15 and 16.5 m/s and 10% of the time spent at 19.5 m/s.

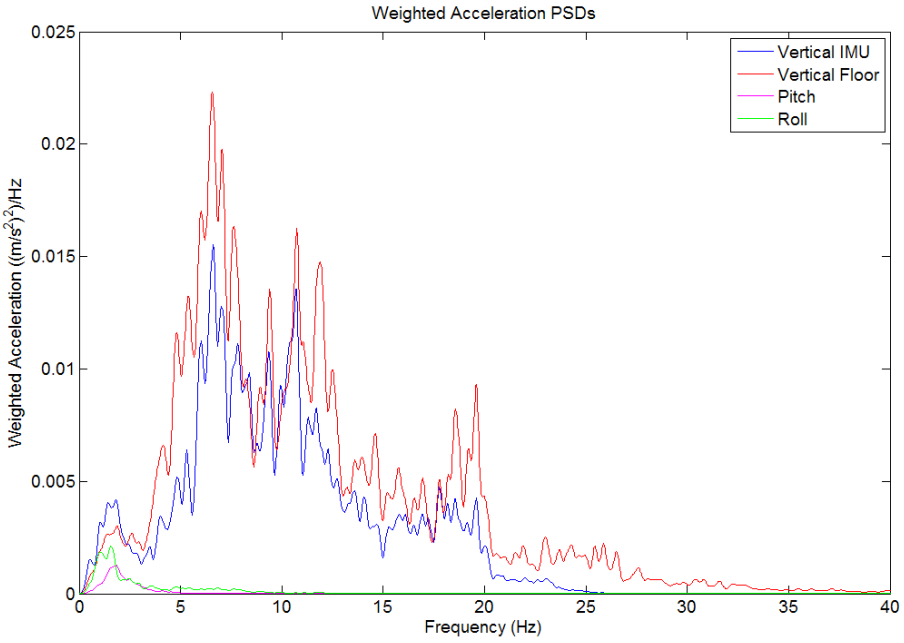

Figure 0-2 – Weighted Body Acceleration - Swindon Section 2/3

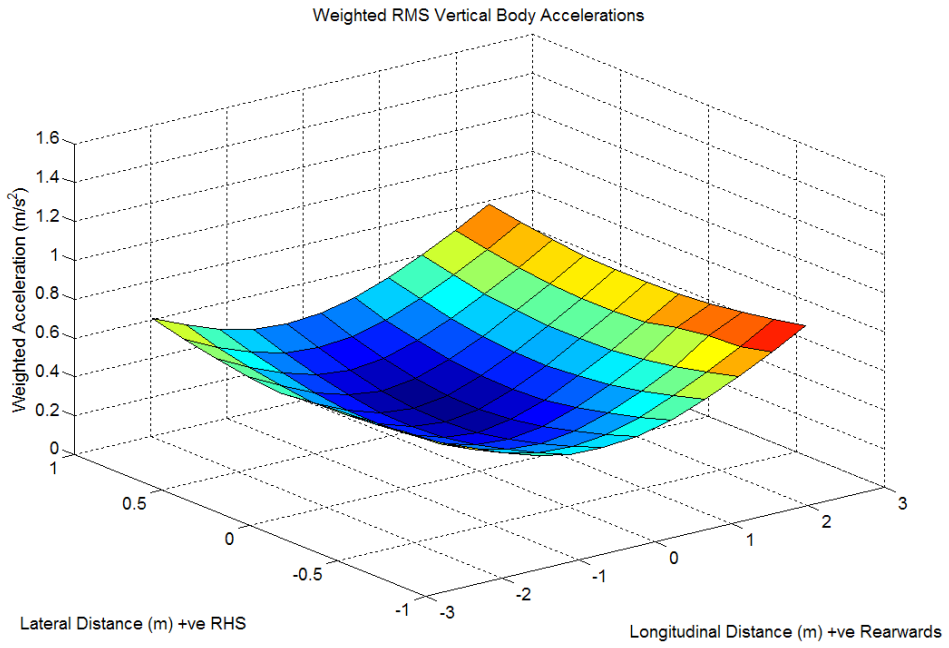

Figure 0-3 – RMS Weighted Vertical Body Acceleration – Swindon Section 2/3

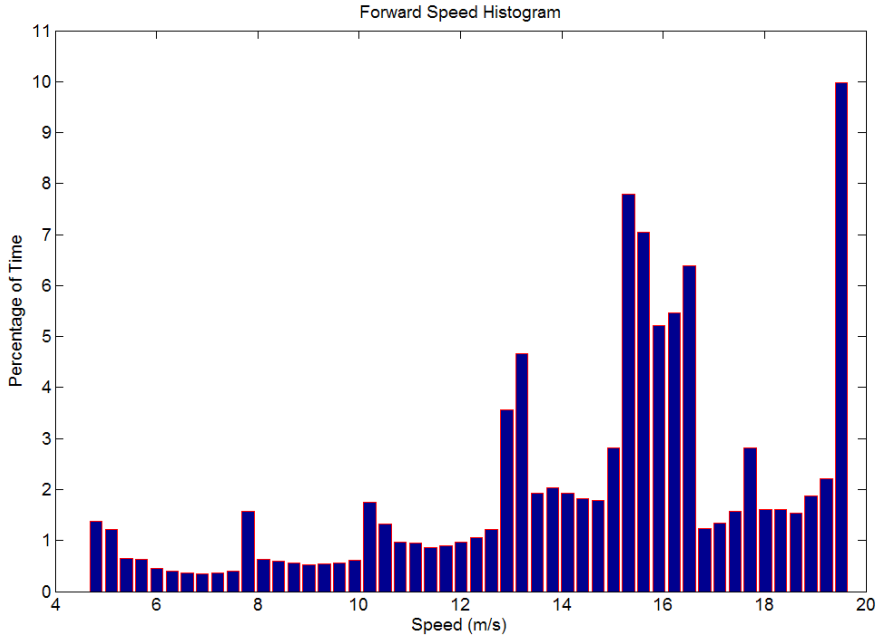

Figure 0-4 – Speed Histogram – Swindon Section 2/3

In Figure 0-5 to Figure 0-8 plots are presented for Swindon section 8/9. The results show much larger low frequency acceleration content for vertical, pitch and roll measures than the section 2/3 case. Once weighted this means that the highest level of discomfort occurs just over 1 Hz, with roll having a much larger influence than in section 2/3. As with section 2/3 there is also high

discomfort levels in the 5 to 12Hz region. The increased level of pitch and roll is also observed in the vertical acceleration surface (Figure 0-7), where as well as the magnitude being larger than section 2/3, the curve is much steeper. The speed histogram in Figure 0-8 shows that this section 8/9 was traversed at a higher speed than section 2/3. The higher speed and roughness will cause a magnitude change of the experienced accelerations, but the cause of the change in frequency distribution is due to the relative PSD gradients of the two road surfaces. Section 2/3 had an exponent of 2.21, whist section 8/9 had an exponent of 2.84, meaning that section 8/9 would be expected to have a higher low frequency content than section 2/3.

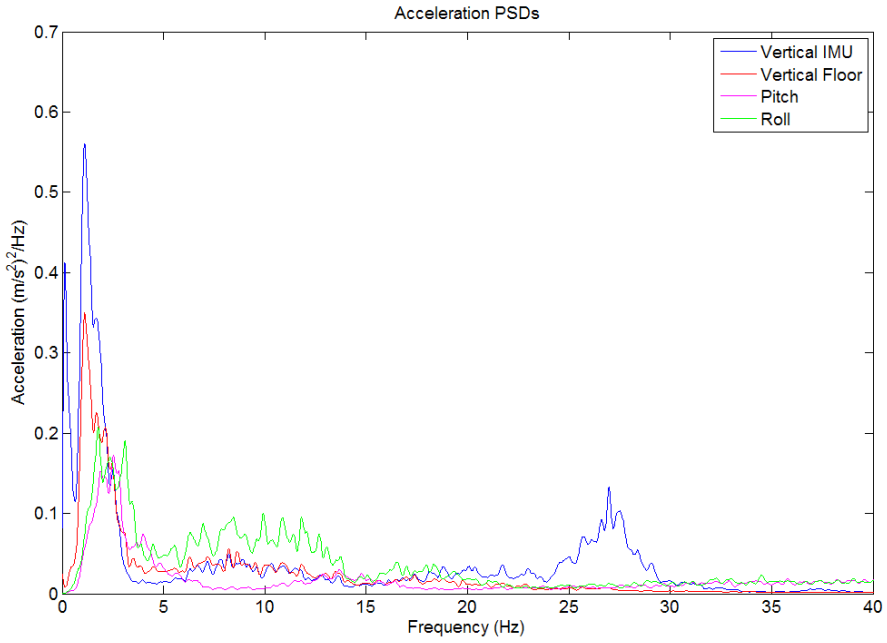

Figure 0-5 – Un-weighted Body Acceleration – Swindon Section 8/9

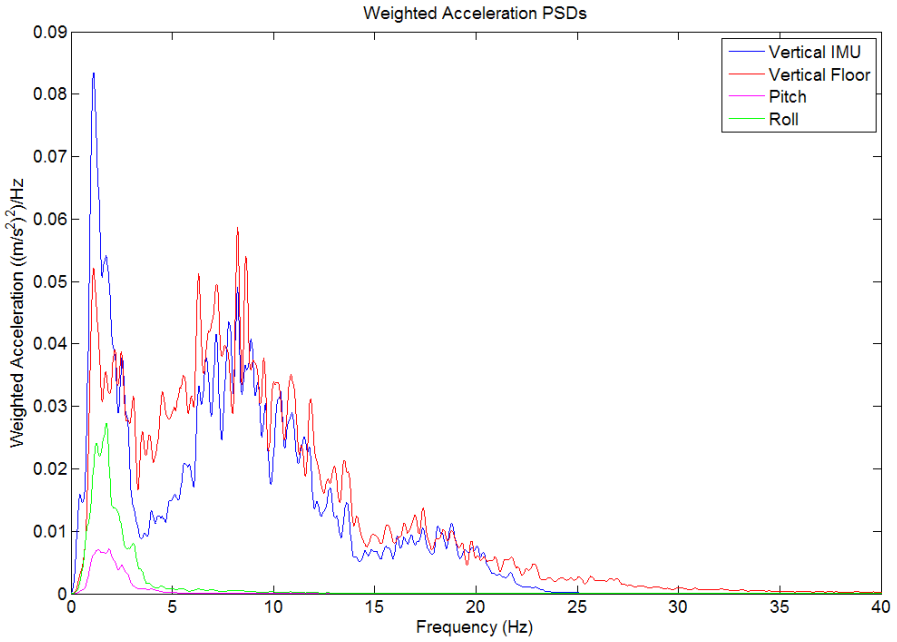

Figure 0-6 – Weighted Body Acceleration – Swindon Section 8/9

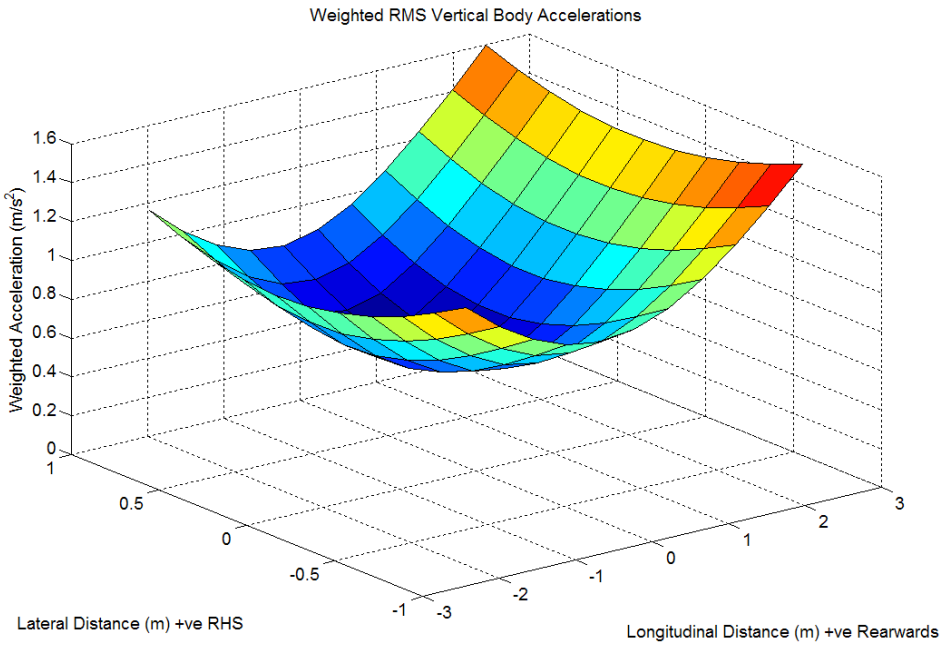

Figure 0-7 – RMS Weighted Vertical Acceleration 3D Map – Swindon Section 8/9

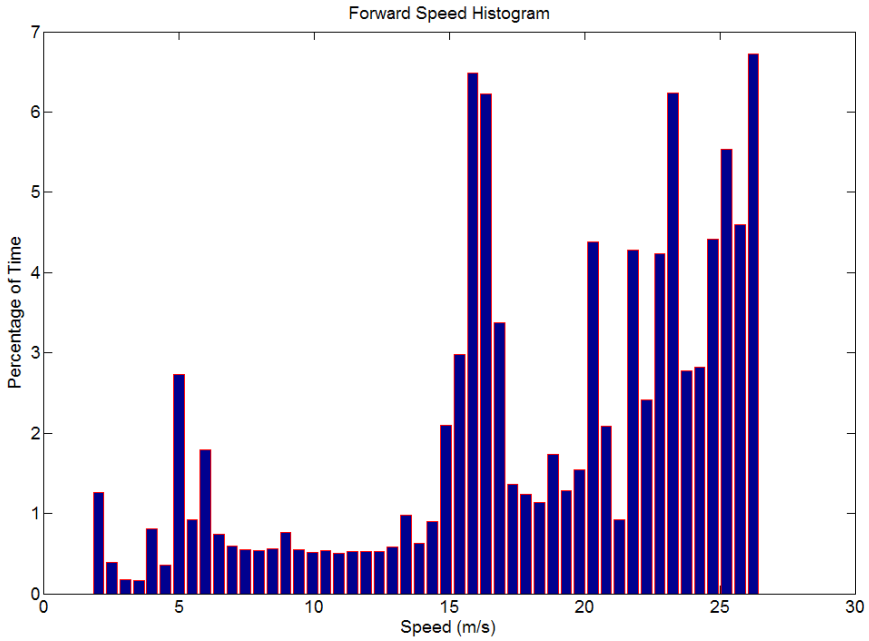

Figure 0-8 – Speed Histogram – Swindon Section 8/9

A third and final Swindon comparison is presented for section 11 in Figure 0-9 to Figure 0-12. In this case the situation is again quite different to section 2/3 and section 8/9. The un-weighted body acceleration PSDs show clearly the wheelbase filtering affects up to around 12Hz, with very dominant pitch behaviour around 2Hz. Once weighted, the discomfort is mostly focussed around the 5-7Hz range due to an almost pure heave input in this frequency range. The 3D RMS weighted vertical acceleration map in Figure 0-11, shows a large variation in discomfort along the longitudinal axis of the vehicle compared to the lateral case, due the large level of pitch. Interestingly lowest discomfort zone is no longer in the lateral centreline of the vehicle. Instead the lowest weighted acceleration RMS is achieved around 0.2m towards the driver's side of the vehicle. Comparison of the rear left and right hub acceleration PSDs (Figure 0-13) showed that the magnitude was larger at the left for quite a wide range of frequencies, meaning that the left-hand-side road input would have been larger. The speed histogram (Figure 0-12) shows that 82% of the time was spent between 11 and 14 m/s, which explains the high level of wheelbase filtering apparent in the body acceleration PSDs.

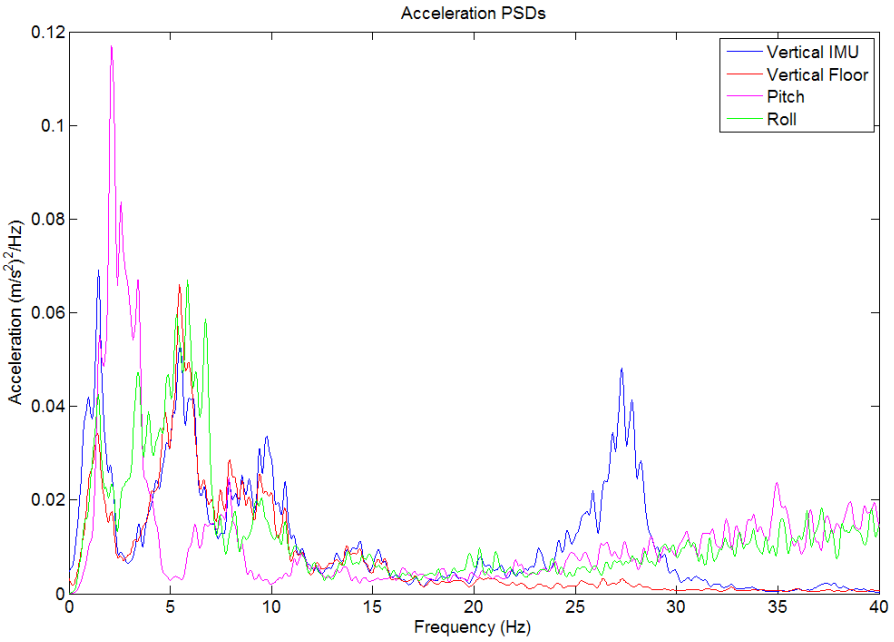

Figure 0-9 – Un-weighted Body Acceleration – Swindon Section 11

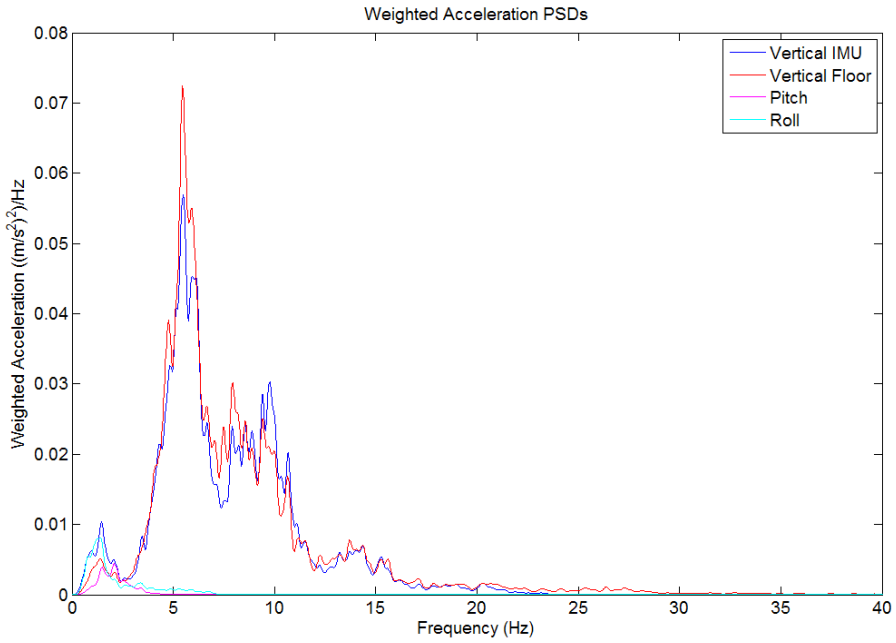

Figure 0-10 – Weighted Body Acceleration – Swindon Section 11

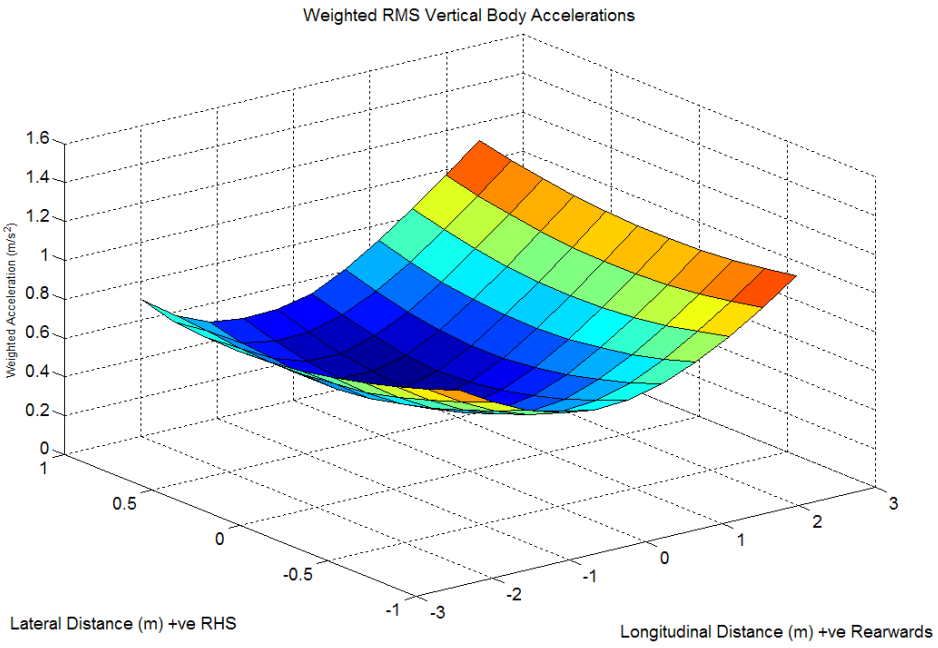

Figure 0-11 – RMS Weighted Vertical Acceleration 3D Map – Swindon Section 11

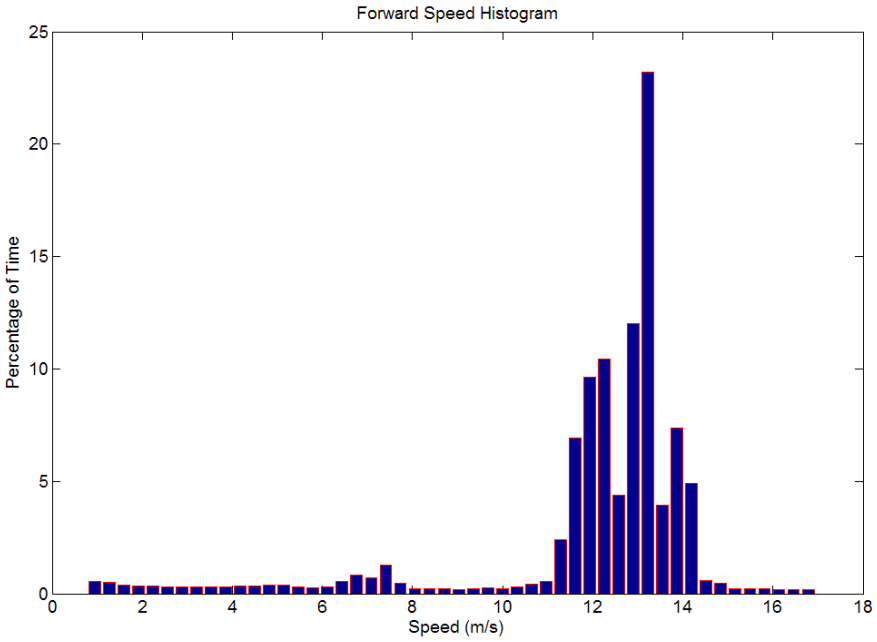

Figure 0-12 – Speed Histogram – Swindon Section 11

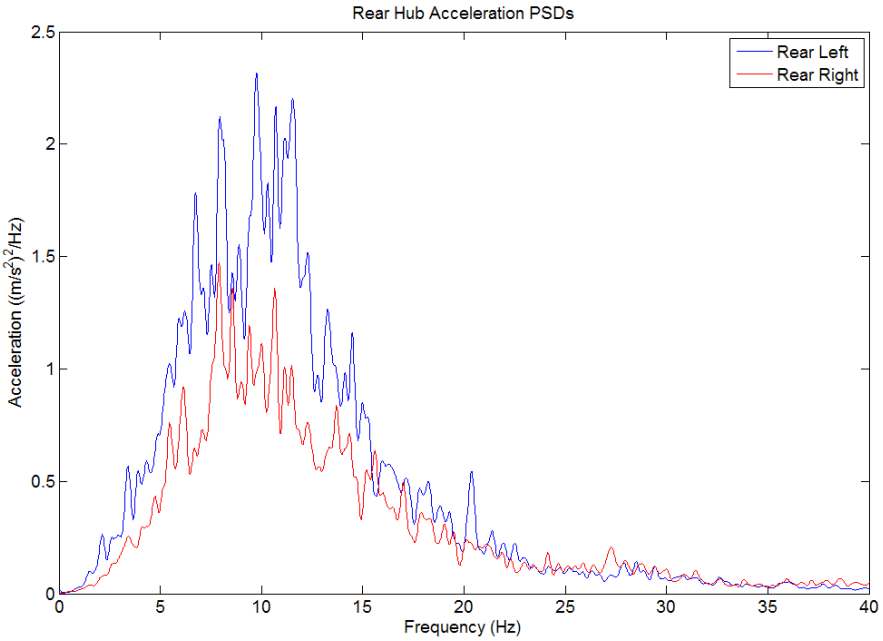

Figure 0-13 – Hub Acceleration PSD Comparison – Swindon Section 11

Analysis of the Offenbach data showed that the frequency distribution of Offenbach section 4 was most like Swindon section 2/3, but with more low frequency dominance. Offenbach section 5 was similar in heave and pitch to Swindon section 8/9, but had much lower roll content. Offenbach Section 9 was most like Swindon section 2/3 in frequency distribution, but with a smaller magnitude. Offenbach section 12 had fairly large low frequency content in comparison to high frequency, but less than in the Swindon section 8/9 case. Unfortunately the floor accelerometer had some interference on occasions causing peaks at 2.15 increments in the frequency domain (Figure 0-14). This cause of this was unknown so only the vertical IMU and pitch and roll IMU could be used for overall comparisons.

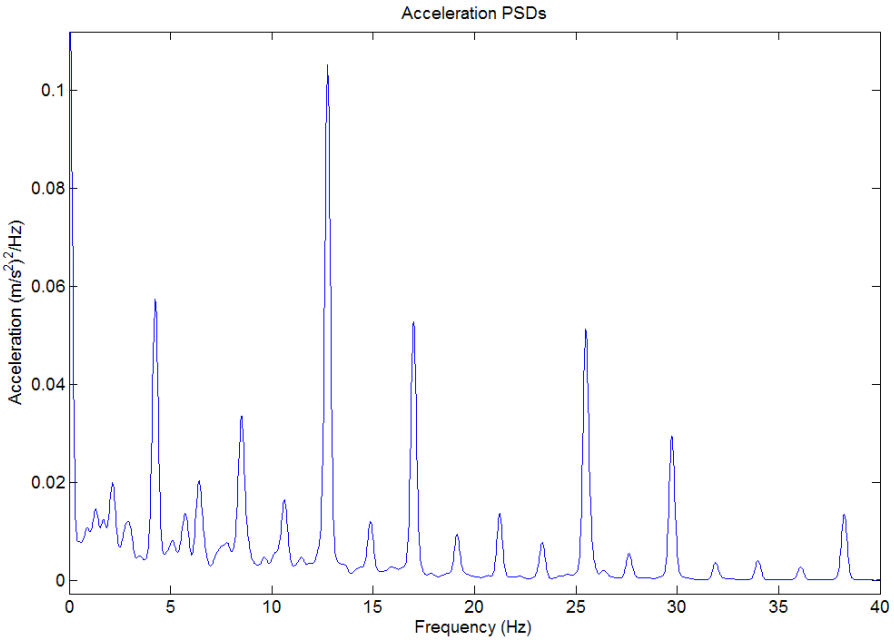

Figure 0-14 – Floor Accelerometer Interference

Generally the Offenbach drive route road surfaces had lower overall amplitude than the Swindon surfaces, but also had higher gradients on average. This led to the majority of the Offenbach sections having a higher dominance of low frequency discomfort (<5Hz) than the Swindon sections. In addition, the variation in discomfort PSD shape was much larger for the Swindon route than in Offenbach. This comes from a larger variation in road gradient of the Swindon drive route in comparison to Offenbach, which can be seen in Table 3-1. This larger variation means that tuning of a vehicle suspension for the best compromise over the entire drive route would be a more difficult task for the Swindon drive route than the Offenbach drive route. In addition tuning a suspension system purely on the Offenbach drive route could produce a vehicle that performs poorly on the Swindon drive route and vice-versa.

The RMS discomfort at the IMU position for the Swindon route and two Offenbach parts are compared below. The RMS discomfort for the Swindon route is close to double that of the Offenbach routes, which were 11% different, to show that this was not purely related to forward speed the three complete route speed histograms are shown in Figure 0-15 to Figure 0-17. The Swindon and Offenbach Part 2 speed histograms show relatively similar speed distributions.

- Swindon overall RMS comfort at 0,0 = 0.503 m/s^2
- Offenbach Part 1 overall RMS comfort at 0,0 = 0.246 m/s^2
- Offenbach Part 2 overall RMS comfort at 0,0 = 0.274 m/s^2

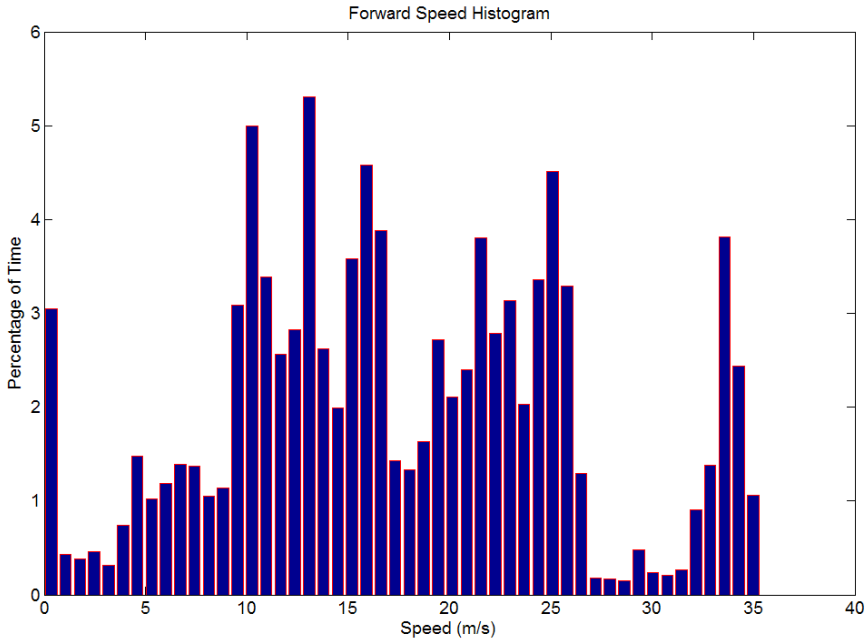

Figure 0-15 – Speed Histogram - Swindon

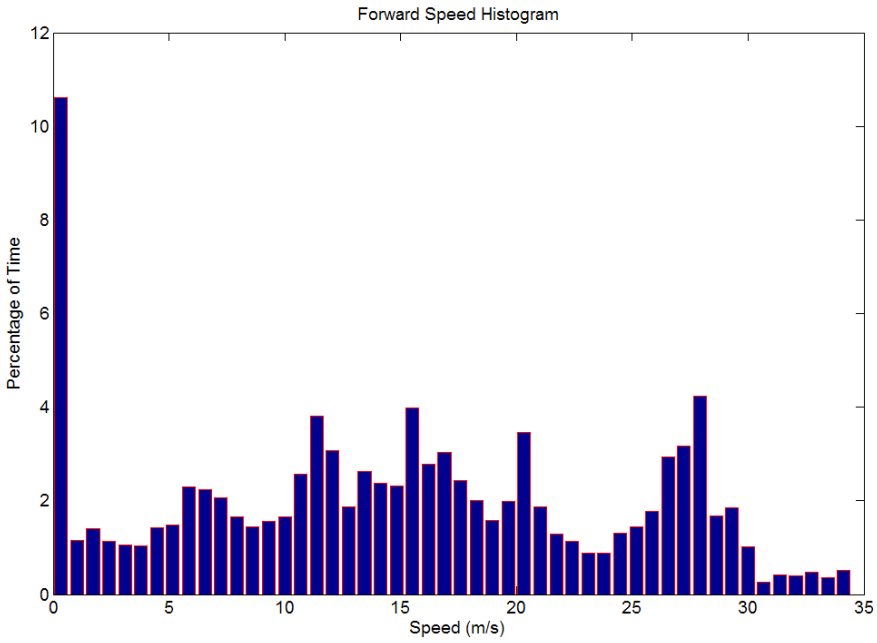

Figure 0-16 – Speed Histogram – Offenbach Part 1

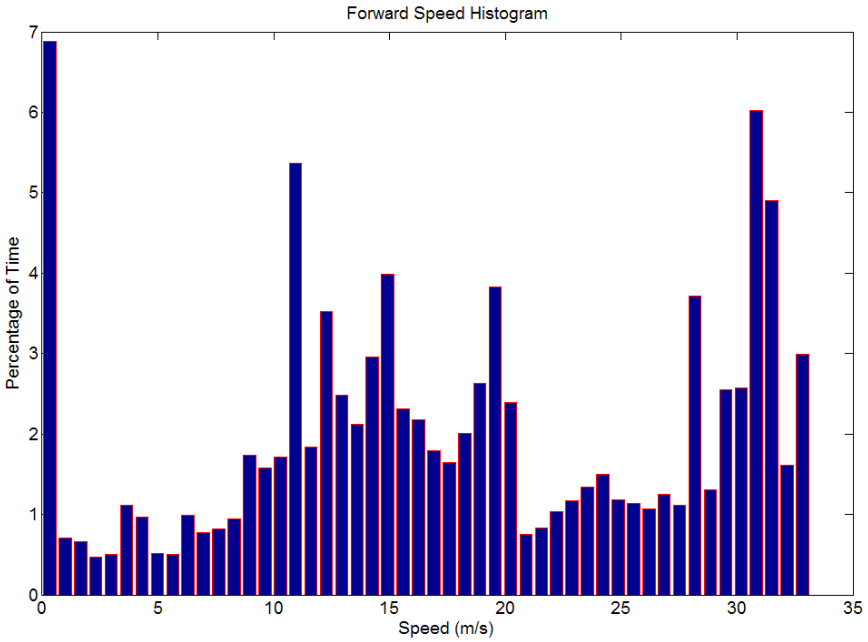

Figure 0-17 – Speed Histogram - Offenbach Part 2